Synthesis and Utilization of Non-ribosomal Amino Acids Consisting of Carbon-Carbon Double Bonds in the Design of Hybrid Peptide Foldamers

विद्या वाचस्पति की
उपाधि की अपेक्षाओं की आंशिक पूर्ति में प्रस्तुत शोध प्रबंध

A thesis submitted in partial fulfillment of the requirements of the degree of Doctor of Philosophy

द्वारा / **By**

सचिन अ. नलावडे Sachin A. Nalawade

पंजीकरण सं. / Registration No.: 20153374

शोध प्रबंध पर्यवेक्षक / Thesis Supervisor: प्रो. एच. एन. गोपी
Prof. H. N. Gopi



भारतीय विज्ञान शिक्षा एवं अनुसंधान संस्थान पुणे
INDIAN INSTITUTE OF SCIENCE EDUCATION AND RESEARCH PUNE

2024

Dedicated to my Family and All Supporters!!!



भारतीय विज्ञान शिक्षा एवं अनुसंधान संस्थान पुणे
INDIAN INSTITUTE OF SCIENCE EDUCATION AND RESEARCH PUNE
डॉ. होमी भाभा मार्ग, पुणे 411008, महाराष्ट्र, भारत | Dr. Homi Bhabha Road, Pune 411008, Maharashtra, India
T +91 20 2590 8001 W www.iiserpune.ac.in

IISER PUNE

CERTIFICATE

This is to certify that the work incorporated in the thesis entitled "**Synthesis and Utilization of Non-ribosomal Amino Acids Consisting of Carbon-Carbon Double Bonds in the Design of Hybrid Peptide Foldamers**" submitted by **Sachin A. Nalawade (ID No. 20153374)** carried out by the candidate at the Indian Institute of Science Education and Research (IISER), Pune, under my supervision. The work presented here or any part of it has not been included in any other thesis submitted previously for the award of any degree or diploma from any other University or Institution.

Date: 15/02/2024

Prof. Hosahudya N. Gopi
(Research Supervisor)
Professor, Department of Chemistry,
IISER-Pune
Pune-411008, India

भारतीय विज्ञान शिक्षा एवं अनुसंधान संस्थान पुणे
INDIAN INSTITUTE OF SCIENCE EDUCATION AND RESEARCH PUNE
डॉ. होमी भाभा मार्ग, पुणे 411008, महाराष्ट्र, भारत | Dr. Homi Bhabha Road, Pune 411008, Maharashtra, India
T +91 20 2590 8001 W www.iiserpune.ac.in

IISER PUNE

Declaration

I hereby declare that the thesis entitled "**Synthesis and Utilization of Non-ribosomal Amino Acids Consisting of Carbon-Carbon Double Bonds in the Design of Hybrid Peptide Foldamers**" submitted for the degree of Doctor of Philosophy in Chemistry at Indian Institute of Science Education and Research (IISER), Pune has not been submitted by me to any other University or Institution. This work was carried out at Indian Institute of Science Education and Research (IISER), Pune, India under the supervision of Prof. Hosahudya N. Gopi.

Date: 16-02-2024

Sachin A. Nalawade
ID: 20153374
Research Fellow
Department of Chemistry,
IISER-Pune
Pune-411008

Acknowledgment

First, I would like to extend my sincere appreciation to my esteemed PhD supervisor **Prof. Hosahudya N. Gopi** for his invaluable guidance and unwavering support throughout my doctoral journey, enabling the successful completion of my research. Prof. Gopi's expertise, dedication, and mentorship have been pivotal in shaping my research and academic growth. His commitment to excellence, tireless efforts, and encouragement have been a constant source of inspiration. I extend my sincere appreciation to Prof. Gopi for his instrumental role in my research and academic success and for being an exceptional supervisor. His influence will continue to resonate in my professional journey. Thank you, Prof. Gopi, for your assistance at every challenging juncture, invaluable support, guidance, and inspiration.

I extend my sincere thanks to our present director Prof. Sunil Bhagwat, and former directors, Prof. Jayant B. Udgaonkar and Prof. K. N. Ganesh for providing outstanding research facilities and infrastructure. I am also thankful to IISER-Pune for granting me a five-year research fellowship. Special appreciation goes to **Prof. Ramakrishna G. Bhat** (IISER-Pune) and **Prof. Hirekodathakallu V. Thulasiram** (NCL-Pune) for being the members of my research advisory committee. Their valuable suggestions and constructive criticism have consistently guided me in the right direction. I also like to express my gratitude for all of the chemistry professors at IISER, Pune, for their support and direction. I am very much thankful to Mr. Ravinder and Mr. Nasa for SC-XRD analysis, Mr. Sandip and Mr. Nitin for NMR analysis, Mr. Prajapathi and Mr. Mahesh for MALDI analysis, Mr. Sandip Kanade for HRMS study. I am also thankful to Mr. Mayuresh, Mr. Thushar, Mr. Ganesh and Mr. Sanjay for the administrative help.

I consider myself fortunate to have incredible labmates, and I express my heartfelt thanks to each one of them. Among the senior lab members, Dr. Anupam Bandyopadhyay, Dr. Sandip Jadhav, and Dr. Sachitanand Mali had already moved on before my arrival in the group. Upon joining, I had the privilege of working alongside Dr. Ganesh (Anna), Dr. Sushil, Dr. Rajkumar, Dr. Anindita, Dr. Rahi, Dr. Veeresh, and Mr. Rupal who were seniors during my early days in the group. Their support has been invaluable since the beginning of my PhD journey, and I consider myself fortunate to have such supportive seniors. In particular, I had the opportunity to work closely with Ganesh Anna. When I joined, Ganesh Anna was in the final year of his PhD and deeply engrossed in completing his research. Despite his busy schedule, he generously

shared his knowledge, guiding me on various fundamental aspects that proved instrumental in navigating my own PhD tenure. I am deeply thankful to my current labmates with whom I have been working closely for over half of my PhD duration include Sanjit Dey, Puneeth Kumar, Manjeet Singh, Saikat Pahan, Souvik Panda, Souvik Roy, Sandip Toraskar and undergraduate students Mona, Abhijit, Sereena, Vivek, Rajat, Nithun, Manish, Devanandan, Keerthivason, Avanthika, Utthara. All my labmates have been remarkably supportive, cultivating a positive and friendly ambiance in the laboratory. I must acknowledge the support I received from everyone, not just in the realm of my research but also on a personal level. Each individual helped in their own capacity, and their assistance has been invaluable. I am really lucky to have such nice second family in my life.

At certain moments in life, we cross paths with individuals who selflessly lend a helping hand without any expectations. I am fortunate to have such individuals in my life, and their assistance has been invaluable during challenging times. My heartfelt gratitude goes to Dr. Srinu Tothadi, Dr. Shiv Pal, and Mr. Rishukumar Panday for their unwavering support and assistance. Without friend's life in campus would be boring, I would like to express my sincere gratitude to all my friends, including Dr. Ganesh Shinde, Dr. Yogeshwar more, Dr. Gijo George, Dr. Ravibhushan Kulkarni, Dr. Shahaji More, Dr. Santosh Shelar, Dr. Laxman Sawase, Dr. Iranna Todkari, Mr. Utreshwar Gavhane Dr. Uday, Dr. Bhavin, and most importantly, the entire IISER-community.

The successful completion of my PhD study stands as a testament to the indispensable role played by my family. No words can adequately capture the profound sacrifices made by my mother Vimal, my father Ashokrao, and my late beloved younger brother Nitin. Their selflessness and dedication surpass any measure; if I were to give my life, it would still be an insufficient token of appreciation. Throughout my PhD tenure, I found myself unable to fulfill my responsibilities towards my parents. Yet, in my absence, my sister, Pratibha, and her husband, Vishnu, stepped in admirably, providing unwavering care and support to our parents. In the demanding pursuit of my academic endeavors, regrettably, I found myself unable to allocate ample time to my beloved family - my wife, Yogita, and our two cherished children, Ansh and Aaradhya, never voiced complaints. Instead, they remained my unwavering support system, patiently awaiting my time and attention.

In closing, I extend my deep appreciation to the elemental forces of nature, recognizing their significant contribution in granting me the resilience and courage necessary to pursue the aspirations of my life.

Sachin A. Nalawade

Contents

Abbreviations……..i

Abstract……..…….iv

Publications……..……v

Chapter 1: Unveiling the Structural Essence: Exploring Protein Structures and the Influence of Non-Ribosomal Amino Acids in Protein-Like Constructions

1.1. Introduction……2

1.2. Protein Structure Mimetics……..5

1.2.1. β- Amino acids in the design of peptide foldamers……...5

1.2.2. γ- Amino acids in the design of peptide foldamers……...8

1.2.3. α, β-unsaturated γ-amino acids in the design of peptide foldamers……11

1.2.3.1. Biological Significance of α, β-unsaturated γ-amino……...11

1.2.3.2. Earlier work on α, β-unsaturated γ-amino acids in the context of foldamers……11

1.3. Chemistry of α,β-unsaturated γ-amino acids……15

1.6. References……16

Chapter 2: Stereoselective Synthesis of Backbone Extended π-Conjugated Amino Esters

2.1. Introduction……...23

2.2. Objective of the current work……24

2.3. Results and discussion……...25

2.4. Conclusion……33

2.5. Experimental details……..33

2.5.1. General information……33

2.5.2. General procedure for the synthesis of Boc-amino allylic alcohol (**2a-2g**) ……34

2.5.3. General Procedure for the synthesis of (*E*)-Boc-α,β-unsaturated γ-amino aldehydes (**3a-3g**) ……37

2.5.4. General Procedure for the synthesis of Ethyl ester of (E)α-β, (E)γ-δ, ε-Amino acids (**4a-4g**) ……37

2.5.5. General Procedure for the Synthesis of (*E, E*)-Carbon-Carbon double bond conjugated allylic alcohols (**5a-5c**) ……40

2.5.6. General Procedure for the Synthesis of (*E*)α-β, (*E*)γ-δ, ε-amino aldehydes (**6a-6c**) …42

2.5.7. General Procedure for the Synthesis of ethyl ester of (E)α-β, (E)γ-δ, (E)ε-ζ, η-amino acids (**7a-7c**) ……43

2.5.8. Synthetic Procedure for the Preparation of homo-dipeptide (**8a**) …….44

2.6. Chiral HPLC Trace of Compounds **2a**, **4a**, **5a**, **7a**, **2e** and **4e**……46

2.7. References…….47

2.8. Appendix……...49

2.8.1. Ortep plot and crystallographic information of compounds **2a-2e**, **4b, 4c, 7a, 7c** and **8a**……..49

2.8.2. ^{1}H NMR, ^{13}C NMR and HRMS spectra of all compounds……59

2.8.3. Copy of the Permission letter from Journal for reuse of figures and diagrams…….....94

Chapter 3: Design of Shortest Helix-Turn-Helix Mimetics from α,γ-Hybrid Peptide Foldamers

3.1. Introduction……...96

3.2. Objective of the current work……97

3.3. Results and discussion……...98

3.3.1. Crystal structure analysis of **P1**……..99

3.3.2. Crystal structure analysis of **P2** and **P3**…….101

3.3.3. Crystal structure analysis of **P4**…….105

3.3.4. Superposition of the peptide **P4** over the helix-turn-helix motif of the 434 repressor DNA-binding domain protein…….108

3.3.5. 2D-NMR (TOCSY & ROESY) analysis of peptides **P1**, **P2** and **P4**, NOE correlations with their solid state structures……109

3.3.5.1. Peptide **P1** 2D-NMR analysis and NOE correlations with its solid state structure….110

3.3.5.2. Peptide **P2** 2D-NMR analysis and NOE correlations with its solid state structure….116

3.3.5.3. Peptide **P4** 2D-NMR analysis and NOE correlations with its solid state structure…123

3.3.6. CD Spectroscopy of peptides **P1**, **P2**, **P3** and **P4**……...129

3.3.7. HPLC trace of peptides **P1**, **P2**, **P3** and **P4**……130

3.4. Conclusion……...130

3.5. Experimental details……131

3.6. References……...141

3.7. Appendix…….144

3.7.1. Ortep plot and crystallographic information of **P1**, **P2**, **P3** and **P4**……145

3.7.2. ^{1}H NMR and mass spectra of peptides **P1**- **P4**……...151

3.7.3. ^{1}H NMR, ^{13}C NMR and HRMS spectra of monomer units……155

3.7.3. Copy of the Permission letter from Journal for reuse of figures and diagrams……...164

Chapter 4: Unveiling Reactivity Patterns in Thiol Addition Reactions on α, β-Unsaturated γ-Amino Acid Amides and Peptides Composed of it

4.1. Introduction……166

4.2. Objective of the current work……..167

4.3. Results and discussion……168

4.3.1. Outcome of the Reaction between Thioacetic acid and (*E*)-α,β-Unsaturated γ-Amino Amides (**1-5, 2'' and 3''**) and ester (**7**)……...169

4.3.1.1. Reaction in the presence of a base: Both α and β addition products were observed in each reactions……169

4.3.1.2. Reaction in absence of a base: Only β addition products were observed in each reactions……178

4.3.1.3. Reaction Under Inert Atmosphere: Only β addition products were observed in the reaction……...181

4.3.2. Outcome of the Reaction between Thiophenol and BocNH-(*E*)-α,β-Unsaturated γ-Phenylalanine Benzyl Amides (**6**)……...182

4.3.3. A concise overview of thioacid and thiol conjugate addition reactions conducted under diverse conditions with various substrates and plausible mechanisms inferred from the experiments……182

4.3.4. Outcome of the thioacetic acid and thiol (thiophenol / ethanethiol) addition reactions on peptide backbone containing (*E*)-α,β-unsaturated γ-amino acids……185

4.3.5. Ramachandran type plot of Peptides **P2a**, **P2b**, **P3** and **P4**……199

4.3.6. CD Spectroscopy of peptides **P2a**, **P2b**, **P3** and **P4**……200

4.4. Conclusion……...201

4.5. Experimental details……201

4.6. References……...227

4.7. Appendix…….230

4.7.1. Ortep plot and crystallographic information of peptide **7B**, **1A**, **1C**, **2C**, **2D**, **3C**, **4C**, **2A**'', **5A**, **P1**, **P2a**, **P2b**, **P3** and **P4**…….230

4.7.2. ^{1}H NMR, ^{13}C NMR, HRMS and MALDI spectra of all compounds and peptides…….244

Chapter 5: α, γ-Hybrid Peptide Foldamers Consisting of γ-Amino Acid with Aromatic Backbone: Role of Chiral and Achiral Amino Acids in Folding Patterns of Hybrid Peptides

5.1. Introduction…….294

5.2. Objective of the current work……..296

5.3. Results and discussion…….296

5.3.1. Crystal structure analysis of **P1**……297

5.3.2. Crystal structure analysis of **P2**……299

5.3.3. Crystal structure analysis of **P3**……301

5.3.4. NMR structure analysis of peptides **P3**, **P4** and **P5** using 2D NMR (TOCSY & ROESY) analysis and DMSO-d_6 titration …….302

5.3.4.1. Peptide **P3** and **P4** NMR structure analysis, using 2D NMR (TOCSY and ROESY) and DMSO-d_6 titration……...303

5.3.4.2. Peptide **P5** NMR structure analysis, using 2D NMR (TOCSY and ROESY) and DMSO-d_6 titration……..315

5.4. Conclusion……...321

5.5. Experimental details……322

5.5.1. General information…….322

5.5.2. Procedure for the synthesis of 2-aminophenyl acetic acid……...323

5.5.3. Synthesis of hybrid peptides containing 2-aminophenyl acetic acid ……..323

5.6. References……...330

5.7. Appendix…….334

5.7.1. Ortep plot and crystallographic information of **5a, P1, P2** and **P3**……..334

5.7.2. ^{1}H NMR and ^{13}C NMR spectra of all compounds……...339

Abbreviations

Ac_2O = Acetic anhydride

Apa = (2-aminophenyl)acetic acid

ACN = Acetonitrile

AcOH = Acetic acid

Aib = α-Amino isobutyric acid

Aic = 4-amino isocaproic acid

aq. = Aqueous

BF_3OEt_2 = Boron trifluoride etherate

Bn = Benzyl

Boc = tert-Butoxycarbonyl

$(Boc)_2O$ = Boc anhydride

^tBu = tertiary Butyl

Calcd. = Calculated

CCDC no. = Cambridge Crystallographic Data Centre number

CIF = Crystallographic Information File

dγ = dehydro gamma

dr = Diastereomeric ratio

DCC = N, N' –Dicyclohexylcarbodiimide

DCM = Dichloromethane

DD = Double Dehydro

DIBAL-H = Diisobutylaluminium hydride

DIPEA = Diisopropylethyl Amine

DMAP = 4-Dimethylaminopyridine

DMF = Dimethylformamide

DMSO = Dimethylsulfoxide

er = Enantiomeric ratio

Et = Ethyl

EtOAc = Ethyl acetate

EtOH = Ethanol

Fmoc = 9-Fluorenylmethoxycarbonyl

Fmoc-OSu = N-(9-Fluorenylmethoxycarbonyloxy) succinimide

g = gram

h = hours

H-bond = Hydrogen bond

HATU = Hexafluorophosphate Azabenzotriazole Tetramethyl Uronium

HBTU = 2-(1H-benzotriazol-1-yl)-1, 1, 3, 3-tetramethyluronium hexafluorophosphate

HCl = Hydrochloric acid

H-T-H = Helix-Turn-Helix

HOBt = Hydroxybenzotriazole

IBX = 2-Idoxybenzoic acid

IR = Infrared Spectroscopy

LAH = Lithium Aluminium Hydride

M = Molar

MALDI-TOF/TOF = Matrix-Assisted Laser Desorption/Ionization-Time of Flight

Me = Methyl

MeOH = Methanol

mg = Milligram

min = Minutes

µL = Micro liter

mL = Milliliter

mM = MilliMolar

mmol = millimoles

MS = Mass Spectroscopy

N = Normal

nM = NanoMolar

NHS = N-hydroxy succinimide

NMP = N-methyl pyrrolidone

NMR = Nuclear Magnetic Resonance

ORTEP = Oak Ridge Thermal-Ellipsoid Plot Program

PG = Protecting Group

ppm = Parts per million

Py = Pyridine

R_f = Retention factor

RP- HPLC = Reversed Phase-High Performance Liquid Chromatography

R_t = Retention time

RT = Room Temperature

TFA = Trifluoroacetic acid

THF = Tetrahydrofuran

UV = Ultraviolet–Visible Spectroscopy

*Z*dγ = *Z*-dehydro gamma

Abstract

Designing protein secondary structure mimetics using non-natural amino acids has significant importance in understanding protein folding, as well as from the perspective of medicinal chemistry. Various backbone-modified synthetic amino acids have been explored over the years to design functional foldamers. These include acyclic beta- and gamma-amino acids, carbocyclic beta- and gamma-amino acids, sugar-modified beta- and gamma-amino acids, and dialkyl beta- and gamma-amino acids. In contrast to saturated gamma-amino acids, alpha, beta-unsaturated gamma-amino acids have been frequently found in many biologically active peptide natural products. Our interest lies in understanding the reactivity and conformational properties of these gamma-amino acids, which consist of carbon-carbon double bonds in the backbone. In this work, we have demonstrated the stereoselective synthesis of amino acids with conjugative multiple double bonds in the backbone using the Wittig reaction. We thoroughly investigated the stereochemistry and substrate scope of the Wittig reaction in the synthesis of conjugative multiple double bonds and successfully isolated amino acids with multiple conjugated double bonds with complete E-selectivity in excellent yields. Furthermore, we explored these amino acids for the design of helix-turn-helix type foldamers. We synthesized a series of helix-turn-helix structures and studied their conformations in single crystals and solution. By combining alpha, gamma and alpha, beta-unsaturated amino acids, we demonstrated the helix-turn-helix motifs in short sequences consisting of seven residues. Additionally, we examined the reactivity of these alpha, beta-unsaturated amino acids in peptides and monomers. Interestingly, we observed stereoselective alpha-addition of thioacids in peptides, while in monomer amides, we observed both beta- and alpha-addition products. Thus, we proved that the stereoselective alpha-addition products are possible in peptides but not in monomer building blocks. We also explored aromatic amino acids to design alpha, gamma-hybrid peptide foldamers and studied their structural analogy with hybrid peptides composed of alpha, beta-unsaturated amino acids with cis double bonds. The alpha, gamma-hybrid peptides composed of alpha and aromatic gamma-amino acids adopt helical structures with alternating H-bond directionality, a feature rarely observed in protein structures. In summary, our work demonstrates the synthesis, reactivity, and conformations of peptides composed of unsaturated amino acids.

Publications

1. **S. A. Nalawade**, M. Singh, D. R. Puneeth Kumar, S. Dey, H. N. Gopi, Stereoselective synthesis of backbone extended π-conjugated amino esters, *Org.Biomol.Chem.* **2023**, *21*, 2586–2595.
2. **S. A. Nalawade**, M. G. Kumar, D. R. Puneeth Kumar, M. Singh, S. Dey, H. N. Gopi, Crystal structure analysis of helix–turn–helix type motifs in α,γ-hybrid peptides, *CrystEngComm*, **2024**, *26*, 913 – 917.
3. **S. A. Nalawade**, S, V. Jadhav, K. M. P. Raja, H. N. Gopi, α, γ-Hybrid peptide Foldamers consisting of γ-amino acid with aromatic backbone: Role of Chiral and Achiral Amino Acids in Folding Patterns of Hybrid peptides, *Submitted*.
4. **S. A. Nalawade**, H. N. Gopi, Unveiling Reactivity Patterns in Thiol Addition Reactions on α, β-unsaturated γ-amino acid amides and peptides Composed of it, *Submitted*.
5. **S. A. Nalawade,** H. N. Gopi, Efficient Synthesis of Trisubstituted Thiophenes via Single Step Reaction with Thioacetic Acid and α,β-Unsaturated γ-Amino Amides, *Manuscript under preparation.*
6. M. G. Kumar, K. Veeresh, **S. A. Nalawade**, R. V. Nithun, H. N. Gopi, Direct Transformation of N-Protected α,β-Unsaturated γ-Amino Amides into γ-Lactams through a Base-Mediated Molecular Rearrangement, *J. Org. Chem.* **2019**, *84*, 15145–15153.
7. D. R. Puneeth Kumar, **S. A. Nalawade**, S. Pahan, M. Singh, D. Senapati, S. Roy, S. Dey, S. Toraskar, S. Raghothama, H. N. Gopi. Proteolytically Stable ααγ-Hybrid Peptides Inhibits the Aggregation and Cytotoxicity of Aβ42, *ACS Chem. Neurosci.,* **2023**, *14*, 3398–3408.
8. M. Singh, **S. A. Nalawade**, D. R. Puneeth Kumar, K. Veeresh, S. Pahan, S. Dey, H. N. Gopi, HBTU Mediated Synthesis of α,β-Unsaturated γ-Lactams from *E*-α,β-Unsaturated γ-Amino Acids, *Eur. J. Org. Chem.*, **2023**, *26*, e202300682.
9. M. Singh, M. Kumar, **S. A. Nalawade**, D. R. Puneeth Kumar, H. N. Gopi, Cyclization of N-Boc-(*E*)-α,β-Unsaturated γ-Amino Acid Active Esters into N-Boc-(*Z*)-α,β-Unsaturated γ-Lactams through *E* → *Z* Isomerization, *Org. Biomol. Chem.*, **2023**, *21*, 3766-3769.
10. D. R. Puneeth Kumar, R. M. Reja, D. K. Senapati, M. Singh, **S. A. Nalawade**, G. George, G. Kaul, A. Akhir, S. Chopra, S. Raghothama, H. N. Gopi, A cationic

amphiphilic peptide chaperone rescues Aβ42 aggregation and cytotoxicity, *RSC Med. Chem*., **2023**, *14*, 332-340.

11. S. Dey, S. Roy, D. R. Puneeth Kumar, **S. A. Nalawade**, M. Singh, S. Panda Mahapatra, H. N. Gopi, Metal-Directed Hierarchical Superhelices from Hybrid Peptide Foldamers. *Under revision*.
12. D. R. Puneeth Kumar, G. George, S. Pahan, S. Dey, **S. A. Nalawade**, U. Bhattacharya, H. N. Gopi, Designing β-Double-Helix Structures from α,γ-Peptidic Foldamers. *Under Preparation*.

Chapter 1

Unveiling the Structural Essence: Exploring Protein Structures and the Influence of Non-Ribosomal Amino Acids in Protein-Like Constructions

1.1. Introduction

Proteins play a fundamental role in maintaining life in all living organisms through their diverse structures and functions. The functions of proteins depend on their three-dimensional structures, which result from the highly ordered arrangement of their polypeptide backbone. The hierarchical structures of proteins are illustrated in Figure 1. Fundamentally, protein structures are primarily categorized at four levels, primary, secondary, tertiary, and quaternary. These structures correspond to distinct processes involved in the formation of functional proteins. The primary structure is linked to assembly, the secondary structure to folding, the tertiary structure to packing, and the quaternary structure to interactions.

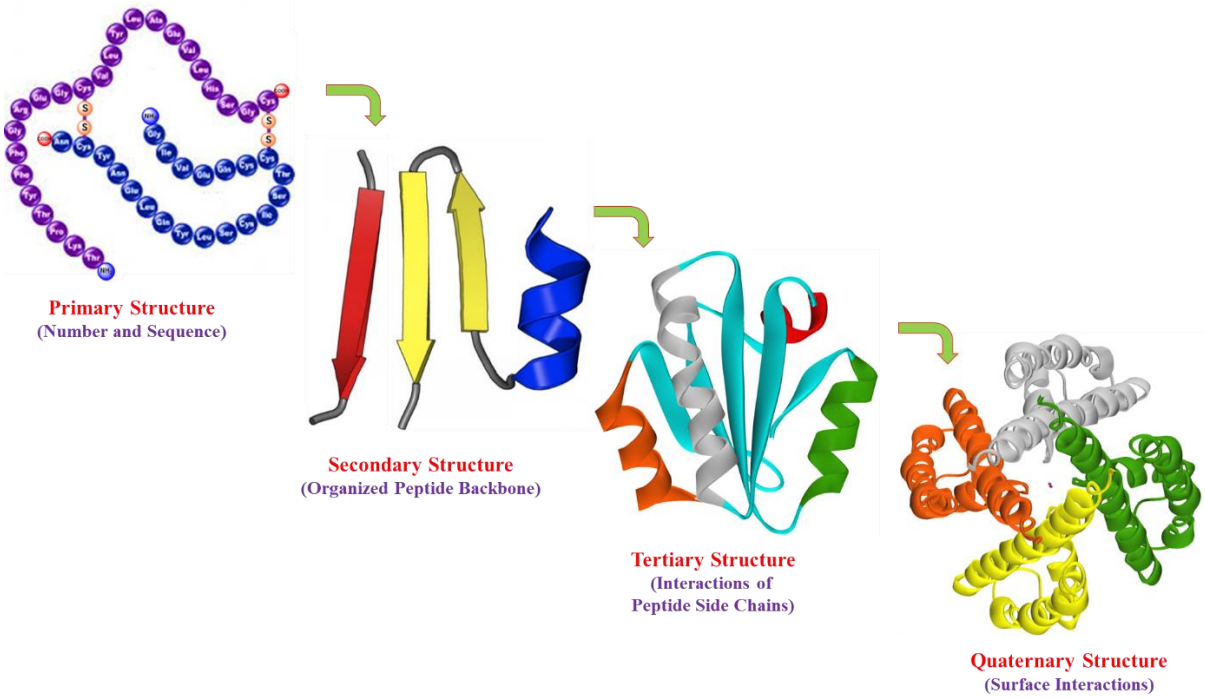


Figure 1: Representation of Hierarchical structures of proteins (PDB codes: 1AIU and 1BL8).

Upon close examination of the tertiary and quaternary structures of proteins, the hyphothetical breakdown of these three-dimensional structures results in secondary structures like α-helices, β-sheets, and β-turns. The combination of one or more secondary structures with specific geometry leads to super-secondary structures or motifs such as β-hairpins, helix-loop-helix, Zinc fingers, β-α-β motifs, leucine zipper, helix-turn-helix, coiled-coils etc. Many of these supersecondary structures are found in transcription factors that interact with DNA. Figure 2 illustrates representative examples of supersecondary structures in proteins.

The primary structure of a protein is determined by the sequence of amino acids that folds into

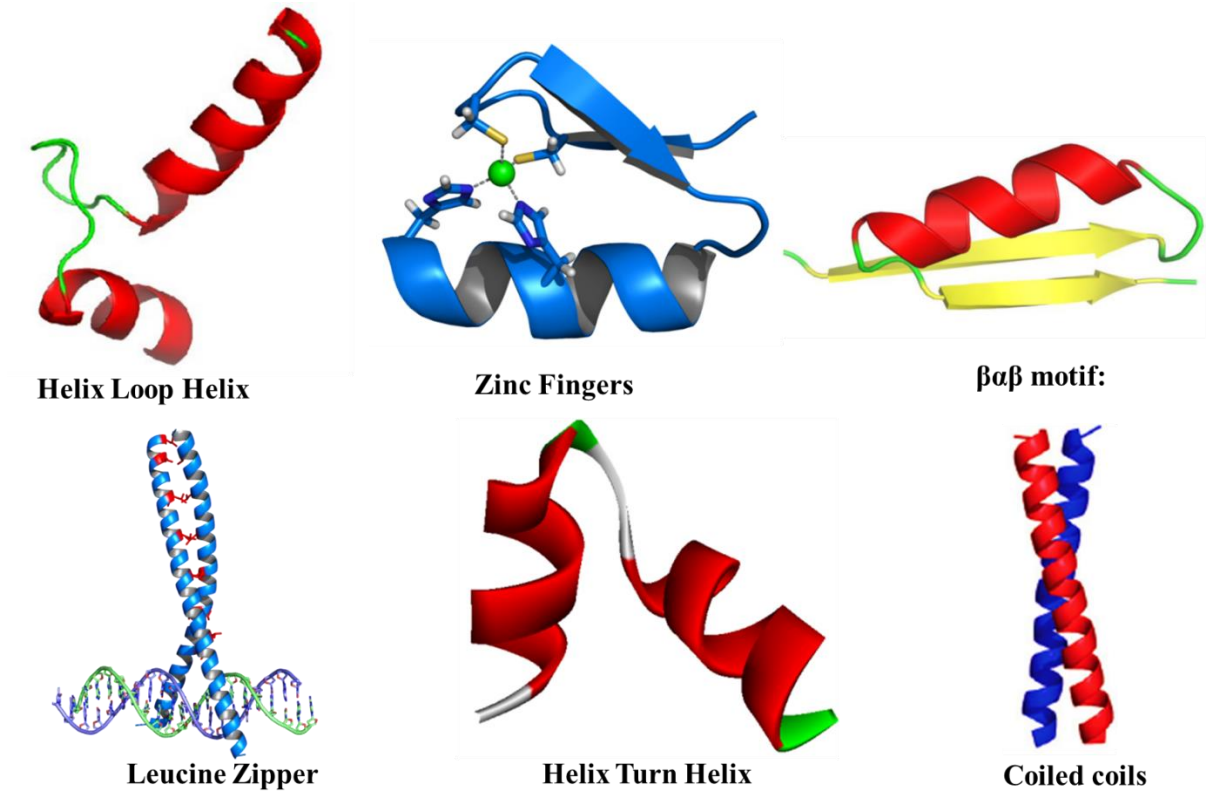


Figure 2: Representative examples of supersecondary structures of proteins.

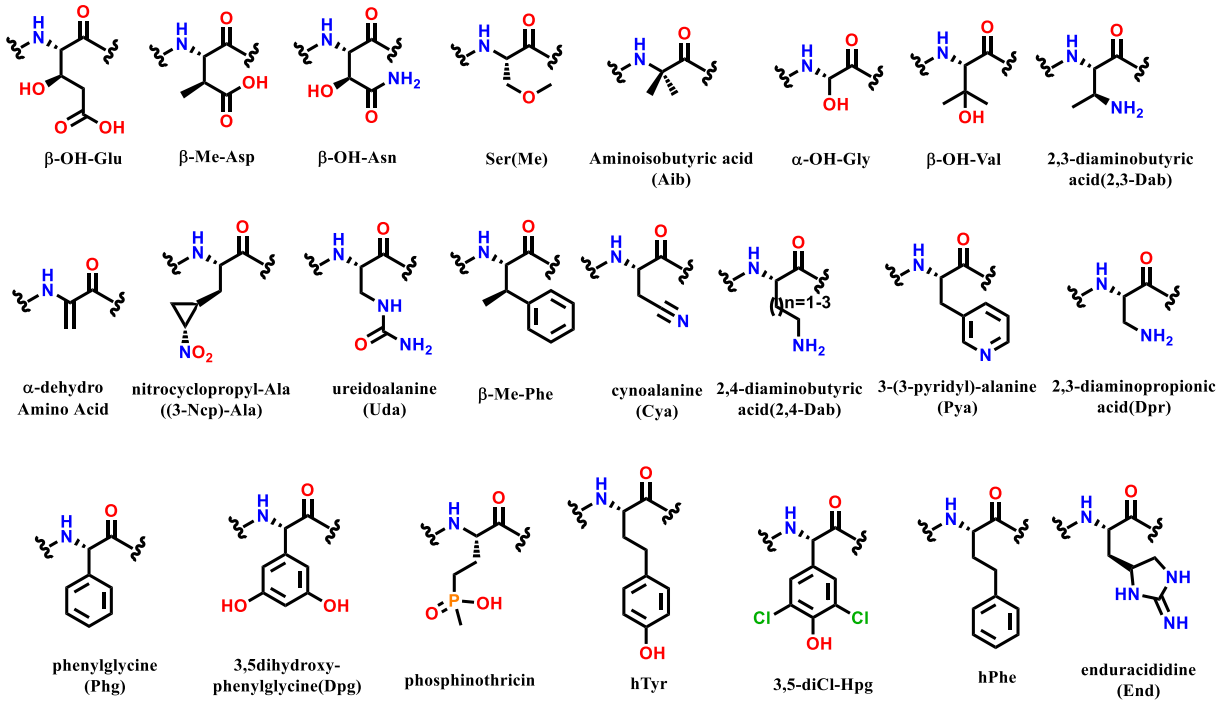


Figure 3: Non-ribosomal α-amino acids present the peptide natural products.

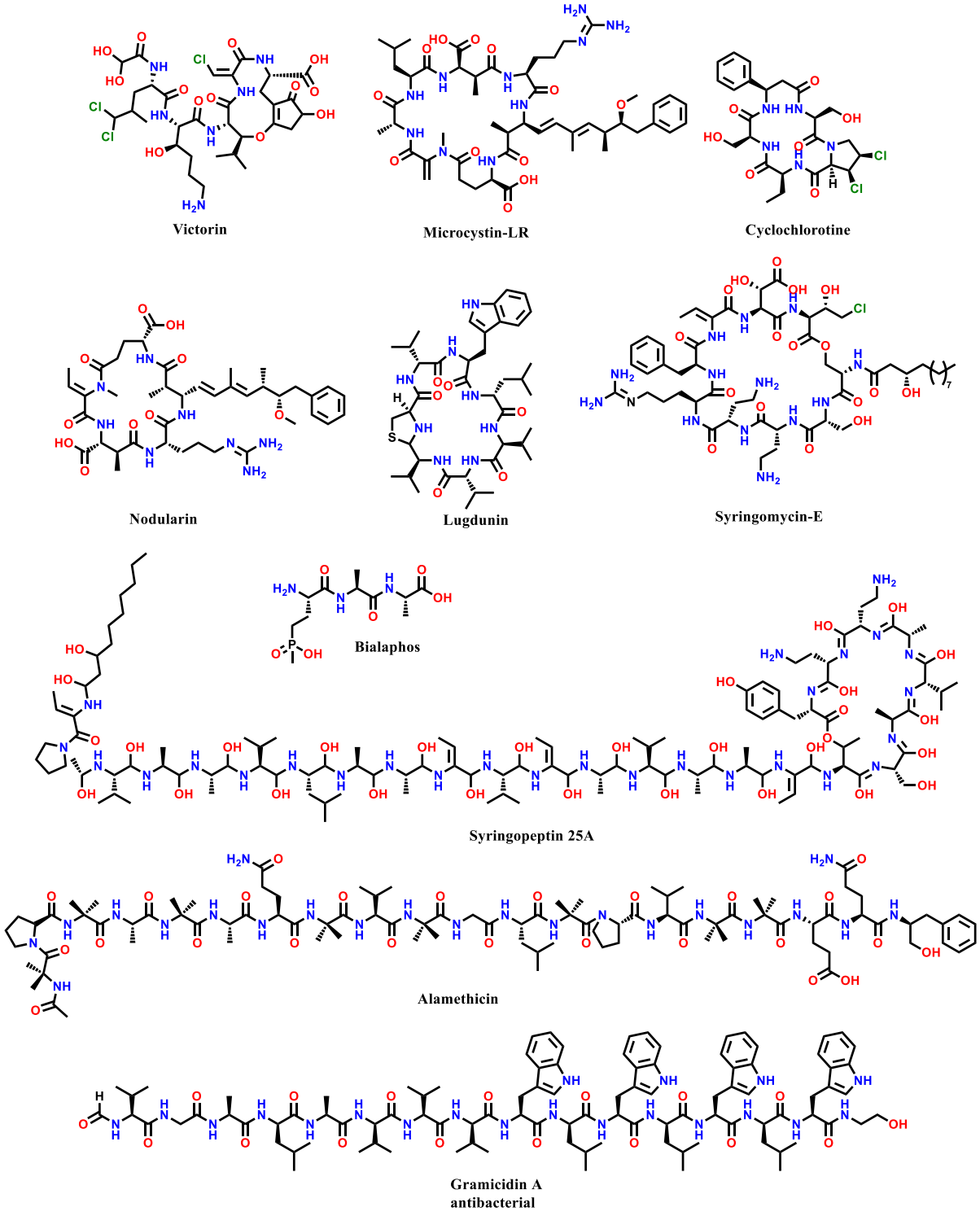


Figure 4: Peptide natural products composed of various non-ribosomal α-amino acids.

intricate secondary, tertiary, and quaternary structures. The combination of two or more tertiary structures leads to quaternary structures. This structural complexity is vital because proteins act as molecular machines, catalysts, and structural components, participating in virtually every

biological process. All proteins are made up of twenty amino acids. Using these twenty amino acids, nature has designed a myriad of proteins to perform specific functions.

In addition to the twenty ribosomal amino acids, a large number of non-ribosomal amino acids, including α- and β-amino acids, have been found in peptide natural products. Some of these amino acids are shown in Figure 3. Peptide natural products consisting of these non-ribosomal amino acids are depicted in Figure 4.

Apart from non-ribosomal α-amino acids such as Aib and α-dehydro amino acids, backbone-homologated β-, γ-, and higher homologue amino acids have been extensively used in the design of protein secondary structure mimetics.

1.2. Protein Structure Mimetics.

The structure and functions of proteins have inspired chemists to address the fundamental question of whether it is possible to construct protein-like structures and functions using non-ribosomal amino acids. The design of protein structure mimetics using synthetic amino acids represents a cutting-edge and innovative approach in the field of molecular biology and structure based drug discovery. In this context, extensive work has been done over the last two decades to replicate or modulate the structural features of natural proteins from various non-natural amino acids. Among the various non-natural amino acids, β- and γ-amino acids have been extensively explored to design protein-like structures because they are closely related to α-amino acids. This innovative strategy of utilization of β- and γ-amino acids holds tremendous potential not only to engineer structures that emulate the functions of their biological counterparts, but also for the development of advanced therapeutics, materials, and tools. Some of these synthetic β- and γ-amino acids explored in the design of protein structure mimetics are shown in Figure 5. Homologation and Double homologation of α-amino acids leads to β- and γ-amino acids respectively. Further depending on the position of the side chain it classified as β^3- and β^2- / γ^2-, γ^3-, and γ^4-, where, number represents the position of side chain (Figure 5).

1.2.1. β- Amino acids in the design of peptide foldamers.

Unlike α-peptides, β-peptides and higher homologue oligomers have demonstrated notable stability against proteolysis and metabolism.[1] This inherent stability renders β-peptides and higher homologue oligomers highly appealing from a biomedical standpoint. Over last twenty years, β-peptides constructed from β-amino acids, have emerged as promising tools for crafting protein secondary structures. In their pioneering investigations, Gellman and colleagues, have

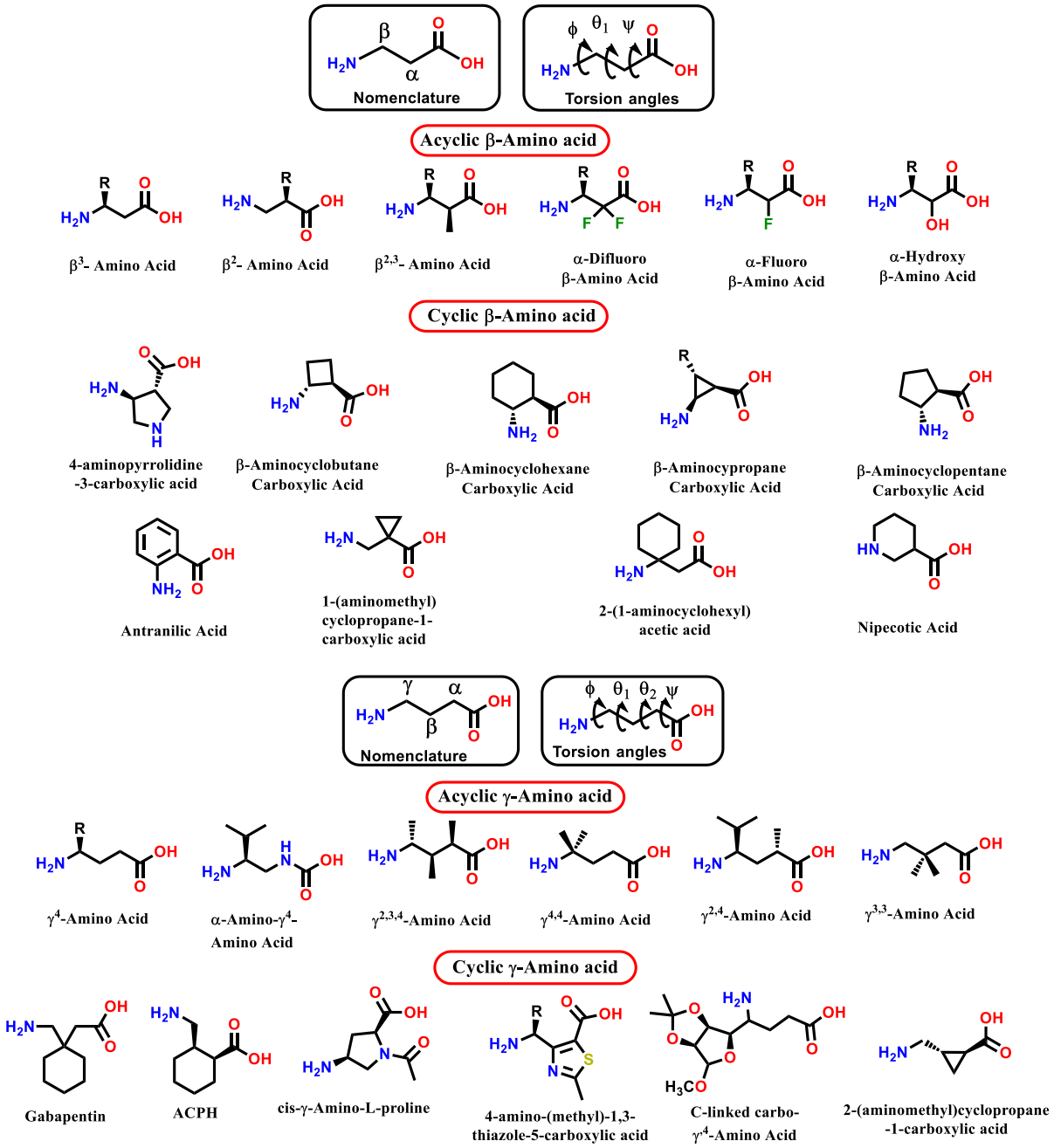


Figure 5: Some of the synthetic acyclic and cyclic β-amino acids and γ-amino acids used in the design of protein structure mimetics.

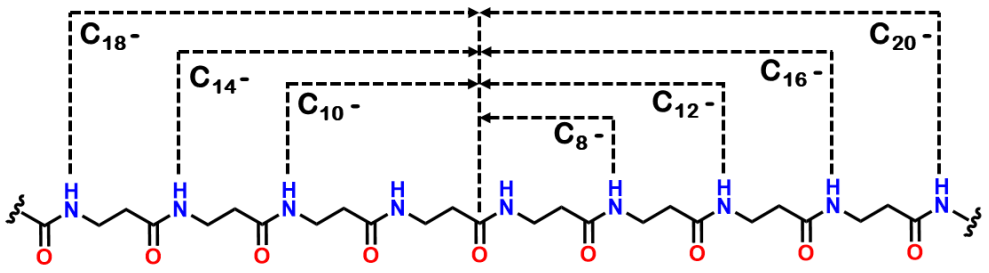


Figure 6: Possible H-bonding patterns in the oligomer of β-peptide foldamers.

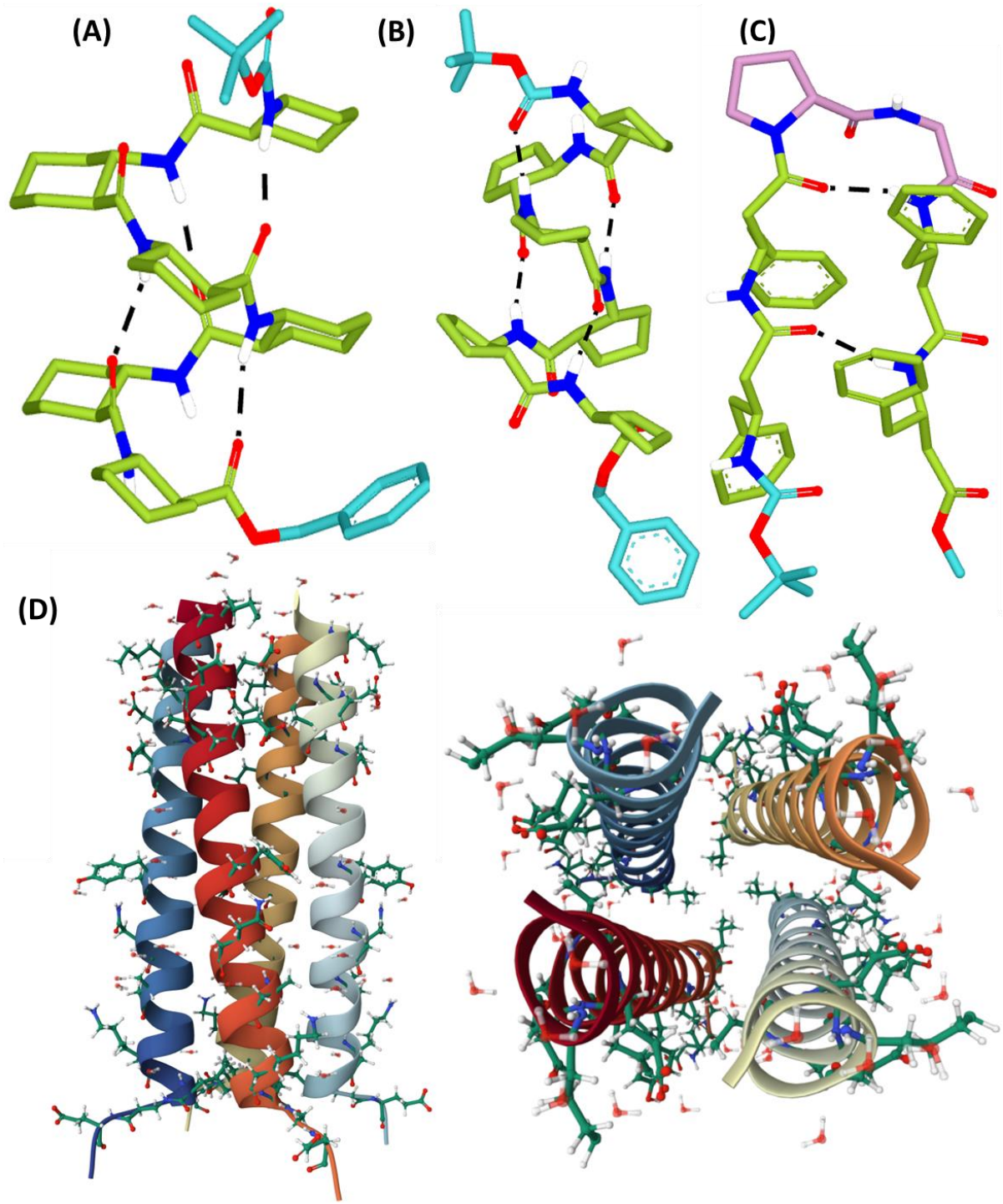


Figure 7: β-peptide structures , (A) C_{14}-helical structure from the homooligomer of *trans*-ACHA β-aminoacid[14a] (B) C_{12}-helical structure from the homooligomer of *trans*-ACPC β-amino acid[14b] (C) β-hairpin conformation constructed from the β^3-amino acids[4a] (D) Quaternary helix bundle structures in α, β-hybrid peptides[15] (PDB - 2OXK).

utilized sterically constrined cyclic β-amino acids in the design of protein structure mimetics.[2] Similarly, Seebach and colleagues have introduced backbone homologated flexible and chiral

β-amino acids and explored the conformational properties of the polypeptides resulting from these amino acids.[3] Further, in their first trial, Balaram and colleagues utilized β- and γ-amino acids along with α-amino acids to design hybrid peptides.[4] The hybrid peptides have shown to display a variety of hydrogen-bonded helical structures and β-hairpin structures.[4a] This exploration of hybrid peptides was subsequently delved deeper by Gellman and other researchers.[5, 6] In continuation, Sharma and Reiser conducted comprehensive research on β-peptide oligomers derived from carbo-β-amino acids[7-9] and cyclic β-amino acids[10], respectively. The groups of Fulop,[11, 12] and Aitken[13] have utilized various types of cyclic β-amino acids in the design of β-peptide helices. Structures gained by peptides composed of β-amino acid units include sheets, turns, and helices. The group of Gellman demonstrated that the oligomer of cyclic *trans*-2-aminocyclohexanecarboxylic acid and (*trans*-ACHA) *trans*-2-amino cyclopentanecarboxylic acid (*trans*-ACPC) adopt 14- and 12-helical conformations, respectively.[14] Furthermore, Gellman demonstrated impressive quaternary helix bundle structures in α, β-hybrid peptides featuring (3α)-β-(2α)-β sequence patterns[15] and $C_{11/11/12}$-helix and $C_{10/11/11}$-helix formation in 1:2 and 2:1 α, β-hybrid peptides.[16] β-peptides and their higher homologues generate a diverse range of helical secondary structures that differ from those observed in alpha-peptides. The helices obtained from the β-peptides are recognized as C_{14}-, C_{12}-, C_{10}-, and C_8- helices based on the intramolecular H-bond pseudocycles.[17-23] The β-peptide helices exhibit distinct polarities compared to α-helices. The structures derived from β-peptides are shown in Figure 7.

1.2.2. γ- Amino acids in the design of peptide foldamers.

In comparison to the extensive research on β-amino acids, γ-amino acids have not been thoroughly investigated. There has been limited exploration of γ-amino acids, and yet, in their early investigations, Seebach[24] and Hanessian[25] identified the C_{14}-helical conformations in

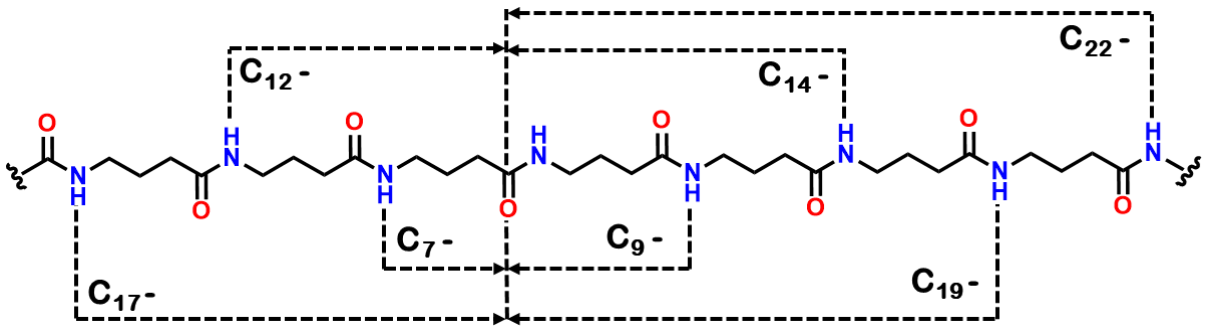


Figure 8: Possible H-bonding pattern in the oligomer of γ-peptide foldamer.

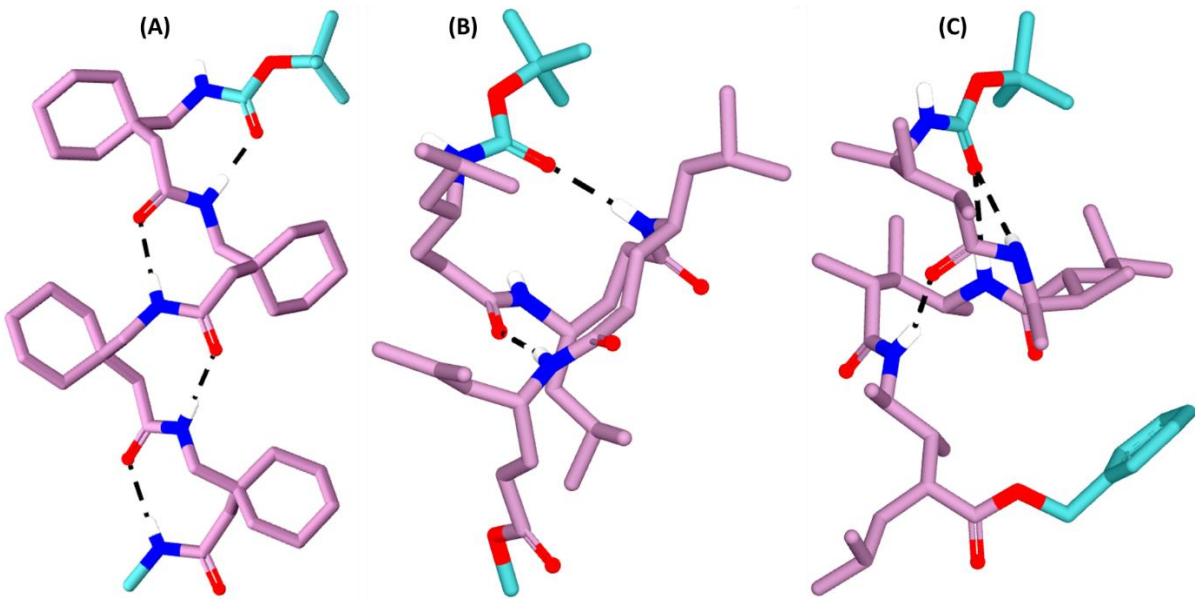


Figure 9: γ-peptide helical structures , (A) C_9-helical structure from the homooligomer of gabapentin[28] (B) C_{14}-helical structure from the homooligomer of monosubstituted γ^4-amino acid[29] (C) C_{14}-helical structure from the homooligomer of 2, 3, 4-substituted γ-amino acids[25]

oligomers of γ^4-amino acids, as well as 2, 3, 4-substituted γ-amino acids. Hofmann and colleagues theoretically speculated a wide range of helical structures from the oligopeptide of unsubstituted γ-amino acids and 1:1 alternating α- and γ- amino acids containing hybrid peptides.[26] The C_9-helix conformation anticipated by Hofmann was experimentally validated by Sharma and Kunwar.[27] In continuation, Balaram and colleagues reported the first crystal structure of the C_9-helix derived from the homooligomers of gabapentin ($\gamma^{3,3}$-amino acid),[28] in contrast to it homooligomers of monosubstituted γ^4-residues (γ^4-Leu, γ^4-Ile, and γ^4-Val) displayed C_{14}-helical conformations.[29] The X-rays structures of γ-peptide C_{14}- and C_9-helices are shown in Figure 9. Balaram and coworkers reported range of helical conformations available to the hybrid peptides composed of gabapentin ($\gamma^{3,3}$-amino acid).[30] Recently, group of Gellman reported the C_{14}-helical organizations in single crystals from the homooligomers of cyclic γ-amino acids.[31] Moreover, Smith and colleagues demonstrated the formation of extended sheet structures from the $\gamma^{2,3}$-cyclopropane amino acids,[32] this extended sheet structure in the solid state is stabilized by characteristics three-centered hydrogen bonds between the carbonyl oxygen and NH group of the amide and one CH of the cyclopropane ring (Figure 10a). Unlike the extended sheets, homooligomers of $\gamma^{2,3}$-*trans*-dioxolane-constrained γ-amino acids have been observed to adopt C_7-helical conformations in solution (Figure 10b).[33] Apart from cyclic and acyclic γ-amino acids, numerous variations of γ-amino acids that

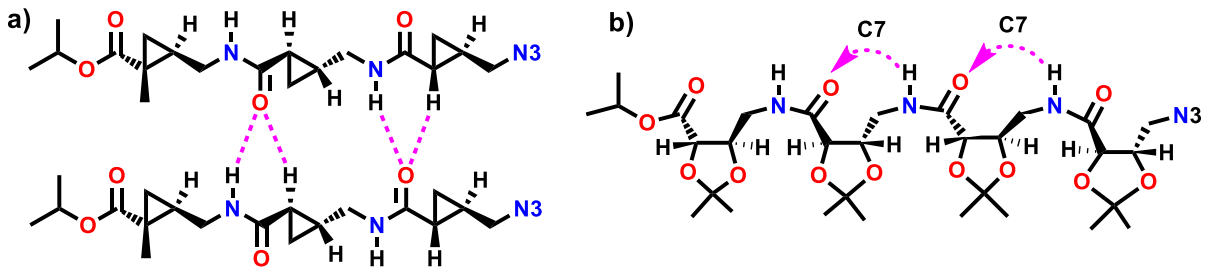


Figure 10: (a) Extended sheet structure of cyclopropane γ-amino acids homooligomer. (b) homooligomers of $\gamma^{2,3}$-*trans*-dioxolane shown C_7 bend-ribbon structure.

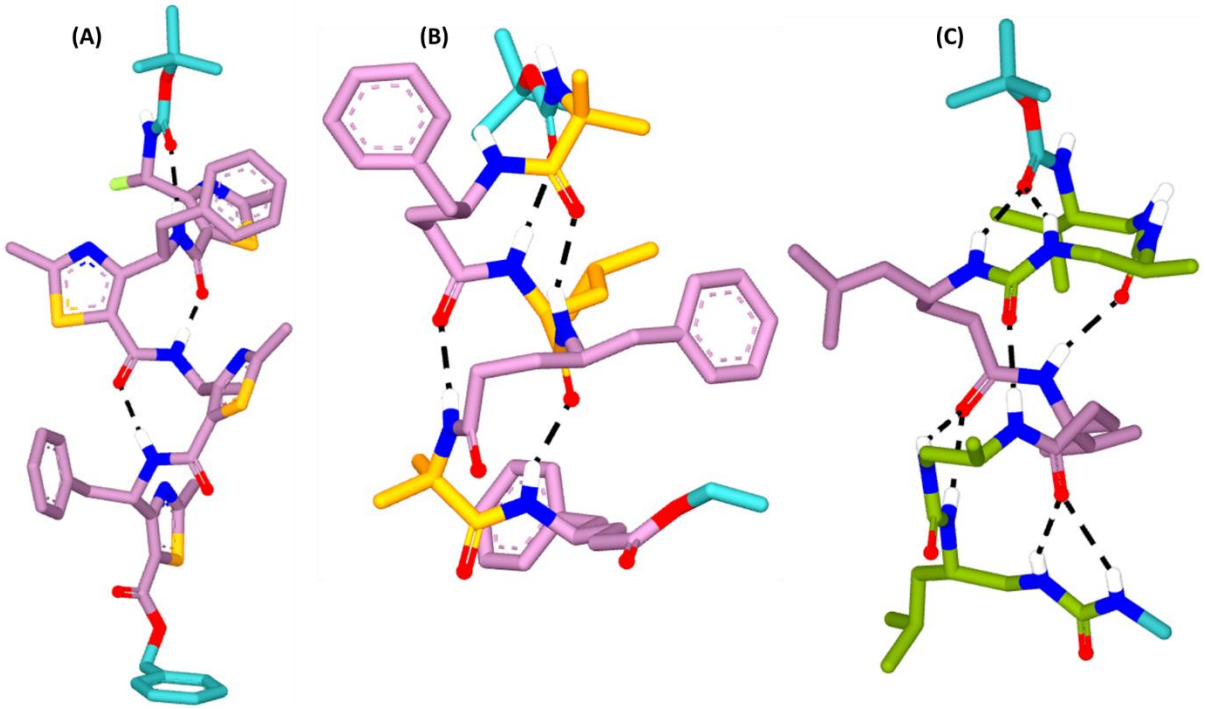


Figure 11: γ-peptide helical structures , (A) C_9-helical structure from the homooligomer of γ-amino acids with thiazole backbone[36] (B) C_{12}-helical conformation from the α,γ^4-hybrid peptide[37] (C) C_{14} helix from γ-amino urea-oligomer[35]

incorporate backbone heteroatoms, such as oxygen (O) and nitrogen (N), have also been reported. Yang and colleagues showed the conformational preferences of both α-aminoxy peptides and β-aminoxy peptides. They confirmed C_8-helical conformations in α-aminoxy peptides and C_9-helices in the case of β-aminoxy peptides.[34] Moreover, Guichard and his research team devised innovative γ-amino acids by substituting the α-carbon with an NH group, resulting in the creation of diverse urea-oligomer peptidomimetics.[35] These urea-moities containing γ-peptides adopted C_{14}-helical conformation similar to that of monosubstituted γ^4-peptide helices. Additionally, Millard reported C_9-helical conformation in the solution and as

well as in the solid state from γ-amino acids with thiazole backbone.[36] The helical structures obtained from the oligomers of γ-amino acids are shown in Figure 11. In addition, our group has also studied the conformations of hybrid peptides composed of α and γ-hybrid peptides.[37]

Contrary to the various unnatural γ-amino acids mentioned above, numerous nonribosomal γ-amino acids, including α, β-unsaturated γ-amino acids, β-keto-γ-amino acids, and β-hydroxy γ-amino acids, have been identified in various biologically active peptide natural products. However, there is limited understanding of the conformational properties of these amino acids. This chapter delves into the exploration of geometrically constrained *trans*-α, β-unsaturated γ-amino acids in the creation of novel peptide foldamers.

1.2.3. α, β-unsaturated γ-amino acids in the design of peptide foldamers

1.2.3.1. Biological Significance of α, β-unsaturated γ-amino acids

In contrast to synthetic γ-amino acids, a variety of γ-amino acids have been found in peptide natural products. These γ-amino acids are synthesized through different biosynthetic pathways. Specifically non-ribosomal amino acids such as (*E*)-α, β-unsaturated γ-amino acids, also known as (*E*)-vinylogous amino acids, are commonly present in various natural products suchas Luminmycin, Miraziridine A, Gallinamide A and Cyclotheonamide A shown in Figure12.[38] Many of them acting as serine and or cysteine protease inhibitors. Furthermore, Schreiber,Clardy, and Fusetani conducted an in-depth mechanistic study, revealing that Cyclotheonamides bind strongly to serine protease and bovine β-trypsin, serving as potent inhibitors.[39] Gallinamide A has exhibited notable effectiveness as an anti-malarial agent.[40] Natural cyclic peptide such as Miraziridine A, inhibits a range of proteases, including papain-like cysteine protease, pepsin-like aspartyl protease and trypsin-like protease.[41,42] The exceptional biological properties and the existence of (*E*)-α, β-unsaturated γ-amino acids residues in these substances have motivated synthetic chemists to create peptide inhibitors directed towards serine and cysteine proteases (Figure 13).[43]

1.2.3.2. Earlier work on α, β-unsaturated γ-amino acids in the context of foldamers

The biological and chemical characteristics of (*E*)-α, β-unsaturated γ-amino acid residues have inspired many biochemists to investigate their conformational behavior, both in monomers and peptides. Our group has been interested in exploring these non-ribosomal amino acids in the design of foldamers. Among the various non-ribosomal γ-amino acids, α,β-unsaturated γ-amino acids have attracted considerable attention because of their functionalizability. These

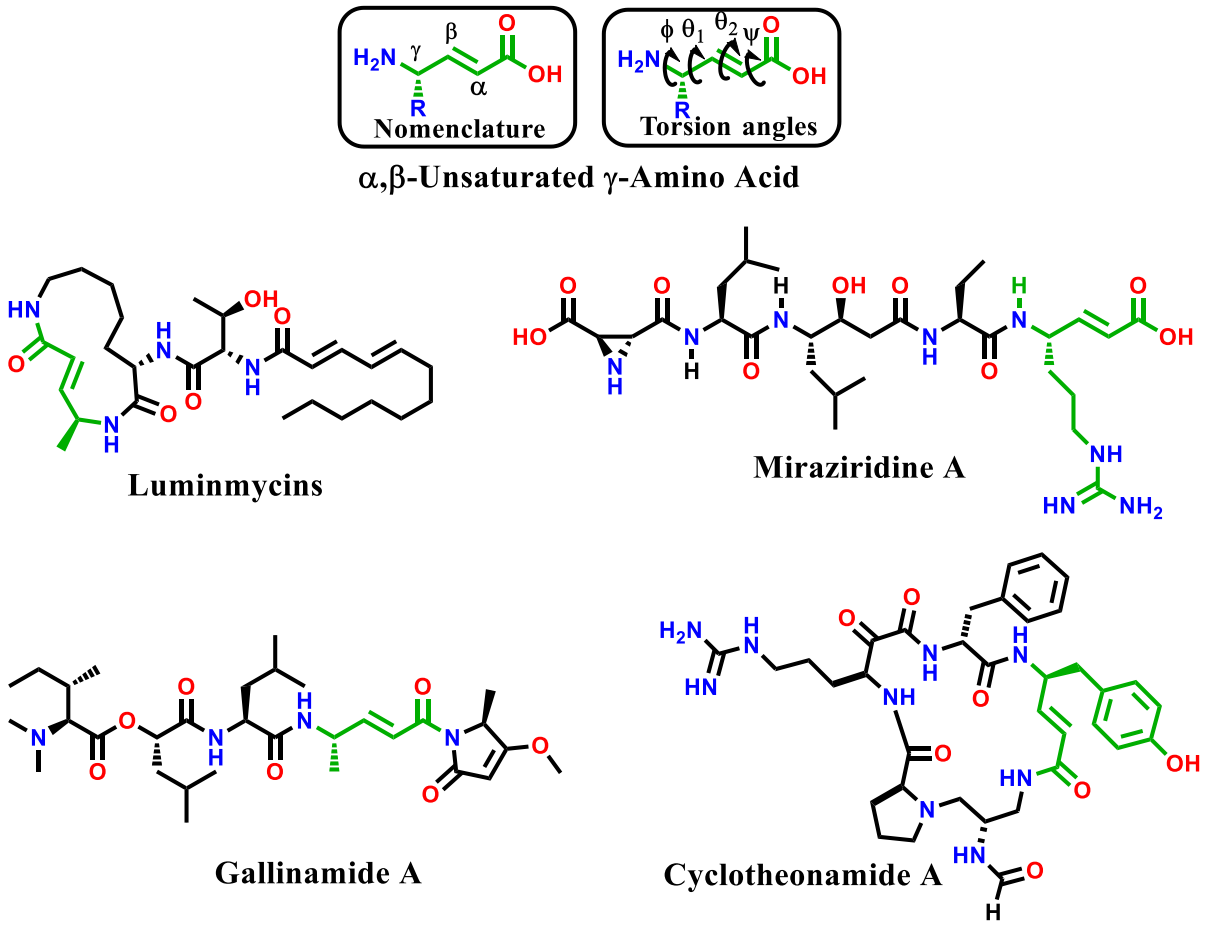


Figure 12: Naturally-occurring peptides containing α, β-unsaturated γ-amino acids.

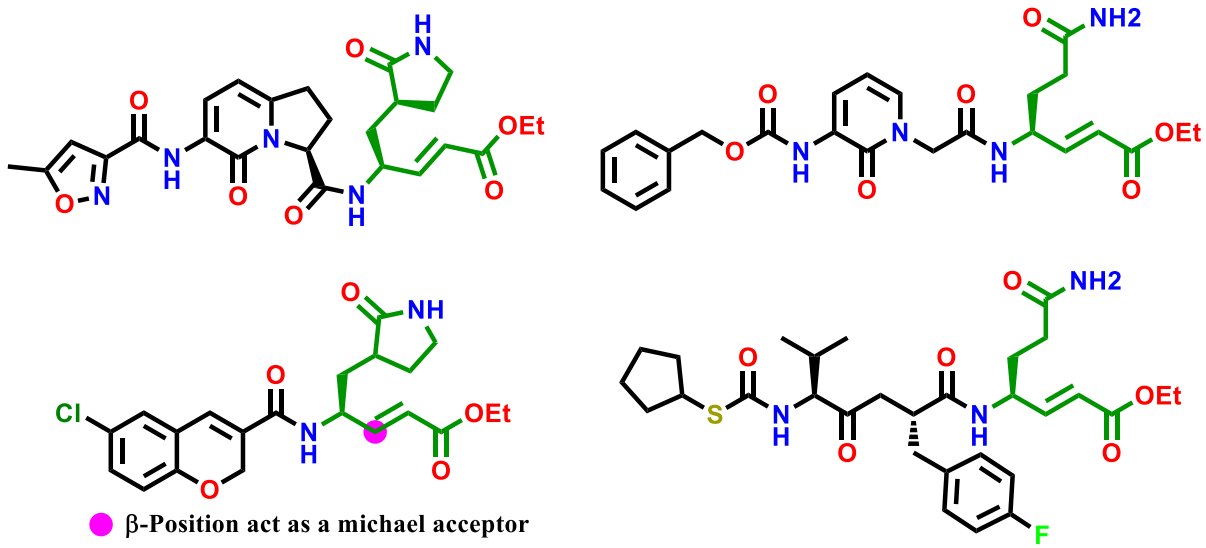


Figure 13: Synthetic peptides with α, β-unsaturated γ-amino acids are employed for different protease inhibitors.

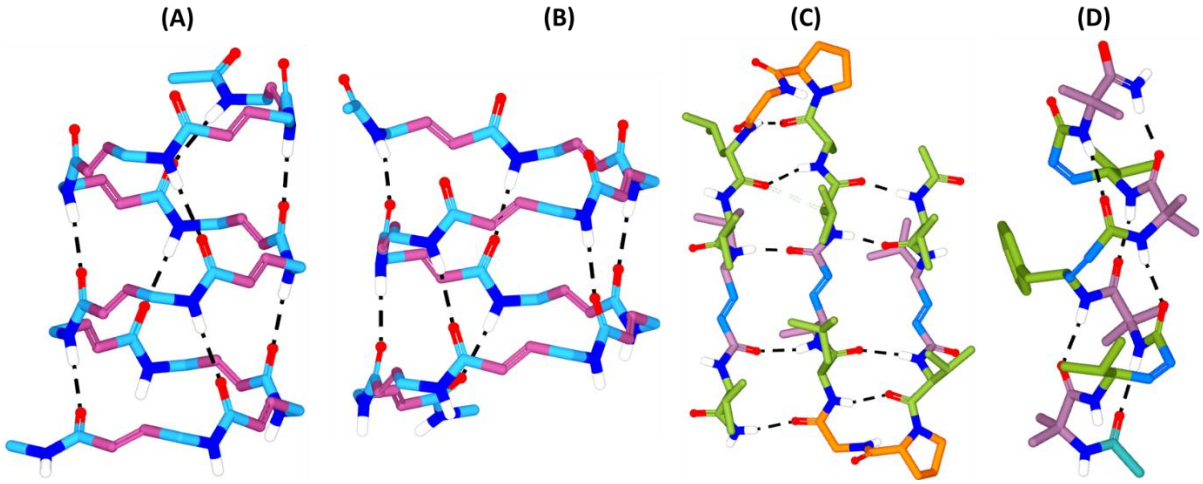


Figure 14: α, β-unsaturated γ-amino acids containing peptide structures, Hofmann theoretically predicted (A) C_{22}- and (B) C_{27}-helical structures from the homooligomer of (*E*)-α,β-unsaturated γ-amino acids[46] (C) Triple stranded β-sheeet structure[53] (D) C_{12}-helical conformation from the alternating α, (*Z*)-α,β-unsaturated γ-amino acids hybrid peptide[57]

α,β-unsaturated γ-amino acids have been used as precursors for the synthesis of γ-amino acids. During their preliminary work, Schreiber and colleagues demonstrated β-sheet type mimetics from dipeptides of unsaturated amino acids.[44] Further, Chakraborty et al. utilized *E*-α,β-unsaturated γ-proline to induce reverse turns.[45] In their pioneering work, Hofmann and colleagues examined the folded structures available to the oligomers of (*E*)-α,β-unsaturated γ-amino acids and (*Z*)-α,β-unsaturated γ-amino acids using theoretical calculations.[46] The oligomers of (*E*)-α,β-unsaturated γ-amino acids have shown to adopt a variety of helical structures with 14- to 27-membered hydrogen-bond pseudocycles. Some of these structures are shown in Figure 14. In contrast, theoretical calculations suggested that the oligomers of (*Z*)-α,β-unsaturated γ-amino acids have shown to adopt helical conformations with seven- and nine-membered hydrogen bond pseudocycles. Maillard and colleagues experimentally demonstrated C_9-helical conformations from the oligomers of hetero-aromatic amino acids, which resemble the *Z*-α,β-unsaturated γ-amino acids.[47] In addition, they also examined the inhibition of hIAPP and $A\beta_{1\text{-}42}$ aggregation and antimicrobial activity using the C_9-helical foldamers[48-50] from the oligomers of hetero-aromatic amino acids, which resemble the *Z*-α,β-unsaturated γ-amino acids.

Our group has been interested in understanding the conformational properties of peptides composed of α,β-unsaturated γ-amino acids. The conformational analysis of (*E*)-α,β-unsaturated γ-amino acids and amides revealed that these amino acids prefer to adopt β-sheet

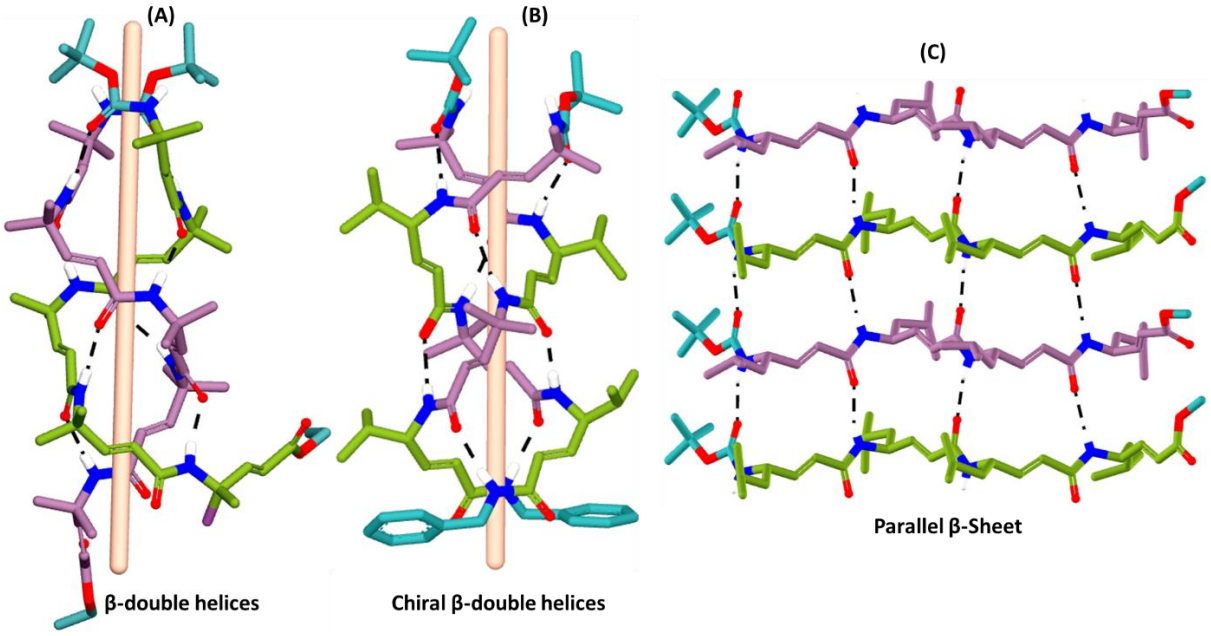


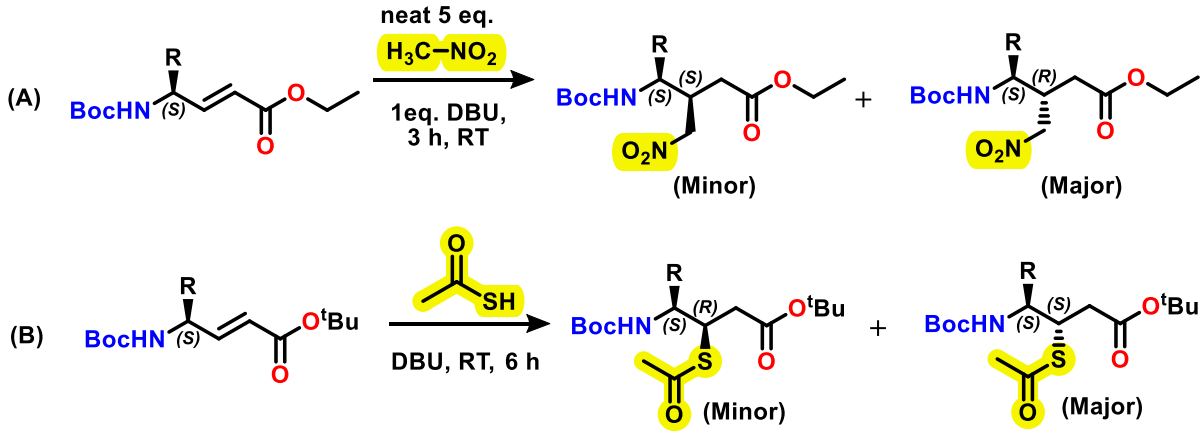
Figure 15: β-double helical structures from (*E*)-α, β-unsaturated γ-amino acids containing peptides, (A) β-double helices from homooligomers of 4,4-dialkyl α,β-unsaturated γ-amino acids.[58] (B) Chiral β-double helices[59] (C) Parallel β-sheeet structure from homooliogomer peptide of chiral (*E*)-α, β-unsaturated γ-amino acids[52a]

type conformations. The local conformations of α,β-unsaturated γ-amino acids can be assigned using the torsion angles φ, θ_1, θ_2, and ψ along the N-Cγ, Cγ-Cβ, Cβ-Cα, and Cα-C(O) bonds, respectively. The local conformations of α,β-unsaturated γ-amino acids are shown in Figure 9. The torsion parameter θ_2 always adopts values close to 180 due to the *trans* configuration of the carbon-carbon double bonds. In addition, the torsion angle ψ also shows values close to 180 due to the s-*cis* conformation along C=C-C=O. The β-sheet promoting nature of (*E*)-α,β-unsaturated γ-amino acids has been explored to design β-hairpins,[51] β-sheets,[52] multi-stranded β-sheets,[53] and miniature β-meanders.[54] In addition, the incorporation of these (*E*)-α,β-unsaturated γ-amino acids in short helix-promoting sequences leads to unusual planar structures.[55] Furthermore, our group has also demonstrated the antimicrobial properties of hybrid lipopeptides composed of (*E*)-vinylogous amino acids.[56] In contrast to the (*E*)-vinylogous amino acids, (*Z*)-vinylogous amino acids have been nicely accommodated in the helical conformations in hybrid peptides composed of alternating α- and *Z*-amino acids.[57] Additionally, our group demonstrated the formation of β-double helices derived from the homooligomers of 4,4-dialkyl α,β-unsaturated γ-amino acids.[58] In β-double helices, the two peptide strands intertwine together and are stabilized through interstrand H-bonds. Moreover, our group has demonstrated the design of chiral double helices composed of chiral (*E*)-α,β-

unsaturated-γ-amino acids along with 4,4-dimethyl α,β-unsaturated γ-amino acids and their applications as ion transporters.[59] Some of these β-double helices are shown in Figure 15.

1.3. Chemistry of α,β-unsaturated γ-amino acids

In addition to their applications in biological and peptide foldameric contexts, (*E*)-α,β-unsaturated-γ-amino acids have been utilized as starting materials in various organic reactions, including epoxidation, Diels-Alder reactions, and Michael addition reactions, leading to generate the diverse γ-amino acids. Plummer et al reported the conjugate addition of nitromethane to N-protected vinylogous amino esters.[60] In continuation, our group examined the diastereoselectivity and the mechanism of nitromethane conjugate addition.[61] This conjugate addition leads to the synthesis of 3,4-disubstituted γ-amino acids. The 3,4-disubstituted γ-amino acids have been further explored in the design of foldamers.[62] Similarly, like the nitromethane Michael addition, thioacetic acid conjugate addition also gave high diastereoselectivity. These thiol-substituted γ-amino acids have been explored in the design of stable β-hairpin structures.[63] The schematic representation of the conjugate addition of nitromethane and thioacetic acid is shown in Scheme 1.



Scheme 1: (A) Nitromethane Michael addition reaction.[61] (B) Thioacetic acid conjugate addition reaction.[63]

Overall, α,β-unsaturated γ-amino acids have served as excellent starting materials for the synthesis of disubstituted γ-amino acids and have also served as excellent building blocks to design foldamers.

As these (*E*)-α,β-unsaturated γ-amino acids have been serving as excellent starting materials to design functional peptides, in this thesis, we sought to investigate the conformational properties of peptides composed of conjugated multiple double bonds in the backbone, stereochemistry

of the synthesis of multiple conjugated double bonds,[52c] conformational analysis of peptides composed of *E*-vinylogous amino acids in the middle of the sequence.[64] In addition, we explored the possibility of thioacetic acid and thiol conjugate addition reactions in peptides composed of *E*-vinylous amino acids and the stereochemistry of the conjugate addition products and conformations of these peptides. Finally, we also investigated the conformations of α,γ-hybrid peptides composed of aromatic γ-amino acid mimetics of *Z*-γ-amino acids. All these results are described in the following chapters.

1.4. References

1. (a) J. Frackenpohl, P. I. Arvidsson, J. V. Schreiber, D. Seebach, *ChemBioChem*, **2001**, *2*, 445-455; (b) C. M. Goodman, S. Choi, S. Shandler, W. F. DeGrado, *Nat. Chem. Biol*. **2007**, *3*, 252-262.
2. D. H. Appella, L. A. Christianson, D. A. Klein, D. R. Powell, X. L. Huang, J. J. Barchi Jr, S. H. Gellman, *Nature* **1997**, *387*, 381-384.
3. P. I. Arvidsson, M. Rueping, D. Seebach, *Chem. Commun*. **2001**, 649-650.
4. (a) I. L. Karle, H. N. Gopi, Balaram, P. *Proc. Natl. Acad. Sci. USA*, **2002**, *99*, 5160-5164; (b) R. S. Roy, I. L. Karle, S. Raghothama, Balaram, P. *Proc. Natl. Acad. Sci. USA*, **2004**, *101*, 16478-16482; (c) I. L. Karle, A. Pramanik, A. Banerjee, S. Bhattacharjya, P. Balaram, *J. Am. Chem. Soc.* **1997**, *119*, 9087-9095.
5. (a) S. De Pol, C. Zorn, C. D. Klein, O. Zerbe, O. Reiser, *Angew. Chem., Int. Ed.* **2004**, *43*, 511–514; (b) A. Hayen, M. A. Schmitt, F. N. Ngassa, K. A. Thomasson, S. H. Gellman, *Angew. Chem., Int. Ed.* **2004**, *43*, 505–510.
6. (a) M. A. Schmitt, S. H. Choi, I. A. Guzei, S. H. Gellman, *J. Am. Chem. Soc.* **2005**, *127*, 13130-13131; (b) M. A. Schmitt, S. H. Choi, I. A. Guzei, S. H. Gellman, *J. Am. Chem. Soc.* **2006**, *128*, 4538-4539.
7. G. V. M. Sharma, V. G. Reddy, A. S. Chander, K. R. Reddy, *Tetrahedron: Asymmetry* **2002**, *13*, 21-24.
8. G. V. M. Sharma, K. R. Reddy, P. R. Krishna, A. R. Sankar, K. Narsimulu, S. K. Kumar, P. Jayaprakash, B. Jagannadh, A. C. Kunwar, *J. Am. Chem. Soc.* **2003**, 53, *125*, 13670-13671;
9. G. V. M. Sharma, K. R. Reddy, P. R. Krishna, A. R. Sankar, P. Jayaprakash, B. Jagannadh, A. C. Kunwar, *Angew. Chem., Int. Ed*. **2004**, *43*, 3961-3965.

10. (a) L. K. A. Pilsl, O. Reiser, *Amino Acids* **2011**, *41*, 709-718; (b) S. De Pol, C. Zorn, C. D. Klein, O. Zerbe, O. Reiser, *Angew. Chem., Int. Ed*. **2004**, *43*, 511-514.
11. (a) A. Hetenyi, I. M. Mandity, T. A. Martinek, G. K. Toth, F. Fulop, *J. Am. Chem. Soc*. **2005**, *127*, 547-553; (b) I. M. Mandity, E. Weber, T. A. Martinek, G. Olajos, G. K.Toth, E. Vass, F. Fulop, *Angew. Chem., Int. Ed*. **2009**, *48*, 2171-2175.
12. (a) T. A. Martinek, G. K. Toth, E. Vass, M. Hollosi, F. Fulop, *Angew. Chem., Int. Ed*. **2002**, *41*, 1718-1721; (b) T. A. Martinek, I. M. Mandity, L. Fulop, G. K. Toth, E. Vass, M. Hollosi, E. Forro, F. Fulop, *J. Am. Chem. Soc*. **2006**, *128*, 13539-13544.
13. C. Fernandes, S. Faure, E. Pereira, V. Thery, V. Declerck, R. Guillot, D. J. Aitken, *Org. Lett*. **2010**, *12*, 3606-3609.
14. (a) D. H. Appella, L. A. Christianson, I. L. Karle, D. R. Powell, S. H. Gellman, *J. Am. Chem. Soc.* **1996**, *118*, 13071-13072; (b) D. H. Appella, L. A. Christianson, I. L. Karle, D. R. Powell, S. H. Gellman, *J. Am. Chem. Soc.* **1999**, *121*, 6206-6212; (c) D. H. Appella, L. A. Christianson, D. A. Klein, M. A. Richards, D. R. Powell, S. H. Gellman, *J. Am. Chem. Soc.* **1999**, *121*, 7574-7581; (d) S. Krauthauser, L. A. Christianson, D. R. Powell, S. H. Gellman *J. Am. Chem. Soc.* **1997**, *119*, 11719-11720; (e) A. Hayen, M. A. Schmitt, F. N. Ngassa, K. A. Thomasson, S. H. Gellman, *Angew. Chem., Int. Ed*. **2004**, *43*, 505-510; (f) S. H. Choi, I. A. Guzei, L. C. Spencer, S. H. Gellman, *J. Am. Chem. Soc*. **2008**, *130*, 6544-6550.
15. (a) W. S. Horne, J. L. Price, J. L. Keck, S. H. Gellman, *J. Am. Chem. Soc*. **2007**, *129*, 4178-4180; (b) M. W. Giuliano, W. S. Horne, S. H. Gellman, *J. Am. Chem. Soc*. **2009**, *131*, 9860-9861.
16. M. A. Schmitt, S. H. Choi, I. A. Guzei, S. H. Gellman, *J. Am. Chem. Soc*. **2006**, *128*, 4538-4539.
17. (a) S. H. Gellman, *Acc. Chem. Res.* **1998**, *31*, 173-180; (b) D. J. Hill, M. J. Mio, R. B. Prince, T. S. Hughes, J. S. Moore, *Chem. Rev*. **2001**, *101*, 3893-4012; (c) R. P. Cheng, S. H. Gellman, W. F. DeGrado, *Chem. Rev*. **2001**, *101*, 3219-3232.
18. (a) J. Venkatraman, S. C. Shankaramma, P. Balaram, *Chem. Rev*. **2001**, *101*, 3131-3152; (b) D. Seebach, A. K. Beck, D. J. Bierbaum, *Chem. Biodiversity* **2004**, *1*, 1111-1239; (c) S. Hecht, I. Huc, *Foldamers: Structure, Properties and Applications*; Wiley-VCH: Weinheim, **2007**.
19. (a) D. Seebach, J. Gardiner, *Acc. Chem. Res.* **2008**, *41*, 1366-1375; (b) C. G. Cummings, A. D. Hamilton, *Curr. Opin. Chem. Biol*. **2010**, *14*, 341-346.

20. (a) E. J. Petersson, A. Schepartz, *J. Am. Chem. Soc*. **2008**, *130*, 821-823; (b) J. L. Price, W. S. Horne, S. H. Gellman, *J. Am. Chem. Soc*. **2010**, *132*, 12378-12387.
21. (a) D. Seebach, V. J. Schreiber, S. Abele, X. Daura, F. W. Gunsteren, *Helv. Chim. Acta* **2000**, *83*, 34-57; (b) D. H. Appella, L. A. Christianson, D. A. Klein, D. R. Powell, X. L. Huang, J. J. Barchi, S. H. Gellman, *Nature* **1997**, *387*, 381-384; (c) P. I. Arvidsson, M. Rueping, D. Seebach, *Chem. Commun*. **2001**, 649-650;
22. (a) X. Daura, D. Bakowies, D. Seebach, J. Fleischhauer, W. F. van Gunsteren, P. Kruger, *Eur. Biophys. J*. **2003**, *32*, 661-670;. (b) A. Hetenyi, I. M. Mandity, T. A. Martinek, G. K. Toth, F. Fulop, *J. Am. Chem. Soc*. **2005**, *127*, 547-553; (c) R. Threlfall, A. Davies, N.M. Howarth, J. Fisher, R. Cosstick, *Chem. Commun*. **2008**, 585-587; (d) F. Rua, S. Boussert, T. Parella, I. Diez-Perez, V. Branchadell, E. Giralt, R. M. Ortuno, *Org. Lett*. **2007**, *9*, 3643-3645.
23. (a) P. I. Arvidsson, N. S. Ryder, H. M. Weiss, G. Gross, O. Kretz, R. Woessner, D. Seebach, *ChemBioChem* **2003**, *4*, 1345-1347; (b) I. M. Mandity, E. Weber, T. A. Martinek, G. Olajos, G. K. Toth, E. Vass, F. Fulop, *Angew. Chem., Int. Ed*. **2009**, *48*, 2171-2175; (c) D. Seebach, S. Abele, K. Gademann, B. Jaun, *Angew. Chem., Int. Ed*. **1999**, *38*, 1595-1597; (d) T. A. Martinek, G. K. Toth, E. Vass, M. Hollosi, F. Fulop, *Angew. Chem., Int. Ed*. **2002**, *41*, 1718-1721; (e) T. A. Martinek, I. M. Mandity, L. Fulop, G. K.Toth, E. Vass, M. Hollosi, E. Forro, F. Fulop, *J. Am. Chem. Soc*. **2006**, *128*, 13539-13544.
24. T. Hintermann, K. Gademann, B. Jaun, D. Seebach, *Helv. Chim. Acta*. **1998**, *81*, 893-1002.
25. S. Hanessian, X. Luo, R. Schaum, S. Michnick, *J. Am. Chem. Soc.* **1998**, *120*, 8569-8570.
26. (a) C. Baldauf, R. Gunther, H. -J. Hofmann, *Helv. Chim. Acta*. **2003**, *86*, 2573-2588; (b) C. Baldauf, R. Gunther, H. -J. Hofmann, *J. Org. Chem.* **2006**, *71*, 1200-1208.
27. a) G. V. M. Sharma, P. Jayaprakash, K. Narsimulu, A. R. Sankar, K. R. Reddy, A. C. Kunwar, *Angew. Chem.Int. Ed.***2006**, *45*, 2944-2947.
28. P. G. Vasudev, N. Shamala, K.Ananda, P. Balaram, *Angew. Chem., Int. Ed*. **2005**, *44*, 4972-4975.
29. K. Basuroy, B. Dinesh, M. B. M. Reddy, S. Chandrappa, S. Raghothama, N. Shamala, P. Balaram, *Org. Lett*. **2013**, *15*, 4866-4869.
30. P. G. Vasudev, K. Ananda, S. Chatterjee, S. Aravinda, N. Shamala, P. Balaram, *J. Am. Chem. Soc.* **2007,** *129*, 4039-4048.
31. L. Guo, W. Zhang, A.G. Reidenbach, M.W. Giuliano, I.A. Guzei, L.C. Spencer, S.H. Gellman, *Angew. Chem. Int. Ed Engl.*, **2011,** *50*, 5843-5846.

32. M. Khurram, N. Qureshi, M. D. Smith, *Chem. Commun*. **2006**, 5006-5008.
33. A. Kothari, M. Khurram, N. Qureshi, E. M. Beck, M. D. Smith, *Chem. Commun*. **2007**, 2814-2816.
34. (a) X. Lee, D. Yang, *Chem. Commun*. **2006**, 3367-3379; (b) F. Chen, N.-Y. Zhu, D. Yang, *J. Am. Chem. Soc.* **2004**, *126*, 15980-15981.
35. (a) N. Pendem, Y. R. Nelli, C. Douat, L. Fischer, M. Laguerre, E. Ennifar, B. Kauffman, G. Guichard, *Angew. Chem. Int. Ed*. **2013**, *52*, 4147-4151; (b) G. W. Collie, K. Pulka-Ziach, C. M. Lombardo, J. Fremaux, F. Rosu, M. Decossas, L. Mauran, O. Lambert, V. Gabelica, C. D. Mackereth, G. Guichard, *Nature Chemistry* **2015**, *7*, 871-878.
36. C. Bonnel, B. Legrand, M. Simon, J. Martinez, J.-L. Bantignies, Y. K. Kang, E. Wenger, F. Hoh, N. Masurier, L. T. Maillard, *Chem. Eur. J.* **2017**, *23*, 17584-17591.
37. (a) A. Bandyopadhyay, S. V. Jadhav, H. N. Gopi, *Chem. Commun*. **2012**, *48*, 7170-7172; (b) S. V. Jadhav, A. Bandyopadhyay, H. N. Gopi, *Org. Biomol. Chem*. **2013**, *11*, 509-514; (c) A. Bandyopadhyay, H. N. Gopi, *Org. Lett*. **2012**, *14*, 2770-2773.
38. (a) N. Fusetani, S. Matsunaga, H. Matsumoto, Y. Takebayashi, *J. Am. Chem. Soc.* 1990, *112*, 7053‑7054; b) J. E. Coleman, E. D. d Silva, F. Kong, R. J. Andersen, T. M. Allen, *Tetrahedron* 1995, *51*, 10653‑10662; c) N. Schaschke, *Bioorg. Med. Chem. Lett.* 2004, *14*, 855‑857; d) R. G. Linington, B. R. Clark, E. E. Trimble, A. Almanza, L.-D. Urena, D. E. Kyle, W. H. Gerwick, *J. Nat. Prod.* 2009, *72*, 14‑17; e) X. Bian, A. Plaza, Y. Zhang, R. Muller, *J. Nat. Prod.* 2012, *75*, 1652–1655; f) J. A. Nieman, J. E. Coleman, D. J. Wallace, E. Piers, L. Y. Lim, M. Roberge, R. J. Andersen, *J. Nat. Prod.* 2003, *66*, 183–199.
39. (a) A. Y. Lee, M. Hagihara, R. Karmacharya, M. W. Albers, S. L. Schreiber, J. Clardy, *J. Am. Chem. Soc.* 1993, *115*, 12619–12620; (b) B. E. Maryanoff, X. Qiu, K. P. Padmanabhan, A. Tulinsky, H. R. A. Jr, P. Andrade-Gordon, M. N. Greco, J. A. Kauffman, K. C. Nicolaou, A. Liu, P. H. Brungs, N. Fusetani, *Proc. Natl. Acad. Sci. USA* 1993, *90*, 8048–8052.
40. (a) R. G. Linington, B. R. Clark, E. E. Trimble, A. Almanza, L.-D. Uren, D. E. Kyle, W. H. Gerwick, *J. Nat. Prod*. **2009**, *72*, 14-17. (b) B. Miller, A. J. Friedman, H. Choi, J. Hogan, J. A. McCammon, V. Hook, W. H. Gerwick, *J. Nat. Prod.* **2014**, *77*, 92–99.
41. Y. Nakao, M. Fujita, K. Warabi, S. Matsunaga, N. Fusetani, *J. Am. Chem. Soc*. **2000**, *122*, 10462-10463.

42. P. Tabares, B. Degel, N. Schaschke, U. Hentschel, T. Schirmeister, *Pharmacognosy Res.* **2012**, *4*, 63−66.

43. (a) R. P. Hanzlik, S. A. Thompson, *J. Med. Chem*. **1984**, *27*, 711-712; (b) H. M. M. Bastiaans, J. L. Van der Baan, H. C. J. Ottenheijm, *J. Org. Chem*. **1997**, *62*, 3880-3889; (c) S. Liu, R. P. Hanzlik, *J. Med. Chem*. **1992**, *35*, 1067-1075; (d) J-S. Kong, S. Venkatraman, K. Furness, S. Nimkar, T. A. Shepherd, Q. M. Wang, J. Aube, R. P. Hanzlik, *J. Med. Chem*. **1998**, *41*, 2579-2587; (e) N. Schaschke, C. P. Sommerhoff, *ChemMedChem* **2010**, *5*, 367-370.

44. M. Hagihara, N. J. Anthony, T. J. Stout, J. Clardy, S. L. Schreiber, *J. Am. Chem. Soc.* **1992**, *114*, 6568-6570.

45. T. K Chakraborty, A. Ghosh, S. K. Kumar, A. C. Kunwar, *J. Org. Chem*. **2003**, *68*, 6459-6462.

46. C. Baldauf, R. Gunther, H.-J. Hofmann, *J. Org. Chem*. **2005**, *70*, 5351-5361.

47. L. Mathieu, B. Legrand, C. Deng, L. Vezenkov, E. Wenger, C. Didierjean, M. Amblard, M.-C. Averlant-Petit, N. Masurier, V. Lisowski, J. Martinez, L.T. Maillard, *Angew. Chem. Int. Ed*. **2013**, *52*, 6006-6010; *Angew. Chem*, **2013**, *125*, 6122-6126.

48. B. Legrand, L. Mathieu, A. Lebrun, S. Andriamanarivo, V. Lisowski, N. Masurier, S. Zirah, Y. K. Kang, J. Martinez, L. T. Maillard, *Chem. Eur. J.* **2014**, *20*, 6713−6720.

49. C. Bonnel, B. Legrand, M. Simon, M. Clavie, A. Masnou, E. Jumas-Bilak, Y. K. Kang, P. Licznar-Fajardo, L. T. Maillard, N. Masurier, *J. Med. Chem.* **2020**, *63*, 9168−9180.

50. J. Kaffy, C. Berardet, L. Mathieu, B. Legrand, M. Taverna, F. Halgand, G. V. D. Rest, L. T. Maillard, S. Ongeri, *Chem. Eur. J.* **2020**, *26*, 14612–14622.

51. A. Bandyopadhyay, S. M. Mali, P. Lunawat, K. M. P. Raja, H. N. Gopi, *Org. Lett*. **2011**, *13*, 4482-4485.

52. (a) K. Veeresh, M. Singh and H. N. Gopi, *Org. Biomol. Chem.*, **2019**, *17*, 9226-9231; (b) S. M. Mali, A. Bandyopadhyay, S. V. Jadhav, M. Ganesh Kumar, H. N. Gopi, *Org. Biomol. Chem*. **2011**, *9*, 6566; (c) S. A. Nalawade, M. Singh, D. R. Puneeth Kumar, S. Dey, H. N. Gopi, *Org.Biomol.Chem*. **2023**, *21*, 2586–2595.

53. (a) A. Bandyopadhyay, R. Misra and H. N. Gopi, *Chem. Commun*., **2016**, *52*, 4938–4941.

54. M. G. Kumar, S. N. Benke, K. M. P. Raja, H. N. Gopi, *Chem. Commun*., **2015**, *51*, 13397-13399.

55. (a) A. Bandyopadhyay, H. N. Gopi, *Org. Lett.*, **2012**, *14*, 2770–2773; (b) Kuruva Veeresh, Hosahudya N. Gopi**,** *Org. Lett.* **2019**, *21*, 4500–4504.
56. S. S. Shankar, S. N. Benke, N. Nagendra, P. L. Srivastava, H. V. Thulasiram, H. N. Gopi, *J. Med. Chem.* **2013**, *56*, 8468-8474.
57. M. G. Kumar, V. J. Thombare, M. M. Katariya, K. Veeresh, K. M. P. Raja and H. N. Gopi, *Angew. Chem. Int. Ed.*, **2016**, *128*, 7978 –7982.
58. R. Misra, S. Dey, R. M. Reja and H. N. Gopi, *Angew. Chem. Int. Ed.*, **2018**, *57*, 1057-1061.
59. S. Pahan, S. Dey, G. George, S. P. Mahapatra, D. R. Puneeth Kumar, H. N. Gopi, *Angew. Chem. Int. Ed.* **2024**, *63*, e202316309.
60. J. S. Plummer, L. A. Emery, M. A. Stier, M. J. Suto, *Tetrahedron Lett*. **1993**, *34*, 7529-7532.
61. M. G. Kumar, S. M. Mali, H. N. Gopi, *Org. Biomol. Chem.*, **2013**, *11*, 803–813.
62. M. G. Kumar, H. N. Gopi, *Org. Lett.* **2015**, *17*, 4738–4741.
63. M. G. Kumar, S. M. Mali, K. M. P. Raja, H. N. Gopi, *Org. Lett.* **2015**, *17*, 230–233.
64. S. A. Nalawade, M. G. Kumar, D. R. Puneeth Kumar, M. Singh, S. Dey, H. N. Gopi, *CrystEngComm*, **2024**, *26*, 913 – 917.

Chapter 2

Stereoselective Synthesis of Backbone Extended π-Conjugated Amino Esters

The original work of this chapter has been published in the "Organic and Biomolecular Chemistry" journal. Here, we adopted the text from Ref. **S. A. Nalawade**, M. Singh, D. R. Puneeth Kumar, S. Dey, H. N. Gopi, *Org.Biomol.Chem*. **2023**, *21*, 2586–2595. with permission from the Royal Society of Chemistry. A copy of the permission letter attached at the end of the chapter.

2.1. Introduction

In addition to the twenty ribosomal amino acids, peptide natural products often contain a diverse array of non-ribosomal amino acids, including α,α-dialkyl amino acids, N-methyl amino acids, β-amino acids, as well as γ- and higher homologue amino acids.[1] Among these non-natural amino acids, α,β-unsaturated γ-amino acids, have gained substantial attention due to their biological applications. Earlier α,β-unsaturated γ-amino acids were considered as non-natural. However, in the 1990s, *E*-vinylogous γ-amino acids were identified in diverse natural secondary metabolites (Figure 1).[2] Additionally, efforts have been made to investigate the conformational properties of these α,β-unsaturated γ-amino acids, aiming to design a diverse array of folded structures.[3] In their preliminary research, Schreiber and colleagues demonstrated the formation of β-sheet type structures from dipeptides derived from α,β-unsaturated γ-amino acids.[4] Prof. grison's group[5] and Prof. Chakraborty's group[6] utilized these amino acids to create β-turn mimetics. Employing ab initio MO theory, Hofmann and co-workers examined the diverse helical structures accessible to both (*E*)- and (*Z*)-vinylogous amino acids.[7] Additionally, Maillard and colleagues reported the formation of 9-helix structures from oligomers of *Z*-vinylogous amino acids.[8] Furthermore, these amino acids serve as precursors for synthesizing γ-amino acids.[9]

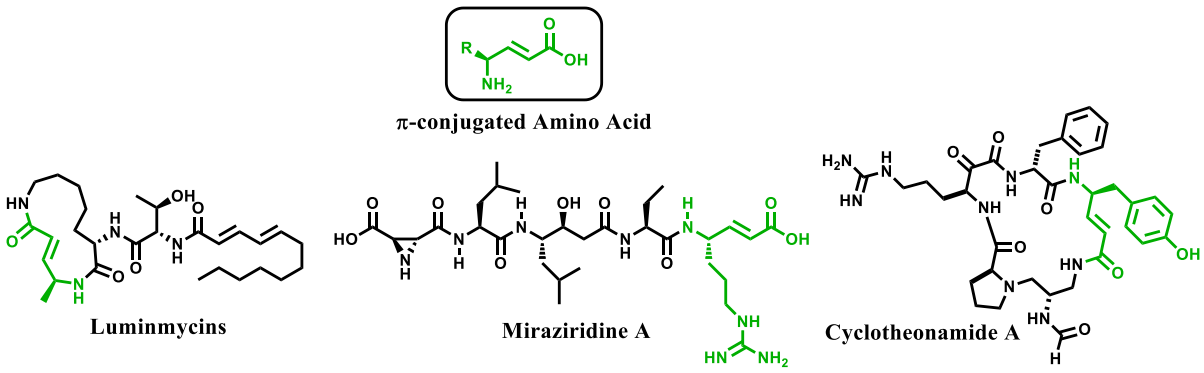


Figure 1: Peptide natural products consist of π-conjugated amino acids with *trans* geometry.

In contrast to α,β-unsaturated γ-amino acids with single backbone double bonds, amino acids featuring multiple backbone double bonds are rarely observed in nature. However, the natural product FR252921 and its analogues, isolated from Pseudomonas fluorescence, comprise an amino acid with three conjugative (*E*,*E*,*E*)-carbon-carbon double bonds (Figure 2).[10] It is an achiral amino acid, its synthesis involves a domino stereoinvertive Suzuki-type coupling and a 4π-electrocyclic ring-opening reaction.[11] However, this type of domino reaction on chiral amino acids would be difficult and pose challenges. Furthermore, various synthetic methods

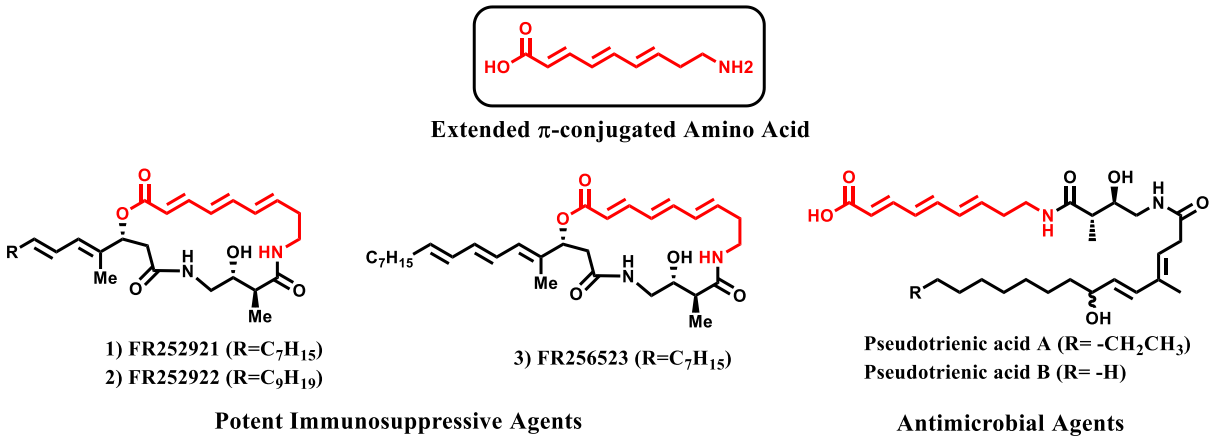


Figure 2: Peptide natural products consist of amino acids with three conjugative double bonds with *trans* geometry.

have been developed for the synthesis of achiral polyene amino acids.[12-15] In our previous work, we documented the synthesis of α,β-unsaturated γ-amino acids with exceptionally high (*E*)-selectivity of carbon-carbon double bonds.[16] In organic synthesis, Wittig[17] and Wittig-Horner[18,19] reactions have been commonly employed for the introduction of double bonds. The stereochemistry of the double bonds in Wittig[17] reactions and Wittig-Horner[18,19] reactions predominantly relies on the stability of the ylides and the reaction conditions. However, it has been rarely studied whether Wittig or Wittig-Horner reactions can effectively be utilized for the synthesis of conjugative multiple double bonds. Nonetheless, Ideses and shani investigated the synthesis of conjugated dienes using the Wittig reaction, observing the formation of both (*E*) and (*Z*) stereoisomers. Furthermore, they noted significant isomerization of the "old" double bond during the synthesis of the "new" double bond.[20]

In continuation, we aimed to assess the applicability of the Wittig reaction for the introduction of multiple double bonds with exclusive (*E*)-selectivity. In this report, we present the synthesis of ethyl esters of N-protected amino acids featuring two and three conjugative backbone double bonds, achieved with complete *E*-selectivity. Additionally, we describe the crystal conformations of amino acids with two and three double bonds, as well as peptides composed of these amino acids.

2.2. Objective of the current Work

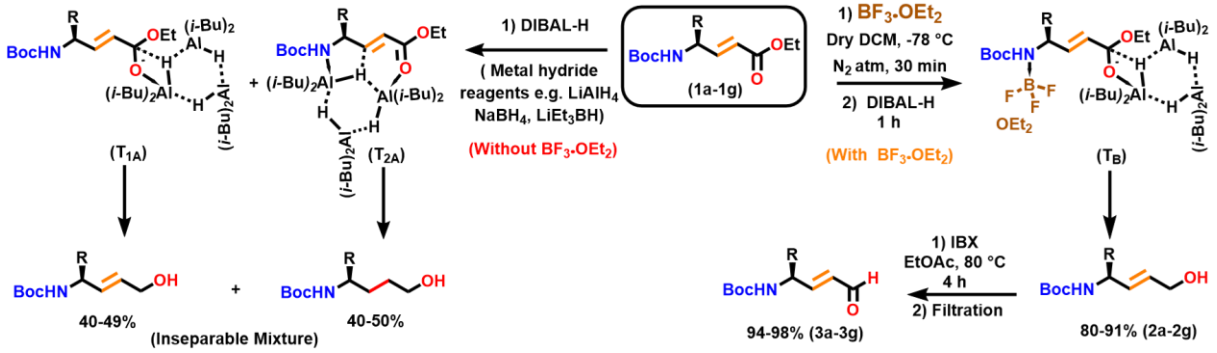
Naturally occurring peptides containing amino acid with multiple conjugative backbone double bonds have found diverse applications in various biological contexts. The primary goal of this study is to explore and demonstrate the utilization of the Wittig reaction for the synthesis of

conjugative multiple double bonds. This investigation aims to contribute insights into the feasibility, efficiency, and selectivity of employing the Wittig reaction for the formation of compounds with multiple conjugative double bonds. The utilization of the Wittig reaction for the synthesis of conjugative multiple double bonds is rare.

In this study, we investigated the viability of the Wittig reaction for constructing two and three carbon-carbon double bonds on the N-protected amino acid backbone. The ethyl esters of N-Boc amino acids with multiple carbon-carbon double bonds in the backbone were successfully isolated in excellent yields, demonstrating exceptional *E*-selectivity of the double bonds. The allylic alcohols of α,β-unsaturated γ-amino esters were selectively synthesized through DIBAL-H and $BF_3.OEt_2$, subsequently transformed into aldehydes using IBX oxidation. Through this protocol, we synthesized ethyl esters of N-Boc-(*E*,*E*)-α,β,γ,δ-unsaturated ε-amino acids with various side-chain functionalities, as well as ethyl esters of N-Boc-(*E*,*E*,*E*)-α,β,γ,δ,ε,ζ-unsaturated η-amino acids, achieving excellent yields. The observed exceptional *E*-selectivity is probably due to the stabilization of the planar transition state of the Wittig reaction through interaction with the double bond *p*-orbitals. Notably, no racemization was observed during the amino acid synthesis. This chapter may serve as an excellent method for synthesizing multiple conjugative carbon-carbon double bonds.

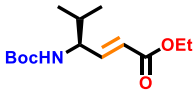
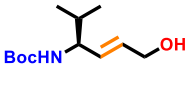
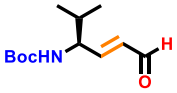
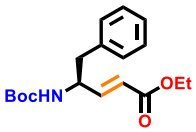
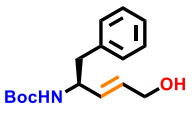
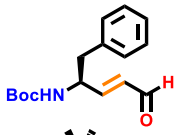
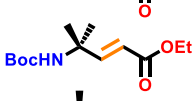
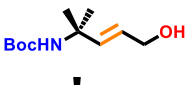
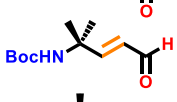
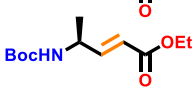
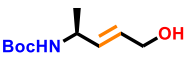
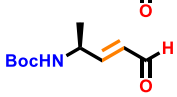
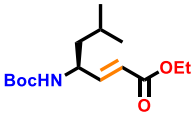
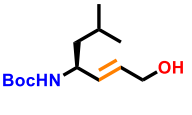
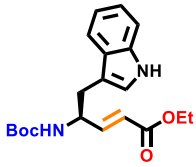
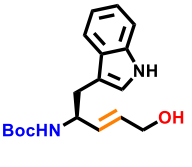
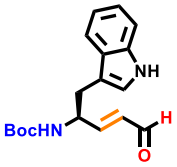
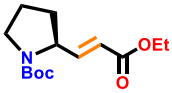
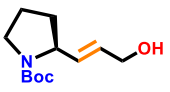
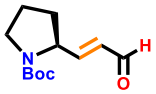
2.3. Results and Discussion

To investigate whether or not the Wittig reaction can be used to synthesize the amino acids with conjugative multiple double bonds and also to evaluate the stereochemistry of these conjugative double bonds, we synthesized ethyl esters of (*E*)-α,β-unsaturated γ-amino acids (**1a-1g**) from Boc-amino aldehydes using a previously reported procedure.[16] The amino acid list is provided in Table 1. We employed the Wittig reaction to synthesize these amino acids and noted the exclusive *E*-selectivity of the double bonds in the synthesis. To introduce an additional double bond to these (*E*)-α,β-unsaturated γ-amino acids, it is essential to convert the ethyl esters of (*E*)-α,β-unsaturated γ-amino acids into corresponding allylic alcohols and subsequently aldehydes. As DIBAL-H is known for the selective reduction of ethyl esters into corresponding alcohols in the presence of conjugated double bonds,[21,22] we anticipated that it can selectively reduce ethyl esters of **1a-1g** to corresponding allylic alcohols **2a-2g**. We treated amino esters **1a-1g** with DIBAL-H for reduction; however, we observed a partial reduction of



Scheme 1: Selective reduction of ethyl esters of α,β-unsaturated γ-amino acids (**1**) to corresponding allylic alcohols (**2**) using DIBAL-H in the presence of $BF_3.OEt_2$ and subsequent IBX oxidation to (*E*)-α,β-unsaturated γ-aldehyde (**3**).

Table 1: Selective reduction of ethyl esters of α,β-unsaturated γ-amino acids (**1**) to corresponding allylic alcohols (**2**) and subsequent IBX oxidation to (*E*)-α,β-unsaturated γ-amino aldehydes (**3**)

Entry	(*E*)-α,β-Unsaturated γ-Amino Ester (1)	((*E*)-Boc-Amino Allylic Alcohol) Product (2)	% Yield of Product (2)	((*E*)-α,β-Unsaturated-γ-Amino Aldehydes) Product (3)	% Yield of Product (3)
a)			84		96
b)			90		97
c)			83		94
d)			86		98
e)			91		98
f)			88		95
g)			80		94

both double bonds with ethyl esters. Approximately 40%-50% of the carbon-carbon double bond-reduced alcohols were isolated, alongside the allylic alcohol. We hypothesized that the amide NH group might be contributing to these undesired outcomes. By capturing the lone pair on nitrogen with a suitable Lewis acid, It may possible to direct the reaction to selectively

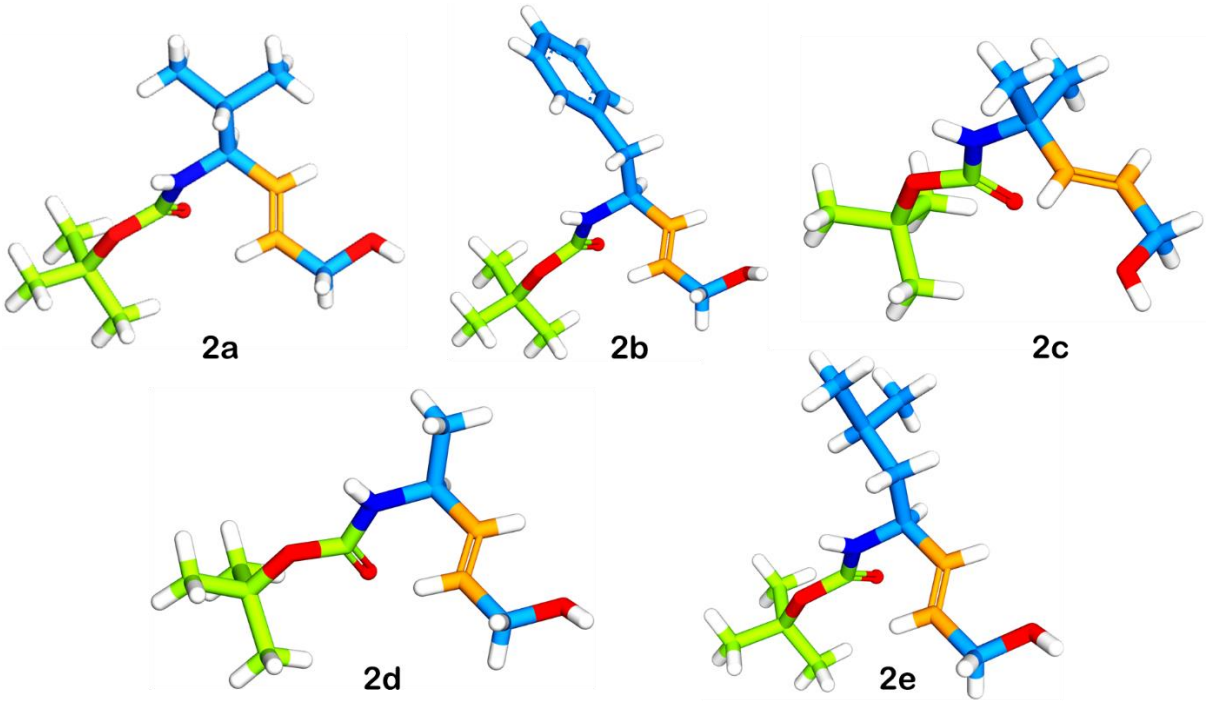
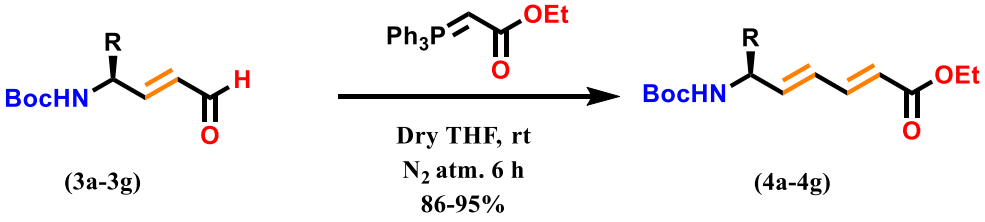


Figure 3: The X-ray diffracted structures of allylic alcohol **2a-2e**.

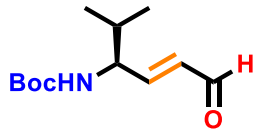
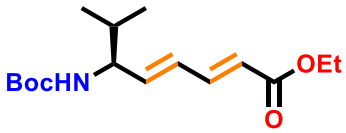
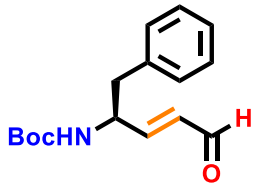
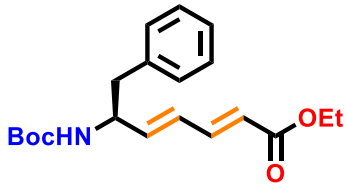
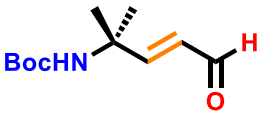
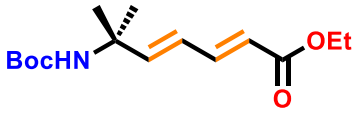
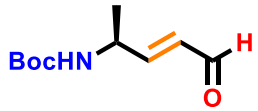
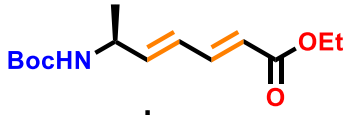
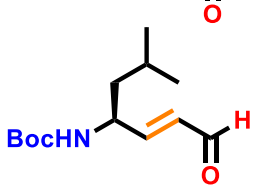
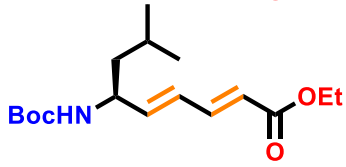
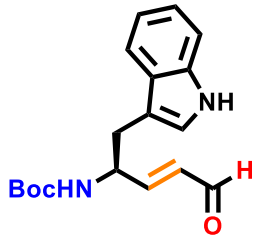
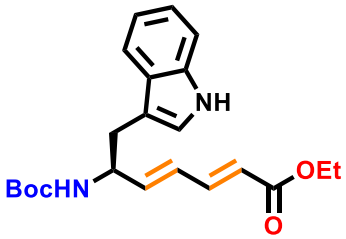
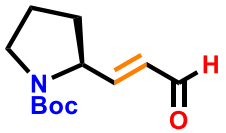
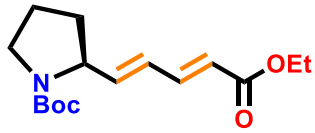
reduce the ethyl esters without affecting the conjugated double bonds. We modified the reduction conditions accordingly. Before introducing DIBAL-H, we treated the ethyl esters of α,β-unsaturated γ-amino acids with $BF_3 \cdot OEt_2$ and stirred the mixture for approximately 30 minutes.[23] The introduction of DIBAL-H to the solution of α,β-unsaturated γ-amino esters in the presence of $BF_3.OEt_2$ resulted exclusively in allylic alcohols. As expected, we observed a selective reduction of ethyl esters, and no conjugated double bonds were reduced. The schematic representation of the reduction of ethyl esters of α,β-unsaturated γ-amino acids is shown in Scheme 1. The allylic alcohols **2a-2g**, were obtained in high yields. Amino acids with sterically hindered side-chains, such as **1a** and **1c**, and the amino acid with a proline side-chain **1g**, exhibited relatively lower yields compared to the amino acids with alanine **1d** and leucine **1e** side-chains as well as aromatic amino acid side-chains **1b** and **1f**. The list of allylic alcohols is detailed in Table 1. We determined the single crystal structures of **2a-2e**, shown in Figure 3.

Since α,β-unsaturated γ-amino aldehydes are essential for the Wittig reaction, we treated the allylic alcohols **2a-2g** with IBX in ethyl acetate at 80 °C for oxidation. Scheme 1 provides a schematic representation of the reaction. All α,β-unsaturated γ-amino aldehydes **3a-3g** were isolated in high yields (see Table 1), and no traces of carboxylic acids were detected in the reaction. These results indicate that allylic alcohols can be readily converted into α,β-unsaturated aldehydes using IBX oxidation without affecting the conjugated carbon-carbon

Table 2: Synthesis of the ethyl esters of ε-amino acids (**4a-4g**) with two conjugative (*E*,*E*)-carbon-carbon double bonds



(3a-3g) (4a-4g)

Entry	(*E*)-α,β-Unsaturated-γ-Amino Aldehydes (3)	((*E*)α,β, (*E*)γ-δ, ε-Amino Esters) Product (4)	% Yield
a)			90
b)			93
c)			88
d)			95
e)			94
f)			86
g)			87

double bonds.The N-Boc-protected α,β-unsaturated γ-aldehydes were immediately used in the Wittig reaction. The aldehydes **3a-3g** underwent treatment with the Wittig ylide in dry THF at room temperature. Following a 6-hour stirring period under an inert atmosphere, the Wittig products **4a-4g** were obtained in highly satisfactory yields. The amino acids featuring two

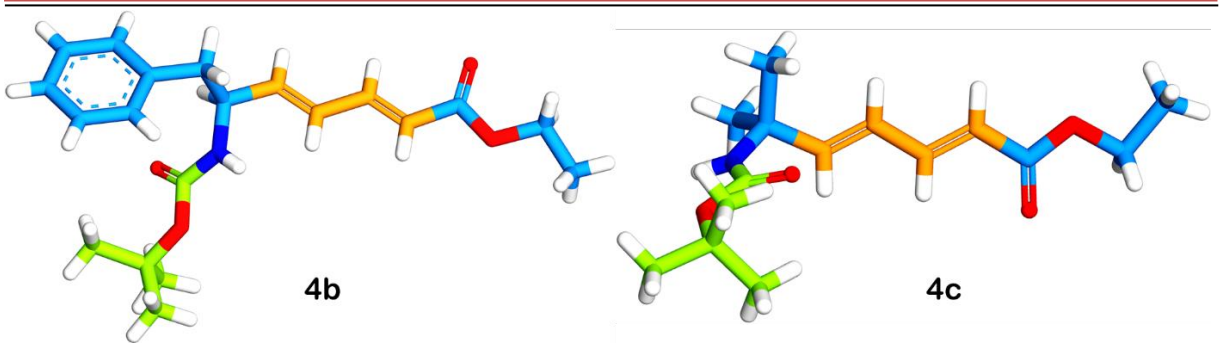
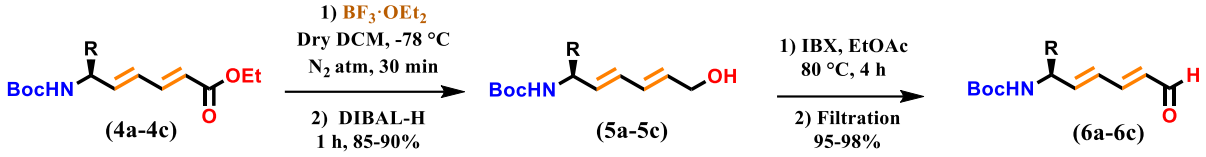


Figure 4: The X-ray diffracted structures of (*E*)α-β, (*E*)γ-δ, ε-amino ethyl esters **4b-4c**.

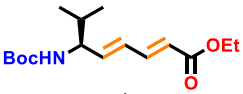
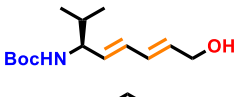
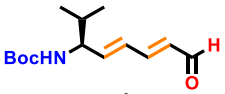
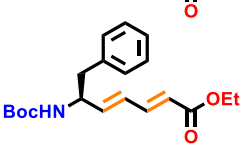
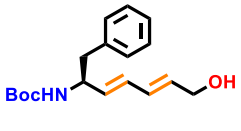
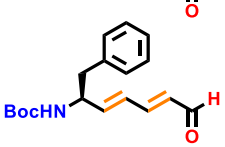
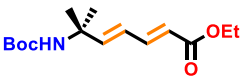
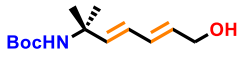
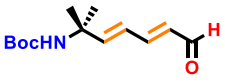
conjugative double bonds were characterized through 1H, 13C, and mass spectral analyses, revealing that the two double bonds exhibited *E*,*E*-stereochemistry. Furthermore, the analysis of product **4f** indicated that there is no necessity for the protection of the indole NH group. Apart from solution characterization, we investigated their structures in single crystals. The X-ray structures of amino acids **4b** and **4c** are depicted in Figure 4. Crystal structure analysis also unveiled that the two conjugative double bonds in the amino acid backbone adopted a *trans*, *trans* geometry. It is worth mentioning that the Wittig reaction exclusively yielded *E*-double bonds in both the starting amino acids and the products. Despite the absence of steric interference from side-chain substituents during the introduction of the second double bond, it may possible to get the mixed stereochemistry, however, we observed a strictly *trans* geometry of the double bonds. The N-protected amino esters with two conjugative *E*,*E*-double bonds are listed in Table 2.

Intrigued by the exclusive *trans* geometry of the two conjugative double bonds, we aimed to explore the possibility of introducing a third double bond using the Wittig reaction, along with investigating the geometry of the newly introduced double bond on the same amino acid backbone. To introduce a third double bond, we needed aldehydes with two conjugated carbon-carbon double bonds. As a proof of concept, we subjected the ethyl esters of (*E*)α-β, (*E*)γ-δ, ε-amino acids **4a-4c** to reduction to obtain the corresponding vinylogous allylic alcohol. We assumed that the same protocol described above could be utilized for the reduction of ethyl esters without affecting the double bonds. The ethyl ester of (*E*)α-β, (*E*)γ-δ, ε-amino acids were stirred with $BF_3.OEt_2$, before the addition of DIBAL-H. The reduction was carried out at -78 °C under an inert atmosphere. We observed a selective reduction of ethyl esters to yield double-bond conjugated allylic alcohols **5a-5c** without affecting the carbon-carbon double bonds. Scheme 2 provides a schematic representation of the reaction. The double-bond conjugated allylic alcohols were obtained in high yields and characterized. The list of these alcohols is



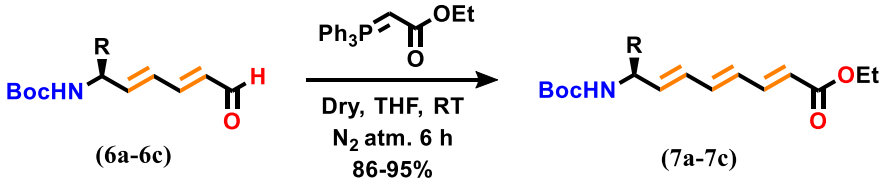
Scheme 2: Synthesis of (*E*,*E*)-double bond conjugated allylic alcohols (**5a-5c**) and corresponding aldehydes (**6a-6c**).

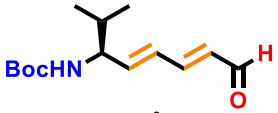
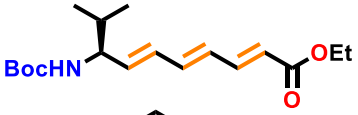
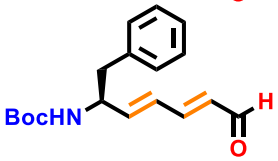
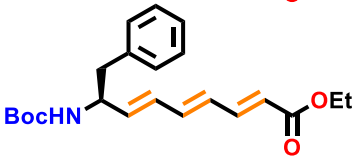
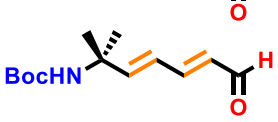
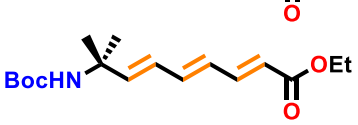
Table 3: Synthesis of (*E*,*E*)-double bond conjugated allylic alcohols (**5**) and corresponding aldehydes (**6**)

Entry	(*E*)α-β, (*E*)γ-δ, ε-Amino Esters (4)	((*E*,*E*) double bond conjugated Allylic Alcohol) Product (5)	% Yield of Product (5)	((*E*)α-β, (*E*)γ-δ, ε-Amino Aldehyde) Product (6)	% Yield of Product (6)
a)			86		96
b)			90		98
c)			85		95

detailed in Table 3. Subsequently, the (*E*,*E*)-carbon-carbon double bond conjugated allylic alcohols underwent IBX oxidation in ethyl acetate, with the reaction mixture stirred at 80 °C

Table 4: Synthesis of the ethyl esters of η-amino acid (**7a-7c**) with three conjugative (*E*,*E*,*E*)-carbon-carbon double bonds.



Entry	(*E*)α-β, (*E*)γ-δ, ε-Amino Aldehyde (6)	((*E*)α-β, (*E*)γ-δ, (*E*)ε-ς, η-Amino Esters) Product (7)	% Yield
a)			88
b)			90
c)			87

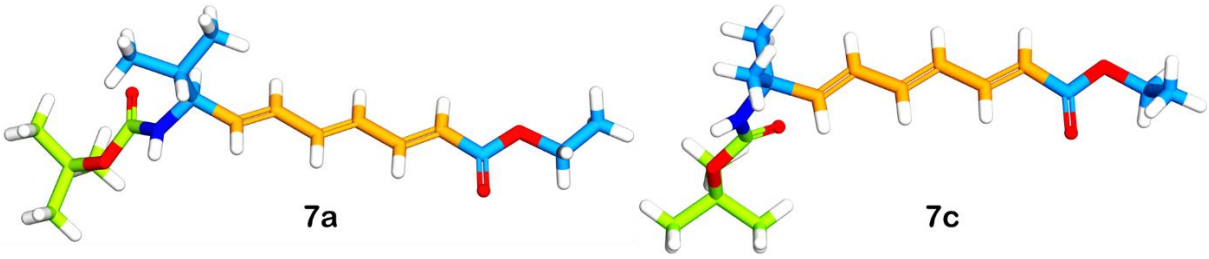


Figure 5: The X-ray diffracted structures of (*E*)α-β, (*E*)γ-δ, (*E*)ε-ζ, η-amino ethyl esters **7a-7c**.

for approximately 4 hours (Scheme 2). The resulting (*E*)α-β, (*E*)γ-δ, ε-amino aldehydes **6a-6c** were isolated in excellent yields and are presented in Table 3. The aldehydes were immediately employed in the Wittig reaction using a stable Wittig ylide. This reaction took place in dry THF under an inert atmosphere at room temperature. The resulting Wittig products **7a-7c** were isolated in high yields (refer to Table 4) and characterized through 1H, 13C, and HR-MS analysis. Additionally, compounds **7a** and **7c** yielded single crystals, and their X-ray diffracted structures are depicted in Figure 5. The structural analysis unveiled that the carbon-carbon double bonds in all three amino acids exhibited a trans geometry. Notably, amino acid **7a** adopted a parallel β-sheet-type structure, stabilized by intermolecular hydrogen bonds formed between the amide NH and CO groups of two amino acid residues. Unlike **7a**, the η-amino acid **7c**, with dimethyl substitutions, adopted a twisted conformation. The dimethyl-substituted α-amino acids favored helical conformations and terminate the β-sheet structure. Notably, the third double bond also adopted a *trans* geometry, despite the potential for the system to adopt a *cis* geometry. The backbone carbon-carbon double bonds in the ε- and η-amino esters displayed remarkable *E*-selectivity. Earlier studies[16] suggested that in the case of γ-amino acids, *E*-selectivity is a result of adopting a planar and less sterically hindered transition state whereas, Z-geometry would involve an energetically unfavorable puckered transition state for amino aldehydes and the ylide. We hypothesized that the remarkable *E*-selectivity observed in

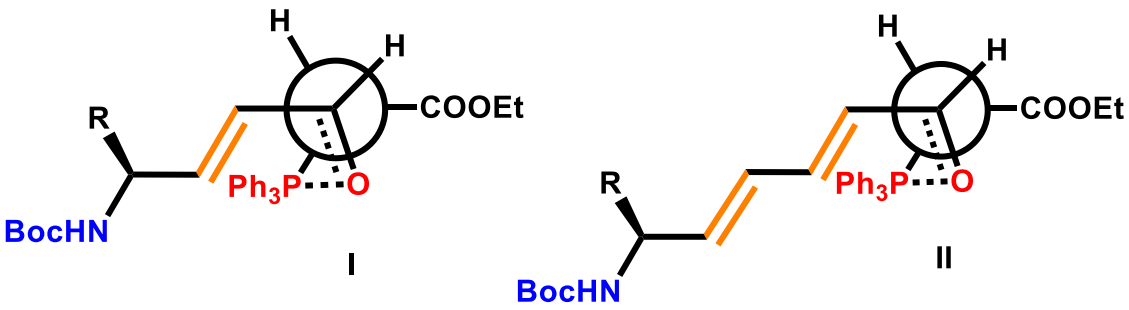
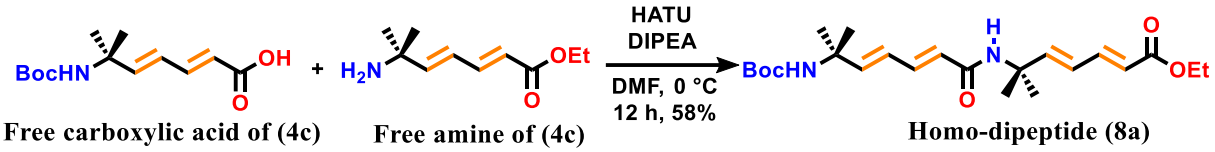


Figure 6: Schematic representation of the planar transition states during the formation of **ε-** (**I**) and **η-** (**II**) amino esters.

both ε and η-amino acids is likely attributed to less steric interactions in the transition state.[24] The schematic depiction of the transition state interactions between the aldehyde and ylide during the formation of ε- and η-amino esters is illustrated in Figure 6.

To investigate whether the amino acids with multiple double bonds can be used to synthesize peptides, we synthesized a dipeptide employing the amino acid **4c**. The reaction is schematically depicted in Scheme 3. A segment of **4c** was subjected to hydrolysis using 1N NaOH, resulting in the isolation of the free carboxylic acid in good yield. Simultaneously, the



Scheme 3: Synthesis of dipeptide (**8a**) using conjugative *trans-trans* double bonds containing ε-amino acids.

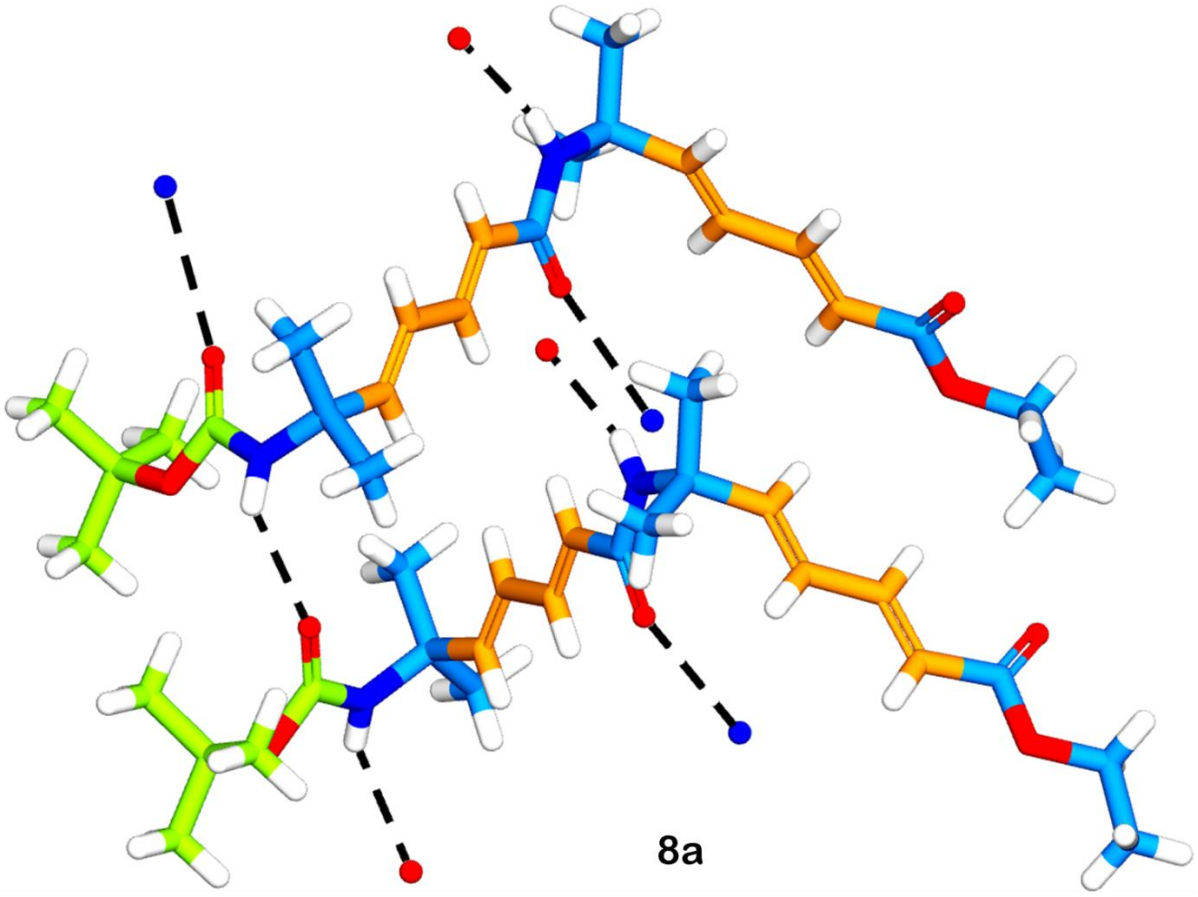


Figure 7: The X-ray diffracted structures of dipeptide **8a**.

Boc group of another portion of **4c** was deprotected using 50% TFA in DCM. The **4c** compound is amenable to both hydrolysis and Boc group deprotection, and no alteration in the geometry of the double bonds was noted during these processes. The free amine and carboxylic acid groups of **4c** were coupled using HATU in the presence of the weak base DIPEA in DMF. The dipeptide **8a** was obtained in a moderate yield after column purification. The peptide's structure was examined in single crystals, and the X-ray diffracted structure of the dipeptide is illustrated in Figure 7. In single crystals, the dipeptide adopted an extended structure.

2.4. Conclusion

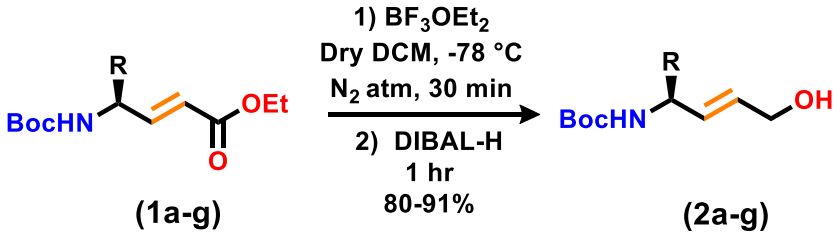
We demonstrated the synthesis of ethyl esters of N-protected amino acids featuring three conjugative backbone carbon-carbon double bonds, originating from *E*-vinylogous amino acids through the application of the Wittig reaction. Additionally, we detailed the selective synthesis of allylic alcohols, without affecting the conjugated carbon-carbon double bonds. All allylic alcohols were successfully isolated in high yields. Furthermore, we demonstrated the oxidation of these allylic alcohols to unsaturated aldehydes. The esters of N-Boc-protected amino acids possessing two and three conjugative double bonds were obtained in excellent yields with maintained chiral integrity. No racemization was detected throughout the synthesis and isolation of these amino acid esters. Additionally, we demonstrated the applicability of these amino acids by synthesizing a dipeptide. The single-crystal conformations of both the amino acids and peptides revealed extended-type conformations. We hypothesized that the remarkable *E*-selectivity of conjugative double bonds is likely a result of the planar transition state combined with the overlap of *p*-orbitals. The allylic alcohols and carbon-carbon double bond-conjugated aldehydes can function as starting materials in diverse organic transformations, while the amino acids can be utilized in constructing peptides and foldamers. In summary, we illustrated the utility of the Wittig reaction in synthesizing conjugative double bonds along the amino acid backbone, with exceptional *E*-selectivity.

2.5. Experimental details

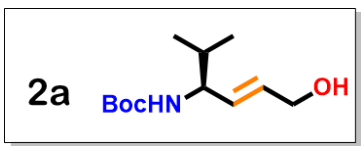
2.5.1. General Information: All amino acids and reagents, including Di-tert-butyl dicarbonate, N,O-Dimethylhydroxylamine hydrochloride, DCC, HOBt, HATU, DIPEA, $LiAlH_4$, PPh_3, Ethyl bromoacetate, DIBAL-H, $BF_3{\cdot}OEt_2$, 2-iodoxybenzoic acid (IBX), THF, DCM, DMF, Ethyl acetate, and ethanol sodium hydroxide (NaOH), were procured from commercial sources. THF was dried over sodium metal and distilled before use. DCM was also dried using CaH_2 and distilled under an inert atmosphere before use. Pet-ether and Ethyl acetate

were distilled prior to use. Column chromatography utilized silica gel (230-400 mesh). ^{1}H NMR and ^{13}C NMR spectra were recorded on 400 MHz and 100 MHz, respectively, using deuterated chloroform ($CDCl_3$) as the internal standard. Chemical shifts (δ) and coupling constants were reported in ppm and Hz, respectively. The mass of all pure molecules was confirmed by a high-resolution mass spectrometer (ESI-QTOF). X-ray data were collected at a 100 K temperature on a Bruker APEX(II) DUO CCD diffractometer using Mo Kα radiation (λ = 0.71073 Å). Specific rotations were recorded using chloroform solvent (Rudolph Analytical Research instrument). The Boc-amino (*E*)-vinylogous ester (**1a-1g**) was synthesized using our previously reported protocol.[16]

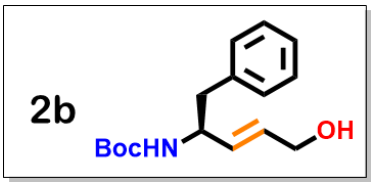
2.5.2. General procedure for the synthesis of Boc-amino allylic alcohol (2a-2g)



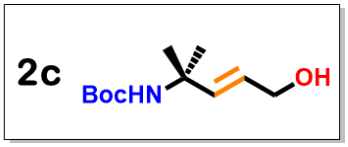
Boc-amino vinylogous ester (**1a-1g**) (20 mmol) was dissolved in anhydrous DCM (100 mL) under a nitrogen atmosphere, cooled to -78 °C, and then $BF_3{\cdot}OEt_2$ (23 mmol) was introduced into the solution. The mixture was stirred at that temperature for 30 minutes. Following this, a 1 M toluene solution of DIBAL-H (70 mmol) was introduced to the reaction mixture, and the resultant blend was stirred at -78 °C for 1 hour. The advancement of the reaction was tracked using TLC. After reaching completion, the reaction mixture was neutralized with a 5% aqueous HCl solution (150 mL). The resulting mixture was permitted to reach room temperature. Subsequently, DCM was evaporated, and the product was extracted with ethyl acetate (150 mL × 3). The ethyl acetate solution obtained through extraction was washed with 10% Na_2CO_3 (200 mL), followed by a brine solution (200 mL). The organic layer was dehydrated using anhydrous Na_2SO_4, and the product was concentrated under reduced pressure. The purified Boc-amino allylic alcohol (**2a-2g**) was then isolated through column chromatography utilizing an ethyl acetate/petroleum ether (1/3) (v/v) solvent system.



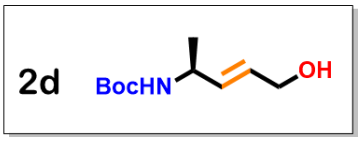
Tert-butyl (*S*,*E*)-(6-hydroxy-2-methylhex-4-en-3-yl)carbamate (2a). White crystalline solid, yield: 3.85 g (84%), mp: 97-99 °C, $[\alpha]_D^{25}$ = +4.201 (*c* = 1 $CHCl_3$). ^1H NMR (400 MHz, $CDCl_3$) δ 5.74 (dtd, *J* = 15.5, 5.6, 1.2 Hz, 1H), 5.59 (ddt, *J* = 15.5, 6.0, 1.2 Hz, 1H), 4.56 (br, 1H), 4.13 (dt, *J* = 5.6, 1.2 Hz, 2H), 3.96 (m, 6.0, 1.2 Hz, 1H), 1.97 (s, 1H, -OH), 1.74 (m, *J* = 6.4, 6.4 Hz, 1H), 1.43 (s, 9H), 0.89 (d, *J* = 6.4 Hz, 3H), 0.87 (d, *J* = 6.4 Hz, 3H). ^{13}C {^1H} NMR (101 MHz, $CDCl_3$) δ 155.77, 130.74, 130.30, 79.43, 77.48, 77.16, 76.84, 63.09, 57.22, 32.54, 28.52, 18.84, 18.23. HRMS (ESI-QTOF) *m/z* calculated value for $C_{12}H_{23}NO_3$ is $[M+Na]^+$ 252.1576 and observed 252.1569.



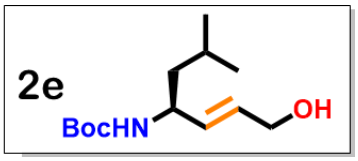
Tert-butyl (*S*, *E*)-(5-hydroxy-1-phenylpent-3-en-2-yl)carbamate (2b). White crystalline solid, yield: 4.99 g (90%), mp: 83-85 °C, $[\alpha]_D^{25}$ = +6.408 (*c* = 1 $CHCl_3$). ^1H NMR (400 MHz, $CDCl_3$) δ 7.31 – 7.27 (m, 2H), 7.23 – 7.16 (m, 3H), 5.71 (dt, *J* = 15.6, 4.4 Hz, 1H), 5.65 (dd, *J* = 15.6, 4.4 Hz, 1H), 4.53 (br, 1H), 4.41 (m, *J* = 6.8, 4.4 Hz, 1H), 4.09 (d, *J* = 4.4 Hz, 2H), 2.83 (d, *J* = 6.8 Hz, 2H), 1.79 (s, 1H, -OH), 1.39 (s, 9H). ^{13}C {^1H} NMR (101 MHz, $CDCl_3$) δ 155.32, 137.50, 131.60, 129.84, 129.64, 128.49, 126.64, 79.65, 77.48, 77.16, 76.84, 63.06, 52.79, 41.79, 28.49. HRMS (ESI-QTOF) *m/z* calculated value for $C_{16}H_{23}NO_3$ is $[M+Na]^+$ 300.1575 and observed 300.1566.



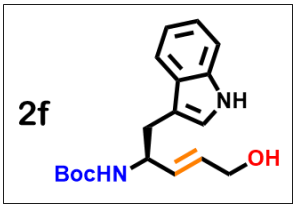
Tert-butyl (*E*)-(5-hydroxy-2-methylpent-3-en-2yl)carbamate (2c). Colourless solid, yield: 3.571 g (83%), mp: 55-57 °C. ^1H NMR (400 MHz, $CDCl_3$) δ 5.81 (dt, *J* = 15.6, 1.3 Hz, 1H), 5.67 (dt, *J* = 15.6, 5.6 Hz, 1H), 4.64 (s, 1H), 4.11 (dd, *J* = 5.6, 1.3 Hz, 2H), 2.26 (s, 1H, -OH), 1.41 (s, 9H), 1.35 (s, 6H). ^{13}C {^1H} NMR (101 MHz, CDCl3) δ 154.64, 138.03, 126.56, 79.27, 77.48, 77.16, 76.84, 63.25, 52.83, 28.55, 27.87. HRMS (ESI-QTOF) *m/z* calculated value for $C_{11}H_{21}NO_3$ is $[M+Na]^+$ 238.1418 and observed 238.1413.



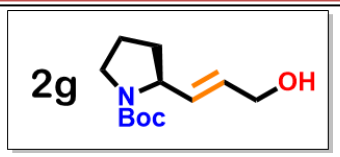
Tert-butyl (*S*,*E*)-(5-hydroxypent-3-en-2-yl)carbamate (2d). Colourless solid, yield: 3.46 g (86%), mp: 42-44 °C, $[\alpha]_D^{25}$ = -10.5 (*c* = 1 $CHCl_3$). ^1H NMR (400 MHz, $CDCl_3$) δ 5.77 – 5.70 (dtd, *J* = 15.6, 5.2, 1.2 Hz,1H), 5.65 (ddt, *J* = 15.6, 4.8, 1.2 Hz, 1H), 4.54 (br, 1H), 4.20 (m, *J* = 6.8, 4.8, 1.2 Hz, 1H), 4.11 (dt, *J* = 5.2, 1.2 Hz, 2H), 2.10 (s, 1H, -OH), 1.42 (s, 9H), 1.20 (d, *J* = 6.8 Hz, 3H). ^{13}C {^1H} NMR (101 MHz, $CDCl_3$) δ 155.32, 133.73, 128.68, 79.55, 77.48, 77.16, 76.84, 63.10, 47.42, 28.55, 21.13. HRMS (ESI-QTOF) *m/z* calculated value for $C_{10}H_{19}NO_3$ is $[M+Na]^+$ 224.1262 and observed 224.1256.



Tert-butyl (*S*,*E*)-(1-hydroxy-6-methylhept-2-en-4-yl)carbamate (2e). White crystalline solid, yield: 4.43 g (91%), mp: 102-104 °C, $[\alpha]_D^{25}$ = -9.136 (*c* = 1 $CHCl_3$). ^1H NMR (400 MHz, $CDCl_3$) δ 5.75 (dtd, *J* = 15.6, 5.6, 1.2 Hz, 1H), 5.58 (ddt, *J* = 15.6, 6.0, 1.2 Hz, 1H), 4.44 (br, 1H), 4.15 (m, *J* = 6.0, 1.2 Hz, 1H), 4.12 (dt, *J* = 5.6, 1.2 Hz, 2H), 1.90 (s, 1H, -OH), 1.65 (m, *J* = 6.4, 6.4 Hz, 1H), 1.43 (s, 9H), 1.35 – 1.27 (m, 2H), 0.92 (d, *J* = 6.4 Hz, 3H), 0.918 (d, *J* = 6.4 Hz, 3H). ^{13}C {^1H} NMR (101 MHz, $CDCl_3$) δ 155.50, 132.95, 129.17, 79.44, 77.48, 77.16, 76.84, 63.09, 50.27, 44.77, 28.54, 24.80, 22.78, 22.51. HRMS (ESI-QTOF) *m/z* calculated value for $C_{13}H_{25}NO_3$ is $[M+Na]^+$ 266.1731 and observed 266.1732.

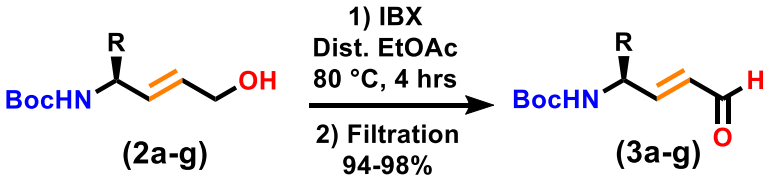


Tert-butyl (*S*,*E*)-(5-hydroxy-1-(1H-indol-3-yl)pent-3-en-2-yl)carbamate (2f). Colourless solid, yield: 5.564 g (88%), mp: 93-95 °C, $[\alpha]_D^{25}$ = +16.236 (*c* = 1 $CHCl_3$). ^1H NMR (400 MHz, $CDCl_3$) δ 8.34 (br, *J* = 1.2 Hz, 1H), 7.59 (d, *J* = 7.6 Hz, 1H), 7.34 (d, *J* = 7.6 Hz, 1H), 7.18 (t, *J* = 7.6 Hz, 1H), 7.11 (t, *J* = 7.6 Hz, 1H), 7.0 (d, *J* = 1.2 Hz, 1H), 5.74 – 5.69 (dd, *J* = 15.6, 4 Hz, 1H), 5.69 – 5.63 (dt, *J* = 15.6, 4.4 Hz, 1H), 4.68 (br, 1H), 4.50 (br, *J* = 4, 5.6 Hz, 1H), 4.03 (d, *J* = 4.4 Hz, 2H), 2.99 (d, *J* = 5.6 Hz, 2H), 1.89 (s, 1H, -OH), 1.41 (s, 9H). ^{13}C {^1H} NMR (101 MHz, $CDCl_3$) δ 155.60, 136.32, 132.41, 129.45, 127.95, 122.99, 122.10, 119.47, 119.12, 111.46, 111.34, 79.65, 77.48, 77.16, 76.84, 63.08, 52.27, 31.28, 28.51. HRMS (ESI-QTOF) *m/z* calculated value for $C_{18}H_{24}N_2O_3$ is $[M+Na]^+$ 339.1684 and observed 339.1686.



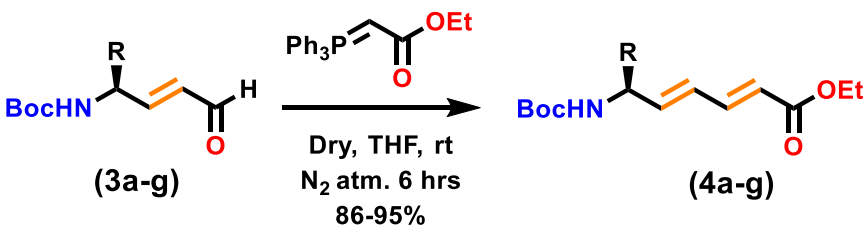
Tert-butyl (*S*,*E*)-2-(3-hydroxyprop-1-en-1-yl)pyrrolidine-1-carboxylate (2g). Colourless liquid, yield: 3.634 g (80%), $[\alpha]_D^{25}$ = -32.536 (*c* = 1 $CHCl_3$). ^1H NMR (400 MHz, $CDCl_3$) δ 5.62 (m, 2H), 4.27 (br, 1H), 4.10 (d, Hz, 2H), 3.36 (br, 2H), 2.13 (s, 1H, -OH), 1.99 (m, 1H), 1.81 (m, 2H), 1.72 – 1.65 (m, 1H), 1.42 (s, 9H). ^{13}C {^1H} NMR (101 MHz, $CDCl_3$) δ 154.77, 132.34, 129.05, 79.38, 77.48, 77.16, 76.84, 63.10, 58.25, 46.75, 46.25, 32.35, 31.82, 28.65, 23.59, 23.01. HRMS (ESI-QTOF) *m/z* calculated value for $C_{12}H_{21}NO_3$ is $[M+Na]^+$ 250.1418 and observed 250.1408.

2.5.3. General Procedure for the synthesis of (*E*)-Boc-α,β-unsaturated γ-amino aldehydes (3a-3g)

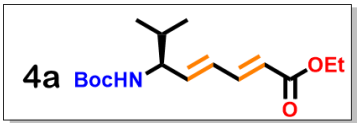


The oxidation of Boc-amino allylic alcohol (**2a-2g**) with 2-iodoxybenzoic acid (IBX) led to the formation of (*E*)-N-Boc-α,β-Unsaturated γ-Amino Aldehydes (**3a-3g**). In this process, 15 mmol of Boc-amino allylic alcohol (**2a-2g**) was dissolved in distilled ethyl acetate (150 mL), and 16.5 mmol of 2-iodoxybenzoic acid (IBX) was added to the solution. The reaction mixture was stirred for 4 hours at 80 °C under reflux using a condenser. The advancement of the reaction was tracked via TLC in an ethyl acetate and petroleum ether (30/70) (v/v) solvent system. Upon completion, the reaction mixture was filtered through a sintered funnel, and the filtrate was concentrated under reduced pressure. The (*E*)-N-Boc-α,β-Unsaturated γ-Amino Aldehydes (**3a-3g**) were obtained in excellent yields and promptly used in the Wittig reaction.

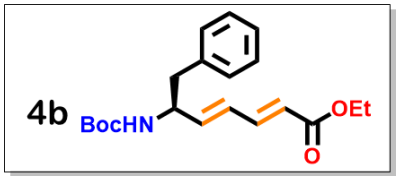
2.5.4. General Procedure for the synthesis of Ethyl ester of (*E*)α-β, (*E*)γ-δ, ε-Amino acids (4a-4g)



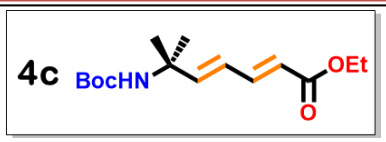
The (*E*)-Boc-α,β-unsaturated γ-aldehyde (**3a-3g**) (14 mmol) was dissolved in anhydrous THF (120 mL) under a nitrogen atmosphere. Subsequently, Wittig ylide (Ph3P=CHCO2Et) (16.8 mmol) was introduced into the solution. The mixture was stirred for approximately 6 hours at room temperature. The advancement of the reaction was tracked using TLC. After the reaction was complete, THF was removed from the reaction mixture by evaporation, and the product, ethyl ester of (*E*)α-β, (*E*)γ-δ, ε-amino acids (**4a-4g**), was purified through column chromatography employing an ethyl acetate/petroleum ether (6/94) (v/v) solvent system.



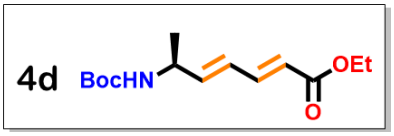
Ethyl (*S*,2*E*,4*E*)-6-((tert-butoxycarbonyl)amino)-7-methylocta-2,4-dienoate (4a). Colourless solid, yield: 3.74 g (90%), mp: 58-60 °C, $[\alpha]_D^{25}$ = -7.616 (*c* = 1 $CHCl_3$). ^1H NMR (400 MHz, $CDCl_3$) *δ* 7.26 (dd, *J* = 15.2, 11.2 Hz, 1H), 6.25 (dd, *J* = 15.2, 11.2 Hz, 1H), 5.98 (dd, *J* = 15.2, 6 Hz, 1H), 5.85 (d, *J* = 15.2 Hz, 1H), 4.57 (br, 1H), 4.18 (q, *J* = 7.2 Hz, 2H), 4.07 (br, *J* = 6 Hz, 1H), 1.82 – 1.76 (m, *J* = 6.8, 6.8 Hz, 1H), 1.43 (s, 9H), 1.28 (t, *J* = 7.2 Hz, 3H), 0.91 - 0.89 (d, *J* = 6.8 Hz, 3H), 0.90 - 0.88 (d, *J* = 6.8 Hz, 3H). ^{13}C {^1H} NMR (101 MHz, $CDCl_3$) *δ* 167.14, 155.57, 143.97, 142.07, 128.62, 121.27, 79.69, 77.48, 77.16, 76.84, 60.44, 57.52, 32.63, 28.50, 18.89, 18.29, 14.41. HRMS (ESI-QTOF) *m/z* calculated value for $C_{16}H_{27}NO_4$ is $[M+Na]^+$ 320.1837 and observed 320.1826.



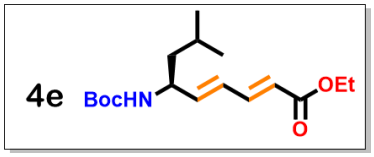
Ethyl (*S*,2*E*,4*E*)-6-((tert-butoxycarbonyl)amino)-7-phenylhepta-2,4-dienoate (4b). White solid, yield: 4.49 g (93%), mp: 81-83 °C, $[\alpha]_D^{25}$ = -12.48 (*c* = 1 $CHCl_3$). ^1H NMR (400 MHz, $CDCl_3$) *δ* 7.30 – 7.14 (m, 6H, aromatic-Ph & vinylic β-proton merged), 6.19 (dd, *J* = 15.4, 10.9 Hz, 1H), 6.02 (dd, *J* = 15.4, 5.2 Hz, 1H), 5.82 (d, *J* = 15.4 Hz, 1H), 4.57 (br, 1H), 4.55 (br, *J* = 5.2, 6.2 Hz, 1H), 4.19 (q, *J* = 7.1 Hz, 2H), 2.86 (d, *J* = 6.2 Hz, 2H), 1.40 (s, 9H), 1.28 (t, *J* = 7.1 Hz, 3H). ^{13}C {^1H} NMR (101 MHz, $CDCl_3$) δ 167.07, 155.16, 143.75, 142.26, 136.84, 129.60, 128.63, 128.12, 126.87, 121.60, 79.90, 77.48, 77.16, 76.84, 60.48, 53.02, 41.48, 28.46, 14.41. HRMS (ESI-QTOF) *m/z* calculated value for $C_{20}H_{27}NO_4$ is $[M+Na]^+$ 368.1837 and observed 368.1830.



Ethyl (2*E*,4*E*)-6-((tert-butoxycarbonyl)amino)-6-methylhepta-2,4-dienoate (4c). White solid, yield: 3.45 g (88%), mp: 70-72 °C. ^{1}H NMR (400 MHz, $CDCl_3$) δ 7.27 (dd, J = 15.6, 10 Hz, 1H), 6.21 (dd, J = 15.2, 10 Hz, 1H), 6.18 – 6.15 (d, J = 15.2 Hz, 1H) 5.83 (d, J = 15.6 Hz, 1H), 4.62 (s, 1H), 4.18 (q, J = 7.2 Hz, 2H), 1.41 (s, 9H), 1.39 (s, 6H), 1.28 (t, J = 7.2 Hz, 3H). ^{13}C {^{1}H} NMR (101 MHz, $CDCl_3$) δ 167.13, 154.38, 148.81, 144.62, 125.18, 121.01, 79.50, 77.48, 77.16, 76.84, 60.38, 53.24, 28.52, 27.73, 14.42. HRMS (ESI-QTOF) *m/z* calculated value for $C_{15}H_{25}NO_4$ is $[M+Na]^+$ 306.1681 and observed 306.1677.

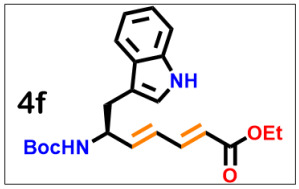


Ethyl (*S*,2*E*,4*E*)-6-((tert-butoxycarbonyl)amino)hepta-2,4-dienoate (4d). Colourless liquid, yield: 3.58 g (95%), $[\alpha]_D^{25}$ = -29.496 (c = 1 $CHCl_3$). ^{1}H NMR (400 MHz, $CDCl_3$) δ 7.22 (dd, J = 15.4, 11.0 Hz, 1H), 6.24 (dd, J = 15.3, 11.0 Hz, 1H), 6.02 (dd, J = 15.3, 5.5 Hz, 1H), 5.85 (d, J = 15.4 Hz, 1H), 4.54 (br, 1H), 4.32 (br, J = 6.8 Hz, 1H), 4.18 (q, J = 7.1 Hz, 2H), 1.43 (s, 9H), 1.27 (t, J = 7.1 Hz, 3H), 1.24 (d, J = 6.8 Hz, 3H). ^{13}C {^{1}H} NMR (101 MHz, $CDCl_3$) δ 167.07, 155.14, 144.30, 143.98, 127.15, 121.53, 79.79, 77.48, 77.16, 76.84, 60.46, 47.69, 28.51, 20.78, 14.41. HRMS (ESI-QTOF) *m/z* calculated value for $C_{14}H_{23}NO_4$ is $[M+Na]^+$ 292.1524 and observed 292.1519.

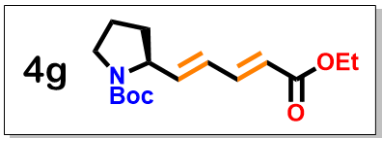


Ethyl (*S*,2*E*,4*E*)-6-((tert-butoxycarbonyl)amino)-8-methylnona-2,4-dienoate (4e). Colourless gummy liquid, yield: 4.1 g (94%), $[\alpha]_D^{25}$ = -10.648 (c = 1 $CHCl_3$). ^{1}H NMR (400 MHz, $CDCl_3$) δ 7.24 (dd, J = 15.4, 11.0 Hz, 1H), 6.26 (dd, J = 15.3, 11.0 Hz, 1H), 5.96 (dd, J = 15.3, 6.2 Hz, 1H), 5.85 (d, J = 15.4 Hz, 1H), 4.44 (br, 1H), 4.25 (br, J = 6.2 Hz, 1H), 4.19 (q, J = 7.1 Hz, 2H), 1.67 – 1.61 (m, J = 6.4, 6.4 Hz, 1H), 1.43 (s, 9H), 1.35 (m, 2H), 1.28 (t, J = 7.1 Hz, 3H), 0.93 – 0.91 (d, J = 6.4 Hz, 3H), 0.92 – 0.90 (d, J = 6.4 Hz, 3H). ^{13}C {^{1}H} NMR (101 MHz, $CDCl_3$) δ 167.12, 155.29, 144.07, 143.81, 127.61, 121.36, 79.72, 77.48, 77.16,

76.84, 60.44, 50.58, 44.37, 28.51, 24.86, 22.81, 22.46, 14.42. HRMS (ESI-QTOF) *m/z* calculated value for $C_{17}H_{29}NO_4$ is $[M+Na]^+$ 334.1994 and observed 334.1991.

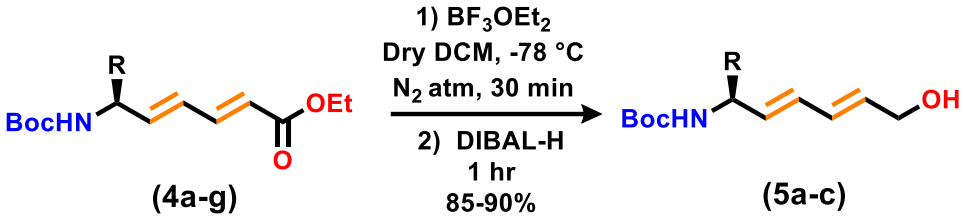


Ethyl (*S*,2*E*,4*E*)-6-((tert-butoxycarbonyl)amino)-7-(1H-indol-3-yl)hepta-2,4-dienoate (4f). Colourless gummy liquid, yield: 4.63 g (86%), $[\alpha]_D^{25}$ = -15.112 (*c* = 1 $CHCl_3$). ^1H NMR (400 MHz, $CDCl_3$) δ 8.19 (br, *J* = 2.4 Hz, 1H), 7.59 (d, *J* = 7.9 Hz, 1H), 7.36 (d, *J* = 7.9 Hz, 1H), 7.25 – 7.20 (dd, *J* = 15.6, 10.8 Hz, 1H), 7.22 – 7.18 (t, *J* = 7.9 Hz, 1H), 7.13 (t, *J* = 7.9 Hz, 1H), 7.00 (d, *J* = 2.4 Hz, 1H), 6.24 (dd, *J* = 15.2, 10.8 Hz, 1H), 6.09 (dd, *J* = 15.2, 5.2 Hz, 1H), 5.81 (d, *J* = 15.6 Hz, 1H), 4.64 (br, 1H, NH), 4.64 (br, *J* = 5.2, 4 Hz, 1H, εCH), 4.19 (q, *J* = 7.1 Hz, 2H), 3.04 (d, *J* = 4 Hz, 2H), 1.41 (s, 9H), 1.28 (t, *J* = 7.1 Hz, 3H). ^{13}C {^1H} NMR (101 MHz, $CDCl_3$) δ 167.17, 155.39, 143.98, 143.26, 136.33, 127.91, 127.81, 123.00, 122.28, 121.35, 119.74, 119.02, 111.31, 110.97, 79.83, 77.48, 77.16, 76.84, 60.47, 52.47, 31.07, 28.47, 14.41. HRMS (ESI-QTOF) *m/z* calculated value for $C_{22}H_{28}N_2O_4$ is $[M+Na]^+$ 407.1946 and observed 407.1944.

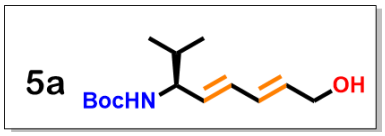


Tert-butyl (*S*)-2-((1*E*,3*E*)-5-ethoxy-5-oxopenta-1,3-dien-1-yl)pyrrolidine-1-carboxylate (4g). Colourless liquid, yield: 3.6 g (87%), $[\alpha]_D^{25}$ = -67.68 (*c* = 1 $CHCl_3$). ^1H NMR (400 MHz, $CDCl_3$) δ 7.25 (dd, *J* = 15.2, 11.0 Hz, 1H, vinylic β-proton), 6.22 – 6.09 (br, 1H, vinylic γ-proton), 6.04 – 5.93 (br, 1H, vinylic δ-proton), 5.82 (d, *J* = 15.2 Hz, 1H, vinylic α-proton), 4.29 (br, 1H), 4.18 (q, *J* = 7.1 Hz, 2H), 3.44 – 3.32 (br, 2H), 2.11 – 1.99 (br, 1H), 1.82 (q, 2H), 1.74 – 1.68 (m, 1H), 1.39 (s, 9H), 1.28 (t, *J* = 7.1 Hz, 3H). ^{13}C {^1H} NMR (101 MHz, $CDCl_3$) δ 167.16, 154.57, 144.04, 143.61, 127.51, 120.94, 79.59, 77.48, 77.16, 76.84, 60.41, 58.65, 46.42, 32.42, 28.57, 23.20, 14.41. HRMS (ESI-QTOF) *m/z* calculated value for $C_{16}H_{25}NO_4$ is $[M+Na]^+$ 318.1680 and observed 318.1680.

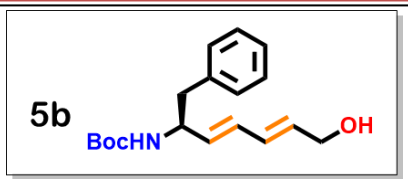
2.5.5. General Procedure for the Synthesis of (*E*,*E*)-Carbon-Carbon double bond conjugated allylic alcohols (5a-5c)



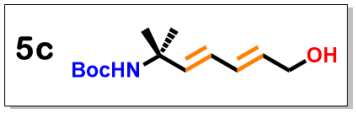
The reduction of the ethyl ester of (*E*)α-β, (*E*)γ-δ, ε-amino acids (**4a-4c**) utilizing $BF_3{\cdot}OEt_2$ and DIBAL-H resulted in the generation of (*E*,*E*)-double bond conjugated allylic alcohols (**5a-5c**). In summary, the ethyl ester of (*E*)α-β, (*E*)γ-δ, ε-amino acids (**4a-4c**) (10 mmol) was dissolved in dry DCM (50 mL) under a nitrogen atmosphere, cooled to -78 °C, and then $BF_3{\cdot}OEt_2$ (11.5 mmol) was introduced into the solution. The reaction mixture was stirred at that temperature for 30 minutes. Subsequently, a 1 M toluene solution of DIBAL-H (35 mmol) was added to the reaction mixture, and the resultant mixture was stirred at -78 °C for 1 hour. The progression of the reaction was tracked by TLC. Upon completion, the reaction mixture was quenched with a 5% aqueous HCl solution (100 mL). The resulting mixture was allowed to warm to room temperature. Afterward, DCM was evaporated, and the product was extracted with ethyl acetate (100 mL × 3). The extracted ethyl acetate solution was washed with 10% Na_2CO_3 (200 mL), followed by a brine (200 mL) solution. The organic layer was then dehydrated using anhydrous Na_2SO_4, and the product was concentrated under reduced pressure. The purified (*E*,*E*)-double bond conjugated allylic alcohols (**5a-5c**) were obtained after column chromatography using an ethyl acetate/petroleum ether (1/3) (v/v) solvent system.



Tert-butyl ((*S*,4*E*,6*E*)-8-hydroxy-2-methylocta-4,6-dien-3-yl)carbamate (5a). Colourless liquid, yield: 2.2 g (86%), $[\alpha]_D^{25}$ = +14.4 (*c* = 1 $CHCl_3$). ^1H NMR (400 MHz, $CDCl_3$) δ 6.23 (ddt, *J* = 14.9, 10.5, 1.4 Hz, 1H), 6.14 (ddd, *J* = 14.8, 10.5, 1.3 Hz, 1H), 5.80 (dt, *J* = 14.9, 5.8 Hz, 1H), 5.56 (dd, *J* = 14.8, 6.5 Hz, 1H), 4.53 (br, 1H), 4.17 (dd, *J* = 5.8, 1.4 Hz, 2H), 3.99 (br, *J* = 6.5, 1.3 Hz, 1H), 1.75 (s, 1H), 1.64 (m, *J* = 6.8, 6.8 Hz, 1H), 1.43 (s, 9H), 0.89 - 0.876 (d, *J* = 6.8 Hz, 3H) 0.884 - 0.87 (d, *J* = 6.8 Hz, 3H). ^{13}C {^1H} NMR (101 MHz, $CDCl_3$) δ 155.63, 133.26, 131.82, 130.89, 130.23, 79.45, 77.48, 77.16, 76.84, 63.39, 57.53, 32.77, 28.54, 18.81, 18.36. HRMS (ESI-QTOF) *m/z* calculated value for $C_{14}H_{25}NO_3$ is $[M+Na]^+$ 278.1728 and observed 278.1725.

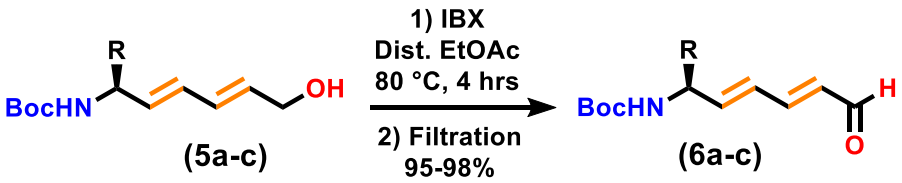


Tert-butyl ((*S*, 3*E*,5*E*)-7-hydroxy-1-phenylhepta-3,5-dien-2-yl)carbamate (5b). Colourless liquid, yield: 2.73 g (90%), $[\alpha]_D^{25}$ = -9.6 (*c* = 1 $CHCl_3$). ^1H NMR (400 MHz, $CDCl_3$) δ 7.31 – 7.26 (m, 2H, -Ph), 7.23 – 7.15 (m, 3H, -Ph), 6.20 (ddt, *J* = 15.0, 10.5, 1.5 Hz, 1H), 6.10 (ddd, *J* = 15.0, 10.5, 1.3 Hz, 1H), 5.77 (dt, *J* = 15.0, 5.7 Hz, 1H), 5.61 (dd, *J* = 15.0, 5.9 Hz, 1H), 4.54 (d, *J* = 8 Hz, 1H), 4.44 (br, *J* = 8, 6.4, 5.9, 1.3 Hz, 1H), 4.15 (dd, *J* = 5.7, 1.5Hz, 2H), 2.83 (d, *J* = 6.4 Hz, 2H), 1.96 (s, 1H), 1.39 (s, 9H). ^{13}C {^1H} NMR (101 MHz, $CDCl_3$) δ 155.30, 137.42, 133.67, 132.25, 130.95, 130.54, 129.73, 129.65, 128.48, 126.62, 79.66, 77.48, 77.16, 76.84, 63.27, 53.00, 41.86, 28.47. HRMS (ESI-QTOF) *m/z* calculated value for $C_{18}H_{25}NO_3$ is $[M+Na]^+$ 326.1731 and observed 326.1731.



Tert-butyl ((3*E*,5*E*)-7-hydroxy-2-methylhepta-3,5-dien-2-yl)carbamate (5c). Colourless liquid, yield: 2 g (85%). ^1H NMR (400 MHz, $CDCl_3$) δ 6.22 (ddt, *J* = 15.2, 10.3, 1.5 Hz, 1H), 6.08 (dd, *J* = 15.4, 10.3 Hz, 1H), 5.83 (d, *J* = 15.4 Hz, 1H), 5.78 (dt, *J* = 15.2, 5.9 Hz,1H), 4.60 (s, 1H), 4.15 (dd, *J* = 5.9, 1.5 Hz, 2H), 1.80 (s, 1H), 1.41 (s, 9H), 1.37 (s, 6H). ^{13}C {^1H} NMR (101 MHz, $CDCl_3$) δ 154.41, 140.45, 131.56, 131.38, 126.46, 79.23, 77.48, 77.16, 76.84, 63.47, 53.07, 28.54, 27.85. HRMS (ESI-QTOF) *m/z* calculated value for $C_{13}H_{23}NO_3$ is $[M+Na]^+$ 264.1575 and observed 264.1572.

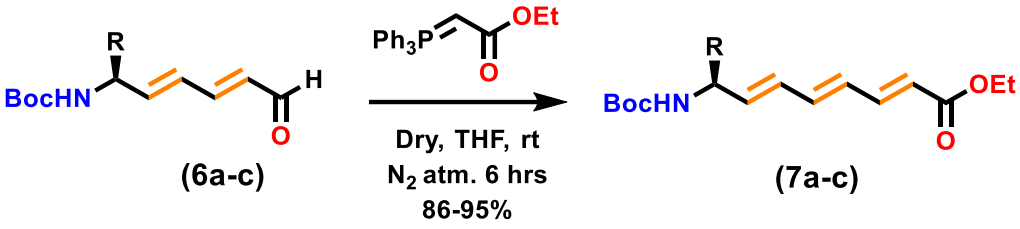
2.5.6. General Procedure for the Synthesis of (*E*)α-β, (*E*)γ-δ, ε-amino aldehydes (6a-6c)



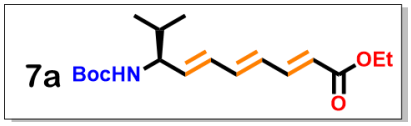
The oxidation of (*E*,*E*)-double bond conjugated allylic alcohols (**5a-5c**) using 2-iodoxybenzoic acid (IBX) resulted in the formation of (*E*)α-β, (*E*)γ-δ, ε-amino aldehydes (**6a-6c**). In this procedure, a solution of (*E*,*E*)-double bond conjugated allylic alcohols (**5a-5c**) (8 mmol) in distilled ethyl acetate (80 mL) was combined with 2-iodoxybenzoic acid (IBX) (8.8 mmol). The reaction mixture was stirred for 4 hours at 80 °C using a reflux condenser. The

advancement of the reaction was monitored using TLC in ethyl acetate and petroleum ether (30/70) (v/v). Upon completion, the reaction mixture was filtered using a sintered funnel, and the filtrate was concentrated under reduced pressure. We isolated (*E*)α-β, (*E*)γ-δ, ε-amino aldehydes (**6a-6c**) in very good yields and promptly utilized them for the subsequent Wittig reaction.

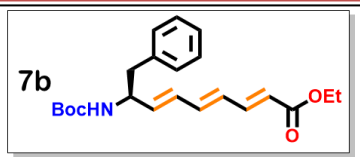
2.5.7. General Procedure for the Synthesis of ethyl ester of (*E*)α-β, (*E*)γ-δ, (*E*)ε-ζ, η-amino acids (7a-7c)



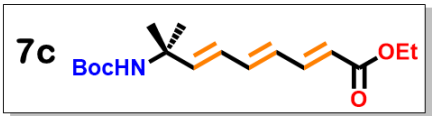
(7a-7c). (*E*)α-β, (*E*)γ-δ, ε-amino aldehydes (**6a-6c**) (7.5 mmol) were dissolved in dry THF (100 mL) under a nitrogen atmosphere. Subsequently, Wittig ylide ($Ph_3P{=}CHCO_2Et$) (9 mmol) was introduced into the solution. The reaction mixture was stirred for 6 hours at room temperature, and the progress of the reaction was monitored using TLC. Upon completion of the reaction, THF was evaporated from the reaction mixture, and the product ethyl ester of (*E*)α-β, (*E*)γ-δ, (*E*)ε-ζ, η-amino acids (**7a-7c**) was purified by column chromatography using an ethyl acetate/petroleum ether (6/94) (v/v) solvent system.



Ethyl (*S*,2*E*,4*E*,6*E*)-8-((tert-butoxycarbonyl)amino)-9-methyldeca-2,4,6-trienoate (7a). White crystalline solid, yield: 2.13 g (88%), mp: 87-89 °C, $[\alpha]_D^{25}$ = -6.32 (*c* = 1 $CHCl_3$). ^1H NMR (400 MHz, $CDCl_3$) *δ* 7.27 (dd, *J* = 15.2, 11, Hz, 1H), 6.52 (dd, *J* = 14.8, 11 Hz, 1H), 6.27 (dd, *J* = 14.8, 11.2 Hz, 1H), 6.22 (dd, *J* = 15.2, 11.2 Hz, 1H), 5.85 (d, *J* = 15.2 Hz, 1H), 5.78 (dd, *J* = 15.2, 6.4 Hz, 1H), 4.57 (m, *J* = 6.4 Hz, 1H), 4.18 (q, *J* = 7.1 Hz, 2H), 4.05 (br, 1H), 1.78 (m, *J* = 6.4, 6.4 Hz, 1H), 1.43 (s, 9H), 1.28 (t, *J* = 7.1 Hz, 3H), 0.91 – 0.89 (d, *J* = 6.4 Hz, 3H), 0.89 – 0.88 (d, *J* = 6.4 Hz, 3H). ^{13}C {^1H} NMR (101 MHz, $CDCl_3$) *δ* 167.20, 155.57, 144.43, 140.01, 137.91, 130.26, 129.72, 121.04, 79.55, 77.48, 77.16, 76.84, 60.39, 57.60, 32.72, 28.50, 18.88, 18.32, 14.40. HRMS (ESI-QTOF) *m/z* calculated value for $C_{18}H_{29}NO_4$ is $[M+Na]^+$ 346.1994 and observed 346.1990.



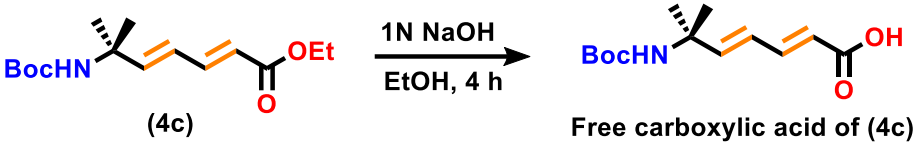
Ethyl (*S*,2*E*,4*E*,6*E*)-8-((tert-butoxycarbonyl)amino)-9-phenylnona-2,4,6-trienoate (7b). White solid, yield: 2.5 g (90%), mp: 89-91 °C, $[\alpha]_D^{25}$ = -8.088 (*c* = 1 $CHCl_3$). ^1H NMR (400 MHz, DMSO-d_6) δ 7.30 – 7.16 (m, 6H, aromatic-Ph & vinylic β-proton merged), 7.07 (d, *J* = 8.4 Hz, 1H, -NH), 6.71 (dd, *J* = 14.8, 10.8 Hz, 1H), 6.39 (dd, *J* = 14.8, 11.4 Hz, 1H), 6.17 (dd, *J* = 15.2, 11.4 Hz, 1H), 5.96 (d, *J* = 15.3, 1H), 5.93 (dd, *J* = 15.2, 6.2 Hz, 1H), 4.26 (m, *J* = 6.2 Hz,1H), 4.12 (q, *J* = 7.1 Hz, 2H), 2.76 (m, 2H), 1.32 (s, 9H), 1.22 (t, *J* = 7.1 Hz, 3H). ^{13}C {^1H} NMR (101 MHz, $CDCl_3$) δ 167.19, 155.19, 144.34, 139.78, 138.19, 137.10, 130.09, 129.76, 129.62, 128.59, 126.79, 121.26, 79.82, 77.16, 60.44, 53.07, 41.69, 28.47, 14.44. HRMS (ESI-QTOF) *m/z* calculated value for $C_{22}H_{29}NO_4$ is $[M+Na]^+$ 394.1994 and observed 394.1993.



Ethyl (2*E*,4*E*,6*E*)-8-((tert-butoxycarbonyl)amino)-8-methylnona-2,4,6-trienoate (7c). White crystalline solid, yield: 2 g (87%), mp: 81-83 °C. ^1H NMR (400 MHz, $CDCl_3$) δ 7.28 (dd, *J* = 15.3, 10.4 Hz, 1H), 6.54 (dd, *J* = 14.9, 10.4 Hz, 1H), 6.26 (dd, *J* = 14.9, 10.6 Hz, 1H), 6.17 (dd, *J* = 15.6, 10.6 Hz, 1H), 6.03 (d, *J* = 15.6 Hz, 1H), 5.84 (d, *J* = 15.3 Hz, 1H), 4.62 (s, 1H), 4.18 (q, *J* = 7.1 Hz, 2H), 1.41 (s, 9H), 1.38 (s, 6H), 1.29 (t, *J* = 7.1 Hz, 3H). ^{13}C {^1H} NMR (101 MHz, $CDCl_3$) δ 167.26, 154.44, 144.82, 144.56, 140.61, 129.52, 126.73, 120.75, 79.41, 77.48, 77.16, 76.84, 60.38, 53.24, 28.53, 27.83, 14.43. HRMS (ESI-QTOF) *m/z* calculated value for $C_{17}H_{27}NO_4$ is $[M+Na]^+$ 332.1837 and observed 332.1833.

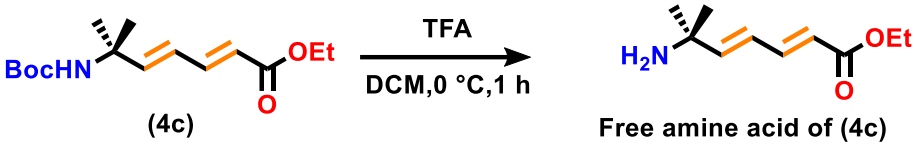
2.5.8. Synthetic Procedure for the Preparation of homo-dipeptide (8a)

The homo-dipeptide was synthesized using the ethyl ester of N-Boc-protected amino acid (**4c**).

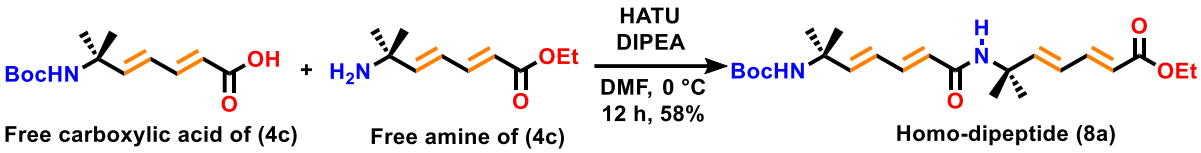


Ethyl ester hydrolysed Free carboxylic acid synthesis of (4c). To a solution of (**4c**) (1 g, 3.53 mmol) in ethanol (10 mL), 8 mL of 1N aqueous NaOH solution was added. The reaction mixture was stirred for 4 hours, and the progress of the reaction was monitored by TLC. After

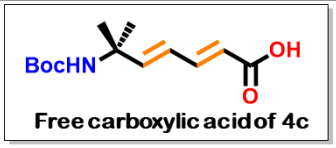
the completion of the reaction, the ethanol solvent was evaporated under reduced pressure. The aqueous layer was diluted with water (50 mL) and then acidified with 5% aqueous HCl, followed by extraction with ethyl acetate (3 x 50 mL). The combined organic layer was washed with brine and dried over anhydrous Na_2SO_4. The organic layer was concentrated under reduced pressure, yielding 856 mg (95%, 3.35 mmol) of the ethyl ester hydrolyzed free carboxylic acid product of (**4c**).



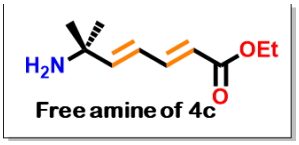
Boc-deprotected Free amine synthesis of (4c). The DCM solution (4 mL) of (**4c**) (1.1 g, 3.88 mmol) was chilled to 0 °C, and then 5 mL of neat Trifluoroacetic acid (TFA) was added. The reaction was stirred for 1 hour at 0 °C. Upon completion of the reaction (monitored by TLC), the solvent was evaporated under reduced pressure. The reaction mixture was subsequently treated with saturated Na_2CO_3 solution under cold conditions. The aqueous layer was extracted with ethyl acetate (3 x 50 mL). The combined organic layer was washed with brine and dried over anhydrous Na_2SO_4. Concentration under reduced pressure yielded 689 mg (97%, 3.76 mmol) of the Boc-deprotected free amine of (**4c**).



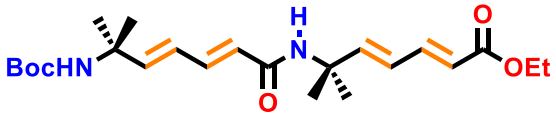
Coupling Reaction. The free carboxylic acid of (**4c**) (856 mg, 3.35 mmol) and HATU (1.27 g, 3.35 mmol) were dissolved in 3 mL of DMF. The resulting solution was chilled to 0 °C, and then DIPEA (1.75 mL, 10 mmol) was introduced. After stirring the mixture for 5 minutes at ice-cooled temperatures, a DMF solution (2 mL) of the Boc-deprotected free amine (1.1 g, 3.88 mmol) from (**4c**) was added to the reaction. The reaction continued at room temperature overnight, monitored by TLC. Upon completion, the reaction mixture was diluted with 120 mL of ethyl acetate. The ethyl acetate layer was successively washed with 5% HCl (3 x 50 mL), 10% Na_2CO_3 (3 x 50 mL), brine (2 x 50 mL), and dried over Na_2SO_4. Concentration under reduced pressure, followed by column chromatography using ethyl acetate/petroleum ether (2/3) (v/v), afforded 815 mg (58%, 1.94 mmol) of the pure homo-dipeptide (**8a**).



Free carboxylic acid of 4c. Colourless gummy liquid, yield: 856 mg (95%). ^{1}H NMR (400 MHz, DMSO-d_6) δ 7.09 (dd, *J* = 15.3, 10.4 Hz, 1H), 6.77 (s, 1H), 6.22 (d, *J* =15.6 Hz, 1H), 6.13 (d, *J* = 15.6, 10.4 Hz, 1H), 5.78 (d, *J* = 15.3 Hz, 1H), 1.32 (s, 9H), 1.24 (s, 6H). ^{13}C NMR (101 MHz, DMSO-d_6) δ 167.69, 154.23, 149.86, 144.34, 124.24, 121.32, 77.52, 52.50, 28.26, 27.19. MALDI/TOF-TOF m/z calculated value for $C_{13}H_{21}NO_4$ is $[M+Na]^+$ 278.1368 and observed 278.1353.



Free amine of 4c. Faint yellow gummy liquid, yield: 689 mg (97%, 3.76 mmol). ^{1}H NMR (400 MHz, CD_3CN) δ 7.17 (dd, *J* = 15.3, 10.5 Hz, 1H), 6.30 (dd, *J* = 15.5, 10.5 Hz, 1H), 6.20 (d, *J* = 15.5 Hz, 1H), 5.82 (d, *J* = 15.3 Hz, 1H), 4.06 (q, *J* = 7.2 Hz, 2H), 3.21 (s, 2H), 1.17 (s, 6H), 1.15 (t, *J* = 7.2 Hz, 3H). ^{13}C NMR (101 MHz, CD_3CN) δ 167.48, 152.14, 145.39, 125.19, 121.76, 60.96, 52.60, 29.40, 14.56. MALDI/TOF-TOF m/z calculated value for $C_{10}H_{17}NO_2$ is $[M+H]^+$ 184.1337 and observed 184.1318.



Homo-dipeptide (8a). White solid, yield: 815 mg (58%). ^{1}H NMR (400 MHz, $CDCl_3$) *δ* 7.25 (dd, *J* = 15.4, 10 Hz, 1H), 7.12 (dd, *J* = 15.2, 10 Hz, 1H), 6.30 (d, *J* = 15.4 Hz, 1H), 6.22 – 6.11 (m, 3H), 5.83 (d, *J* = 15.2 Hz, 1H), 5.77 (d, *J* = 15.2 Hz, 1H), 5.69 (s, 1H), 4.71 (s, 1H), 4.17 (q, *J* = 7.1 Hz, 2H), 1.47 (s, 6H), 1.40 (s, 9H), 1.36 (s, 6H), 1.26 (t, *J* = 7.1 Hz, 3H). ^{13}C {^{1}H} NMR (101 MHz, $CDCl_3$) *δ* 166.97, 165.42, 154.31, 147.83, 147.47, 144.45, 140.81, 125.28, 124.92, 123.78, 121.07, 79.49, 77.36, 77.04, 76.73, 60.24, 54.11, 53.10, 28.38, 27.37, 14.27. MALDI/TOF-TOF *m/z* calculated value for $C_{23}H_{36}N_2O_5$ is $[M+Na]^+$ 443.25 and observed 443.24.

2.6. Chiral HPLC Trace of Compounds 2a, 4a, 5a, 7a, 2e and 4e :

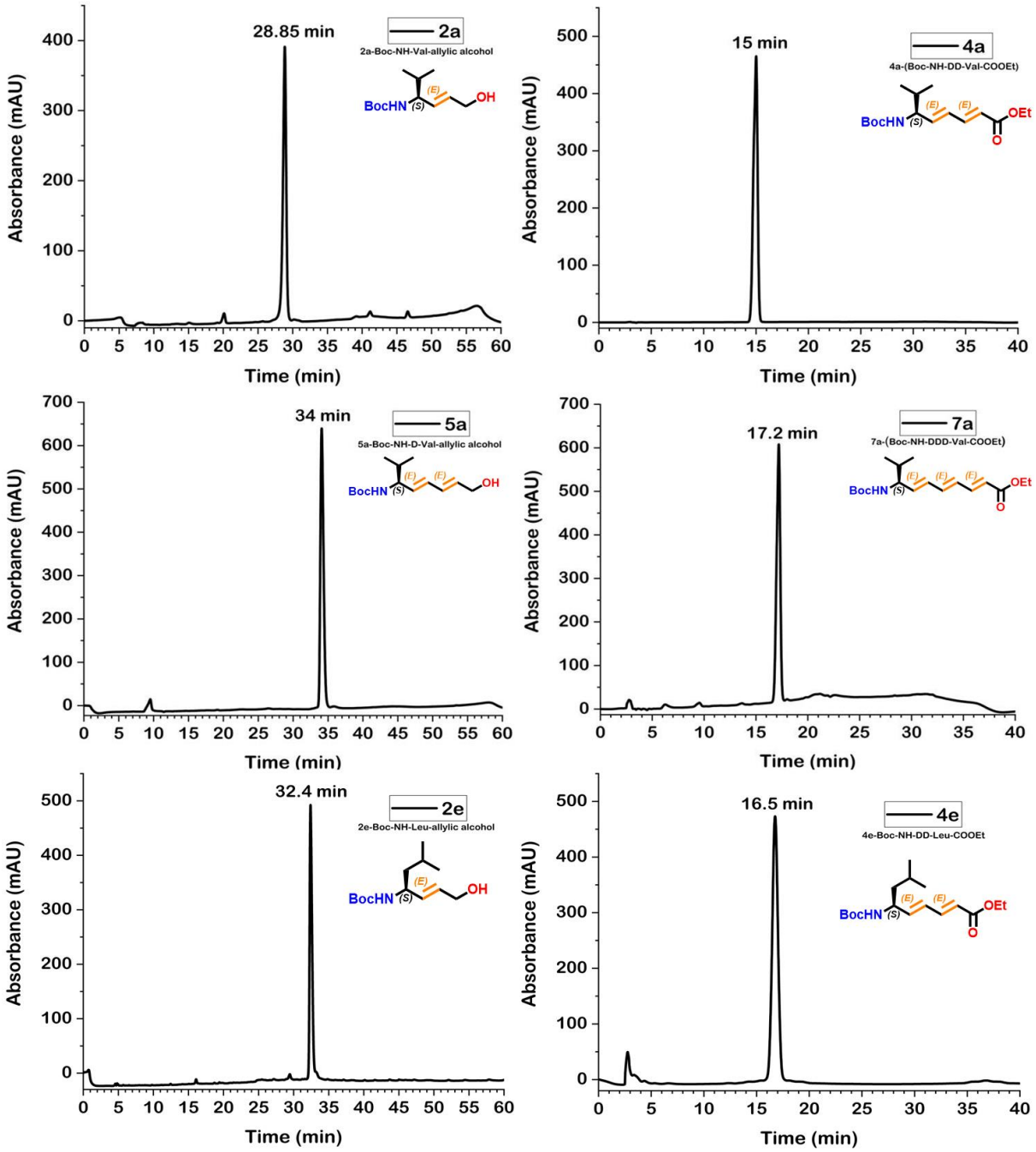


Figure 8: Chiral HPLC trace of Compounds **2a, 4a, 5a, 7a, 2e** and **4e**. The HPLC was performed on the DAICEL CHIRALPAK-IC column using an n-hexane/isopropanol (95/5) solvent system at isocratic mode with a flow rate of 1 mL/min.

2.7. References

CCDC numbers of **2a-2e**, **4b**, **4c**, **7a**, **7c** and **8a** are 2213473 – 2213482.

1. (a) M. A. T. Blaskovich, *J. Med. Chem.*, **2016**, *59*, 10807−10836; (b) L. Zhang, C. Wang, K. Chen, W. Zhong, Y. Xu, I. Molnár, *Nat. Prod. Rep.*, **2022**:

10.1039/D2NP00036A; (c) D. Seebach, A. K. Beck, D. Bierbaum, *Chem. Biodiversity*, **2004**, *1*, 1111– 1239; (d) P. G. Vasudev, S. Chatterjee, N. Shamala, P. Balaram, *Chem. Rev.*, **2011**, *111*, 657– 687.

2. (a) N. Schaschke, *Bioorg. Med. Chem. Lett.*, **2004**, *14*, 855–857; (b) R. G. Linington, B. R. Clark, E. E. Trimble, A. Almanza, L.-D.Ureña, D. E. Kyle, W. H. Gerwick, *J. Nat. Prod.*, **2009**, *72*, 14–17; (c) T. Conroy, J. T. Guo, N. Elias, K. M. Cergol, J. Gut, J. Legac, L. Khatoon, Y. Liu, S. McGowan, P. J. Rosenthal, N. H. Hunt, R. J. Payne, *J. Med. Chem.*, **2014**, *57*, 10557–10563; (d) B. E. Maryanoff, H.-C. Zhang, M. N. Greco, K. A. Glover, J. A. Kauffman, P. Andrade-Gordon, *Bio. Med. Chem.*, **1995**, ***3***, 1025-1038; (e) J. A. Nieman, J. E. Coleman, D. J. Wallace, E. Piers, L. Y. Lim, M. Roberge, R. J. Andersen, *J. Nat. Prod*., **2003**, *66*, 183-199.
3. B. Legrand, L. T. Maillard, *ChemPlusChem* **2021**, *86*, 629–645.
4. M. Hagihara, N. J. Anthony, T. J. Stout, J. Clardy, S. L. Schreiber, *J. Am. Chem. Soc*., **1992**, *114*, 6568–6570.
5. (a) C. Grison, S. Geneve, E. ´ Halbin, P. Coutrot, Tetrahedron, **2001**, *57*, 4903–4923; (b) C. Grison, P. Coutrot, S. Geneve, C. Didierjean, M. Marraud, *J. Org. Chem*., **2005**, *70*, 10753–10764.
6. T. K. Chakraborty, A. Ghosh, S. K. Kumar, A. C. Kunwar, *J. Org. Chem.*, **2003**, *68*, 6459–6462.
7. C. Baldauf, R. Gunther, H. J. Hofmann, *J. Org. Chem*., **2005**, *70*, 5351–5361.
8. L. Mathieu, B. Legrand, C. Deng, L. Vezenkov, E. Wenger, C. Didierjean, M. Amblard, M. C. Averlant-Petit, N. Masurier, V. Lisowski, J. Martinez, L. T. Maillard, *Angew. Chem. Int. Ed. Engl.* **2013**, *52*, 6006–6010.
9. (a) M. Brenner, D. Seebach, *Helv. Chim. Acta*, **2001**, *84*, 1181–1189; (b) S.V. Jadhav, R. Misra, S. K. Singh, H. N. Gopi, *Chem. Eur. J*., **2013**, *19*, 16256-16262.
10. K. Fujine, M. Tanaka, K. Ohsumi, M. Hashimoto, S. Takase, H. Ueda, M. Hino, T. Fujii, *J. Antibiot.*, **2003**, *56*, 55−61.
11. Y. Chen, G. Coussanes, C. Souris, P. Aillard, D. Kaldre, K. Runggatscher, S. Kubicek, G. D. Mauro, B. Maryasin, N. Maulide, *J. Am. Chem. Soc*., **2019**, *141*, 13772−13777.
12. J. R. Falck, A. He, H. Fukui, H. Tsutsui, A. Radha, *Angew. Chem. Int. Ed.*, **2007**, *46*, 4527–4529.
13. D. Amans, V. Bellosta, J. Cossy, *Org. Lett*., **2007**, *9*, 4761–4764.
14. J. S. Yadav, S. Sengupta, *Eur. J. Org. Chem*., **2013**, 376–388.

15. D. Amans, V. Bellosta, J. Cossy, *Chem. Eur. J.*, **2009**, *15*, 3457 – 3473.
16. S. M. Mali, A. Bandyopadhyay, S. V. Jadhav, M. Ganesh Kumar, H. N. Gopi, *Org. Biomol. Chem*., **2011**, *9*, 6566–6574.
17. (a) G. Wittig, *Science*, **1980**, *210*, 600–604; (b) A. D. Abell, M. K. Edmonds, in *Modern Carbonyl Olefination* (Ed.: T. Takeda), Wiley-VCH, Weinheim, Germany, **2004**, pp. 1–17; (c) B. E. Maryanoff, A. B. Reitz, *Chem. Rev*. **1989**, *89*, 863-927
18. O. I. Kolodiazhnyi, Phosphorus Ylides, Chemistry and Application in Organic Synthesis, Wiley-VCH, Weinheim, Germany, **1999**.
19. W. S. Wadsworth, W. D. Emmons, *J. Am. Chem. Soc*., **1961**, *83*, 1733–1738.
20. R. ldeses, A. Shani, *Tetrahedron*, **1989**, *45*, 3523-3534.
21. M. Yoshida, H. Otaka, T. Doi, *Eur. J. Org. Chem*., **2014**, 6010–6016.
22. T. Tomioka, Y. Yabe, T. Takahashi, T. K. Simmons, *J. Org. Chem*., **2011**, *76*, 4669–4674.
23. T. Moriwake, S. Hamano, D. Miki, S. Saito, S. Torii, *Chemistry Letters*, **1986**, *15*, 815-818.
24. R. Robiette, J. Richardson, V. K. Aggarwal, J. N. Harvey, *J. Am. Chem. Soc*. **2005**, *127*, 13468-13469.
25. (a) G. M. Sheldrick, *Acta Crystallogr. Sect A.* **1990**, *46*, 467-473; (b) G. M. Sheldrick, SHELXL-97, Program for Crystal Structure Solution and Refinement, Universität Göttingen (Germany) **1997**.

2.8. Appendix

S. No	Content	Page No
2.8.1.	**Ortep plot and crystallographic information 2a-2e, 4b, 4c, 7a, 7c, and 8a**	**49**
2.8.2	**^{1}H, ^{13}C NMR and HRMS spectra of all compounds**	**59**
2.8.3.	**Copy of the Permission letter from Journal for reuse of figures and diagrams**	**94**

2.8.1. Ortep plot and crystallographic information 2a-2e, 4b, 4c, 7a, 7c, and 8a

2.8.1.1. Ortep plot of 2a-2e, 4b, 4c, 7a, 7c, and 8a

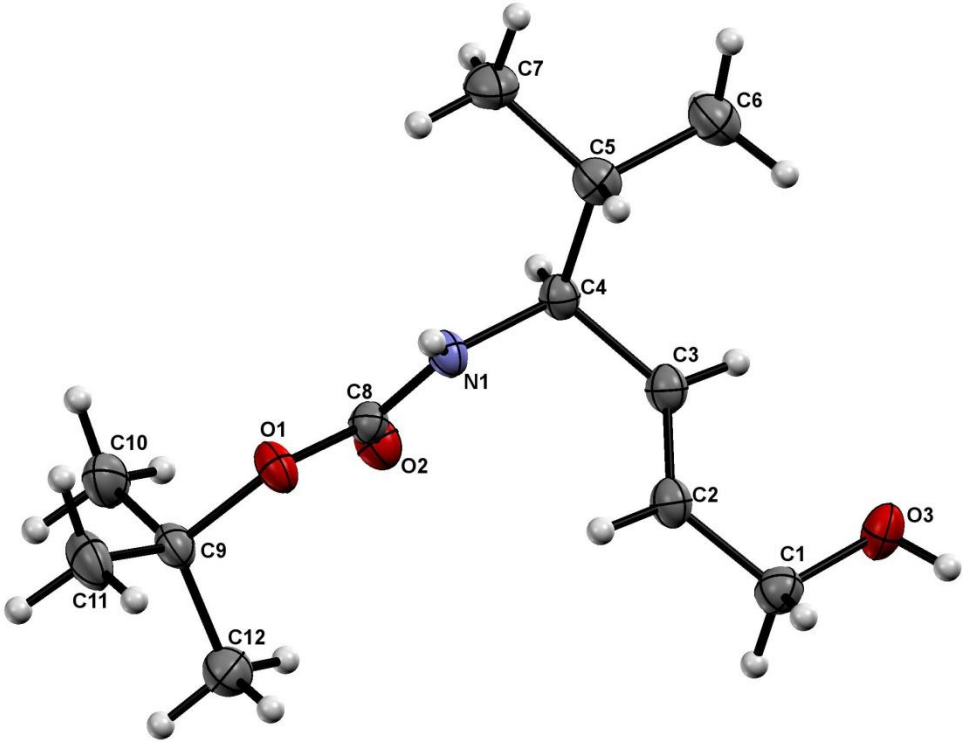


Figure 9: ORTEP diagram of compound **2a**. All H-atoms are not labeled for clarity. Ellipsoids are drawn at 50% probability. (CCDC no 2213473)

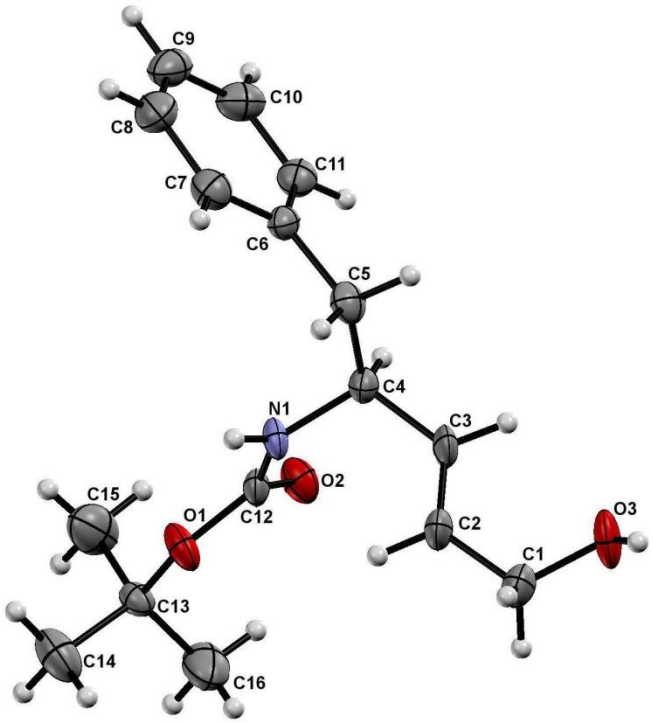


Figure 10: ORTEP diagram of compound **2b**. All H-atoms are not labeled for clarity. Ellipsoids are drawn at 50% probability. (CCDC no 2213474)

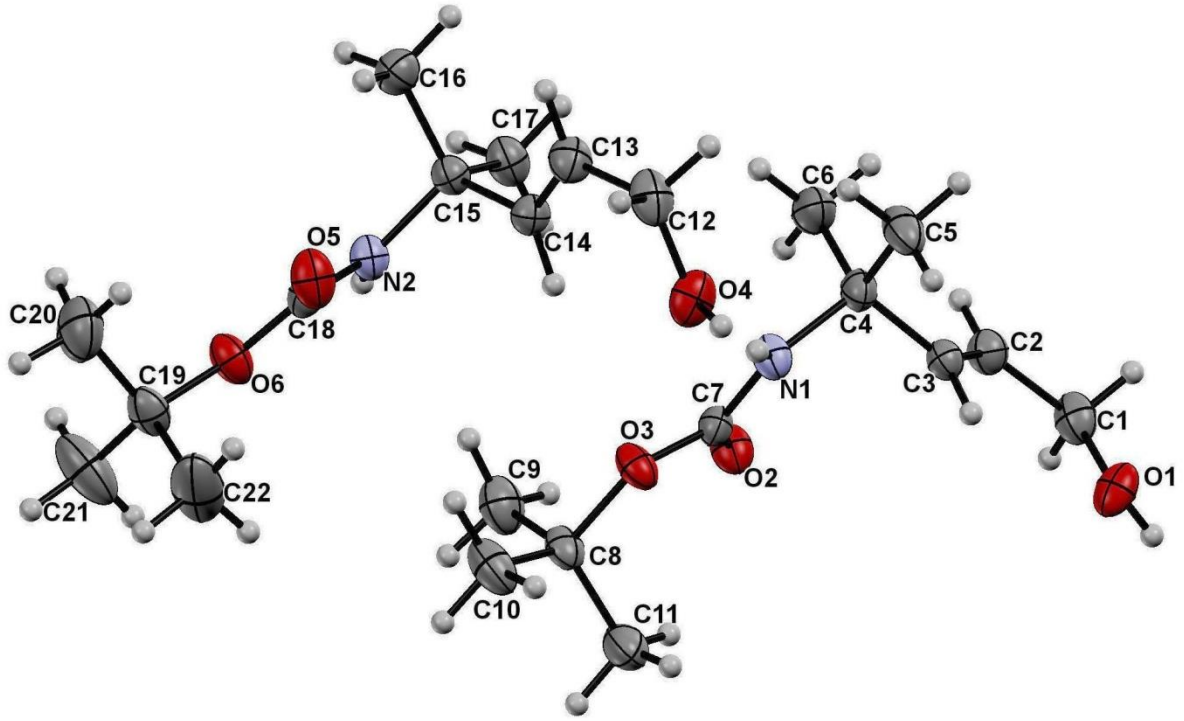


Figure 11: ORTEP diagram of compound **2c**. All H-atoms are not labeled for clarity. Two molecules appeared in the asymmetric unit. Ellipsoids are drawn at 50% probability. (CCDC no 2213475)

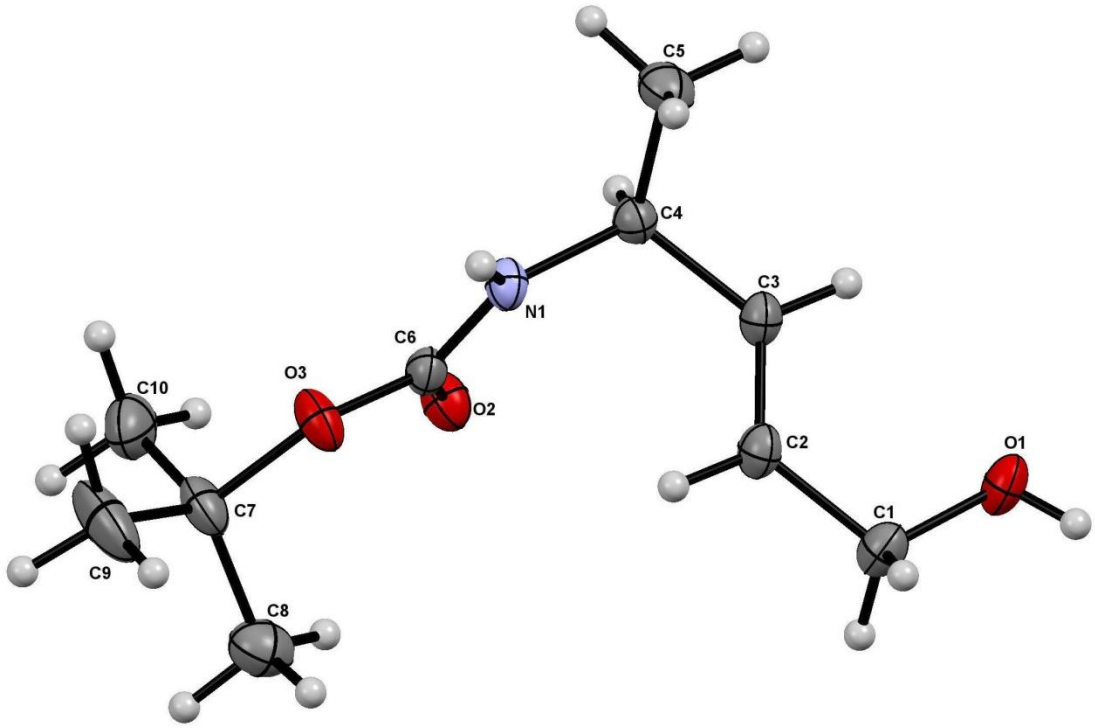


Figure 12: ORTEP diagram of compound 2**d**. All H-atoms are not labeled for clarity. Ellipsoids are drawn at 50% probability. (CCDC no 2213476)

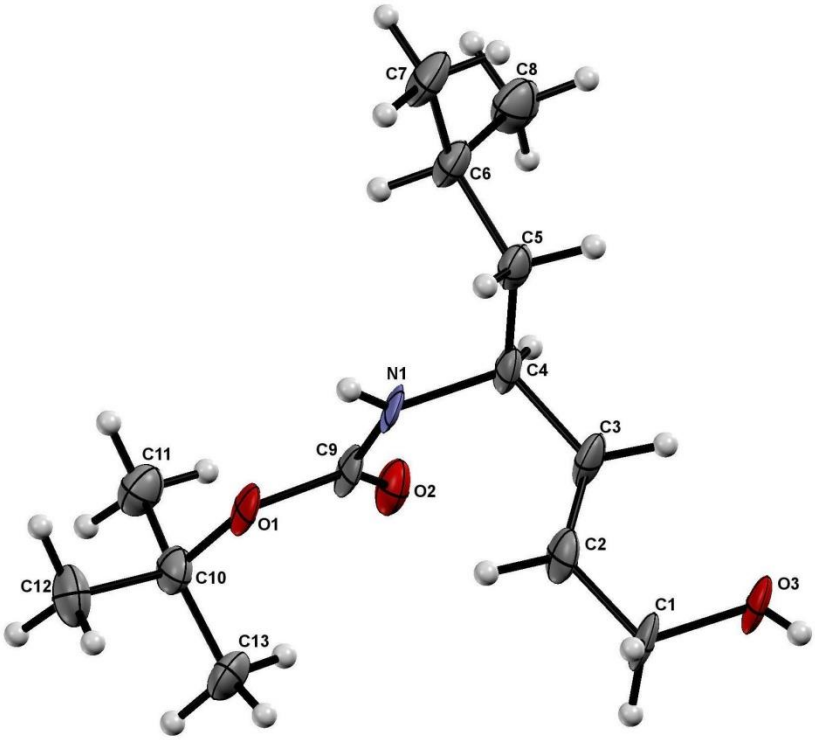


Figure 13: ORTEP diagram of compound **2e**. All H-atoms are not labeled for clarity. Ellipsoids are drawn at 50% probability. (CCDC no 2213477)

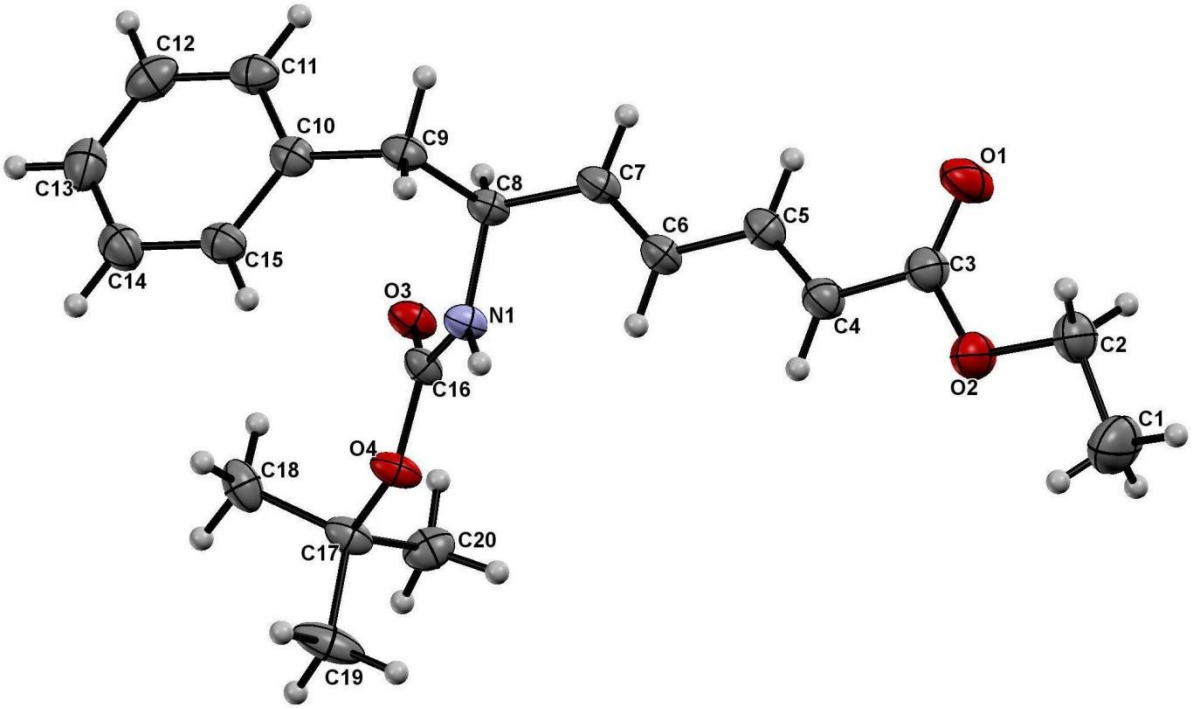


Figure 14: ORTEP diagram of compound **4b**. All H-atoms are not labeled for clarity. Ellipsoids are drawn at 50% probability. (CCDC no 2213478)

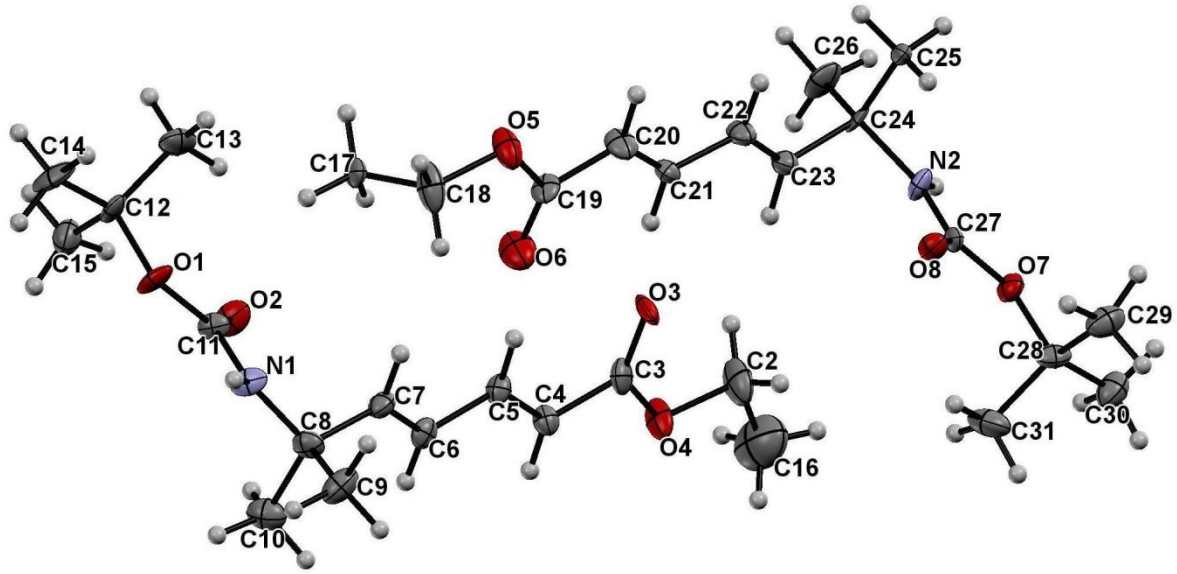


Figure 15: ORTEP diagram of compound **4c**. All H-atoms are not labeled for clarity. Two molecules appeared in the asymmetric unit. Ellipsoids are drawn at 50% probability. (CCDC no 2213479)

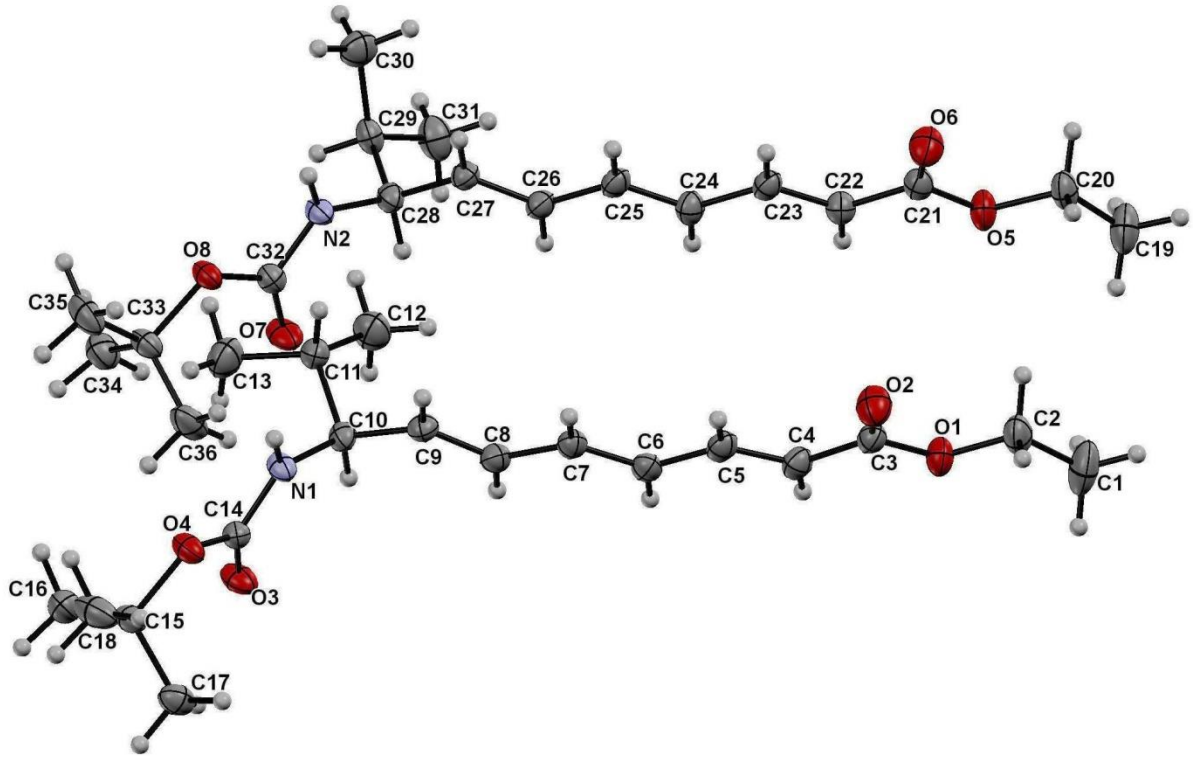


Figure 16: ORTEP diagram of compound **7a**. All H-atoms are not labeled for clarity. Two molecules appeared in the asymmetric unit. Ellipsoids are drawn at 50% probability. (CCDC no 2213480)

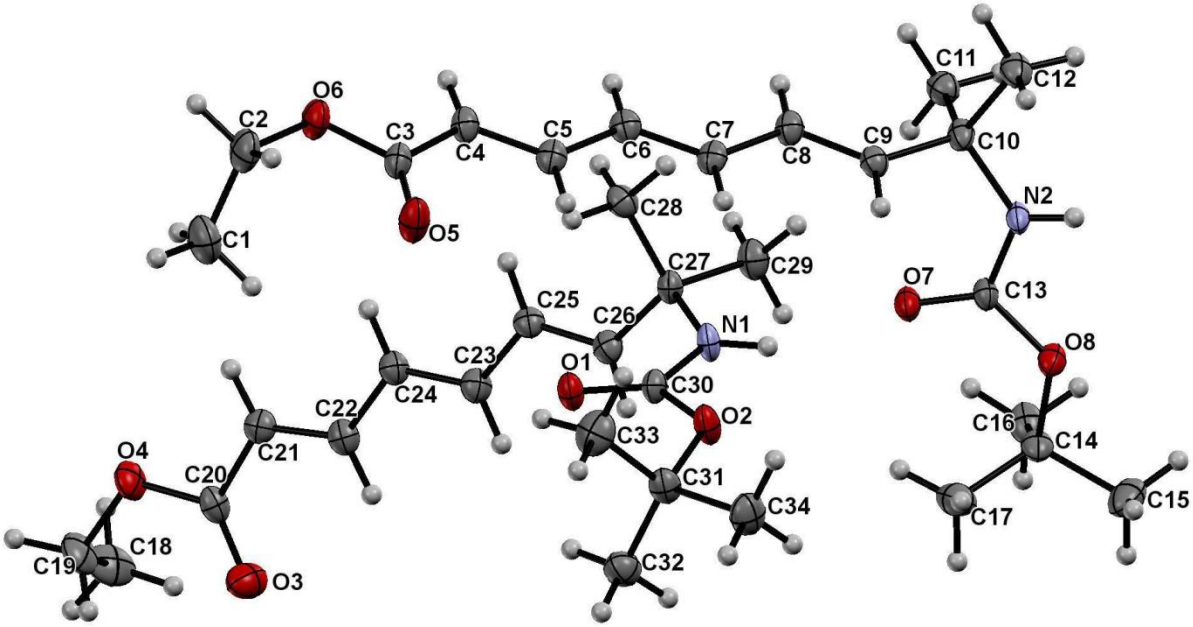


Figure 17: ORTEP diagram of compound **7c**. All H-atoms are not labeled for clarity. Two molecules appeared in the asymmetric unit. Ellipsoids are drawn at 50% probability. (CCDC no 2213481)

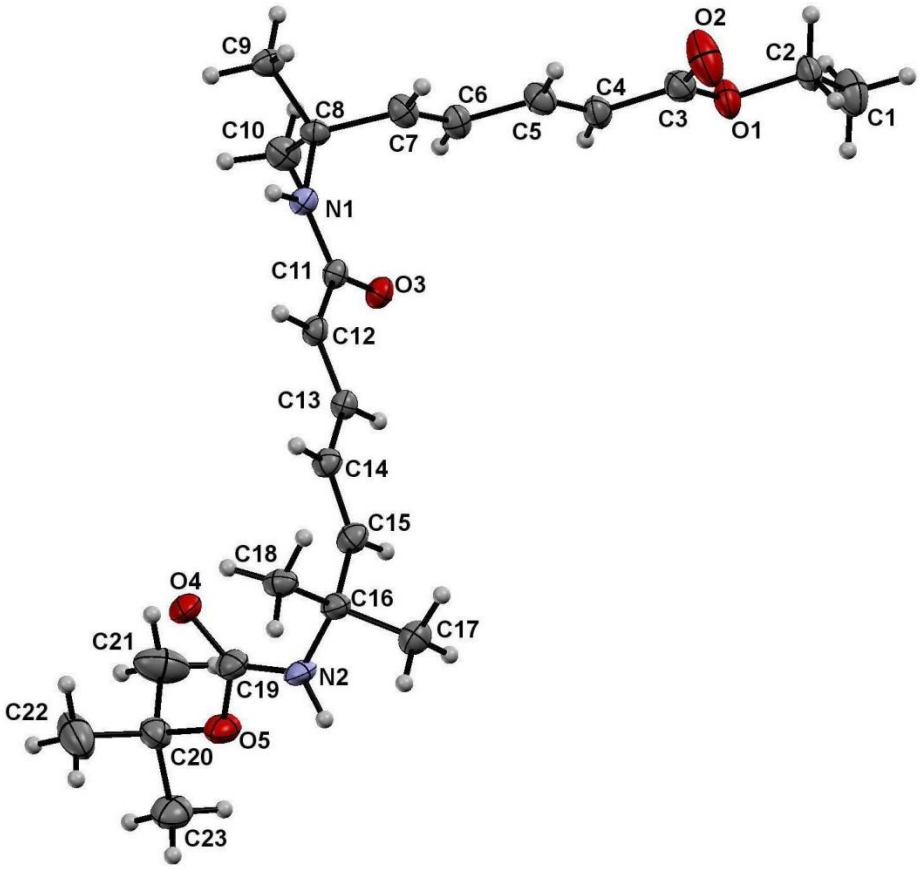


Figure 18: ORTEP diagram of compound **8a**. All H-atoms are not labeled for clarity. Ellipsoids are drawnat 50% probability. (CCDC no 2213482)

2.8.1.2. crystallographic information 2a-2e, 4b, 4c, 7a, 7c, and 8a

Compound 2a: Colourless needle shape Crystals of 2a were grown by slow evaporation from a solution of dichloromethane and n-heptane. A good quality single crystal (0.3 × 0.05 × 0.05 mm) was mounted on the head of a goniometer using a loop with a small amount of paraffin oil. The X-ray diffraction data of a single crystal were collected at 100K temperature on a Bruker APEX(II) DUO CCD diffractometer using Cu K_α radiation (λ = 1.54178 Å), ω-scans (2θ = 149.64), for a total of 12047 independent reflections. Space group P 21 21 21, a = 6.3864(10), b = 10.5866(17), c = 19.684(3), β = 90, V = 1330.8(4) Å^3, Orthorhombic, Z = 4 for chemical formula C_{12} H_{23} N O_3, with one molecule in asymmetric unit; ρ calcd = 1.145 gcm^{-3}, μ = 0.655 mm^{-1}, F (000) = 504.0, Rint= 0.0499. The structure was obtained by direct methods using SHELXL-97.[25] The final R value was 0.0416 (wR2 = 0.0791) 2590 observed reflections ($F0 \geq 4\sigma$ (|F0|)) and 152 variables, S = 1.062. The largest difference peak and hole were 0.195 and -0.167 eÅ^3, respectively.

Compound 2b: Colourless rod shape Crystals of 2b were grown by slow evaporation from a solution of ethyl acetate and n-hexane. A good quality single crystal (0.2 × 0.1 × 0.1 mm) was mounted on the head of a goniometer using a loop with a small amount of paraffin oil. The X-ray diffraction data of a single crystal were collected at 100K temperature on a Bruker APEX(II) DUO CCD diffractometer using Mo K_α radiation (λ = 0.71073 Å), ω-scans (2θ = 56.824), for a total of 68381 independent reflections. Space group P 21 21 21, a = 6.061(2), b = 12.023(4), c = 21.699(7), β = 90, V = 1581.3(8) Å^3, Orthorhombic, Z = 4 for chemical formula C_{16} H_{23} N O_3, with one molecule in asymmetric unit; ρ calcd = 1.165 gcm^{-3}, μ = 0.080 mm^{-1}, F (000) = 600.0, Rint= 0.1671. The structure was obtained by direct methods using SHELXL-97.[25] The final R value was 0.0865 (wR2 = 0.0657) 3927 observed reflections ($F0 \geq 4\sigma$ (|F0|)) and 185 variables, S = 1.940. The largest difference in peak and hole were 0.223 and -0.218 eÅ^3, respectively.

Compound 2c: Colourless plate shape Crystals of 2c were grown by slow evaporation from a solution of dichloromethane and n-heptane. A good quality single crystal (0.52 × 0.41 × 0.31 mm) was mounted on the head of a goniometer using a loop with a small amount of paraffin oil. The X-ray diffraction data of a single crystal were collected at 100K temperature on a Bruker APEX(II) DUO CCD diffractometer using Mo K_α radiation (λ = 0.71073 Å), ω-scans (2θ = 52.698), for a total of 35186 independent reflections. Space group P -1, a = 9.165(2), b = 10.586(3), c = 13.936(3), β = 108.378(7), V = 1282.1(5) $Å^3$, Triclinic, Z = 4 for chemical formula C_{11} H_{21} N O_3, with two molecules in asymmetric unit; ρ calcd = 1.115 gcm^{-3}, μ = 0.080 mm^{-1}, F (000) = 472.0, Rint= 0.0765. The structure was obtained by direct methods using SHELXL-97.[25] The final R value was 0.0941 (wR2 = 0.1383) 5120 observed reflections ($F0 \geq 4\sigma$ (|F0|)) and 284 variables, S = 1.152. The largest difference peak and hole were 0.251 and -0.250 $eÅ^3$, respectively.

Compound 2d: Colourless Plate shape Crystals of 2d were grown by slow evaporation from a solution of dichloromethane and n-heptane. A good quality single crystal (0.7 × 0.6 × 0.5 mm) was mounted on the head of a goniometer using a loop with a small amount of paraffin oil. The X-ray diffraction data of a single crystal were collected at 100K temperature on a Bruker APEX(II) DUO CCD diffractometer using Mo K_α radiation (λ = 0.71073 Å), ω-scans (2θ = 56.688), for a total of 17718 independent reflections. Space group P 21 21 21, a = 6.5455(12), b = 9.445(2), c = 19.264(4), β = 90, V = 1191.0(4) $Å^3$, Orthorhombic, Z = 4 for chemical formula C_{10} H_{19} N O_3, with one molecule in asymmetric unit; ρ calcd = 1.122 gcm^{-3}, μ = 0.082 mm^{-1}, F (000) = 440.0, Rint= 0.0488. The structure was obtained by direct methods using SHELXL-97.[25] The final R value was 0.0352 (wR2 = 0.0781) 2966 observed reflections ($F0 \geq 4\sigma$ (|F0|)) and 133 variables, S = 0.995. The largest difference peak and hole were 0.175 and -0.186 $eÅ^3$, respectively.

Compound 2e: Colourless plate shape Crystals of 2e were grown by slow evaporation from a solution of ethyl acetate and n-hexane. A good quality single crystal (0.4 × 0.3 × 0.2 mm) was mounted on the head of a goniometer using a loop with a small amount of paraffin oil. The X-ray diffraction data of a single crystal were collected at 100K temperature on a Bruker APEX(II) DUO CCD diffractometer using Mo K_α radiation (λ = 0.71073 Å), ω-scans (2θ =

48.998), for a total of 15175 independent reflections. Space group P 21 21 2, a = 11.178(7), b = 21.505(13), c = 6.138(4), β = 90, V = 1475.4(15) Å^3, Orthorhombic, Z = 4 for chemical formula C_{13} H_{25} N O_3, with one molecule in asymmetric unit; ρ calcd = 1.095 gcm^{-3}, μ = 0.077 mm^{-1}, F (000) = 536.0, Rint= 0.1319. The structure was obtained by direct methods using SHELXL-97.[25] The final R value was 0.0942 (wR2 = 0.2125) 2434 observed reflections ($F0 \geq 4\sigma$ (|F0|)) and 149 variables, S = 1.021. The largest difference peak and hole were 0.484 and -0.311 eÅ^3, respectively.

Compound 4b: Colourless plate shape Crystals of 4b were grown by slow evaporation from a solution of dichloromethane and n-heptane. A good quality single crystal (0.33 × 0.25 × 0.17 mm) was mounted on the head of a goniometer using a loop with a small amount of paraffin oil. The X-ray diffraction data of a single crystal were collected at 100K temperature on a Bruker APEX(II) DUO CCD diffractometer using Mo K_α radiation (λ = 0.71073 Å), ω-scans (2θ = 56.702), for a total of 27968 independent reflections. Space group C 2, a = 35.93(5), b = 5.117(8), c = 10.707(16), β = 92.39(3), V = 1967(5) Å^3, Monoclinic, Z = 4 for chemical formula C_{20} H_{27} N O_4, with one molecule in asymmetric unit; ρ calcd = 1.166 gcm^{-3}, μ = 0.081 mm^{-1}, F (000) = 744.0, Rint= 0.0730. The structure was obtained by direct methods using SHELXL-97.[25] The final R value was 0.0522 (wR2 = 0.1352) 4866 observed reflections ($F0 \geq 4\sigma$ (|F0|)) and 231 variables, S = 0.679. The largest difference peak and hole were 0.278 and -0.242 eÅ^3, respectively.

Compound 4c: Colourless plate shape Crystals of 4c were grown by slow evaporation from a solution of dichloromethane and n-heptane. A good quality single crystal (0.42 × 0.30 × 0.22 mm) was mounted on the head of a goniometer using a loop with a small amount of paraffin oil. The X-ray diffraction data of a single crystal were collected at 100K temperature on a Bruker APEX(II) DUO CCD diffractometer using Mo K_α radiation (λ = 0.71073 Å), ω-scans (2θ = 56.844), for a total of 63821 independent reflections. Space group P c, a = 9.1906(18), b = 18.987(4), c = 9.7142(16), β = 100.338(6), V = 1667.6(5) Å^3, Monoclinic, Z = 4 for chemical formula C_{15} H_{25} N O_4, with two molecules in asymmetric unit; ρ calcd = 1.129 gcm^{-3}, μ = 0.081 mm^{-1}, F (000) = 616.0, Rint= 0.1210. The structure was obtained by direct methods using SHELXL-97.[25] The final R value was 0.0866 (wR2 = 0.1342) 8309 observed reflections ($F0 \geq$

4σ (|F0|)) and 374 variables, S = 0.997. The largest difference peak and hole were 0.749 and -0.406 eÅ^3, respectively.

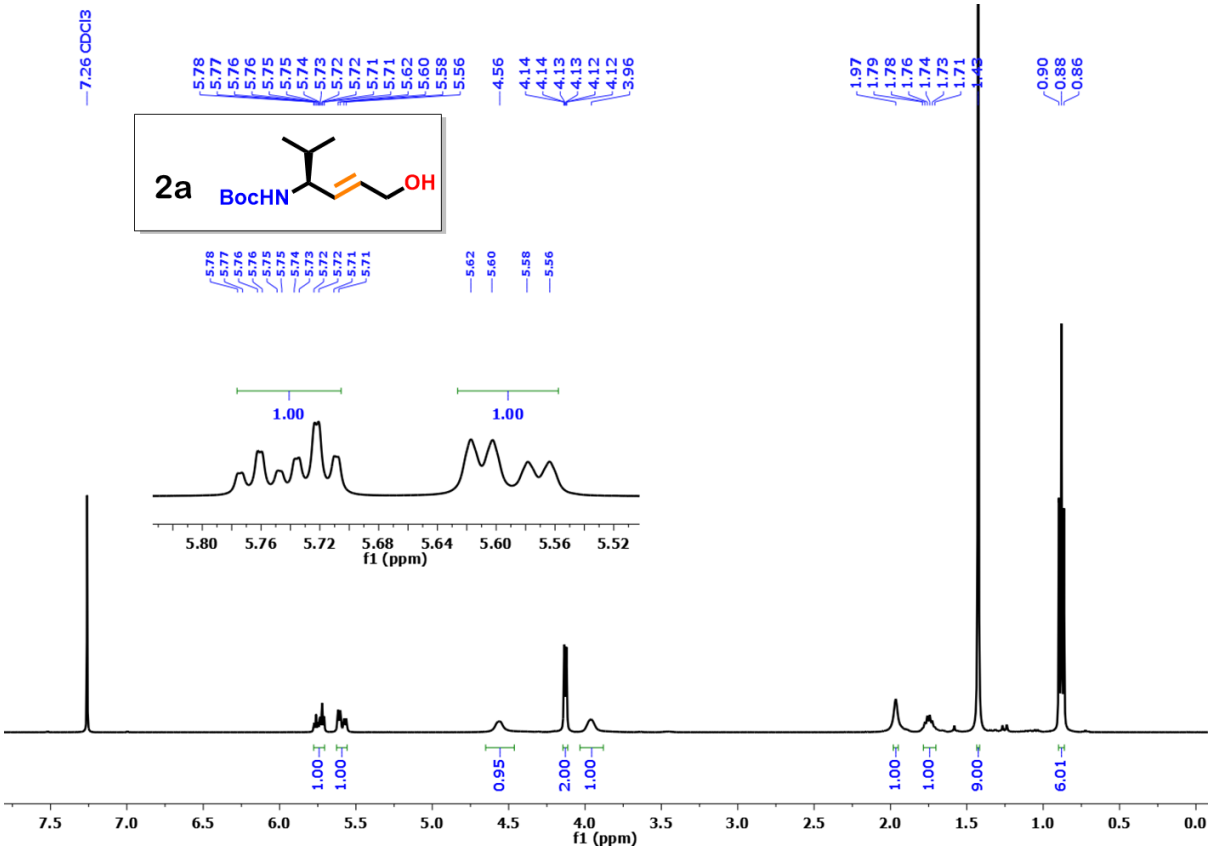
Compound 7a: Colourless plate shape Crystals of 7a were grown by slow evaporation from a solution of dichloromethane and n-heptane. A good quality single crystal (0.28 × 0.21 × 0.17 mm) was mounted on the head of a goniometer using a loop with a small amount of paraffin oil. The X-ray diffraction data of a single crystal were collected at 100K temperature on a Bruker APEX(II) DUO CCD diffractometer using Mo K_α radiation (λ = 0.71073 Å), ω-scans (2θ = 57.14), for a total of 25003 independent reflections. Space group P -1, a = 10.171(4), b = 11.307(4), c = 18.203(6), β = 78.945(8), V = 1922.9(12) Å^3, Triclinic, Z = 4 for chemical formula C_{18} H_{29} N O_4, with two molecules in asymmetric unit; ρ calcd = 1.117 gcm^{-3}, μ = 0.078 mm^{-1}, F (000) = 704.0, Rint= 0.0976. The structure was obtained by direct methods using SHELXL-97.[25] The final R value was 0.0681 (wR2 = 0.1411) 9658 observed reflections (*F0* ≥ 4σ (|F0|)) and 428 variables, S = 0.919. The largest difference peak and hole were 0.324 and -0.253 eÅ^3, respectively.

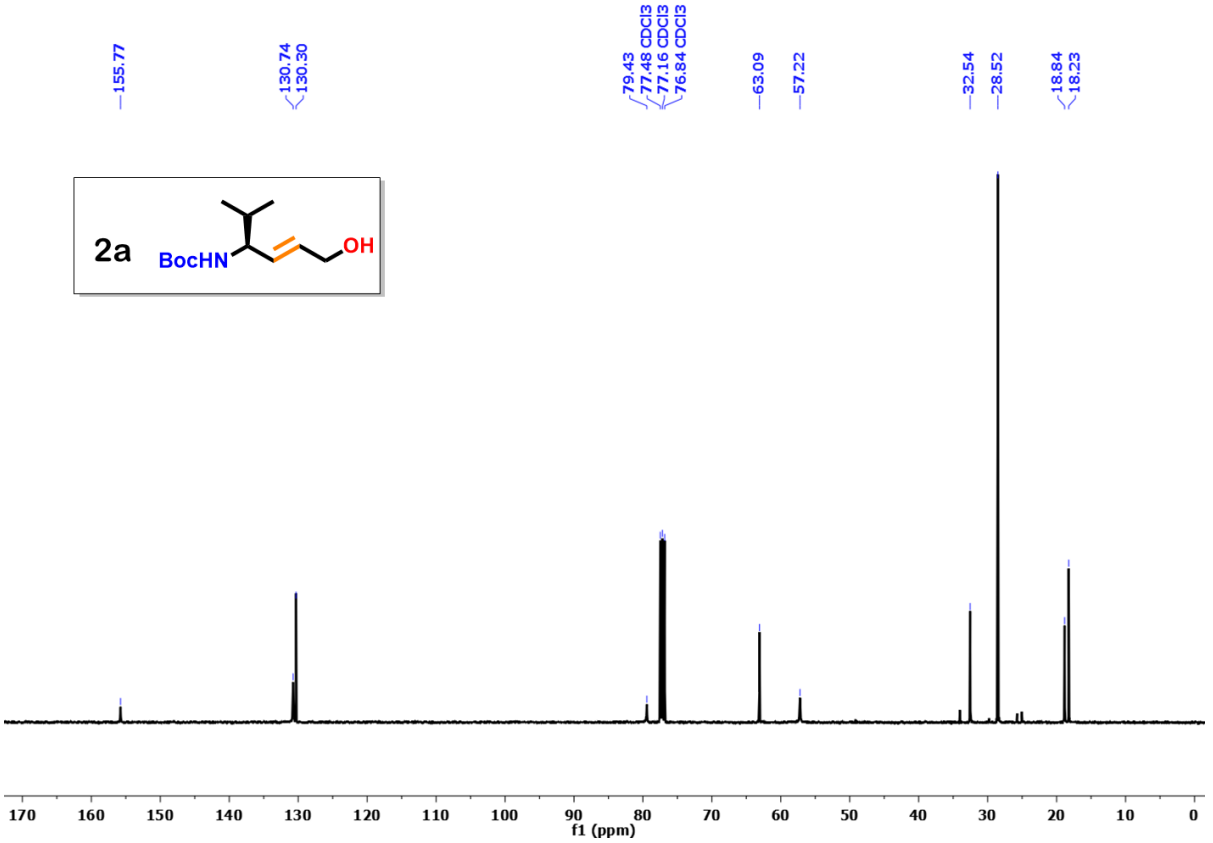
Compound 7c: Colourless rod shape Crystals of 7c were grown by slow evaporation from a solution of dichloromethane and n-heptane. A good quality single crystal (0.38 × 0.15 × 0.14 mm) was mounted on the head of a goniometer using a loop with a small amount of paraffin oil. The X-ray diffraction data of a single crystal were collected at 100K temperature on a Bruker APEX(II) DUO CCD diffractometer using Mo K_α radiation (λ = 0.71073 Å), ω-scans (2θ = 56.844), for a total of 78922 independent reflections. Space group P 21/c, a = 9.880(3), b = 20.895(7), c = 18.293(6), β = 105.188(10), V = 3645(2) Å^3, Monoclinic, Z = 8 for chemical formula C_{17} H_{27} N O_4, with two molecules in asymmetric unit; ρ calcd = 1.128 gcm^{-3}, μ = 0.079 mm^{-1}, F (000) = 1344.0, Rint= 0.1187. The structure was obtained by direct methods using SHELXL-97.[25] The final R value was 0.0619 (wR2 = 0.1811) 9130 observed reflections (*F0* ≥ 4σ (|F0|)) and 410 variables, S = 0.726. The largest difference peak and hole were 0.339 and -0.311 eÅ^3, respectively.

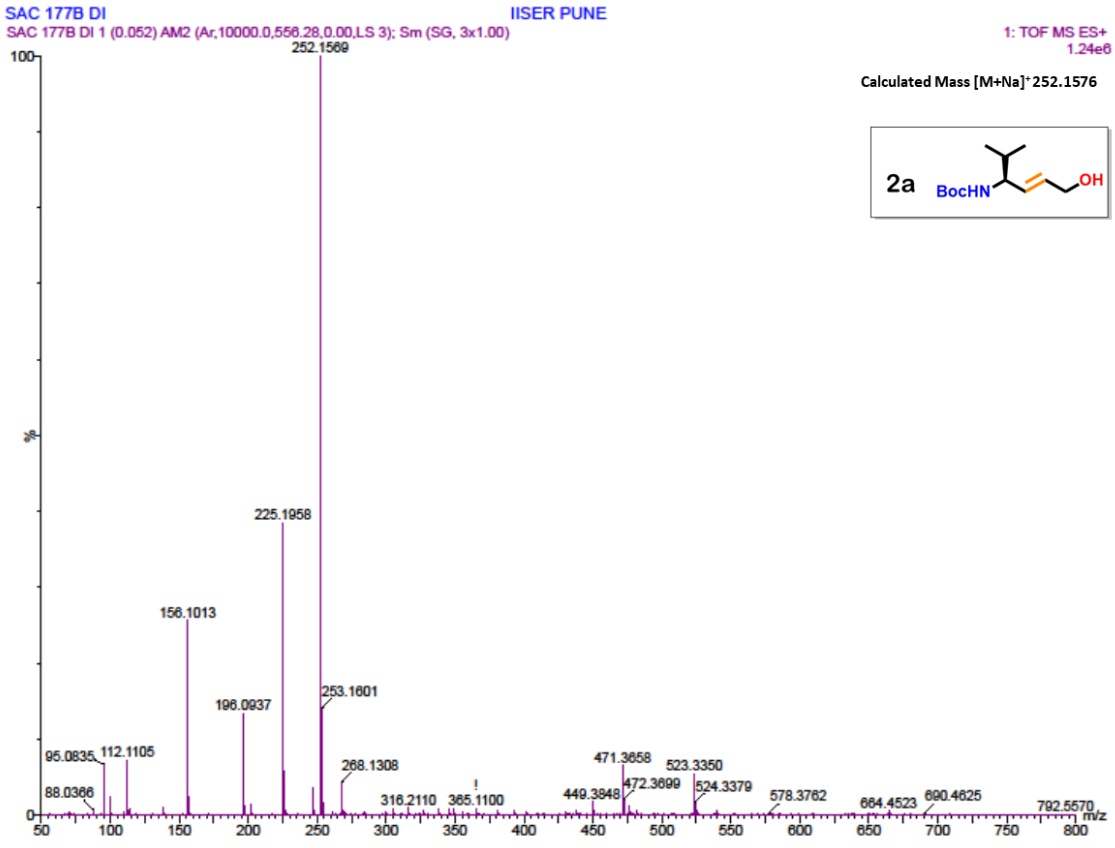
Compound 8a: Colourless plate shape Crystals of 8a were grown by slow evaporation from a solution of methanol and water. A good quality single crystal (0.2× 0.09 × 0.05 mm) was mounted on the head of a goniometer using a loop with a small amount of paraffin oil. The X-

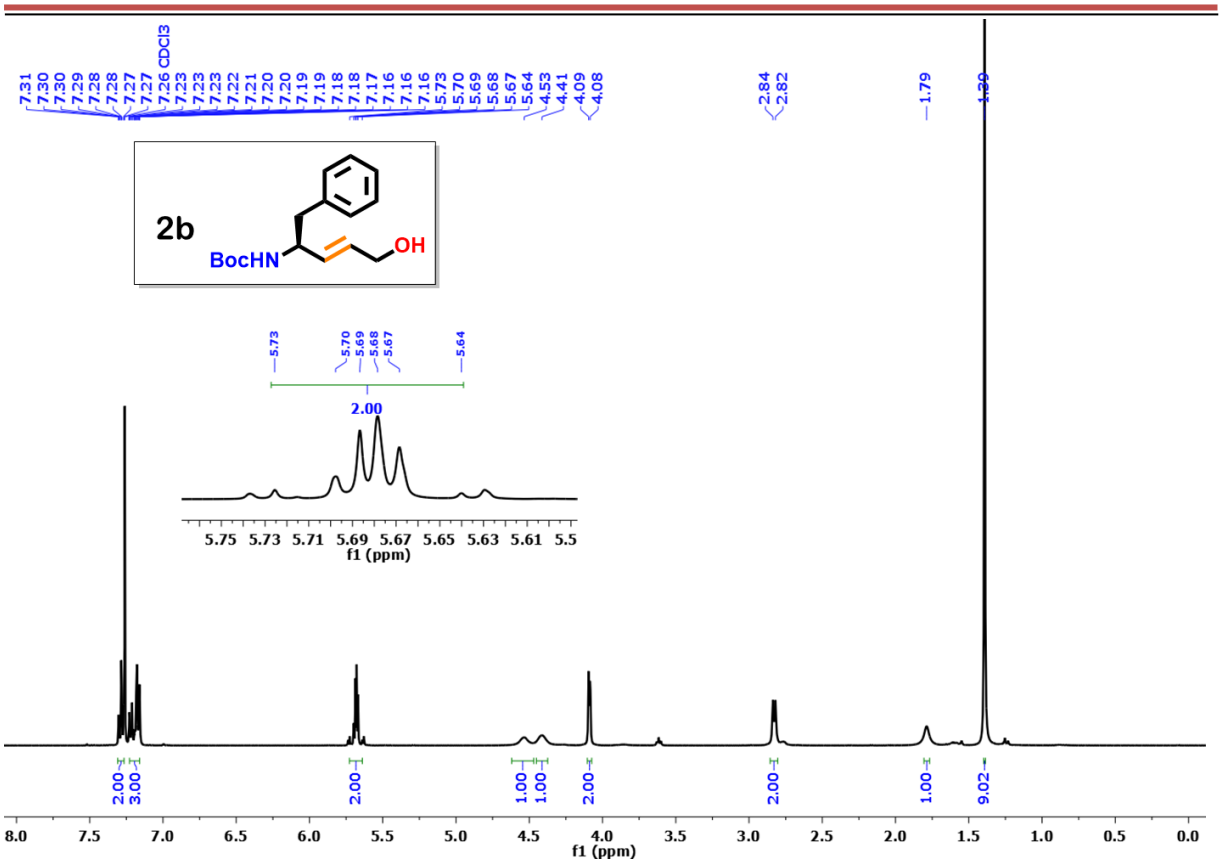
ray diffraction data of a single crystal were collected at 100K temperature on a Bruker APEX(II) DUO CCD diffractometer using Mo K_α radiation (λ = 0.71073 Å), ω-scans (2θ = 57.312), for a total of 33779 independent reflections. Space group P n a 21, a = 9.447(4), b = 7.160(3), c = 36.118(16), β = 90, V = 2443.1(19) Å^3, Orthorhombic, Z = 4 for chemical formula C_{23} H_{36} N_2 O_5, with one molecule in asymmetric unit; ρ calcd = 1.143 gcm^{-3}, μ = 0.080 mm^{-1}, F (000) = 912, Rint= 0.0837. The structure was obtained by direct methods using SHELXL-97.[25] The final R value was 0.0652 (wR2 = 0.1504) 6159 observed reflections ($F0 \geq 4\sigma$ (|F0|)) and 280 variables, S = 1.041. The largest difference peak and hole were 0.477 and -0.238 eÅ^3, respectively.

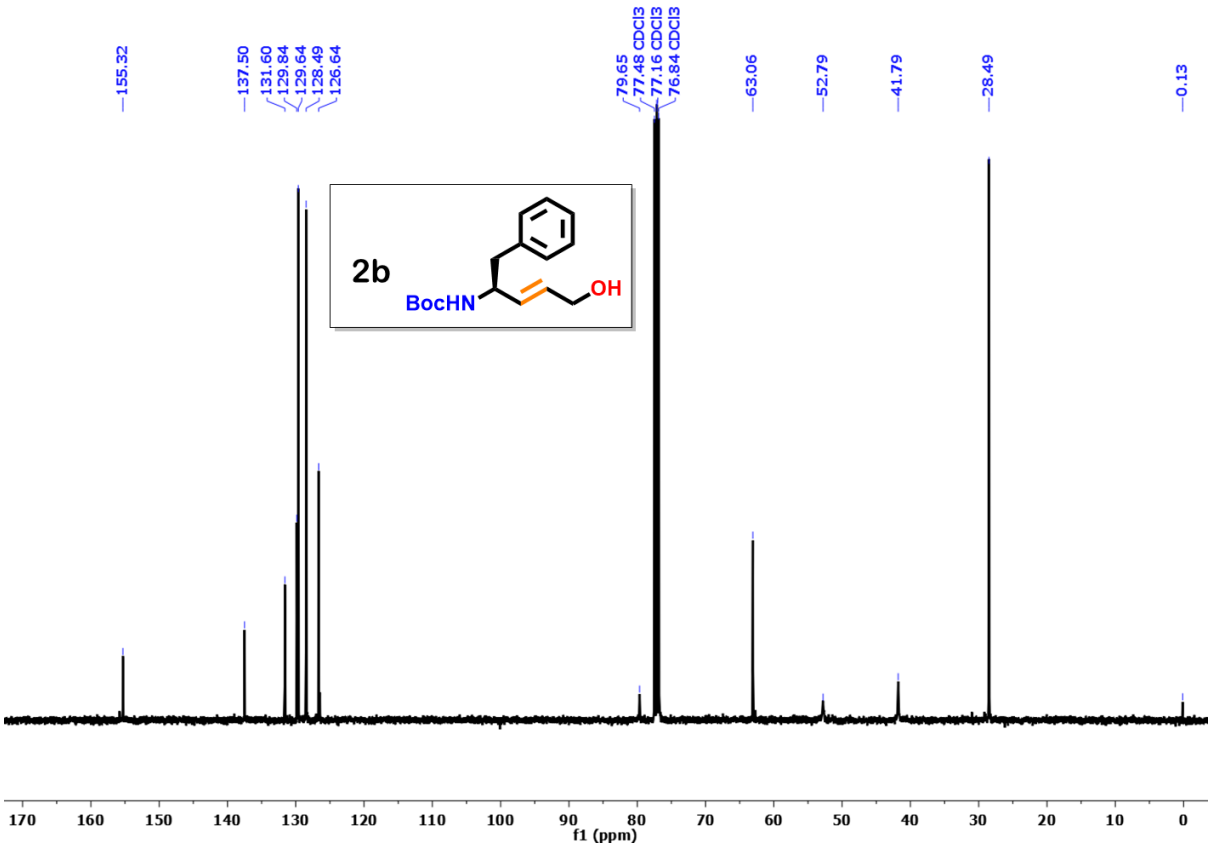
2.8.2. ^{1}H NMR, ^{13}C NMR and HRMS Spectra of all Compounds

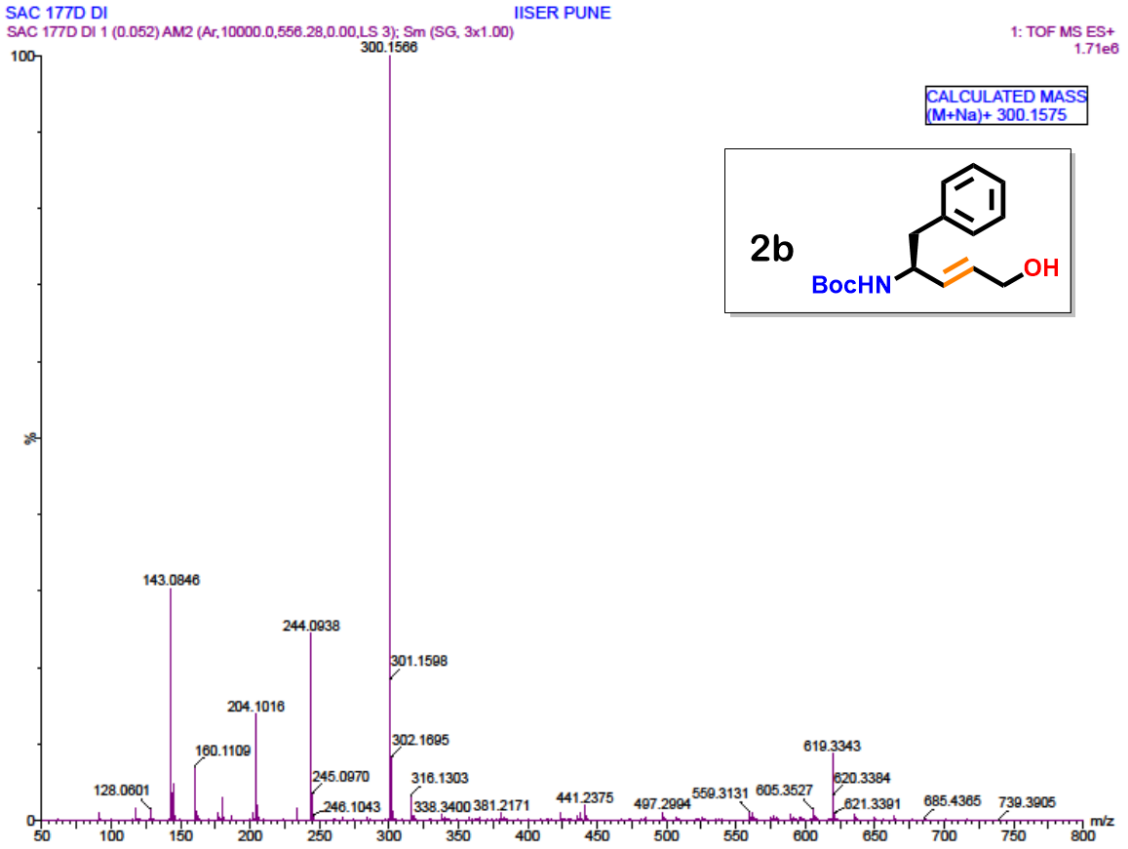


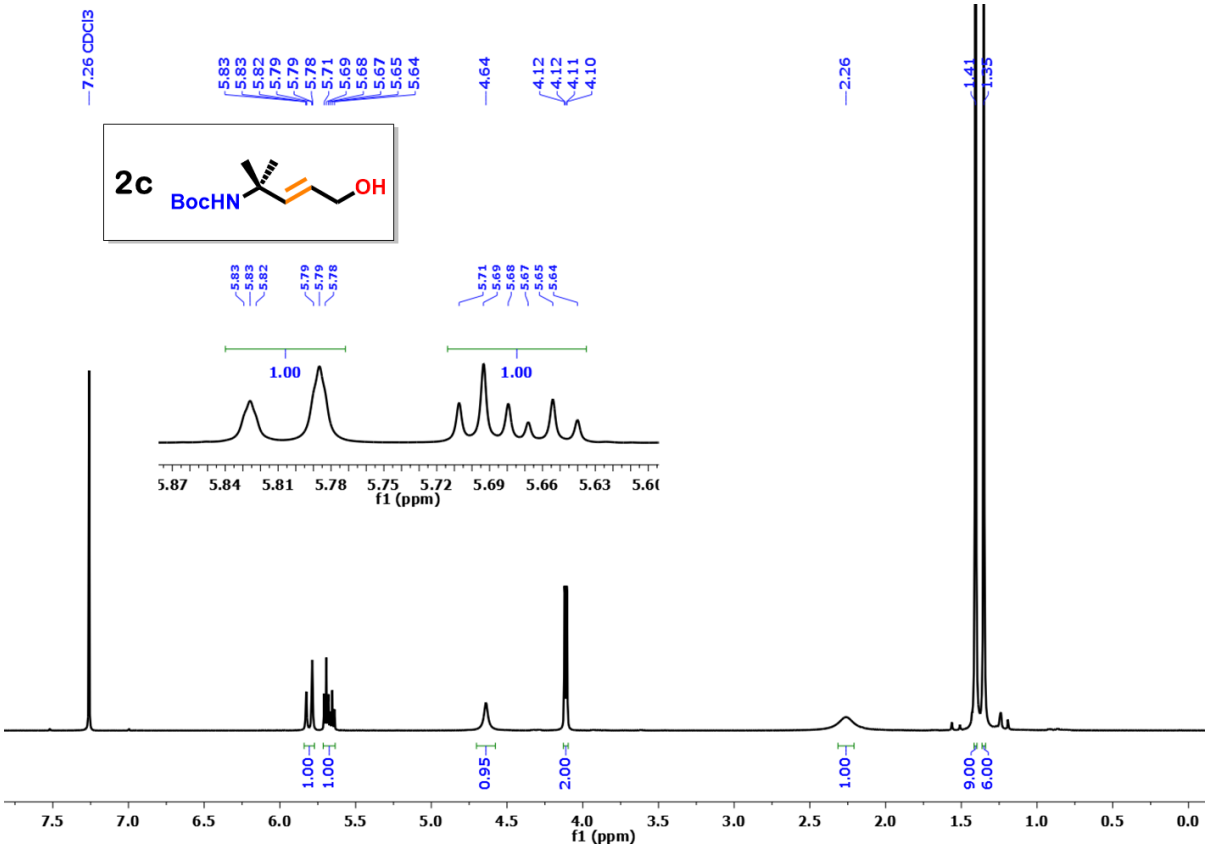

155.77
130.74
130.30
79.43
77.48 CDCl3
77.16 CDCl3
76.84 CDCl3
63.09
57.22
32.54
28.52
18.84
18.23
2a
BocHN
OH
170 160 150 140 130 120 110 100 90 80 70 60 50 40 30 20 10 0
f1 (ppm)

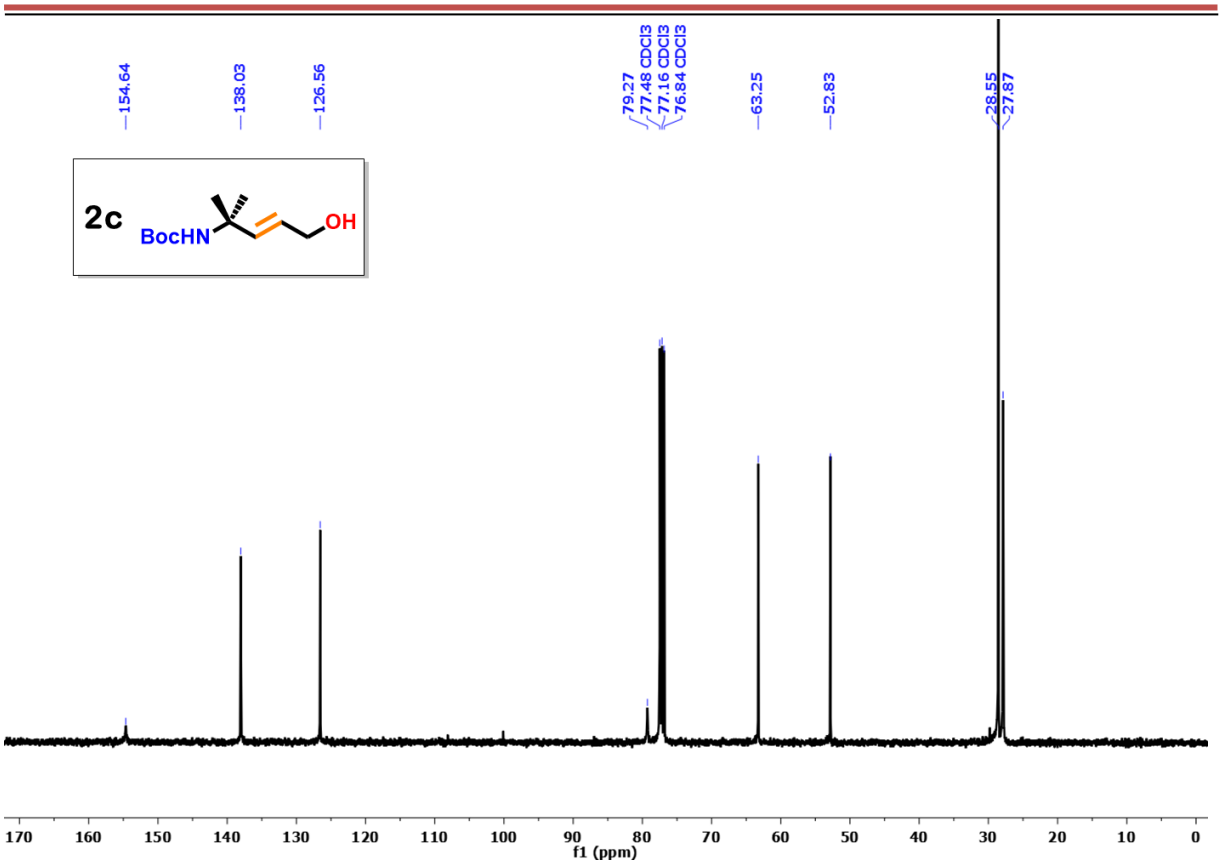

SAC 177B DI
IISER PUNE
SAC 177B DI 1 (0.052) AM2 (Ar,10000.0,556.28,0.00,LS 3); Sm (SG, 3x1.00)
1: TOF MS ES+
1.24e6
Calculated Mass [M+Na]+ 252.1576
2a
BocHN
OH
100
%
0
252.1569
225.1958
156.1013
253.1601
196.0937
95.0835
112.1105
88.0366
268.1308
316.2110
365.1100
449.3848
471.3658
472.3699
523.3350
524.3379
578.3762
664.4523
690.4625
792.5570
50 100 150 200 250 300 350 400 450 500 550 600 650 700 750 800
m/z

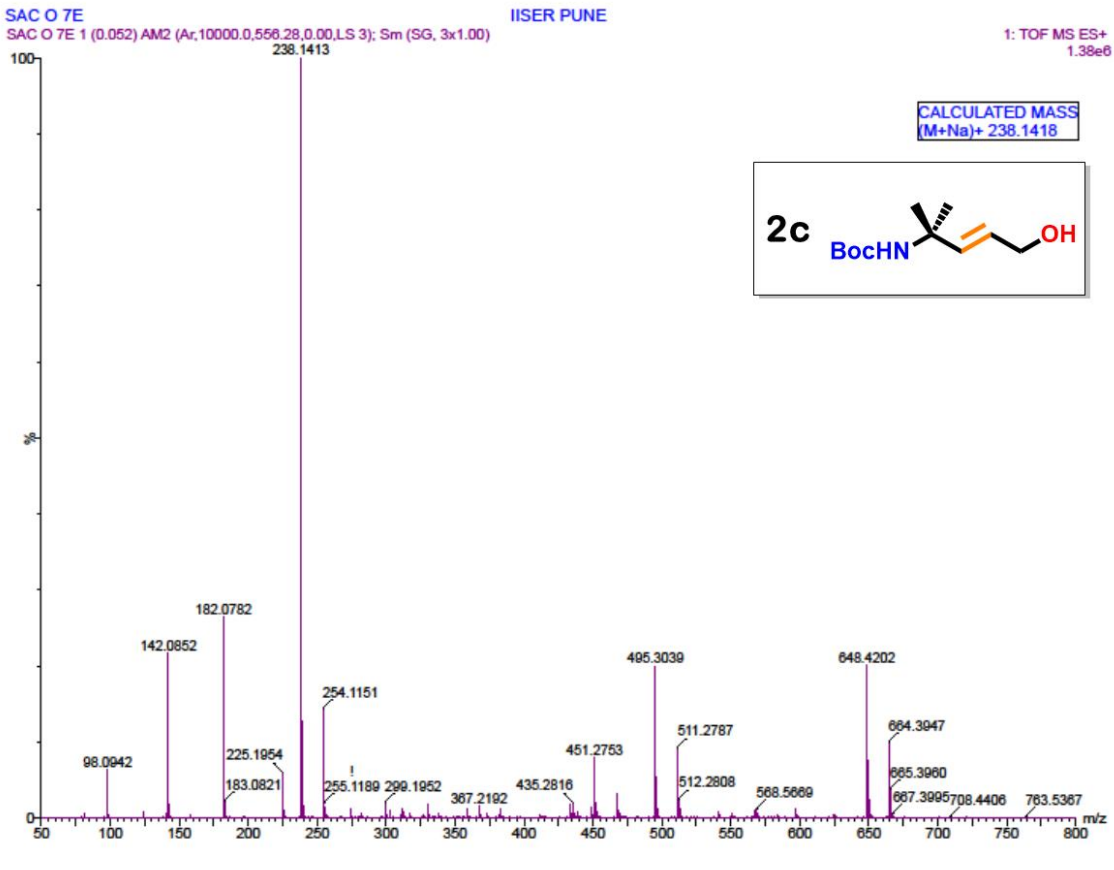

2b
BocHN
OH
f1 (ppm)

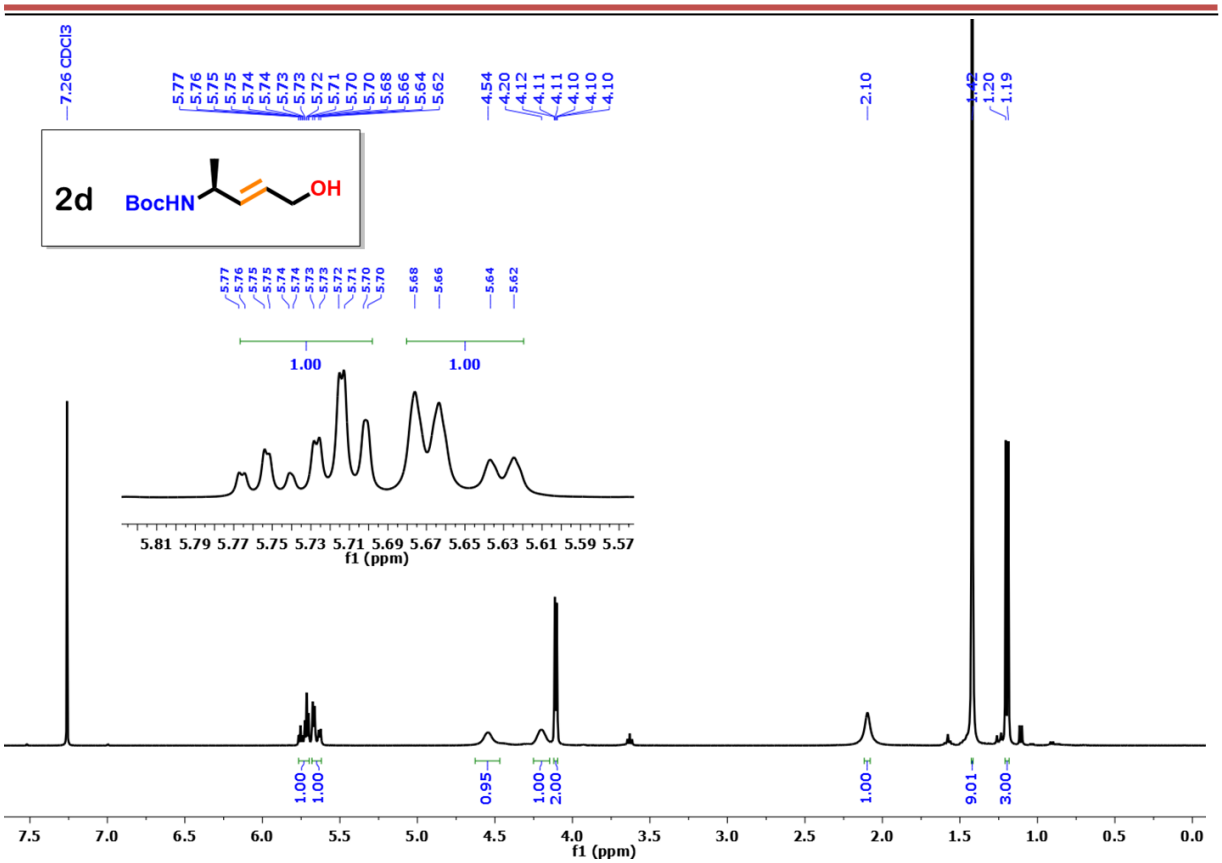

2b
BocHN
OH
f1 (ppm)

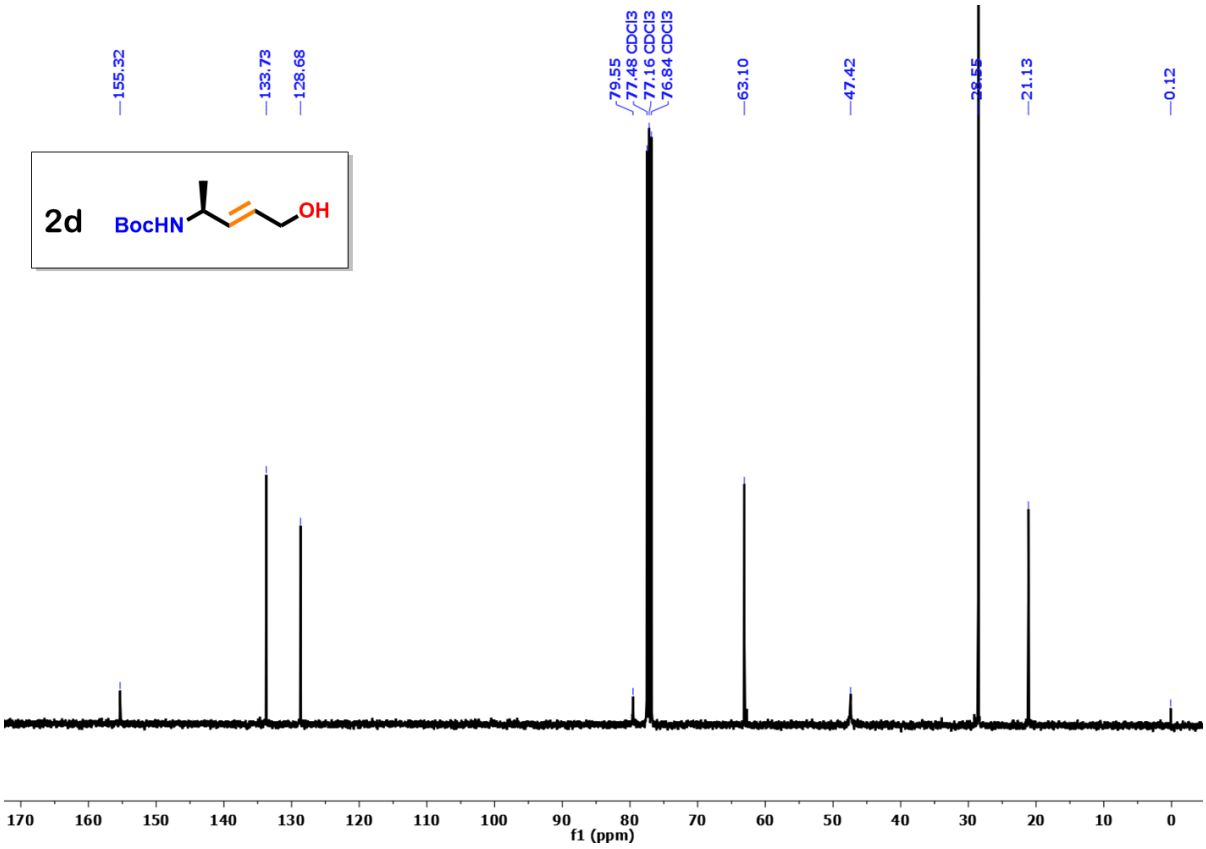

SAC 177D DI
IISER PUNE
SAC 177D DI 1 (0.052) AM2 (Ar,10000.0,556.28,0.00,LS 3); Sm (SG, 3x1.00)
1: TOF MS ES+
1.71e6
CALCULATED MASS
(M+Na)+ 300.1575
2b
BocHN
OH
300.1566
143.0846
244.0938
301.1598
204.1016
160.1109
302.1695
619.3343
245.0970
316.1303
620.3384
128.0601
246.1043
338.3400
381.2171
441.2375
497.2994
559.3131
605.3527
621.3391
685.4365
739.3905
m/z

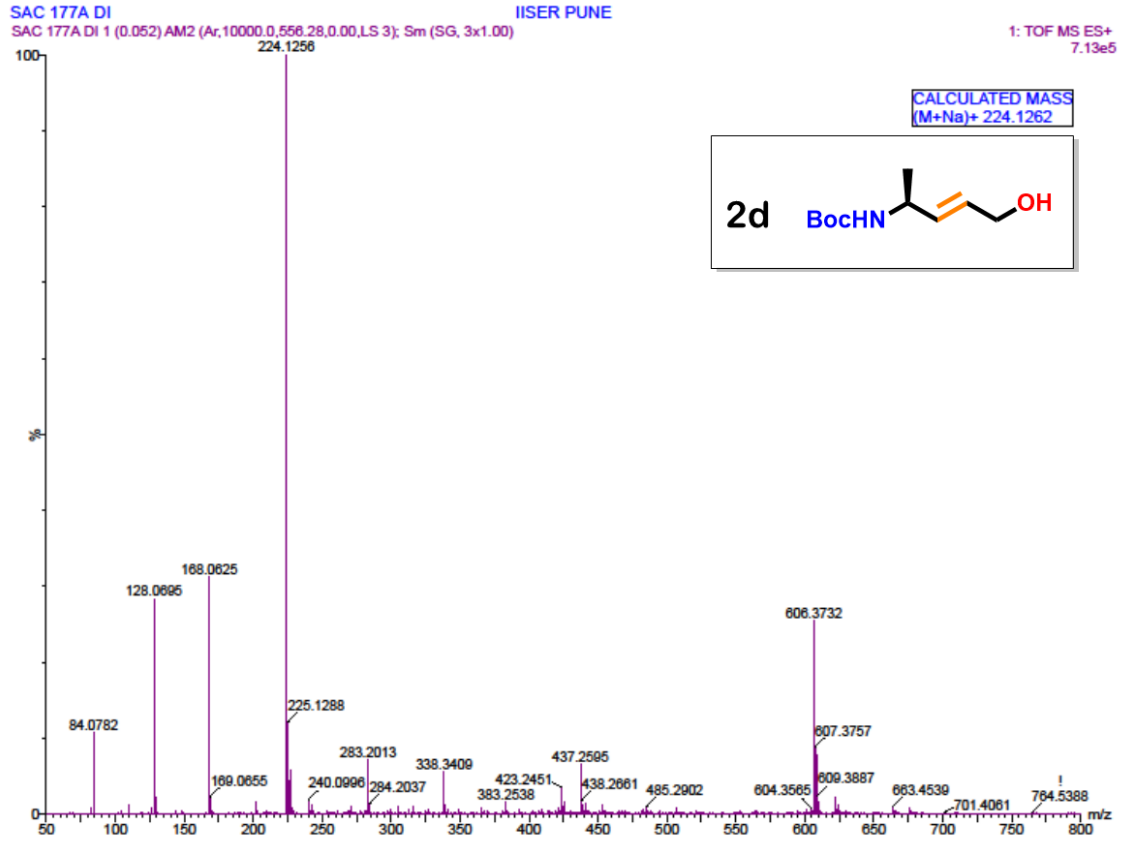

7.26 CDCl3
5.83
5.83
5.82
5.79
5.79
5.78
5.71
5.69
5.68
5.67
5.65
5.64
4.64
4.12
4.12
4.11
4.10
2.26
1.41
1.35
2c
BocHN
OH
1.00
1.00
f1 (ppm)
1.00
1.00
0.95
2.00
1.00
9.00
6.00
f1 (ppm)

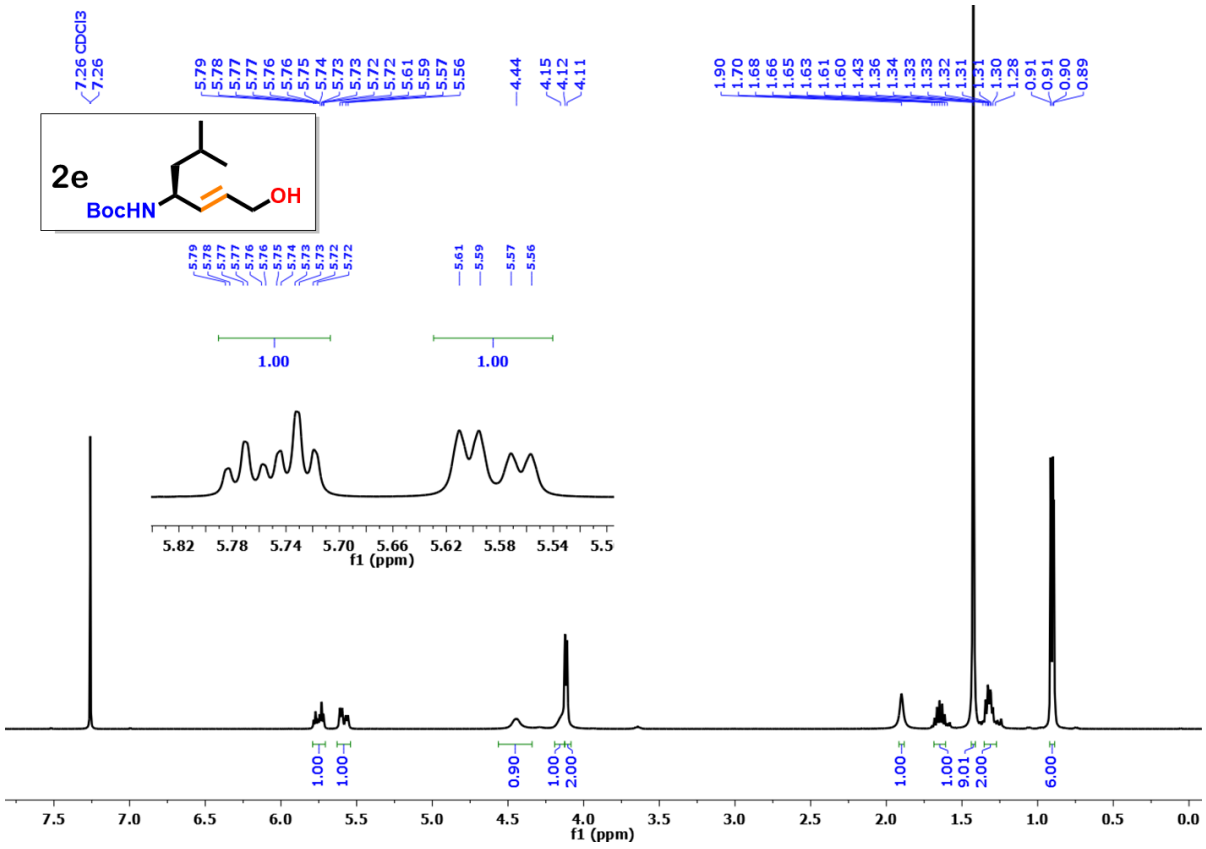

154.64
138.03
126.56
79.27
77.48 CDCl3
77.16 CDCl3
76.84 CDCl3
63.25
52.83
28.55
27.87
2c
BocHN
OH
f1 (ppm)

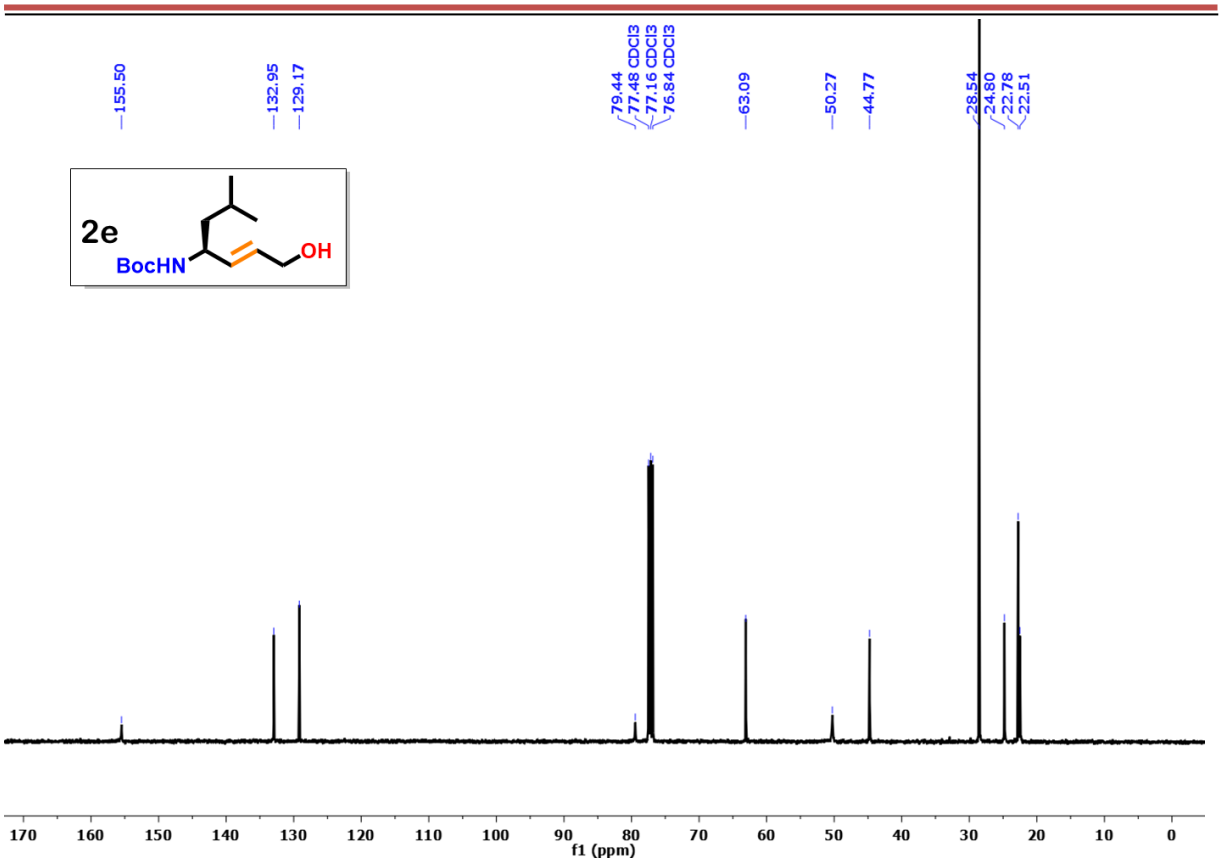

SAC O 7E
IISER PUNE
SAC O 7E 1 (0.052) AM2 (Ar,10000.0,556.28,0.00,LS 3); Sm (SG, 3x1.00)
1: TOF MS ES+
1.38e6
CALCULATED MASS
(M+Na)+ 238.1418
2c
BocHN
OH
238.1413
182.0782
142.0852
254.1151
495.3039
648.4202
511.2787
664.3947
451.2753
225.1954
98.0942
183.0821
512.2808
665.3960
255.1189
299.1952
435.2816
568.5669
667.3995
708.4406
763.5367
367.2192
%
m/z

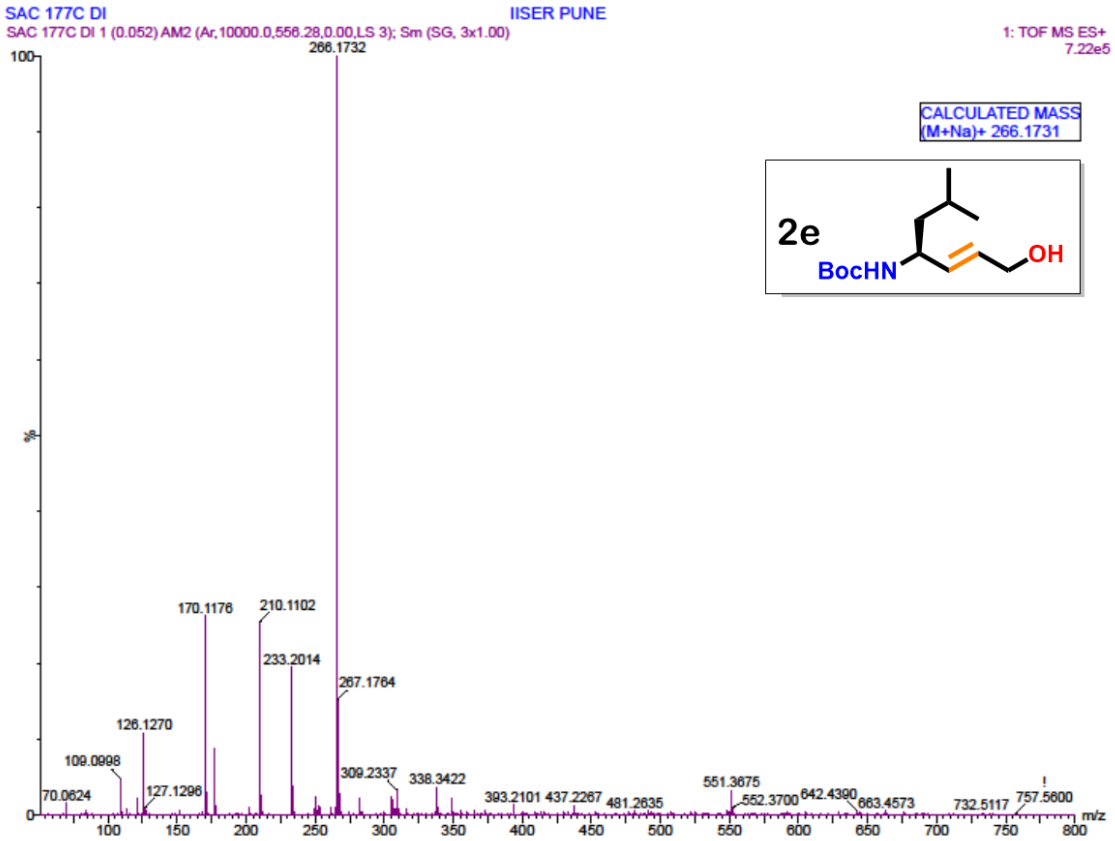

7.26 CDCl3
5.77
5.76
5.75
5.75
5.74
5.74
5.73
5.72
5.71
5.70
5.70
5.68
5.66
5.64
5.62
4.54
4.20
4.12
4.11
4.11
4.10
4.10
4.10
2.10
1.42
1.20
1.19
2d
BocHN
OH
1.00
1.00
5.81 5.79 5.77 5.75 5.73 5.71 5.69 5.67 5.65 5.63 5.61 5.59 5.57
f1 (ppm)
1.00
1.00
0.95
1.00
2.00
1.00
9.01
3.00
7.5 7.0 6.5 6.0 5.5 5.0 4.5 4.0 3.5 3.0 2.5 2.0 1.5 1.0 0.5 0.0
f1 (ppm)

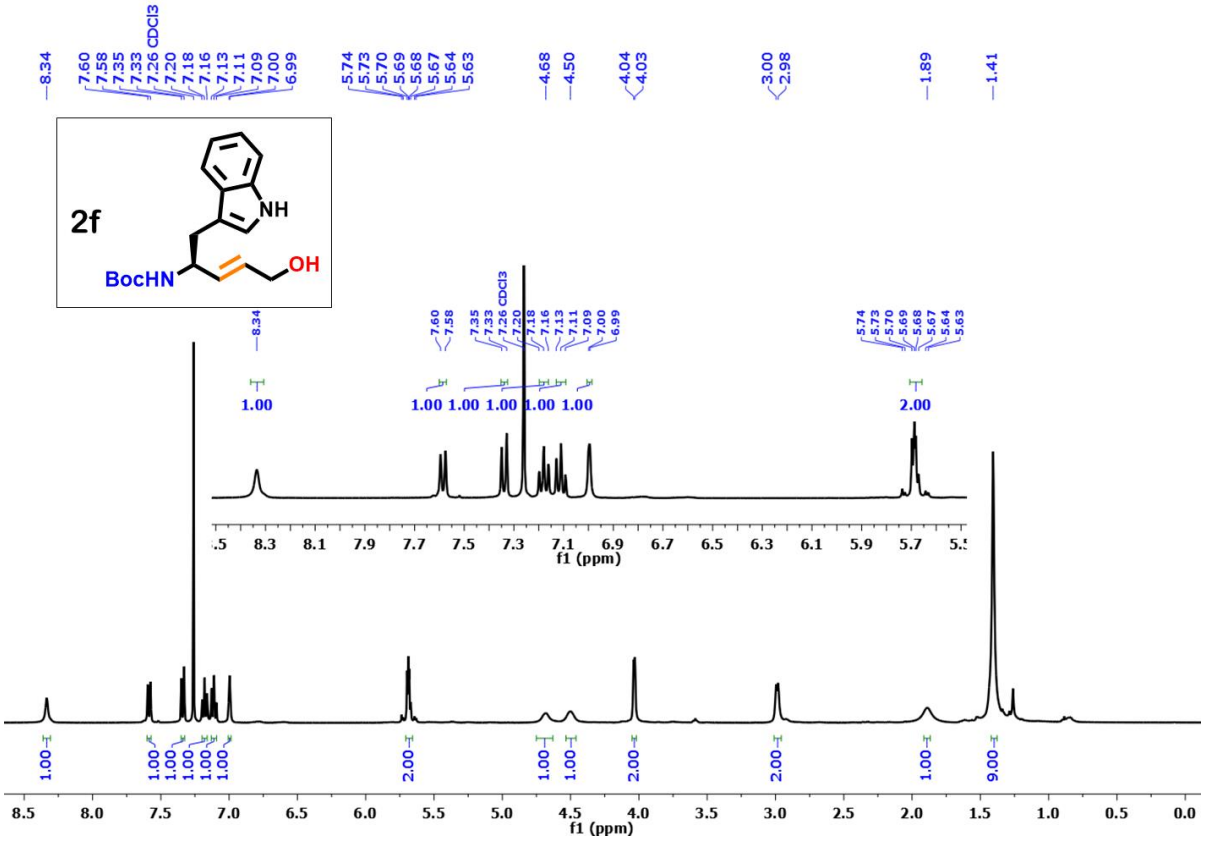

155.32
133.73
128.68
79.55
77.48 CDCl3
77.16 CDCl3
76.84 CDCl3
63.10
47.42
28.55
21.13
0.12
2d
BocHN
OH
170 160 150 140 130 120 110 100 90 80 70 60 50 40 30 20 10 0
f1 (ppm)

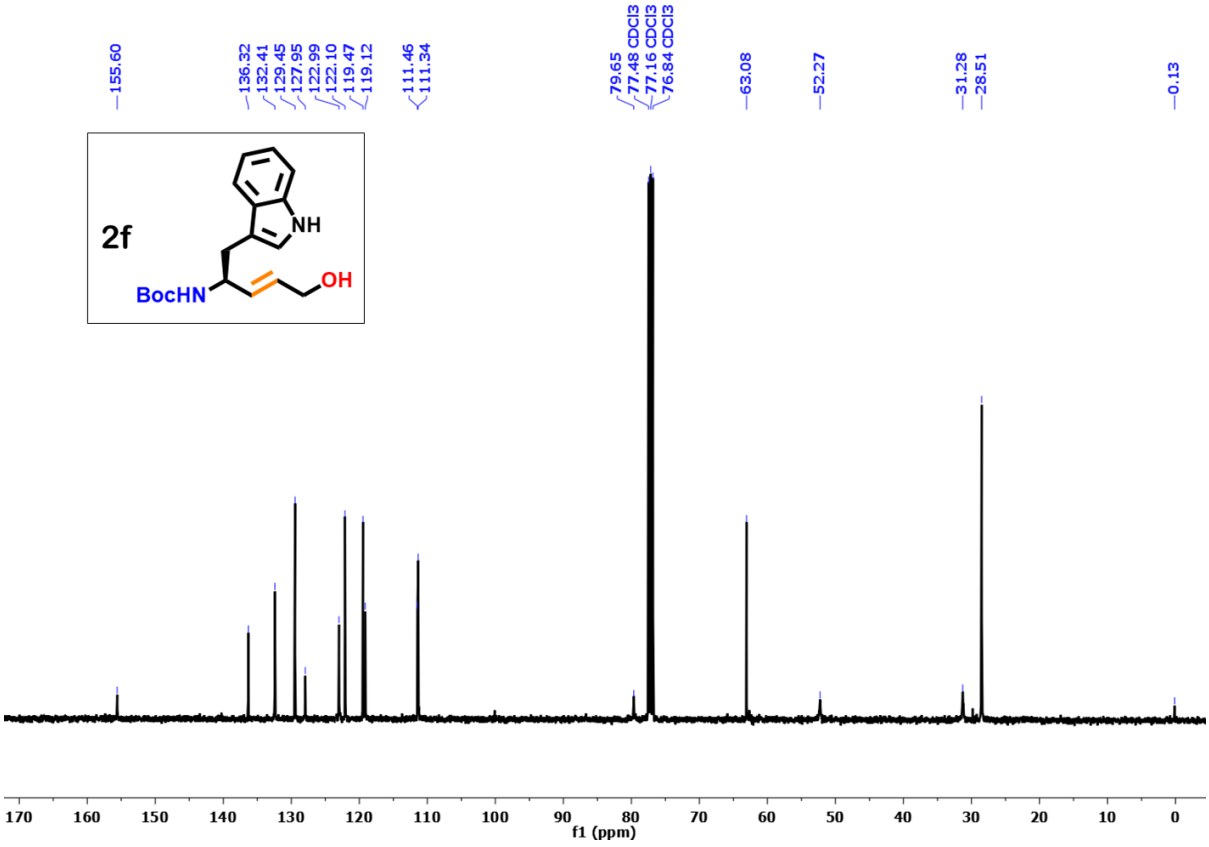

SAC 177A DI
IISER PUNE
SAC 177A DI 1 (0.052) AM2 (Ar,10000.0,556.28,0.00,LS 3); Sm (SG, 3x1.00)
1: TOF MS ES+
7.13e5
CALCULATED MASS
(M+Na)+ 224.1262
2d
BocHN
OH
224.1256
168.0625
128.0695
84.0782
225.1288
283.2013
338.3409
606.3732
607.3757
437.2595
609.3887
m/z

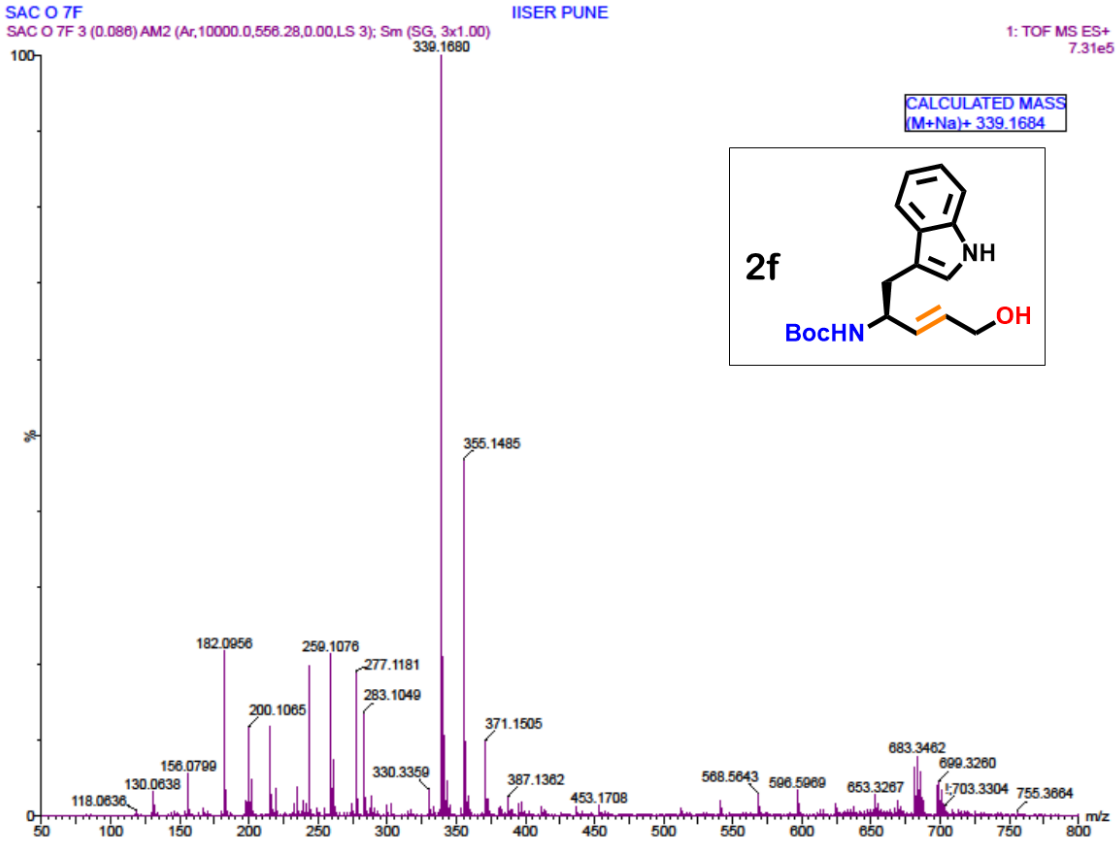

2e
BocHN
OH
7.26 CDCl3
1.00
1.00
f1 (ppm)

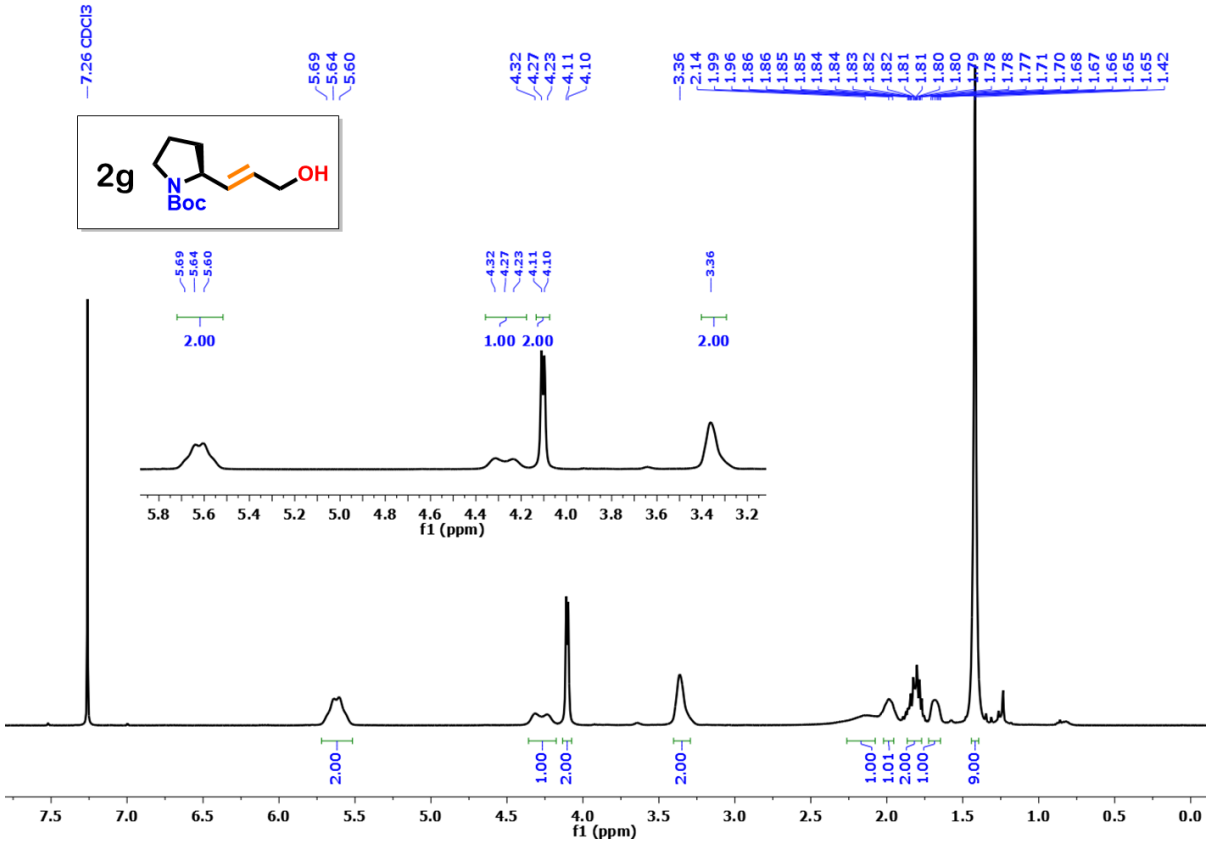

155.50
132.95
129.17
79.44 CDCl3
77.48 CDCl3
77.16 CDCl3
76.84 CDCl3
63.09
50.27
44.77
28.54
24.80
22.78
22.51
2e
BocHN
OH
f1 (ppm)

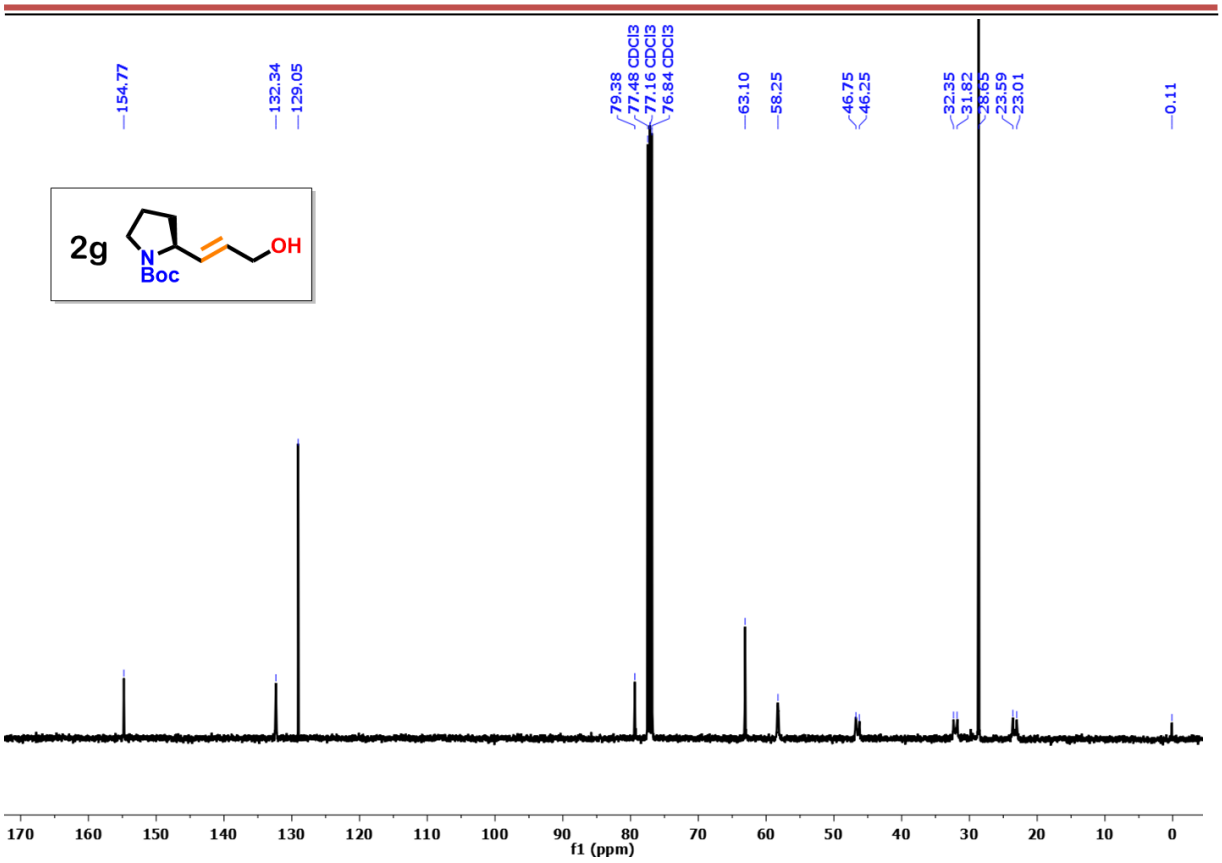

SAC 177C DI
IISER PUNE
SAC 177C DI 1 (0.052) AM2 (Ar,10000.0,556.28,0.00,LS 3); Sm (SG, 3x1.00)
1: TOF MS ES+
7.22e5
CALCULATED MASS
(M+Na)+ 266.1731
2e
BocHN
OH
266.1732
170.1176
210.1102
233.2014
267.1764
126.1270
109.0998
70.0624
127.1296
309.2337
338.3422
393.2101
437.2267
481.2635
551.3675
552.3700
642.4390
663.4573
732.5117
757.5600
%
m/z

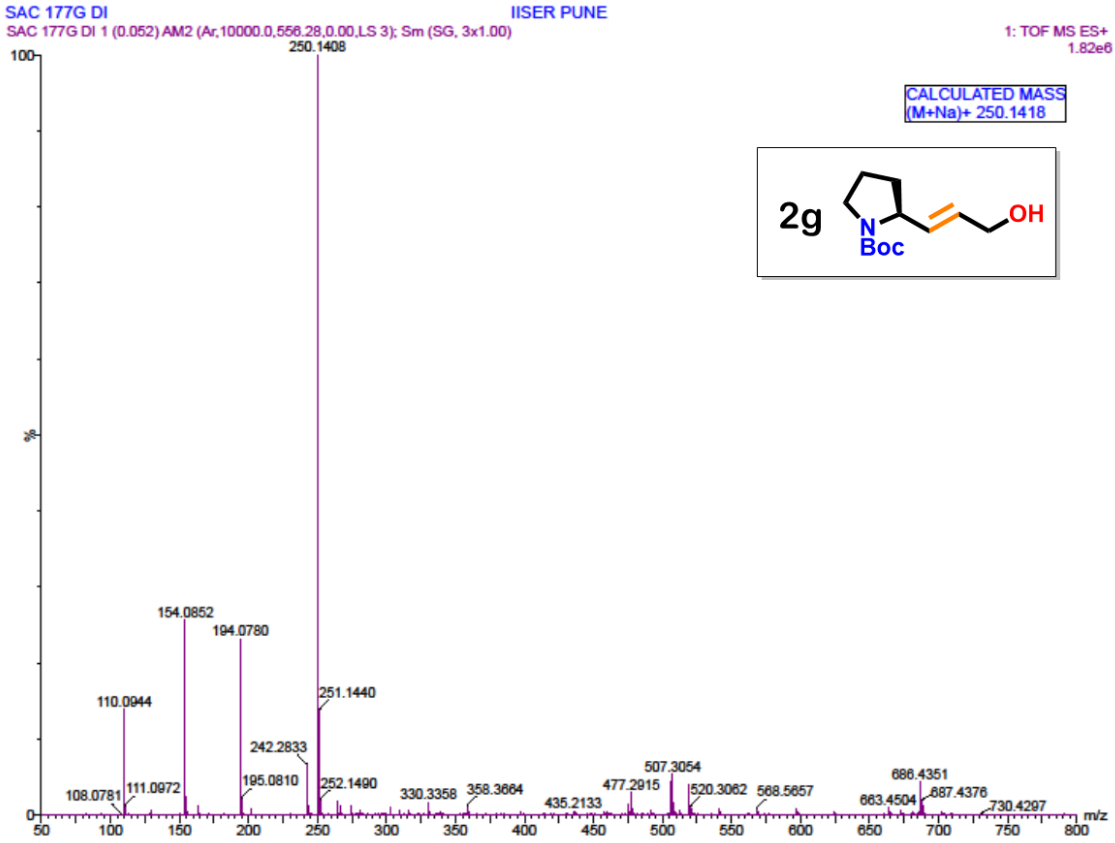

8.34
7.60
7.58
7.35
7.33
7.26 CDCl3
7.20
7.18
7.16
7.13
7.11
7.09
7.00
6.99
5.74
5.73
5.70
5.69
5.68
5.67
5.64
5.63
4.68
4.50
4.04
4.03
3.00
2.98
1.89
1.41
2f
NH
BocHN
OH
1.00
1.00 1.00 1.00 1.00 1.00
2.00
f1 (ppm)
1.00
1.00
1.00
1.00
1.00
2.00
2.00
1.00
1.00
2.00
2.00
1.00
9.00
f1 (ppm)

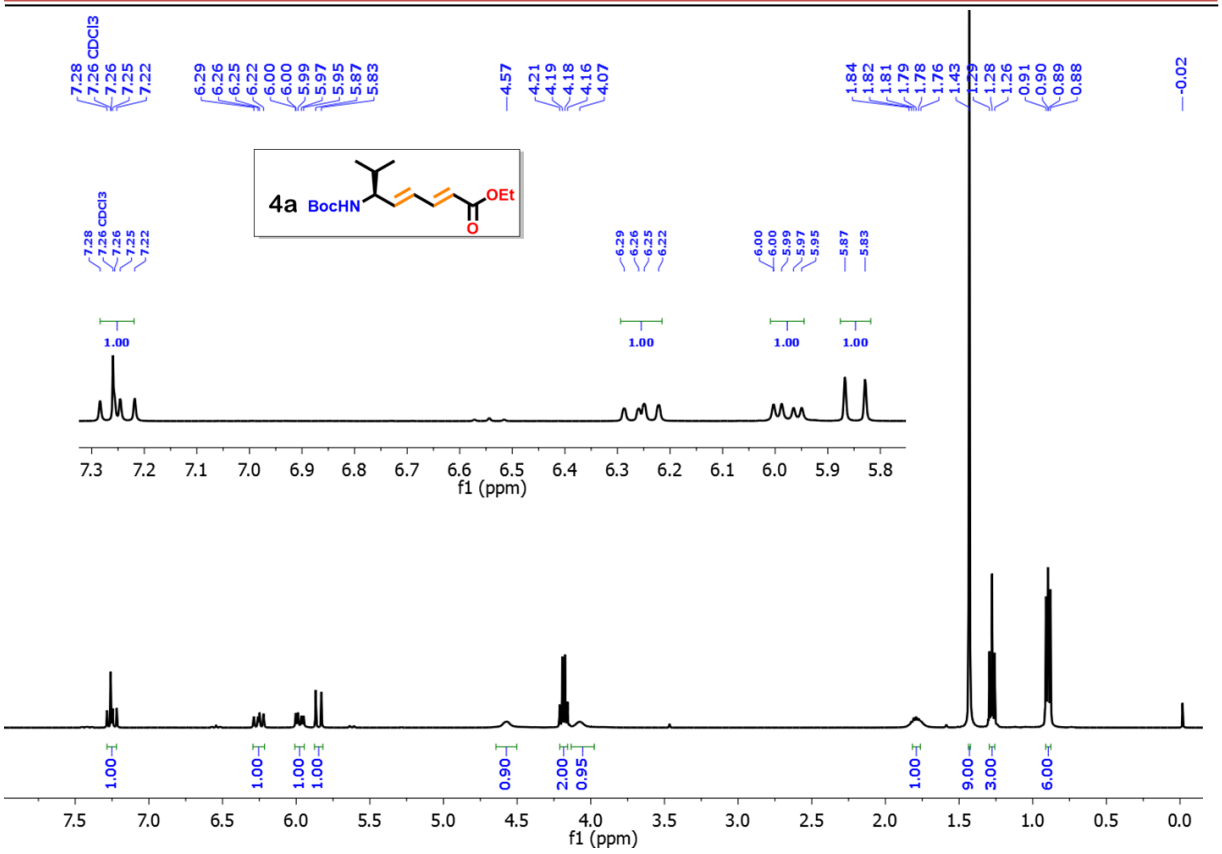

155.60
136.32
132.41
129.45
127.95
122.99
122.10
119.47
119.12
111.46
111.34
79.65
77.48 CDCl3
77.16 CDCl3
76.84 CDCl3
63.08
52.27
31.28
28.51
0.13
2f
NH
BocHN
OH
f1 (ppm)

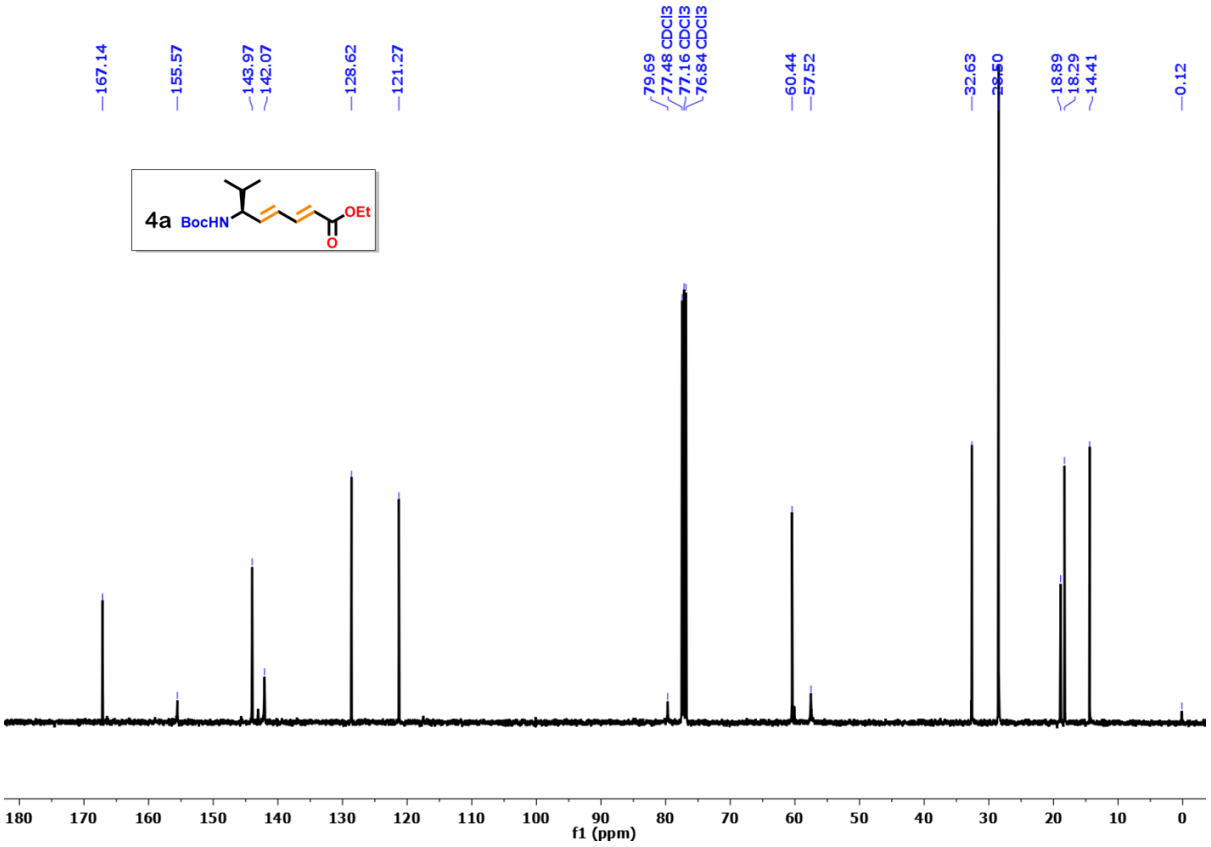

SAC O 7F
IISER PUNE
SAC O 7F 3 (0.086) AM2 (Ar,10000.0,556.28,0.00,LS 3); Sm (SG, 3x1.00)
1: TOF MS ES+
7.31e5
CALCULATED MASS
(M+Na)+ 339.1684
2f
NH
BocHN
OH
339.1680
355.1485
182.0956
259.1076
277.1181
283.1049
200.1065
371.1505
156.0799
130.0638
118.0636
330.3359
387.1362
453.1708
568.5643
596.5969
653.3267
683.3462
699.3260
703.3304
755.3664
%
m/z

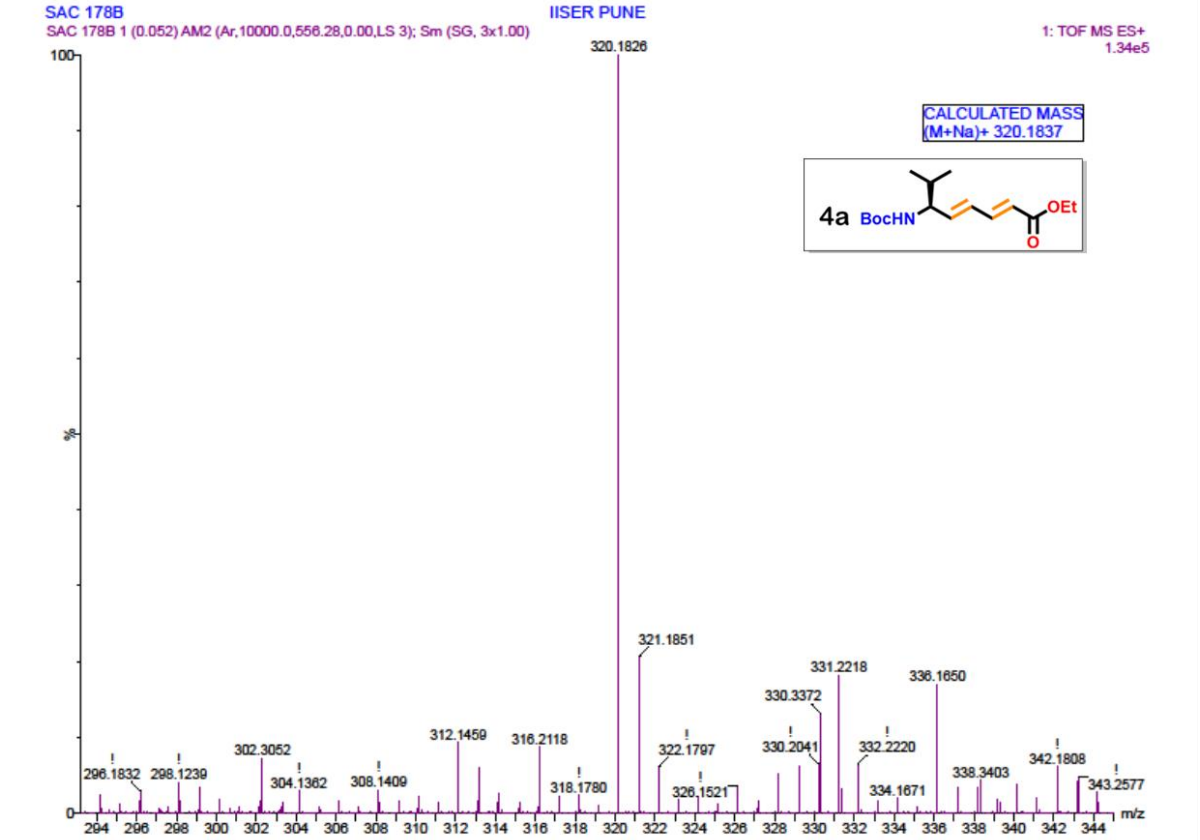

7.26 CDCl3
2g
N
Boc
OH
2.00
1.00
2.00
2.00
f1 (ppm)

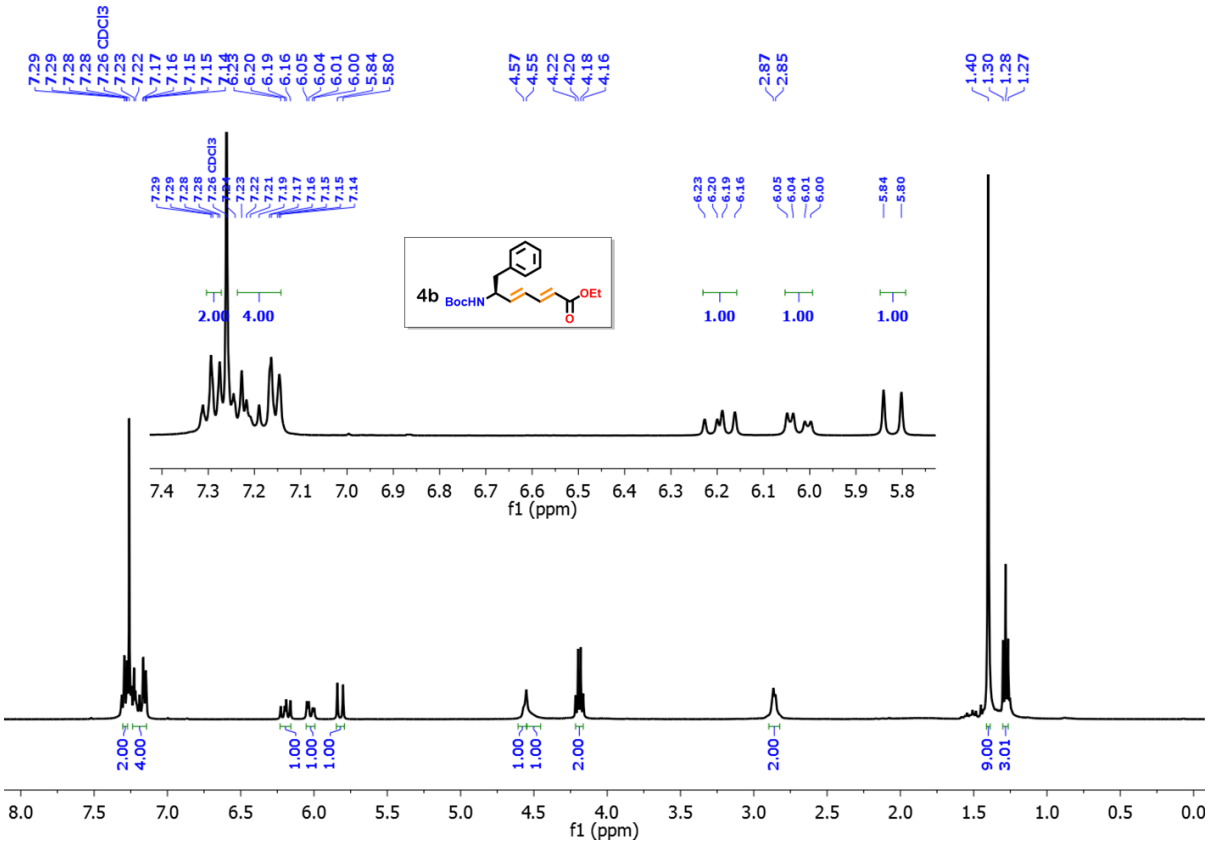

154.77
132.34
129.05
79.38 CDCl3
77.48 CDCl3
77.16 CDCl3
76.84 CDCl3
63.10
58.25
46.75
46.25
32.35
31.82
28.65
23.59
23.01
0.11
2g
N
Boc
OH
f1 (ppm)

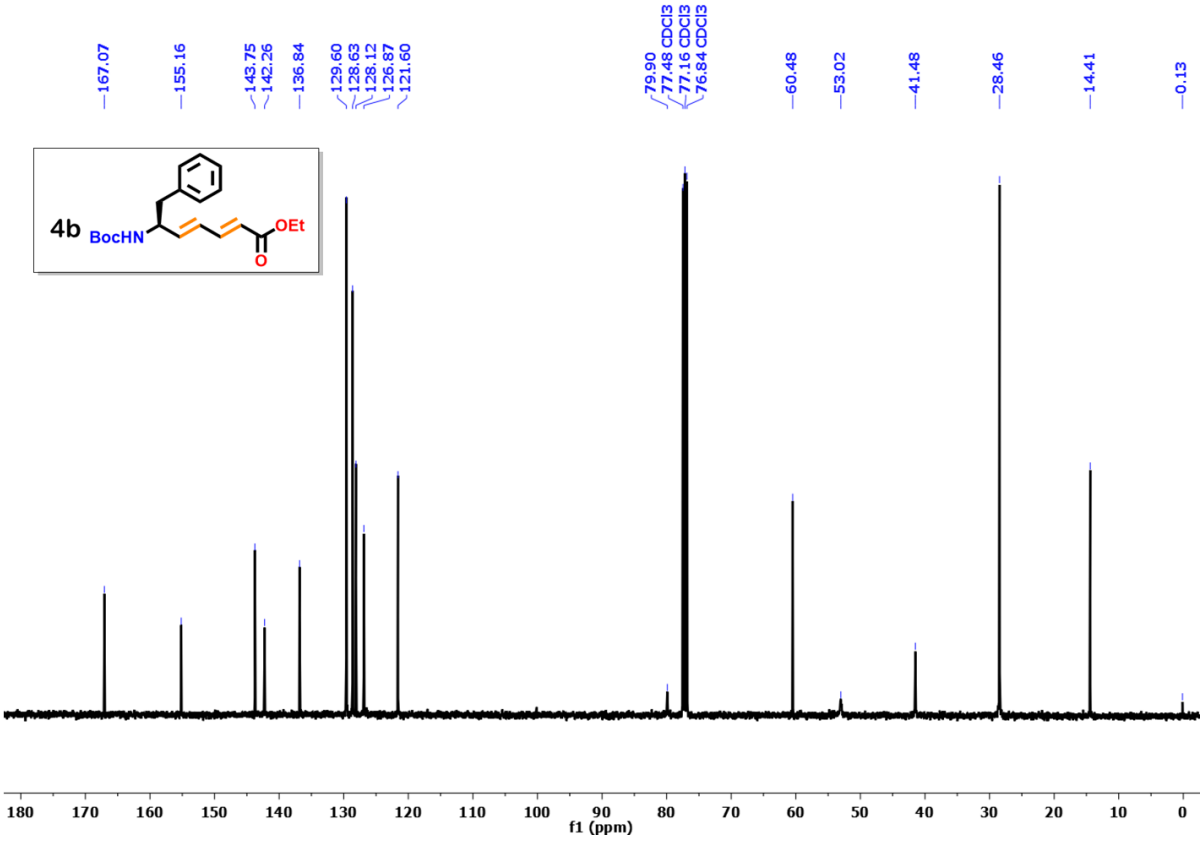

SAC 177G DI
IISER PUNE
SAC 177G DI 1 (0.052) AM2 (Ar,10000.0,556.28,0.00,LS 3); Sm (SG, 3x1.00)
1: TOF MS ES+
1.82e6
CALCULATED MASS
(M+Na)+ 250.1418
2g
N
Boc
OH
250.1408
154.0852
194.0780
110.0944
251.1440
242.2833
195.0810
252.1490
108.0781
111.0972
330.3358
358.3664
435.2133
477.2915
507.3054
520.3062
568.5657
663.4504
686.4351
687.4376
730.4297
%
m/z

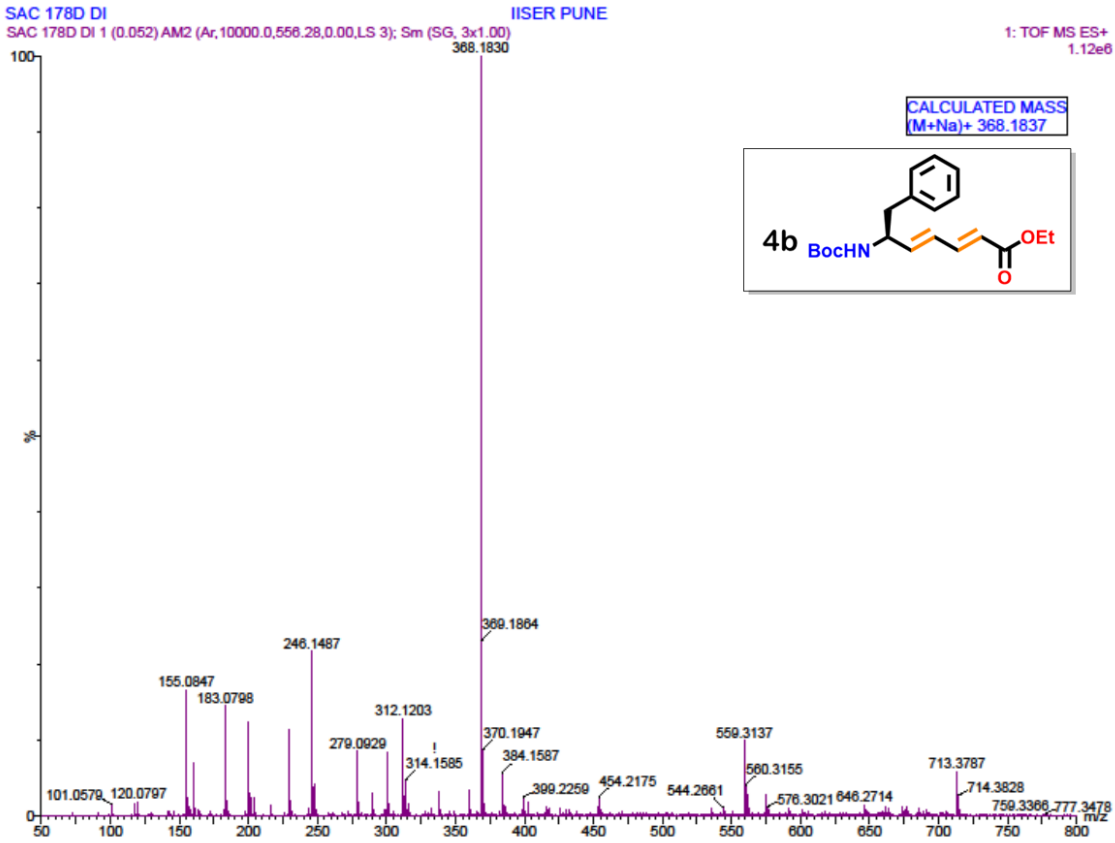

7.28 CDCl3
7.26
7.26
7.25
7.22
6.29
6.26
6.25
6.22
6.00
6.00
5.99
5.97
5.95
5.87
5.83
4.57
4.21
4.19
4.18
4.16
4.07
1.84
1.82
1.81
1.79
1.78
1.76
1.43
1.29
1.28
1.26
0.91
0.90
0.89
0.88
-0.02
4a BocHN
OEt
O
1.00
1.00
1.00
1.00
f1 (ppm)
0.90
2.00
0.95
1.00
9.00
3.00
6.00
f1 (ppm)

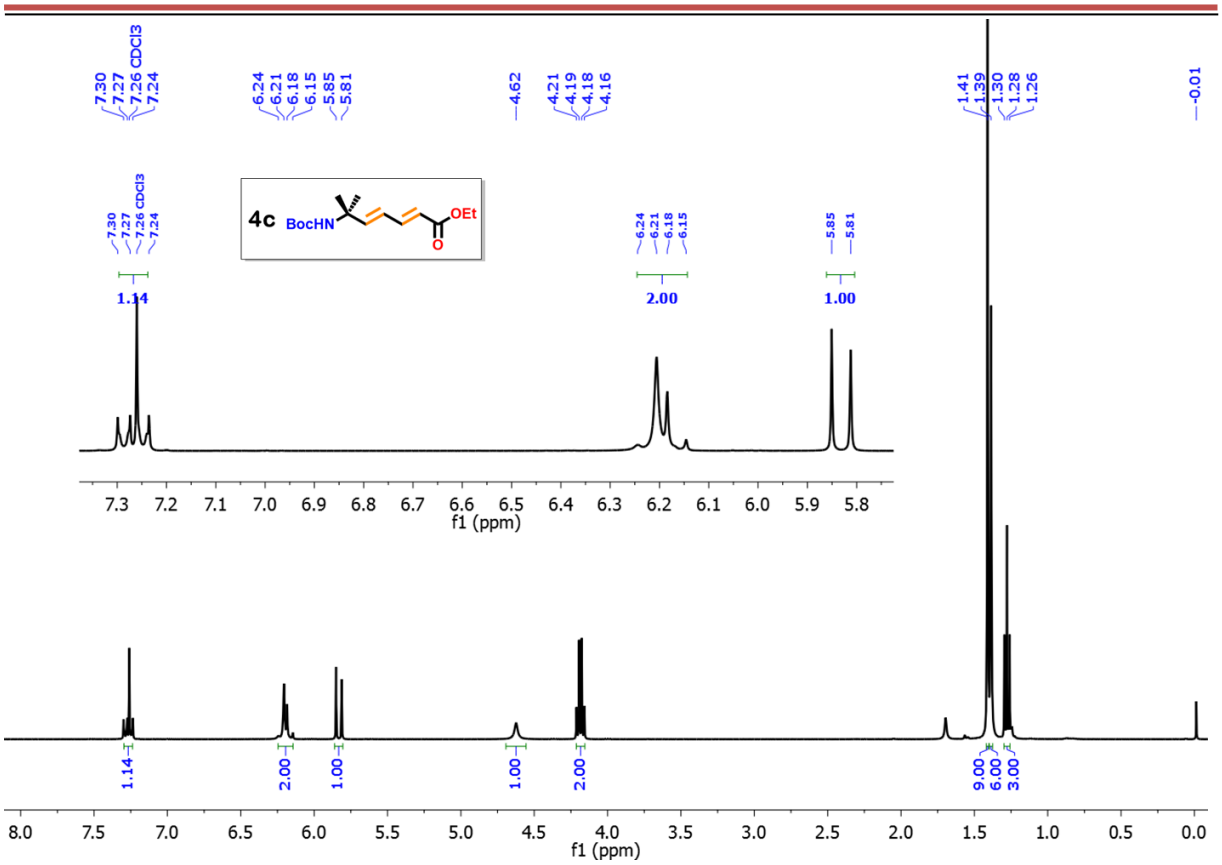

167.14
155.57
143.97
142.07
128.62
121.27
79.69
77.48 CDCl3
77.16 CDCl3
76.84 CDCl3
60.44
57.52
32.63
28.50
18.89
18.29
14.41
0.12
4a BocHN
OEt
O
f1 (ppm)

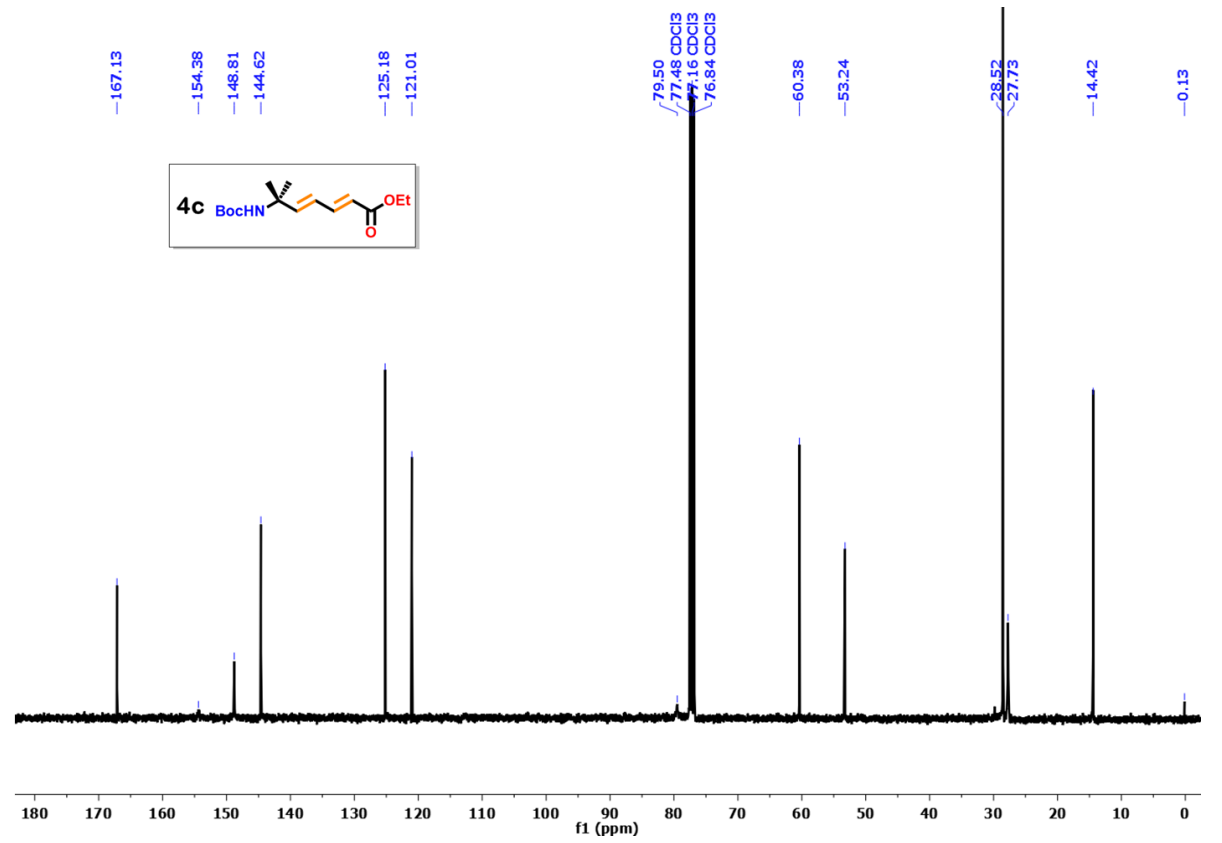

SAC 178B
IISER PUNE
SAC 178B 1 (0.052) AM2 (Ar,10000.0,556.28,0.00,LS 3); Sm (SG, 3x1.00)
1: TOF MS ES+
1.34e5
CALCULATED MASS
(M+Na)+ 320.1837
4a BocHN OEt
320.1826
321.1851
331.2218
330.3372
336.1650
330.2041
332.2220
322.1797
342.1808
338.3403
312.1459
316.2118
302.3052
296.1832
298.1239
304.1362
308.1409
318.1780
326.1521
334.1671
343.2577
%
m/z

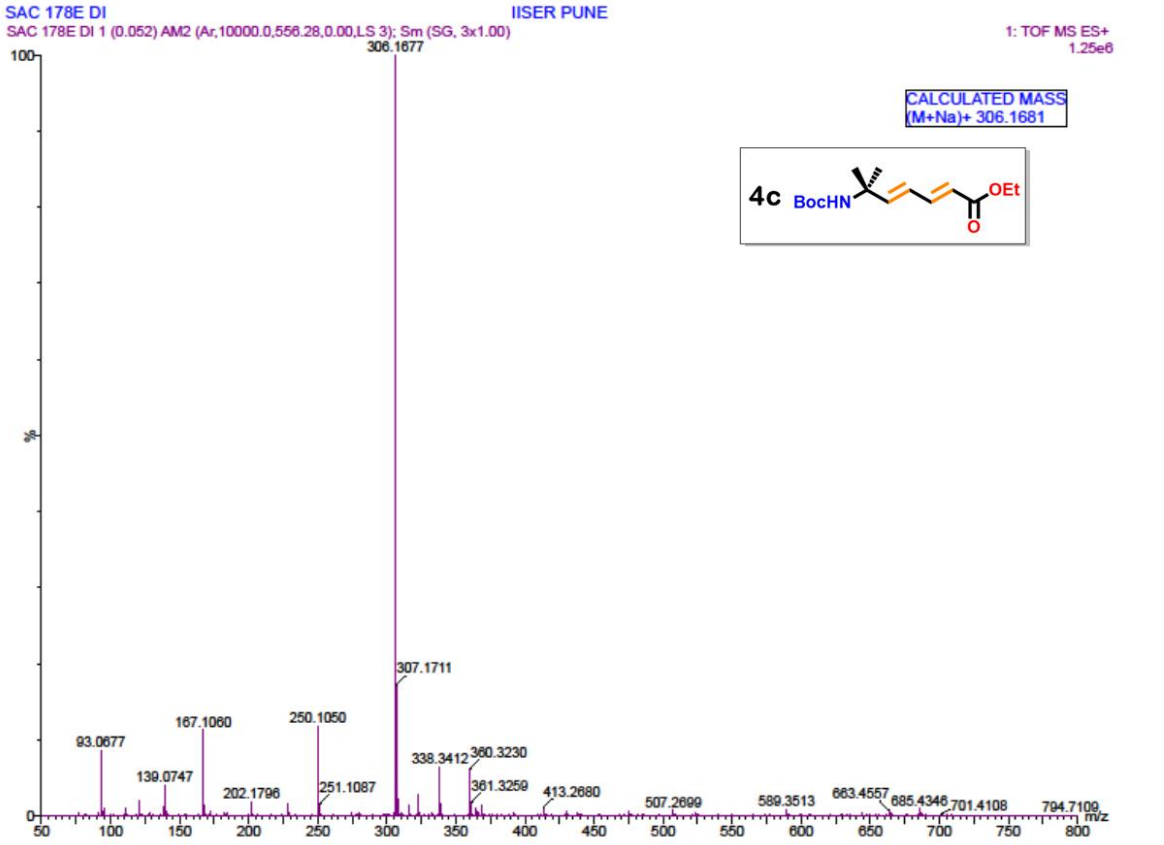

4b BocHN OEt
f1 (ppm)
f1 (ppm)

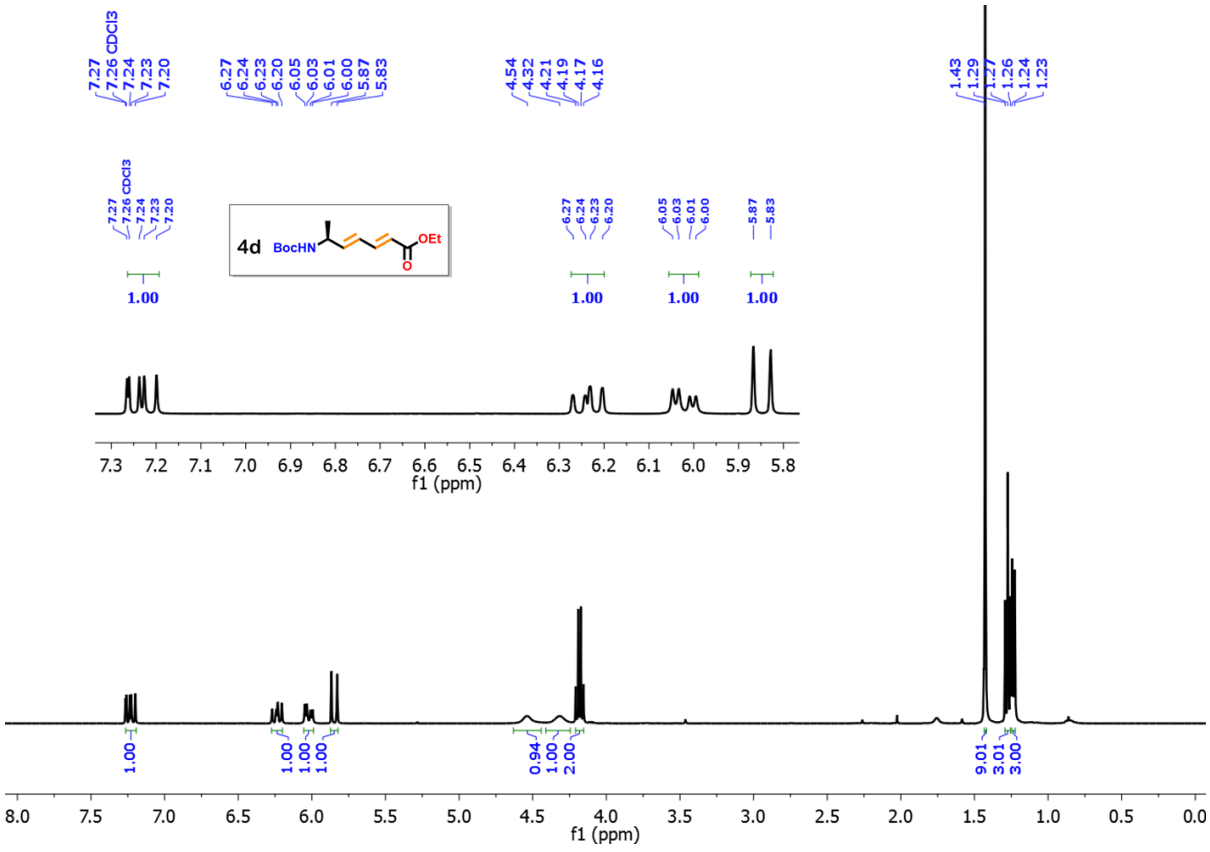

167.07
155.16
143.75
142.26
136.84
129.60
128.63
128.12
126.87
121.60
79.90
77.48 CDCl3
77.16 CDCl3
76.84 CDCl3
60.48
53.02
41.48
28.46
14.41
0.13
4b
BocHN
OEt
O
f1 (ppm)

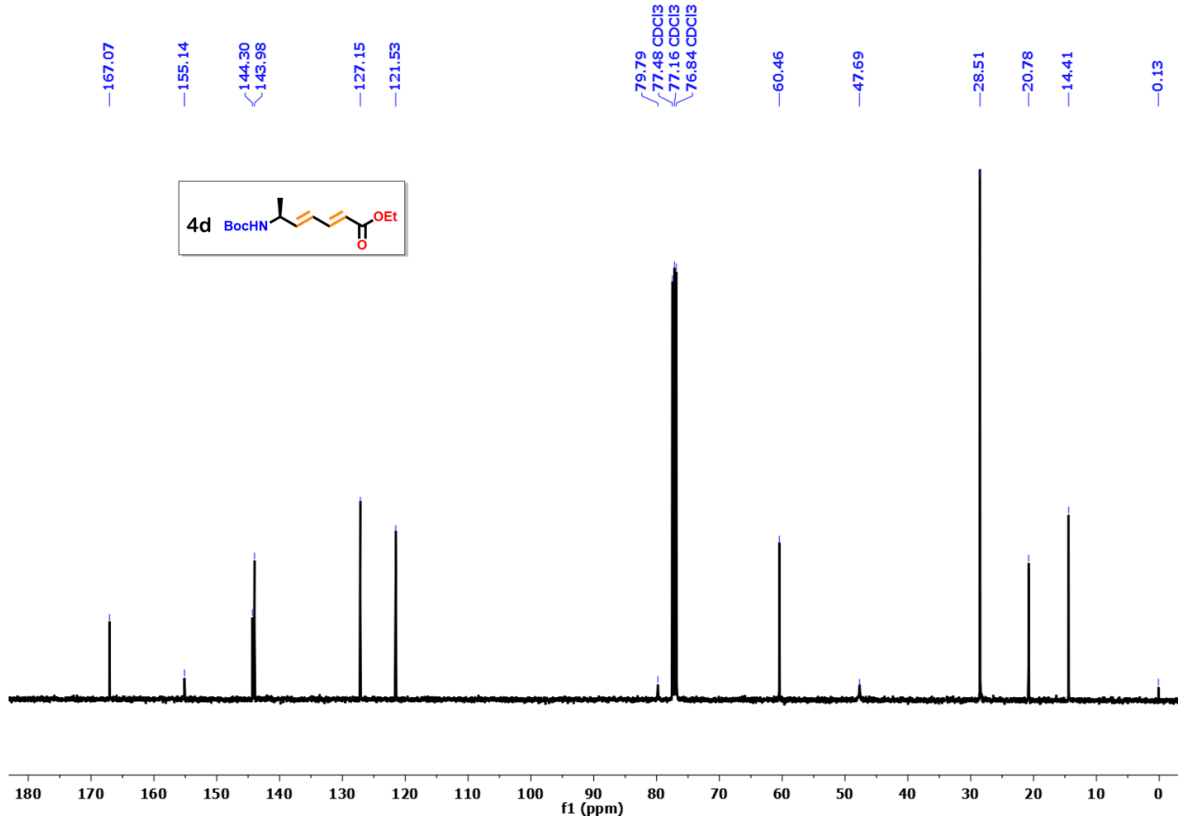

SAC 178D DI
IISER PUNE
SAC 178D DI 1 (0.052) AM2 (Ar,10000.0,556.28,0.00,LS 3); Sm (SG, 3x1.00)
1: TOF MS ES+
1.12e6
CALCULATED MASS
(M+Na)+ 368.1837
4b
BocHN
OEt
O
368.1830
369.1864
246.1487
155.0847
183.0798
312.1203
279.0929
314.1585
370.1947
384.1587
399.2259
454.2175
544.2661
559.3137
560.3155
576.3021
646.2714
713.3787
714.3828
759.3366
777.3478
101.0579
120.0797
%
m/z

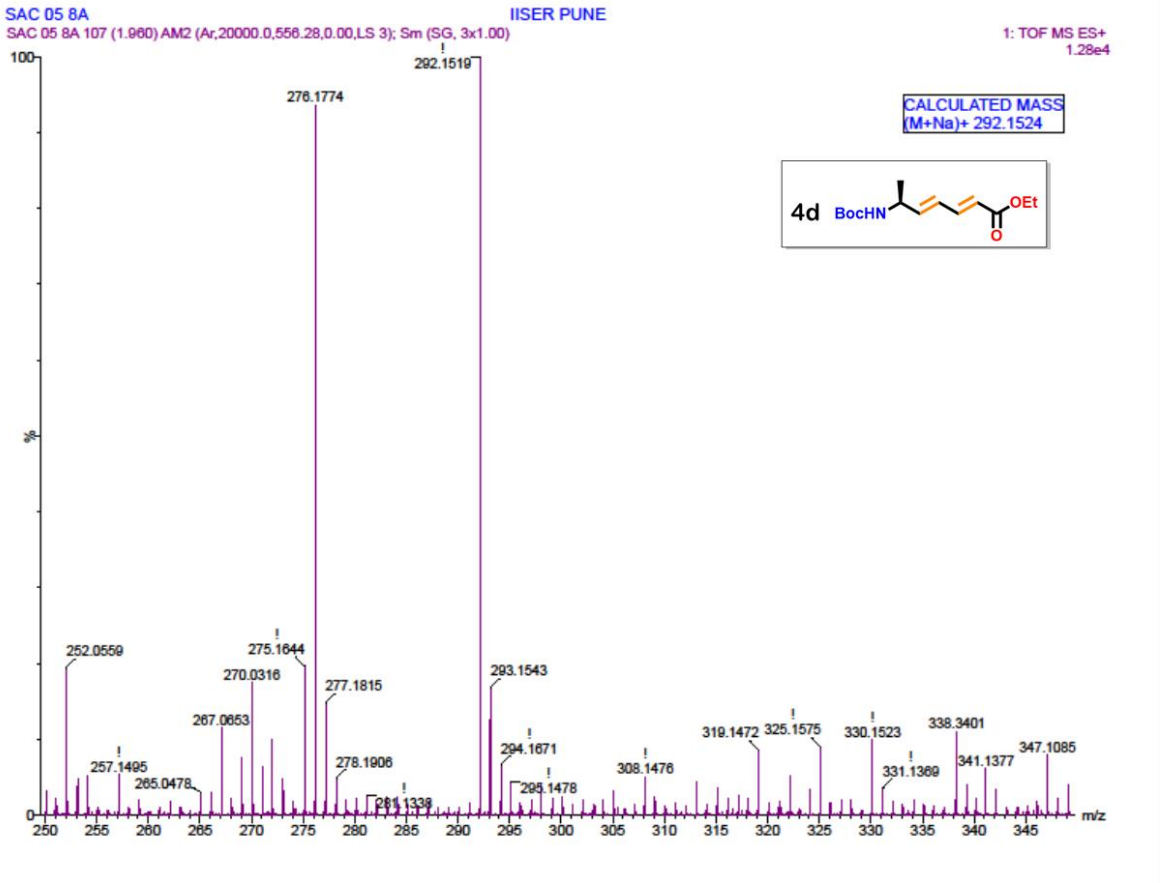

7.30
7.27
7.26 CDCl3
7.24
6.24
6.21
6.18
6.15
5.85
5.81
4.62
4.21
4.19
4.18
4.16
1.41
1.39
1.30
1.28
1.26
-0.01
4c
BocHN
OEt
O
1.14
2.00
1.00
f1 (ppm)

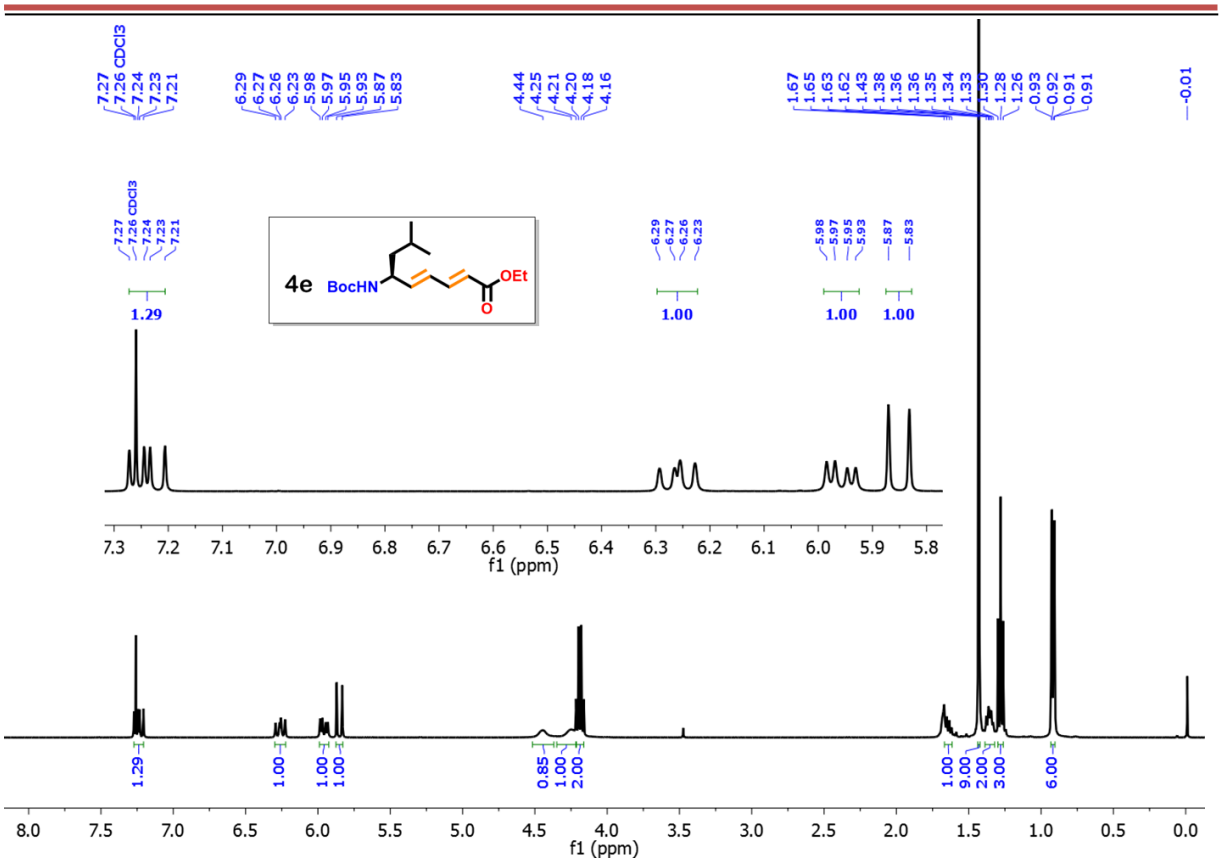

167.13
154.38
148.81
144.62
125.18
121.01
79.50
77.48 CDCl3
77.16 CDCl3
76.84 CDCl3
60.38
53.24
28.52
27.73
14.42
-0.13
4c
BocHN
OEt
O
f1 (ppm)

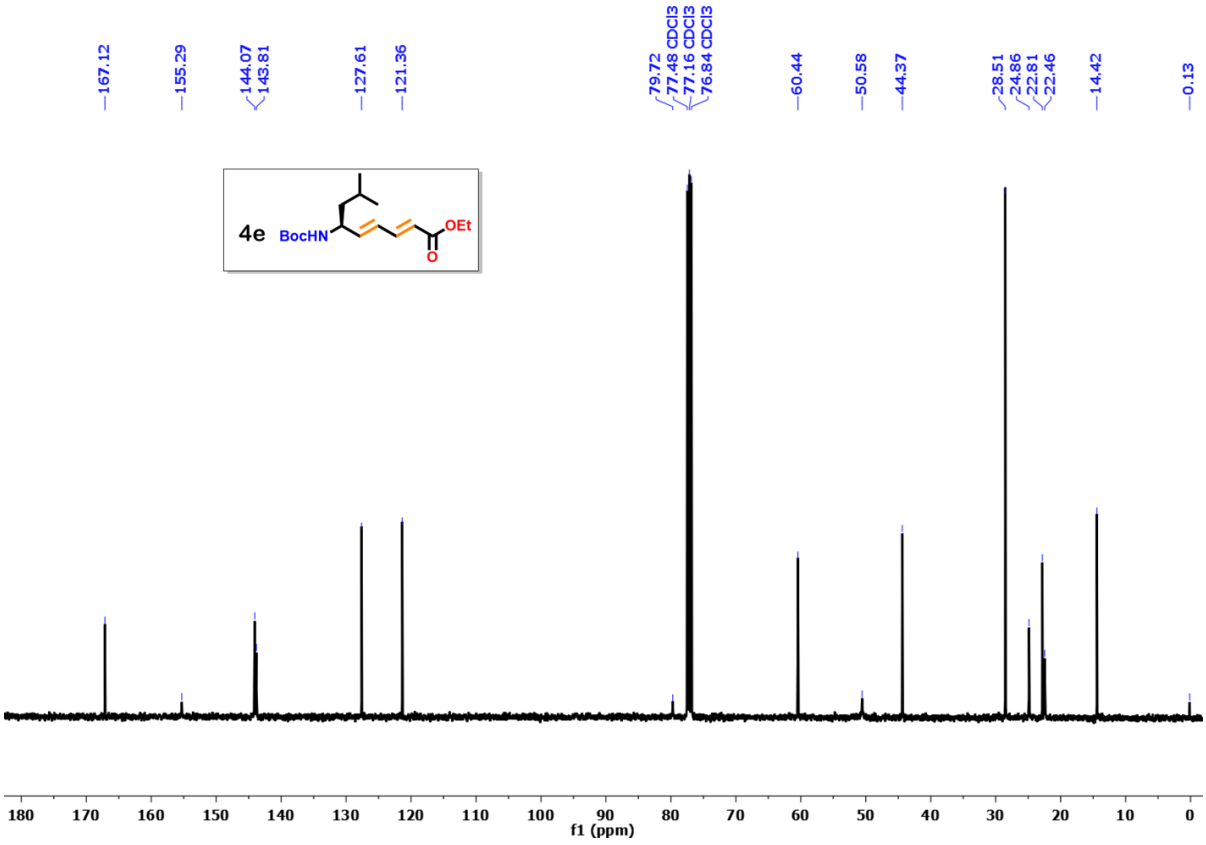

SAC 178E DI
IISER PUNE
SAC 178E DI 1 (0.052) AM2 (Ar,10000.0,556.28,0.00,LS 3); Sm (SG, 3x1.00)
1: TOF MS ES+
1.25e6
306.1677
CALCULATED MASS
(M+Na)+ 306.1681
4c BocHN OEt O
307.1711
167.1060
250.1050
93.0677
338.3412
360.3230
139.0747
361.3259
202.1796
251.1087
413.2680
507.2699
589.3513
663.4557
685.4346
701.4108
794.7109
m/z

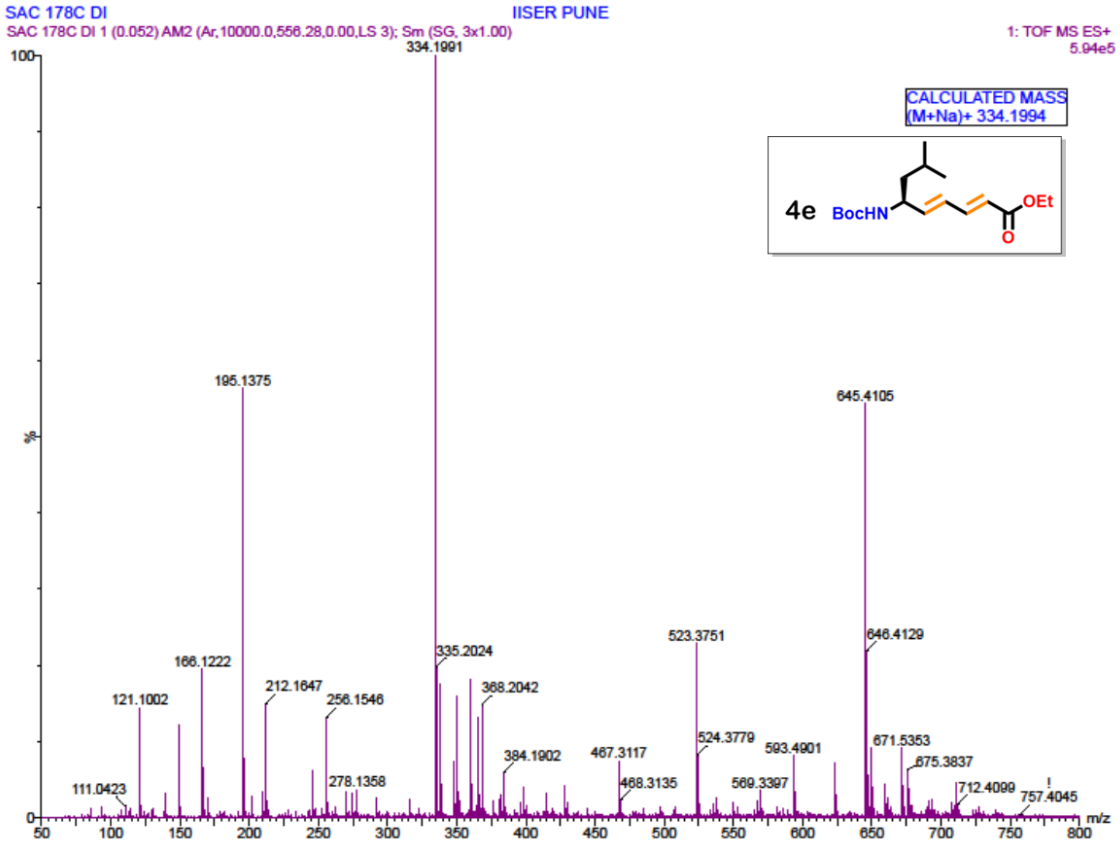

7.27 CDCl3
7.26
7.24
7.23
7.20
6.27
6.24
6.23
6.20
6.05
6.03
6.01
6.00
5.87
5.83
4.54
4.32
4.21
4.19
4.17
4.16
1.43
1.29
1.27
1.26
1.24
1.23
4d BocHN OEt O
1.00
f1 (ppm)
f1 (ppm)

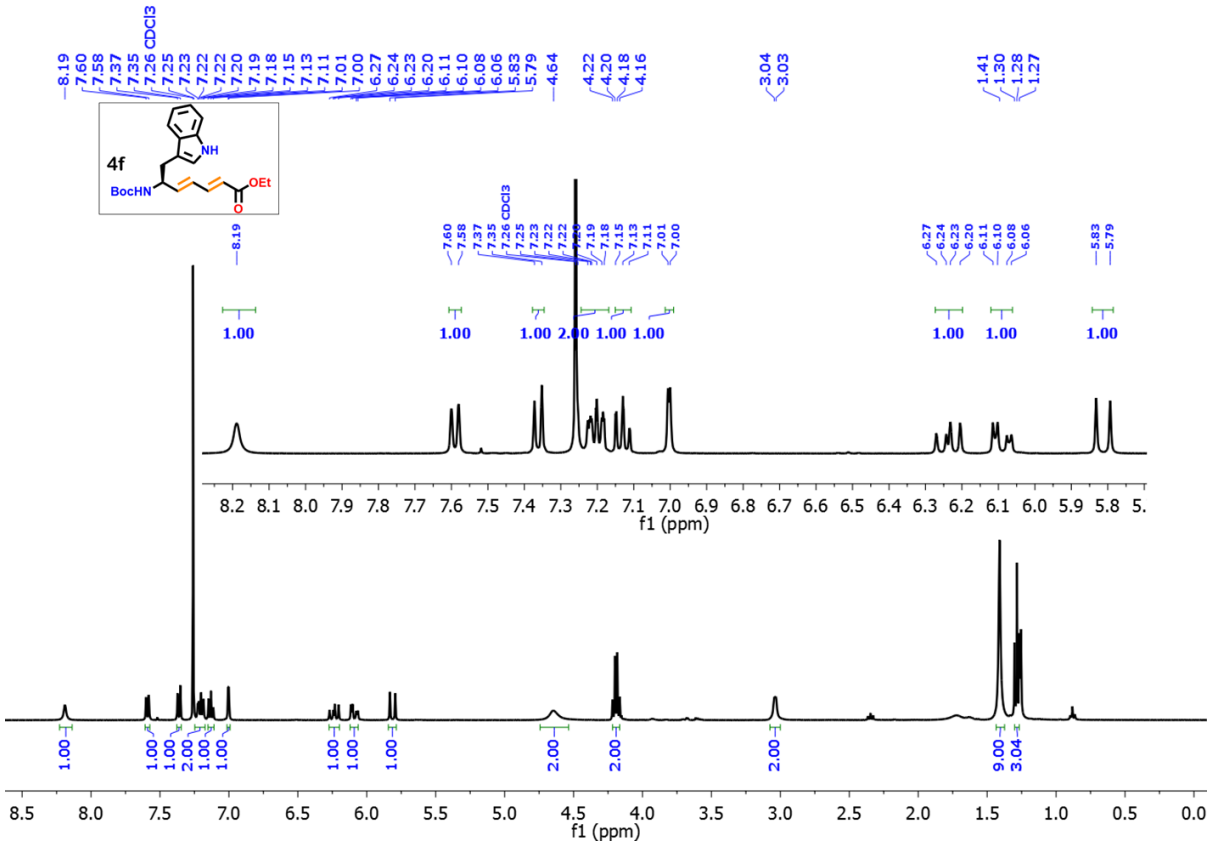

167.07
155.14
144.30
143.98
127.15
121.53
79.79
77.48 CDCl3
77.16 CDCl3
76.84 CDCl3
60.46
47.69
28.51
20.78
14.41
0.13
4d BocHN OEt O
f1 (ppm)

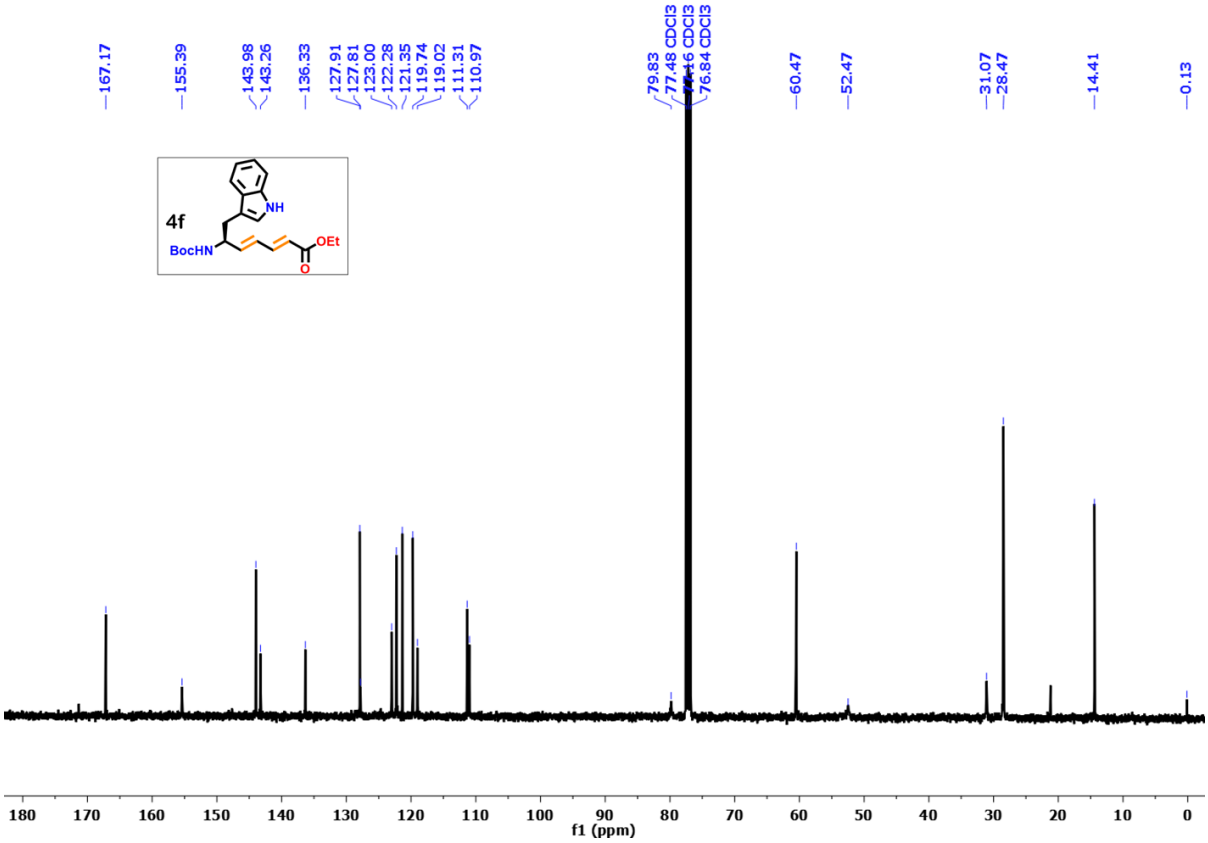

SAC 05 8A
IISER PUNE
SAC 05 8A 107 (1.960) AM2 (Ar,20000.0,556.28,0.00,LS 3); Sm (SG, 3x1.00)
1: TOF MS ES+
1.28e4
CALCULATED MASS
(M+Na)+ 292.1524
4d BocHN OEt O
292.1519
276.1774
252.0559
275.1644
270.0316
277.1815
293.1543
267.0653
294.1671
257.1495
278.1906
265.0478
295.1478
308.1476
319.1472
325.1575
330.1523
338.3401
331.1369
341.1377
347.1085
%
m/z

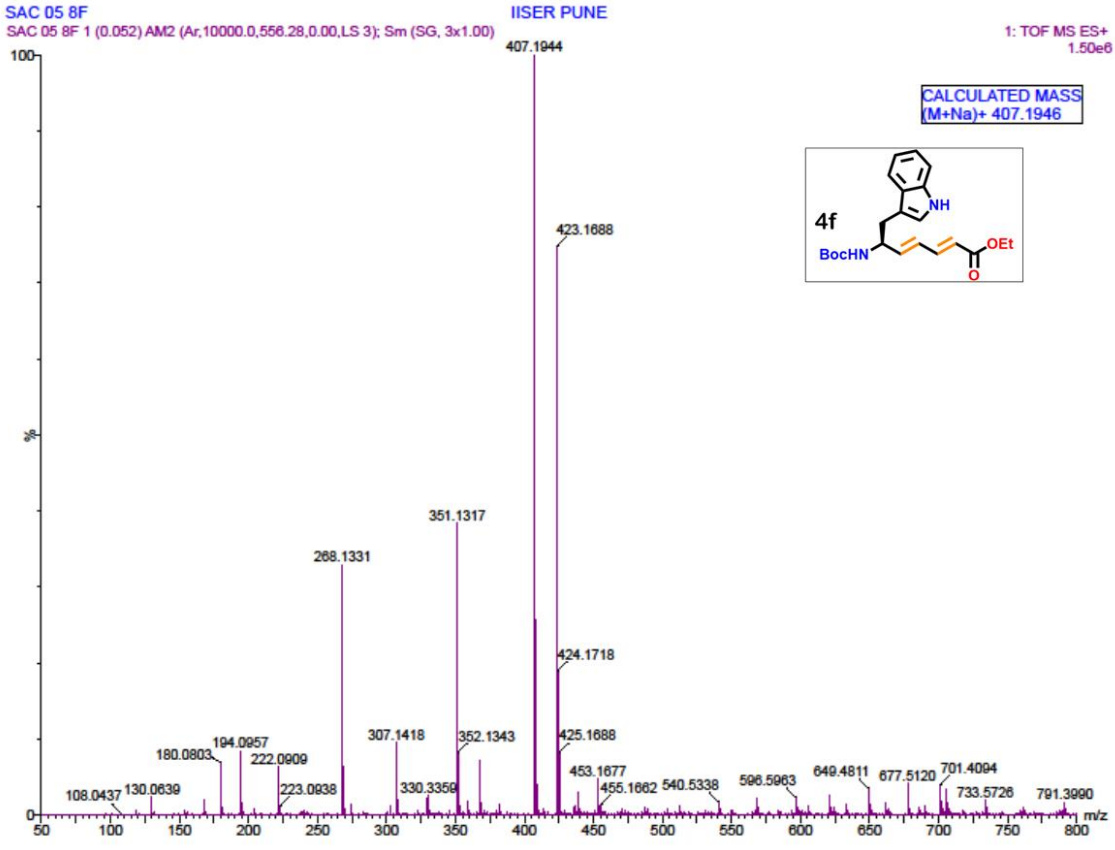

4e
BocHN
OEt
O
f1 (ppm)

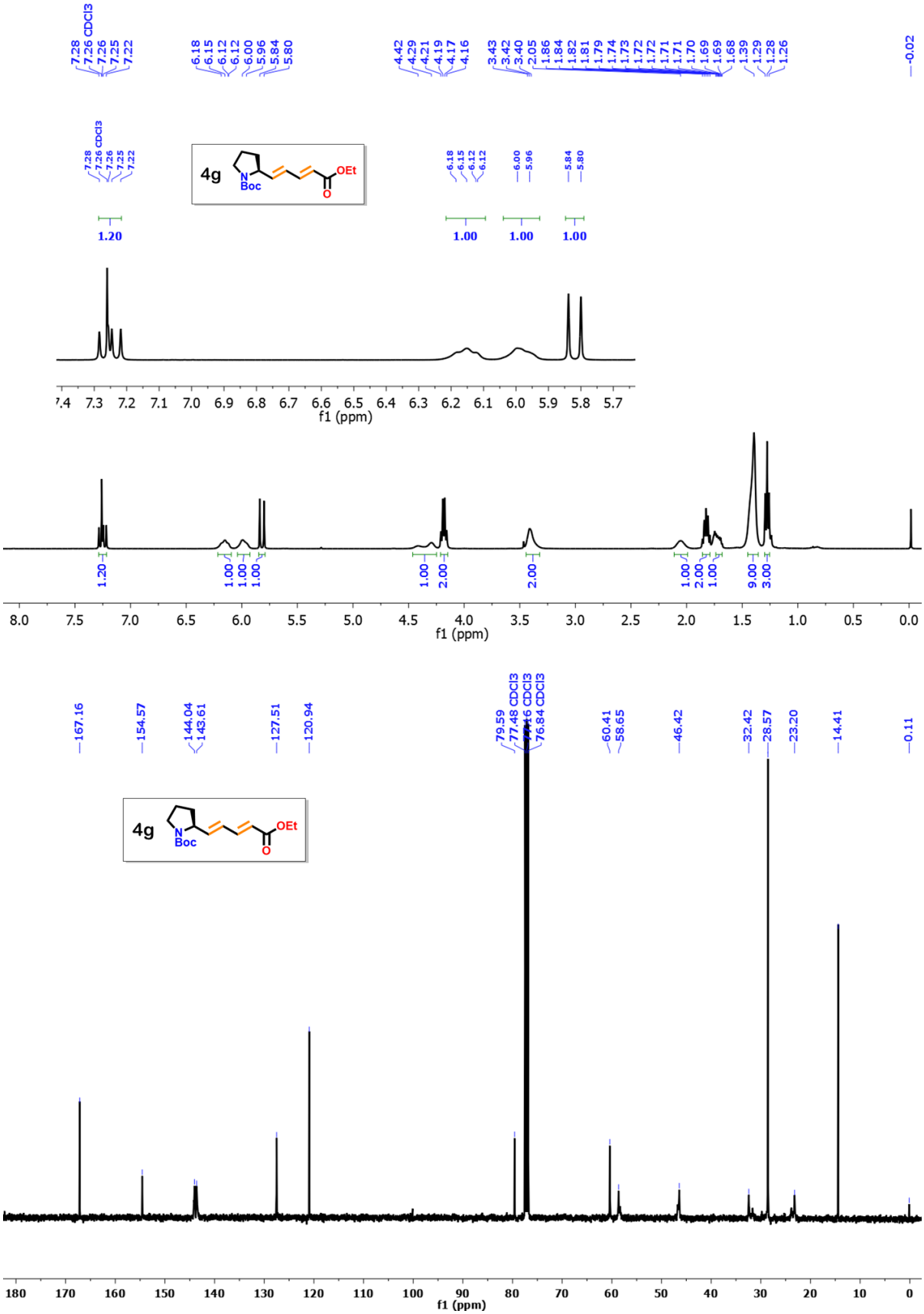

4e
BocHN
OEt
O
f1 (ppm)

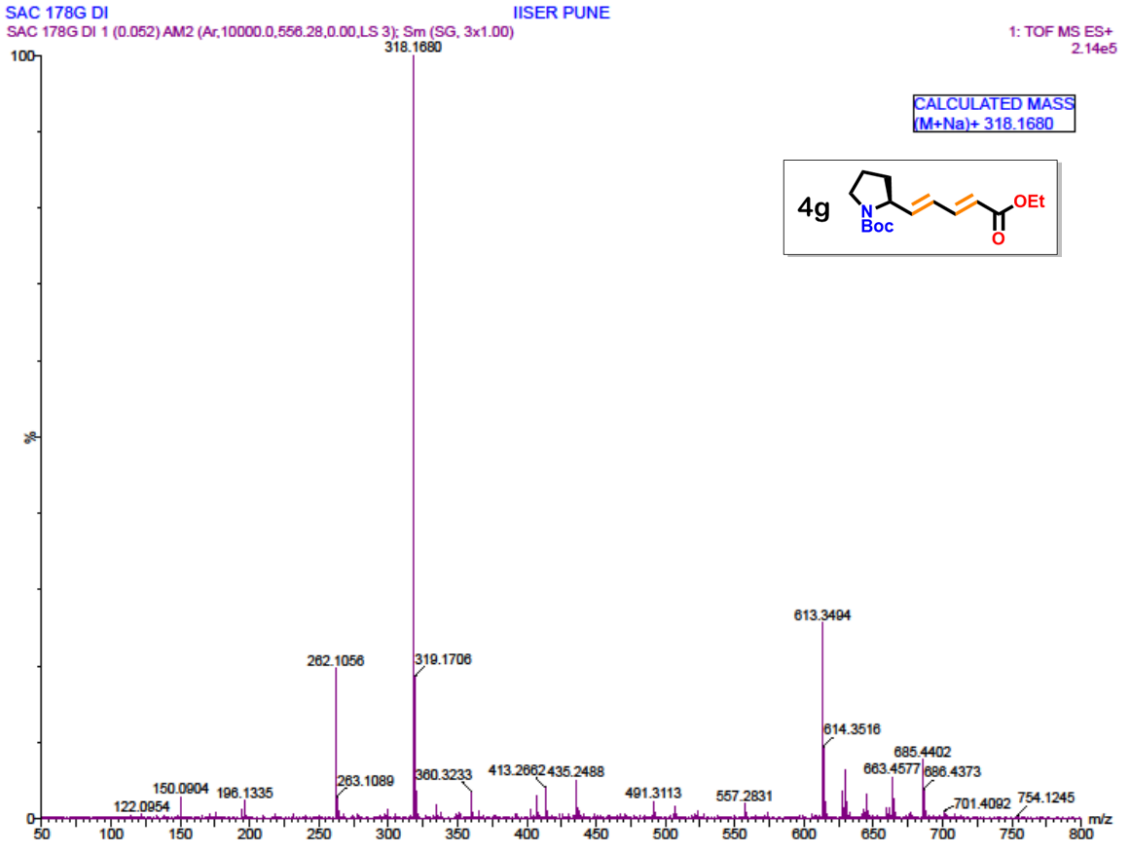

SAC 178C DI
IISER PUNE
SAC 178C DI 1 (0.052) AM2 (Ar,10000.0,556.28,0.00,LS 3); Sm (SG, 3x1.00)
1: TOF MS ES+
5.94e5
CALCULATED MASS
(M+Na)+ 334.1994
4e
BocHN
OEt
O
334.1991
195.1375
645.4105
523.3751
646.4129
335.2024
166.1222
212.1647
368.2042
121.1002
256.1546
524.3779
593.4901
671.5353
384.1902
467.3117
675.3837
278.1358
468.3135
569.3397
712.4099
757.4045
111.0423
%
m/z

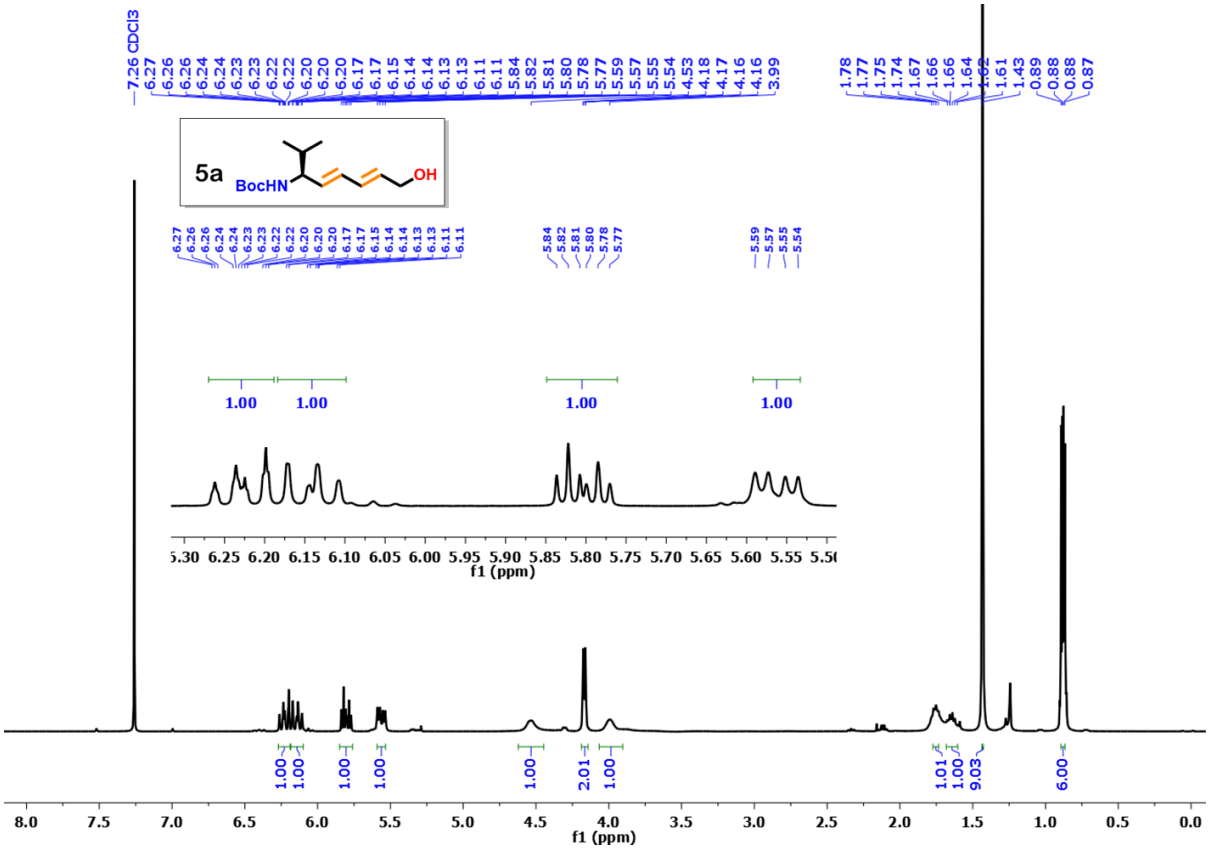

CDCl3
4f
NH
BocHN
OEt
O
f1 (ppm)

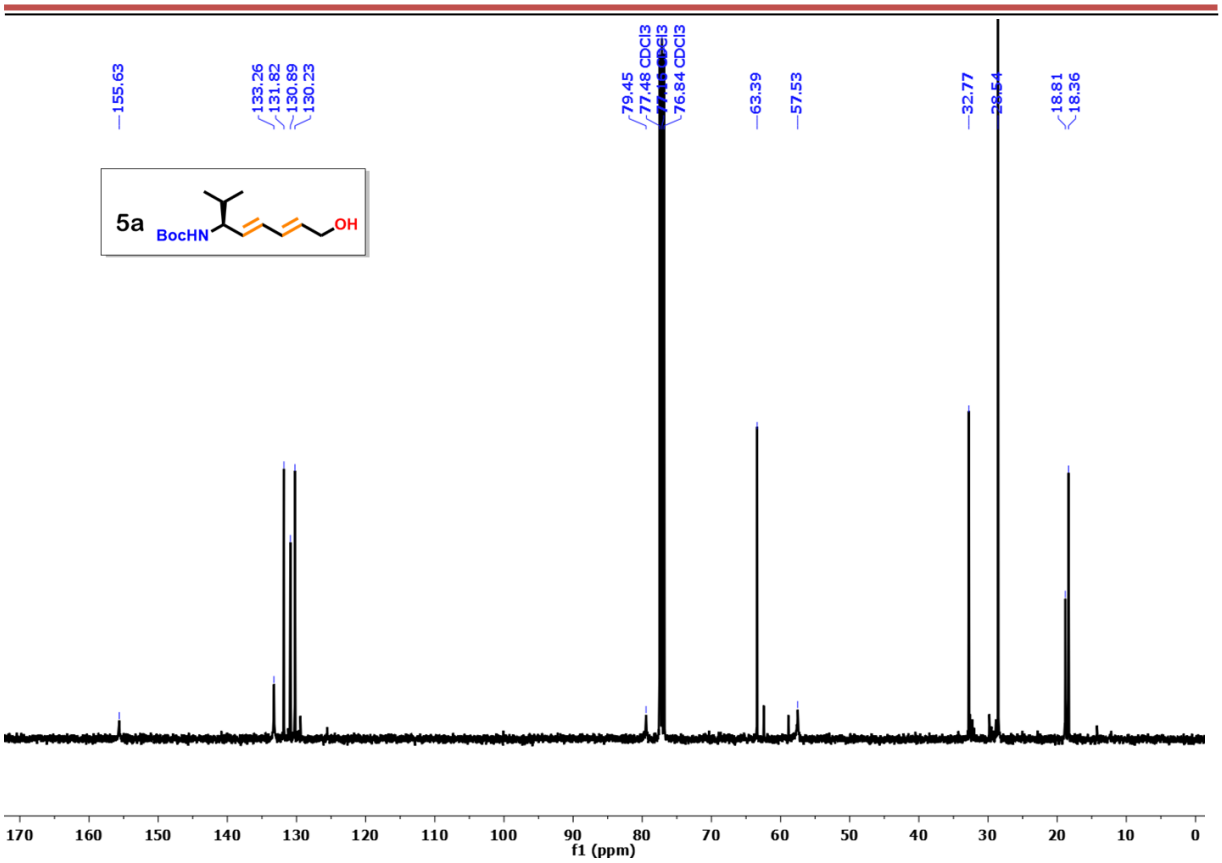

167.17
155.39
143.98
143.26
136.33
127.91
127.81
123.00
122.28
121.35
119.74
119.02
111.31
110.97
79.83
77.48 CDCl3
76.84 CDCl3
60.47
52.47
31.07
28.47
14.41
0.13
4f
NH
BocHN
OEt
O
f1 (ppm)

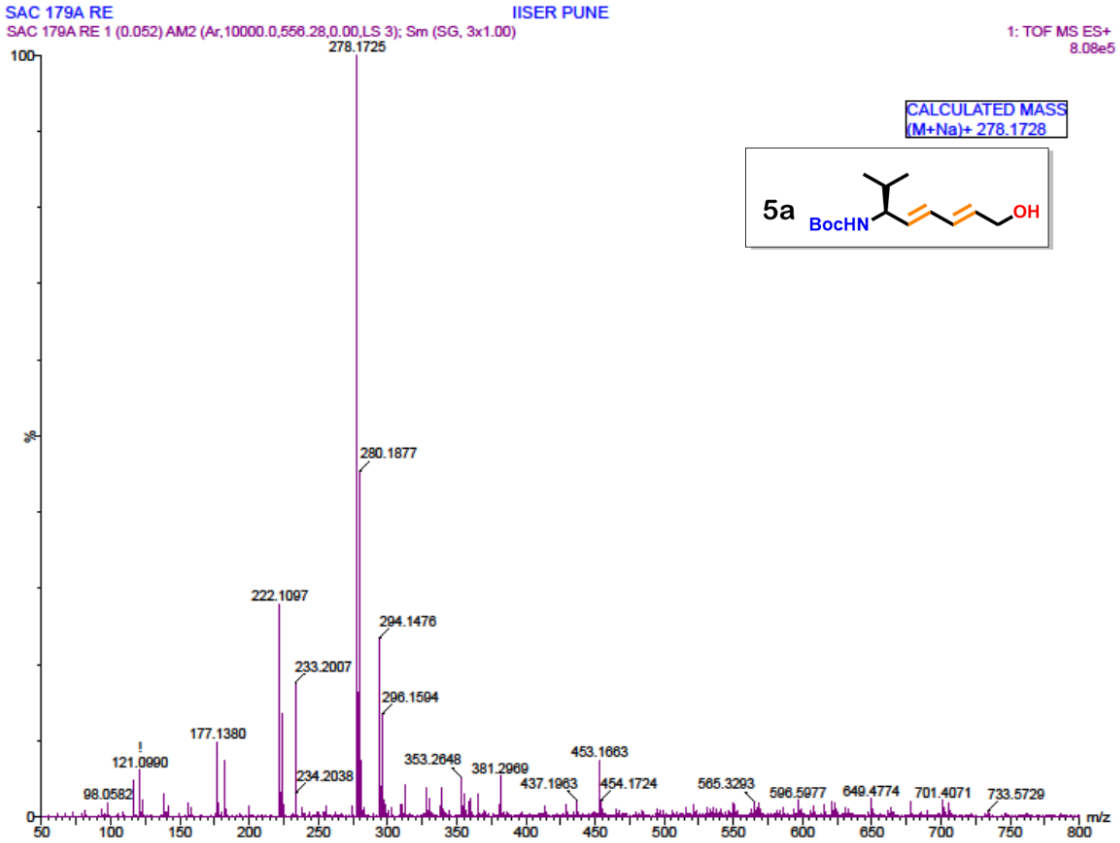

SAC 05 8F
IISER PUNE
SAC 05 8F 1 (0.052) AM2 (Ar,10000.0,556.28,0.00,LS 3); Sm (SG, 3x1.00)
1: TOF MS ES+
1.50e6
CALCULATED MASS
(M+Na)+ 407.1946
4f
NH
BocHN
OEt
O
407.1944
423.1688
351.1317
268.1331
424.1718
425.1688
307.1418
352.1343
194.0957
180.0803
222.0909
223.0938
108.0437
130.0639
330.3359
453.1677
455.1662
540.5338
596.5963
649.4811
677.5120
701.4094
733.5726
791.3990
%
m/z

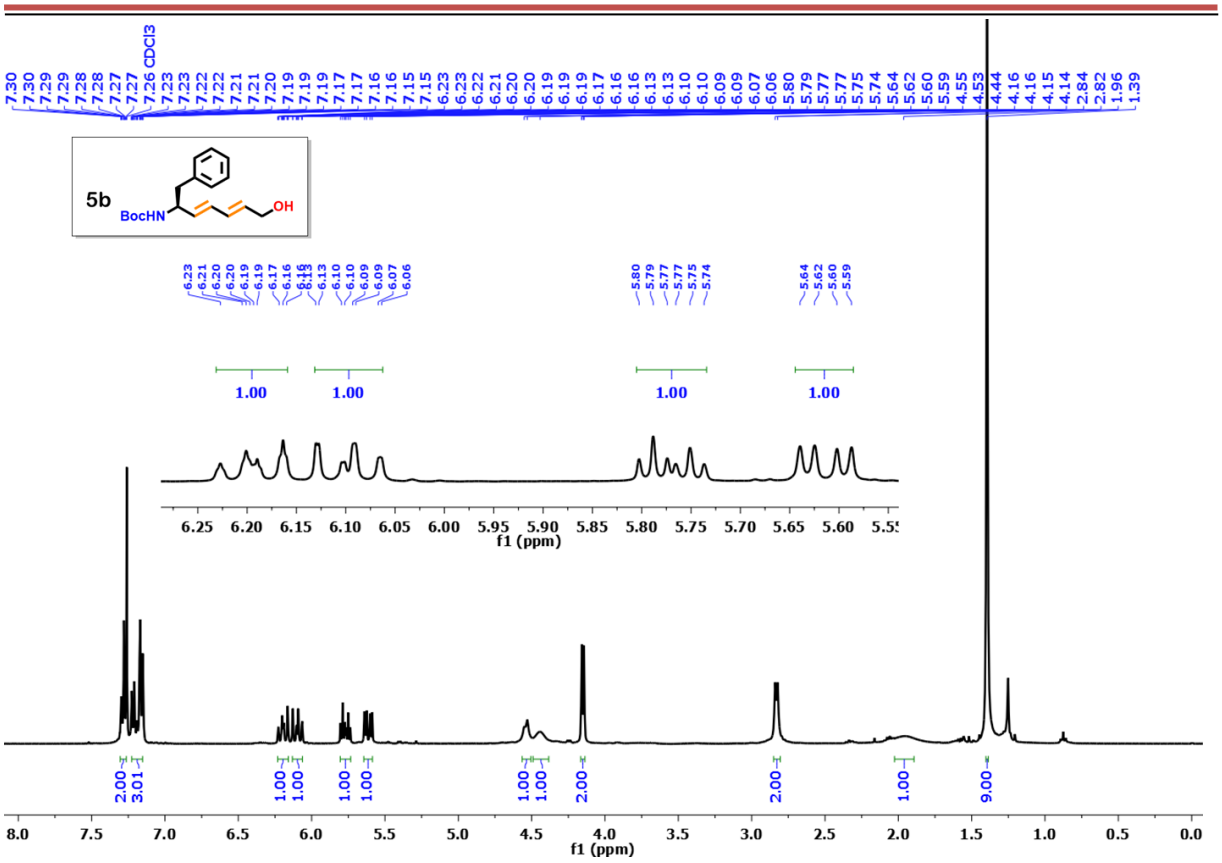

7.28
7.26 CDCl3
7.26
7.25
7.22
6.18
6.15
6.12
6.12
6.00
5.96
5.84
5.80
4.42
4.29
4.21
4.19
4.17
4.16
3.43
3.42
3.40
2.05
1.86
1.84
1.82
1.81
1.79
1.74
1.73
1.72
1.72
1.71
1.71
1.70
1.69
1.69
1.68
1.39
1.29
1.28
1.26
-0.02
4g
Boc
OEt
O
1.20
1.00
1.00
1.00
f1 (ppm)
1.20
1.00
1.00
1.00
2.00
2.00
1.00
2.00
1.00
9.00
3.00
f1 (ppm)
167.16
154.57
144.04
143.61
127.51
120.94
79.59
77.48 CDCl3
77.16 CDCl3
76.84 CDCl3
60.41
58.65
46.42
32.42
28.57
23.20
14.41
0.11
4g
Boc
OEt
O
f1 (ppm)

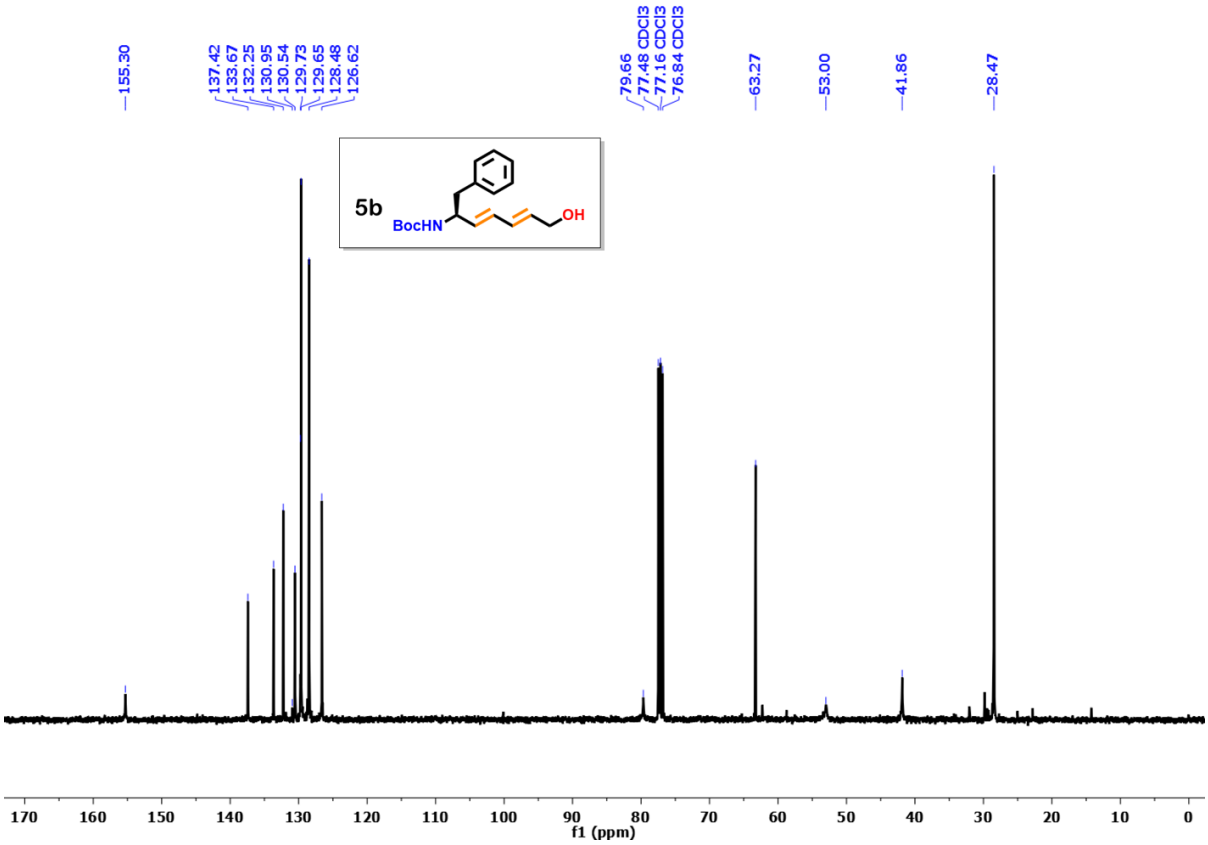

SAC 178G DI
IISER PUNE
SAC 178G DI 1 (0.052) AM2 (Ar,10000.0,556.28,0.00,LS 3); Sm (SG, 3x1.00)
1: TOF MS ES+
2.14e5
CALCULATED MASS
(M+Na)+ 318.1680
4g
Boc
OEt
O
318.1680
613.3494
262.1056
319.1706
614.3516
685.4402
663.4577
686.4373
360.3233
413.2662
435.2488
263.1089
150.0904
196.1335
122.0954
491.3113
557.2831
701.4092
754.1245
%
m/z

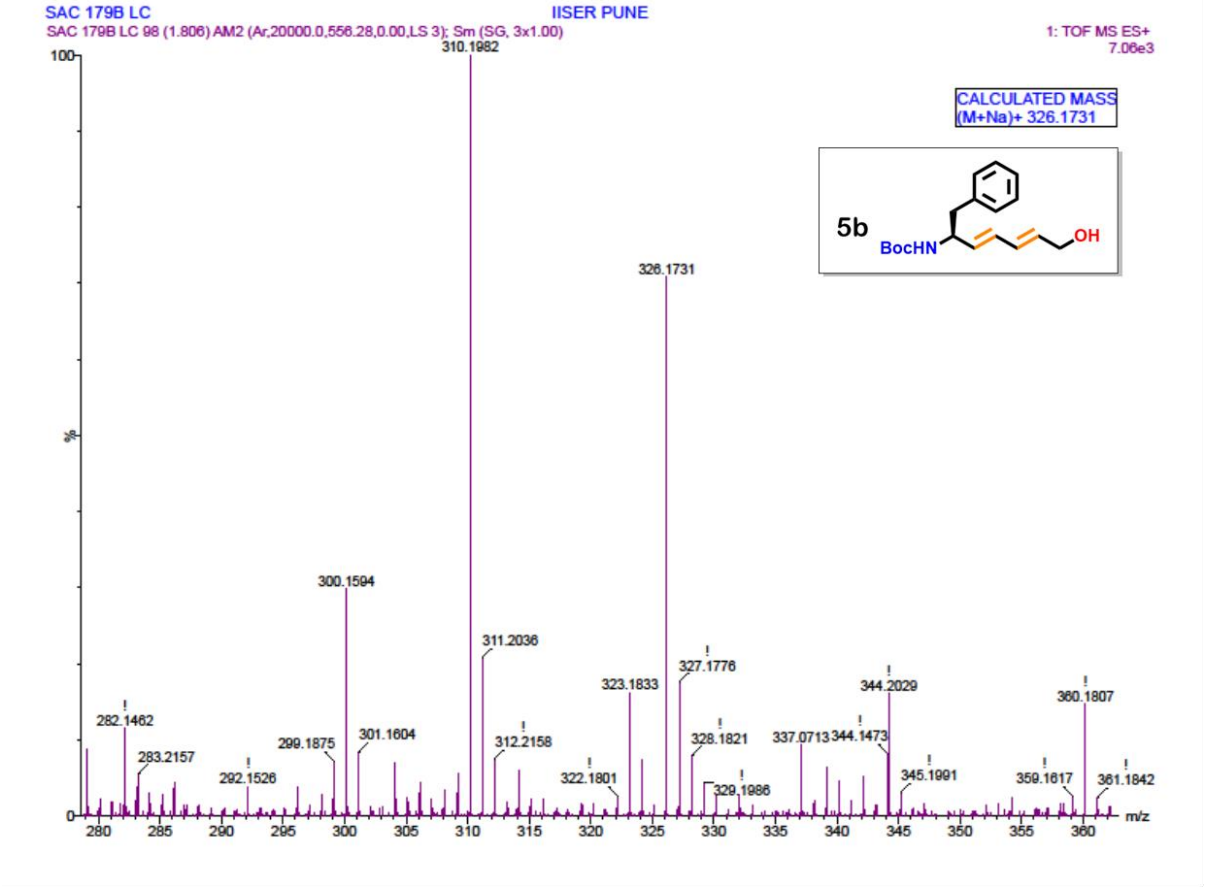

7.26 CDCl3
5a
BocHN
OH
1.00
1.00
1.00
1.00
f1 (ppm)
1.00
1.00
1.00
1.00
1.00
2.01
1.00
1.01
1.00
9.03
6.00
f1 (ppm)

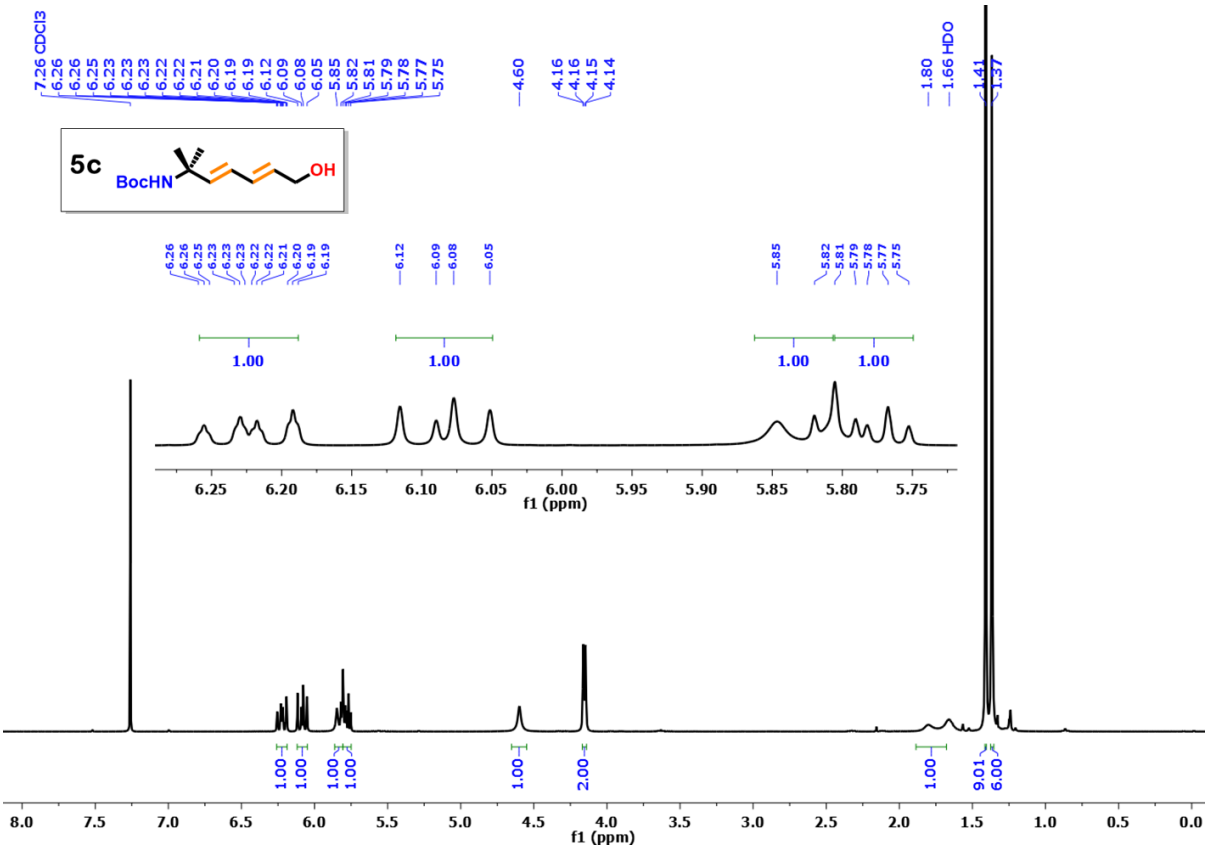

155.63
133.26
131.82
130.89
130.23
79.45
77.48 CDCl3
76.84 CDCl3
63.39
57.53
32.77
28.54
18.81
18.36
5a
BocHN
OH
f1 (ppm)

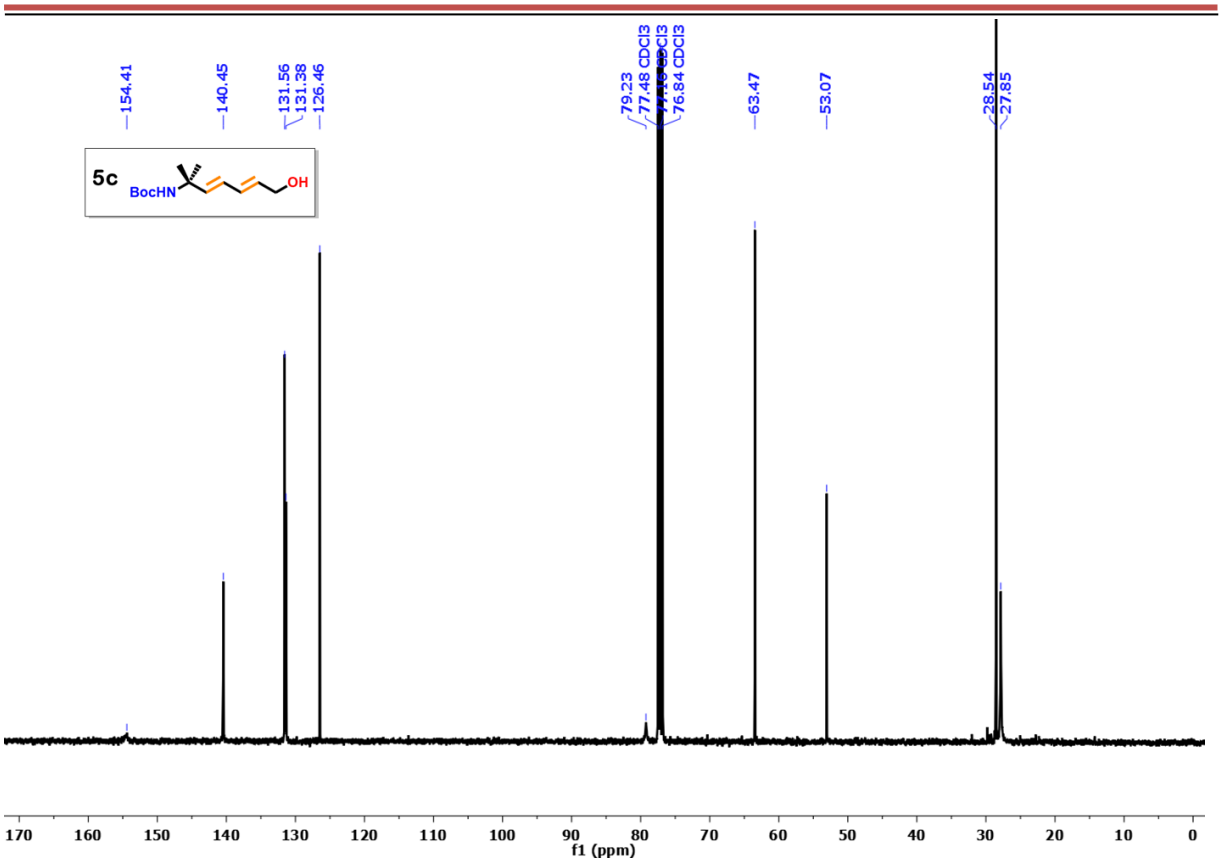

SAC 179A RE
IISER PUNE
SAC 179A RE 1 (0.052) AM2 (Ar,10000.0,556.28,0.00,LS 3); Sm (SG, 3x1.00)
1: TOF MS ES+
8.08e5
CALCULATED MASS
(M+Na)+ 278.1728
5a
BocHN
OH
278.1725
280.1877
222.1097
294.1476
233.2007
296.1594
177.1380
121.0990
98.0582
234.2038
353.2648
381.2969
437.1963
453.1663
454.1724
565.3293
596.5977
649.4774
701.4071
733.5729
%
m/z

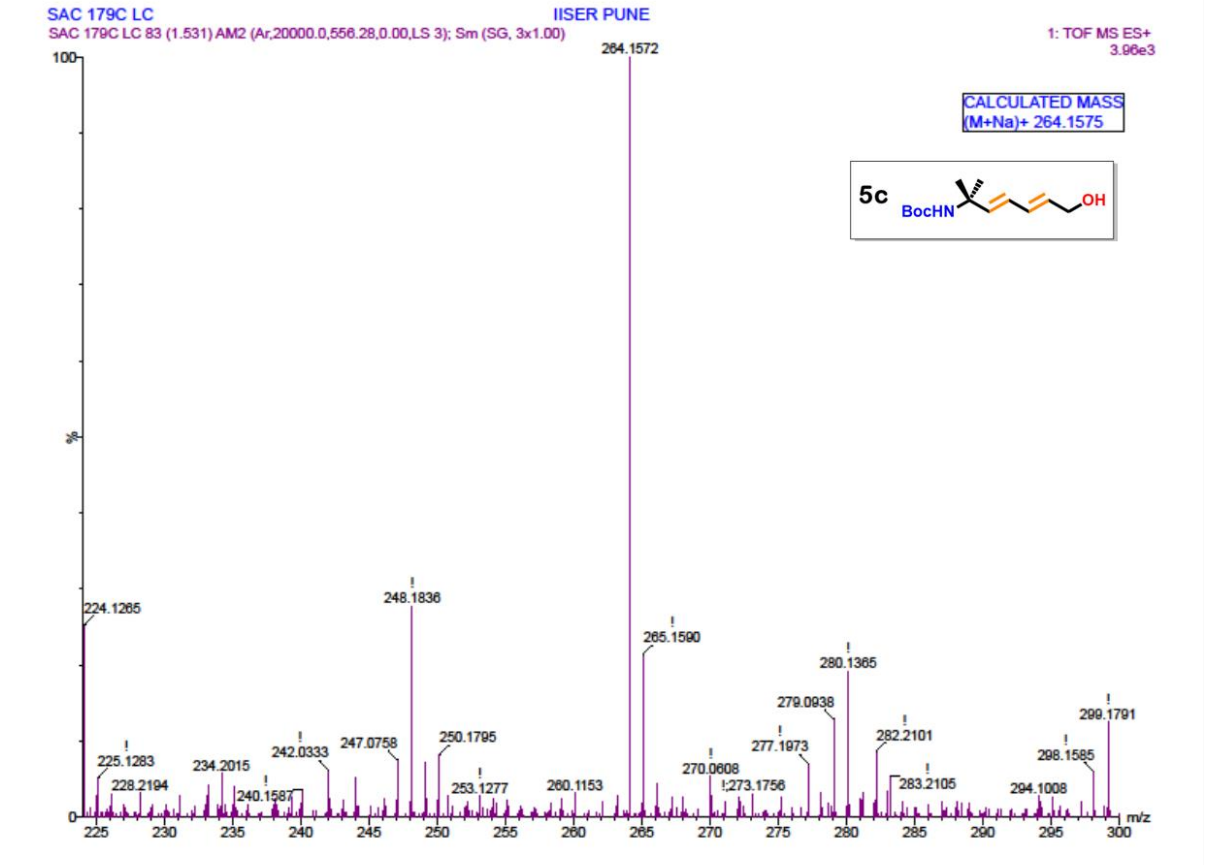

5b
BocHN
OH
f1 (ppm)

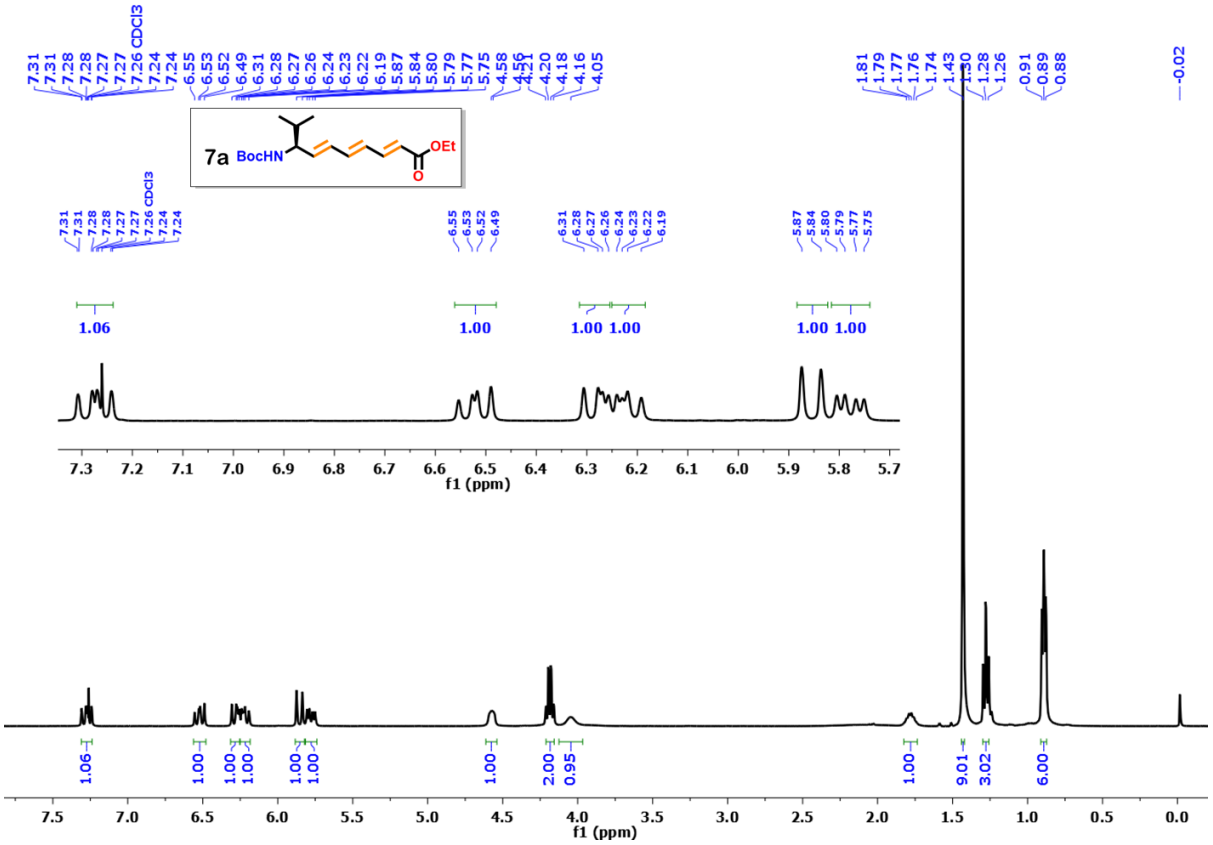

5b
BocHN
OH
f1 (ppm)

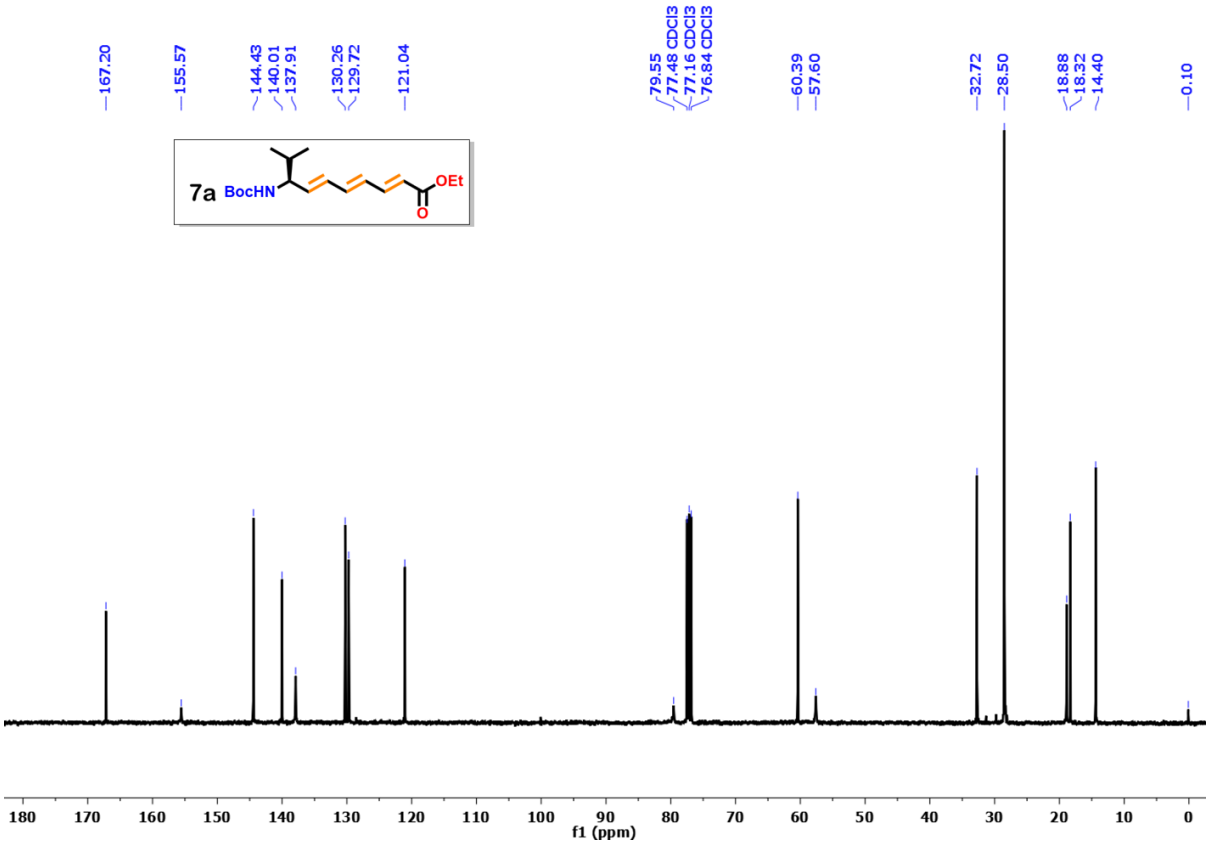

SAC 179B LC
IISER PUNE
SAC 179B LC 98 (1.806) AM2 (Ar,20000.0,556.28,0.00,LS 3); Sm (SG, 3x1.00)
1: TOF MS ES+
7.06e3
CALCULATED MASS
(M+Na)+ 326.1731
5b
BocHN
OH
310.1982
326.1731
300.1594
311.2036
327.1776
323.1833
344.2029
360.1807
282.1462
283.2157
299.1875
301.1604
312.2158
328.1821
337.0713
344.1473
345.1991
292.1526
322.1801
329.1986
359.1617
361.1842
%
m/z

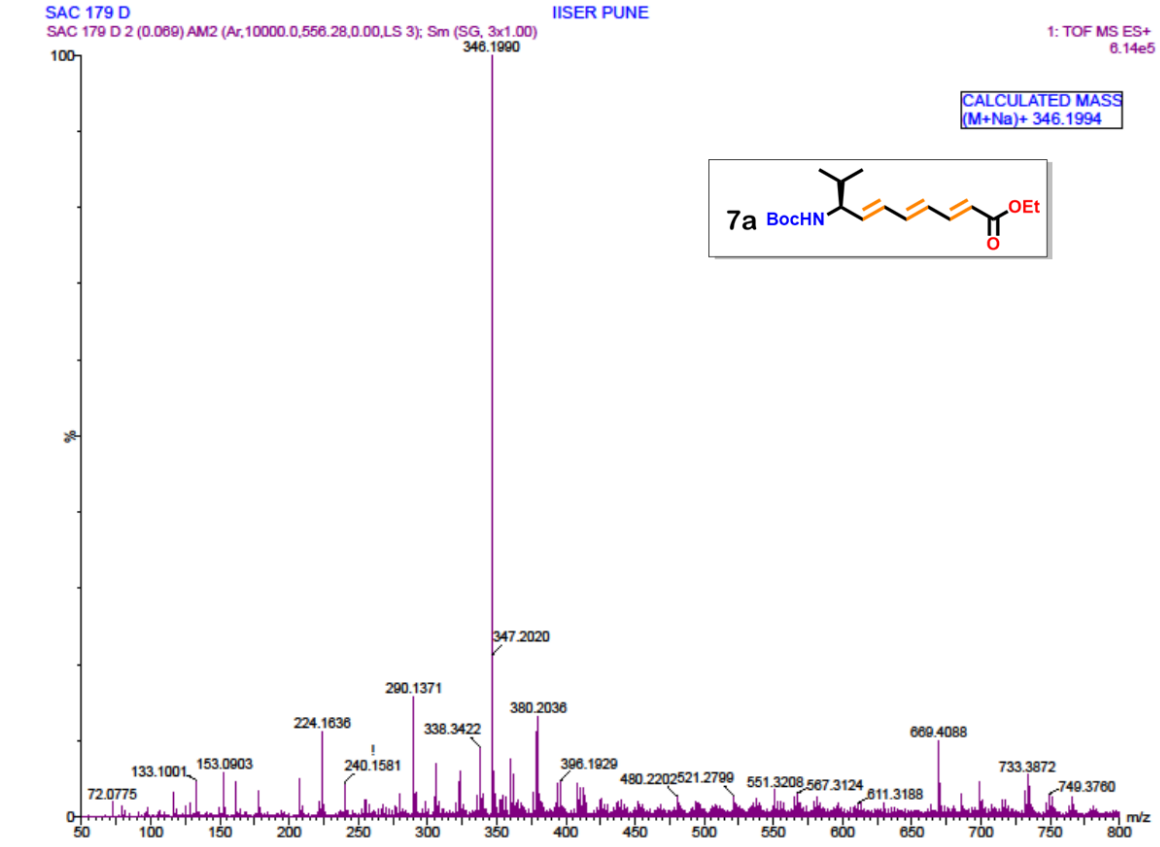

7.26 CDCl3
1.80 HDO
1.41
1.37
5c
BocHN
OH
1.00
1.00
1.00
1.00
f1 (ppm)
1.00
1.00
1.00
1.00
2.00
1.00
9.01
6.00
f1 (ppm)

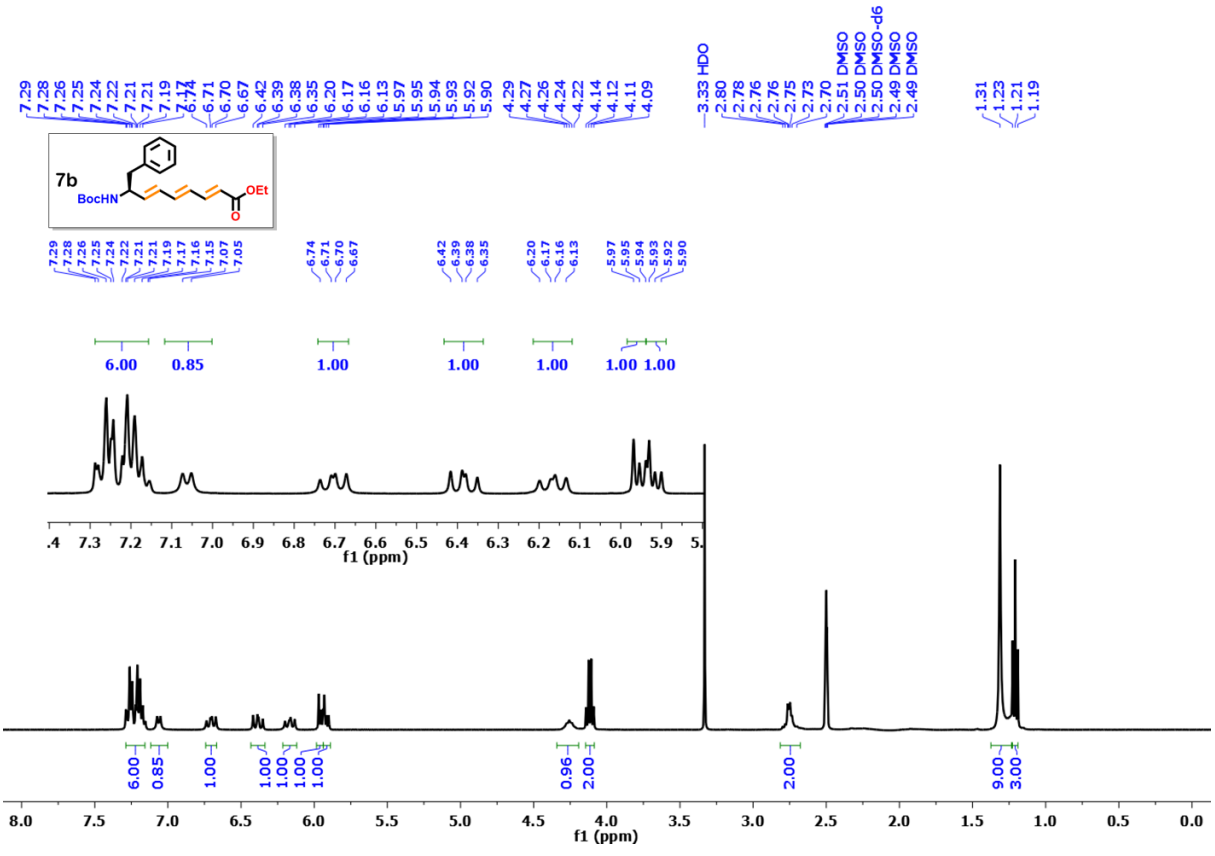

154.41
140.45
131.56
131.38
126.46
79.23
77.48 CDCl3
77.16 CDCl3
76.84 CDCl3
63.47
53.07
28.54
27.85
5c
BocHN
OH
f1 (ppm)

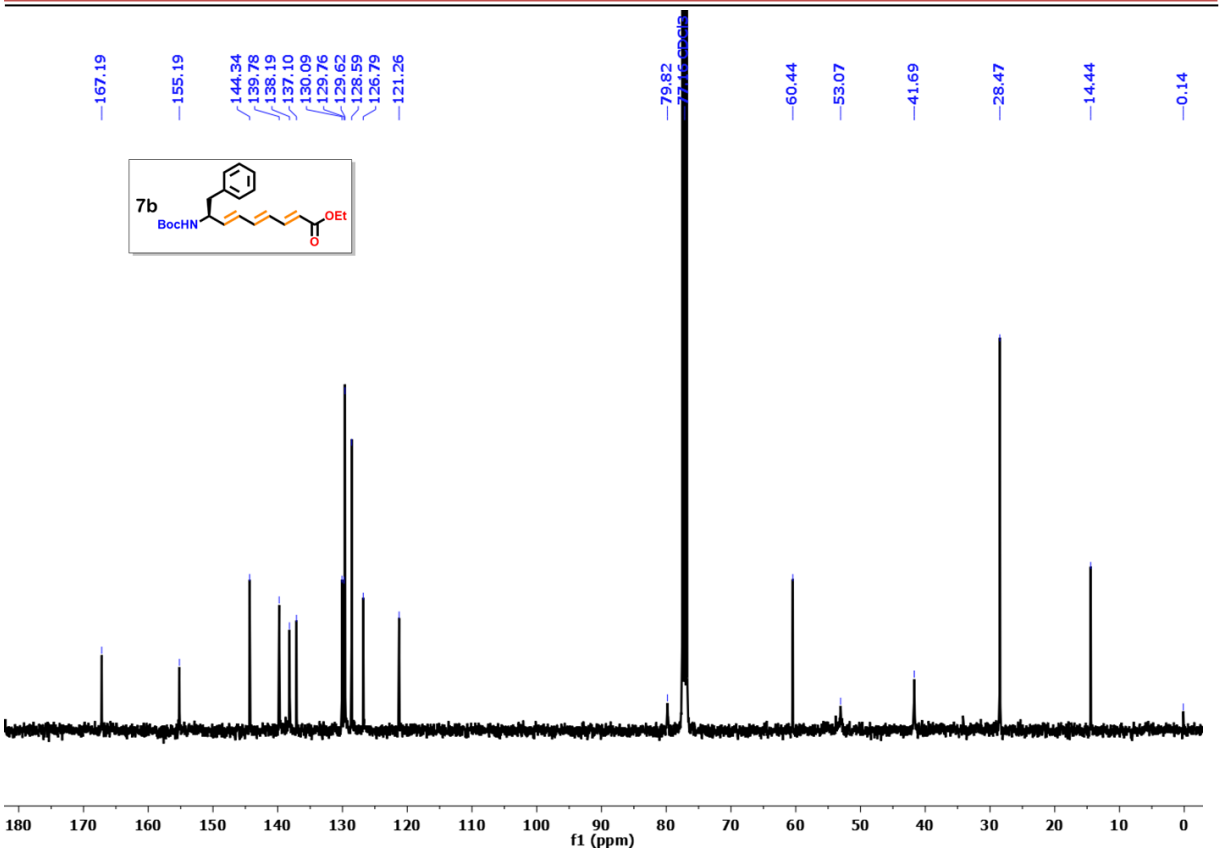

SAC 179C LC
IISER PUNE
SAC 179C LC 83 (1.531) AM2 (Ar,20000.0,556.28,0.00,LS 3); Sm (SG, 3x1.00)
1: TOF MS ES+
3.96e3
CALCULATED MASS
(M+Na)+ 264.1575
5c
BocHN
OH
264.1572
248.1836
224.1265
265.1590
280.1365
279.0938
299.1791
282.2101
277.1973
298.1585
225.1283
247.0758
250.1795
242.0333
234.2015
228.2194
240.1587
253.1277
260.1153
270.0608
273.1756
283.2105
294.1008
%
m/z

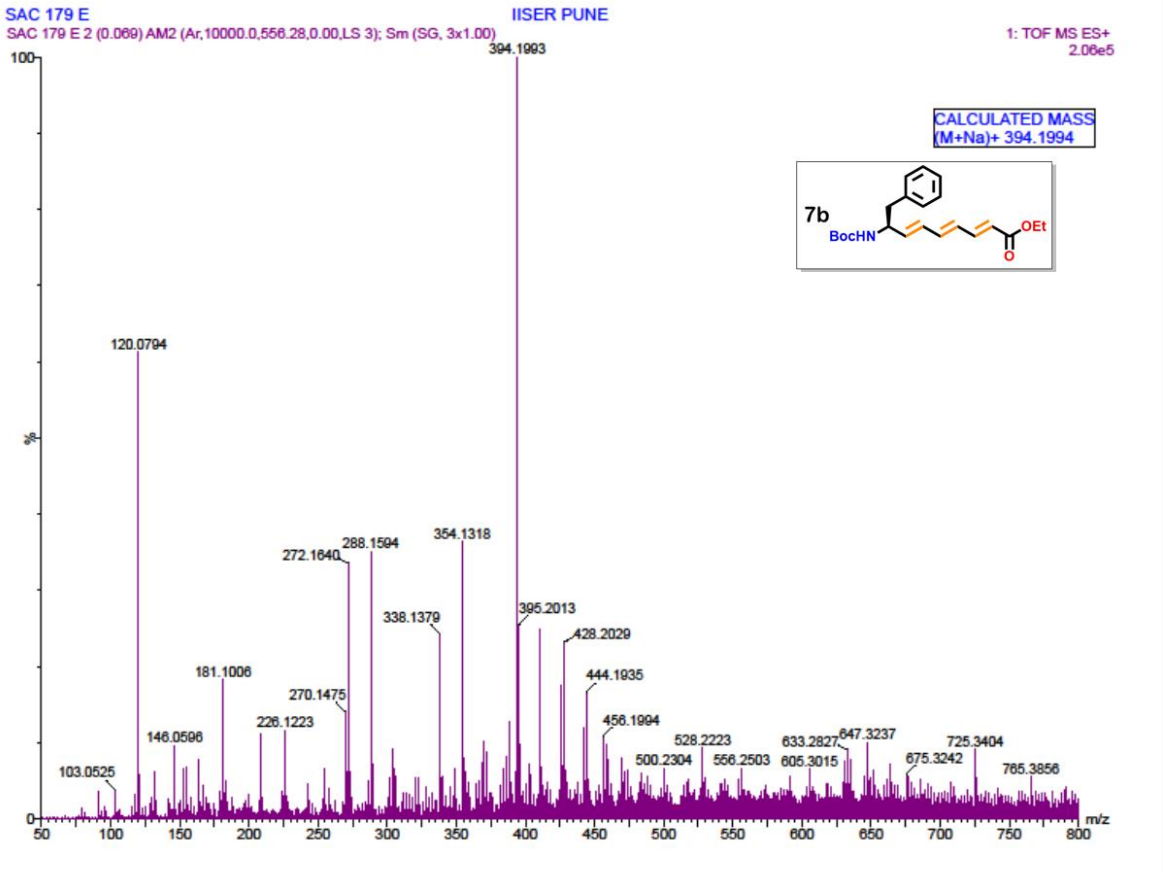

7a BocHN OEt O
f1 (ppm)

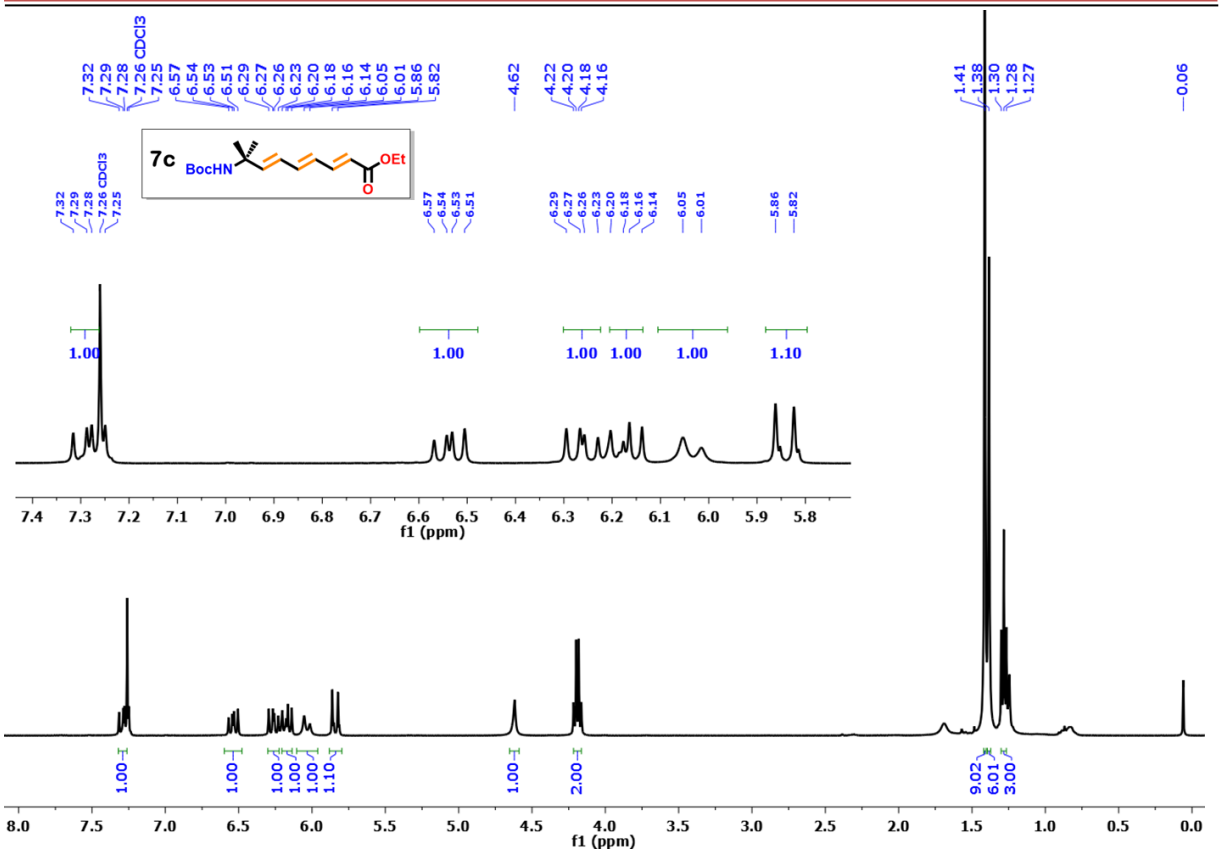

7a BocHN OEt O
f1 (ppm)

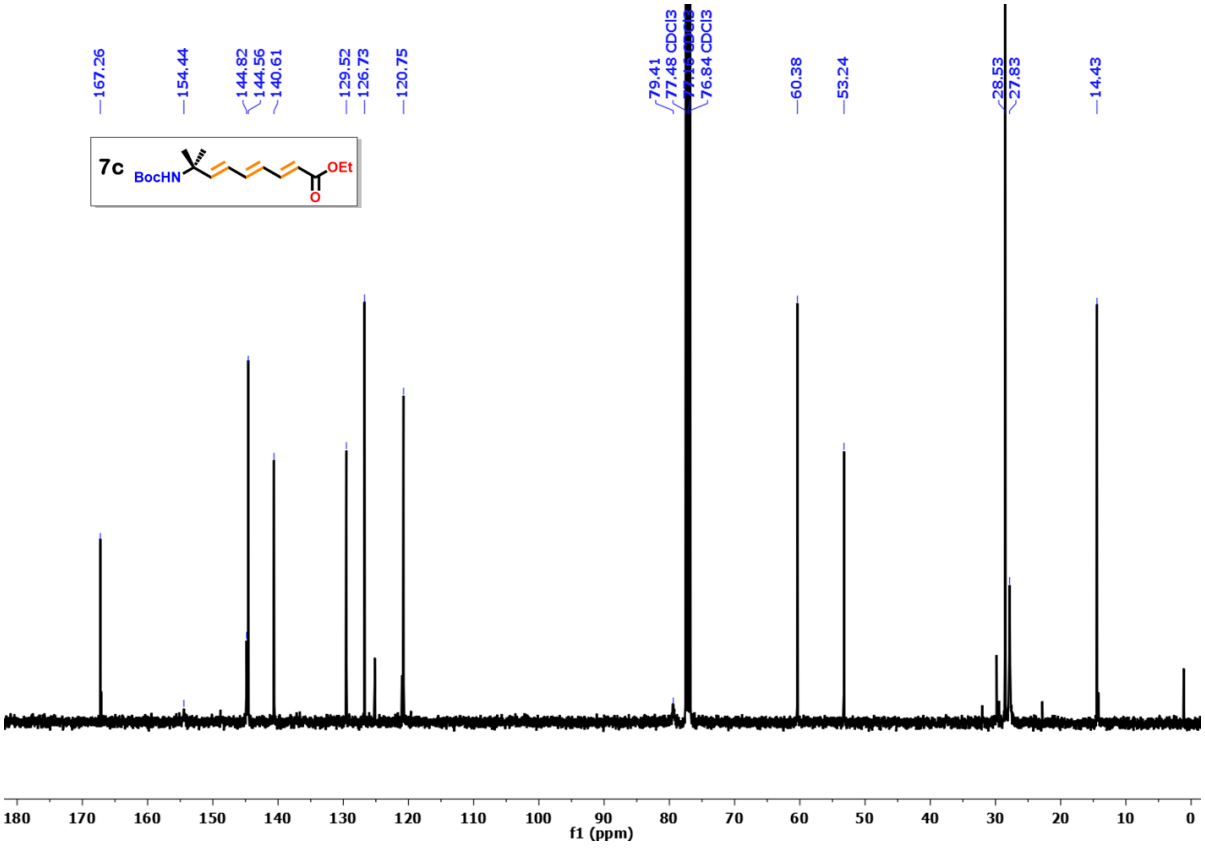

SAC 179 D
IISER PUNE
SAC 179 D 2 (0.069) AM2 (Ar,10000.0,556.28,0.00,LS 3); Sm (SG, 3x1.00)
1: TOF MS ES+
6.14e5
CALCULATED MASS
(M+Na)+ 346.1994
7a BocHN OEt O
346.1990
347.2020
290.1371
380.2036
338.3422
224.1636
240.1581
396.1929
669.4088
733.3872
749.3760
153.0903
133.1001
72.0775
480.2202
521.2799
551.3208
567.3124
611.3188
%
m/z

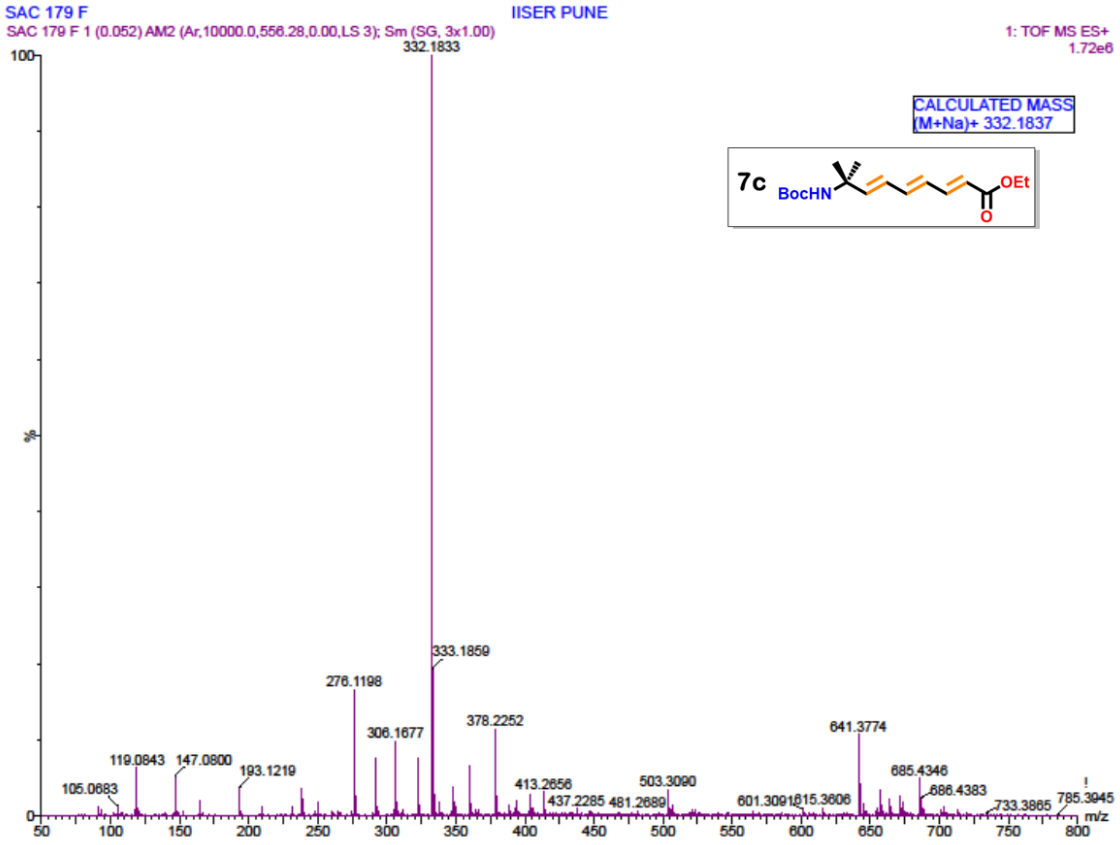

7b BocHN OEt O
HDO
DMSO
DMSO-d6
6.00
0.85
1.00
1.00
1.00
1.00
1.00
f1 (ppm)
0.85
0.96
2.00
9.00
3.00

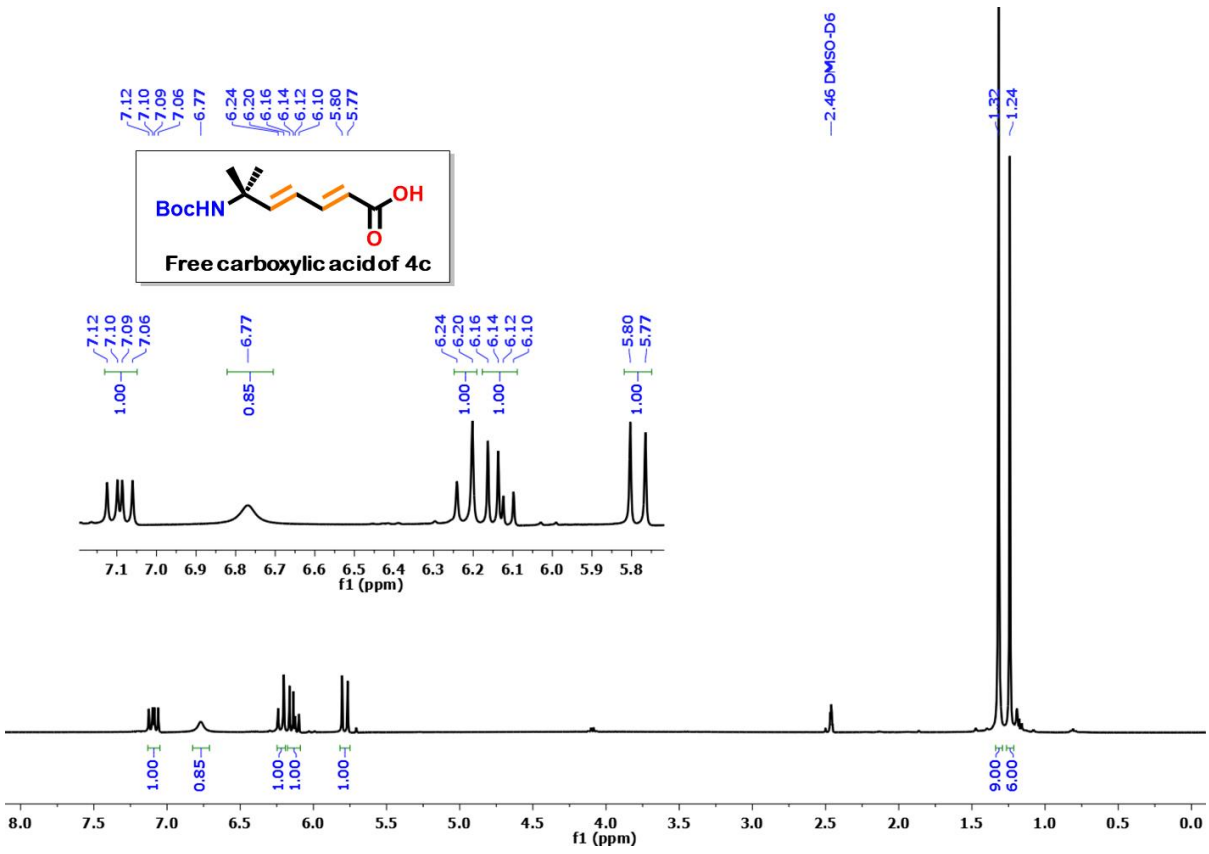

167.19
155.19
144.34
139.78
138.19
137.10
130.09
129.76
129.62
128.59
126.79
121.26
79.82
60.44
53.07
41.69
28.47
14.44
0.14
7b
BocHN
OEt
O
f1 (ppm)

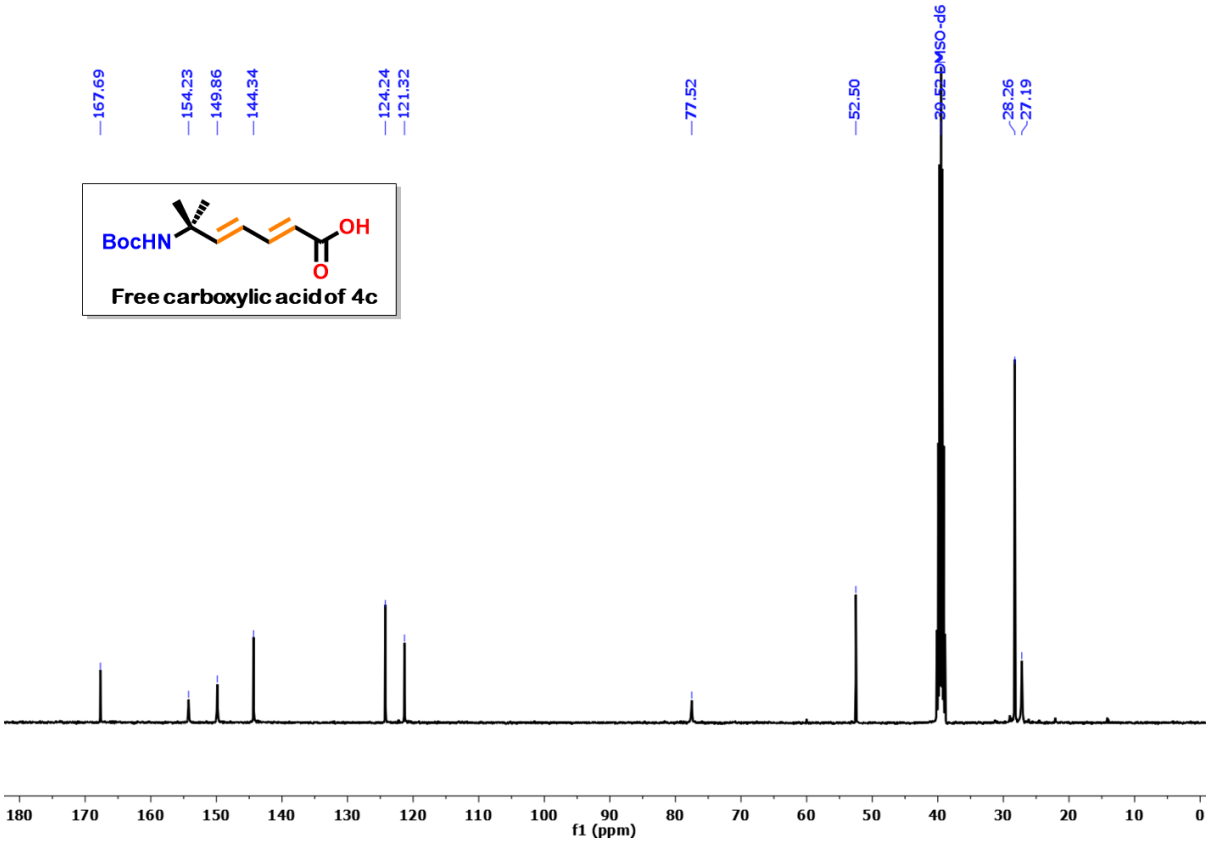

SAC 179 E
IISER PUNE
SAC 179 E 2 (0.069) AM2 (Ar,10000.0,556.28,0.00,LS 3); Sm (SG, 3x1.00)
1: TOF MS ES+
2.06e5
CALCULATED MASS
(M+Na)+ 394.1994
7b
BocHN
OEt
O
394.1993
120.0794
354.1318
288.1594
272.1640
338.1379
395.2013
428.2029
444.1935
181.1006
270.1475
456.1994
226.1223
146.0596
528.2223
633.2827
647.3237
725.3404
500.2304
556.2503
605.3015
675.3242
765.3856
103.0525
%
m/z

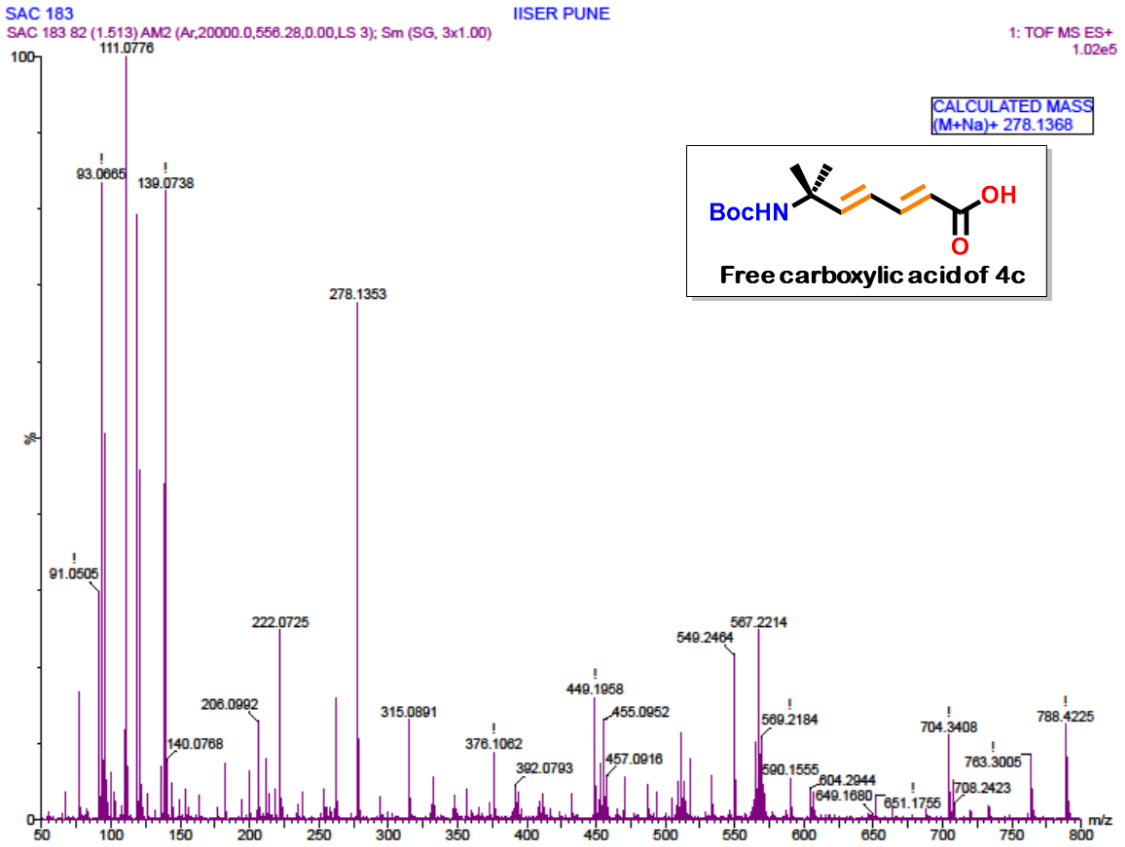

7c
BocHN
OEt
O
f1 (ppm)

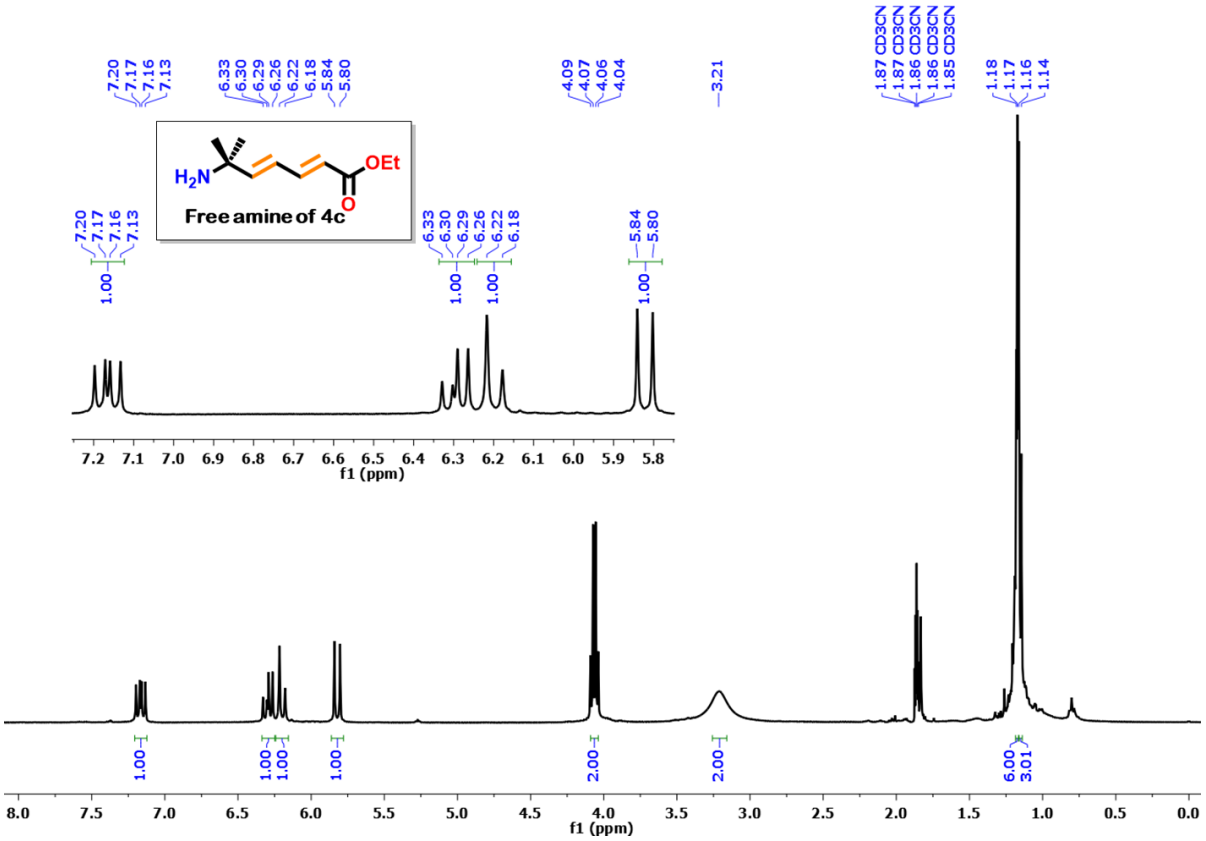

7c
BocHN
OEt
O
f1 (ppm)

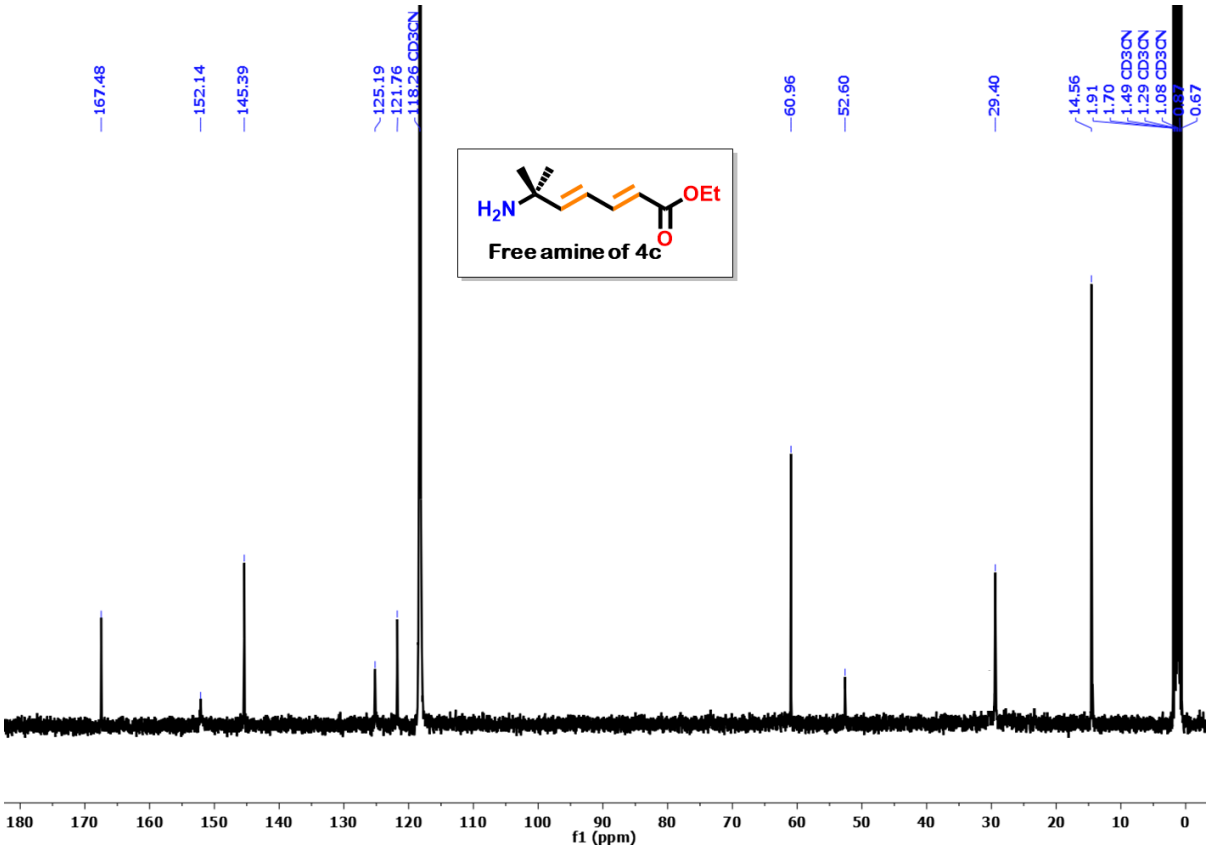

SAC 179 F
IISER PUNE
SAC 179 F 1 (0.052) AM2 (Ar,10000.0,556.28,0.00,LS 3); Sm (SG, 3x1.00)
1: TOF MS ES+
1.72e6
CALCULATED MASS
(M+Na)+ 332.1837
7c
BocHN
OEt
O
332.1833
333.1859
276.1198
306.1677
378.2252
641.3774
119.0843
147.0800
193.1219
105.0683
413.2656
437.2285
481.2689
503.3090
601.3091
615.3606
685.4346
686.4383
733.3865
785.3945
%
m/z

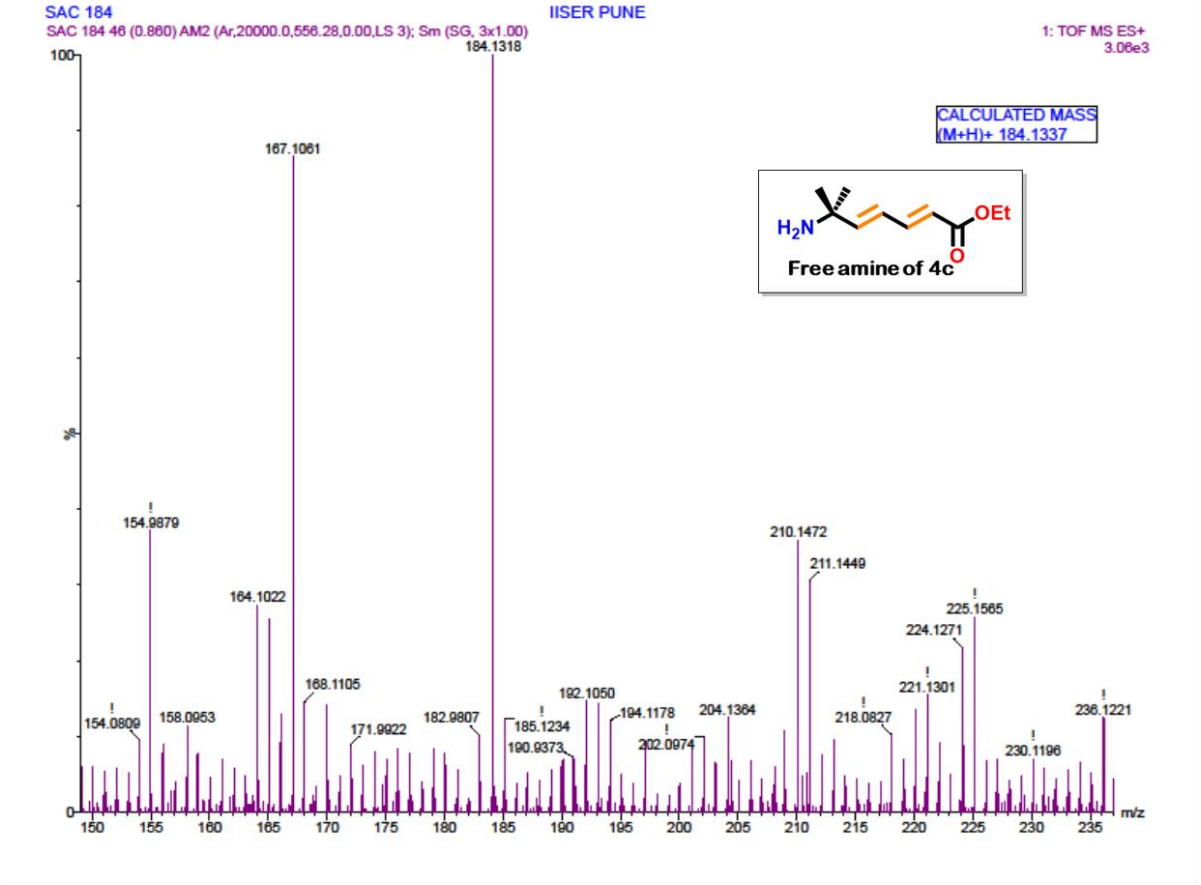

BocHN
OH
O
Free carboxylic acid of 4c
2.46 DMSO-D6
f1 (ppm)

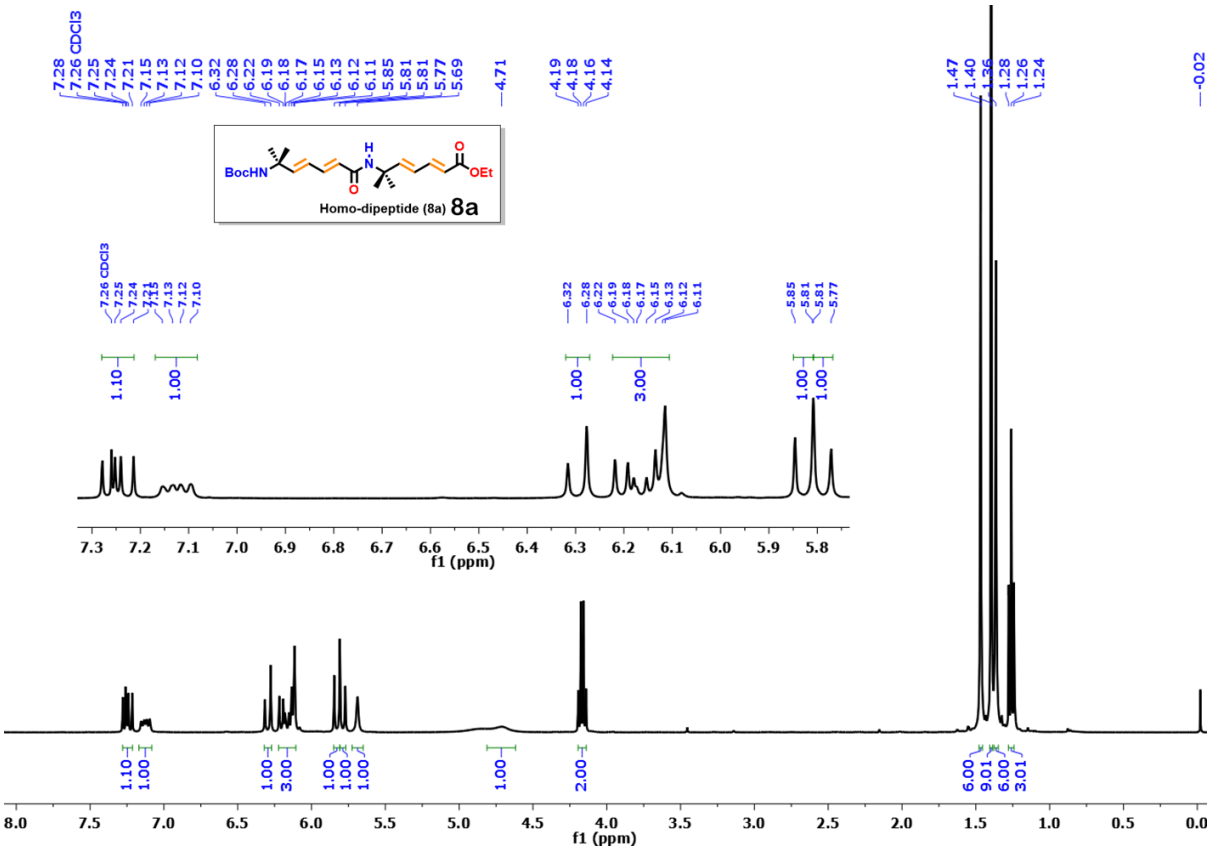

167.69
154.23
149.86
144.34
124.24
121.32
77.52
52.50
39.52 DMSO-d6
28.26
27.19
BocHN
OH
O
Free carboxylic acid of 4c
180 170 160 150 140 130 120 110 100 90 80 70 60 50 40 30 20 10 0
f1 (ppm)

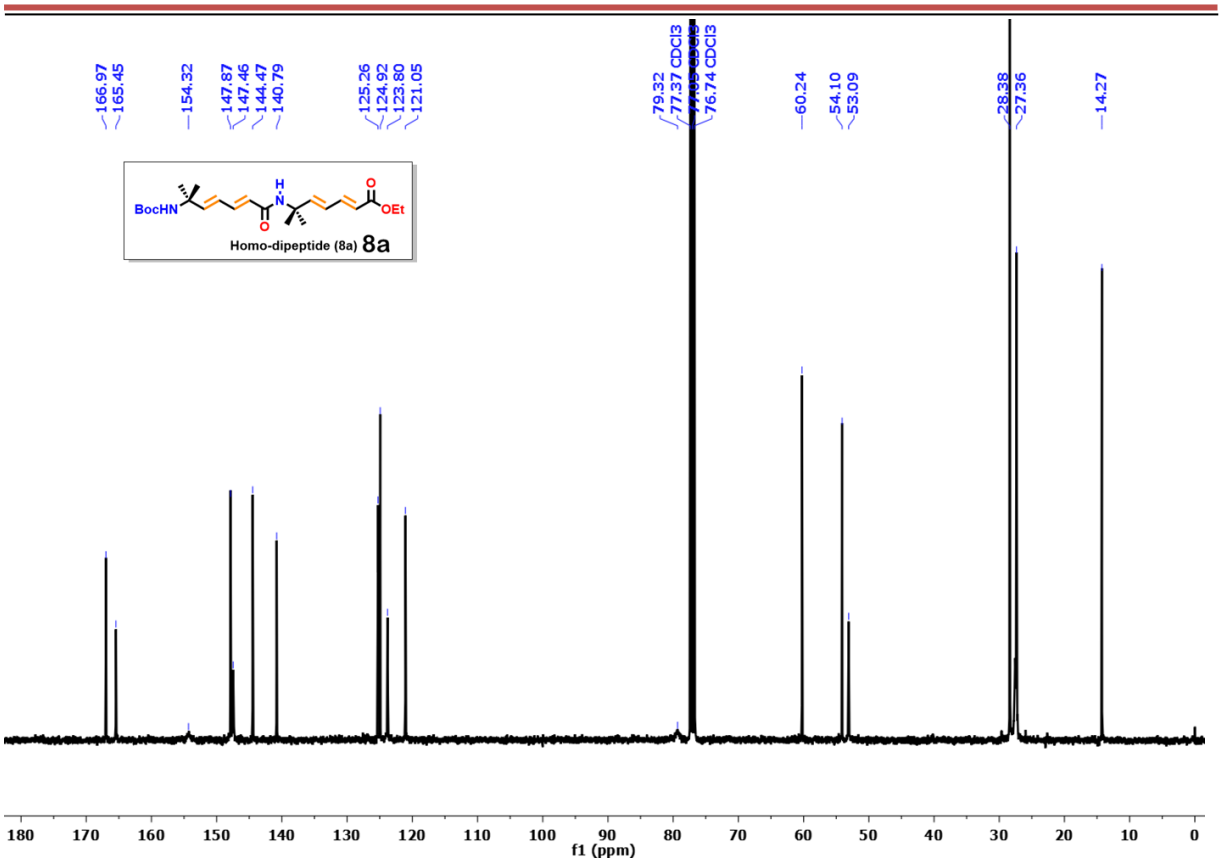

SAC 183
IISER PUNE
SAC 183 82 (1.513) AM2 (Ar,20000.0,556.28,0.00,LS 3); Sm (SG, 3x1.00)
1: TOF MS ES+
1.02e5
CALCULATED MASS
(M+Na)+ 278.1368
BocHN
OH
O
Free carboxylic acid of 4c
111.0776
93.0665
139.0738
278.1353
91.0505
222.0725
206.0992
140.0768
315.0891
376.1062
392.0793
449.1958
455.0952
457.0916
549.2464
567.2214
569.2184
590.1555
604.2944
649.1680
651.1755
704.3408
708.2423
763.3005
788.4225
%
m/z

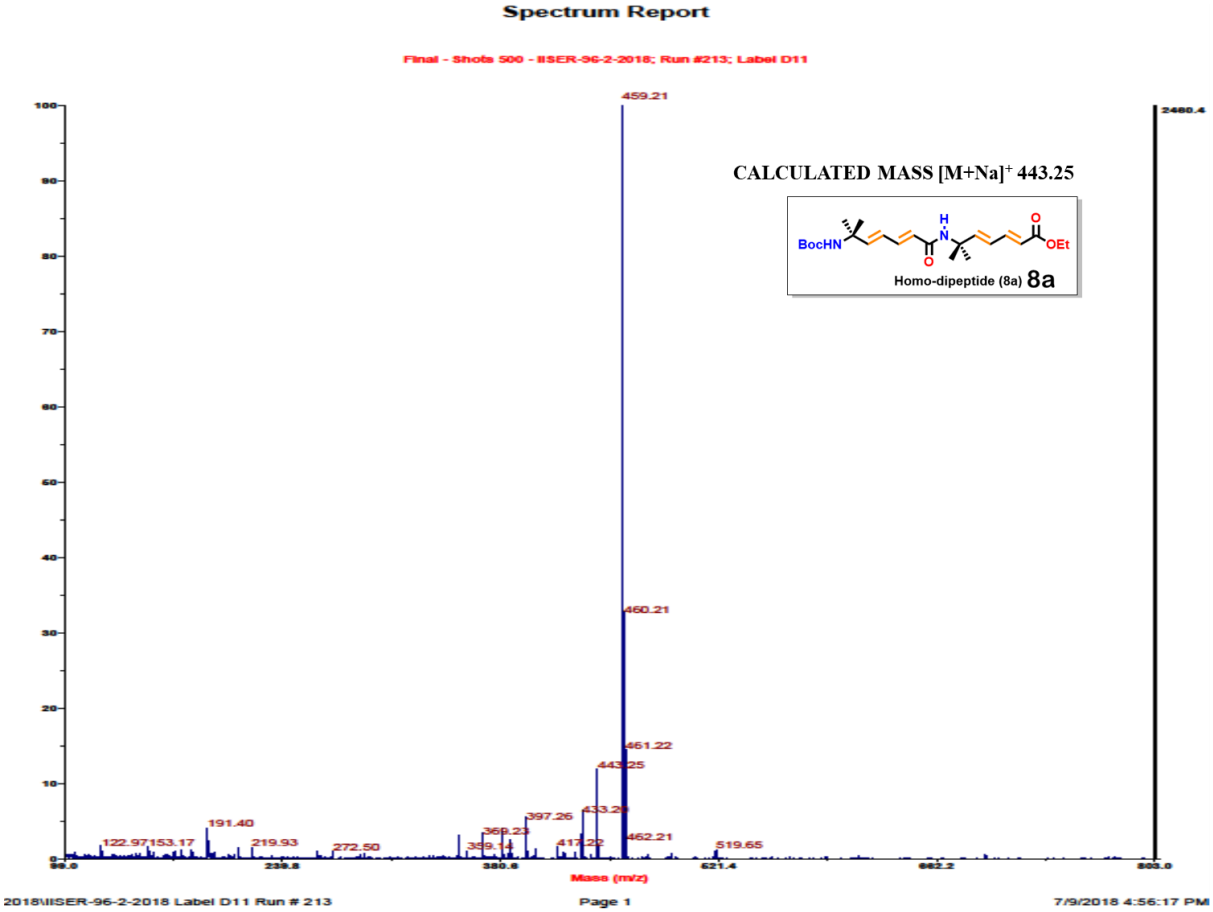

Free amine of 4c
f1 (ppm)


Free amine of 4c
f1 (ppm)

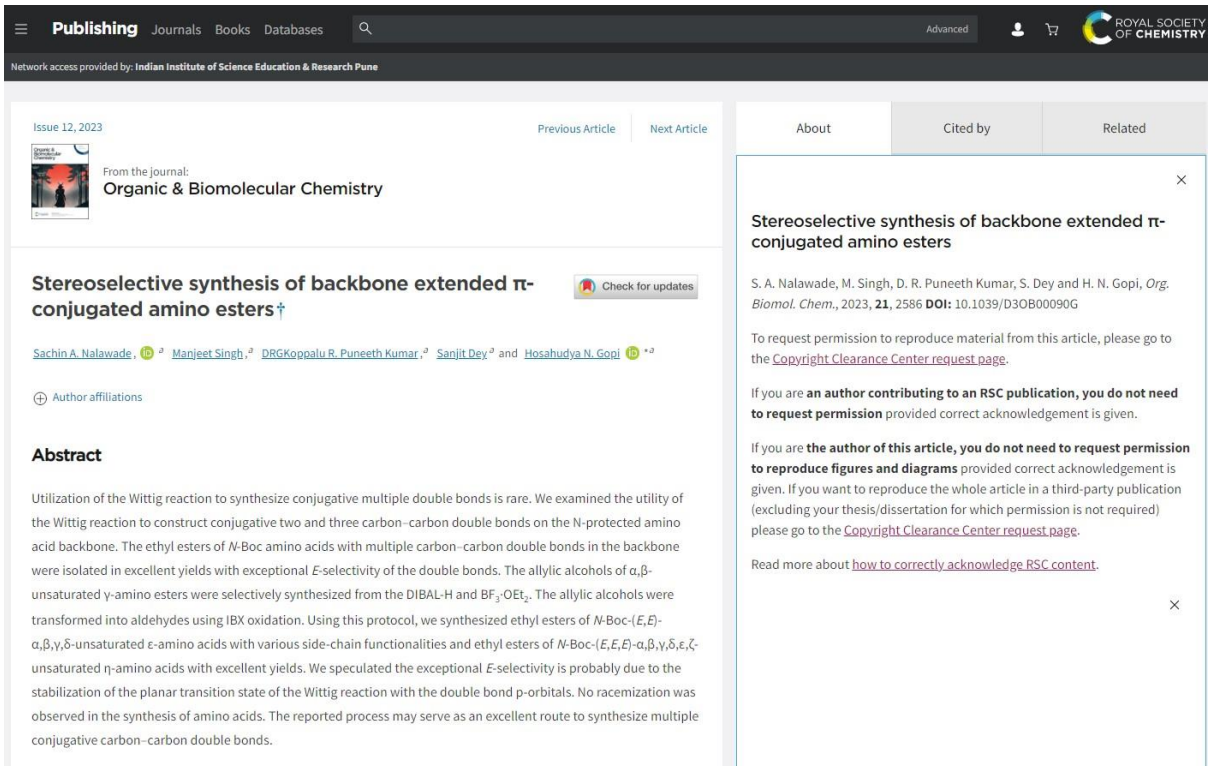

SAC 184
SAC 184 46 (0.860) AM2 (Ar,20000.0,556.28,0.00,LS 3); Sm (SG, 3x1.00)
IISER PUNE
1: TOF MS ES+
3.06e3
CALCULATED MASS
(M+H)+ 184.1337
Free amine of 4c
184.1318
167.1061
154.9879
164.1022
168.1105
154.0809
158.0953
171.9922
182.9807
185.1234
190.9373
192.1050
194.1178
202.0974
204.1364
210.1472
211.1449
218.0827
221.1301
224.1271
225.1565
230.1196
236.1221
%
m/z


Homo-dipeptide (8a) 8a
f1 (ppm)


166.97
165.45
154.32
147.87
147.46
144.47
140.79
125.26
124.92
123.80
121.05
79.32
77.37 CDCl3
76.74 CDCl3
60.24
54.10
53.09
28.38
27.36
14.27
BocHN
OEt
Homo-dipeptide (8a) 8a
f1 (ppm)


Spectrum Report
Final - Shots 500 - IISER-96-2-2018; Run #213; Label D11
459.21
460.21
461.22
443.25
CALCULATED MASS [M+Na]+ 443.25
BocHN
OEt
Homo-dipeptide (8a) 8a
Mass (m/z)
2018\IISER-96-2-2018 Label D11 Run # 213
Page 1
7/9/2018 4:56:17 PM

2.8.3. Copy of the Permission letter from Journal for reuse of figures and diagrams.



Publishing Journals Books Databases Advanced ROYAL SOCIETY OF CHEMISTRY

Network access provided by: Indian Institute of Science Education & Research Pune

Issue 12, 2023 Previous Article Next Article

From the journal: Organic & Biomolecular Chemistry

Stereoselective synthesis of backbone extended π-conjugated amino esters†

Check for updates

Sachin A. Nalawade, Manjeet Singh, DRGKoppalu R. Puneeth Kumar, Sanjit Dey and Hosahudya N. Gopi

Author affiliations

Abstract

Utilization of the Wittig reaction to synthesize conjugative multiple double bonds is rare. We examined the utility of the Wittig reaction to construct conjugative two and three carbon–carbon double bonds on the N-protected amino acid backbone. The ethyl esters of *N*-Boc amino acids with multiple carbon–carbon double bonds in the backbone were isolated in excellent yields with exceptional *E*-selectivity of the double bonds. The allylic alcohols of α,β-unsaturated γ-amino esters were selectively synthesized from the DIBAL-H and $BF_3{\cdot}OEt_2$. The allylic alcohols were transformed into aldehydes using IBX oxidation. Using this protocol, we synthesized ethyl esters of *N*-Boc-(*E*,*E*)-α,β,γ,δ-unsaturated ε-amino acids with various side-chain functionalities and ethyl esters of *N*-Boc-(*E*,*E*,*E*)-α,β,γ,δ,ε,ζ-unsaturated η-amino acids with excellent yields. We speculated the exceptional *E*-selectivity is probably due to the stabilization of the planar transition state of the Wittig reaction with the double bond p-orbitals. No racemization was observed in the synthesis of amino acids. The reported process may serve as an excellent route to synthesize multiple conjugative carbon–carbon double bonds.

About Cited by Related

Stereoselective synthesis of backbone extended π-conjugated amino esters

S. A. Nalawade, M. Singh, D. R. Puneeth Kumar, S. Dey and H. N. Gopi, *Org. Biomol. Chem.*, 2023, **21**, 2586 **DOI:** 10.1039/D3OB00090G

To request permission to reproduce material from this article, please go to the Copyright Clearance Center request page.

If you are **an author contributing to an RSC publication, you do not need to request permission** provided correct acknowledgement is given.

If you are **the author of this article, you do not need to request permission to reproduce figures and diagrams** provided correct acknowledgement is given. If you want to reproduce the whole article in a third-party publication (excluding your thesis/dissertation for which permission is not required) please go to the Copyright Clearance Center request page.

Read more about how to correctly acknowledge RSC content.

Chapter 3

Design of Shortest Helix-Turn-Helix Mimetics from α,γ-Hybrid Peptide Foldamers

The original work of this chapter has been published in the "CrystEngComm" journal. Here, we adopted the text from Ref. **S. A. Nalawade**, M. G. Kumar, D. R. Puneeth Kumar, M. Singh, S. Dey, H. N. Gopi, *CrystEngComm*, **2024**, *26*, 913 – 917. with permission from the Royal Society of Chemistry. A copy of the permission letter attached at the end of the chapter.

3.1. Introduction

The design of protein structures from the non-ribosomal amino acid building blocks and organic templates has attracted considerable attention over the years due to their promising applications in medicinal chemistry, catalysis and material sciences.[1] In comparison to the protein secondary structures, the design of protein supersecondary structure mimetics is a challenging task because it requires a sequence that folds into a predictable fashion. Among the various protein super secondary structures, the helix-turn-helix motif is most abundant in protein structures and ubiquitous in transcription factors.[2] It plays a significant role in DNA binding and repair,[3] calcium binding motifs[4] and protein-protein interactions.[5] In contrast to β-hairpins,[6,7] no tight turns have been recognized in helix-turn-helix motifs. Quite often helices are connected by loosely structured sequences of amino acids. The stabilization of the helix-turn-helix motifs is commonly governed by the global constraints of the protein three-dimensional structures. Extensive efforts have been made in the literature to design helix-turn-helix motifs using natural and non-ribosomal amino acid templates outside the protein context. Huc and colleagues recently designed and studied antiparallel helix-turn-helix motifs from aromatic oligomamides (Figure **1a** and **1b**).[8] Berlicki and co-workers designed helix-loop-helix motifs using β-amino acids and connection between two helices were also constructed using cisACPC (cis-2-aminocyclopentanecarboxylic acid) (Figure **1c**) residues, they have studied the hydrolase activity.[9,10] Balaram and colleagues design two helix motifs by connecting two helical structures using the ε-aminocaproic acid (Figure **1d**).[11,12] Sharma and

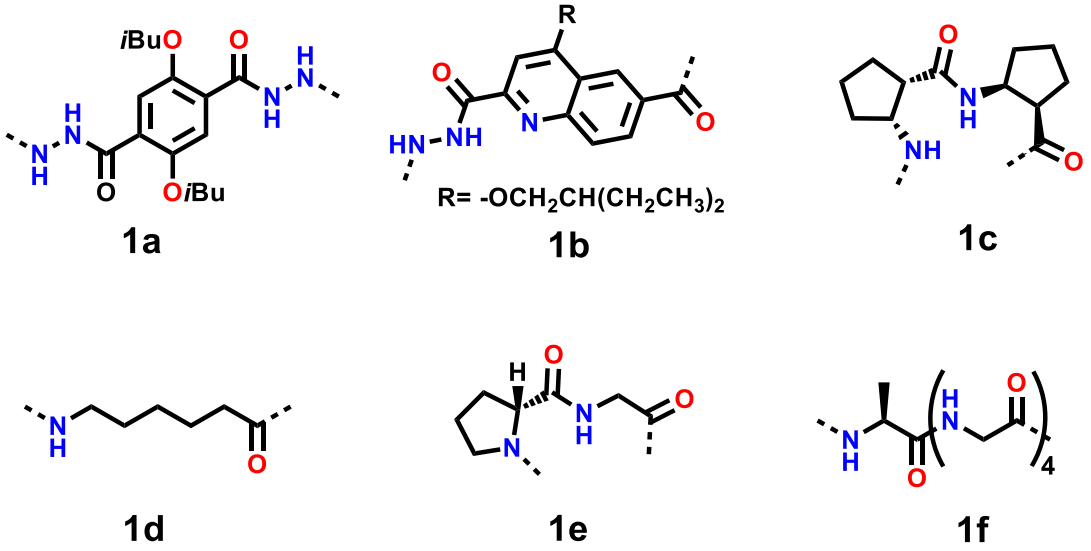


Figure 1: Turn or loop segment used in the literature for design of helix-turn-helix motif.

colleagues designed the anti-parallel helix-turn-helix motifs using D-Pro-Gly as a loop (Figure **1e**).[13] Ramagopal et al designed helix-turn-helix by connecting left-handed and right-handed helices by a loop consisting of L-Ala-$(Gly)_4$ residues (Figure**1f**).[14] In addition, efforts have also been made to design hairpin-helix motifs with short loop sequences.[15] In comparison to the β-hairpins design, there is not much success in the design of helix-turn-helix motifs.

We have been interested in understanding the conformational properties of peptides composed of α- and γ-amino acids. Both theoretical[16] and experimental[17] studies suggested that 12-helix is stable conformation of α,γ-hybrid peptides. In addition to the saturated γ-amino acids, unsaturated γ-amino acids have also been used peptide foldamers. Schreiber and co-workers reported the extended sheet type structures constructed from the oligopeptides of *E*-vinylogous amino acids[18] (Figure **2a** and **2g**) and β-turn generated using proline *E*-vinylogous amino acids (Figure **2b** and **2c**).[19] Maillard and team demonstrated the construction of C_9-helical structures using oligomers of new (*Z*) double bond containing thiazole-based γ-amino acid (Figure **2d**).[20] Previously, we reported miniature β-meander type motifs by judiciously placing α,β-unsaturated γ-amino acids (Figure **2g**) in the peptide sequences.[21] Due to the conformational restrictions of carbon-carbon double bonds, the α,β-unsaturated γ-amino

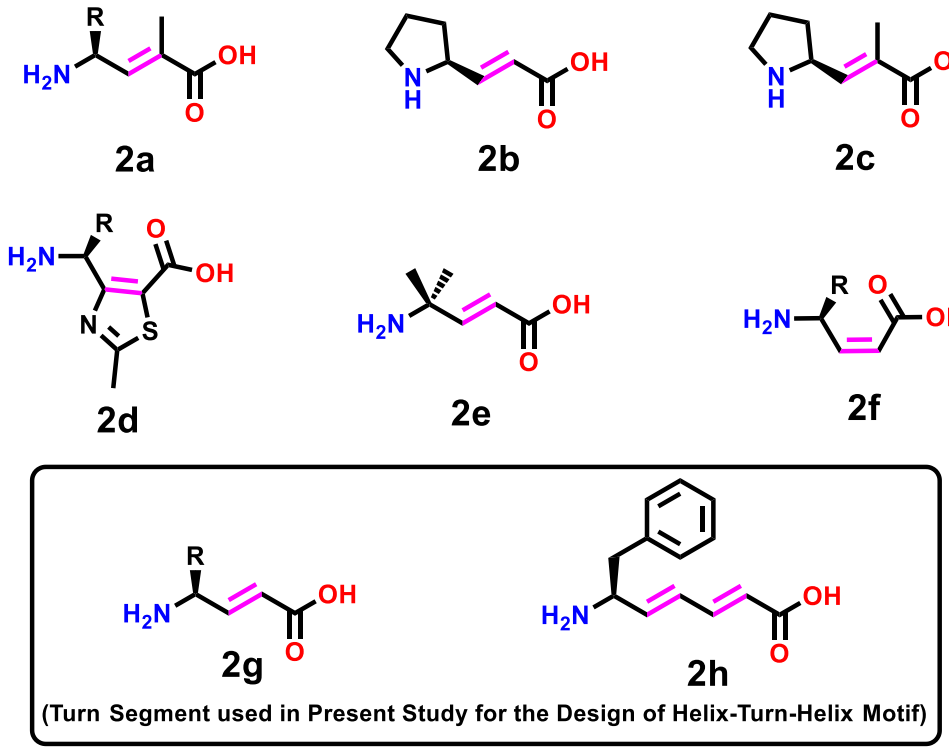


Figure 2: *Z*- and *E*-vinylogous amino acids used in the synthesis of foldamers.

acids are prone to adopt β-sheet type conformations[22,23] and we explored this property to design β-double helices using achiral *E*-vinylogous $\gamma^{4,4}$ dimethyl amino acid (Figure **2e**).[24] In addition, we demonstrated excellent accommodation of (*Z*)-α,β-unsaturated γ-amino acids (Figure **2f**) into helical foldamers.[25] Aligned with these investigations, we aimed to explore the π-conjugated amino acids (Figure **2g** and **2h**) in the design of organized protein supersecondary structural mimetics.

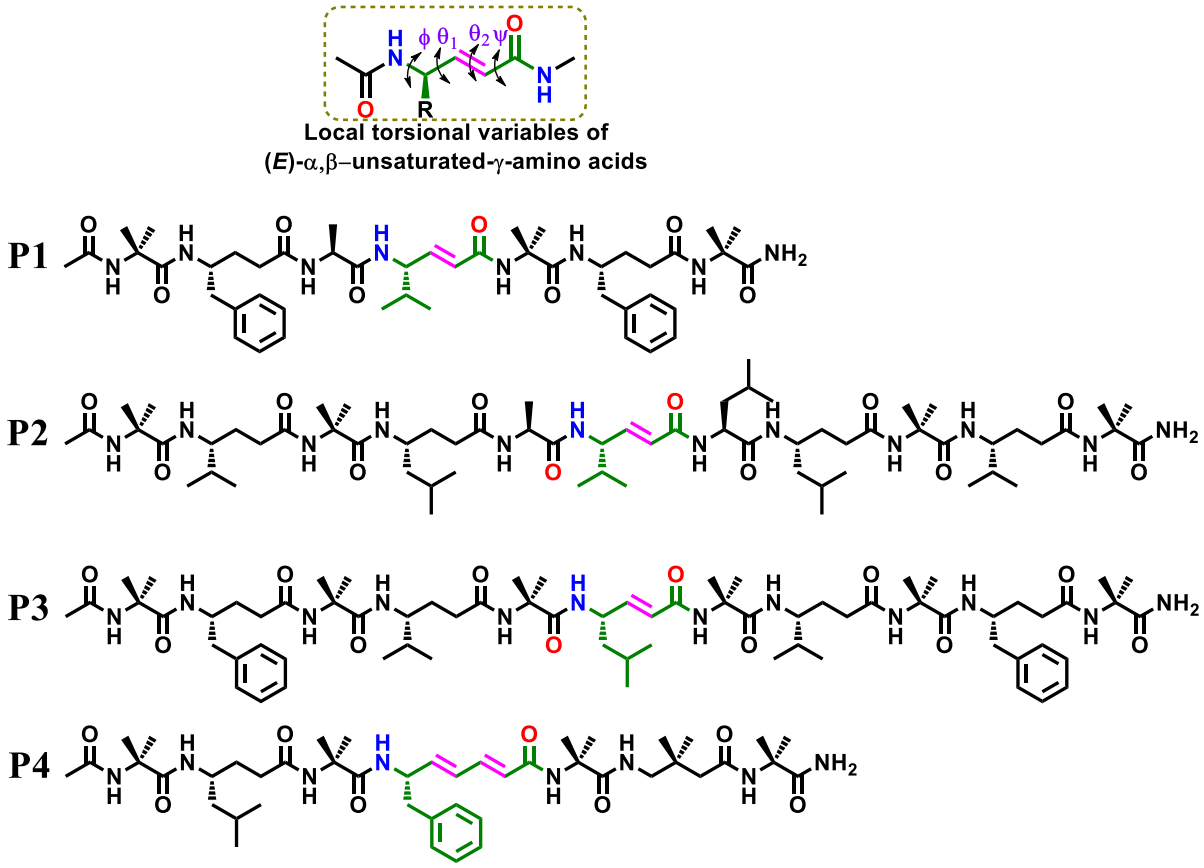
3.2. Objective of the current work

The emulation of protein supersecondary structures through short synthetic peptide sequences is of paramount significance in the realms of synthetic protein design, catalysis, and drug discovery. Verity of unnatural amino acids have been employed as building block in the design of such supersecondary structures.[26] In the preceding chapter, we devloped a strategy for synthesizing backbone extended π-conjugated amino acids (Figure **2h**).[27] Our focus was on creating functional, well-folded supersecondary structures using these π-conjugated amino acids. Based on earlier results, we postulated that the β-sheet-promoting and turn-inducing characteristics of (E)-vinylogous amino acids could be effectively harnessed to design highly organized and compact miniature Helix-turn-Helix mimetics. This will extends beyond the conventional secondary structures such as helices, β-sheets, and turns. Here, we are reporting the design, single crystal and solution conformations of helix-turn-helix mimetics using the short α,γ-hybrid peptides, and (*E*)- α,β-unsaturated γ-amino acids as well as (*E, E*)-αβ, γδ-unsaturated ε-amino acids. In the design of helix-turn -helix, unsaturated amino acids served as rigid linkers to connect two individual helices. By varying the number of trans double bonds at the central unsaturated residue, the positioning of the helices can be adjusted.

3.3. Results and discussion

In order to understand the conformations of peptides with *E*-vinylogous amino acids at the center, we designed α,γ-hybrid peptides **P1**-**P4**. The sequences of these peptides are shown in Scheme 1. The sequences **P1**, **P2** and **P3** consist of 1:1 alternating α- and γ-amino acids and α,β-unsaturated γ-amino acid at the middle of the sequence, while **P4** consists of an unsaturated amino acid with two conjugative *trans* double bonds. The α,γ-hybrid peptides have been shown to adopt helical conformations in very short sequences.[28,29]

All N-protected γ-amino acids were synthesized using the Wittig reaction as reported earlier.[27]



Scheme 1: Designed α,γ-hybrid peptide sequences of the helix-turn-helix motif mimetics.

Peptides were synthesized using the solid phase method on Rink amide resin. After completion of the synthesis, peptides were cleaved from the resin using TFA and purified by reverse phase HPLC.

3.3.1. Crystal structure analysis of P1

As single crystal structures unambiguously provide structural information, we subjected all peptides for crystallization in various solvent combinations. Peptide **P1** was crystallized using aqueous methanol and its X-ray diffracted single crystal structure is shown in Figure 3. It is striking to notice that a short seven-residue peptide adopted a three-dimensional helix-turn-helix type motif in single crystals. The detailed structure analysis revealed that the tripeptides at the N- and C-terminus sequences adopted right-handed 12-helix conformations, which are stabilized by the two consecutive 12-membered H-bonds ($i \rightarrow i+3$). At the N-terminal helix, two N-terminus amide NH groups and two amide CO groups at the C-terminus of this short helix are exposed for intermolecular H-bonding. Similarly, at the C-terminus tripeptide helix, the two amide NH groups at the N-terminus and two CO groups at the C-terminus are not

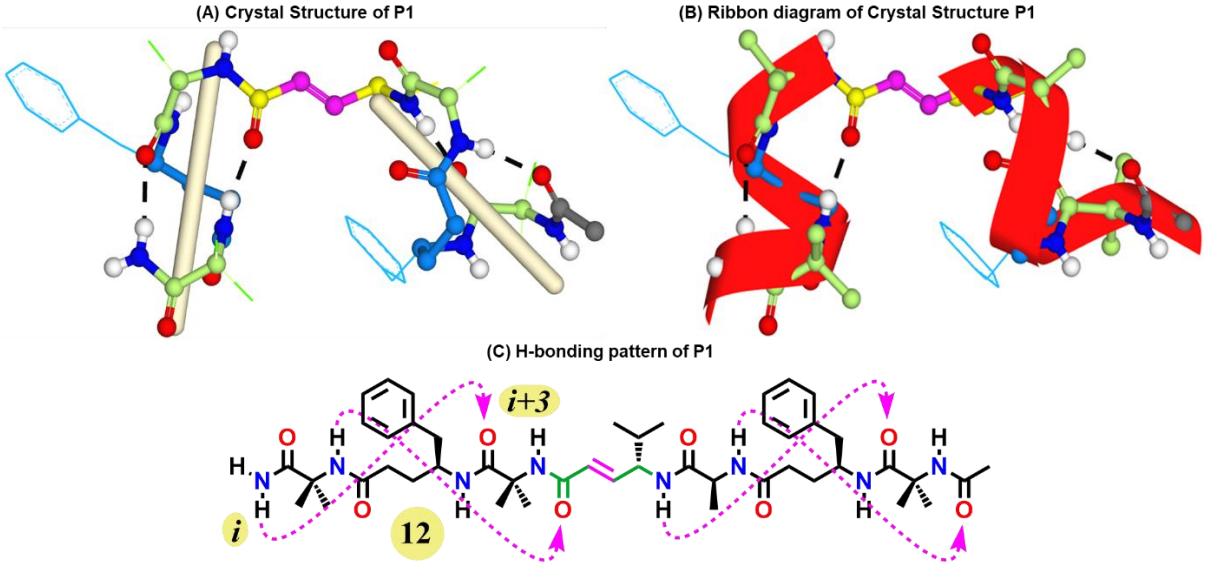


Figure 3. (A) Single-crystal X-ray diffracted structure of **P1**. (B) Ribbon diagram of crystal structure **P1** depicting helix-turn-helix motif of protein. All amino acid side chains and hydrogen atoms (except N-H and vinylogous hydrogens) are omitted for clarity. (C) Schematic representation of intramolecular hydrogen bonding pattern in helix-turn-helix motif mimetics **P1**.

Table 1: Hydrogen bonding Parameters of Peptide **P1**

Intra-molecular H-bonds of peptide **P1**				
D-H.....A	**d(D-H)**	**d(H.....A) (Å)**	**d(D.....A) (Å)**	**<(N-H.....O) (°)**
N(3)-H(3A).....O(1)	0.88	2.04	2.91	168.8
N(4)-H(4).....O(2)	0.88	1.85	2.70	163
N(7)-H(7).....O(5)	0.88	1.98	2.85	170
N(8)-H(8B).....O(6)	0.88	2.11	2.97	166.4
Intermolecular H-bonds of peptide **P1**				
N(1)-H(1).....O(8)#	0.88	2.01	2.85	160.1
N(8)-H(8A).....O(6)*	0.88	2.12	2.87	141.8
[D = Donor, A = Acceptor, H = Hydrogen, d = distance in Å, < = angle in (°)] Symmetry operations used to generate equivalent atoms: # -x+1/2,y+1/2,-z+1 * -x+1,y,-z+1				

involved in the intramolecular H-bonding and are exposed for intermolecular H-bonding with other helices. The exposed amide NH and the C-terminus CO groups are involved in the intermolecular H-bonding with two different helix-turn-helix type motifs. In addition, the C-terminal amide NH_2 and the CO of the fifth residue are involved in the symmetrical intermolecular H-bonds with the same functional groups of the other helix-turn-helix type motif. Hydrogen bonding Parameters of Peptide **P1** is shown in Table 1. The analysis of the

torsion angle parameters revealed that the Aib residues displayed average ϕ and ψ angles, -54±1° and -48±5°, respectively. The Ala residue displayed ϕ and ψ angles -69° and -34°, respectively. The local torsion parameters of the γ-residues can be measured with two additional parameters θ_1 (N-**C$^{\gamma}$-C$^{\beta}$**-C$^{\alpha}$) and θ_2 (C$^{\gamma}$-**C$^{\beta}$-C$^{\alpha}$**-C'') along with ϕ and ψ values as shown in Scheme 1. The torsion angle parameters of peptide **P1** are tabulated in Table 2.

Table 2: Torsional angle parameters of peptide **P1**.

Peptide P1	ϕ	θ_1	θ_2	Ψ	ω
Aib (1)	-54	-	-	-52	178
γPhe (2)	-119	58	60	-128	-171
Ala (3)	-69	-	-	-34	-172
dγVal (4)	**-81**	**121**	**-176**	**-169**	**-178**
Aib (5)	-53	-	-	-49	-178
γPhe (6)	-125	57	66	-111	-178
Aib (7)	-55	-	-	-43	-

The average torsion angles of γ-Phe residues ϕ, θ_1, θ_2 and ψ were found to be -122±4°, +57±1°, +63±4° and -120±9°, respectively. The γ-amino acids adopted *gauche, gauche* conformations along C$^{\gamma}$-C$^{\beta}$ and C$^{\beta}$-C$^{\alpha}$ bonds. In contrast to the saturated γ-amino acids, the α,β-unsaturated γ-amino acid incorporated at the middle of the sequence displayed torsion parameters -81°, +121°, -176° and -169° for ϕ, θ_1, θ_2 and ψ, respectively. In contrast to the saturated γ-residues, the unsaturated γ-amino acid adopted extended type conformation. The rigid conformation of unsaturated amino acid forced the molecule to adopt a helix-turn-helix type motif.

3.3.2. Crystal structure analysis of P2 and P3

Inspired by the results of **P1**, we designed eleven residues α,γ-hybrid peptides **P2** and **P3** consisting of α,β-unsaturated γ-amino acid in the middle to understand whether or not other sequences can display helix-turn-helix type motifs. The single crystals of **P2** and **P3** were obtained from the slow evaporation of the peptide solution in aqueous methanol. The single crystal structure of **P2** and **P3** is shown in Figure 4. and Figure 5. respectively. Remarkably, peptide **P2** and **P3** also adopted a helix-turn-helix type motif in single crystals. The five residues at the N-terminus and the five residues at the C-terminus of both peptide **P2** and **P3** adopted two independent right-handed 12-helix conformations. Each independent 12-helix isstabilized by four consecutive 12-membered ($i \rightarrow i+3$) H-bonds. In both independent 12-

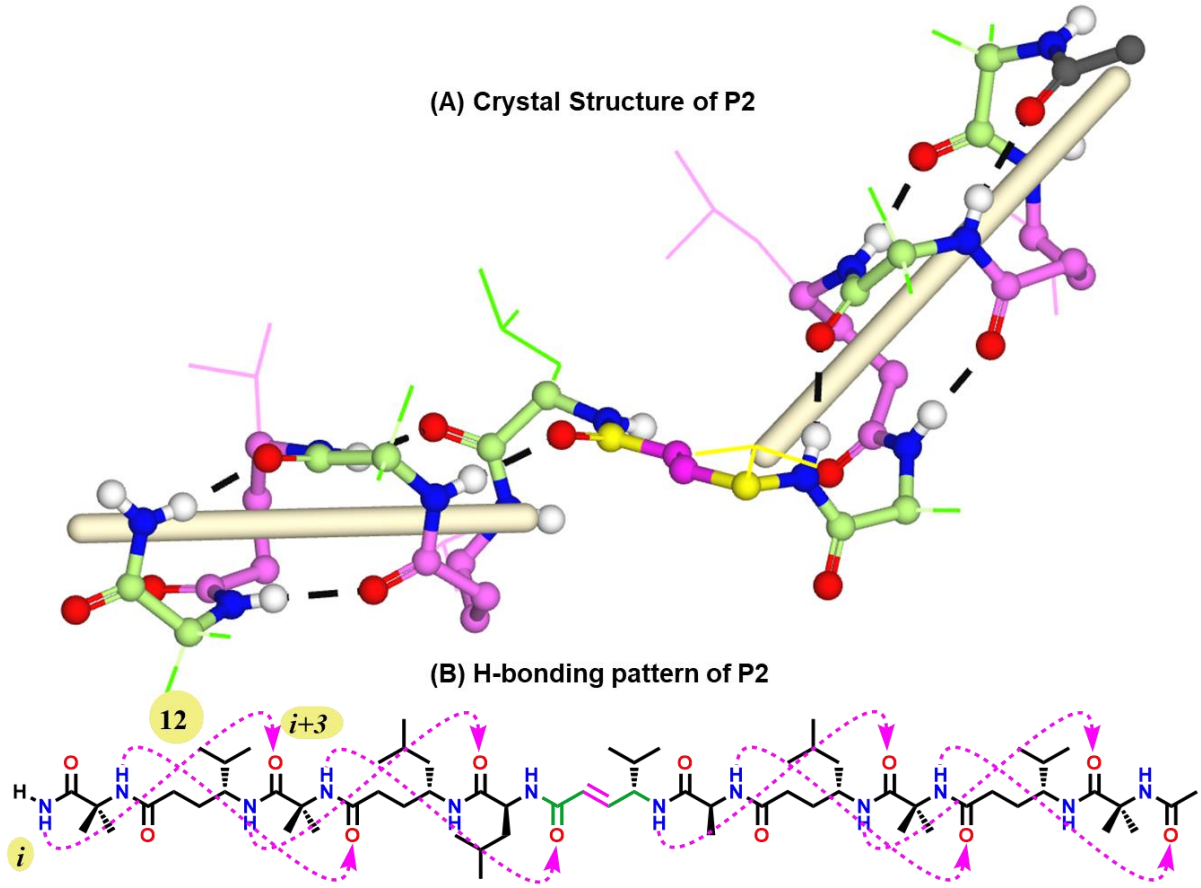


Figure 4. (A) Single-crystal X-ray diffracted structure of **P2**. All amino acid side chains are shown in thin line. Hydrogen atoms (except N-H) are omitted for clarity. (B) Schematic representation of intramolecular hydrogen bonding pattern in helix-turn-helix motif of **P2**.

helices, two amide NH groups at the N-terminus and two CO groups at the C-terminus are exposed for intermolecular H-bonds. The intramolecular 12-membered H-bonding pattern of **P1** and **P2** is shown in Figure 4. and Figure 5. respectively. In contrast to **P1**, two helices in **P2** and **P3** are bridged by the solvent methanol.

In case of peptide **P2** solvent Methanol is bridged through H-bonds between CO of γ-Leu 4 and the NH of Leu 7. The H-bonding parameters of peptide **P2** are tabulated in the Table 3. Further, we examined the torsion angle parameters of **P2** (Table 4). The average ϕ and ψ values of α-amino acid residues in **P2** were found to be -62±7° and -38±6°, respectively. Similarly, the average torsion angles of γ-residues ϕ, θ_1, θ_2 and ψ were found to be -124±4°, +50±2°, +62±2° and -120±6°, respectively. In addition, the torsion parameters ϕ, θ_1, θ_2 and ψ for the α,β-unsaturated γ-amino acid was to be -110°, +6°, -177°, and +179°, respectively.

In case of peptide **P3** solvent Methanol is bridged through H-bonds between CO of γ-Val 4

Table 3: Hydrogen bonding Parameters of Peptide **P2**

Intra-molecular H-bonds of peptide **P2**				
D-H.....A	**d(D-H)**	**d(H.....A) (Å)**	**d(D.....A) (Å)**	**<(N-H.....O) (°)**
N(3)-H(3).....O(1)	0.88	2.05	2.911	164.8
N(4)-H(4).....O(2)	0.88	2.04	2.902	166.6
N(5)-H(5).....O(3)	0.88	1.93	2.807	175.2
N(6)-H(6).....O(4)	0.88	2.03	2.872	159.7
N(9)-H(9).....O(7)	0.88	2.01	2.881	168.4
N(10)-H(10A).....O(8)	0.88	2.05	2.875	156.4
N(11)-H(11).....O(9)	0.88	2.04	2.918	172.3
N(12)-H(12D).....O(10)	0.88	1.99	2.850	165.7
Intermolecular H-bonds of peptide **P2**				
N(1)-H(1).....O(6)#	0.88	2.01	2.875	168.6
N(2)-H(2).....O(12)*	0.88	2.07	2.870	150.6
N(12)-H(12C).....O(6)$	0.88	2.12	2.993	170.7
N(7)-H(7).....O(14) (MeOH solvent)	0.88	2.07	2.941	172.8
(MeOH solvent)O(14)-H(14).....O(5)	0.84	1.87	2.671	157.8
Symmetry operations used to generate equivalent atoms: # x+1,y,z * x+1,y,z-1 $ x,y,z+1				

Table 4: Torsional angle parameters of peptide **P2**.

Peptide P2	ϕ	θ_1	θ_2	Ψ	ω
Aib (1)	-59	-	-	-39	-175
γVal (2)	-124	48	65	-118	-175
Aib (3)	-58	-	-	-45	-173
γLeu (4)	-119	49	62	-129	-164
Ala (5)	-69	-	-	-30	-170
dγVal (6)	**-110**	**6**	**-177**	**179**	**-172**
Leu (7)	-71	-	-	-30	-179
γLeu (8)	-126	49	60	-114	-174
Aib (9)	-55	-	-	-41	-172
γVal (10)	-128	53	61	-120	-172
Aib (11)	-57	-	-	-42	-

and the NH of Aib 7. The H-bond parameters are tabulated in the Table 5. Further, we examined the torsion angle parameters of **P3** (Table 6). The average ϕ and ψ values of α-amino acid residues were found to be -57±3° and -40±3°, respectively. Similarly, the average torsion angles of γ-residues ϕ, θ_1, θ_2 and ψ were found to be -127±4°, +52±4°, +61±3° and -118±2°, respectively. In addition, the torsion parameters ϕ, θ_1, θ_2 and ψ for the α,β-unsaturated γ-amino acid was to be -92°, +3°, +177°, and +174°, respectively. The difference between the structures

of **P1** and **P2**, **P3** is the value of θ_1. In **P1**, θ_1 was to be +121° whereas in **P2** and **P3** it is close to 0°. Overall, the undecapeptide **P2** and **P3** also adopted helix-turn-helix type motif in single crystals similar to that of **P1**.

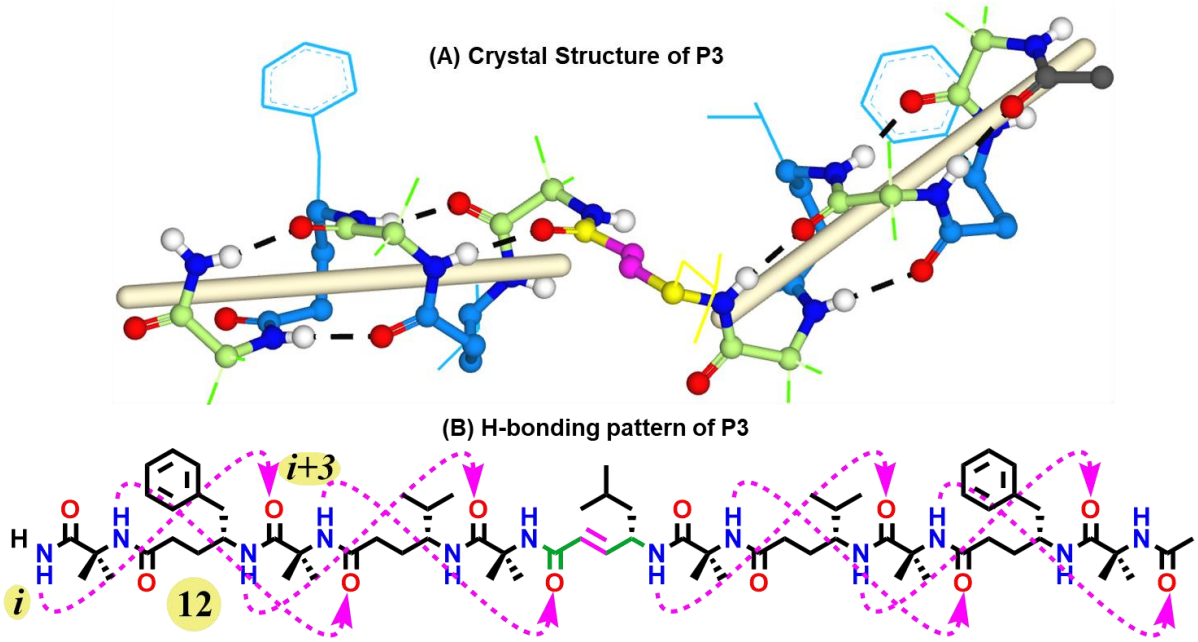


Figure 5. (A) Single-crystal X-ray diffracted structure of **P3**. All amino acid side chains are shown in thin line. Hydrogen atoms (except N-H) are omitted for clarity. (B) Schematic representation of intramolecular hydrogen bonding pattern in helix-turn-helix motif **P3**.

Table 5: Hydrogen bonding Parameters of Peptide **P3**

Intra-molecular H-bonds of peptide **P3**				
D-H.....A	**d(D-H)**	**d(H.....A) (Å)**	**d(D.....A) (Å)**	**<(N-H.....O) (°)**
N(3)-H(3).....O(1)	0.88	2.05	2.92	174
N(4)-H(4).....O(2)	0.88	2.02	2.87	164
N(5)-H(5).....O(3)	0.88	2.16	3.03	171
N(6)-H(6).....O(4)	0.88	2.06	2.88	154
N(9)-H(9).....O(7)	0.88	2.02	2.89	172
N(10)-H(10A).....O(8)	0.88	2.09	2.92	157
N(11)-H(11).....O(9)	0.88	2.09	2.96	172
N(12)-H(12D).....O(10)	0.88	2.05	2.91	164
Intermolecular H-bonds of peptide **P3**				
N(2)-H(2).....O(12)*	0.88	2.05	2.92	174
N(7)-H(7).....O(58) (MeOH solvent)	0.88	2.02	2.87	164
(MeOH solvent)O(58)-H(58).....O(5)	0.84	2.16	3.03	171
Symmetry operations used to generate equivalent atoms * 1+x,-1+y,z				

Table 6: Torsional angle parameters of peptide **P3**.

Peptide P3	ϕ	θ_1	θ_2	Ψ	ω
Aib (1)	-57	-	-	-42	-175
γPhe (2)	-123	52	60	-120	-171
Aib (3)	-58	-	-	-41	-173
γVal (4)	-127	56	58	-118	-175
Aib (5)	-56	-	-	-39	-168
dγLeu (6)	**-92**	**3**	**177**	**174**	**-177**
Aib (7)	-59	-	-	-36	-172
γVal (8)	-130	46	65	-118	-174
Aib (9)	-57	-	-	-41	-174
γPhe (10)	-127	55	62	-117	-175
Aib (11)	-54	-	-	-43	-

3.3.3. Crystal structure analysis of P4

Motivated by the remarkable conformations of peptides **P1, P2** and **P3** we hypothesized that the two helices can be pushed further away from one another if we introduce additional double bonds at the central residue. Based on this hypothesis, we designed a seven-residue peptide **P4** consisting of an unsaturated amino acid with two conjugative carbon-carbon backbone double bonds in the middle of the sequence. In addition, we replaced the C-terminal γ-amino acid with 3,3-dialkyl γ-amino acid (Scheme 1). The C-terminal α,γ- hybrid peptide sequence is achiral in nature. Recently we reported ambidextrous helices from α,γ-hybrid peptides consisting of 1:1 alternating Aib and 3,3-dimethyl amino acids.[30]

The single crystals of peptide **P4** were obtained after the slow evaporation of its solution in aqueous methanol. The single crystal structure of **P4** is shown in Figure 6. Two molecules were found in the asymmetric unit. The α,γ- hybrid sequences at the N- and C-terminus of **P4** adopted independent 12-helix conformations, stabilized by two consecutive intramolecular 12-membered H-bonds. As hypothesized the peptide adopted helix-turn-helix type conformation in single crystals. In comparison with **P1**, **P2** and **P3** the two helices in **P4** have pushed away from one another. Both helices in **P4** are perpendicular to one another. This type of perpendicular orientation of helices is rarely observed in the designed synthetic peptides. Interestingly, the C-terminal achiral peptide adopted both left and right-handed helical conformations in the single crystals. In one of the molecules in the asymmetric unit, both N- and C-terminal sequences adopted right-handed helices, whereas, in another molecule, the N-

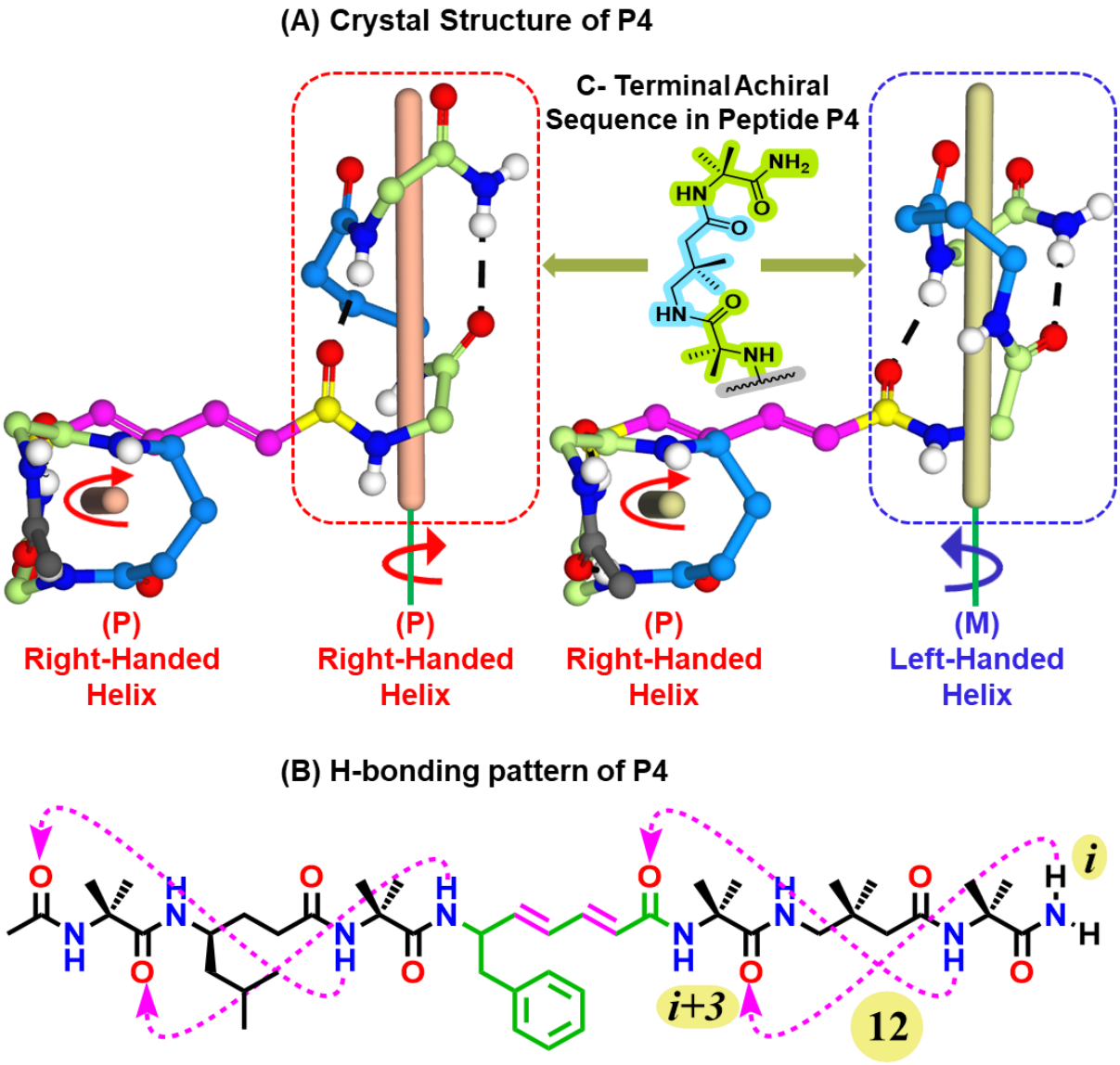


Figure 6. (A) Single-crystal X-ray diffracted structure of **P4**. All amino acid side chains and hydrogen atoms (except N-H) are omitted for clarity. (B) Schematic representation of intramolecular hydrogen bonding pattern in helix-turn-helix motif mimetics **P4**.

terminal sequence adopted a right-handed helix and the C-terminal sequence adopted a left-handed helix. The two helices are stabilized by two consecutive 12-membered ($i \rightarrow i+3$) intramolecular H-bonds. As observed in **P1**, at the N-terminal helix of **P4**, two amide NH groups at N-terminus and two CO groups at the C-terminus are exposed for intermolecular H-bonds. Similarly, at the C-terminus helix, two N-terminus amide NH groups and two C-terminus CO groups are exposed to intermolecular H-bonds. The C-terminus CO-NH_2 group is involved in the intermolecular H-bonding with the CO of Aib5 of another C-terminus helix.

Table 7: Hydrogen bonding Parameters of Peptide **P4**

Intra-molecular H-bonds of peptide **P4** (Molecule 1) (P) right and (M) left handed helix				
D-H.....A	d(D-H)	d(H.....A) (Å)	d(D.....A) (Å)	<(N-H.....O) (°)
N(6)-H(6).....O(8)	0.88	2.00	2.876(15)	171.7
N(5)-H(5).....O(7)	0.88	2.12	2.962(18)	161.4
N(2)-H(2).....O(4)	0.88	2.03	2.885(16)	162.4
N(1)-H(1B).....O(3)	0.88	2.16	3.024(17)	168.5
Intermolecular H-bonds of peptide **P4** (Molecule 1) (P) right and (M) left handed helix				
N(8)-H(8).....O(5)$	0.88	2.17	3.006(17)	157.9
N(4)-H(4).....O(10)*	0.88	2.04	2.918(14)	176.7
N(1)-H(1A).....O(9)#	0.88	2.16	3.012(14)	161.9
N(12)-H(12).....O(2)	0.88	2.05	2.928(14)	174.9
N(9)-H(9A).....O(1)@	0.88	2.10	2.959(14)	165.6
Symmetry operations used to generate equivalent atoms: # -x,y+1/2,-z+2 * x+1,y,z $ x,y-1,z @ -x,y-1/2,-z+2				
Intra-molecular H-bonds of peptide **P4** (Molecule 2) both (P) right-handed helix				
N(14)-H(14).....O(16)#	0.88	1.99	2.867(16)	172.1
N(13)-H(13).....O(15)*	0.88	2.08	2.903(17)	156.2
N(10)-H(10).....O(12)$	0.88	1.99	2.854(16)	165.6
N(9)-H(9B).....O(11)$	0.88	2.15	3.024(17)	172.4
Intermolecular H-bonds of peptide **P4** (Molecule 2) both (P) right-handed helix				
N(16)-H(16).....O(13)$	0.88	2.01	2.873(17)	167.3
N(12)-H(12).....O(2)	0.88	2.05	2.928(14)	174.9
N(9)-H(9A).....O(1)@	0.88	2.10	2.959(14)	165.6
N(4)-H(4).....O(10)*	0.88	2.04	2.918(14)	176.7
N(1)-H(1A).....O(9)#	0.88	2.16	3.012(14)	161.9
Symmetry operations used to generate equivalent atoms: # -x,y+1/2,-z+2 * x+1,y,z				

In the C-terminus helix, the NH of Aib5 is involved in the intermolecular H-bonding with CO of the 3, 3-dialkyl-γ-amino acid residue. The terminal CO-NH_2 group is involved in the intermolecular H-bonding with the same functional group of another helix. The H-bonding parameters of peptide **P4** are tabulated in the Table 7. The average ϕ and ψ torsion parameters of the α-residues in the right-handed helix are -54±4° and -42±6°, respectively (Table 8). Whereas the average ϕ and ψ values of the α-residues in the left-handed helix were found to be 55±8 and 43±9, respectively. The γ-residues in the right-handed helix displayed the ϕ, θ_1, θ_2 and ψ values -125±5°, +49±7°, +63±4° and -115±6°, respectively. In contrast, the achiral γ-residue nicely accommodated into the left-handed 12-helix with the ϕ, θ_1, θ_2 and ψ values +130°, -54°, -56°, and +105°, respectively. Overall, with the introduction of an additional double bond, it is possible to move the helices further apart from one another.

Table 8: Torsional angle parameters of peptide **P4**.

(Molecule 1) (P) Right and (M) Left handed helix							
Peptide P4 (Molecule1)	ϕ	θ_1	θ_2	θ_3	θ_4	Ψ	ω
Aib (1)	-57	-	-	-	-	-38	-171
γLeu (2)	-124	47	63	-	-	-116	-173
Aib (3)	-55	-	-	-	-	-43	-172
(E,E)ddεPhe (4)	**-102**	**3**	**179**	**-180**	**179**	**180**	**168**
Aib (5)	61	-	-	-	-	34	176
Adb (6)	130	-54	-56	-	-	105	175
Aib (7)	49	-	-	-	-	52	-
(Molecule 2) both (P) Right handed helix							
Peptide P4 (Molecule2)	ϕ	θ_1	θ_2	θ_3	θ_4	Ψ	ω
Aib (1)	-55	-	-	-	-	-39	-173
γLeu (2)	-120	43	67	-	-	-120	-175
Aib (3)	-52	-	-	-	-	-47	-167
(E,E)ddεPhe (4)	**-115**	**28**	**-176**	**-175**	**-178**	**-160**	**-178**
Aib (5)	-58	-	-	-	-	-35	-177
Adb (6)	-130	57	59	-	-	-108	-176
Aib7	-50	-	-	-	-	-51	-

3.3.4. Superposition of the peptide P4 over the helix-turn-helix motif of the 434 repressor DNA-binding domain protein

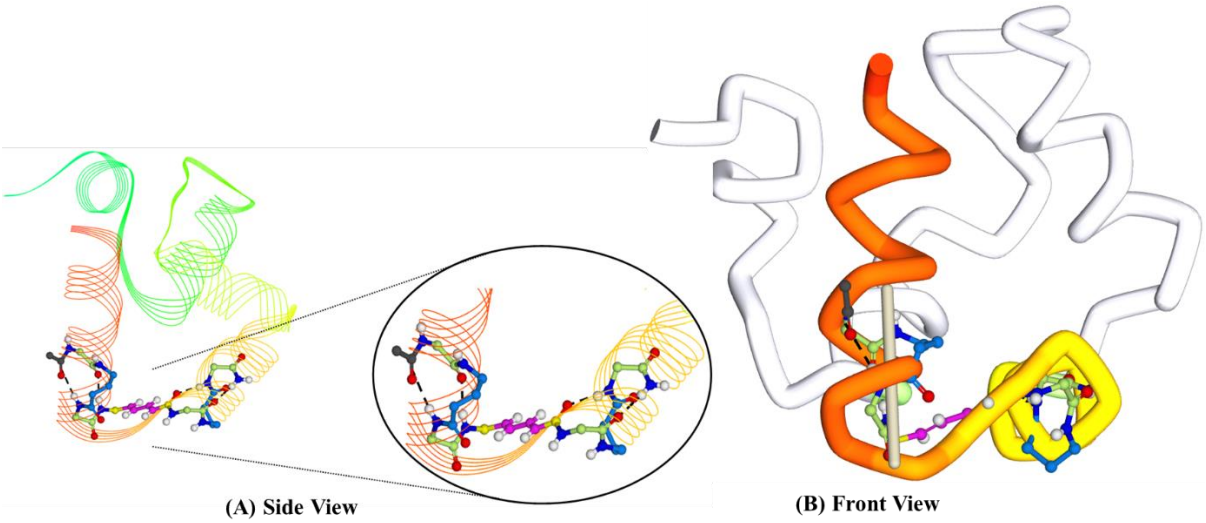


Figure 7: Superposition of the peptide **P4** (shown in ball and stick model) over the helix-turn-helix motif of the 434 repressor DNA-binding domain derived in solution [PDB 2R63]. (A)

Side view of superimposed Peptide **P4** and Protein (depicted as a line ribbon). (B) Peptide **P4** and Protein (represented as a cylindrical coil) superimposed in a frontal view, depicting perpendicular orientation of both helices with each other.

In order to understand whether or not the observed helix-turn-helix type motifs mimic the structures of natural helix-turn-helix motif domains, we superimposed the crystal structure of **P4** over the 434 repressor DNA-binding domain solution structure.[31] The overlay of the two structures is shown in Fig. 5. The conformation of **P4** observed in single crystals is nicely superposed over the helix-turn-helix structure of 434 repressor DNA-binding domain. However, the length of the helices in **P4** is very short and also the intramolecular H-bond pattern in the α,γ-hybrid helices is different from that of the α-helices.

3.3.5. 2D-NMR (TOCSY & ROESY) analysis of peptides P1, P2 and P4, NOE correlations with their solid state structures

In addition to the solid-state crystal structure in hand, We further studied the solution conformations of Peptides **P1**, **P2** and **P4** in CD_3OH using 2D NMR (TOCSY & ROESY) analysis. The amino acid residues and their positions in the peptide sequence were identified using TOCSY and ROESY spectra, respectively. The examination of the ROESY spectra of all three peptides revealed the existence of strong sequential NHi↔NHi+1 contacts along the helices. In addition, NHi↔NHi+1 interactions were not observed between the two helices at the unsaturated amino acids, due to its extended rigid conformation.

Thorough examination of the solid-state crystal structures reveals that the overall conformation of these peptides rises through well-defined helical arrangements centered around the unsaturated amino acid residue. The identification of significant long-range NOEs at the central unsaturated amino acid residue is meaningful, as it validates the conformational similarity of these peptides in the solution state. We validated the existence of long-range NOEs between protons separated by a distance of (i↔i+3) centered at the unsaturated amino acid residue. In the case of **P1**, along with the sequential NHi↔NHi+1 NOEs, we observed long-range NOEs between the $2C^{\gamma}H$↔4NH, $4C^{\alpha}H$↔6NH, $4C^{\beta}H$↔7NH, and $6C^{\gamma}H$↔8NH (See Table 10). In the case of **P2**, we observed strong sequential NOEs between NHi↔NHi+1 residues and long-range NOEs between the $2C^{\gamma}H$↔5NH, $4C^{\gamma}H$↔6NH, $4C^{\gamma}H$↔$6C^{\alpha}H$, $4C^{\gamma}H$↔7NH, $6C^{\alpha}H$↔6NH and the medium NOE between $6C^{\beta}H$↔9NH (See Table 12). In **P4**, along with the strong sequential NOEs between NHi↔NHi+1, we observed NOEs between $2C^{\gamma}H$↔4NH,

2C$^{\gamma}$H↔4C$^{\gamma}$H and weak NOEs between 2C$^{\gamma}$H↔4C$^{\alpha}$H (See Table 14). The distance observed between the NOEs in solution is consistent with the distance observed in the crystal structures. Moreover, though we observed left- and right-handed helices in the crystal structure of **P4**, we observed right-handed helix conformations of both helices in solution. Based on the NOEs observed in the solution NMR, we speculated that all three peptides adopted helix-turn-helix type conformations in solution similar to the crystal structures.

The 2D NMR analysis (TOCSY & ROESY) of all three peptides (**P1**, **P2**, and **P4**) in CD3OH is presented sequentially below. The crucial NOEs observed in the 2D-NMR along with the distance are given below in the Table 10, 12 and 14 for peptide **P1**, **P2** and **P4** respectively.

3.3.5.1. Peptide P1 2D-NMR analysis and NOE correlations with its solid state structure

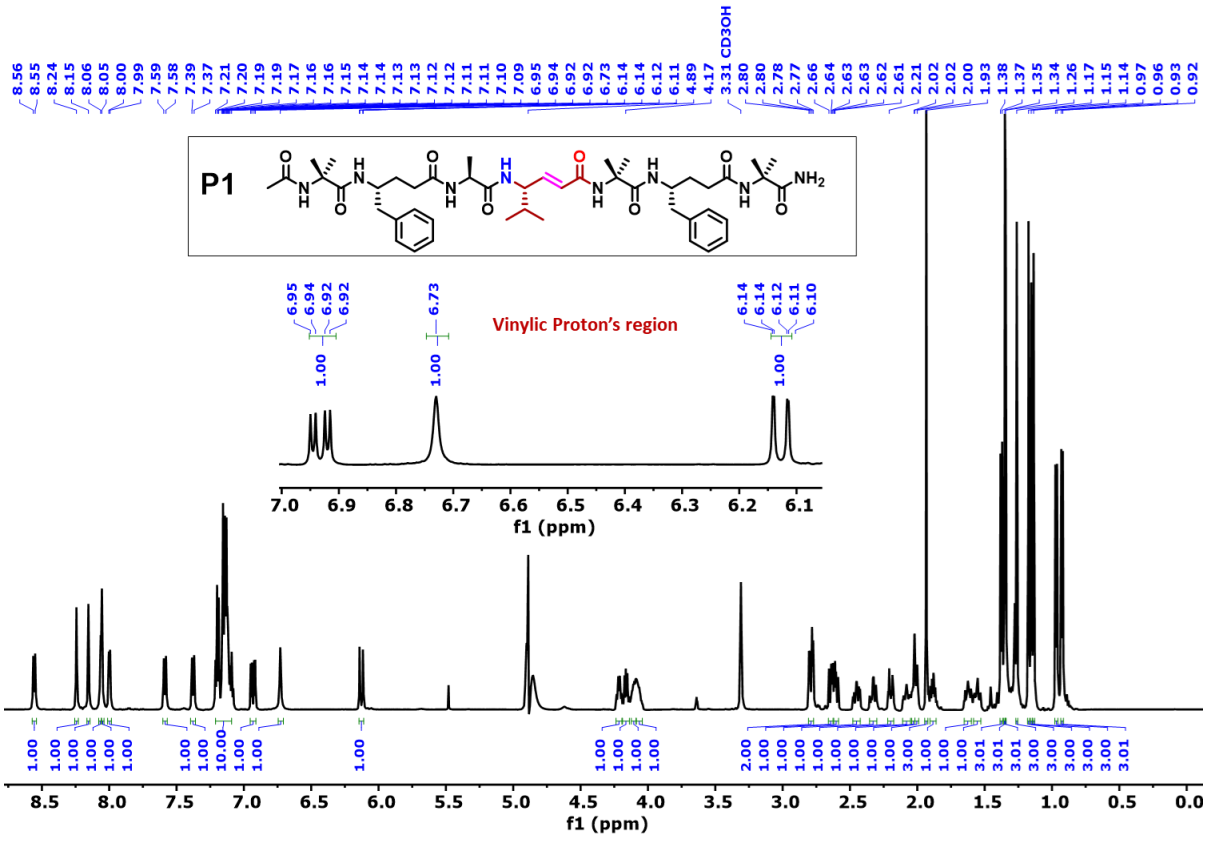


Figure 8: ^{1}H NMR spectrum of peptide **P1** in CD_3OH.

Characterization Data of P1

^{1}H NMR (600 MHz, CD_3OH) δ 8.56 (d, *J* = 8.5 Hz, 1H), 8.24 (s, 1H), 8.15 (s, 1H), 8.06 (s, 1H), 8.05 (s, 1H), 8.00 (d, *J* = 5.7 Hz, 1H), 7.59 (d, *J* = 9.7 Hz, 1H), 7.38 (d, *J* = 9.6 Hz, 1H), 7.21 – 7.09 (m, 10H$_{Aromatic}$), 6.93 (dd, *J* = 15.3, 5.4 Hz, 1H), 6.73 (s, 1H), 6.13 (dd, *J* = 15.3,

1.8 Hz, 1H), 4.21 (m, 1H), 4.16 (m, 1H), 4.10 (m, 1H), 4.07 (m, 1H), 2.79 (dd, *J* = 13.7, 5.2 Hz, 2H), 2.64 (dd, *J* = 13.7, 9.9 Hz, 1H), 2.61 (dd, *J* = 13.7, 9.4 Hz, 1H), 2.45 (ddd, *J* = 14.3, 11.8, 4.7 Hz, 1H), 2.33 (m, 1H), 2.20 (dt, *J* = 14.3, 4.7 Hz, 1H), 2.08 (m, 1H), 2.03 (m, 1H), 2.00 (m, 1H), 1.93 (s, 3H), 1.88 (m, 1H), 1.62 (m, 1H), 1.55 (m, 1H), 1.38 (d, *J* = 7.3 Hz, 3H), 1.35 (s, 3H), 1.34 (s, 3H), 1.26 (s, 3H), 1.17 (s, 3H), 1.15 (s, 3H), 1.14 (s, 3H), 0.97 (d, *J* = 6.7 Hz, 3H), 0.93 (d, *J* = 6.7 Hz, 3H). **MALDI (TOF/TOF)** *m/z* calculated value for $C_{46}H_{68}N_8O_8$ [M+Na^+] is 883.5052 and observed at 883.5010.

Table 9. ^{1}H NMR Chemical Shifts assignment (ppm) of **P1** in CD_3OH at 298 K.

Residues	NH	$_\alpha$CH	$_\beta$CH	$_\gamma$CH	$_\delta$CH	$_\varepsilon$CH	CH_{term}
(N-Terminus) -$COCH_3$	—	—	—	—	—	—	1.93
Aib(1)	8.15	—	1.17 (3H) 1.14 (3H)	—	—	—	—
γPhe(2)	7.38	2.45(1H) 2.20 (1H)	2.08 (1H) 1.62 (1H)	4.07	Benzylic 2.79(1H) 2.64 (1H)	Aromatic 7.21-7.09 (5H)	—
Ala(3)	8.00	4.16	1.38 (3H)	—	—	—	—
dγVal(4)	8.56	6.13	6.93	4.21	1.88	0.97 (3H) 0.93 (3H)	
Aib(5)	8.24	—	1.26 (3H) 1.15 (3H)	—	—	—	—
γPhe(6)	7.59	2.33 (1H) 2.03 (1H)	2.00 (1H) 1.55 (1H)	4.10	Benzylic 2.79 (1H) 2.61 (1H)	Aromatic 7.21-7.09 (5H)	—
Aib(7)	8.05	—	1.35 (3H) 1.34 (3H)	—	—	—	—
-NH_2 (C-Terminus)	8.06[a] 6.73[b]	—	—	—	—	—	—

[a] $CONH_2$ Proton involved in Hydrogen bonding. [b] $CONH_2$ Proton is not involved in Hydrogen bonding. Aromatic protons are shown in $_\varepsilon$CH column. Chemical shift assigned by using TOCSY and ROESY spectra.

Assignment of chemical shifts using TOCSY and ROESY spectra

The amino acid residues and their positions in the peptide sequence were identified using TOCSY and ROESY spectra, respectively. The TOCSY spectrum was used to identify amino acids in the sequence of the peptides.

A) Partial TOCSY spectrum analysis of peptide P1 in CD_3OH

Below partial TOCSY spectrum showing the amino acid residues in peptide P1

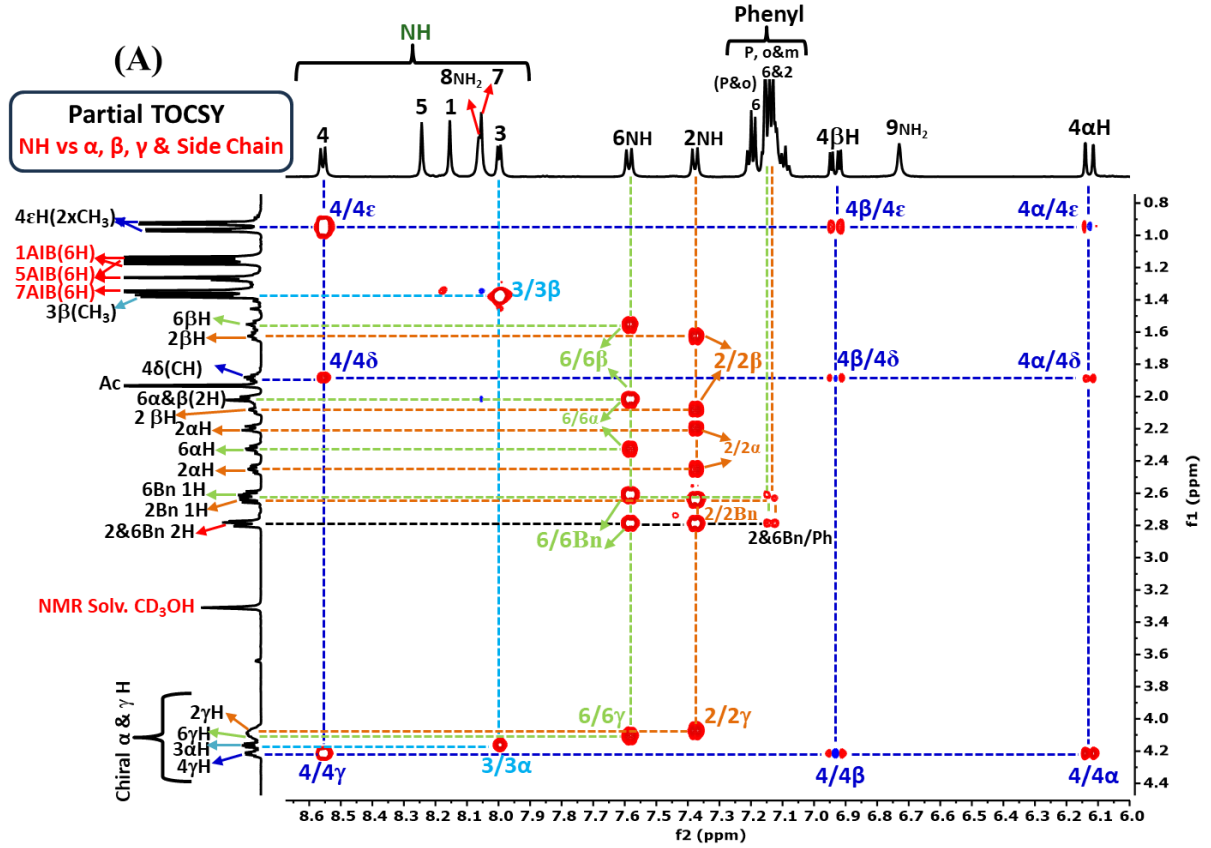
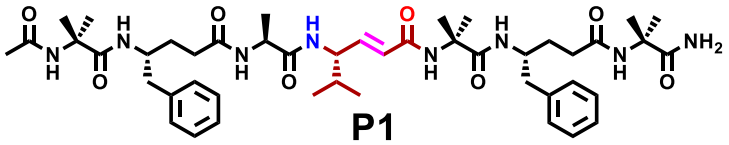
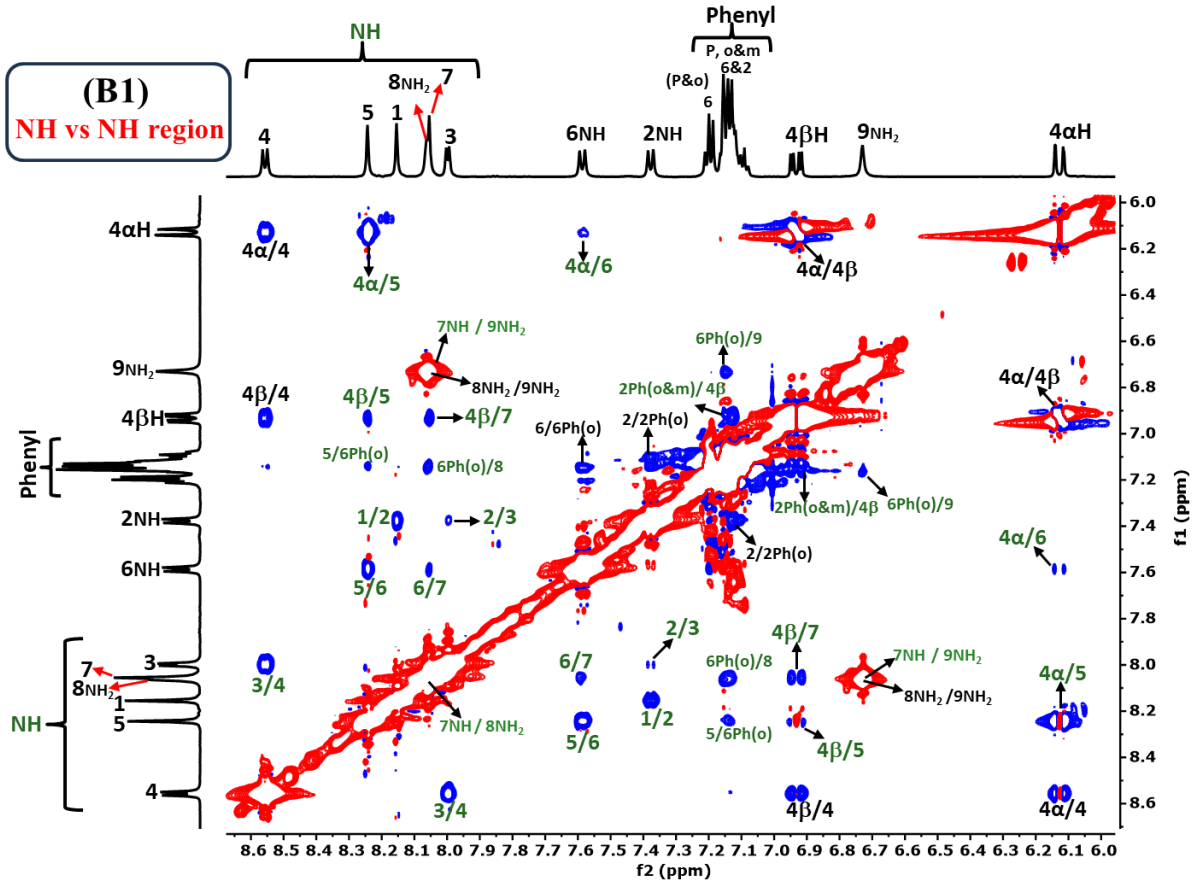


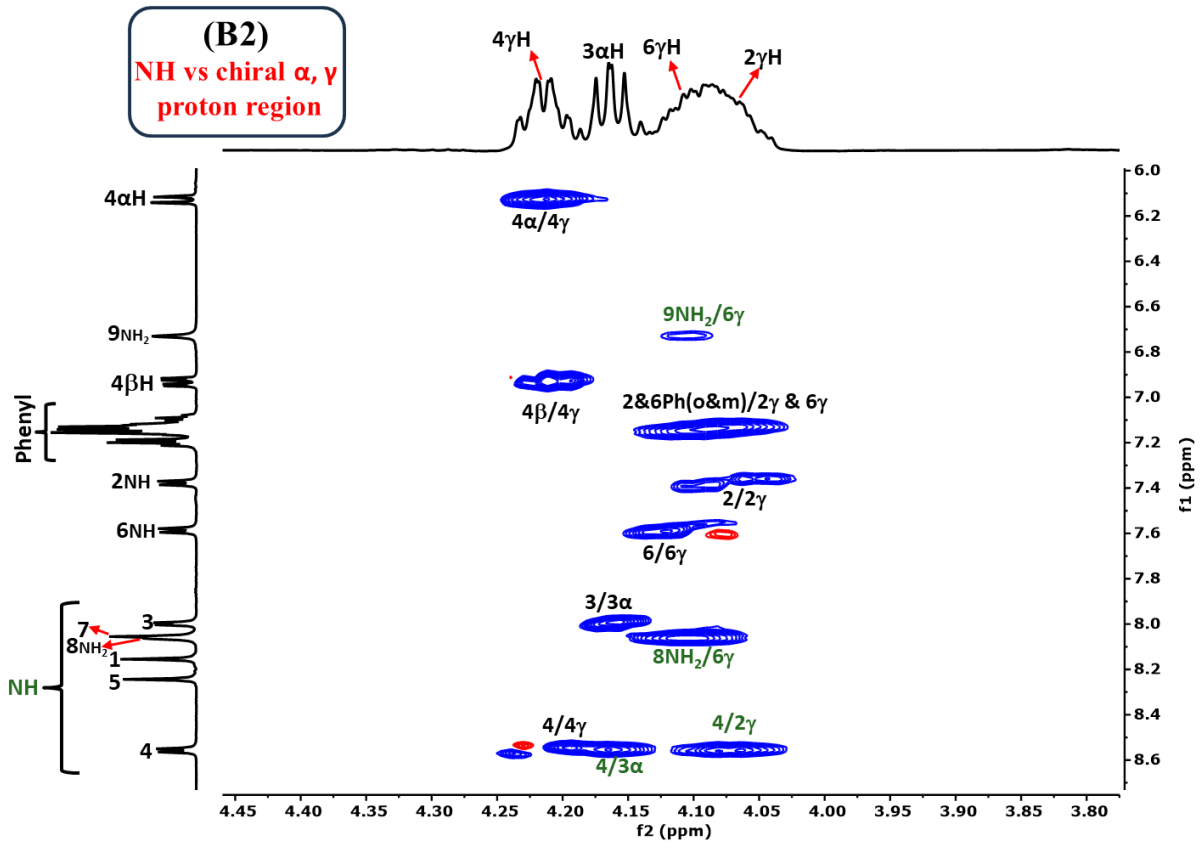
Figure 9: (A) Partial TOCSY spectrum (NH vs α, β, γ, Backbone & Side Chain protons) of peptide **P1** showing correlation between intra residue protons.

B) Partial ROESY spectrum analysis of Peptide P1 in CD_3OH

The below ROESY spectrums (B1) and (B2) depicting the NH↔NH, NH↔chiral $C_\alpha H$, $C_\gamma H$ interactions respectively. The **inter** and intra-residue NOEs are marked with **green** and black labels respectively. Crystal structure of peptide **P1** (B3) depicting observed distance between the protons responsible for **inter** residue NOEs marked with **green** color shown below in partial spectrum B1 and B2.




(B1)
NH vs NH region
NH
Phenyl
P, o&m
6&2
(P&o)
6
4
5
1
8NH2
7
3
6NH
2NH
4βH
9NH2
4αH
4α/4
4α/5
4α/6
4α/4β
4β/4
4β/5
4β/7
7NH / 9NH2
8NH2 /9NH2
6Ph(o)/9
2Ph(o&m)/ 4β
6/6Ph(o)
2/2Ph(o)
5/6Ph(o)
6Ph(o)/8
1/2
2/3
5/6
6/7
3/4
7NH / 8NH2
f1 (ppm)
f2 (ppm)


(B2)
NH vs chiral α, γ
proton region
4γH
3αH
6γH
2γH
4α/4γ
9NH2/6γ
4β/4γ
2&6Ph(o&m)/2γ & 6γ
2/2γ
6/6γ
3/3α
8NH2/6γ
4/4γ
4/2γ
4/3α
Phenyl
NH
f1 (ppm)
f2 (ppm)

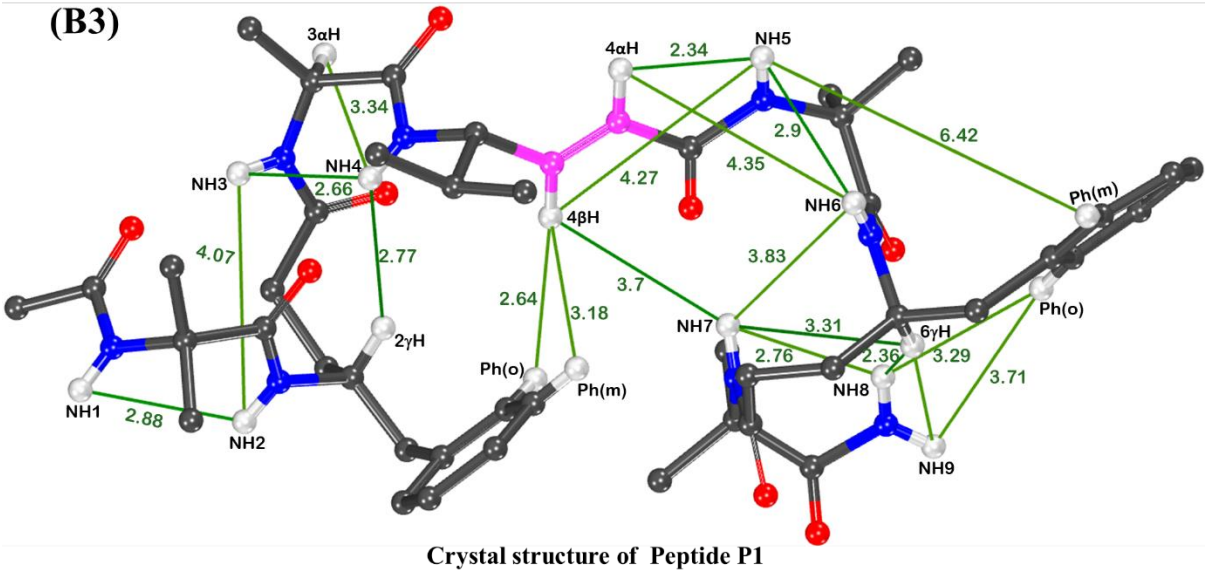


Figure 10: (**B1**) NH vs NH region of peptide **P1** ROESY spectrum in CD_3OH. (**B2**) NH vs Chiral α, and γ protons region of ROESY spectrum of peptide **P1** in CD_3OH. (**B3**) Crystal structure of peptide P1 (B3) depicting observed distance between the protons responsible for **inter** residue NOEs marked with **green** color shown in partial ROESY spectrum B1 and B2. (**inter** -residue NOEs are marked with **green** labels in the ROESY spectrum (B1) and (B2)).

Table 10: NOEs Observed in NH↔NH and NH↔C_αH/ C_βH /C_γH Region of Peptide **P1** in CD_3OH and the distance observed between respective protons in its crystal structure.

C) List of Inter-residue NOEs (marked with green labels) in partial ROESY spectrum (**B1**) and (**B2**) of peptide **P1** in CD_3OH.							
Residue	**H-atom**	**Residue**	**H-atom**	**NOE observed**	**Type of NOE**	**Protons Region**	**Distance in crystal structure (Å)**
Aib (1)	NH	γPhe (2)	NH	Strong	NH/NH (1/2)	**(Inter-Residue NOE) NH vs NH region (Fig. 8: B1)**	2.88
γPhe (2)	NH	Ala (3)	NH	Very Weak	NH/NH (2/3)		4.07
Ala (3)	NH	(*E*)-dγVal (4)	NH	Strong	NH/NH (3/4)		2.66
Aib (5)	NH	γPhe (6)	NH	Strong	NH/NH (5/6)		2.9
γPhe (6)	NH	Aib (7)	NH	Weak	NH/NH (6/7)		3.83
Aib (7)	NH	$CONH_2$ (8)	NH (Intra H-Bonded)	Strong (at Diagonal)	NH/NH (7/8)		2.76
Aib (7)	NH	$CONH_2$ (9)	NH	Medium (Merged in Tocsy Signal)	NH/NH (7/9)		4.09

(E)-dγVal (4)	α CH (Backbone)	Aib (5)	NH	Very Strong	αCH/NH (4/5)	**(Inter-Residue NOE) NH vs NH region (Fig. 8: B1)**	2.34
(E)-dγVal (4)	α CH (Backbone)	Aib (6)	NH	Very Weak	αCH/NH (4/6)		4.35
γPhe (2)	Phenyl (o & m) CH (side-chain)	(*E*)-dγVal (4)	β CH (Backbone)	Strong	Ph(o & m)/βCH (2/4)		2.64 (ortho) 3.18 (meta)
(E)-dγVal (4)	β CH (Backbone)	Aib (5)	NH	Medium	βCH/NH (4/5)		4.27
(E)-dγVal (4)	β CH (Backbone)	Aib (7)	NH	Medium	βCH/NH (4/7)		3.7
γPhe (6)	Phenyl (ortho) CH (side-chain)	$CONH_2$ (8)	NH (intra H-Bonded)	Medium	Ph(o)/NH (6/8)		3.29 (ortho)
γPhe (6)	Phenyl (ortho) CH (side-chain)	$CONH_2$ (9)	NH	Medium	Ph(o)/NH (6/9)		3.71 (ortho)
Aib (5)	NH	γPhe (6)	Phenyl (ortho) CH (side-chain)	Very Weak	NH/ Ph(o) (5/6)		6.42
$CONH_2$(9)	NH	γPhe (6)	γ CH (Backbone)	Medium	NH /γCH (9/6)	**(Inter-Residue NOE) NH vs γ & α CH region (Fig. 8: B2)**	3.25
$CONH_2$(8)	NH (intra H-Bonded)	γPhe (6)	γ CH (Backbone)	Very Strong	NH /γCH (8/6)		2.36
(E)-dγVal (4)	NH	Ala (3)	α CH (Backbone)	Strong	NH /αCH (4/3)		3.34
(E)-dγVal (4)	NH	γPhe (2)	γ CH (Backbone)	Strong	NH /γCH (4/2)		2.77

D) Intra-residue NOEs (marked with **black** labels) in partial ROESY spectrum (**B1**) and (**B2**) of peptide **P1** in CD_3OH.

Residue	**H-atom**	**Residue**	**H-atom**	**NOE observed**	**Protons Region**	**Distance in crystal structure (Å)**
(E)-dγVal (4)	α CH (Backbone)	(*E*)-dγVal (4)	NH	Strong	**(Intra-Residue NOE) NH vs NH region (Fig. 8: B1)**	4.43
(E)-dγVal (4)	β CH (Backbone)	(*E*)-dγVal (4)	NH	Strong		2.97
(E)-dγVal (4)	α CH (Backbone)	(*E*)-dγVal (4)	β CH (Backbone)	Very Strong		2.69
γPhe (2)	NH	γPhe (2)	Phenyl (ortho) CH (side-chain)	Strong		3.03 & 4.77 (ortho)
γPhe (6)	NH	γPhe (6)	Phenyl (ortho) CH	Medium		3.83 &4.19 (ortho)
$CONH_2$ (8)	NH (Intra H-Bonded)	$CONH_2$ (9)	NH	Strong		1.48
(E)-dγVal (4)	α CH	(*E*)-dγVal (4)	γ CH (Backbone)	Strong	**(Intra-Residue NOE) NH vs γ & α CH region (Fig. 8: B2)**	2.31
(E)-dγVal (4)	β CH (Backbone)	(*E*)-dγVal (4)	γ CH (Backbone)	Strong		2.84
γPhe (2)	Phenyl (o & m) CH (side-chain)	γPhe (2)	γ CH (Backbone)	Very Strong		3.96 & 2.79 (ortho)

					(Intra-Residue NOE) NH vs γ & α CH region (Fig. 8: B2)	4.54 & 5.38 (meta)
γPhe (6)	Phenyl (o & m) CH (side-chain)	γPhe (6)	γ CH (Backbone)	Very Strong		2.38 & 4.62 (ortho) 4.67 &6.16 (meta)
γPhe (2)	NH	γPhe (2)	γ CH (Backbone)	Medium		2.75
γPhe (6)	NH	γPhe (6)	γ CH (Backbone)	Medium		2.75
Ala (3)	NH	Ala (3)	α CH (side-chain)	Strong		2.56
(E)-dγVal (4)	NH	(*E*)-dγVal (4)	γ CH (Backbone)	Strong		2.76

3.3.5.2. Peptide P2 2D-NMR analysis and NOE correlations with its solid state structure

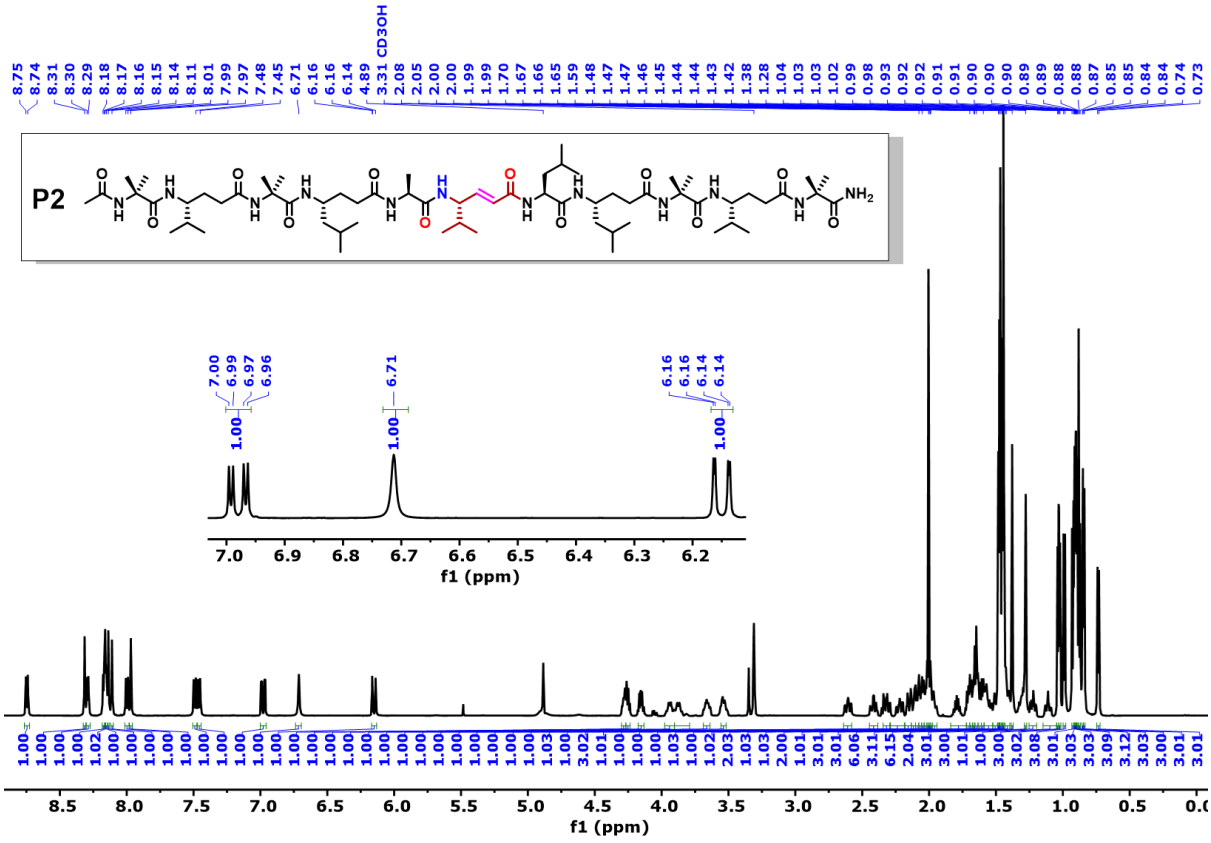


Figure 11: ^{1}H NMR spectrum of peptide **P2** in CD_3OH.

Characterization Data of P2

^{1}H NMR (600 MHz, CD_3OH) δ 8.75 (d, *J* = 8.5 Hz, 1H), 8.31 (s, 1H), 8.29 (d, *J* = 6.3 Hz, 1H), 8.17 (d, *J* = 5.0 Hz, 1H), 8.16 (s, 1H), 8.15 (s, 1H), 8.14 (s, 1H), 8.11 (s, 1H), 8.00 (d, *J* = 9.8 Hz, 1H), 7.97 (s, 1H), 7.49 (d, *J* = 9.7 Hz, 1H), 7.46 (d, *J* = 9.9 Hz, 1H), 6.98 (dd, *J* = 15.2,

4.3 Hz, 1H), 6.71 (s, 1H), 6.15 (dd, *J* = 15.2, 2.0 Hz, 1H), 4.28 (m, 1H), 4.25 (m, 1H), 4.15 (m, 1H), 3.94 (m, 1H), 3.87 (m, 1H), 3.67 (m, 1H), 3.54 (m, 1H), 2.61 (ddd, *J* = 14.3, 12.3, 4.2 Hz, 1H), 2.42 (m, 1H), 2.32 (m, 1H), 2.22 (m, 1H), 2.15 (dt, *J* = 12.3, 3.4 Hz, 1H), 2.11 (m, 1H), 2.09 (m, 1H), 2.07 (m, 1H), 2.05 (m, 1H), 2.03 (m, 1H), 2.00 (s, 3H), 1.99 (s, 1H), 1.98 (m, 1H), 1.96 (m, 1H), 1.79 (m, 1H), 1.71 (m, 1H), 1.69 (m, 1H), 1.67 (m, 1H), 1.65 (m, 2H), 1.61 (m, 1H), 1.56 (m, 2H), 1.51 (m, 1H), 1.48 (s, 3H), 1.47 (s, 3H), 1.466 (s, 6H), 1.46 (br, 1H), 1.45 (s, 3H), 1.44 (s, 6H), 1.41 (m, 2H), 1.38 (s, 3H), 1.28 (s, 3H), 1.23 (m, 1H), 1.11 (m, 1H), 1.04 (d, *J* = 4.7 Hz, 3H), 1.02 (d, *J* = 4.7 Hz, 3H), 0.99 (d, *J* = 6.6 Hz, 3H), 0.93 (d, *J* = 6.6 Hz, 3H), 0.91 (d, *J* = 4.5 Hz, 3H), 0.91 (d, *J* = 4.5 Hz, 3H), 0.90 (d, *J* = 5 Hz, 3H), 0.89 (d, *J* = 6.5 Hz, 3H), 0.87 (d, *J* = 5 Hz, 3H), 0.85 (d, *J* = 6.4 Hz, 3H), 0.84 (d, *J* = 6.5 Hz, 3H), 0.74 (d, *J* = 6.4 Hz, 3H). **MALDI (TOF/TOF)** *m/z* calculated value for $C_{64}H_{116}N_{12}O_{12}$ [M+Na^+] is 1267.87 and observed at 1267.94.

Table 11. ^{1}H NMR Chemical Shifts assignment (ppm) of **P2** in **CD_3OH** at 298 K.

Residues	*NH*	*$_\alpha$CH*	*$_\beta$CH*	*$_\gamma$CH*	*$_\delta$CH*	*$_\varepsilon$CH*	*$_\zeta$CH*	*CH_{term}*
-$COCH_3$	—	—	—	—	—	—	—	2.00
Aib(1)	8.31	—	1.466(6H)	—	—	—	—	—
γVal(2)	7.46	2.32 (1H) 2.11 (1H)	2.07 (1H) 1.61 (1H)	3.54	1.51	0.90 (3H) 0.87 (3H)	—	—
Aib(3)	8.14	—	1.38 (3H) 1.28 (3H)	—	—	—	—	—
γLeu(4)	8.17	2.61 (1H) 2.15(1H)	2.05 (1H) 1.67 (1H)	3.87	1.56 (1H)	1.11 (1H)	0.85(3H) 0.74(3H)	—
Ala(5)	8.16	4.15 (1H)	1.45 (3H)	—	—	—	—	—
dγVal(6)	8.75	6.15 (1H)	6.98 (1H)	4.28	2.03 (1H)	1.04 (3H) 1.02 (3H)	—	—
Leu(7)	8.29	4.25 (1H)	1.65 (2H)	1.79	0.99 (3H) 0.93 (3H)	—	—	—
γLeu(8)	7.49	2.22 (1H) 2.09 (1H)	1.98 (1H) 1.46 (1H)	3.94	1.41 (2H)	1.23 (1H)	0.89(3H) 0.84(3H)	—
Aib(9)	8.11	—	1.48 (3H) 1.47 (3H)	—	—	—	—	—
γVal(10)	8.00	1.99 (1H) 1.99 (1H)	1.96 (1H) 1.71 (1H)	3.67	1.69 (1H)	0.91 (3H) 0.91 (3H)	—	—
Aib(11)	7.97	—	1.44 (6H)	—	—	—	—	—

-NH₂	8.15[a] 6.71[b]	—	—	—	—	—	—	—

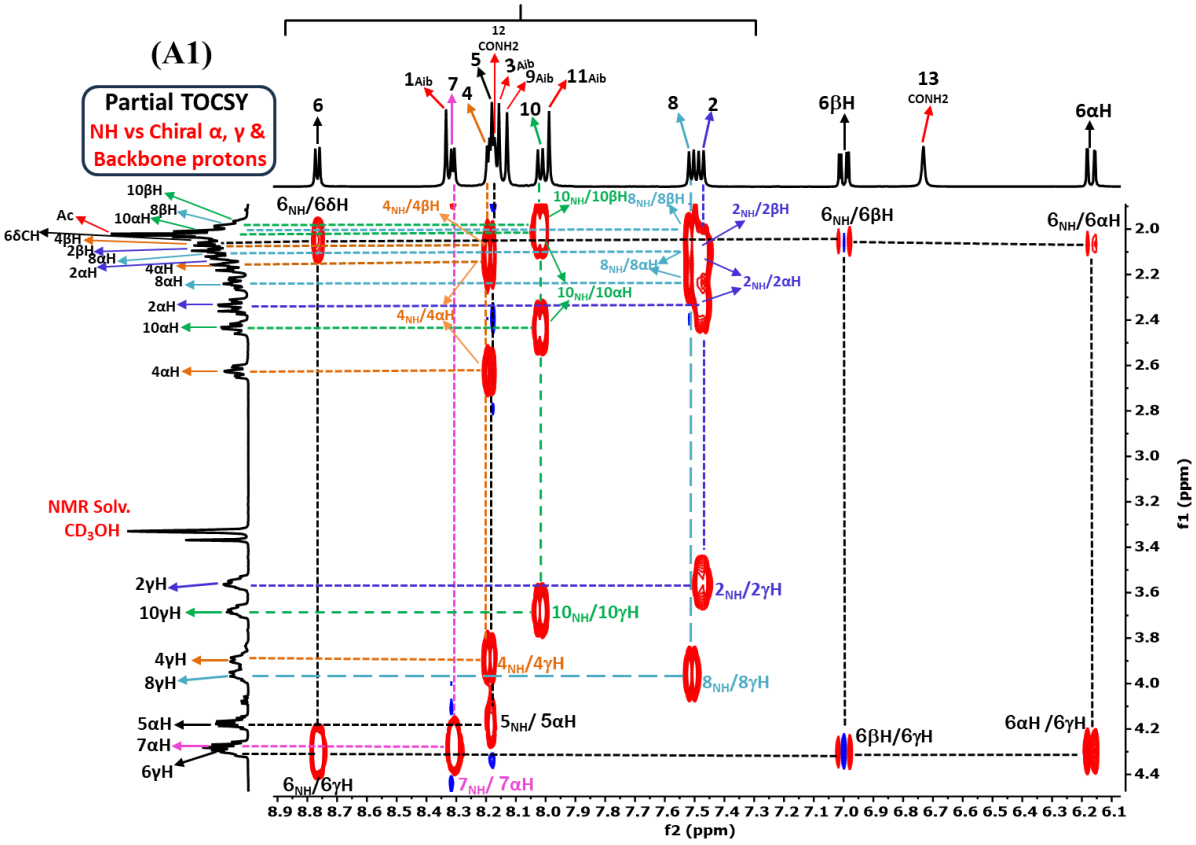
[a] $CONH_2$ Proton involved in Hydrogen bonding. [b] $CONH_2$ Proton is not involved in Hydrogen bonding. Chemical shift assigned by using TOCSY and ROESY spectra.

Assignment of chemical shifts using TOCSY and ROESY spectra

The amino acid residues and their positions in the peptide sequence were identified using TOCSY and ROESY spectra, respectively. The TOCSY spectrum was used to identify amino acids in the sequence of the peptides.

A) Partial TOCSY spectrum analysis of peptide P2 in CD_3OH

Below partial TOCSY spectrum showing the amino acid residues in peptide **P2**.



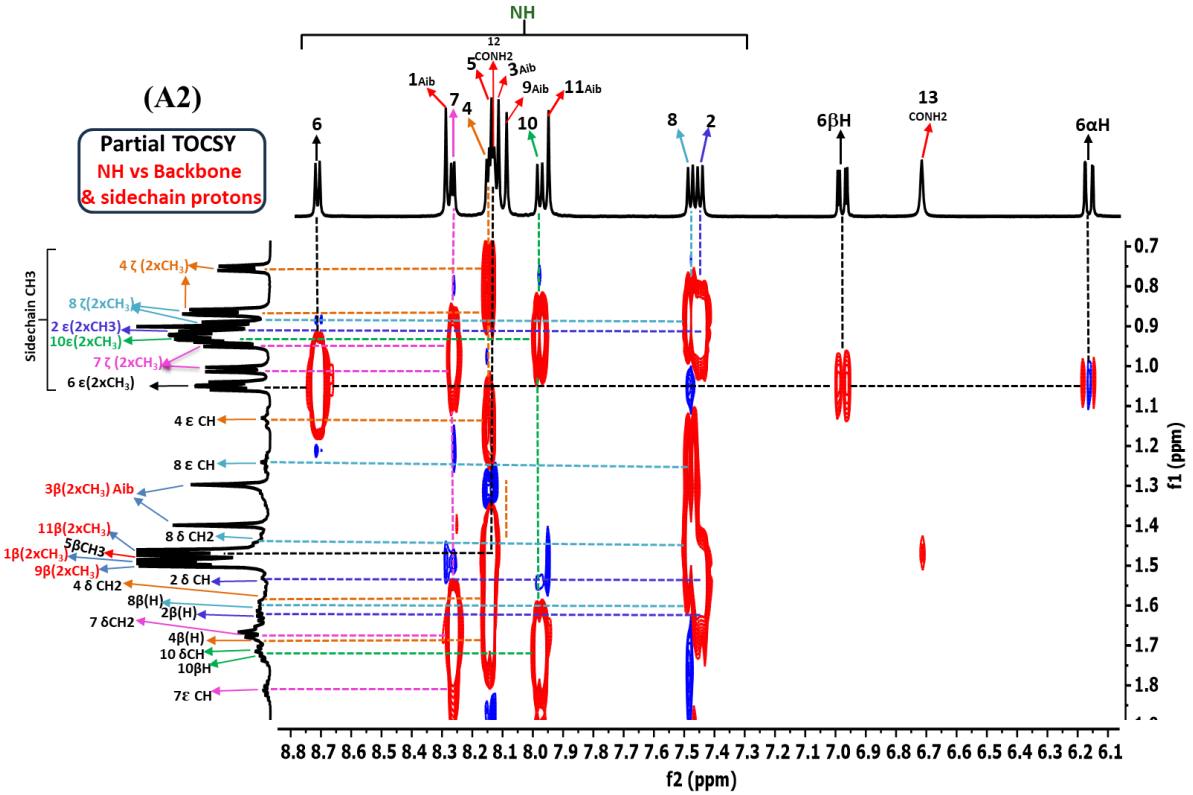
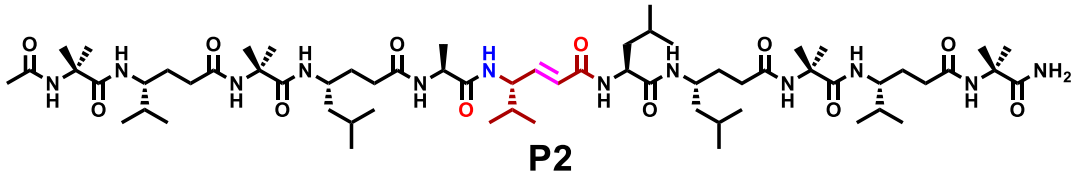


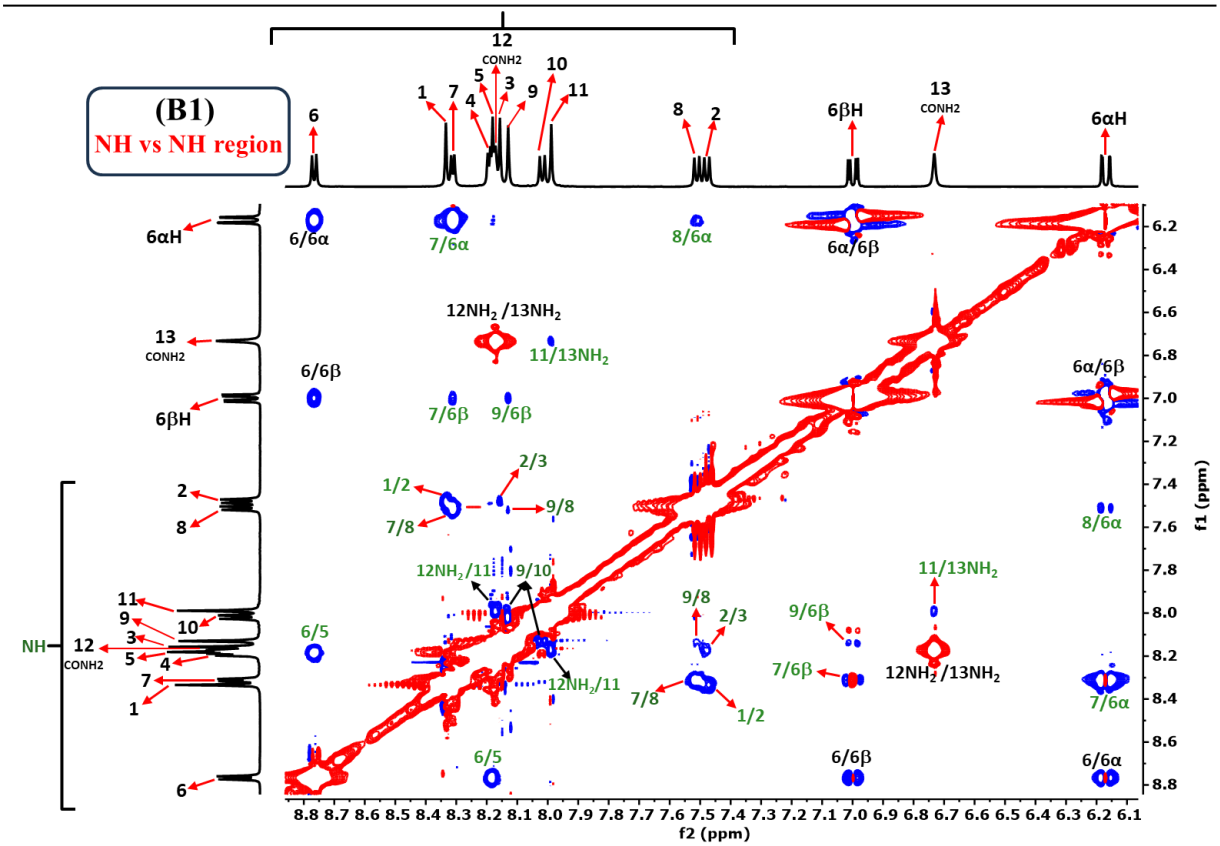
Figure 12: (A1) NH vs α, β, γ & Backbone protons and (A2) NH vs Backbone and sidechain protons are Partial TOCSY spectra of peptide **P2** showing correlation between intra residue protons.

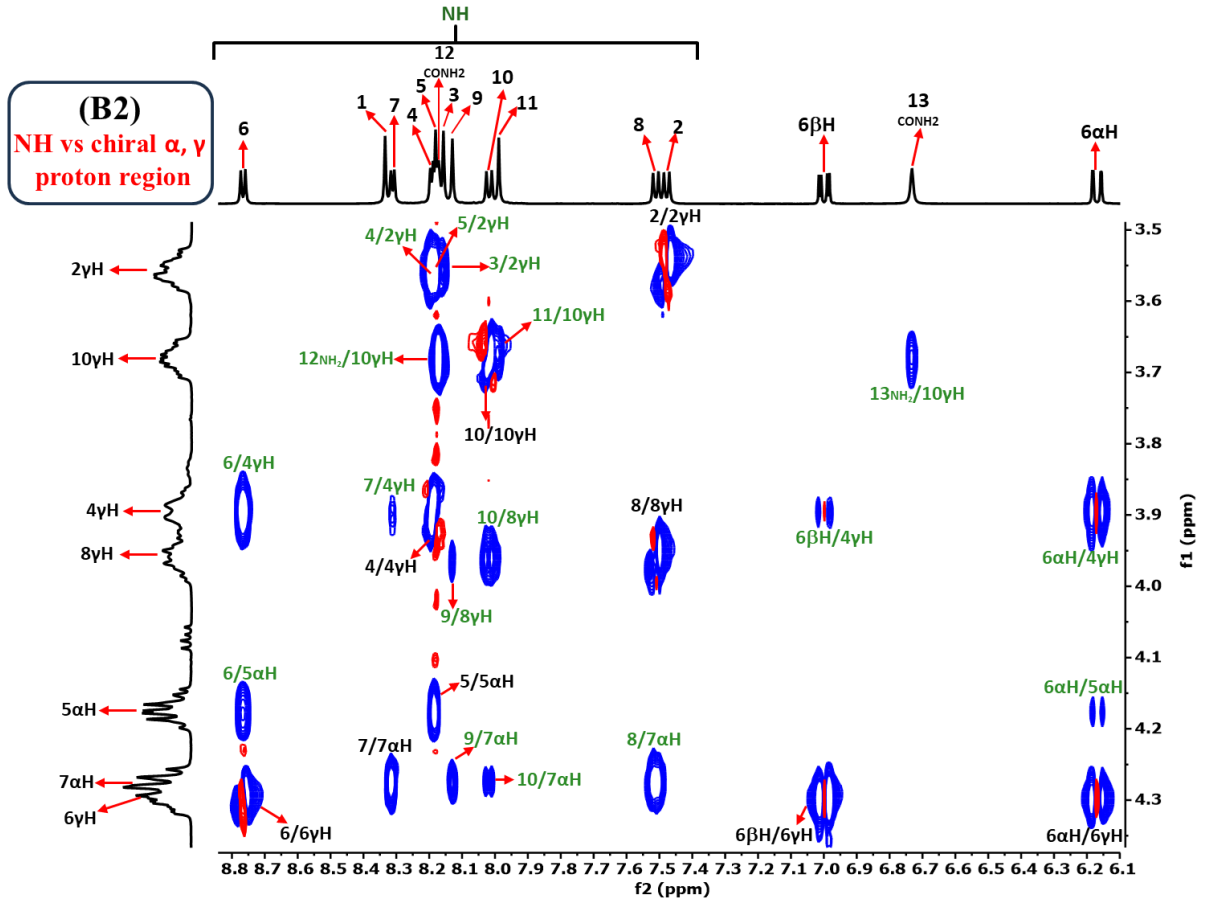
B) Partial ROESY spectrum analysis of peptide P2 in CD_3OH

The below ROESY spectrums (B1) and (B2) depicting the NH↔NH, NH↔chiral $C_\alpha H$, $C_\gamma H$ interactions respectively. The **inter** and intra-residue NOEs are marked with **green** and black labels respectively. Crystal structure of peptide **P2** (B3) depicting observed distance between the protons responsible for **inter** residue NOEs marked with **green** color shown below in partial spectrum B1 and B2.



P2


(B1)
NH vs NH region
f2 (ppm)
f1 (ppm)


(B2)
NH vs chiral α, γ proton region
f2 (ppm)
f1 (ppm)

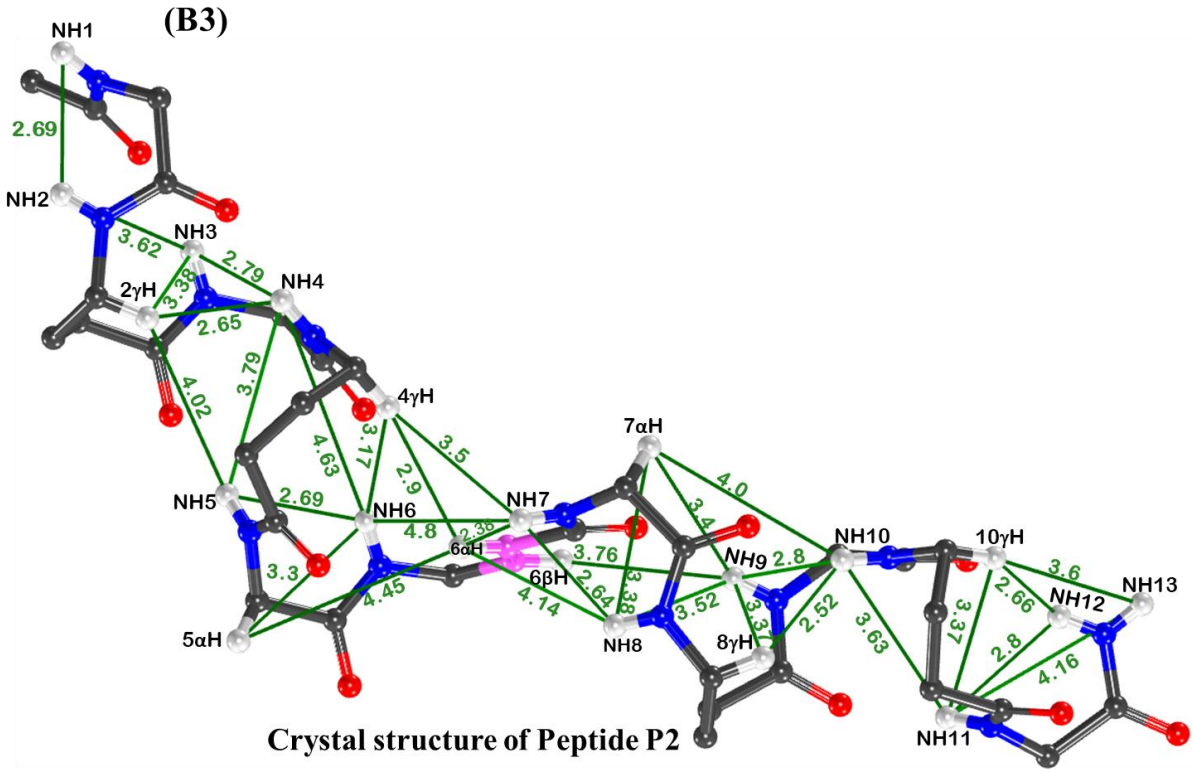


Figure 13: (**B1**) NH vs NH region of peptide **P2** ROESY spectrum in CD_3OH. (**B2**) NH vs Chiral α, and γ protons region in ROESY spectrum of peptide **P2** in CD_3OH. (**B3**) Crystal structure of peptide **P2** depicting the distance between inter residue NOE corresponding protons in the ROESY spectrum B1 and B2. (inter-residue NOEs marked with green labels in the ROESY spectrum (B1) and (B2)).

Table 12: NOEs Observed in NH↔NH and NH↔$C_\alpha H$/ $C_\beta H$ /$C_\gamma H$ Region of Peptide **P2** in CD_3OH and the distance observed between respective protons in its crystal structure.

C) List of Inter-residue NOEs (marked with **green** labels) in partial ROESY spectrum (**B1**) and (**B2**) of peptide **P2** in CD_3OH.							
Residue	**H-atom**	**Residue**	**H-atom**	**NOE observed**	**Type of NOE**	**Protons Region**	**Distance in crystal structure (Å)**
Aib (1)	NH	γVal (2)	NH	Strong	NH/NH (1/2)	**(Inter-Residue NOE) NH vs NH region (Fig. 11: B1)**	2.69
γVal (2)	NH	Aib (3)	NH	Weak	NH/NH (2/3)		3.62
Aib (3)	NH	γLeu (4)	NH	Strong (at Diagonal)	NH/NH (3/4)		2.79
γLeu (4)	NH	Ala (5)	NH	Weak (at Diagonal)	NH/NH (4/5)		3.79
Ala (5)	NH	(*E*)-dγVal (6)	NH	Strong	NH/NH (5/6)		2.69

Leu (7)	NH	γLeu (8)	NH	Very Strong	NH/NH (7/8)	**(Inter-Residue NOE) NH vs NH region (Fig. 11: B1)**	2.64
γLeu (8)	NH	Aib (9)	NH	Very Weak	NH/NH (8/9)		3.52
Aib (9)	NH	γVal (10)	NH	Strong	NH/NH (9/10)		2.80
γVal (10)	NH	Aib (11)	NH	Weak (at Diagonal)	NH/NH (10/11)		3.63
Aib (11)	NH	$CONH_2$ (12)	NH (intra H-Bonded)	Strong	NH/NH (11/12)		2.80
Aib (11)	NH	$CONH_2$ (13)	NH	Weak	NH/NH (11/13)		4.16
Leu (7)	NH	(*E*)-dγVal (6)	β CH (Backbone)	Weak	NH/ *β*CH (7/6)		4.24
Aib (9)	NH	(*E*)-dγVal (6)	β CH (Backbone)	Very Weak	NH/ *β*CH (9/6)		3.77
Leu (7)	NH	(*E*)-dγVal (6)	α CH (Backbone)	Very Strong	NH/ *α*CH (7/6)		2.38
γLeu (8)	NH	(*E*)-dγVal (6)	α CH (Backbone)	Very Weak	NH/ *α*CH (8/6)		4.14
(E)-dγVal (6)	NH	γLeu (4)	γ CH (Backbone)	Strong	NH/ *γ*CH (6/4)	**(Inter-Residue NOE) NH vs γ & α CH region (Fig. 11: B2)**	3.17
(E)-dγVal (6)	NH	Ala (5)	α CH (Backbone)	Strong	NH/ *α*CH (6/5)		3.3
Leu (7)	NH	γLeu (4)	γ CH (Backbone)	Weak	NH/ *γ*CH (7/4)		3.5
γLeu (4)	NH	γVal (2)	γ CH (Backbone)	Very Strong	NH/ *γ*CH (4/2)		2.65
Ala (5)	NH	γVal (2)	γ CH (Backbone)	Very Weak	NH/ *γ*CH (5/2)		4.02
$CONH_2$ (12)	NH (intra H-Bonded)	γVal (10)	γ CH (Backbone)	Very Strong	NH/ *γ*CH (12/10)		2.66
Aib (3)	NH	γVal (2)	γ CH (Backbone)	Medium	NH/ *γ*CH (3/2)		3.38
Aib (9)	NH	γLeu (8)	γ CH (Backbone)	Medium	NH/ *γ*CH (9/8)		3.37
Aib (9)	NH	Leu (7)	α CH (Backbone)	Medium	NH/ *α*CH (9/7)		3.43
γVal (10)	NH	γLeu (8)	γ CH (Backbone)	Strong	NH/ *γ*CH (10/8)		2.526
γVal (10)	NH	Leu (7)	α CH (Backbone)	Weak	NH/ *α*CH (10/7)		4.06
Aib (11)	NH	γVal (10)	γ CH (Backbone)	Medium	NH/ *γ*CH (11/10)		3.38
γLeu (8)	NH	Leu (7)	α CH (Backbone)	Strong	NH/ *α*CH (8/7)		3.38
(E)-dγVal (6)	β CH (Backbone)	γLeu (4)	γ CH (Backbone)	Weak	βCH / *γ*CH (6/4)		4.94
$CONH_2$ (13)	NH	γVal (10)	γ CH (Backbone)	Medium	NH/ *γ*CH (13/10)		3.61

(E)-dγVal (6)	α CH (Backbone)	γLeu (4)	γ CH (Backbone)	Strong	α CH/ γ CH (6/4)		2.91
(E)-dγVal (6)	α CH (Backbone)	Ala (5)	α CH (Backbone)	Weak	α CH/ α CH (6/5)		4.456

D) Intra-residue NOEs (marked with **black** labels) in partial ROESY spectrum (**B1**) and (**B2**) of peptide **P2** in CD_3OH.

Residue	**H-atom**	**Residue**	**H-atom**	**NOE observed**	**Protons Region**	**Distance in crystal structure (Å)**
(E)-dγVal (6)	NH	(*E*)-dγVal (6)	α CH (Backbone)	Strong	**(Intra-Residue NOE) NH vs NH region (Fig. 11: B1)**	2.57
(E)-dγVal (6)	NH	(*E*)-dγVal (6)	β CH (Backbone)	Medium		3.64
$CONH_2$ (12)	NH (Intra H-Bonded)	$CONH_2$ (13)	NH	Very Strong		1.52
(E)-dγVal (6)	α CH (Backbone)	(*E*)-dγVal (6)	β CH (Backbone)	Very Strong		2.76
(E)-dγVal (6)	NH	(*E*)-dγVal (6)	γ CH (Backbone)	Strong	**(Intra-Residue NOE) NH vs chiral γ & α CH region (Fig. 11: B2)**	2.78
Leu (7)	NH	Leu (7)	α CH (Backbone)	Strong		2.70
γLeu (4)	NH	γLeu (4)	γ CH (Backbone)	Very Strong		2.80
Ala (5)	NH	Ala (5)	α CH (Backbone)	Strong		2.68
γVal (10)	NH	γVal (10)	γ CH (Backbone)	Very Strong		2.79
γVal (2)	NH	γVal (2)	γ CH (Backbone)	Strong		2.78
γLeu (8)	NH	γLeu (8)	γ CH (Backbone)	Very Strong		2.77
(E)-dγVal (6)	β CH (Backbone)	(*E*)-dγVal (6)	γ CH (Backbone)	Very Strong		2.44
(E)-dγVal (6)	α CH (Backbone)	(*E*)-dγVal (6)	γ CH (Backbone)	Medium		3.29

3.3.5.3. Peptide P4 2D-NMR analysis and NOE correlations with its solid state structure

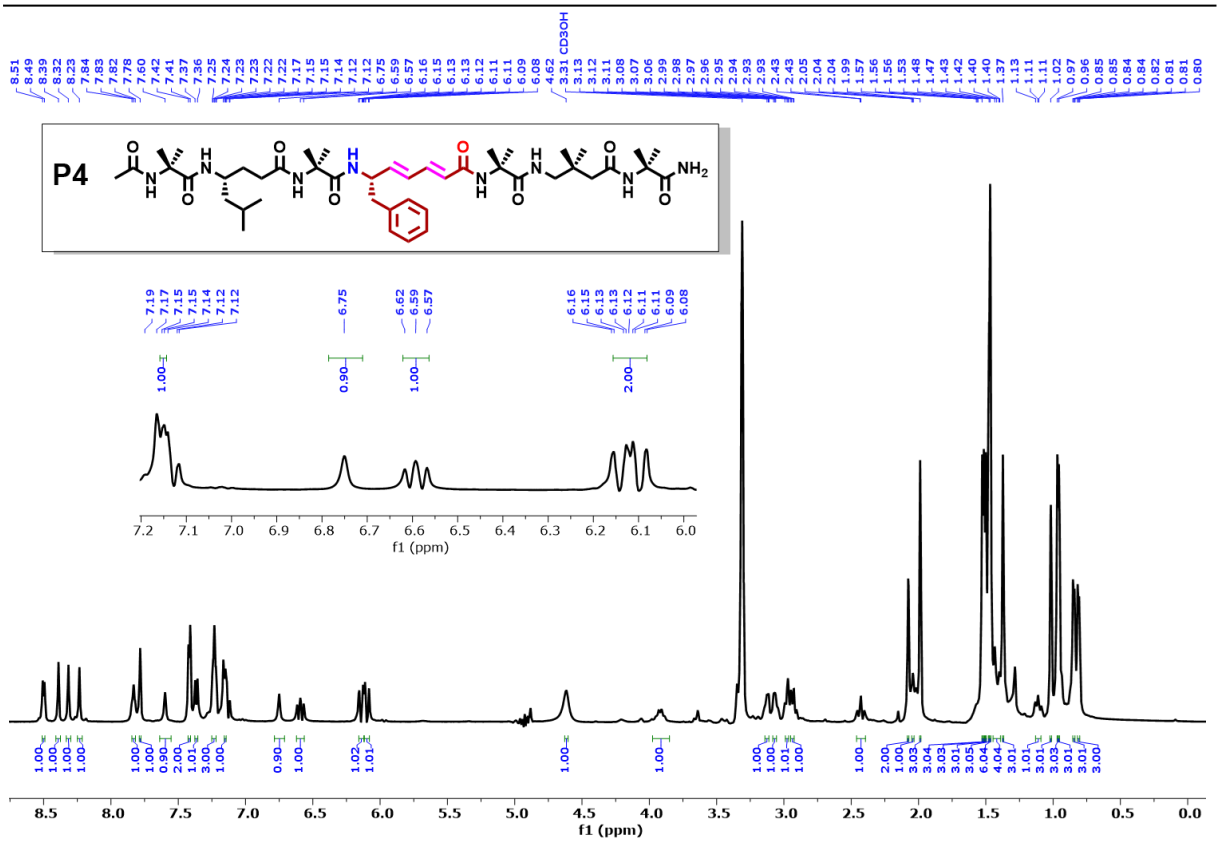


Figure 14: ^{1}H NMR spectrum of peptide **P4** in CD_3OH.

Characterization Data of P4

^{1}H NMR (600 MHz, CD_3OH) δ 8.50 (d, *J* = 8.5 Hz, 1H), 8.39 (s, 1H), 8.32 (s, 1H), 8.23 (s, 1H), 7.83 (t, *J* = 7.2 Hz, 1H), 7.78 (s, 1H), 7.60 (s, 1H), 7.42 (d, *J* = 8.0 Hz, 2H), 7.37 (d, *J* = 11.0 Hz, 1H), 7.23 (dt, *J* = 7.9, 3.7 Hz, 3H), 7.15 (m, 1H), 6.75 (s, 1H), 6.59 (m, 1H), 6.14 (m, 1H), 6.10 (m, 1H), 4.62 (s, 1H), 3.91 (m, 1H), 3.13 (t, *J* = 6.6 Hz, 1H), 3.07 (t, *J* = 6.6 Hz, 1H), 2.99 – 2.96 (m, 1H), 2.95 – 2.93 (m, 1H), 2.46 – 2.39 (m, 1H), 2.08 (s, 2H), 2.04 (br, 1H), 1.99 (s, 3H), 1.53 (s, 3H), 1.51 (s, 3H), 1.50 (s, 3H), 1.48 (s, 3H), 1.47 (s, 6H), 1.43 – 1.42 (m, 4H), 1.37 (s, 3H), 1.11 (m, 1H), 1.02 (s, 3H), 0.97 (s, 3H), 0.96 (s, 3H), 0.84 (m, 3H), 0.81 (m, 3H). **MALDI (TOF/TOF)** *m/z* calculated value for $C_{45}H_{72}N_8O_8$ [M+Na^+] is 875.60 and observed at 875.68.

Table 13. ^{1}H NMR Chemical Shifts assignment (ppm) of **P4** in CD_3OH at 298 K.

Residues	*NH*	*$_{\alpha}$CH*	*$_{\beta}$CH*	*$_{\gamma}$CH*	*$_{\delta}$CH*	*$_{\varepsilon}$CH*	*CH_{term}*
-$COCH_3$	—	—	—	—	—	—	1.99(3H)
Aib(1)	8.39	—	1.53 (3H) 1.51 (3H)	—	—	—	—
γLeu(2)	7.37	2.43(1H) 2.04(1H)	1.42(2H)	3.91(1H)	1.42(1H) 1.11(1H)	1.42(1H)	Sidechain 0.84(3H)

							0.81(3H)
Aib(3)	7.78	—	1.37 (3H) 1.02 (3H)	—	—	—	—
ddεPhe(4)	8.50	6.10(1H)	7.15(1H)	6.59(1H)	6.14(1H)	4.62(1H)	Benzylic 2.98(1H) 2.94(1H) Aromatic 7.42 (O) 7.23(M,P)
Aib(5)	8.32	—	1.50 (3H) 1.48 (3H)	—	—	—	—
γAdp(6)	7.83	2.08(2H)	Sidechain 0.97 (3H) 0.96 (3H)	3.13(1H) 3.07(1H)	—	—	—
Aib(7)	8.23	—	1.47 (6H)	—	—	—	—
-NH₂	7.60[a] 6.75[b]	—	—	—	—	—	—

[a] $CONH_2$ Proton involved in Hydrogen bonding. [b] $CONH_2$ Proton is not involved in Hydrogen bonding. Aromatic protons are shown in CH_{term} column. Chemical shift assigned by using TOCSY and ROESY spectra.

Assignment of chemical shifts using TOCSY and ROESY spectra

The amino acid residues and their positions in the peptide sequence were identified using TOCSY and ROESY spectra, respectively. The TOCSY spectrum was used to identify amino acids in the sequence of the peptides.

A) Partial TOCSY spectrum analysis of peptide P4 in CD_3OH

The below partial TOCSY spectrum showing the amino acid residues in peptide **P4**.

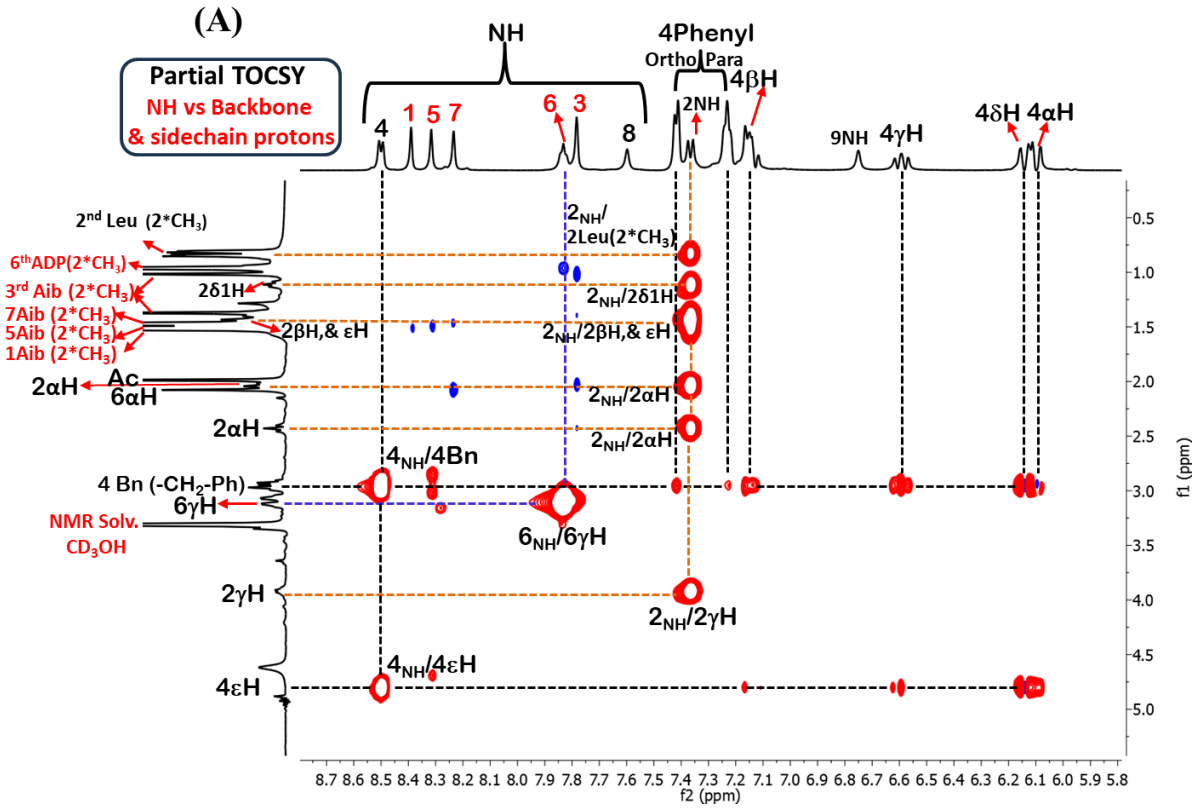
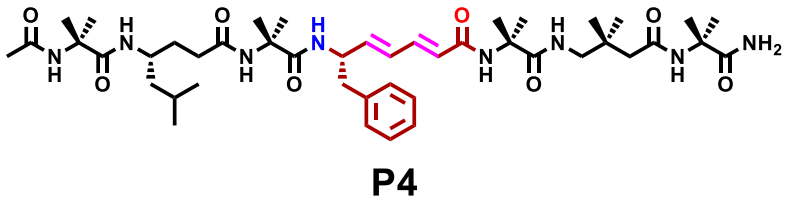


Figure 15: (A) Partial TOCSY spectrum (NH vs α, β, γ, Backbone & Side Chain protons) of peptide **P4** showing correlation between intra residue protons.

B) Partial ROESY spectrum analysis of peptide P4 in CD_3OH

The below partial ROESY spectrum (B1) depicting the NH↔NH, NH↔C_αH/ C_βH /chiral C_γH interactions respectively. The **inter** and intra-residue NOEs are marked with **green** and black labels respectively.



P4

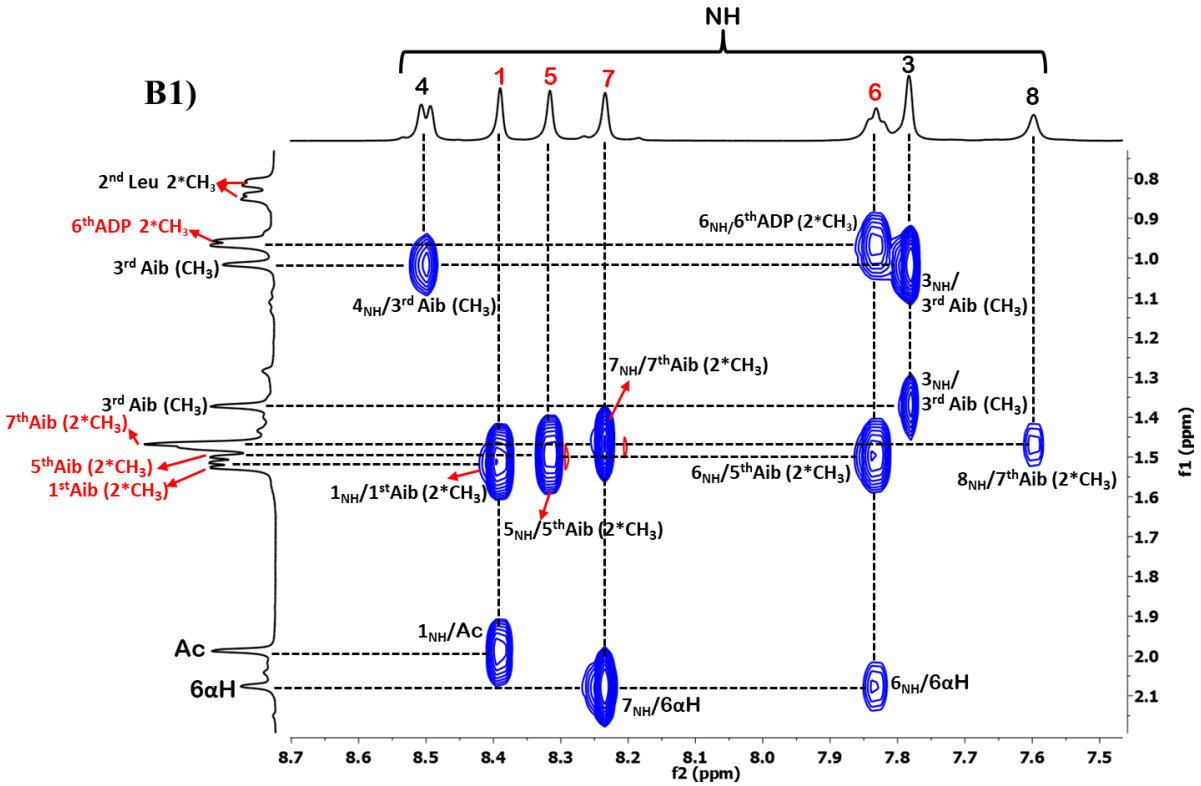
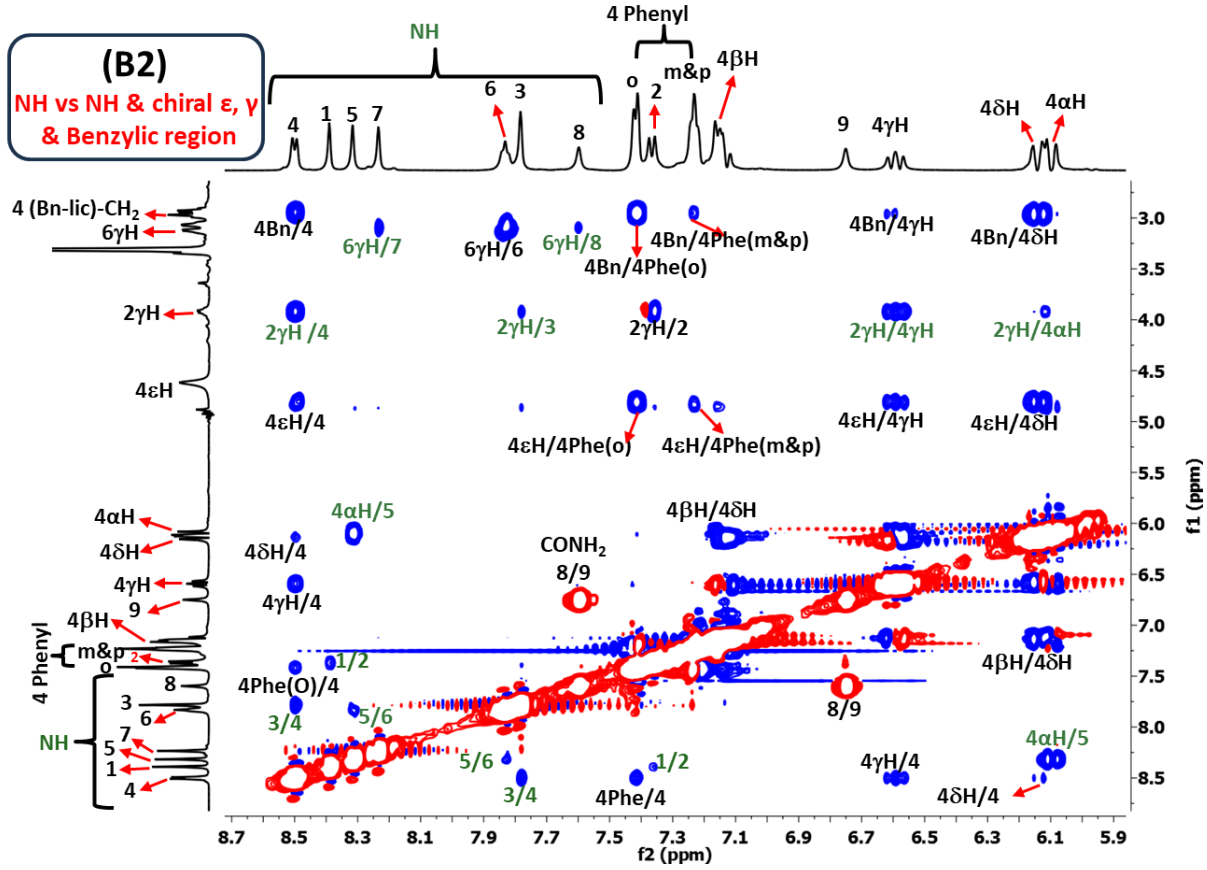
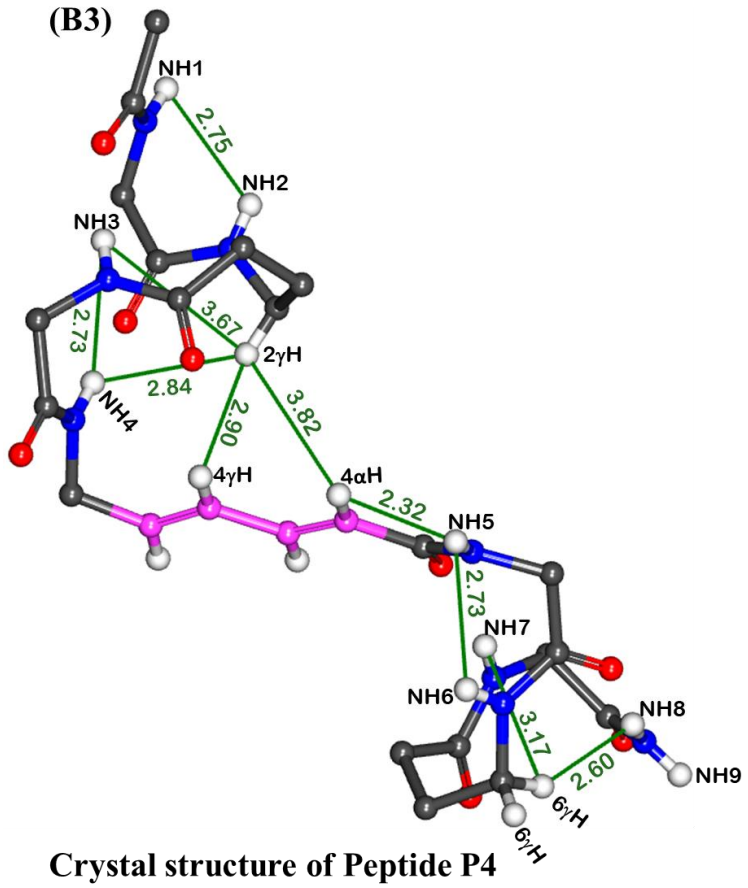


Figure 16: (B1) The Partial ROESY spectrum of peptide **P4** is used to identify the achiral Aib and Adp amino acids. The NH and side-chain protons of Aib residues are labelled in Red.





Crystal structure of Peptide P4

Figure 17: (**B2**) is the partial ROESY spectrum of peptide **P4** in CD_3OH showing sequential NOEs of NH↔NH and NH↔C_αH/ C_βH /chiral C_γH. (**B2**) Crystal structure of peptide **P4** depicting the distance between inter residue NOE corresponding protons in the ROESY spectrum (B1). (**inter**-residue NOEs marked with **green** labels in the ROESY spectrum (B1)).

Table 14: NOEs Observed in NH↔NH and NH↔C_αH/ C_βH /chiral C_γH region of ROESY spectrum of Peptide **P4** and the distance observed between respective protons in its crystal structure.

C) List of Inter-residue NOEs (marked with green labels) in partial ROESY spectrum (**B1**) of peptide **P4** in CD_3OH.							
Residue	**H-atom**	**Residue**	**H-atom**	**NOE observed**	**Type of NOE**	**Protons Region**	**Distance in crystal structure (Å)**
Aib (1)	NH	γLeu (2)	NH	Weak	NH*i*↔NH*i+1*	**(Inter-Residue NOE) NH vs NH/C_αH/ C_βH /chiral C_γH region (Fig. 15: B2)**	2.75
γLeu (2)	*γ* CH	Aib (3)	NH	Weak	*γ*CH*i*↔NH*i+1*		3.67
γLeu (2)	*γ* CH	(*E*,*E*)-ddεPhe (4)	NH	Strong	*γ*CH*i*↔NH*i+2*		2.84
γLeu (2)	*γ* CH	(*E*,*E*)-ddεPhe (4)	*γ* CH	Strong	*γ*CH*i*↔*γ*CH*i+2*		2.90
γLeu (2)	*γ* CH	(*E*,*E*)-ddεPhe (4)	*α* CH	Weak	*γ*CH*i*↔*α*CH*i+2*		3.82
Aib (3)	NH	(*E*,*E*)-ddεPhe (4)	NH	Medium	NH*i*↔NH*i+1*		2.73
(E,E)-ddεPhe (4)	*α* CH	Aib (5)	NH	Strong	*α*CH*i*↔NH*i+1*		2.32
Aib (5)	NH	Adb (6)	NH	Weak	NH*i*↔NH*i+1*		2.73
Adb (6)	*γ* CH	Aib (7)	NH	Medium	*γ*CH*i*↔NH*i+1*		3.17
Adb (6)	*γ* CH	$CONH_2$ (NH8)	NH	Weak	*γ*CH*i*↔NH*i+2*		2.6

D) Intra-residue NOEs (marked with **black** labels) in partial ROESY spectrum (**B1**) of peptide **P4** in CD_3OH.						
Residue	**H-atom**	**Residue**	**H-atom**	**NOE observed**	**Protons Region**	**Distance in crystal structure (Å)**
γLeu (2)	*γ* CH	γLeu (2)	NH	Strong	**(Intra-Residue NOE) NH vs NH/CαH/ CβH /chiral CγH region (Fig. 15: B2)**	2.77
(E,E)-ddεPhe (4)	Benzyl CH_2	(*E*,*E*)-ddεPhe (4)	NH	Strong		2.66
(E,E)-ddεPhe (4)	Benzyl CH_2	(*E*,*E*)-ddεPhe (4)	Phenyl (o) H	Very Strong		2.30
(E,E)-ddεPhe (4)	Benzyl CH_2	(*E*,*E*)-ddεPhe (4)	Phenyl(m&p) H	Weak		4.51 (m) 5.57 (p)
(E,E)-ddεPhe (4)	Benzyl CH_2	(*E*,*E*)-ddεPhe (4)	*γ* CH	Weak		2.31
(E,E)-ddεPhe (4)	Benzyl CH_2	(*E*,*E*)-ddεPhe (4)	*δ* CH	Very Strong		2.55
(E,E)-ddεPhe (4)	*ε* CH	(*E*,*E*)-ddεPhe (4)	NH	Medium		2.75

(E,E)-ddεPhe (4)	ε CH	(*E*,*E*)-ddεPhe (4)	Phenyl (o) H	Strong		2.46
(E,E)-ddεPhe (4)	ε CH	(*E*,*E*)-ddεPhe (4)	Phenyl(m&p) H	Weak		5.58(m) 5.94(p)
(E,E)-ddεPhe (4)	ε CH	(*E*,*E*)-ddεPhe (4)	γ CH	Medium		2.98
(E,E)-ddεPhe (4)	ε CH	(*E*,*E*)-ddεPhe (4)	δ CH	Very Strong		2.58
(E,E)-ddεPhe (4)	Phenyl(o) H	(*E*,*E*)-ddεPhe (4)	NH	Medium		3.60
(E,E)-ddεPhe (4)	γ CH	(*E*,*E*)-ddεPhe (4)	NH	Medium		2.75
(E,E)-ddεPhe (4)	δ CH	(*E*,*E*)-ddεPhe (4)	NH	Weak		3.50
(E,E)-ddεPhe (4)	β CH	(*E*,*E*)-ddεPhe (4)	δ CH	Very Strong		2.50
Adb (6)	γ CH	Adb (6)	NH	Very Strong		2.75
$CONH_2$ (NH8)	NH	$CONH_2$ (NH9)	NH	Very Strong		1.49

3.3.6. CD Spectroscopy of peptides P1, P2, P3 and P4

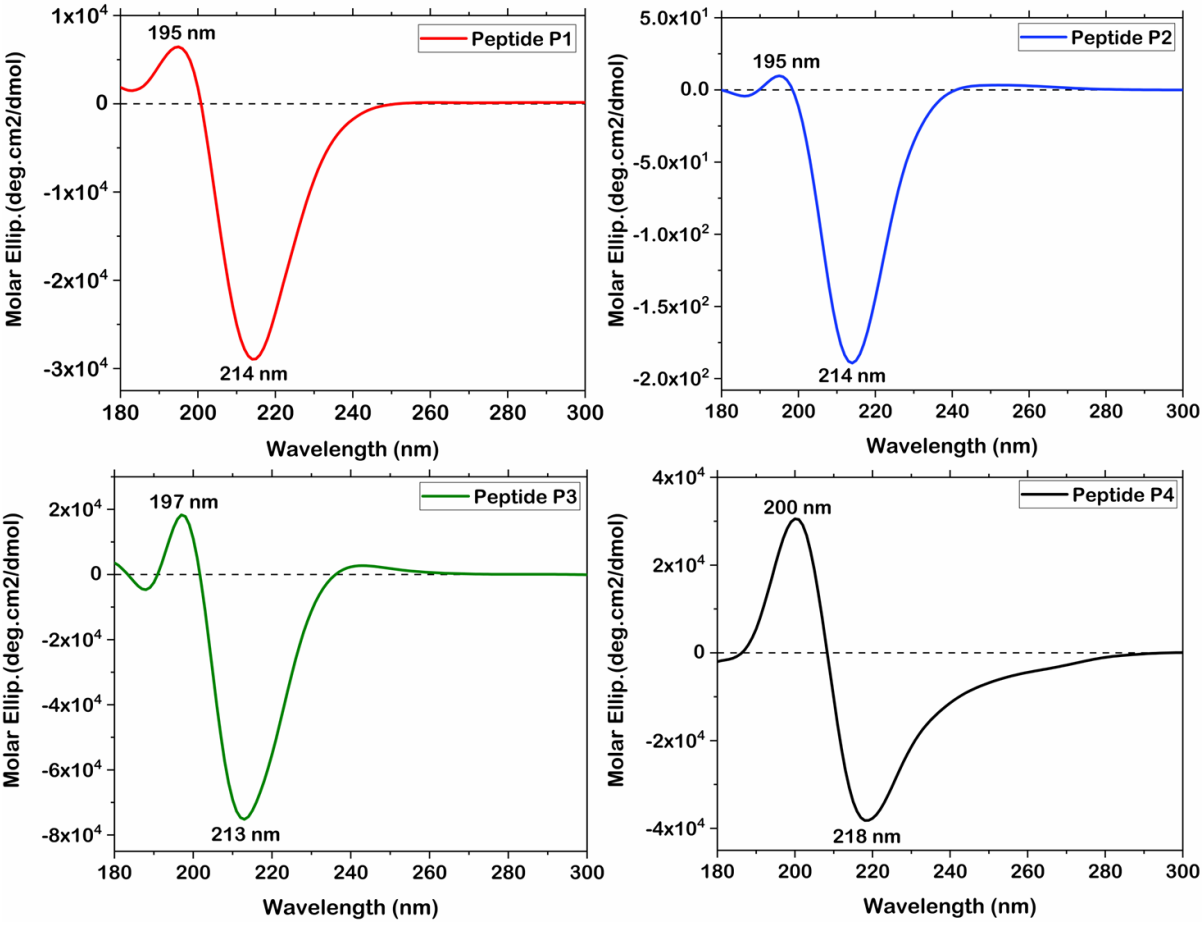


Figure 18: CD Spectra of peptides **P1, P2, P3**, and **P4** in methanol (CH_3OH) at a concentration of 1mg/mL.

The circular dichroism analysis revealed that both **P1, P2** and **P3** exhibited similar spectra, displaying CD minima at 214 nm. However, **P4** CD spectrum in methanol is slightly deviated spectrum compared to **P1, P2** and **P3**, likely due to its conjugated two double bonds. **P4** showed a red-shifted CD minimum at 218 nm.

3.3.7. HPLC trace of peptides P1, P2, P3, and P4

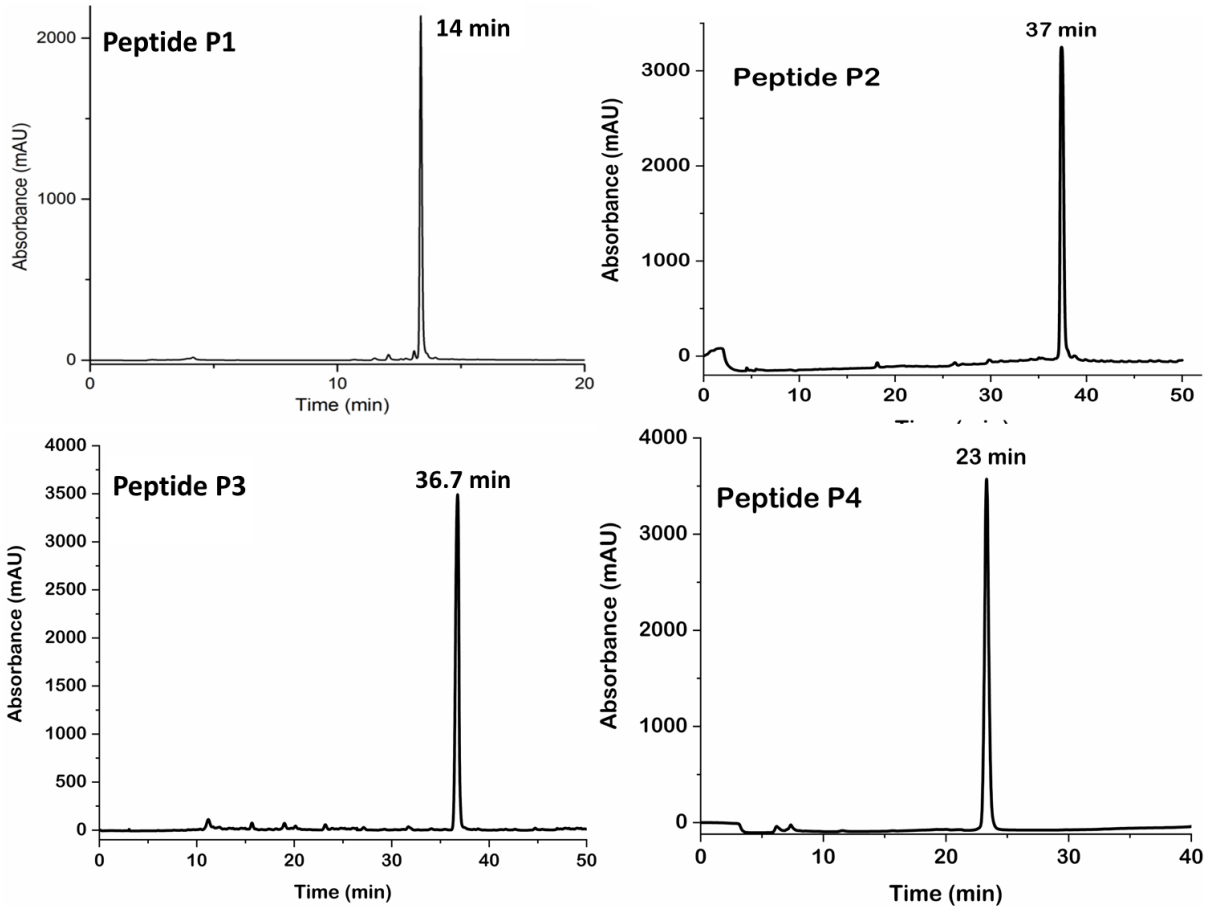


Figure 19: Reverse-phase-HPLC profiles of peptides **P1**, **P2, P3** and **P4** on a C-18 column using methanol/water gradients at a flow rate of 2.0 mL/min. Eluted compounds were detected by the UV absorbance at 220 nm.

3.4. Conclusion

In conclusion, we demonstrated the helix-turn-helix motifs in the designed α,γ-hybrid peptides consisting of α,β-unsaturated γ-amino acids in the middle of the sequence. The helices were separated by a conformationally rigid,α,β-unsaturated γ-amino acids. The helices can be moved apart by introducing additional double bonds in linker amino acids. The amide NH and CO groups of the linker amino acids are involved in helix stabilization through H-bonds. The helices are oriented almost perpendicular to one another mimicking the natural helix-turn-helix

structures. Though efforts have been made in the literature to design anti-parallel helix-turn-helix motifs[32], however, the design of helices with perpendicular orientation is rare. The superposition of the short synthetic sequence over the natural helix-turn-helix structure provides an opportunity to design three-dimensional structures in short peptide sequences. The structures and design principles reported here can be explored to construct a variety of unexplored supersecondary structural mimetics.

3.5. Experimental details

3.5.1. Materials, methods, and general experimental details

All amino acids, Di-tert-butyl dicarbonate, N,O-Dimethylhydroxylamine hydrochloride, DCC, HOBt, DIPEA, $LiAlH_4$, PPh_3, Ethyl bromoacetate, Pd/C (Palladium on carbon), Sodium hydroxide (NaOH), FMOC-Succinimide (FMOC-OSu), DIBAL-H, BF_3OEt_2, 2-iodoxybenzoic acid (IBX), Acetic anhydride, Knorr-Amide resin, MeOH, THF, DCM, and Ethyl acetate, were purchased from the commercial sources. THF was dried over sodium metal and distilled before use. DCM was also dried using CaH_2 and distilled under an inert atmosphere before use. MeOH, Pet-ether, and Ethyl acetate were distilled before use. Column chromatography was performed on silica gel (230-400 mesh). Final peptides were purified on reverse phase HPLC (C-18 column, MeOH/H2O 70:30-95:5 as gradient with flow rate 2.00 mL/min). ^{1}H NMR (1D and 2D NMR) spectra were recorded on 600 MHz, 500 MHz, and 400 MHz (or ^{13}C on 100 MHz) using residual solvents as internal standards (CD_3OH *δH* 3.31 *ppm*, *δC* 49.0 *ppm*, $CDCl_3$ *δH* 7.26 *ppm*, *δC* 77.3 *ppm*). The chemical shifts (*δ*) and coupling constants were reported in ppm and Hz respectively. The mass of all pure peptides was confirmed by Matrix Assisted LASER Desorption Ionization mass spectrometer (MALDI-TOF/TOF). Single crystal XRD data for peptide structure determination were collected from an X-ray diffractometer using Mo-Kα (λ = 0.71073 Å) graphite monochromated radiation.

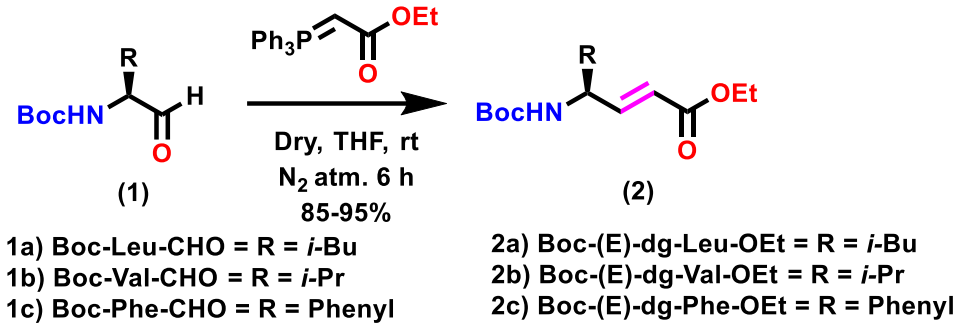
3.5.2. Procedures for building blocks synthesis and its characterization

A. Synthesis of Fmoc-NH-(*E*)-α, β-unsaturated γ-amino acids (4):

Fmoc-NH-(*E*)-α, β-Unsaturated γ-amino acids were synthesized by following three steps (AI – AIII) :

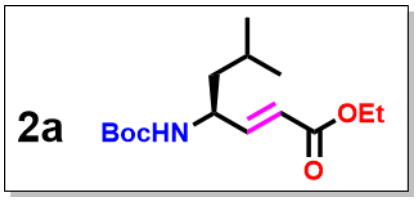
AI. Synthesis of Boc-NH-(*E*)-α, β-unsaturated γ-amino ethyl esters (2): Boc-NH-(*E*)-α, β-Unsaturated γ-amino ethyl esters (2) were synthesized using our reported protocol.**[1]** briefly; boc-amino aldehyde (**1**) (10 mmol) was dissolved in dry THF (180 ml) under N_2 atmosphere.

Then Wittig ylide (PPh_3=$CHCO_2Et$) (36 mmol) was added to the above solution. The reaction mixture was stirred for 6 h at room temperature. The progress of the reaction was monitored by using TLC. Upon completion of the reaction, THF was evaporated from the reaction mixture, and the product Boc-NH-(*E*)-α, β-unsaturated γ-amino ethyl ester (**2**) was purified by column chromatography using ethyl acetate in pet ether (5%) solvent system.



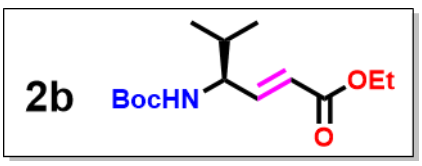
Scheme 2: Synthesis of Boc-NH-(*E*)-α, β-Unsaturated γ-amino ethyl esters (**2**).[1]

ethyl (*S*,*E*)-4-((tert-butoxycarbonyl)amino)-6-methylhept-2-enoate (2a):



^{1}H NMR (400 MHz, Chloroform-*d*) δ 6.81 (dd, *J* = 15.6, 5.4 Hz, 1H, βC*H*), 5.90 (d, *J* = 15.5 Hz, 1H, αC*H*), 4.48 (d, *J* = 8.8 Hz, 1H, N*H*), 4.36 – 4.28 (m, 1H, γC*H*), 4.18 (q, *J* = 7.1 Hz, 2H, -O-CH_2-), 1.71 – 1.64 (m, 1H, -εC*H*-$(CH_3)_2$), 1.43 (s, 9H, *Boc*), 1.37 (t, *J* = 7.4 Hz, 2H, -δCH_2-CH-$(CH_3)_2$), 1.27 (t, *J* = 7.1 Hz, 3H,-O-CH_2-CH_3), 0.92 (d, 6H, -CH-(ζCH_3)$_2$). **^{13}C NMR** (101 MHz, CHLOROFORM-*D*) δ 166.56, 155.22, 149.04, 120.53, 79.81, 77.47, 77.15, 76.83, 60.55, 49.92, 43.95, 28.47, 24.83, 22.83, 14.34. **HRMS** (ESI-QTOF) m/z calculated value for $C_{15}H_{27}NO_4$ is [M+Na] 308.1837 and observed 308.1845.

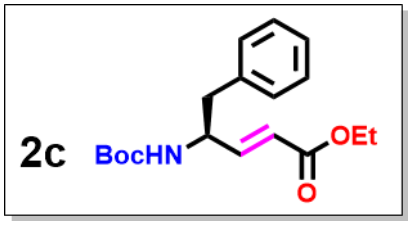
ethyl (*S*,*E*)-4-((tert-butoxycarbonyl)amino)-5-methylhex-2-enoate (2b):



^{1}H NMR (400 MHz, Chloroform-*d*) δ 6.85 (dd, *J* = 15.6, 5.5 Hz, 1H, βC*H*), 5.91 (dd, *J* = 15.7, 1.7 Hz, 1H, αC*H*), 4.56 (d, *J* = 9.2 Hz, 1H, N*H*), 4.24 – 4.12 (m, 3H, γC*H* & -O-CH_2-), 1.91 –

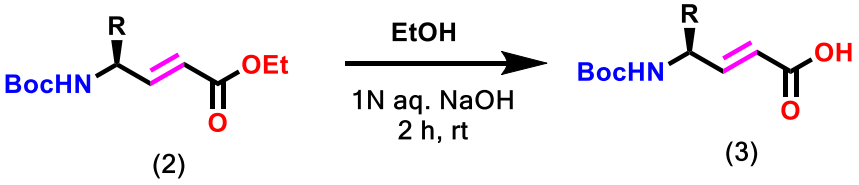
1.81 (m, 1H, -δC*H*-(CH_3)$_2$), 1.44 (s, 9H, *Boc*), 1.28 (t, *J* = 7.1 Hz, 3H, -O-CH_2-C*H*$_3$), 0.94 (d, *J* = 6.7 Hz, 3H, -CH-(εC*H*$_3$)$_2$, 0.91 (d, *J* = 6.9 Hz, 3H, -CH-(εC*H*$_3$)$_2$). **^{13}C NMR** (100 MHz, $CDCl_3$) δ 166.43, 155.51, 147.51, 121.64, 79.85, 77.48, 77.16, 76.84, 60.58, 56.82, 32.40, 28.50, 19.00, 18.13, 14.38. **HRMS** (ESI-QTOF) m/z calculated value for $C_{14}H_{25}NO_4$ is [M+Na] 294.1681 and observed 294.1663.

ethyl (*S*,*E*)-4-((tert-butoxycarbonyl)amino)-5-phenylpent-2-enoate (2c):



^{1}H NMR (400 MHz, Chloroform-*d*) δ 7.31 – 7.27 (m, 2H, Aromatic ortho), 7.25 – 7.15 (m, 3H, Aromatic meta & para), 6.90 (dd, *J* = 15.7, 4.8 Hz, 1H, βC*H*), 5.85 (dd, *J* = 15.7, 1.6 Hz, 1H, αC*H*), 4.61 (s, 1H, N*H*), 4.55 (s, 1H, γC*H*), 4.17 (d, *J* = 7.1 Hz, 2H, -O-C*H*$_2$-CH_3), 2.93 – 2.84 (m, 2H, *Benzylic*), 1.39 (s, 9H, *Boc*), 1.27 (t, *J* = 7.1 Hz, 3H, -O-CH_2-C*H*$_3$). **^{13}C NMR** (101 MHz, $CDCl_3$) δ 166.17, 154.96, 147.59, 136.40, 129.40, 128.57, 126.86, 121.10, 79.86, 77.36, 77.04, 76.73, 60.46, 52.28, 40.88, 28.30, 14.22. **HRMS** (ESI-QTOF) m/z calculated value for $C_{18}H_{25}NO_4$ is [M+Na] 342.1681 and observed 342.1688.

AII. Ethyl ester hydrolysis reaction: Purified Boc-NH-(*E*)-α, β-Unsaturated γ-amino ethyl ester (**2**) (8 mmol) was dissolved in 10 mL of EtOH and then 10 ml of 1N aq. NaOH solution was added to the reaction mixture. The reaction mixture was stirred at that temperature for 2 h. The progress of the reaction was monitored by TLC. After completion of the ethyl ester hydrolysis reaction, EtOH was removed under a *vacuum*. The residue was acidified with 5 % aq. HCl solution (25 ml). The hydrolyzed acid product (3) was extracted with ethyl acetate (40 x 3). The extracted ethyl acetate solution was washed with brine (150 ml) solution. The organic layer was then dried over anhydrous Na_2SO_4 and the product was concentrated under reduced pressure.



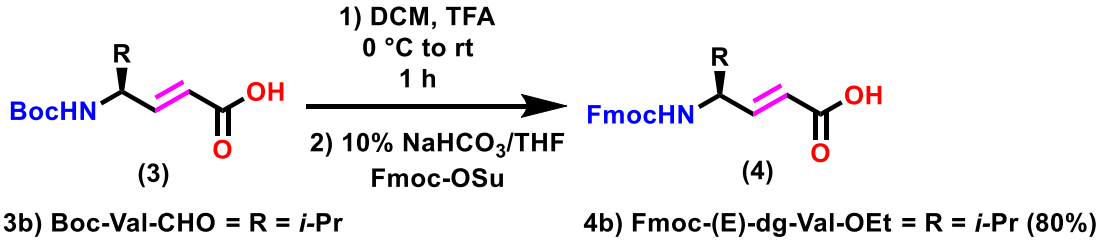
(2) (3)

2a) Boc-(E)-dg-Leu-OEt = R = *i*-Bu
2b) Boc-(E)-dg-Val-OEt = R = *i*-Pr
2c) Boc-(E)-dg-Phe-OEt = R = Phenyl

3a) Boc-(E)-dg-Leu-OH = R = *i*-Bu
3b) Boc-(E)-dg-Val-OH = R = *i*-Pr
3c) Boc-(E)-dg-Phe-OH = R = Phenyl

Scheme 3: Synthesis of Boc-NH-(*E*)-α, β-Unsaturated γ-amino acids (**3**).[1]

AIII. Boc deprotection and Fmoc protection reaction: The Boc-NH-(*E*)-α, β-Unsaturated γ-amino acid (**3**) (8 mmol) was dissolved in 5 mL of DCM and then 12 mL of TFA was added to the reaction mixture at 0 °C. After 1 h, TFA was re moved under a *vacuum*. The residue was dissolved in 22 mL of 10% $NaHCO_3$ (adjusts pH to ~8). The solution of Fmoc-OSu (8 mmol) in 30 mL of THF was added slowly to the reaction mixture and stirred overnight at room temperature. After completion of the reaction, the reaction mixture was acidified with 5% aq. HCl solution and extracted with ethyl acetate (40 x 3). The extracted ethyl acetate solution was washed with brine (150 ml) solution. The organic layer was then dried over anhydrous Na_2SO_4 and the product was concentrated under reduced pressure to give the white solid product of Fmoc-(*E*)-α, β- Unsaturated γ-amino acids (**4**) in 78-80% yields, which were directly used for solid-phase peptide synthesis without further purifications.



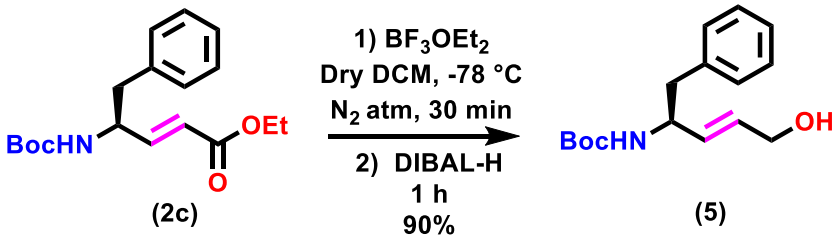
Scheme 4: Synthesis of Fmoc-NH-(*E*)-α, β-Unsaturated γ-amino acids (**4**).

B. Synthesis of Fmoc-NH-(*E*,*E*)-αβ, γδ-unsaturated ε-phenylalanine[2] (9):

Fmoc-NH-(*E*, *E*)-αβ, γδ-unsaturated ε-Phenylalanine amino acid (**9**) were synthesized using our reported protocol.[2] Briefly, synthesis is shown in following five steps (I – V), starting from the above synthesized Boc-(*E*)-dγ-Phe-OEt (**2c**).

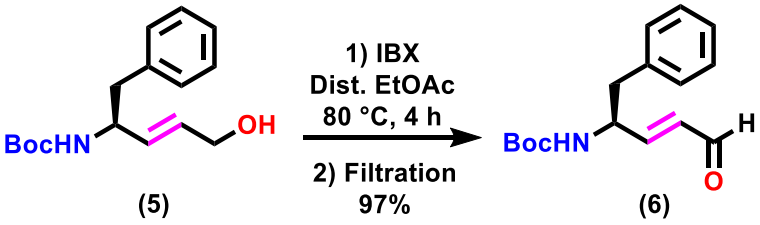
B1. Procedure for the synthesis of Boc-amino-phenylalanine-allylic alcohol[2] (5): Boc-NH-(*E*)-α,β-Unsaturated γ-phenylalanine ethyl ester (**2c**) (10 mmol) was dissolved in dry DCM (50 ml) under N_2 atmosphere, cooled to -78 °C then $BF_3.OEt_2$ (11.5 mmol) was added to the solution. The reaction mixture was stirred at that temperature for 30 min. Then, DIBAL-H of 1 M Toluene solution (35 mmol) was added to the reaction mixture and the resultant reaction mixture was stirred at -78 °C for 1 h. The progress of the reaction was monitored by TLC. After completion, the reaction mixture was quenched with 5 % aqueous HCl solution (80 ml). The resultant reaction mixture was allowed to warm up to room temperature. Then DCM was evaporated and the product was extracted with ethyl acetate (70 ml X 3). The extracted ethyl acetate solution was washed with 10 % Na_2CO_3 (100 ml) followed by brine (100 ml) solution.

The organic layer was then dried over anhydrous Na_2SO_4 and the product was concentrated under reduced pressure. The pure product Boc-amino-phenylalanine-allylic alcohol (**5**) was isolated after the column chromatography using EtOAc / pet ether (1:3) solvent system.



Scheme 5: Synthesis of Boc -Amino Phenylalanine Allylic Alcohol (**5**).

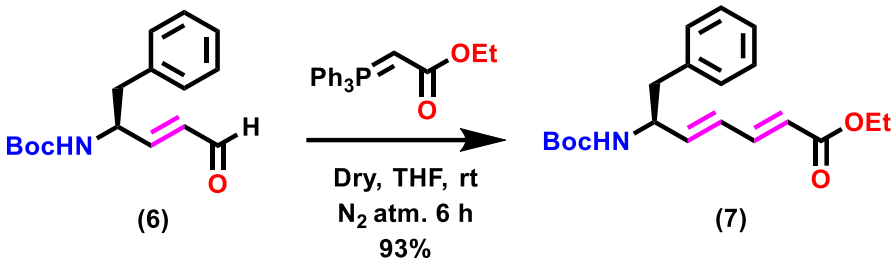
BII. Procedure for the synthesis of Boc-amino-phenylalanine-vinylogous aldehyde[2] (6): The oxidation of Boc-amino phenylalanine allylic alcohol (**5**) using *o*-Iodoxybenzoic acid (IBX) resulted in the formation of Boc-amino phenylalanine vinylogous aldehyde (**6**). In the event, to a solution of Boc-amino phenylalanine allylic alcohol (**5**) (8 mmol) in dist. Ethyl acetate (80 ml) was added *o*-Iodoxybenzoic acid (IBX) (9.5 mmol). The reaction mixture was stirred for 4 h at 80 °C using a reflux condenser. The progress of the reaction was monitored using TLC in 30% (ethyl acetate in pet ether) solvent system. After completion, the reaction mixture was filtered using a sintered funnel, the filtrate is our product (**6**) which was concentrated under reduced pressure. The IBX and IBX-derived by-products are insoluble in ethyl acetate at room temperature i.e. no further purification is required beyond simple filtration. The IBX permits clean oxidation of phenylalanine allylic alcohol (**5**) to Phenylalanine-vinylogous Aldehyde (**6**) in ethyl acetate solvent. Due to the less stability of α, β-unsaturated aldehyde, we further immediately used it for the next Wittig reaction.



Scheme 6: Synthesis of Boc-Amino-Phenylalanine-vinylogous Aldehyde (**6**).

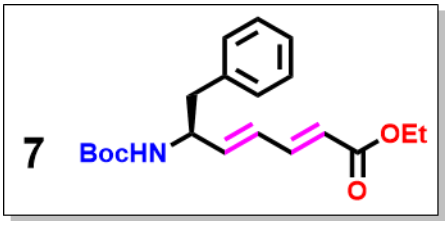
BIII. Procedure for the synthesis of Boc-NH-(*E*, *E*)-αβ, γδ-unsaturated ε-phenylalanine Ester[2] (7): Boc-amino phenylalanine vinylogous aldehyde (**6**) (6 mmol) was dissolved in dry THF (80 ml) under N_2 atmosphere. Then Wittig ylide (PPh_3=$CHCO_2Et$) (7.2 mmol) was added

to the above solution. The reaction mixture was stirred for 6 h at room temperature. The progress of the reaction was monitored by using TLC. Upon completion of the reaction, THF was evaporated from the reaction mixture, and the product Boc-NH-(*E*, *E*)-αβ, γδ-unsaturated ε-phenylalanine ester (**7**) was purified by column chromatography using ethyl acetate in pet ether (6%) solvent system.



Scheme 7: Synthesis of Boc-NH-(*E*, *E*)-αβ, γδ-unsaturated ε-Phenylalanine Ester (**7**).

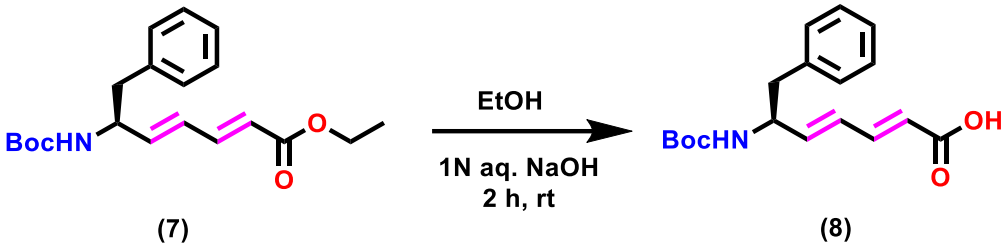
(*S*, 2*E*, 4*E*)-ethyl 6-((*tert*-butoxycarbonyl)amino)-7-phenylhepta-2,4-dienoate (7):



White solid, yield: 4.49g (93%), mp: 81 °C, $[\alpha]_D^{25}$ = -12.48 (c = 1 $CHCl_3$). **^{1}H NMR** (400 MHz, Chloroform-*d*) δ 7.32 – 7.29 (m, 2H, aromatic), 7.26 – 7.23 (m, 1H, aromatic), 7.23 – 7.19 (m, 1H, aromatic), 7.17 – 7.14 (m, 2H, aromatic1H & βC*H* merged), 6.20 (dd, *J* = 15.3, 10.9 Hz, 1H, γC*H*), 6.03 (dd, *J* = 15.4, 5.1 Hz, 1H, δC*H*), 5.82 (d, *J* = 15.3 Hz, 1H, αC*H*), 4.54 (s, 2H, N*H* & εC*H* merged), 4.19 (q, *J* = 7.1 Hz, 2H, -O-C*H*$_2$-CH$_3$), 2.87 (t, *J* = 5.1 Hz, 2H, *Benzylic*), 1.41 (s, 9H, *Boc*), 1.29 (t, *J* = 7.1 Hz, 3H, -O-CH$_2$-C*H*$_3$). **^{13}C NMR** (100 MHz, $CDCl_3$) δ 166.95, 155.04, 143.63, 142.14, 136.72, 129.47, 128.51, 128.00, 126.75, 121.48, 79.78, 77.36, 77.04, 76.72, 60.36, 52.90, 41.36, 28.33, 14.29. **HRMS** (ESI-QTOF) m/z calculated value for $C_{20}H_{27}NO_4$ is [M+Na] 368.1837 and observed 368.1830.

BIV. Ethyl ester hydrolysis reaction[2]: Purified Boc-NH-(*E*, *E*)-αβ, γδ-unsaturated ε-Phenylalanine Ester (**7**) (5 mmol) was dissolved in 10 mL of EtOH and then 10 ml of 1N aq. NaOH solution was added to the reaction mixture. The reaction mixture was stirred at that temperature for 3 h. The progress of the reaction was monitored by TLC. After completion of

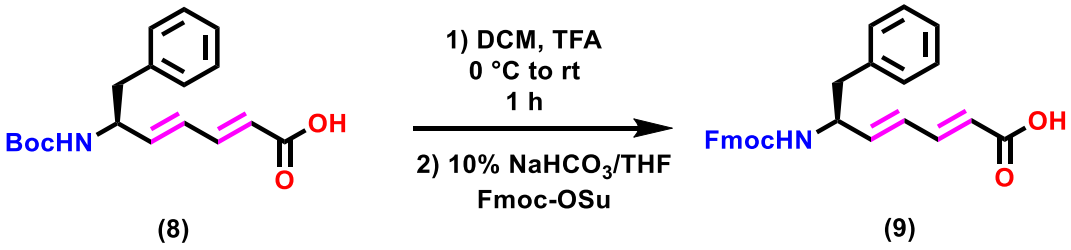
the ethyl ester hydrolysis reaction, EtOH was removed under a *vacuum.* The residue was acidified with 5 % aq. HCl solution (25 ml). The hydrolyzed acid product (**8**) was extracted with ethyl acetate (40 x 3). The extracted ethyl acetate solution was washed with brine (100 ml) solution. The organic layer was then dried over anhydrous Na_2SO_4 and the product was concentrated under reduced pressure.



(7) (8)

Scheme 8: Synthesis of Boc-NH-(*E*, *E*)-αβ, γδ-unsaturated ε-Phenylalanine Acid (**8**).

BV. Boc deprotection and Fmoc protection reaction: The Boc-NH-(*E*, *E*)-αβ, γδ-unsaturated ε-Phenylalanine acid (**8**) (5 mmol) was dissolved in 4 mL of DCM and then 10 mL of TFA was added to the reaction mixture at 0 °C. After 1 h, TFA was removed under a *vacuum*. The residue was dissolved in 15 mL of 10% $NaHCO_3$ (adjusts pH to ~8). The solution of Fmoc-OSu (5 mmol) in 22 mL of THF was added slowly to the reaction mixture and stirred overnight at room temperature. After completion of the reaction, the reaction mixture was acidified with 5% aq. HCl solution and extracted with ethyl acetate (30 x 3). The extracted ethyl acetate solution was washed with brine (100 ml) solution. The organic layer was then dried over anhydrous Na_2SO_4 and the product was concentrated under reduced pressure to give the white solid product of Fmoc-NH-(*E*, *E*)-αβ, γδ-unsaturated ε -Phenylalanine acid (**9**) in 79% yields, which were directly used for solid-phase peptide synthesis without further purifications.



(8) (9)

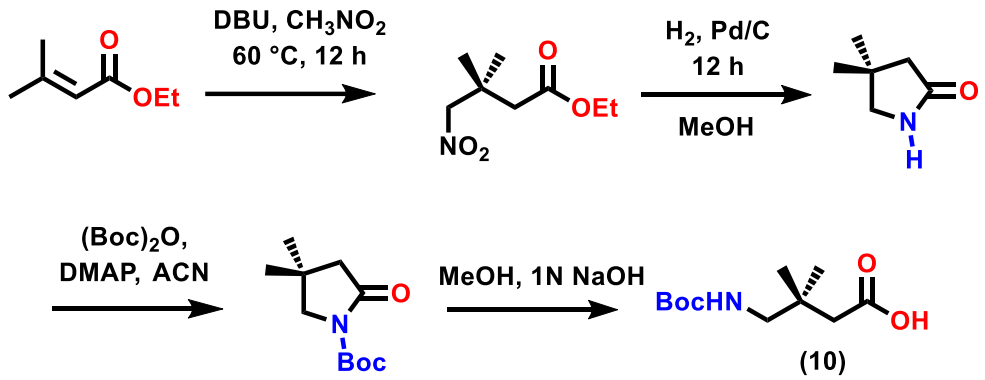
Scheme 9: Synthesis of Fmoc-NH-(*E*, *E*)-αβ, γδ-unsaturated ε-Phenylalanine Acid (**9**).

C. Synthesis of Fmoc-NH-3,3-dimethyl-butanoic acid (Fmoc-Adb)[3] (11):

Boc-NH-3,3-Dimethyl-Butanoic Acid (Boc-Adb) (**10**) was synthesized using our reported protocol.[3] Briefly, Ethyl 3,3-dimethyl acrylate (10 mmol) was dissolved in neat nitromethane

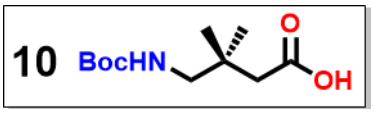
(50 mmol) and 1,8-diazabicyclo[5.4.0]undec-7-ene (DBU) base (15 mmol) were added. The reaction mixture was heated at 60 °C overnight. After completion of the reaction, nitromethane was evaporated under reduced pressure. The residue is acidified with 20 % aq. HCl solution. The acidic aqueous layer was extracted with ethyl acetate (40 x 3). The extracted ethyl acetate solution was washed with brine (100 ml) solution, and then dried over anhydrous Na_2SO_4 and the product was concentrated under reduced pressure.

The product, 3,3-dimethyl-4-nitro-butyric acid ethyl ester (1.5 g, 8 mmol) and activated Pd/C (20% by weight) in MeOH (18 mL) and acetic acid (3 mL) was stirred at room temperature in the presence of hydrogen. After completion of the reaction (24 h), Pd/C was filtered through the pad of celite and the filtrate was concentrated under reduced pressure to get 4,4-dimethyl-2-pyrrolidinone as oil. The amide NH group of 4,4-dimethyl-2-pyrrolidinone was further protected with the Boc group and then hydrolyzed using NaOH in MeOH to get the final product Boc-NH-3,3-Dimethyl-Butanoic Acid (Boc-Adb) (**10**) (1.38 g, 75%).



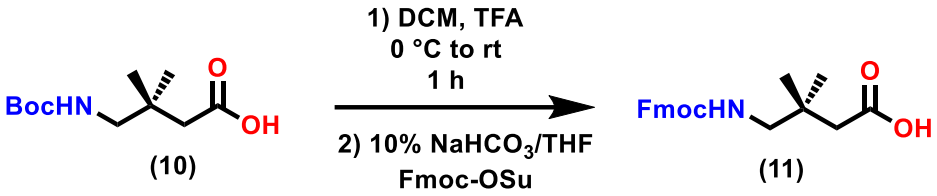
Scheme 10: Synthesis of Boc-NH-3,3-Dimethyl-Butanoic Acid (Boc-Adb) (**10**)[3].

4-((tert-butoxycarbonyl)amino)-3,3-dimethylbutanoic acid (10):



^{1}H NMR (400 MHz, Chloroform-*d*) δ 4.99 (t, *J* = 7.0 Hz, 1H, N*H*), 3.06 (d, *J* = 6.9 Hz, 2H, -NH-γCH_2-), 2.23 (s, 2H, -αCH_2-COOH), 1.44 (s, 9H, *Boc*), 1.00 (s, 6H, -C(CH_3)$_2$). **^{13}C NMR** (101 MHz, $CDCl_3$) δ 175.91, 157.13, 80.04, 77.35, 77.04, 76.72, 49.71, 44.05, 34.99, 28.34, 25.61. **HRMS** (ESI-QTOF) m/z calculated value for $C_{11}H_{21}NO_4$ is [M+Na] 254.1368 and observed 254.1359.

Boc deprotection and Fmoc protection reaction: Boc-NH-3,3-Dimethyl-Butanoic Acid (Boc-Adb) (**10**) (5 mmol) was dissolved in 4 mL of DCM and then 10 mL of TFA was added to the reaction mixture at 0 °C. After 1 h, TFA was removed under a *vacuum*. The residue was dissolved in 15 mL of 10% $NaHCO_3$ (adjusts pH to ~8). The solution of Fmoc-OSu (5 mmol) in 22 mL of THF was added slowly to the reaction mixture and stirred overnight at room temperature. After completion of the reaction, the reaction mixture was acidified with 5% aq. HCl solution and extracted with ethyl acetate (30 x 3). The extracted ethyl acetate solution was washed with brine (100 ml) solution. The organic layer was then dried over anhydrous Na_2SO_4 and concentrated under reduced pressure to give the white solid product, Fmoc-NH-3,3-Dimethyl-Butanoic Acid (Fmoc-Adb) (11). which were directly used for solid-phase peptide synthesis without further purifications.



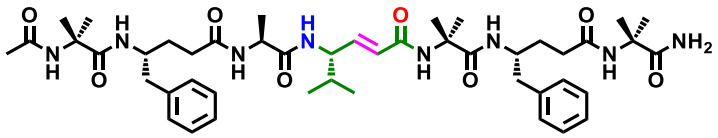
Scheme 11: Synthesis of Fmoc-NH-3,3-Dimethyl-Butanoic Acid (Fmoc-Adb) (**11**).

3.5.2. General procedure for the solid phase synthesis of peptides P1-P4:

Peptides were synthesized at 0.2 mmol scales on Knorr-Amide resin using standard Fmoc-chemistry. HBTU/HOBT was used as a standard coupling reagent. To avoid Michael addition of HOBT, we carried out-coupling reactions of *E*-vinylogous γ-amino acids only with HBTU.[7] Reaction time for Fmoc-deprotections and couplings of amino acids were 45 min and 1.5 h, respectively. The final Fmoc-deprotected amine was acylated using Acetic anhydride and pyridine base (Ac_2O/Py). After completion of the synthesis, peptides were cleaved from the resin using 20 mL of TFA/TIPS/Phenol/H_2O (88:2:5:5). After peptide cleavage, the resin was filtered out using the sintered funnel. The filtrate (which contains peptide) was evaporated under reduced pressure to give the crude peptide products. Peptides were further precipitated out using cold diethyl ether and purified through reverse phase HPLC on the C-18 column using MeOH/H_2O gradient. The purity of peptides were further confirmed using an analytical C-18 column in the same MeOH/H_2O gradient system. The mass of peptides were confirmed by MALDI TOF/TOF.

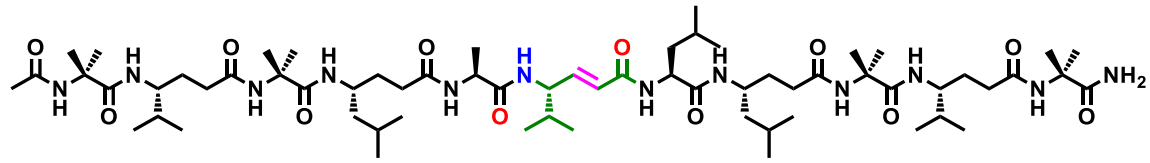
3.5.3. Characterization data of peptides P1, P2, P3 and P4

Peptide P1:

P1 

^{1}H NMR (600 MHz, CD_3OH) δ 8.56 (d, *J* = 8.5 Hz, 1H), 8.24 (s, 1H), 8.15 (s, 1H), 8.06 (s, 1H), 8.05 (s, 1H), 8.00 (d, *J* = 5.7 Hz, 1H), 7.59 (d, *J* = 9.7 Hz, 1H), 7.38 (d, *J* = 9.6 Hz, 1H), 7.21 – 7.09 (m, $10H_{Aromatic}$), 6.93 (dd, *J* = 15.3, 5.4 Hz, 1H), 6.73 (s, 1H), 6.13 (dd, *J* = 15.3, 1.8 Hz, 1H), 4.21 (m, 1H), 4.16 (m, 1H), 4.10 (m, 1H), 4.07 (m, 1H), 2.79 (dd, *J* = 13.7, 5.2 Hz, 2H), 2.64 (dd, *J* = 13.7, 9.9 Hz, 1H), 2.61 (dd, *J* = 13.7, 9.4 Hz, 1H), 2.45 (ddd, *J* = 14.3, 11.8, 4.7 Hz, 1H), 2.33 (m, 1H), 2.20 (dt, *J* = 14.3, 4.7 Hz, 1H), 2.08 (m, 1H), 2.03 (m, 1H), 2.00 (m, 1H), 1.93 (s, 3H), 1.88 (m, 1H), 1.62 (m, 1H), 1.55 (m, 1H), 1.38 (d, *J* = 7.3 Hz, 3H), 1.35 (s, 3H), 1.34 (s, 3H), 1.26 (s, 3H), 1.17 (s, 3H), 1.15 (s, 3H), 1.14 (s, 3H), 0.97 (d, *J* = 6.7 Hz, 3H), 0.93 (d, *J* = 6.7 Hz, 3H). **MALDI (TOF/TOF)** *m/z* calculated value for $C_{46}H_{68}N_8O_8$ $[M+Na^+]$ is 883.5052 and observed at 883.5010.

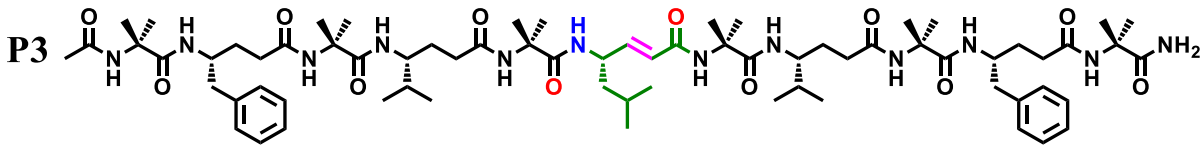
Peptide P2:

P2 

^{1}H NMR (600 MHz, CD_3OH) δ 8.75 (d, *J* = 8.5 Hz, 1H), 8.31 (s, 1H), 8.29 (d, *J* = 6.3 Hz, 1H), 8.17 (d, *J* = 5.0 Hz, 1H), 8.16 (s, 1H), 8.15 (s, 1H), 8.14 (s, 1H), 8.11 (s, 1H), 8.00 (d, *J* = 9.8 Hz, 1H), 7.97 (s, 1H), 7.49 (d, *J* = 9.7 Hz, 1H), 7.46 (d, *J* = 9.9 Hz, 1H), 6.98 (dd, *J* = 15.2, 4.3 Hz, 1H), 6.71 (s, 1H), 6.15 (dd, *J* = 15.2, 2.0 Hz, 1H), 4.28 (m, 1H), 4.25 (m, 1H), 4.15 (m, 1H), 3.94 (m, 1H), 3.87 (m, 1H), 3.67 (m, 1H), 3.54 (m, 1H), 2.61 (ddd, *J* = 14.3, 12.3, 4.2 Hz, 1H), 2.42 (m, 1H), 2.32 (m, 1H), 2.22 (m, 1H), 2.15 (dt, *J* = 12.3, 3.4 Hz, 1H), 2.11 (m, 1H), 2.09 (m, 1H), 2.07 (m, 1H), 2.05 (m, 1H), 2.03 (m, 1H), 2.00 (s, 3H), 1.99 (s, 1H), 1.98 (m, 1H), 1.96 (m, 1H), 1.79 (m, 1H), 1.71 (m, 1H), 1.69 (m, 1H), 1.67 (m, 1H), 1.65 (m, 2H), 1.61 (m, 1H), 1.56 (m, 2H), 1.51 (m, 1H), 1.48 (s, 3H), 1.47 (s, 3H), 1.466 (s, 6H), 1.46 (br, 1H), 1.45 (s, 3H), 1.44 (s, 6H), 1.41 (m, 2H), 1.38 (s, 3H), 1.28 (s, 3H), 1.23 (m, 1H), 1.11 (m, 1H), 1.04 (d, *J* = 4.7 Hz, 3H), 1.02 (d, *J* = 4.7 Hz, 3H), 0.99 (d, *J* = 6.6 Hz, 3H), 0.93 (d, *J* = 6.6 Hz, 3H), 0.91 (d, *J* = 4.5 Hz, 3H), 0.91 (d, *J* = 4.5 Hz, 3H), 0.90 (d, *J* = 5 Hz, 3H), 0.89 (d, *J* = 6.5 Hz, 3H), 0.87 (d, *J* = 5 Hz, 3H), 0.85 (d, *J* = 6.4 Hz, 3H), 0.84 (d, *J* = 6.5 Hz, 3H), 0.74 (d, *J* =

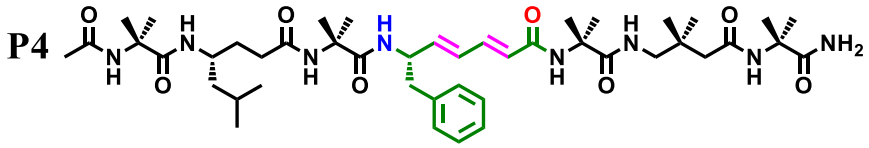
6.4 Hz, 3H). **MALDI (TOF/TOF)** *m/z* calculated value for $C_{64}H_{116}N_{12}O_{12}$ [M+Na^+] is 1267.87 and observed at 1267.94.

Peptide P3:



^{1}H NMR (600 MHz, $CDCl_3$) δ 8.97 (d, *J* = 6 Hz, 1H), 8.82 (s, 1H), 8.21 (d, *J* = 9.6 Hz, 1H), 8.09 (s, 1H), 8.02 (s, 1H), 8.01 (d, *J* = 5.4 Hz, 1H), 7.88 (s, 1H), 7.76 (s, 1H), 7.40 (s, 1H), 7.35 (s, 1H), 7.22 (m, 7H), 7.15 (m, 3H), 7.00 (d, *J* = 9.6 Hz, 1H), 6.79 (d, *J* = 9.6 Hz, 1H), 6.74 (dd, *J* = 15 Hz, *J* = 3 Hz, 1H), 6.37 (d, *J* = 15 Hz, 1H), 5.23 (s, 1H), 4.53 (s, 1H), 4.18 (m, 1H), 4.09 (m, 1H), 3.63 (m, 1H), 3.59 (m, 1H), 2.82 (m, 4H), 2.70 (m, 1H), 2.50 (m, 2H), 2.33 (m, 2H), 2.23 (m, 3H), 2.15 (m, 3H), 2.07 (m, 6H), 2.03 (s, 3H), 1.79 (m, 3H), 1.61 (m, 4H), 1.55 (s, 6H), 1.52 (s, 3H), 1.49 (s, 5H), 1.47 (s, 4H), 1.41 (s, 5H), 1.39 (s, 4H), 1.25 (s, 7H), 1.23 (s, 3H), 0.88 (m, 9H), 0.85 (s, 2H), 0.84 (s, 3H). **MALDI (TOF/TOF)** *m/z* calculated value for $C_{70}H_{112}N_{12}O_{12}$ [M+Na^+] is 1336.72 and observed at 1336.01.

Peptide P4:



1H NMR (600 MHz, CD_3OH) δ 8.50 (d, *J* = 8.5 Hz, 1H), 8.39 (s, 1H), 8.32 (s, 1H), 8.23 (s, 1H), 7.83 (t, *J* = 7.2 Hz, 1H), 7.78 (s, 1H), 7.60 (s, 1H), 7.42 (d, *J* = 8.0 Hz, 2H), 7.37 (d, *J* = 11.0 Hz, 1H), 7.23 (dt, *J* = 7.9, 3.7 Hz, 3H), 7.15 (m, 1H), 6.75 (s, 1H), 6.59 (m, 1H), 6.14 (m, 1H), 6.10 (m, 1H), 4.62 (s, 1H), 3.91 (m, 1H), 3.13 (t, *J* = 6.6 Hz, 1H), 3.07 (t, *J* = 6.6 Hz, 1H), 2.99 – 2.96 (m, 1H), 2.95 – 2.93 (m, 1H), 2.46 – 2.39 (m, 1H), 2.08 (s, 2H), 2.04 (br, 1H), 1.99 (s, 3H), 1.53 (s, 3H), 1.51 (s, 3H), 1.50 (s, 3H), 1.48 (s, 3H), 1.47 (s, 6H), 1.43 – 1.42 (m, 4H), 1.37 (s, 3H), 1.11 (m, 1H), 1.02 (s, 3H), 0.97 (s, 3H), 0.96 (s, 3H), 0.84 (m, 3H), 0.81 (m, 3H). **MALDI (TOF/TOF)** *m/z* calculated value for $C_{45}H_{72}N_8O_8$ [M+Na^+] is 875.60 and observed at 875.68.

3.6. References

CCDC numbers 2226520 (for **P1**), 2226522 (for **P2**), 2226521 (for **P3**) and 2226523 (for **P4**).

1. S. Hecht, I. Huc, *Foldamers: Structure, Properties, and Applications*, Wiley-VCH,Weinheim, **2007**, pp. 1–435; b) G. Guichard, I. Huc, *Chem. Commun.* **2011**, *47*, 5933–5941; c) T. A. Martinek, F. Fülöp, *Chem. Soc. Rev.* **2012**, *41*, 687–702; d) S. Rinaldi, *Molecules* **2020**, *25*, 3276; e) C. M. Goodman, S. Choi, S. Shandler, W. F. DeGrado, *Nat. Chem. Biol.* **2007,** *3*, 252–262; f) D. J. Hill, M. J. Mio, R. B. Prince, T. S. Hughes, J. S. Moore, *Chem. Rev.* **2001**, *101*, 3893–4012; g) R. P. Cheng, S. H. Gellman, W. F. DeGrado, *Chem. Rev.* **2001**, *101*, 3219–3232; h) B. Legrand, L. T. Maillard, *ChemPlusChem* **2021**, *86*, 629–645; i) P. G. Vasudev, S. Chatterjee, N. Shamala, P. Balaram, *Chem. Rev.* **2011**, *111*, 657–687; j) S. H. Yoo, H. -S. Lee, *Acc. Chem. Res.* **2017**, *50*, 832–841; k) Z. C. Girvin, S. H. Gellman, *J. Am. Chem. Soc.* **2020**, *142*, 17211–17223; l) B. Legrand, J. Aguesseau-Kondrotas, M. Simon, L. Maillard, *Catalysts* **2020**, *10*, 700.
2. a) S. Jones, *Genome Biol.* **2004**, *5*, 226; b) L. Aravind, V. Anantharaman, S. Balaji, M. M. Babu, L. M. Iyer, *FEMS Microbiol. Rev.* **2005**, *29*, 231–262.
3. M. Pellegrini-Calace, J. M. Thornton, *Nucleic Acids Res.* **2005**, *33*, 2129–2140.
4. A. Lewit-Bentley, S. Réty, *Curr. Opin. Struct. Biol.* **2000,** *10*, 637–643.
5. M. E. Massari, C. Murre, *Mol. Cell. Biol.* **2000**, *20*, 429–440.
6. a) C. M. Venkatachalam, *Biopolymers* **1968**, *6*, 1425–1436; b) J. S. Richardson, *Adv. Protein Chem.* **1981**, *34*, 167–339; c) K. Gunasekaran, C. Ramakrishnan, P. Balaram, *Protein Engineering, Design and Selection* **1997**, *10*, 1131–1141.
7. J. Venkatraman, S. C. Shankaramma, P. Balaram, *Chem. Rev.* **2001**, *101*, 3131–3152.
8. a) D. Mazzier, S. De, B. Wicher, V. Maurizot, I. Huc, *Chem. Sci.* **2019**, *10*, 6984–6991; b) D. Mazzier, S. De, B. Wicher, V. Maurizot, I. Huc, *Angew. Chem. Int. Ed.* **2020**, *59*, 1606–1610.
9. K. Ożga, M. Drewniak-Świtalska, E. Rudzińska-Szostak, Ł. Berlicki, *ChemPlusChem* **2021**, *86*, 646–649.
10. M. Drewniak, E. Węglarz-Tomczak, K. Ożga, E. Rudzińska-Szostak, K. Macegoniuk, J. M. Tomczak, M. Bejger, W. Rypniewski, Ł. Berlicki, *Bioorg. Chem.* **2018**, *81*, 356–361.
11. a) I. L. Karle, A. Banerjee, P. Balaram, *Folding Des.* **1997**, *2*, 203–210; b) A. Banerjee, S. Raghothama, P. Balaram, *J. Chem. Soc., Perkin Trans. 2* **1997**, 2087–2094.

12. I. L. Karle, J. L. Flippen-Anderson, M. Sukumar, K. Uma, P. BaIaram, *J. Am. Chem. Soc.* **1991**, *113*, 3952–3956.
13. G. V. M. Sharma, V. Subash, K. Narsimulu, A. R. Sankar, A. C. Kunwar, *Angew. Chem. Int. Ed.* **2006**, *45*, 8207–8210.
14. U. A. Ramagopal, S. Ramakumar, D. Sahal, V. S. Chauhan, *Proc. Natl. Acad. Sci. USA* **2001**, *98*, 870–874.
15. I. L. Karle, C. Das, P. Balaram, *Proc. Natl. Acad. Sci. USA* **2000**, *97*, 3034–3037.
16. a) C. Baldauf, R. Günthe, H.-J. Hofmann, *J. Org. Chem*. **2006**, *71*, 1200-1208; b) C. Baldauf, R. Günthe, H.-J. Hofmann, *Biopolymers*, **2006**, *84*, 408-413.
17. a) S. Chatterjee, P. G. Vasudev, S. Raghothama, C. Ramakrishnan, N. Shamala, P. Balaram, *J. Am. Chem. Soc*. **2009**, *131*, 5956-5965; b) L. Guo, Y. Chi, A. M. Almeida, I. A. Guzei, B. K. Parker, S. H. Gellman, *J. Am. Chem. Soc*. **2009**, *131*, 16018-16020; c) A. Bandyopadhyay, S. V. Jadhav, H. N. Gopi, *Chem. Commun*. **2012**, *48*, 7170-7172; e) G. V. M. Sharma, N. Chandramouli, M. Choudhary, P. Nagendar, K. V. S. Ramakrishna, A. C. Kunwar, P. Schramm, H.-J. Hofmann, *J. Am. Chem. Soc*. **2009**, *131*, 17335-17344; f) B. F. Fisher, L. Guo, B. S. Dolinar, I. A. Guzei, S. H. Gellman, *J. Am. Chem. Soc*. **2015**, *137*, 6484-6487; B. F. Fisher, S. H. Gellman, *J. Am. Chem. Soc*. **2016**, *138*, 10766-10769.
18. Hagihara, M.; Anthony, N. J.; Stout, T. J.; Clardy, J.; Schreiber S. L. *J. Am. Chem. Soc.* **1992**, *114*, 6568.
19. (a) Grison, C.; Coutrot, P.; Ge´neve, S.; Didierjean, C.; Marraud, M. *J. Org. Chem*. **2005**, *70*, 10753. (b) Grison, C.; Ge´neve, S.; Halbin, E.; Coutrot, P. *Tetrahedron* **2001**, *57*, 4903.
20. (a) Mathieu, L.; Legrand, B.; Deng, C.; Vezenkov, L.; Wenger, E.; Didierjean, C.; Amblard, M.; Averlant-Petit, M.-C.; Masurier, N.; Lisowski, V.; Martinez, J.; Maillard, L. T. *Angew. Chem. Int. Ed.* **2013**, *52*, 6006.
21. M. Ganesh Kumar, S. N. Benke, K. M. P. Raja, H. N. Gopi, *Chem. Commun.* **2015**, *51*, 13397–13399.
22. M. Hagihara, N. J. Anthony, T. J. Stout, J. Clardy, S. L. Schreiber, *J. Am. Chem. Soc.* **1992**, *114*, 6568–6570.
23. K. Veeresh, M. Singh, H. N. Gopi, *Org. Biomol. Chem.* **2019**, *17*, 9226–9231.
24. R. Misra, S. Dey, R. M. Reja, H. N. Gopi, *Angew. Chem., Int. Ed.* **2018**, *57*, 1057–1061.
25. M. Ganesh Kumar, V. J. Thombare, M. M. Katariya, K. Veeresh, K. M. P. Raja, H. N. Gopi, *Angew. Chem. Int. Ed.* **2016**, *55*, 7847–7851.

26. a) S. H. Gellman, *Acc. Chem. Res*. **1998**, *31*, 173-180; b) J. Venkatraman, S. C. Shankaramma, P. Balaram, *Chem. Rev*. **2001**, *101*, 3131-3152; c) D. Seebach, A. K. Beck, D. J. Bierbaum, *Chem. Biodiversity*, **2004**, *1*,1111-1239; d) R. P. Cheng, S. H. Gellman, W. F. De Grado, *Chem. Rev*. **2001**, *101*, 3219-3232; e) D. J. Hill, M. J. Mio, R. B. Prince, T. S. Hughes, J. S. Moore, *Chem. Rev.* **2001**, *101*, 3893–4012; f) F. Fülöp, T. A. Martinek, G. K. Tóth, *Chem. Soc. Rev*. **2006**, *35*, 323-334; g) S. Hecht, I.Huc, *Foldamers: Structure, Properties and Applications*, Wiley-VCH, Weinheim, **2007**; h) C. M. Goodman, S. Choi, S. Shandler, W. F. DeGrado, *Nat. Chem. Biol*. **2007**, *3*, 252-262; i) W. S. Horne, S. H. Gellman, *Acc. Chem. Res*. **2008**, *41*, 1399-1408; j) D. Seebach, J. Gardiner, *Acc. Chem. Res*. **2008**, *41*, 1366-1375.
27. S. A. Nalawade, M. Singh, D. R. Puneeth Kumar, S. Dey, H. N. Gopi, *Org.Biomol.Chem*. **2023**, *21*, 2586–2595.
28. R. Misra, A. Saseendran, S. Dey, H. N. Gopi, *Angew. Chem. Int. Ed.* **2019**, *58*, 2251–2255.
29. S. Dey, R. Misra, A. Saseendran, S. Pahan, H. N. Gopi, *Angew. Chem. Int. Ed.* **2021**, *60*, 9863–9868.
30. R. Misra, G. George, A. Saseendran, S. Raghothama, H. N. Gopi, *Chem. Asian J.* **2019**, *14*, 4408 – 4414.
31. K. Pervushin, M. Billeter, G. Siegal, K. Wüthrich, *J. Mol. Biol.* **1996**, *264*, 1002–1012.
32. N. Pendem, Y.-R. Nelli, L. Cussol, C. Didierjean, B. Kauffmann, C. Dolain, G. Guichard, *Chem. Eur. J.* **2023,** 29, e202300087.
33. (a) G. M. Sheldrick, Phase annealing in *SHELX*-90: direct methods for larger structures. *Acta Crystallogr.* **1990**, *A46*, 467-473; (b) G. M.Sheldrick, SHELXL-97, Program for Crystal Structure Solution and Refinement, Universität Göttingen (Germany) **1997**.
34. A. L. Spek, *Acta Crystallogr*. PLATON, an integrated tool for the analysis of the results of a single crystal structure determination. **1990**, *A46*, C34.
35. The solvent mask (void determination) in OLEX is based on: J.- S. Jiang, A. T. Brünger, Protein hydration observed by X-ray diffraction. Solvation properties of penicillopepsin and neuraminidase crystal structures. *J. Mol. Biol*. **1994**, *243*, 100-115.

3.7. Appendix

S. No	Content	Page No
3.7.1.	**Ortep plot and crystallographic information of peptide P1, P2, P3 and P4**	**145**

3.7.2	**^{1}H NMR and mass spectra of peptides P1- P4**	**151**
3.7.3	**^{1}H NMR, ^{13}C NMR and HRMS spectra of monomer units**	**155**
3.7.4.	**Copy of the Permission letter from Journal for reuse of figures and diagrams**	**163**

3.7.1. Ortep plot and crystallographic information of peptide P1, P2, P3 and P4

3.7.1.1. ORTEP diagrams of peptides P1, P2, P3 and P4

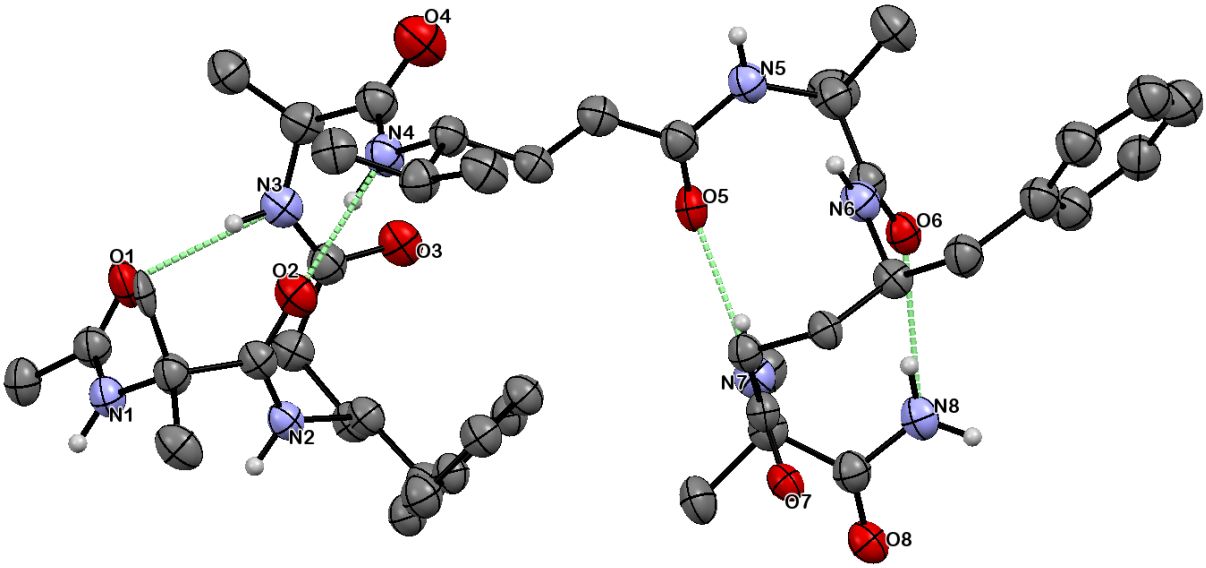


Figure 20: ORTEP diagram of **P1** [Ac-Aib-*γ*Phe-Ala-(*E*)d*γ*Val-Aib-*γ*Phe-Aib-$CONH_2$], with labelled heteroatoms. H-bonding is represented by dotted lines in light green colour. The side-chain and backbone H-atoms are not shown for clarity (except N-H). Ellipsoids are drawn at 50% probability. (symmetry operations: N8 = 1-x,y,1-z; O6 = 1-x,y,1-z; N1 = 1/2-x,-1/2+y,1-z; O8 = 1/2-x,1/2+y,1-z). [(*E*)d*γ*Val = (*E*)-α, β-unsaturated γ-Valine[1]] (**CCDC no : 2226520**)

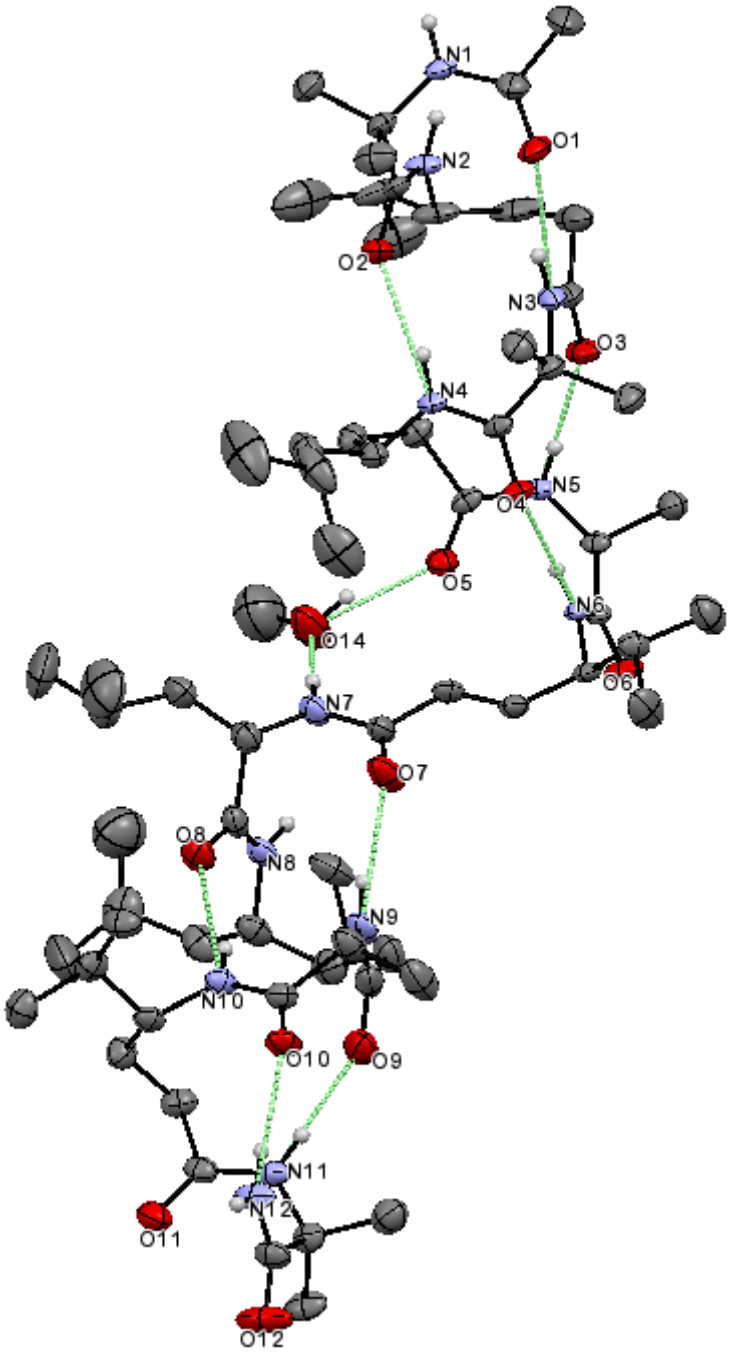


Figure 21: ORTEP diagram of **P2** [Ac-Aib-*γ*Val-Aib-*γ*Leu-Ala-(*E*)d*γ*Val-Leu-*γ*Leu-Aib-*γ*Val-Aib-$CONH_2$], with labelled heteroatoms. H-bonding is represented by dotted lines in light green colour. The side-chain and backbone H-atoms are not shown for clarity (except N-H). Ellipsoids are drawn at 50% probability. (symmetry operations: N1 = -1+x,y,z; N2 = -1+x,y,1+z; N12 = x,y,-1+z; O6 = x,y,1+z); O12 = 1+x,y,-1+z; O6 = 1+x,y,z). [(*E*)d*γ*Val = (*E*)-α, β-unsaturated γ-Valine[1]] (**CCDC no : 2226522**)

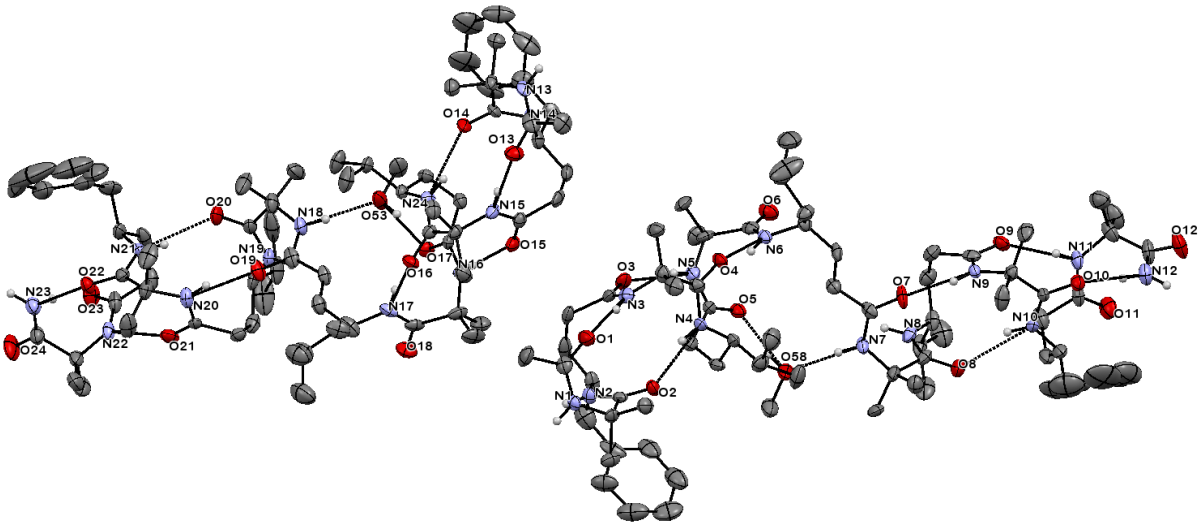


Figure 22: ORTEP diagram of **P3** [Ac-Aib-*γ*Phe-Aib-*γ*Val-Aib-(*E*)d*γ*Leu-Aib-*γ*Val-Aib-*γ*Phe-Aib-$CONH_2$] with labelled heteroatoms. H-bonding is represented by dotted lines. The side-chain and backbone H-atoms are not shown for clarity. Ellipsoids are drawn at 50% probability. (symmetry operations: N2 = -1+x,1+y,z; O12 = 1+x,-1+y,z; N14 = -1+x,-1+y,z; O24 = 1+x,1+y,z). [(*E*)d*γ*Leu = (*E*)-α, β-unsaturated γ^4-Leucine] (**CCDC no : 2226521**)

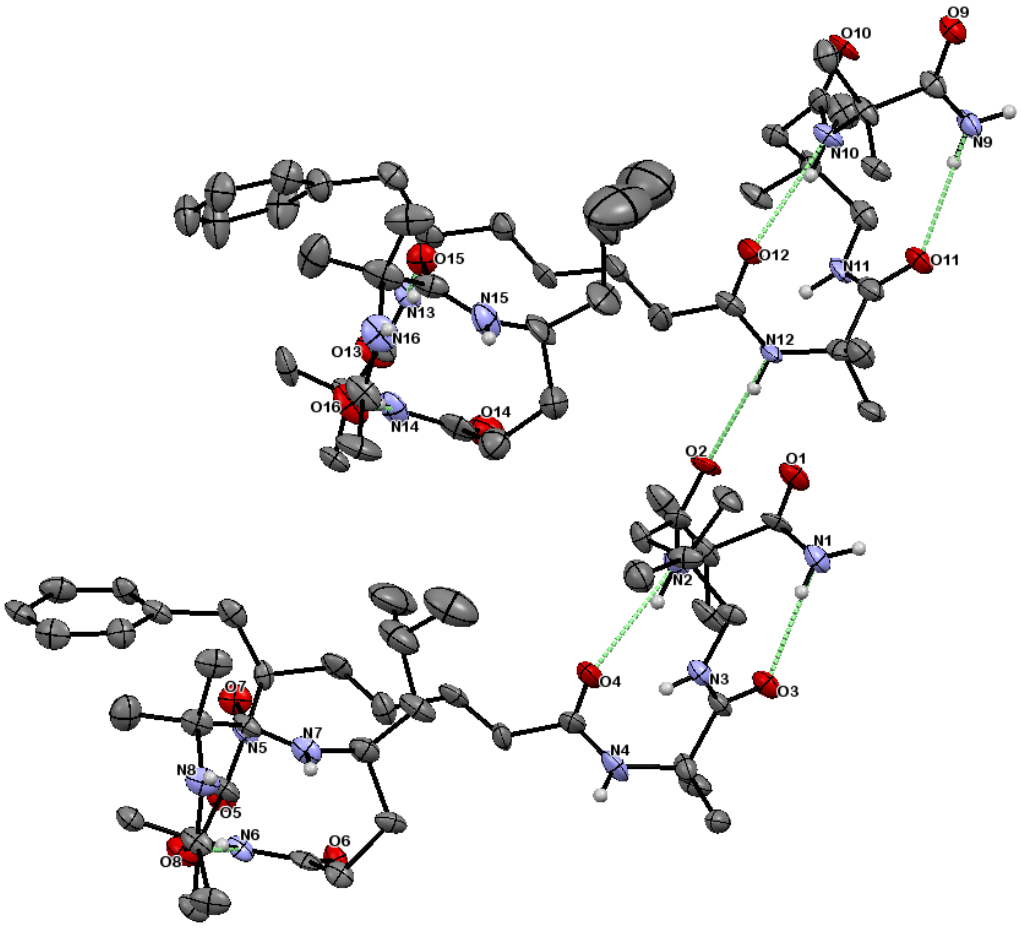


Figure 23: ORTEP diagram of **P4** [Ac-Aib-*γ*Leu-Aib-(*E*,*E*)-dd*ε*Phe-Aib-Adb-Aib-$CONH_2$], with labelled heteroatoms. H-bonding is represented by dotted lines in light green colour. The side-chain and backbone H-atoms are not shown for clarity (except N-H). Ellipsoids are drawn at 50% probability. (symmetry operations: O5 = x,-1+y,z; N8 = x,1+y,z; O10 = 1+x,y,z; O9 = -x,1/2+y,2-z; N9 = -x,1/2+y,2-z; N4 = -1+x,y,z; O1 = -x,-1/2+y,2-z; N1 = -x,-1/2+y,2-z; O13 = x,-1+y,z; N16 = x,1+y,z). [(*E*,*E*)dd*ε*Phe = (*E*,*E*)-αβ, γδ-unsaturated ε-Phenylalanine[2]; Adb = 4-amino-3,3-dimethyl-butanoic acid[3]] (**CCDC no : 2226523**)

3.7.1.2. Crystallographic information of peptides P1, P2, P3 and P4

Crystal structure analysis of Ac-Aib-*γ*Phe-Ala-(*E*)d*γ*Val-Aib-*γ*Phe-Aib-$CONH_2$ (P1): Colourless rod shape Crystals of **P1** were grown by slow evaporation from an aqueous solution of methanol. A good quality single crystal (0.13 × 0.08 × 0.05mm) was mounted on the head of a goniometer using a loop with a small amount of paraffin oil. The X-ray diffraction data of a single crystal were collected at 100K temperature on a Bruker APEX(II) DUO CCD diffractometer using Mo Kα radiation (λ = 0.71073 Å), *ω*-scans (2*θ* = 39.992), for a total of 17071 independent reflections. Space group C 2, a = 33.21(5), b = 10.160(13), c = 16.17(2), *β* = 112.22(3), V = 5051(11) $Å^3$, Monoclinic, Z = 4 for chemical formula $C_{46}\ H_{68}\ N_8\ O_8$ with one molecule in asymmetric unit; *ρ* calcd = 1.132 gcm^{-3}, *μ* = 0.078 mm^{-1}, F (000) = 1856.0, Rint= 0.2784. The structure was obtained by direct methods using SHELXL-97.[33] The final R value was 0.1038 (wR2 = 0.2341) 4549 observed reflections (*F0* ≥ 4*σ* (|F0|)) and 571 variables, S = 0.857. The largest difference peak and hole were 0.327 and -0.253 $eÅ^3$, respectively.

The diffracted single crystal was a small-sized and the quality of diffraction was poor. Several datasets were collected on single crystals from different groups and one of the highest quality is reported herein.

There is some partially occupied solvent molecule also present in the asymmetric unit. A significant amount of time was invested in identifying and refining the disordered molecule. Option SQUEEZE of program PLATON[34] was used to correct the diffraction data for diffuse scattering effects and to remove the contributions of the disordered solvent molecules from the structure factors. PLATON calculated the upper limit of volume that can be occupied by the solvent to be 461 $Å^3$ of the unit cell volume. The program calculated 148 electrons in the unit cell for the diffuse species. No data are given for the diffusely scattering species. Outputs of the SQUEEZE report are appended in CIF file **P1**.

Crystal structure analysis of Ac-Aib-γVal-Aib-γLeu-Ala-(*E*)dγVal-Leu-γLeu-Aib-γVal-Aib-CONH$_2$ (P2): Colourless plate shape Crystals of **P2** were grown by slow evaporation from the aqueous solution of methanol. A good quality single crystal (0.25 × 0.12 × 0.1 mm) was mounted on the head of a goniometer using a loop with a small amount of paraffin oil. The X-ray diffraction data of a single crystal were collected at 100K temperature on a Bruker APEX(II) DUO CCD diffractometer using Mo Kα radiation (λ = 0.71073 Å), *ω*-scans (2*θ* = 56.65), for a total of 43572 independent reflections. Space group P 21, a = 14.637(8), b = 19.378(9), c = 16.197(7), *β* = 104.947(16), V = 4439(4) Å^3, Monoclinic, Z = 2 for chemical formula C_{64} H_{116} N_{12} O_{12}, C H_4 O with one methanol molecule in asymmetric unit; *ρ* calcd = 0.956 gcm^{-3}, *μ* = 0.067mm^{-1}, F (000) = 1396, Rint= 0.0384. The crystal structure was solved by direct methods using SHELXL-97.[33] The final R value was 0.0531 (wR2 = 0.1158) 21737 observed reflections ($F0 \geq 4\sigma$ (|F0|)) and 837 variables, S = 1.053. The largest difference peak and hole were 0.442 and -0.275 eÅ^3, respectively.

There is some partially occupied solvent molecule also present in the asymmetric unit. A significant amount of time was invested in identifying and refining the disordered molecule. The solvent masks option in program Olex2-1.2[35] serves as an alternative to SQUEEZE which is implemented in PLATON[34]. The solvent masks option in program Olex2-1.2[6] was used to correct the diffraction data for diffuse scattering effects and to remove the contributions of the disordered solvent molecules from the structure factors. The Olex2-solvent mask calculated the upper limit of volume that can be occupied by the solvent to be 1193 Å^3, or 26.9% of the unit cell volume. The program calculated 159 electrons in the unit cell for the diffuse species. No data are given for the diffusely scattering species. Outputs of the Olex2-solvent mask (SQUEEZE) report are appended in CIF file **P2**.

Crystal structure analysis of Ac-Aib-γPhe-Aib-γVal-Aib-(*E*)dγLeu-Aib-γVal-Aib-γPhe-Aib-CONH$_2$ (P3): Colourless plate shape Crystals of **P3** were grown by slow evaporation from the aqueous solution of methanol. A good quality single crystal (0.15 × 0.08 × 0.06 mm) was mounted on the head of a goniometer using a loop with a small amount of paraffin oil. The X-ray diffraction data of a single crystal were collected at 100K temperature on a Bruker APEX(II) DUO CCD diffractometer using Mo Kα radiation (λ = 0.71073 Å), *ω*-scans (2*θ* = 56.726), for a total of 117312 independent reflections. Space group P 1 21 1, a = 10.2313(15), b = 22.906(3), c = 36.932(5), *β* = 90.172(5), V = 8655(2) Å^3, Monoclinic, Z = 4 for chemical formula C_{70} H_{112} N_{12} O_{12}, C H_4 O with two P2 molecules and two methanol molecules in

asymmetric unit; ρ calcd = 1.033 gcm^{-3}, μ = 0.071mm^{-1}, F (000) = 2920, Rint= 0.0481. The crystal structure was solved by direct methods using SHELXL-97[33] and refined using Olex2-1.2. The final R value was 0.0914 (wR2 = 0.2372) 42019 observed reflections ($F0 \geq 4\sigma$ (|F0|)) and 1771 variables, S = 1.026. The largest difference peak and hole were 0.421 and -0.351 eÅ^{3}, respectively.

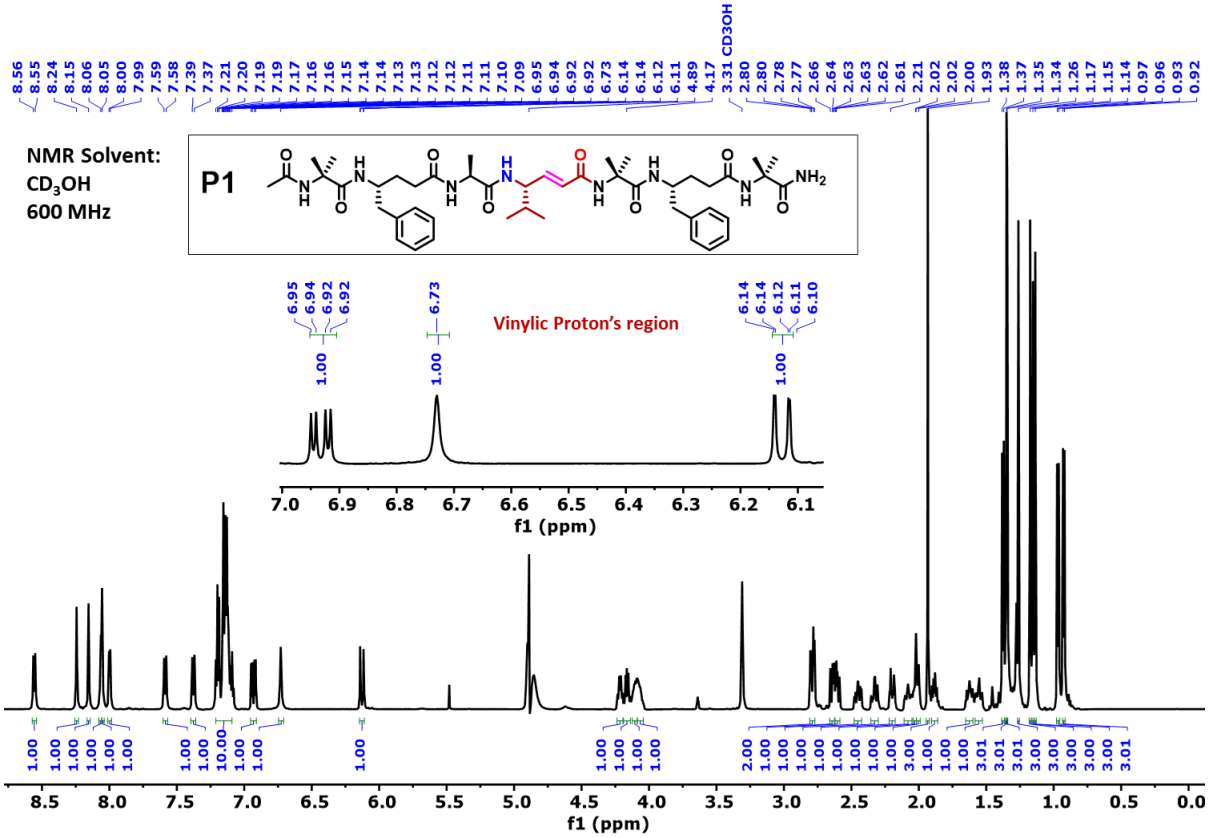
There is some partially occupied solvent molecule also present in the asymmetric unit. A significant amount of time was invested in identifying and refining the disordered molecule. The solvent masks option in program Olex2-1.2[35] serves as an alternative to SQUEEZE which is implemented in PLATON[34]. The solvent masks option in program Olex2-1.2[4] was used to correct the diffraction data for diffuse scattering effects and to remove the contributions of the disordered solvent molecules from the structure factors. The Olex2-solvent mask calculated the upper limit of volume that can be occupied by the solvent to be 1646.3 Å^{3}, or 19 % of the unit cell volume. The program calculated 385 electrons in the unit cell for the diffuse species. No data are given for the diffusely scattering species. Outputs of the Olex2-solvent mask (SQUEEZE) report are appended in CIF file **P3**.

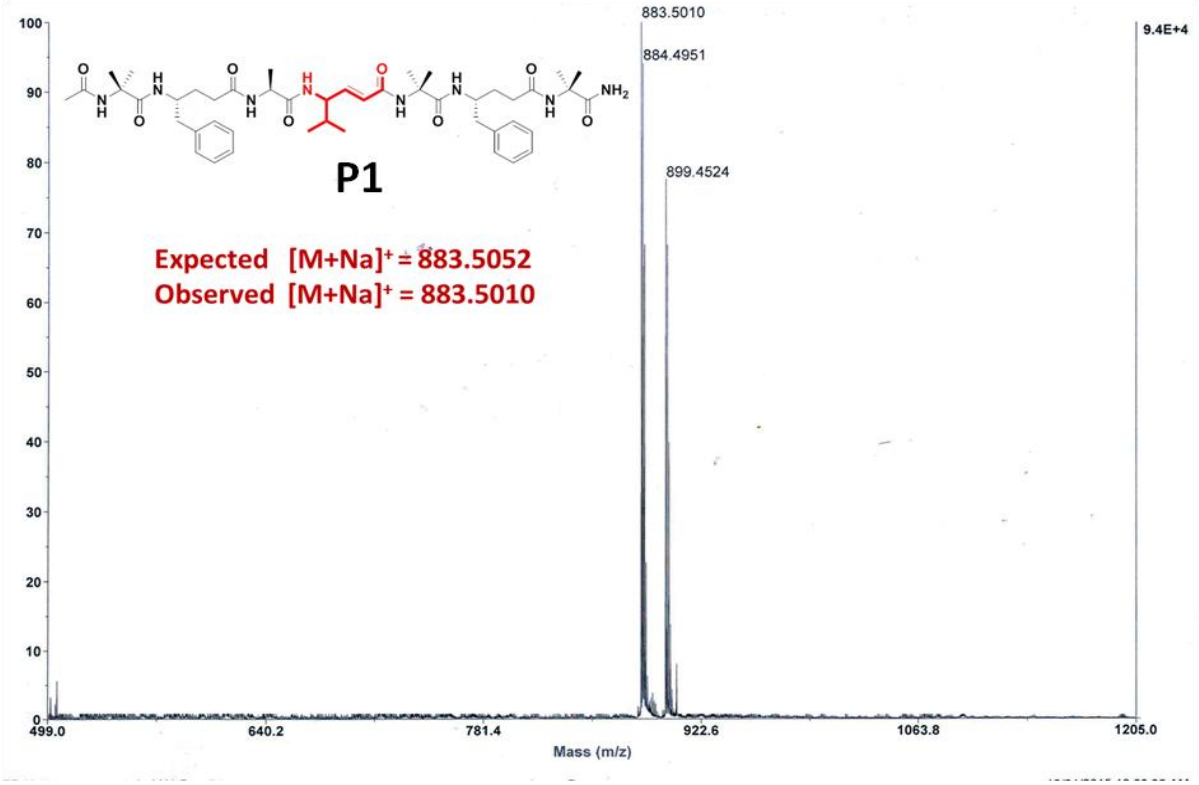
Crystal structure analysis of Ac-Aib-γLeu-Aib-(*E*, *E*)ddγPhe-Aib-Adb-Aib-CONH$_2$ (P4): Colourless needle shape Crystals of **P4** were grown by slow evaporation from the aqueous solution of methanol. A good quality single crystal (0.12 × 0.09 × 0.07 mm) was mounted on the head of a goniometer using a loop with a small amount of paraffin oil. The X-ray diffraction data of a single crystal were collected at 100K temperature on a Bruker APEX(II) DUO CCD diffractometer using Mo Kα radiation (λ = 0.71073 Å), ω-scans (2θ = 56.666), for a total of 66655 independent reflections. Space group P 21, a = 17.73(10), b = 10.52(6), c = 28.85(16), β = 99.42(8), V = 5309(50) Å^{3}, Monoclinic, Z = 4 for chemical formula C_{45} H_{72} N_8 O_8 with two molecule in asymmetric unit; ρ calcd = 1.067 gcm^{-3}, μ = 0.074 mm^{-1}, F (000) = 1848, Rint= 0.1393. The structure was obtained by direct methods using SHELXL-97.[33] The final R value was 0.1070 (wR2 = 0.2415) 22799 observed reflections ($F0 \geq 4\sigma$ (|F0|)) and 1109 variables, S = 1.028. The largest difference peak and hole were 0.949 and -0.386 eÅ^{3}, respectively.

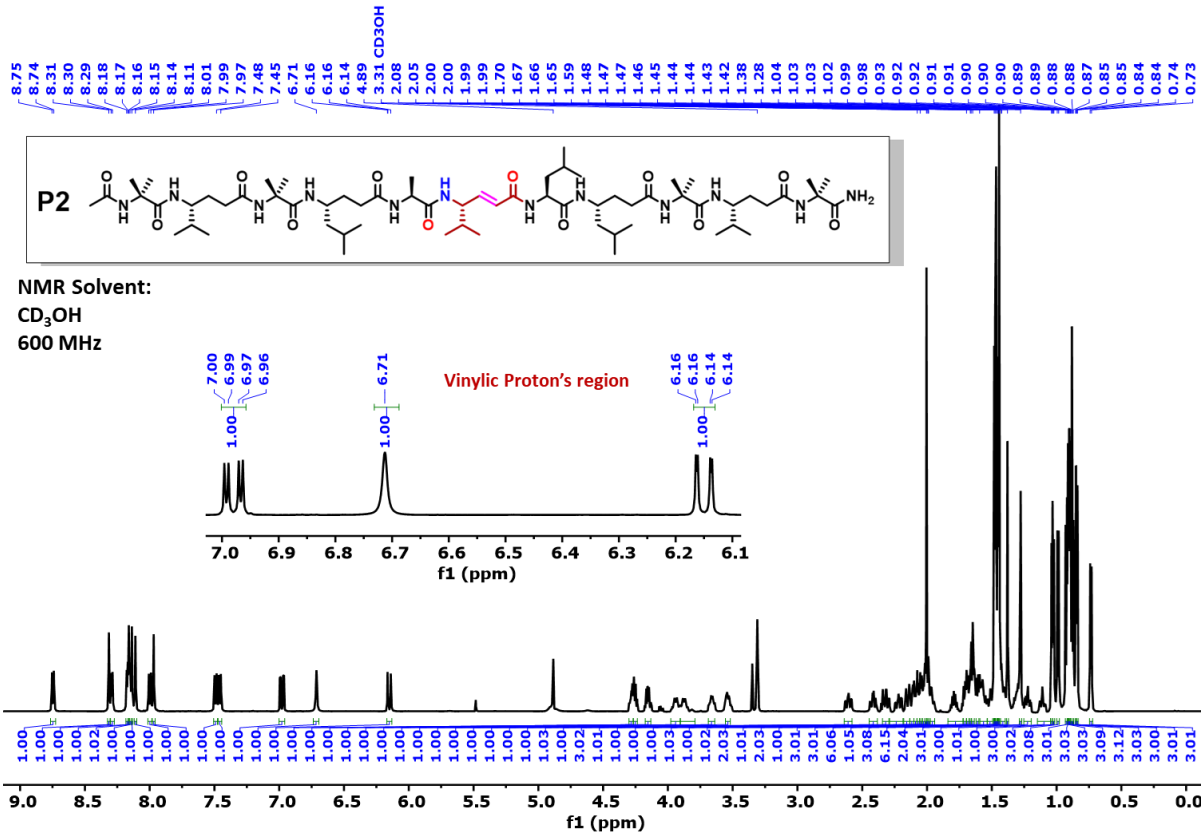
The diffracted single crystal was a small-sized and the quality of diffraction was poor. Several datasets were collected on single crystals from different groups and one of the highest quality is reported herein.

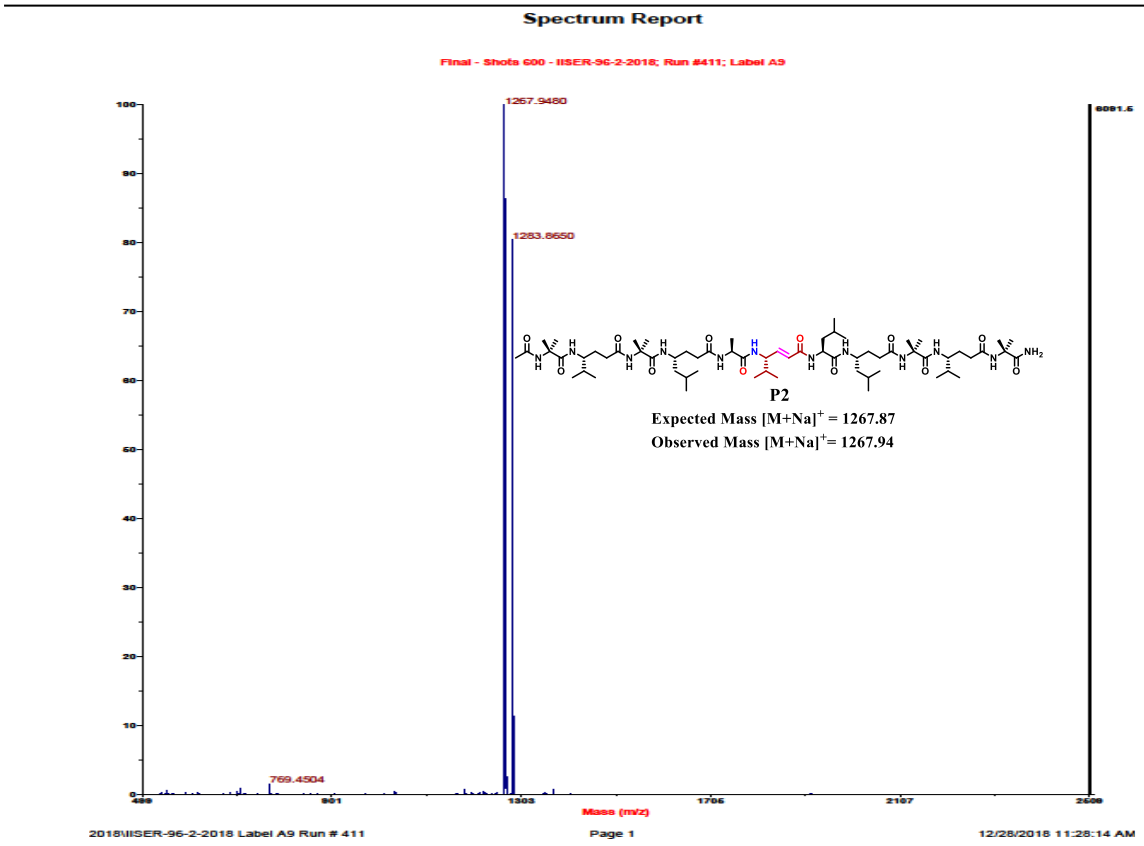
There is some partially occupied solvent molecule also present in the asymmetric unit. A significant amount of time was invested in identifying and refining the disordered molecule. Option SQUEEZE of program PLATON[34] was used to correct the diffraction data for diffuse scattering effects and to remove the contributions of the disordered solvent molecules from the structure factors. PLATON calculated the upper limit of volume that can be occupied by the solvent to be 732 Å^3 of the unit cell volume. The program calculated 203 electrons in the unit cell for the diffuse species. No data are given for the diffusely scattering species. Outputs of the SQUEEZE report are appended in CIF file **P3**.

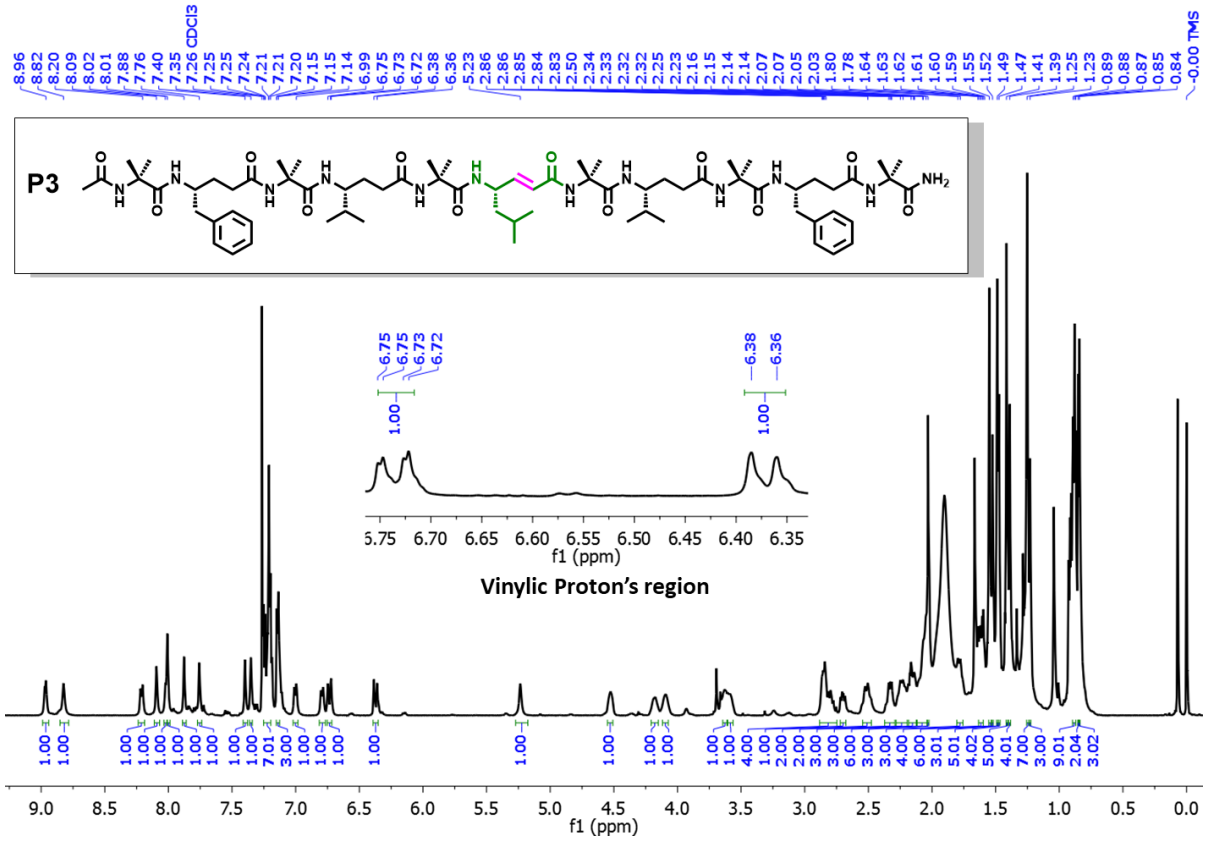
3.7.2. ^{1}H NMR and mass spectra of peptides P1- P4

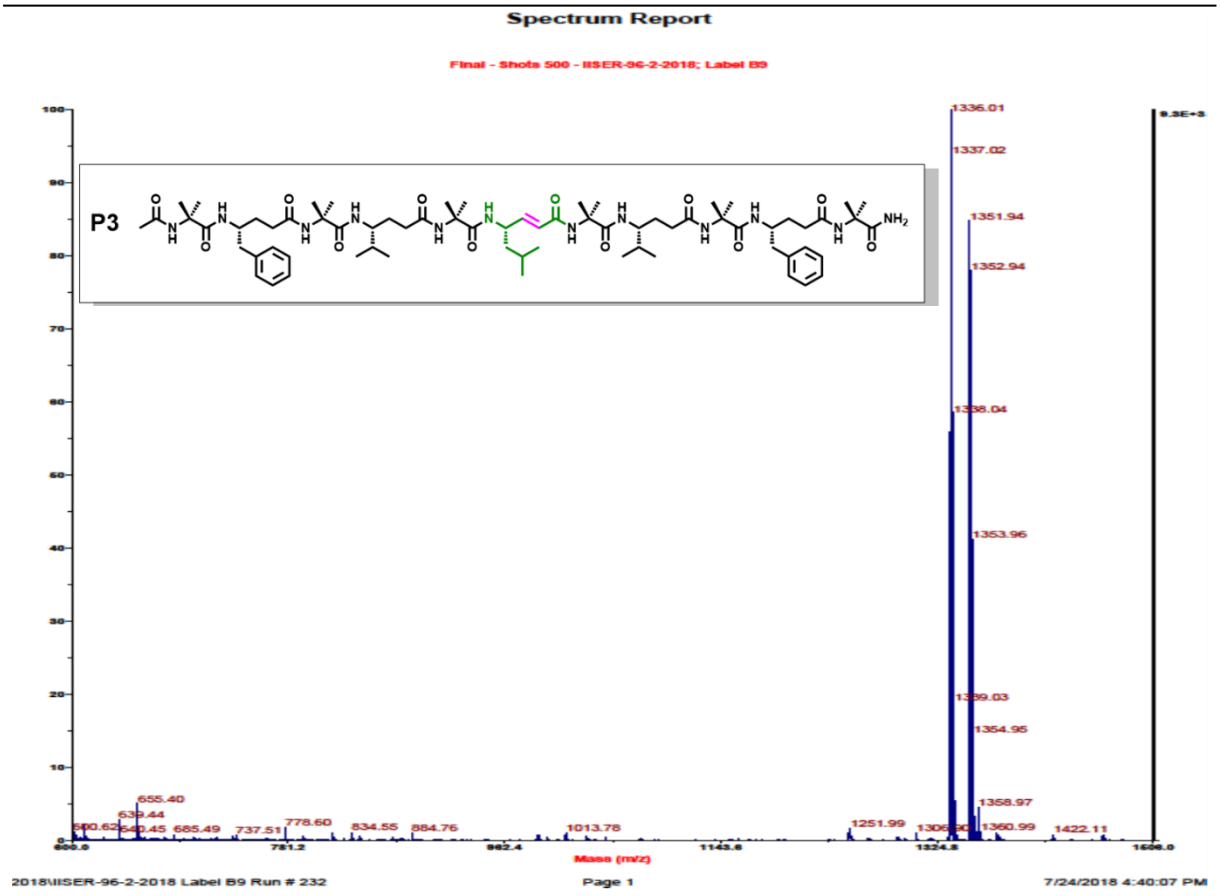


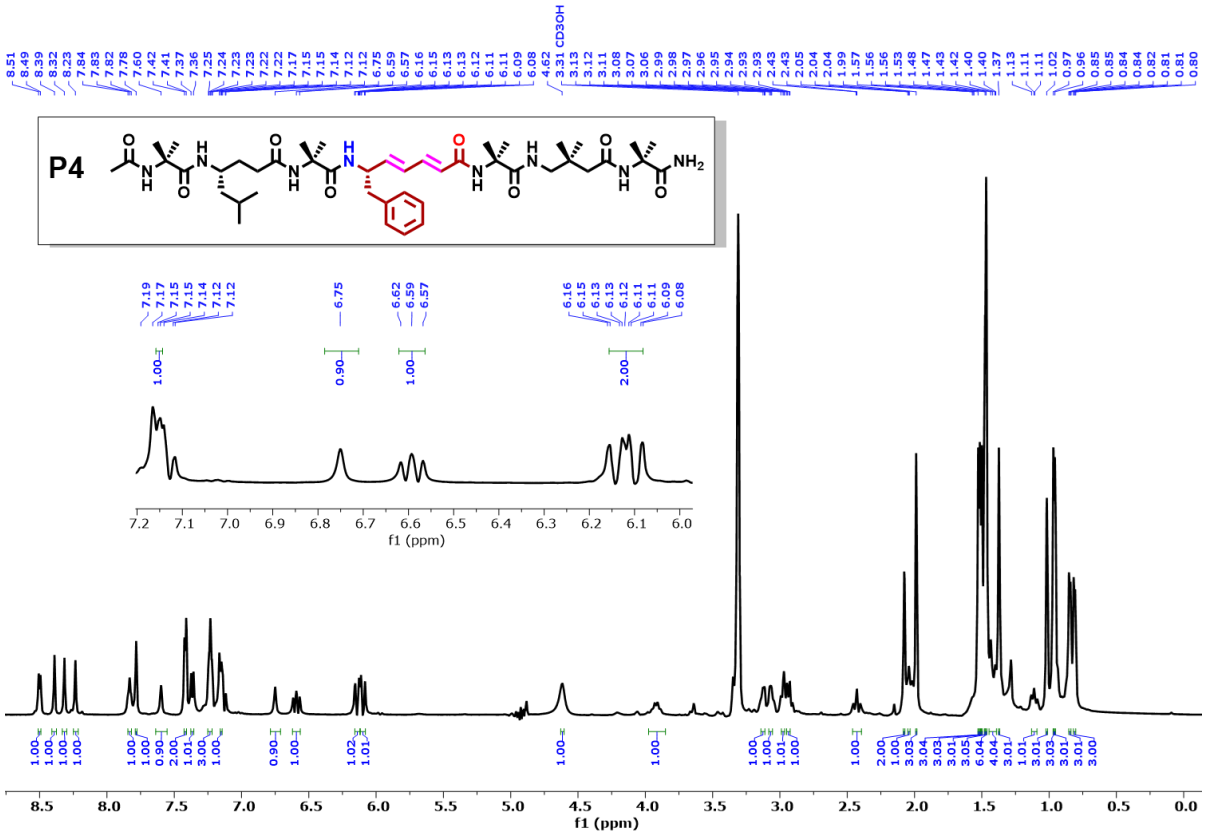

883.5010
884.4951
899.4524
9.4E+4
P1
Expected [M+Na]+ = 883.5052
Observed [M+Na]+ = 883.5010
Mass (m/z)

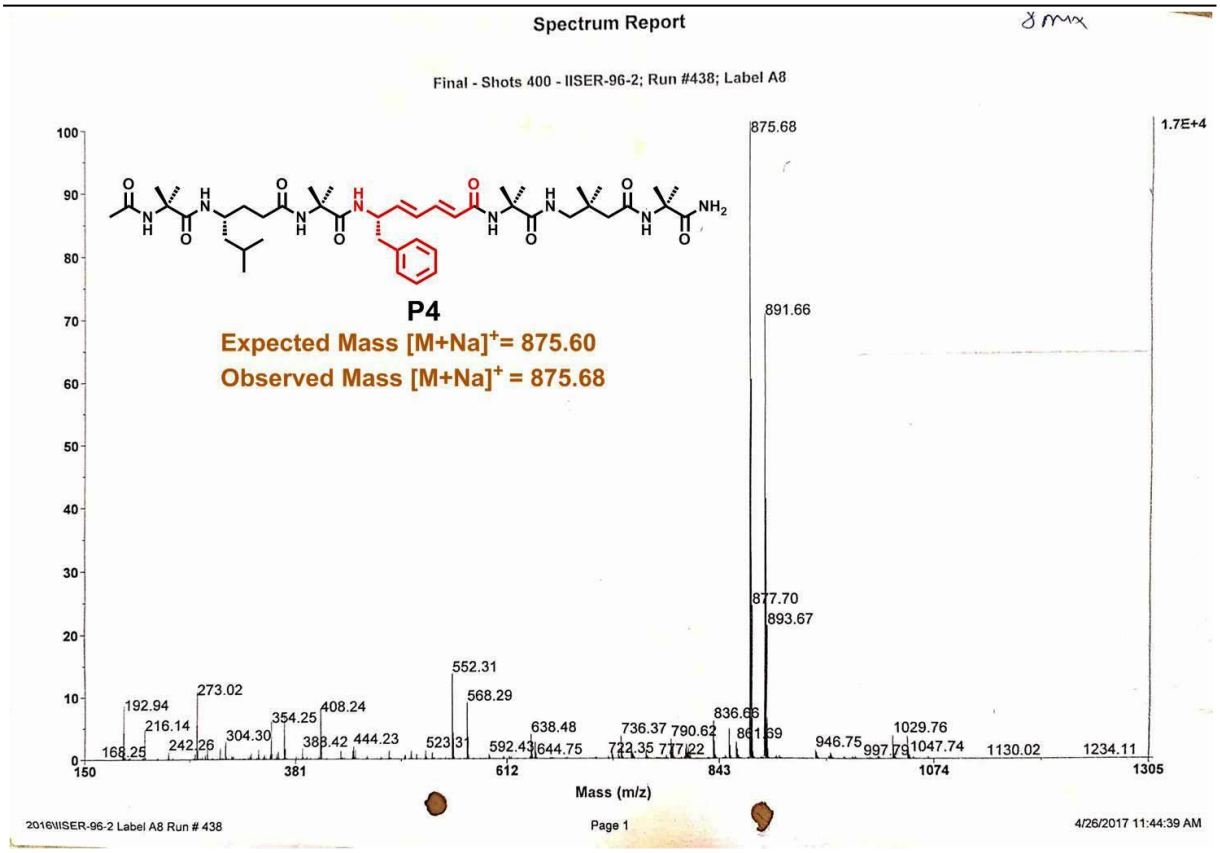

CD3OH
P2
NMR Solvent:
CD3OH
600 MHz
Vinylic Proton's region
f1 (ppm)


Spectrum Report
Final - Shota 600 - IISER-96-2-2018; Run #411; Label A9
1267.9480
1283.8650
769.4504
P2
Expected Mass [M+Na]+ = 1267.87
Observed Mass [M+Na]+= 1267.94
Mass (m/z)
2018\IISER-96-2-2018 Label A9 Run # 411
Page 1
12/28/2018 11:28:14 AM

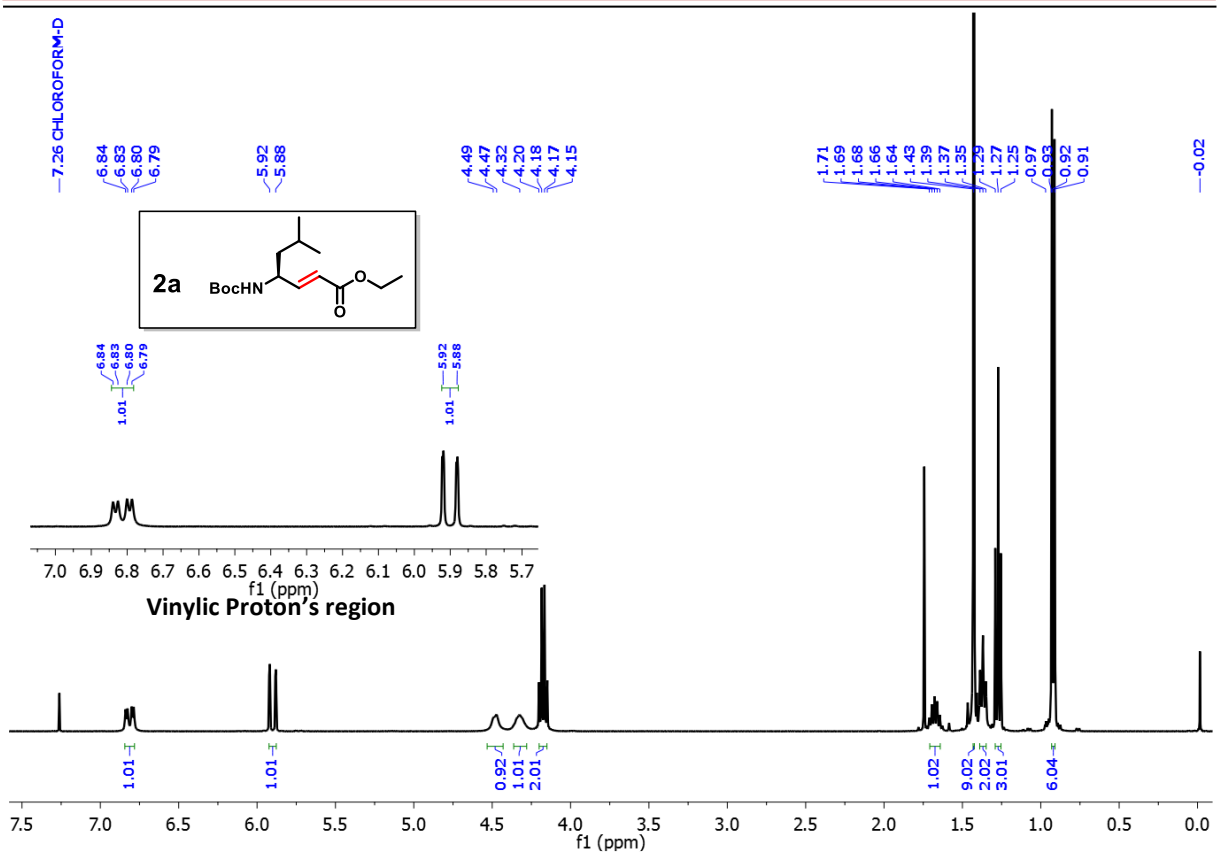

CDCl3
TMS
P3
Vinylic Proton's region
f1 (ppm)

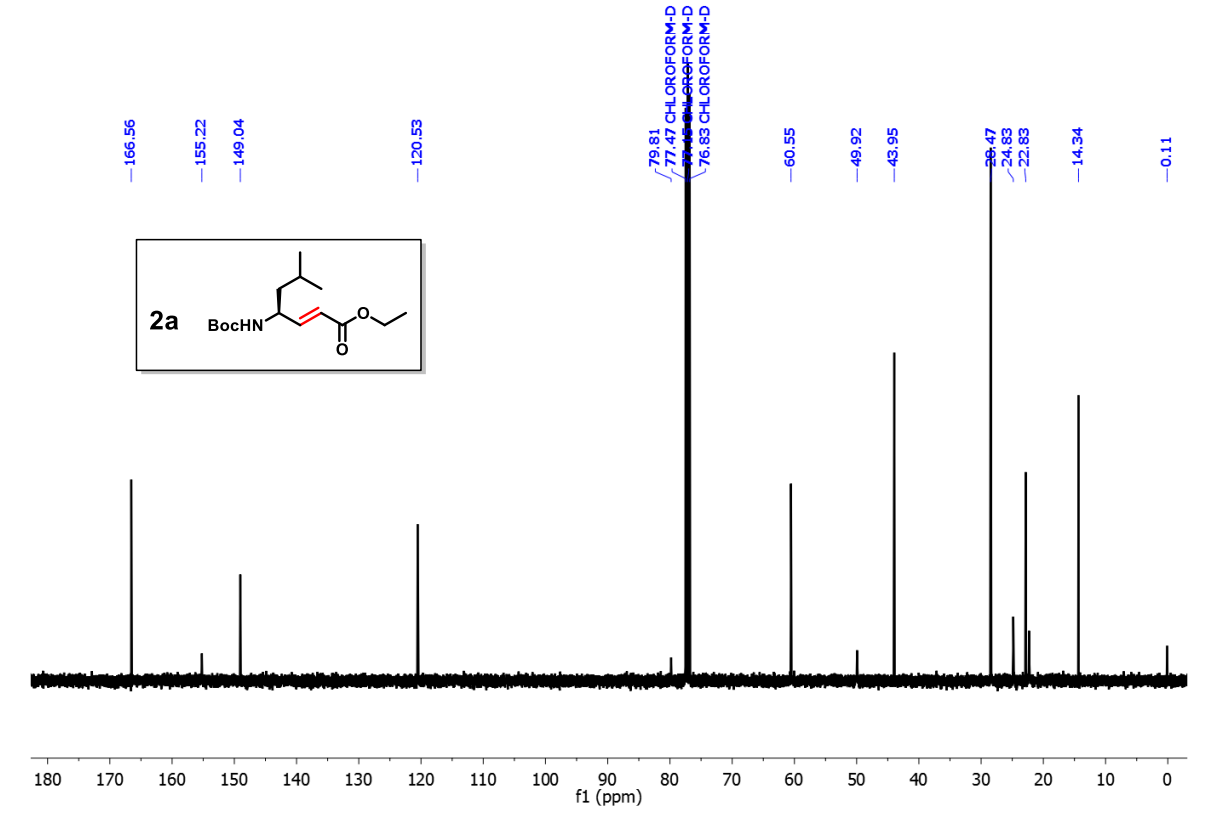

Spectrum Report
Final - Shots 500 - IISER-96-2-2018; Label B9
P3
1336.01
1337.02
1351.94
1352.94
1338.04
1353.96
1339.03
1354.95
1358.97
1360.99
1422.11
655.40
639.44
685.49
737.51
778.60
834.55
884.76
1013.78
1251.99
Mass (m/z)
2018\IISER-96-2-2018 Label B9 Run # 232
Page 1
7/24/2018 4:40:07 PM

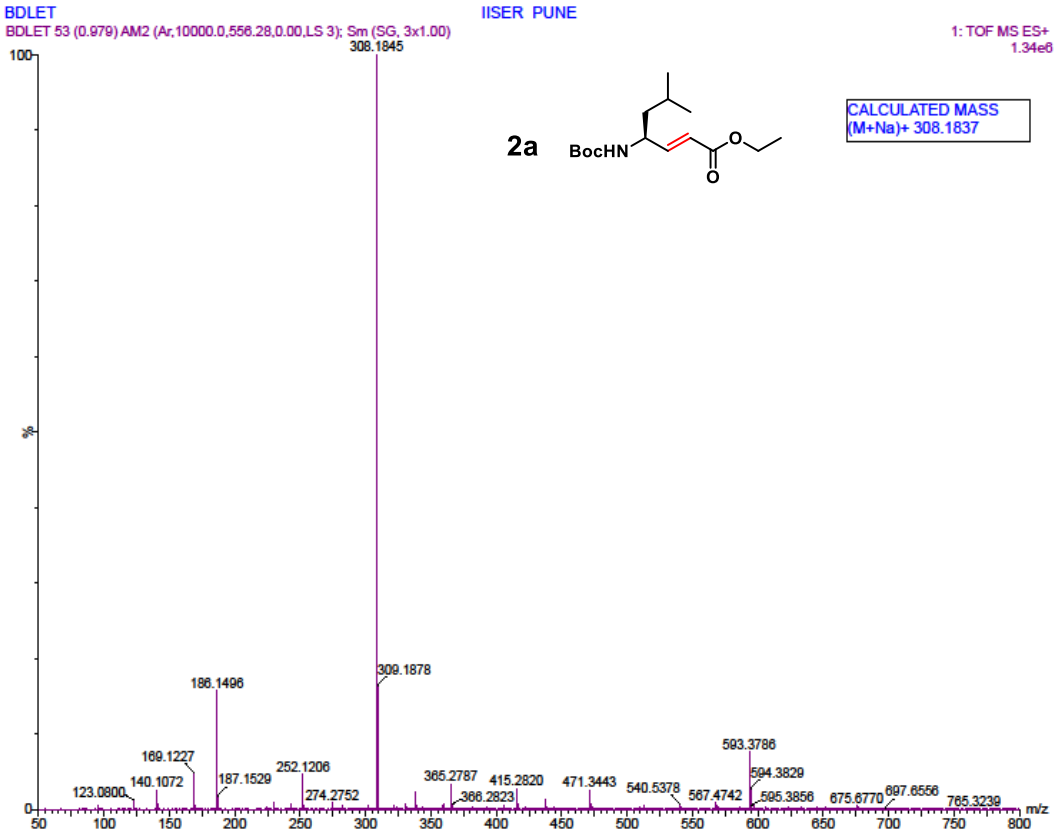

P4
f1 (ppm)

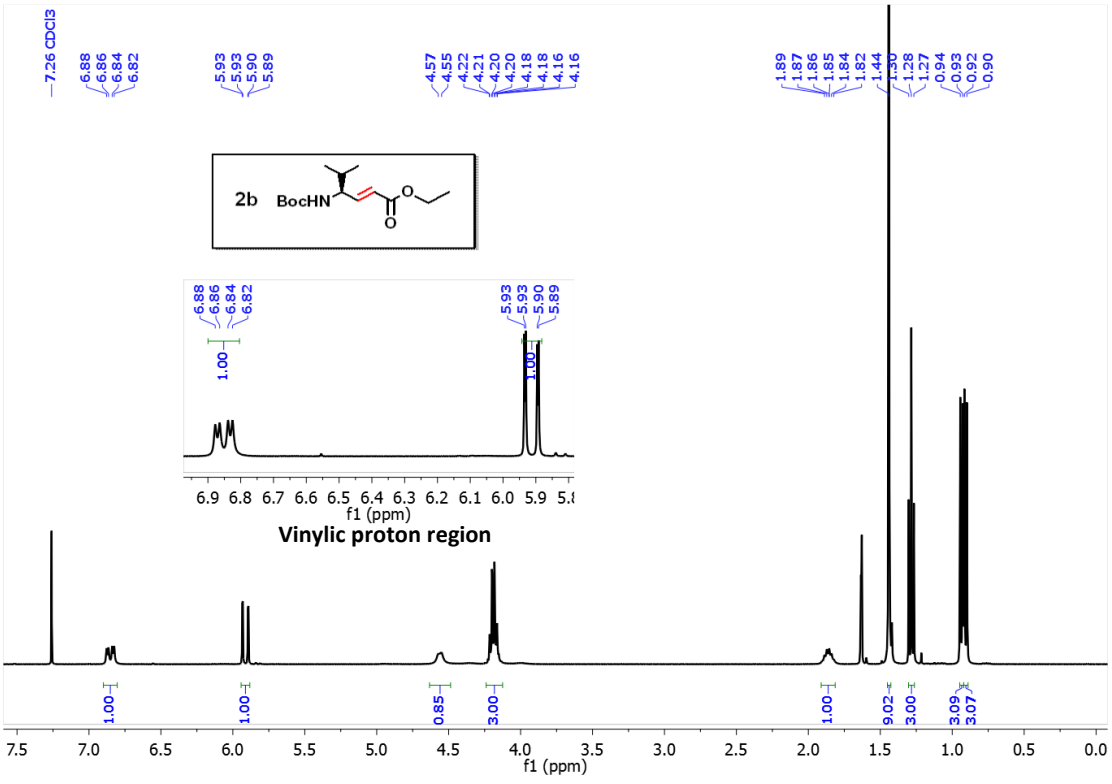


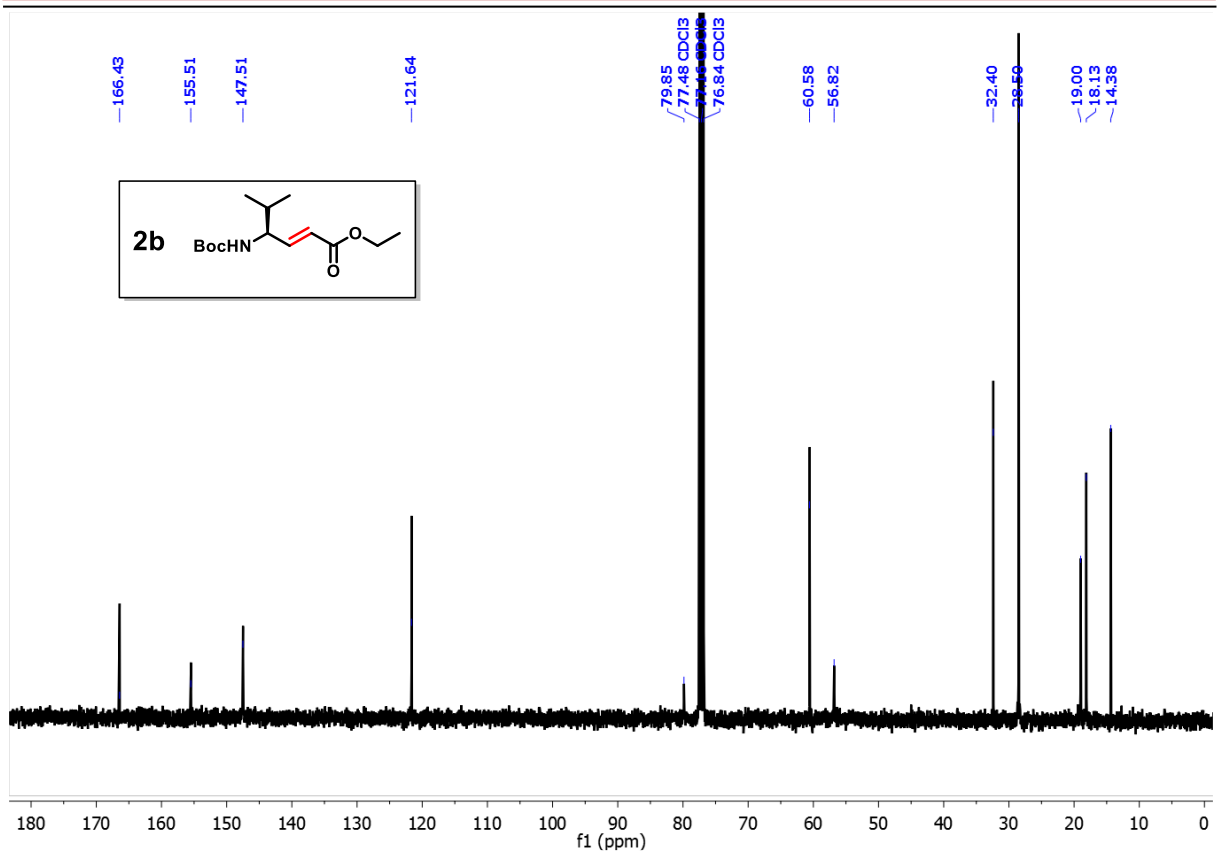
3.7.3. ^{1}H NMR, ^{13}C NMR and HRMS spectra of monomer units

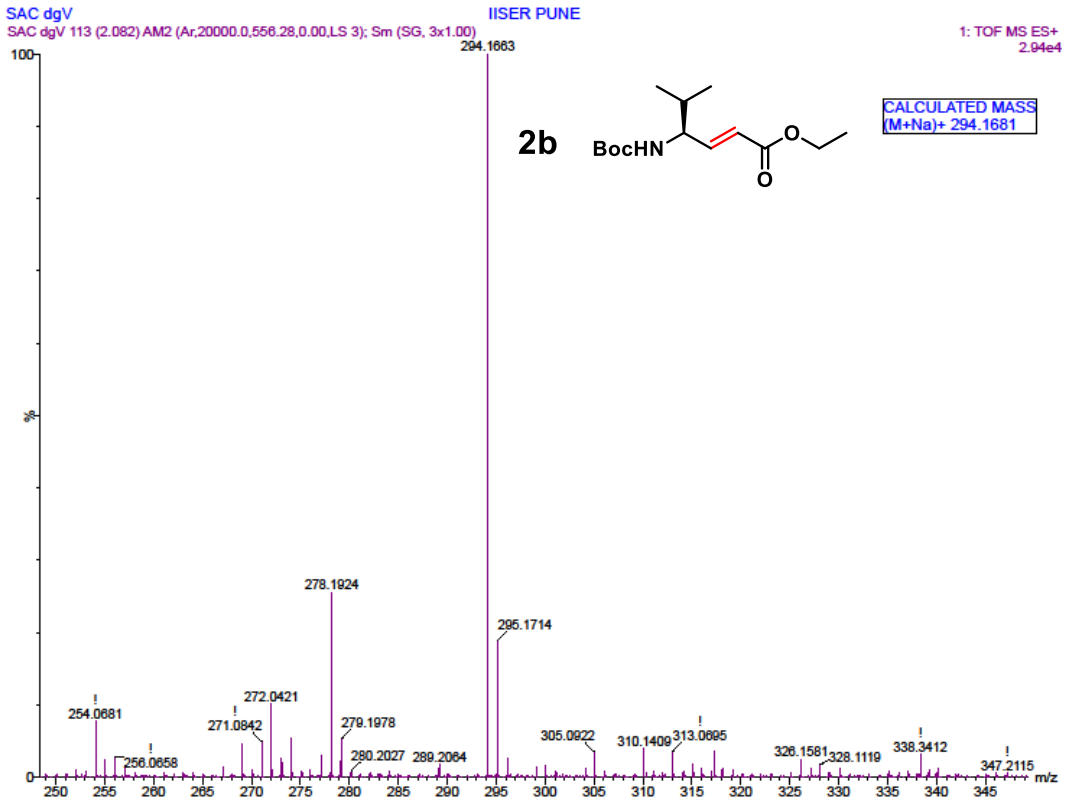

7.26 CHLOROFORM-D
6.84
6.83
6.80
6.79
5.92
5.88
4.49
4.47
4.32
4.20
4.18
4.17
4.15
1.71
1.69
1.68
1.66
1.64
1.43
1.39
1.37
1.35
1.29
1.27
1.25
0.97
0.93
0.92
0.91
-0.02
2a
BocHN
O
O
1.01
1.01
Vinylic Proton's region
f1 (ppm)
1.01
1.01
0.92
1.01
2.01
1.02
9.02
2.02
3.01
6.04
f1 (ppm)

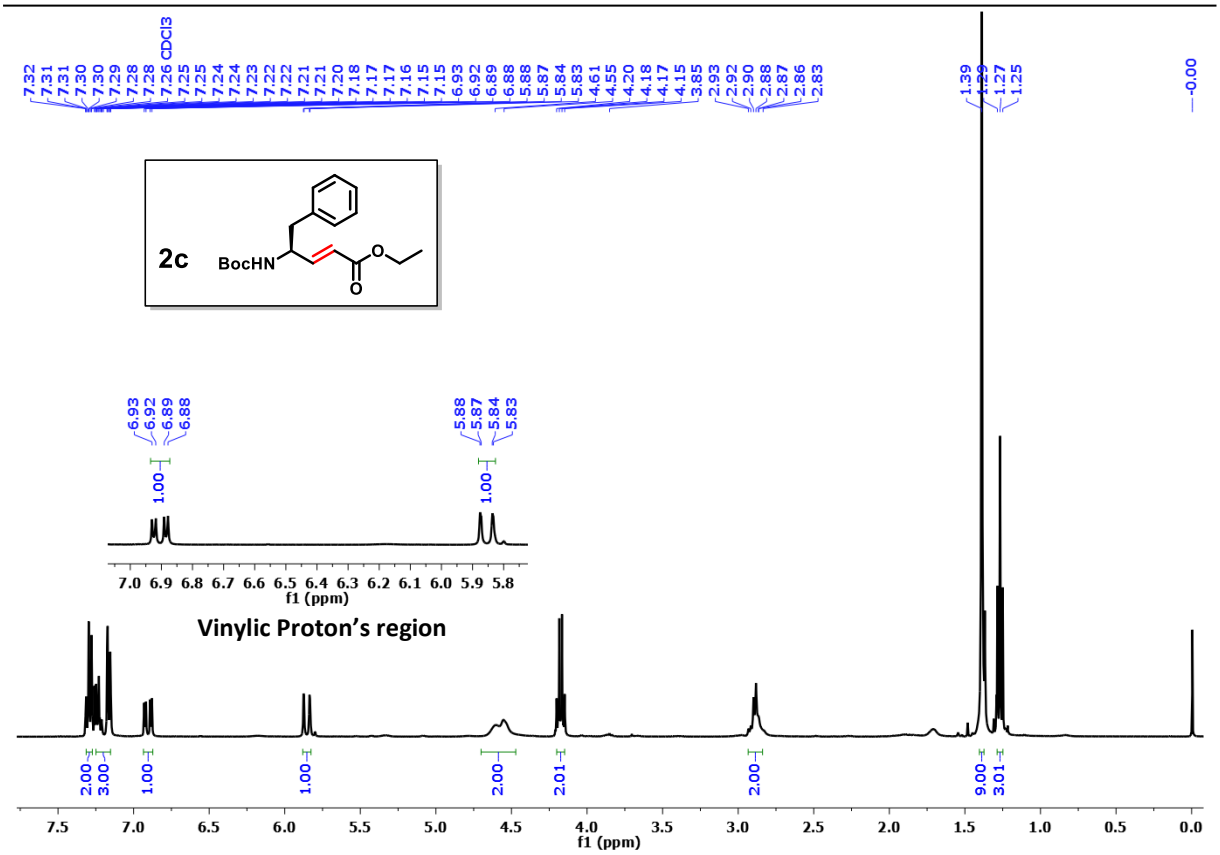

166.56
155.22
149.04
120.53
79.81
77.47 CHLOROFORM-D
76.83 CHLOROFORM-D
60.55
49.92
43.95
28.47
24.83
22.83
14.34
0.11
2a
BocHN
O
O
f1 (ppm)

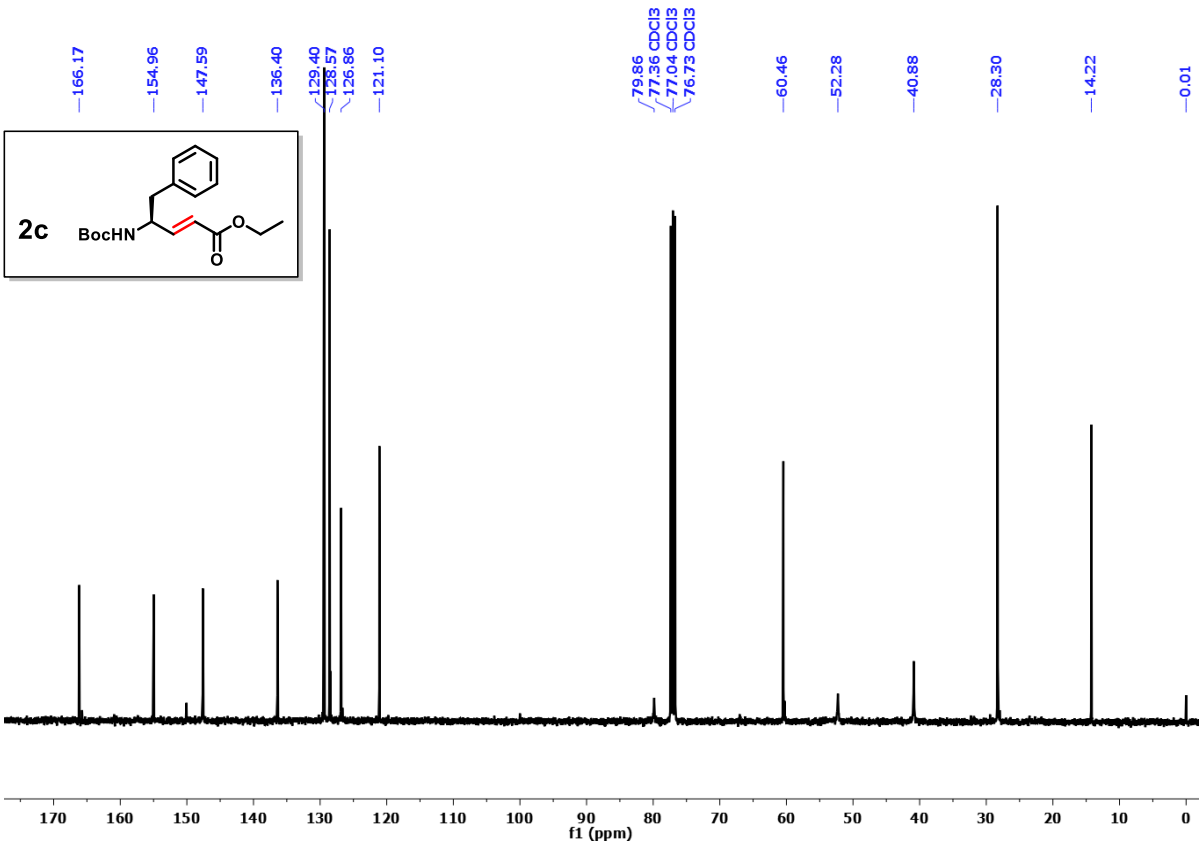

BDLET
IISER PUNE
BDLET 53 (0.979) AM2 (Ar,10000.0,556.28,0.00,LS 3); Sm (SG, 3x1.00)
1: TOF MS ES+
1.34e6
2a
BocHN
CALCULATED MASS
(M+Na)+ 308.1837
308.1845
309.1878
186.1496
169.1227
140.1072
123.0800
187.1529
252.1206
274.2752
365.2787
366.2823
415.2820
471.3443
540.5378
567.4742
593.3786
594.3829
595.3856
675.6770
697.6556
765.3239
m/z

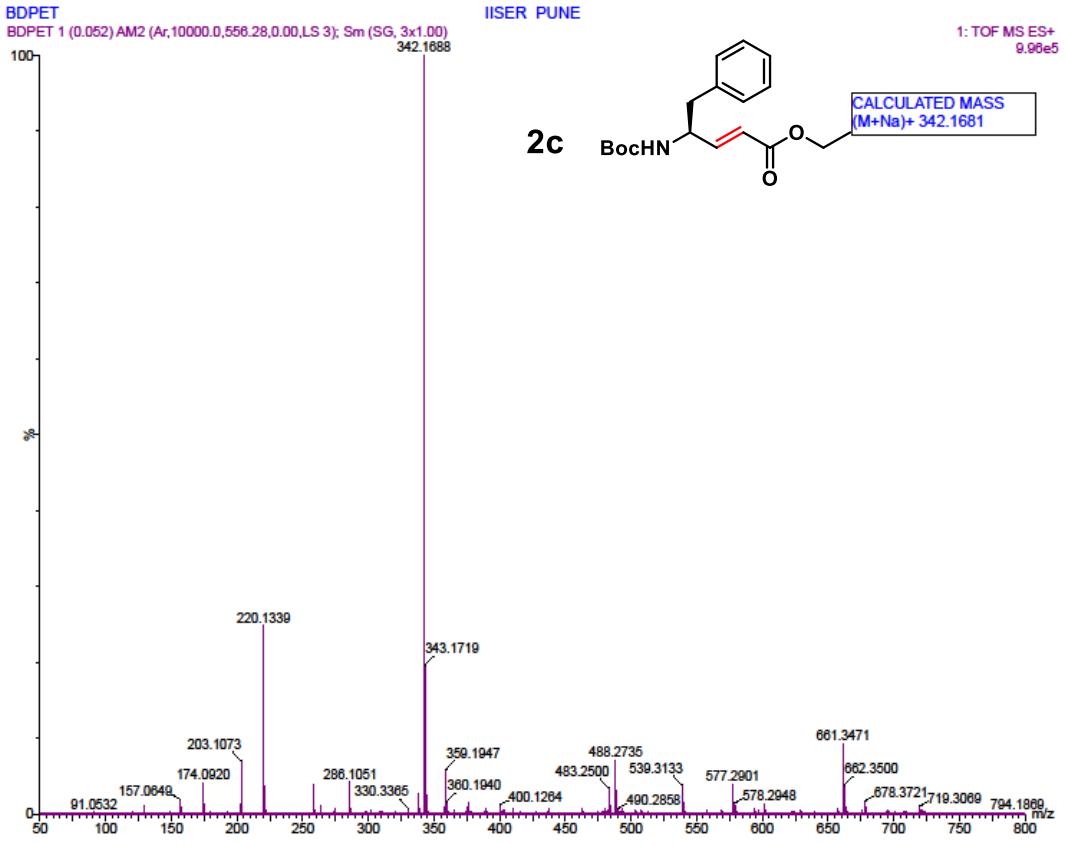

7.26 CDCl3
2b
BocHN
Vinylic proton region
f1 (ppm)

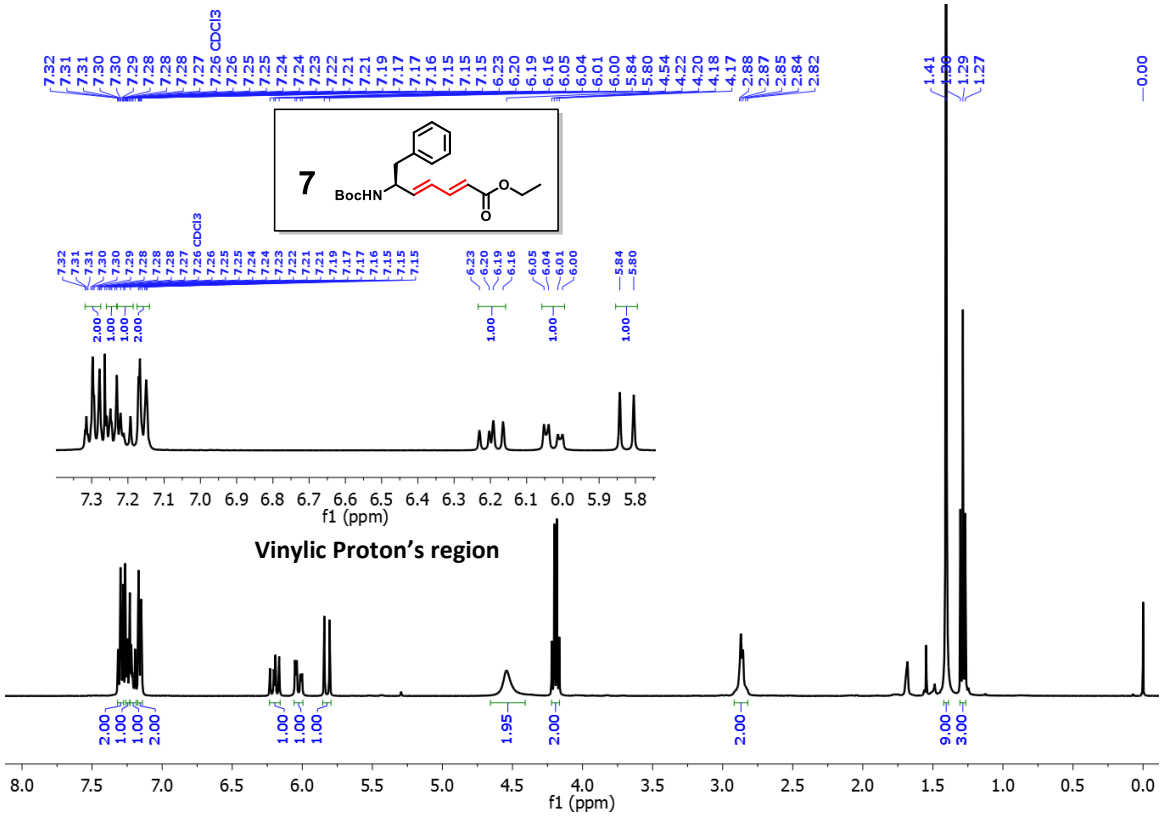

166.43
155.51
147.51
121.64
79.85
77.48 CDCl3
76.84 CDCl3
60.58
56.82
32.40
28.50
19.00
18.13
14.38
2b
BocHN
O
O
180 170 160 150 140 130 120 110 100 90 80 70 60 50 40 30 20 10 0
f1 (ppm)

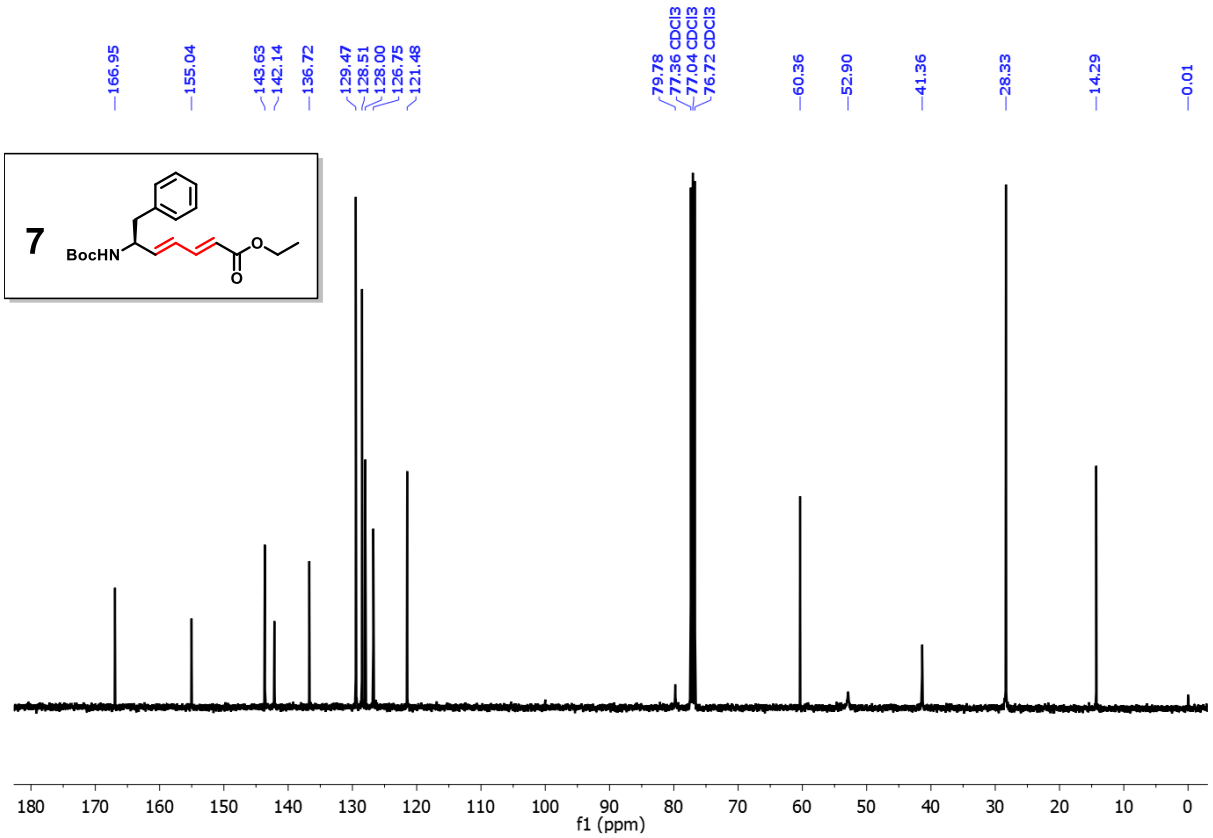

SAC dgV
IISER PUNE
SAC dgV 113 (2.082) AM2 (Ar,20000.0,556.28,0.00,LS 3); Sm (SG, 3x1.00)
1: TOF MS ES+
2.94e4
100
%
0
294.1663
278.1924
295.1714
272.0421
254.0681
271.0842
279.1978
256.0658
280.2027
289.2064
305.0922
310.1409
313.0695
326.1581
328.1119
338.3412
347.2115
m/z
250 255 260 265 270 275 280 285 290 295 300 305 310 315 320 325 330 335 340 345
2b
BocHN
O
O
CALCULATED MASS
(M+Na)+ 294.1681

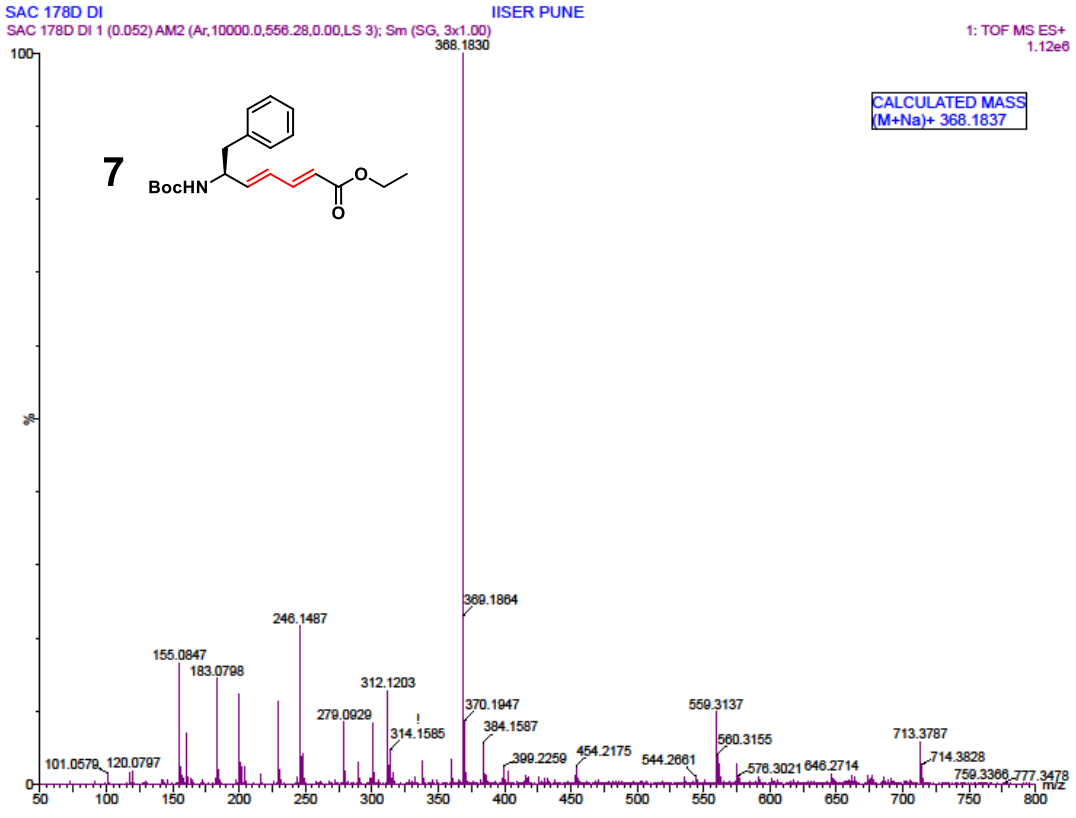

2c
BocHN
O
O
Vinylic Proton's region
f1 (ppm)

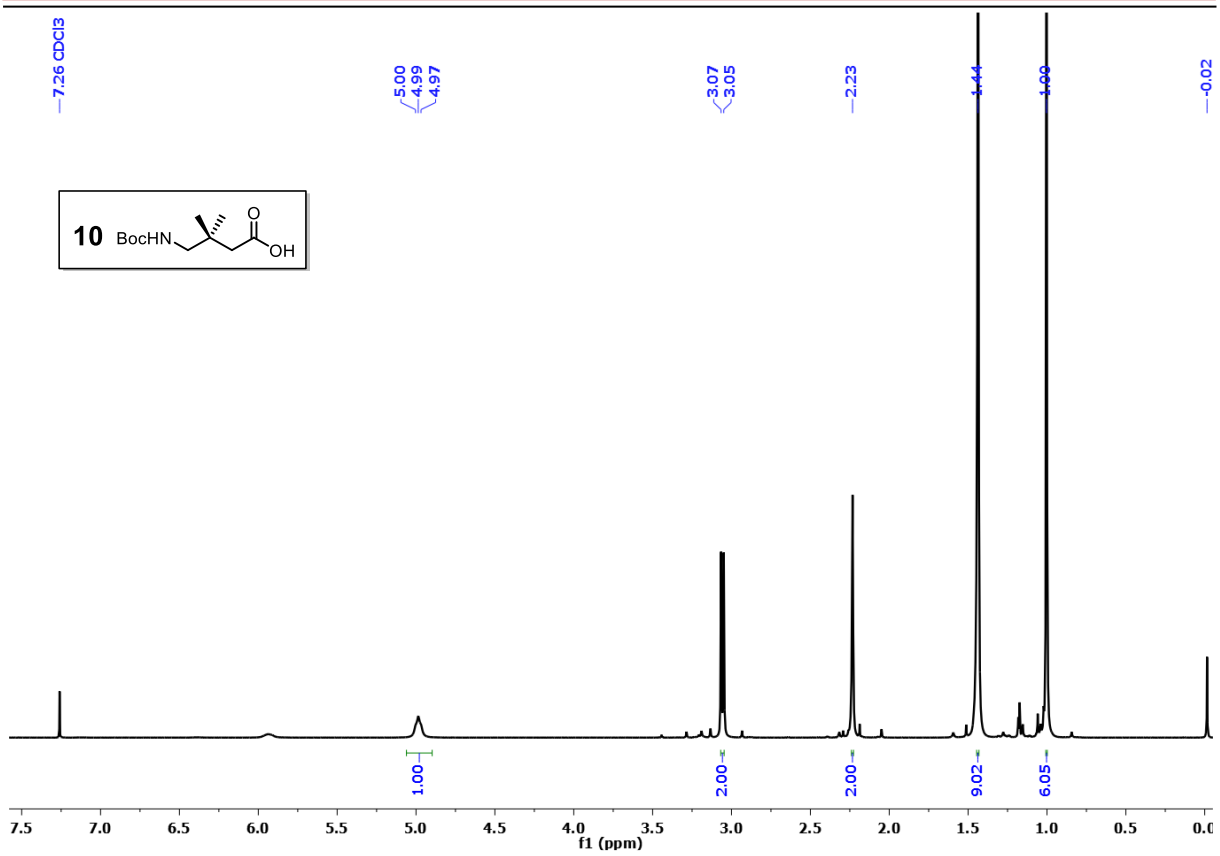

2c
BocHN
O
O
f1 (ppm)

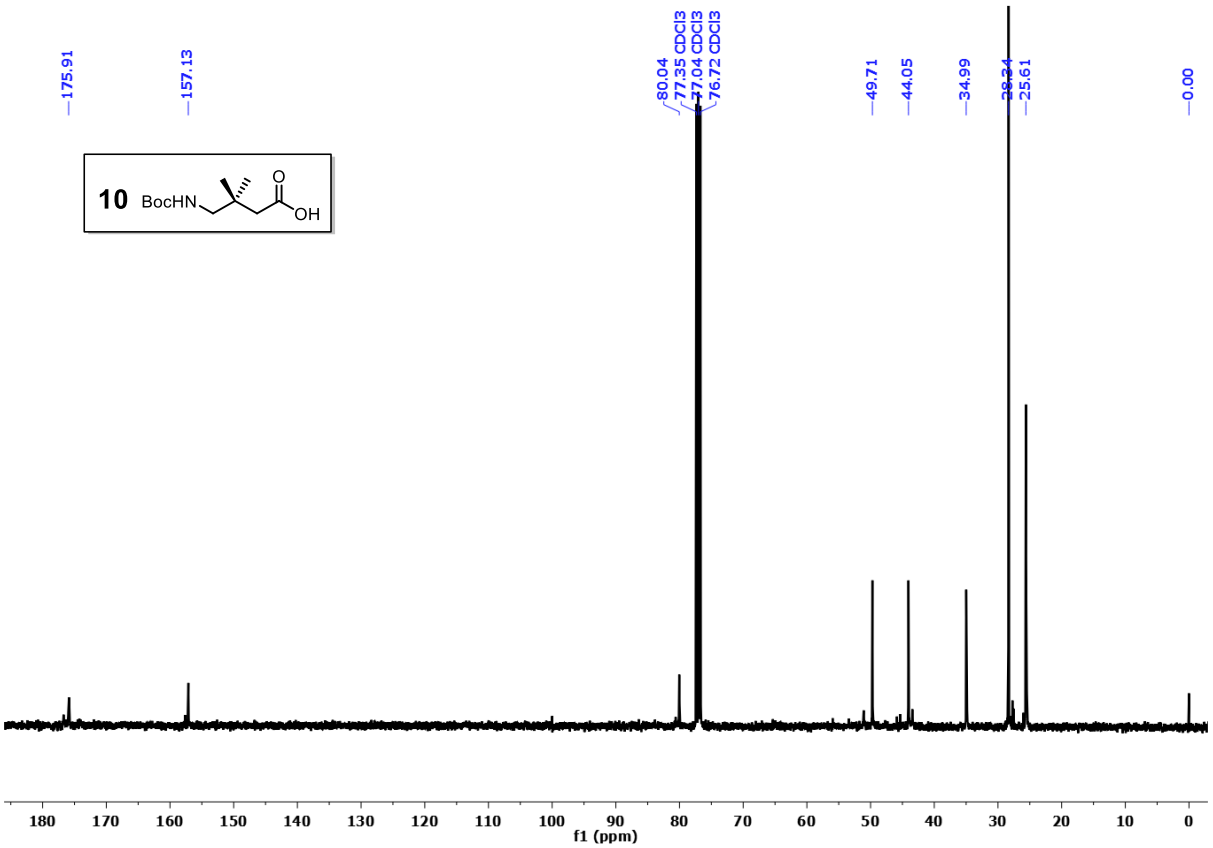

BDPET
IISER PUNE
BDPET 1 (0.052) AM2 (Ar,10000.0,556.28,0.00,LS 3); Sm (SG, 3x1.00)
1: TOF MS ES+
9.96e5
2c
BocHN
CALCULATED MASS
(M+Na)+ 342.1681
342.1688
220.1339
343.1719
203.1073
359.1947
174.0920
286.1051
488.2735
539.3133
661.3471
483.2500
577.2901
662.3500
157.0649
330.3365
360.1940
400.1264
578.2948
678.3721
91.0532
490.2858
719.3069
794.1869
m/z

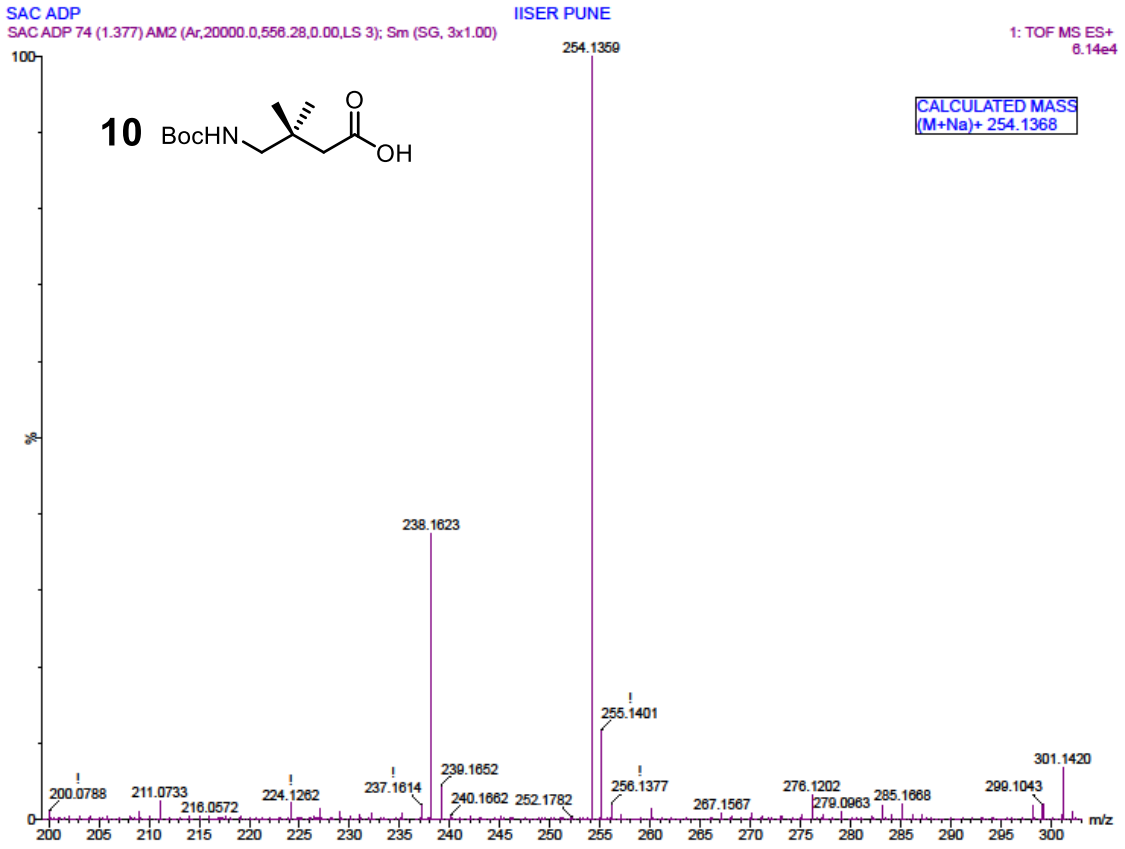

7
BocHN
CDCl3
f1 (ppm)
Vinylic Proton's region


166.95
155.04
143.63
142.14
136.72
129.47
128.51
128.00
126.75
121.48
79.78
77.36 CDCl3
77.04 CDCl3
76.72 CDCl3
60.36
52.90
41.36
28.33
14.29
0.01
7
BocHN
O
O
180 170 160 150 140 130 120 110 100 90 80 70 60 50 40 30 20 10 0
f1 (ppm)

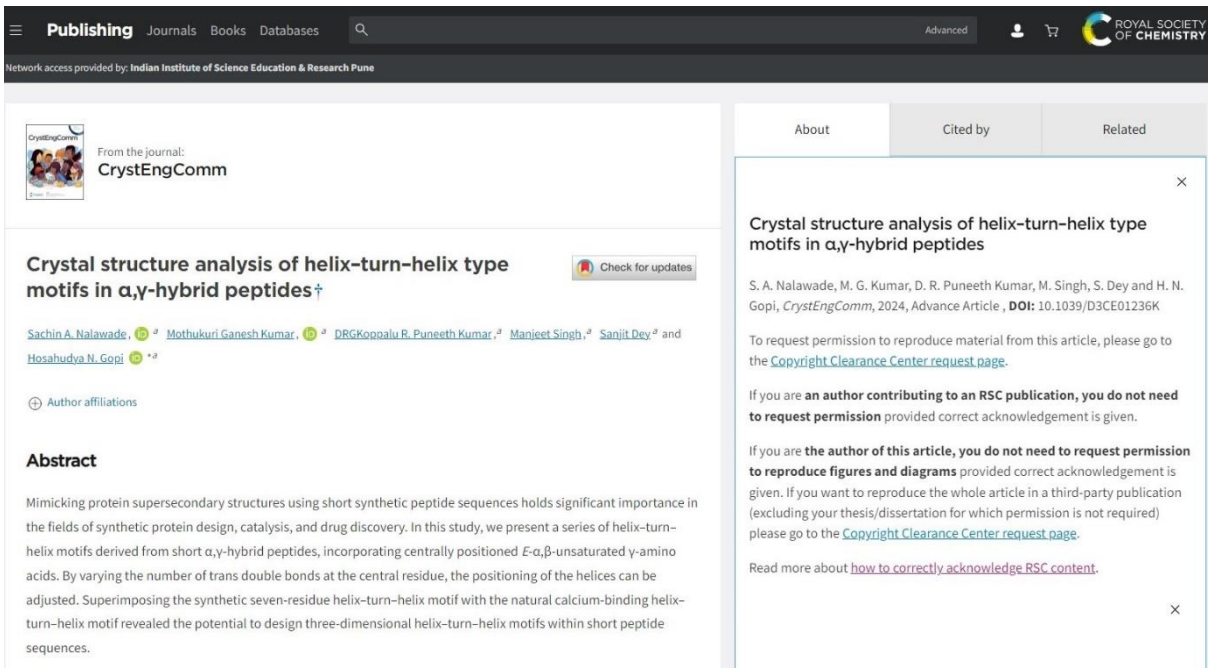

SAC 178D DI
IISER PUNE
SAC 178D DI 1 (0.052) AM2 (Ar,10000.0,556.28,0.00,LS 3); Sm (SG, 3x1.00)
1: TOF MS ES+
1.12e6
CALCULATED MASS
(M+Na)+ 368.1837
7
BocHN
O
O
100
%
0
368.1830
369.1864
246.1487
155.0847
183.0798
312.1203
279.0929
314.1585
370.1947
384.1587
559.3137
560.3155
713.3787
714.3828
454.2175
399.2259
544.2661
576.3021
646.2714
759.3366
777.3478
101.0579
120.0797
50 100 150 200 250 300 350 400 450 500 550 600 650 700 750 800
m/z


7.26 CDCl3
5.00
4.99
4.97
3.07
3.05
2.23
1.44
1.00
-0.02
10 BocHN OH
1.00
2.00
2.00
9.02
6.05
f1 (ppm)


175.91
157.13
80.04
77.35 CDCl3
77.04 CDCl3
76.72 CDCl3
49.71
44.05
34.99
28.24
25.61
0.00
10 BocHN OH
f1 (ppm)



3.7.4. Copy of the Permission letter from Journal for reuse of figures and diagrams.



Chapter 4

Unveiling Reactivity Patterns in Thiol Addition Reactions on α, β-unsaturated γ-amino acid amides and peptides Composed of it

4.1. Introduction

The post-synthetic chemical modification of peptides represents a compelling and attractive strategy, aimed at imparting functional diversity, enhancing stability, and precisely modulating their activities. Within this domain, numerous synthetic methodologies have arisen, facilitating the alteration and diversification of native amino acids.[1, 2] These methodologies involve the integration of various functionalities, such as thiols (-SH), amines (-NH2), carboxylic acids (-COOH), and aromatic side chains, thereby contributing to the enrichment of the chemical profile of peptides.[3] Furthermore, the introduction of synthetic amino acids featuring a diverse array of side-chain functional groups, including azides, alkynes, and nitro groups, has facilitated biocompatible modifications.[4] This advancement has significantly broadened the spectrum of attainable modifications, providing researchers and chemists with unprecedented precision in tailoring peptides. These modifications offer avenues for applications across diverse fields, spanning therapeutic[5, 6] development to materials science.[7, 8] However, compared to side-chain conjugation, fewer efforts have been directed towards backbone conjugation in peptides.

Sulfur is a constituent of numerous biologically active and pharmaceutical compounds (Figure 1).[9] Notably, around twenty percent of FDA-approved drugs incorporate sulfur atoms,[10] underscoring the significance of establishing new carbon-sulfur bonds as a pivotal area of exploration. The utilization of thio-functional groups in post-synthetic modifications provides a powerful tool for customizing peptide properties, ultimately leading to the development of novel and improved peptide-based materials and compounds.[11] Our research focus has been centered on the design of protein secondary structure mimetics utilizing non-ribosomal α,β-unsaturated γ-amino acids. These amino acids have proven to be instrumental in the creation of a diverse array of folded structures. The conjugate addition, a fundamental organic reaction facilitating the selective addition of various functional groups to the β-carbon of α,β-unsaturated carbonyl compounds, positions these compounds as pivotal reactive intermediates in organic chemistry.[12] In a previous study, we elucidated the synthesis of 1,4-conjugate addition products derived from alkyl esters of α,β-unsaturated γ-amino acids, subsequently utilizing these products in the design of helix and β-hairpin mimetics.[13]

Motivated by the stereoselective conjugate addition of nucleophiles to α,β-unsaturated γ-amino acid esters under mild conditions, our investigation was directed towards exploring the feasibility of analogous conjugate addition reactions on peptides incorporating α,β-unsaturated amino acids. The primary objective of this exploration was to generate a diverse array of

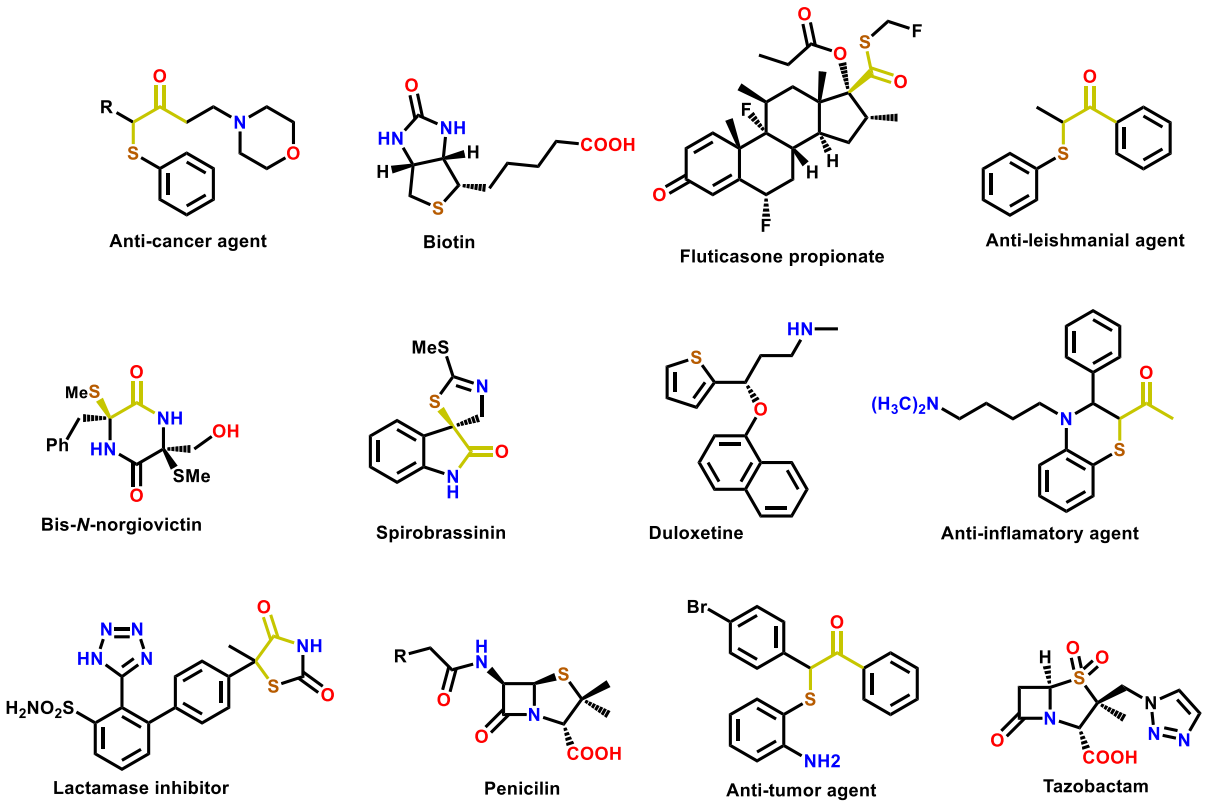


Figure 1: Sulfur atom bearing bioactive compounds, drugs and natural products.

conjugated peptides from a common starting material. Furthermore, considering the relatively limited exploration of conjugate addition reactions on α,β-unsaturated amides in comparison to esters and aldehydes, our study aimed to assess the suitability of amides of α,β-unsaturated γ-amino acids as substrates for the conjugate addition reaction. An additional aspect of our investigation involved the detailed examination of the stereochemistry inherent in the resulting conjugated products.

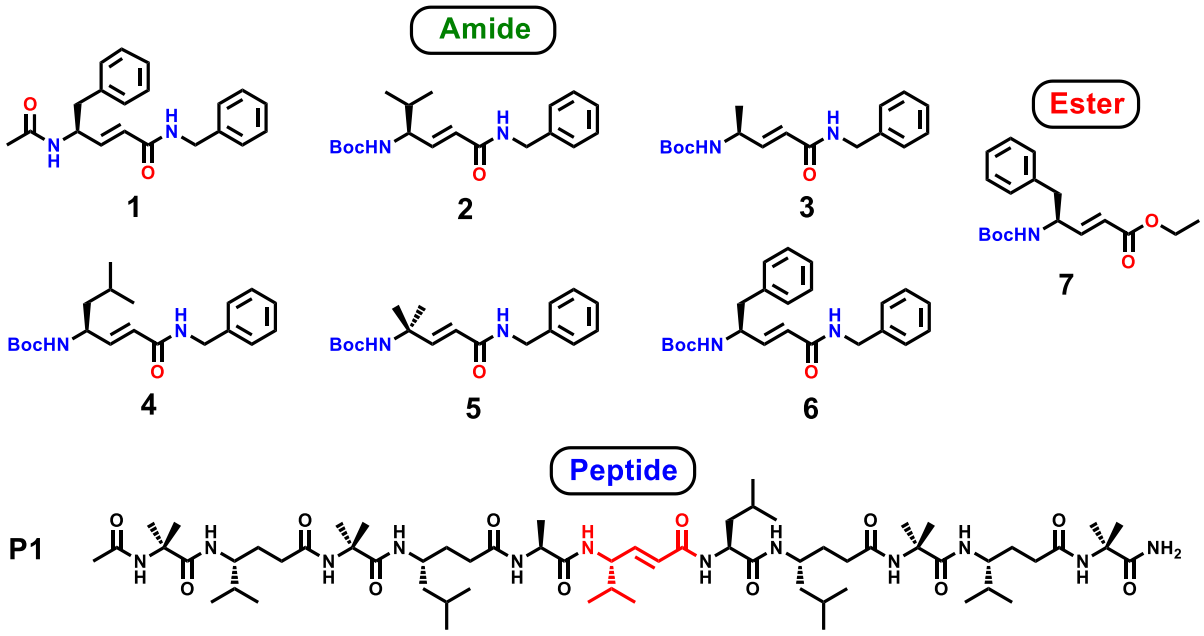
4.2. Objective of the current work

In this chapter, we studied the thioacid addition products derived from N-protected α,β-unsaturated γ-amino acid amides and peptides containing α,β-unsaturated γ-amino acids. In contrast to the predominant β-addition products observed in the esters of α,β-unsaturated γ-amino acids,[13] the α,β-unsaturated amides exhibited a notable divergence, yielding both α- and β-addition products. Surprisingly, in the context of peptides, the thioacid addition reaction predominantly yielded stereoselective α-addition product as the major product. while thiol addition reactions favored stereoselective β-addition product. All products were isolated, and their conformations were studied in single-crystals. Interestingly, unlike the two-helix motifs observed in the starting peptide, both α- and β-addition products of peptides adopted helical

conformations in single crystals, indicating the structural adaptability of α,γ-hybrid peptides. The objective of the thio addition on the α,β-unsaturated amides is to investigate and characterize the resultant products, aiming to understand the regioselectivity and stereochemistry of thioacid addition to these α,β-unsaturated amides. This exploration seeks to elucidate the impact of the amide functional group on the reaction outcome, contributing valuable insights into the reactivity of α,β-unsaturated amides compared to other related compounds. Furthermore, the study aims to contribute to the broader understanding of the synthetic potential and structural adaptability of peptides containing α,β-unsaturated amino acids in the context of thio addition reactions.

4.3. Results and discussion

To investigate the reactivity of N-protected *E*-α,β-unsaturated γ-amino acid amides, we synthesized the benzylamide derivatives (**1-6**) of N-protected α,β-unsaturated-γ-amino acids, along with the control ethyl ester (**7**). Scheme 1 provides an illustration of all the N-protected α,β-unsaturated derivatives synthesized. Additionally, for the exploration of potential post-synthetic conjugate additions on peptides incorporating α,β-unsaturated amino acids, we synthesized the α,γ-hybrid peptide undecapeptide **P1**. This peptide incorporates (*E*)-α,β-unsaturated γ-amino acid within the middle of its sequence. All (*E*)-α,β-unsaturated amino acids[14, 15] and γ-amino acids[16, 17] were synthesized following established procedures, isolated



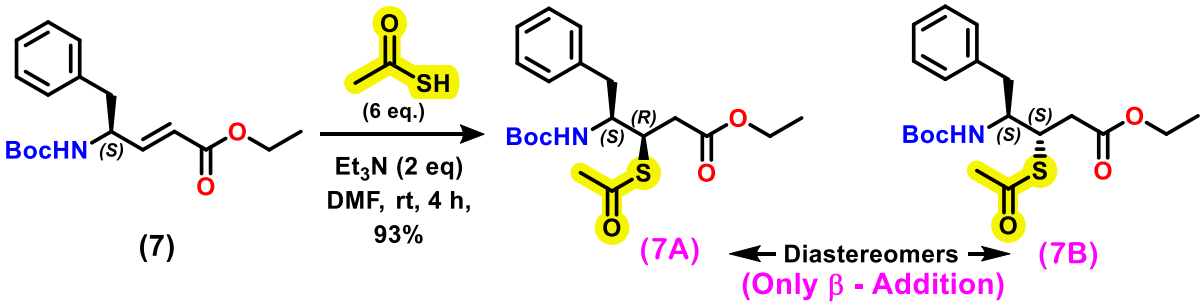
Scheme 1: Sequences of N-protected (*E*)-α,β-unsaturated γ-amino acid amides and α,γ-hybrid peptides composed (*E*)-α,β-unsaturated γ-amino acid at middle of the sequence.

in satisfactory yields, and subjected to characterization. Peptide **P1** was synthesized using the solid-phase method, subsequently purified through RP-HPLC, and thoroughly characterized.

4.3.1. Outcome of the Reaction between Thioacetic acid and (*E*)-α,β-Unsaturated γ-Amino Amides (1-5, 2'' and 3'') and ester (7).

4.3.1.1. <u>Reaction in the presence of a base</u>: Both α and β addition products were observed in each reactions

We initiated the conjugate addition reaction of N-acetyl-protected amide **1** using thioacid as a nucleophile and Et_3N as a base in DMF solvent. Under identical conditions, the control ethyl ester **7** was also subjected to the conjugate addition reaction. Surprisingly, **1** did not yield the 1,4-addition product at room temperature due to the weak reactivity of the conjugated double bonds. In contrast, ester **7** produced conjugate addition products with a 93% yield. Schematic representation of this reaction is given in Scheme 2. Notably, among the two addition products, the (*S*, *S*) anti-addition isomer (**7B)** with respect to the side-chain was the major product



Scheme 2: Conjugate addition of thioacid to BocNH-(*E*)-α,β-Unsaturated γ-Phenylalanine Ethyl Ester **(7)**. Only β-addition addition products were observed in the reaction.

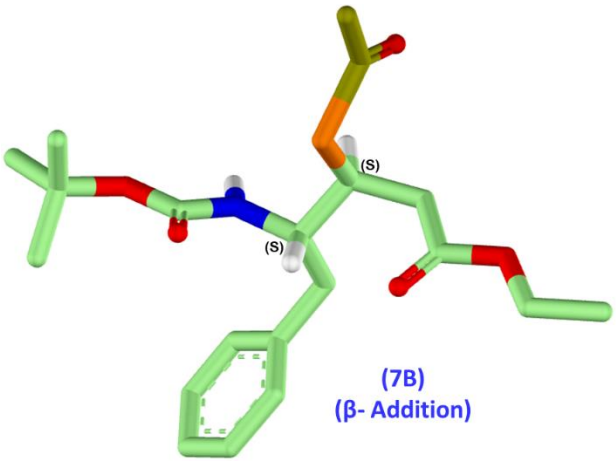
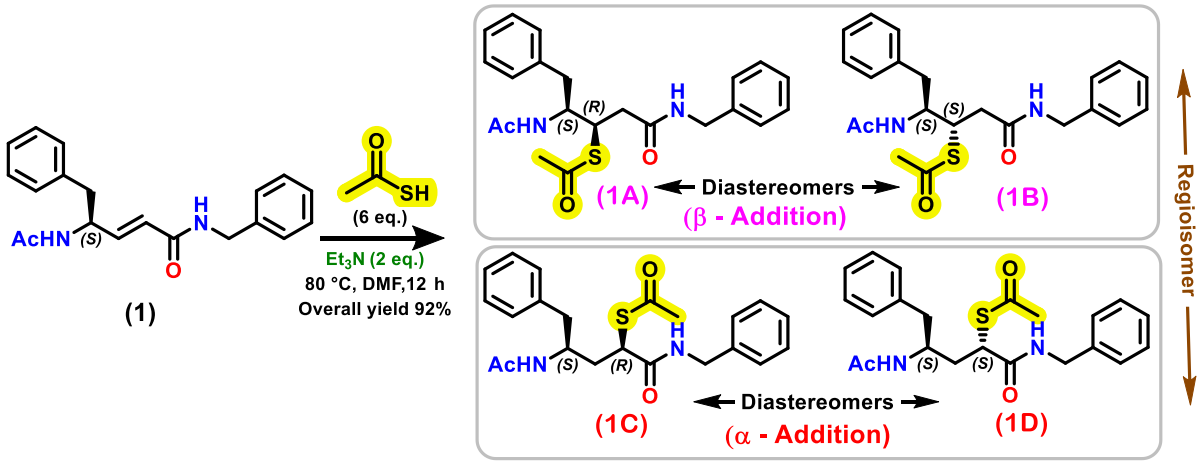


Figure 2: Crystal structures of thioacetic acid β-addition product **7B.**

compared to the (*S, R*) syn-addition isomer (**7A**). X-ray diffracted structure of **7B** is shown in Figure 2.

To enhance the reactivity of **1**, the reaction was conducted at 80°C and stirred for about 12 hours, resulting in complete consumption of the starting material. Remarkably, contrary to ester **7**, the conjugate addition reaction of amide **1** produced both α-addition and β-addition products with a 92% yield. Scheme 3 illustrates a schematic representation of this reaction. The observation of the α-addition product in the conjugate addition reaction was unexpected. All four diastereoisomers were separated using RP-HPLC, and their chromatographic profile is depicted in Figure 3.



Scheme 3: Conjugate addition of thioacid to N-acetyl protected *E*-α,β-unsaturated γ-amino acid amide. Both β-addition and α-addition products were observed in the reaction.

Among these diastereoisomers, one β-addition product **1A** and one α-addition product **1C** were isolated as single crystals, and their X-ray diffracted structures are presented in Figure 4. Moreover, the distinct differentiation of all four diastereoisomers was evident in the 1H NMR analysis shown in Figure 5.

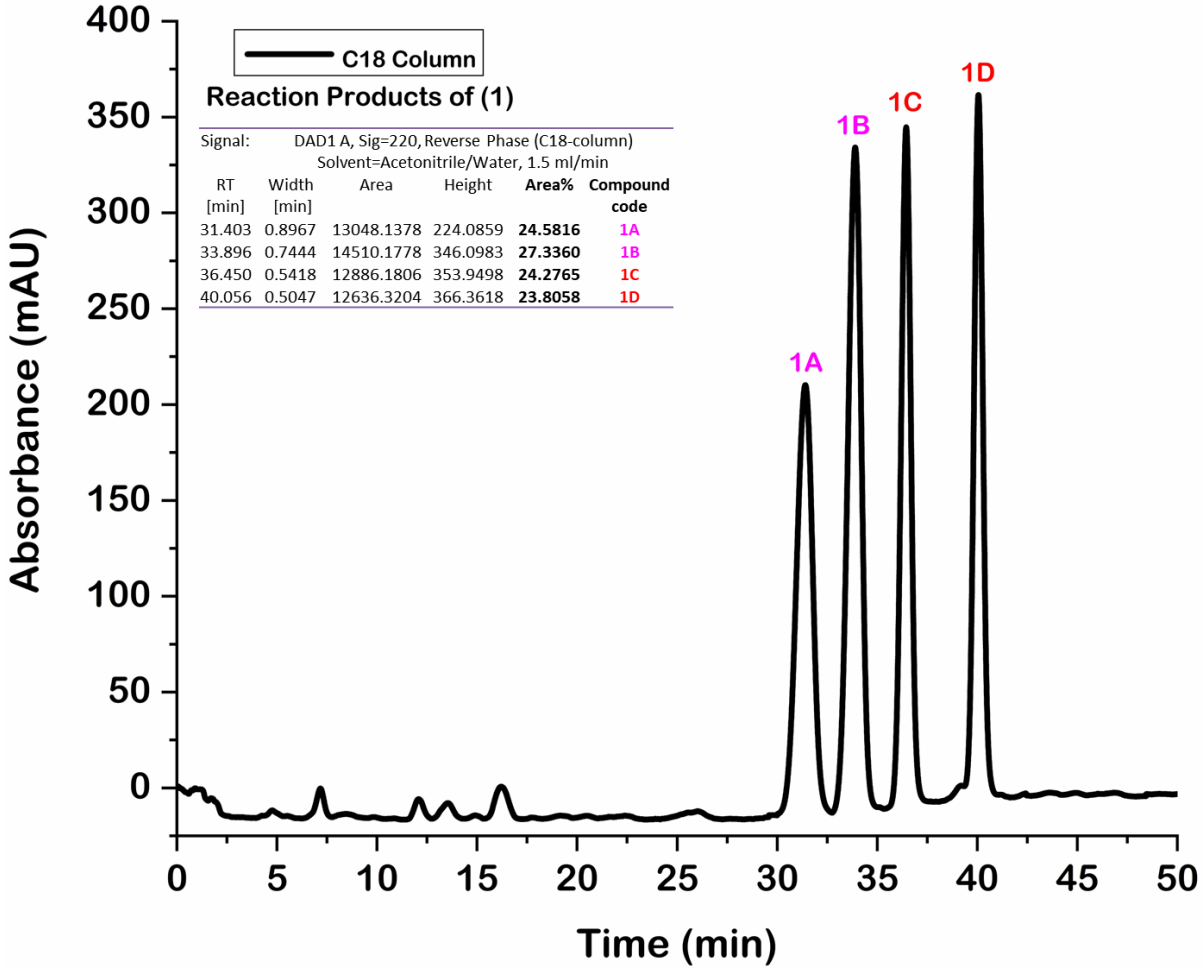


Figure 3: RP-HPLC profile depicting four diastereoisomers obtained in the conjugated addition reaction of **1** with thioacetic acid.

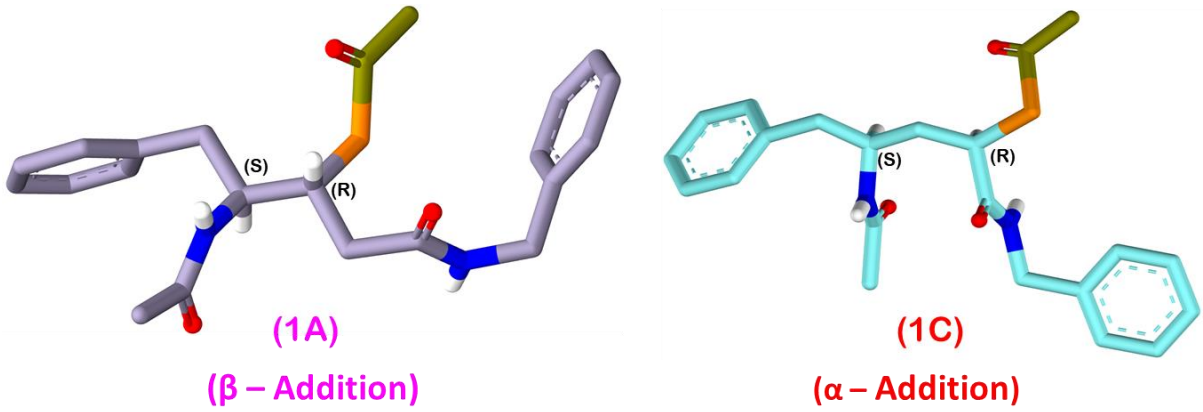


Figure 4: Crystal structures of thioacetic acid β-addition product **1A** and α-addition product **1C**.

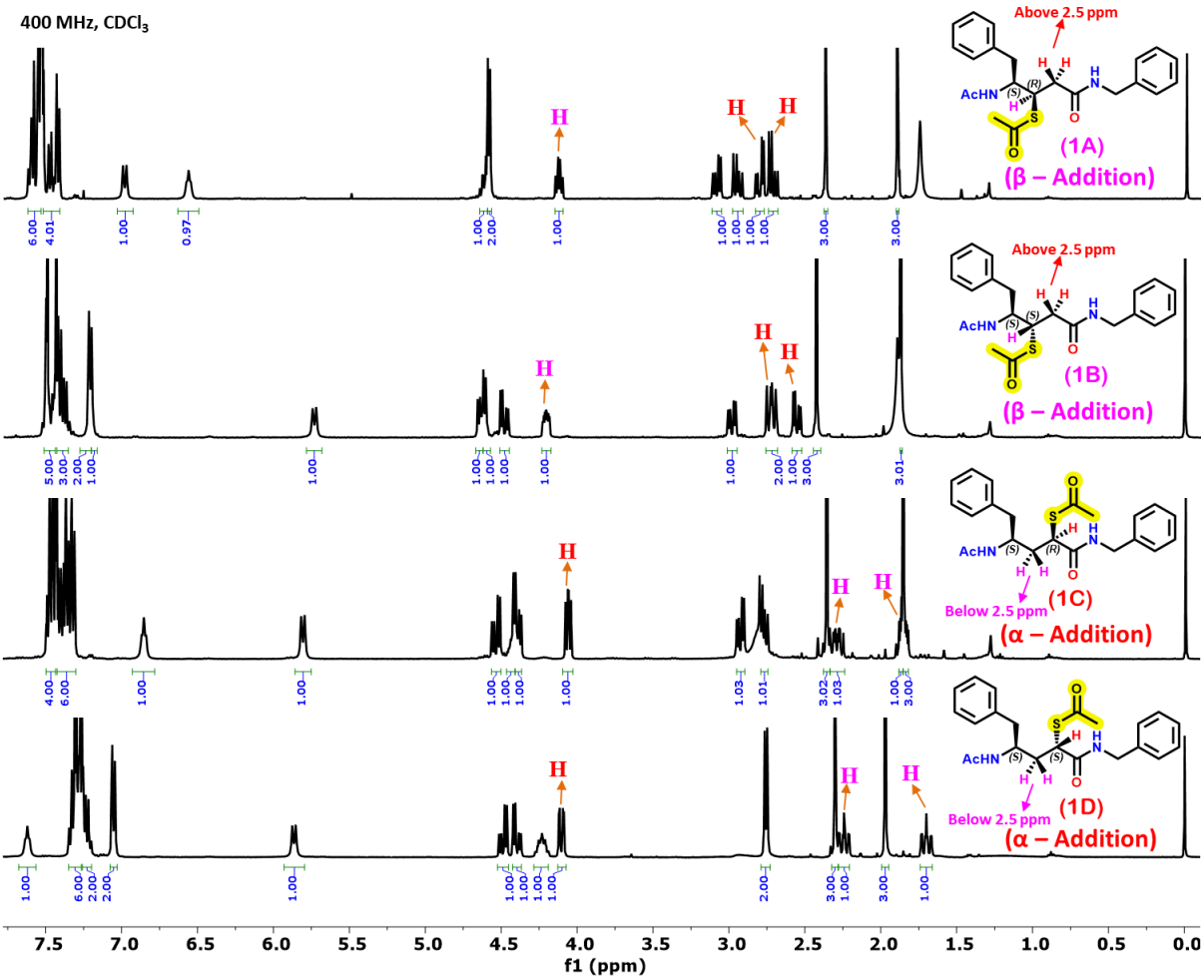
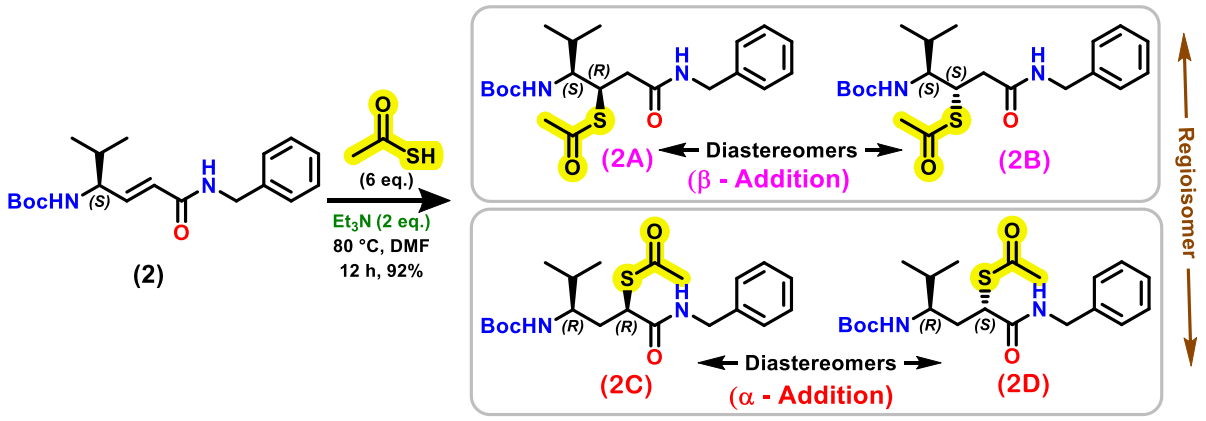


Figure 5: Overlayed ^{1}H NMR Spectra of **1A - 1D** showing the NMR difference of α- addition (**1A** & **1B**) and β- addition (**1C** & **1D**) products

Inspired by the presence of both α-addition and β-addition products in (*E*)-vinylogous amide **1**, we extended our investigation to **2**, incorporating a Valine side chain, for thioacid conjugate addition reaction in the presence of a base (Et_3N) and DMF solvent. Similar to **1**, compound **2**



Scheme 4: A schematic representation of thioacetic acid addition reaction of amide **2**.

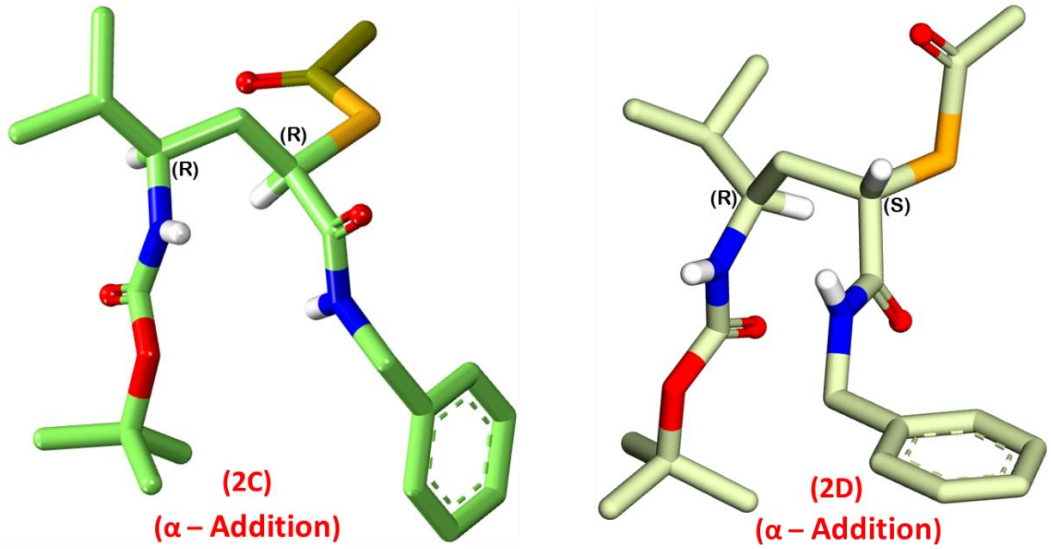


Figure 6: Crystal structures of thioacetic acid α-addition product **2C** and **2D**.

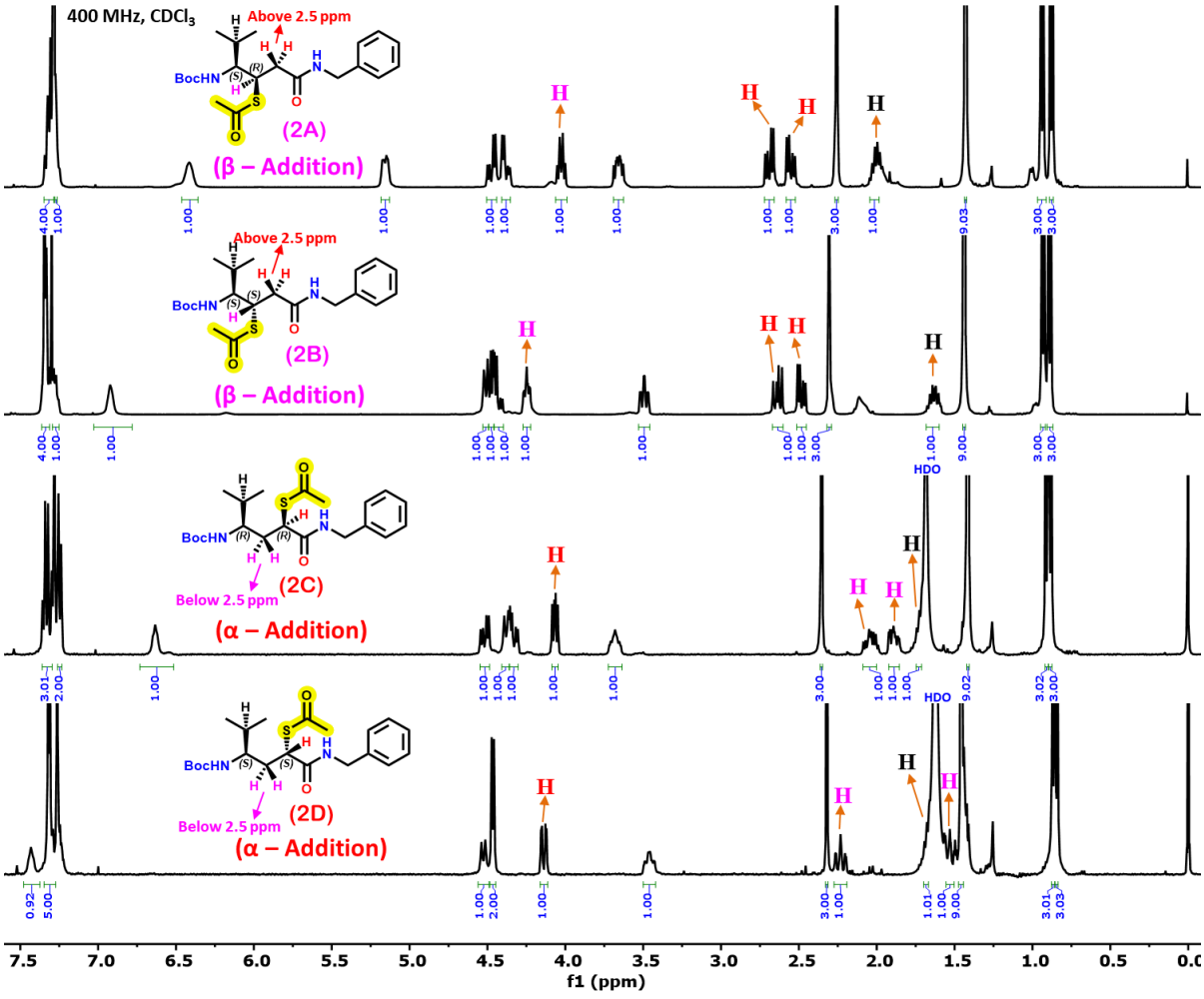
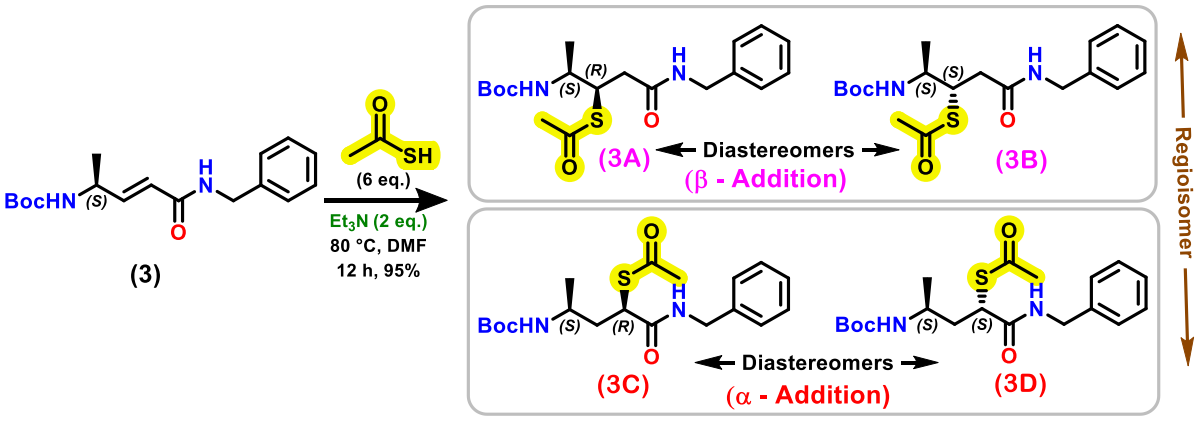


Figure 7: Overlayed ^{1}H NMR Spectra of **2A - 2D** showing NMR difference of α- addition (**2A** & **2B**) and β- addition (**2C** & **2D**) products.

yielded α-addition and β-addition products in equal proportions under heated conditions at 80°C in an open atmosphere. The schematic representation of the thioacetic acid addition reaction is shown Scheme 4. Subsequently, all four diastereoisomers (**2A-2D**) were isolated and characterized. After repeated attempts of crystallization we got single crystal of α-addition products **2C** with (*R, R*) and **2D** with (*S, R*) stereochemistry shown in Figure 6. The distinct differentiation of all four diastereoisomers (**2A-2D**) was evident in the 1H NMR analysis shown in Figure 7.

Additionally, N-Boc-protected amides **3** with an alanine side-chain and **4** with a leucine side-chain were subjected to thioacid conjugate addition in the presence of a base (Et_3N) at 80°C. Similar to **1** and **2**, both **3** and **4** produced an equal mixture of α- and β-addition products. All four diastereoisomeric products of amide **3** and amide **4** were isolated and characterized. Below is given the detailed analysis of all four diastereoisomeric products of each amide **3** and amide **4**, sequentially.

Schematic representation of thioacetic acid addition reaction of amide **3** is shown in Scheme 5. We attempted to get single crystal of amide **3** reaction products (**3A-3D),** only α-addition product **3C** (*S, R*) is crystallised is shown in Figure 8. Figure 9 is the overlayed ^{1}H NMR Spectra of **3A - 3D** showing NMR signal difference of α- addition (**3A** & **3B**) and β- addition (**3C** & **3D**) products.



Scheme 5: A schematic representation of thioacetic acid addition reaction of amide **3**.

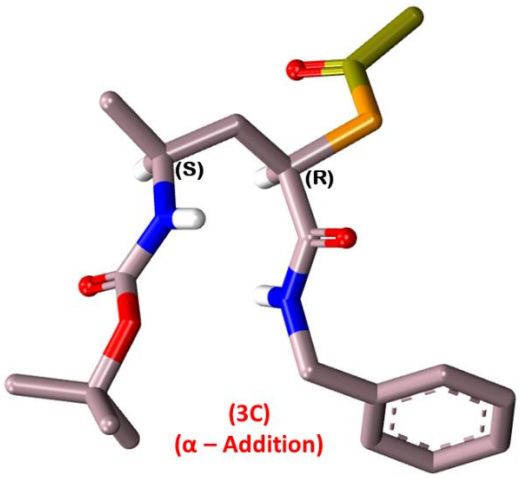


Figure 8: Crystal structures of thioacetic acid α-addition product **3C**.

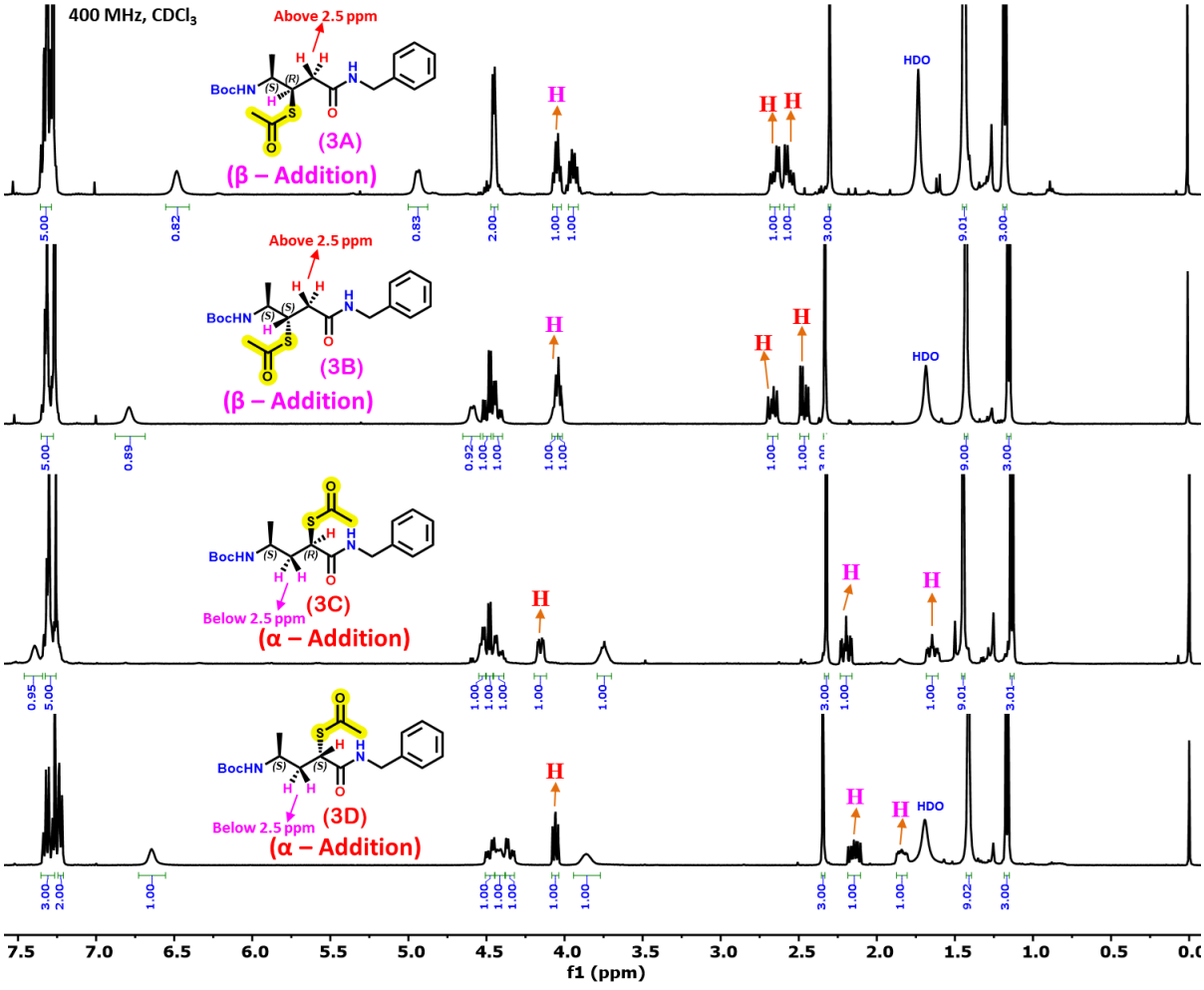
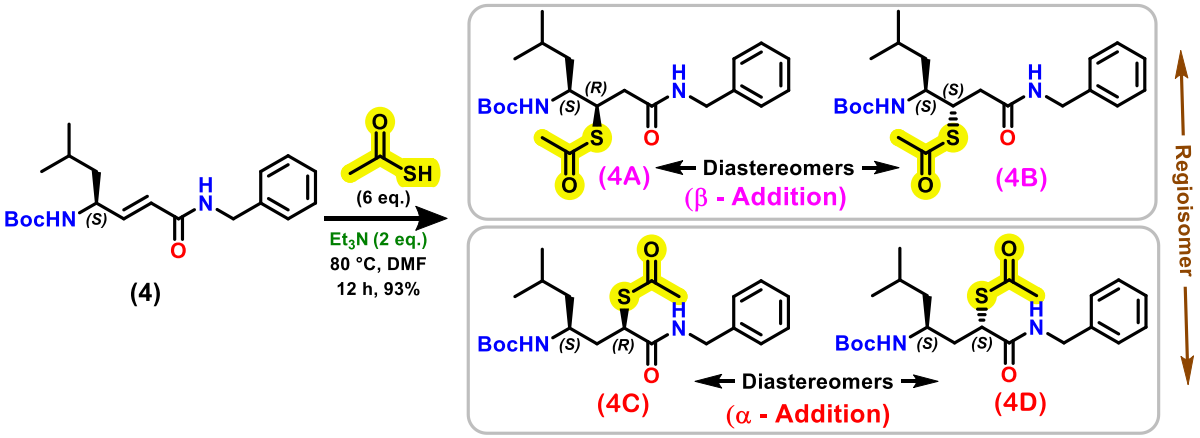


Figure 9: Overlayed ^{1}H NMR Spectra of **3A - 3D** showing NMR difference of α- addition (**3A** & **3B**) and β- addition (**3C** & **3D**) products.

Schematic representation of thioacetic acid addition reaction of amide **4** is shown in Scheme

6. RP-HPLC profile depicting four diastereoisomers obtained in the conjugated addition reaction of **4** with thioacetic acid is shown in Figure 10. We attempted to get single crystal of amide **4** reaction products (**4A-4D**)**,** but only one α-addition product **4C (*S, R*)** is crystallised is shown in Figure 11. The overlayed ^{1}H NMR Spectra of **4A - 4D** showing NMR signal difference of α- addition (**4A** & **4B**) and β- addition (**4C** & **4D**) products (Figure 12).



Scheme 6: A schematic representation of thioacetic acid addition reaction of amide **4**.

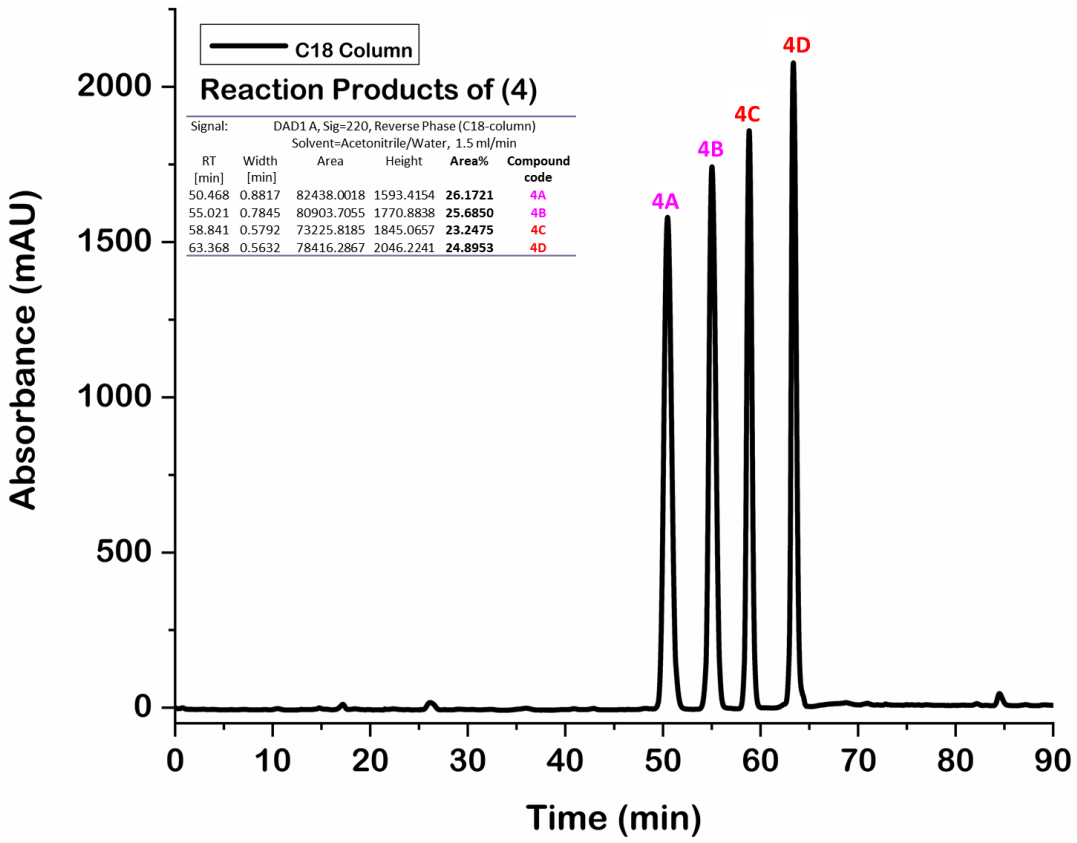


Figure 10: RP-HPLC profile depicting four diastereoisomers obtained in the conjugated addition reaction of **4** with thioacetic acid.

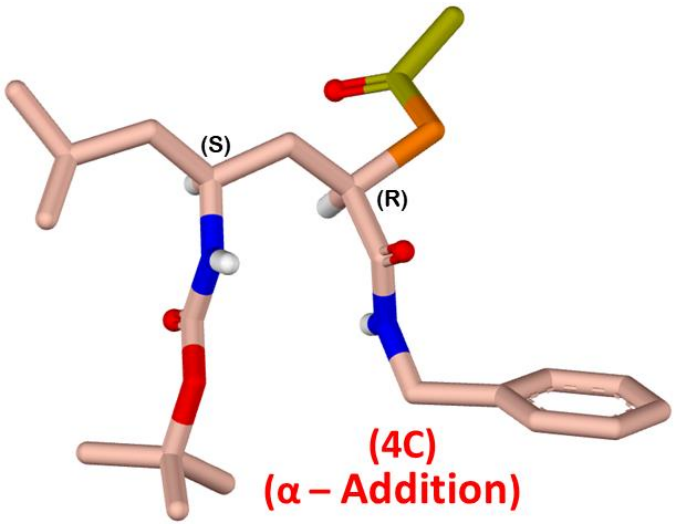


Figure 11: Crystal structures of thioacetic acid α-addition product **4C**.

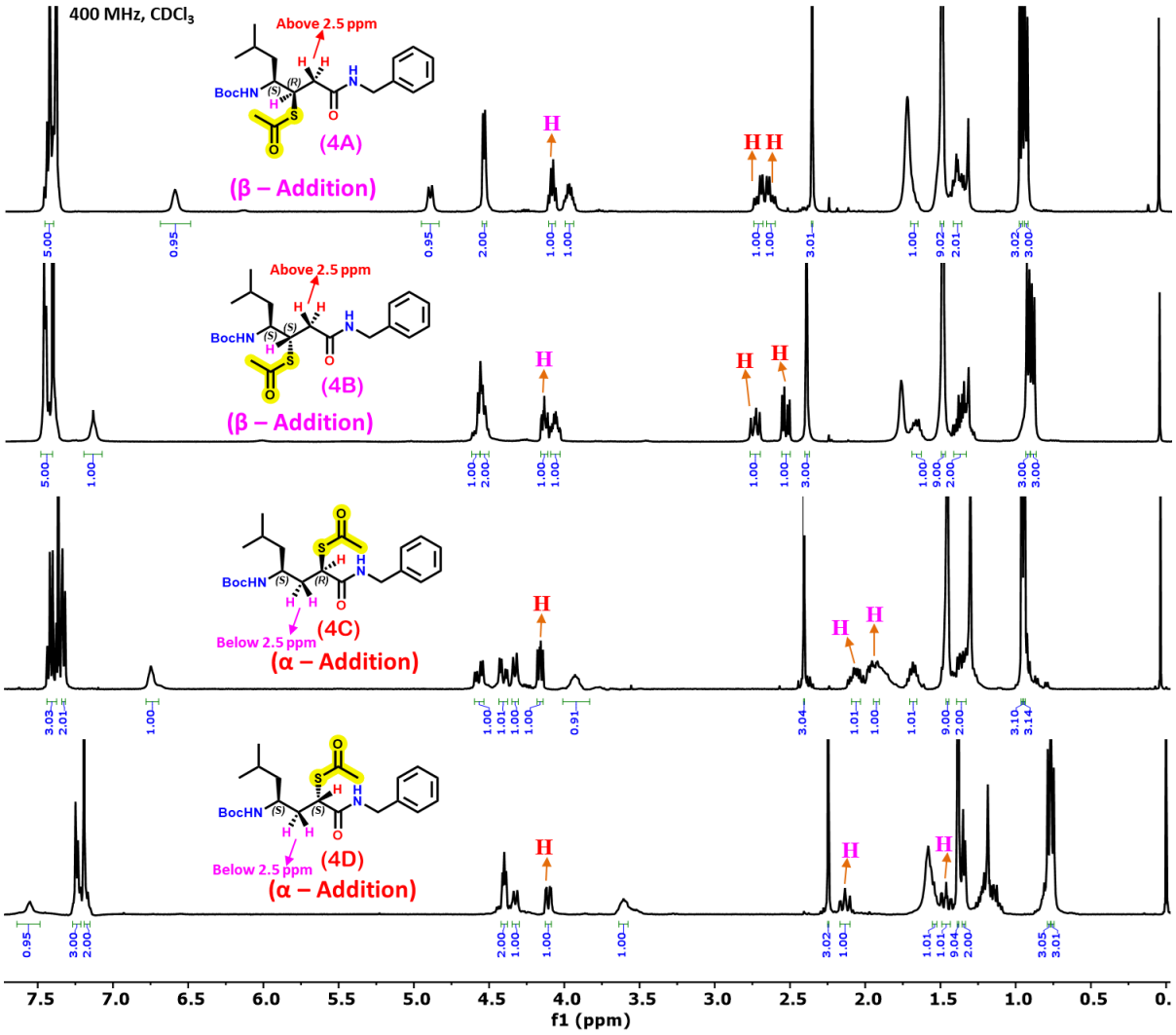
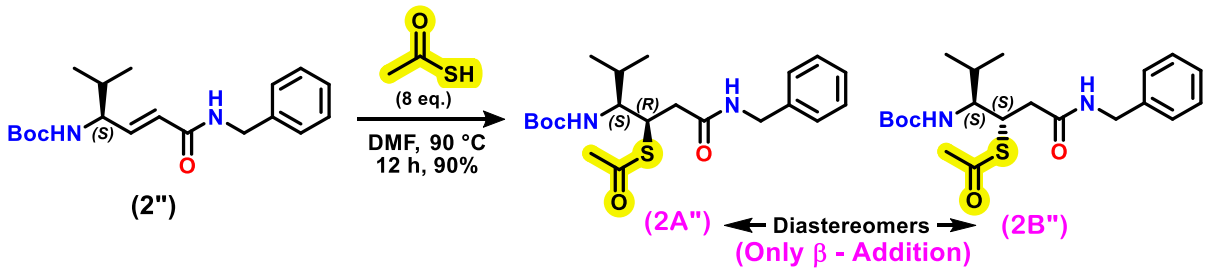


Figure 12: Overlayed ^{1}H NMR Spectra of **4A - 4D** showing NMR difference of α- addition (**4A** & **4B**) and β- addition (**4C** & **4D**) products.

4.3.1.2. <u>Reaction in absence of a base</u>: Only β addition products were observed in each reactions.

Motivated by the presence of both α- and β-addition products, we sought to investigate the reaction conditions favoring α-addition products. To comprehend the role of the base in the α-addition of thioacetic acid, we conducted the thioacetic acid conjugate addition reaction in the absence of triethylamine. The reaction mixture, comprising Amide **2''**, thioacetic acid, and DMF solvent, was stirred for approximately 12 hours at 80 °C. Surprisingly, the reaction exclusively yielded β-addition products. We isolated both products and characterized it.



Scheme 7: Conjugate addition of thioacetic acid on amide **2''** in the absence of base, only β-addition products were isolated.

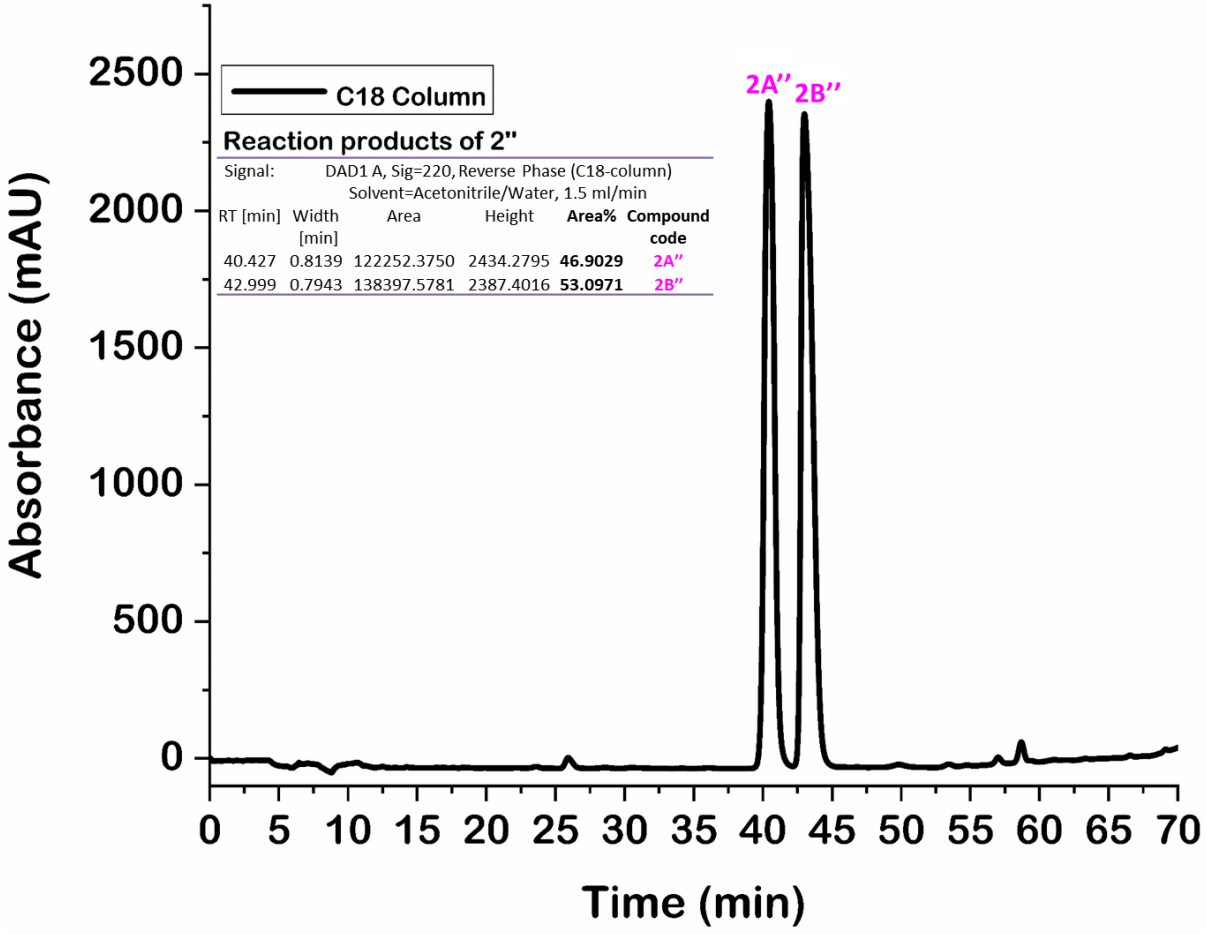


Figure 13: RP-HPLC profile depicting two diastereoisomers obtained in the conjugated addition reaction of amide **2''** with thioacetic acid in the absence of base. Only β-addition products were isolated.

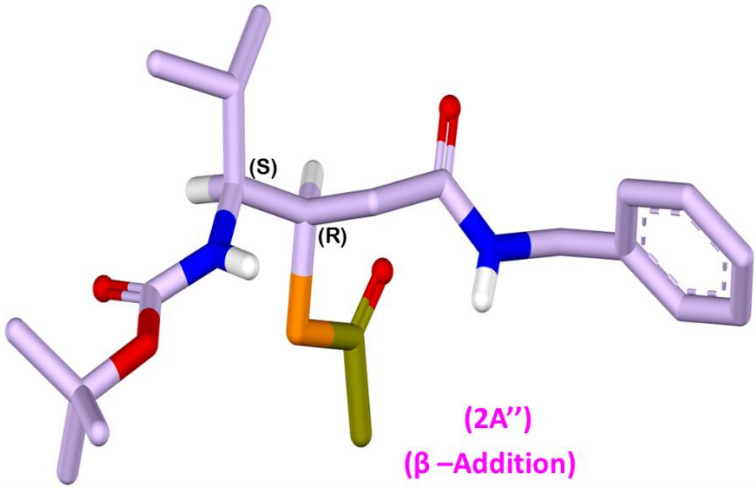
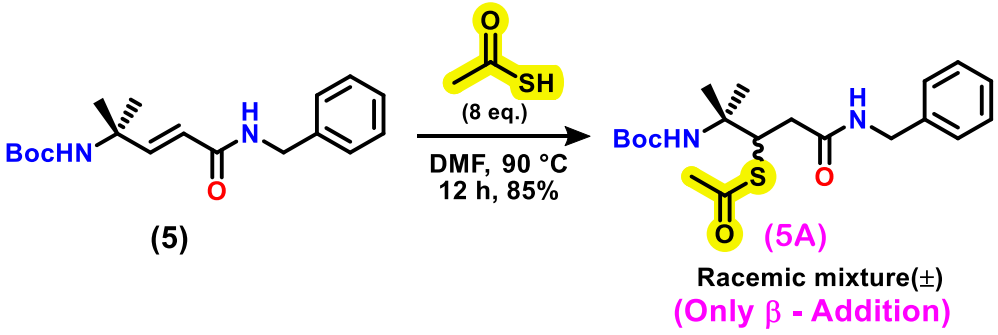


Figure 14: Crystal structures of thioacetic acid β-addition product **2A''**.

Scheme 7 illustrates a schematic representation of this reaction, RP-HPLC profile and the crystal structure of the β-addition product **2A''** is depicted in Figure 13 and Figure 14 respectively.

In the aforementioned reaction, the absence of a base resulted in the non-observation of an α-addition product. These findings underscore the pivotal role of base presence for the manifestation of the α-addition reaction within the defined experimental parameters. To validate the reproducibility of exclusively β-addition products in the reaction conducted without the presence of a base, we performed one more reaction in the absence of base, using



Scheme 8: Conjugate addition of thioacetic acid on amide **5.** In the absence of base, only β-addition products were isolated.

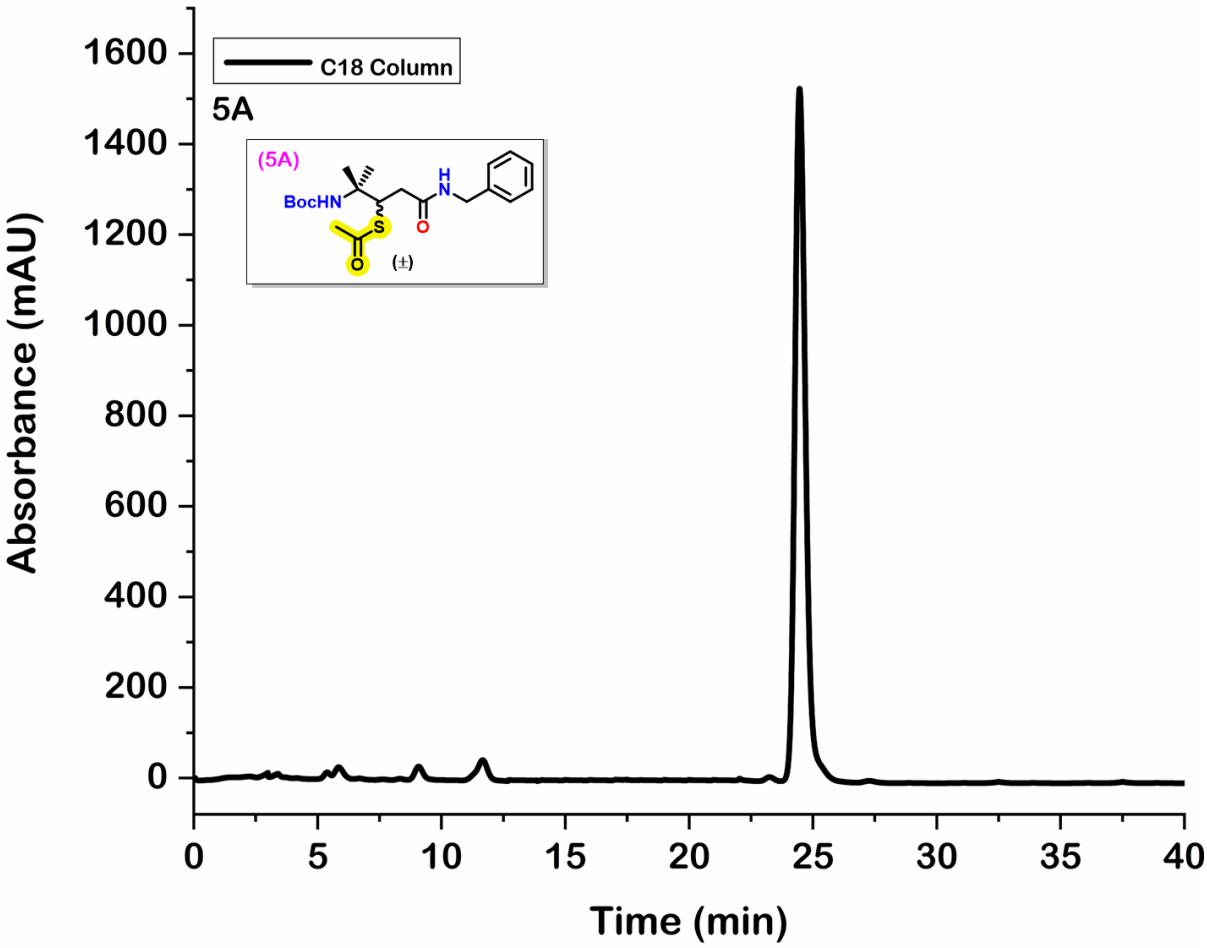


Figure 15: Reverse phase-HPLC profile of product **5A** on C-18 column.

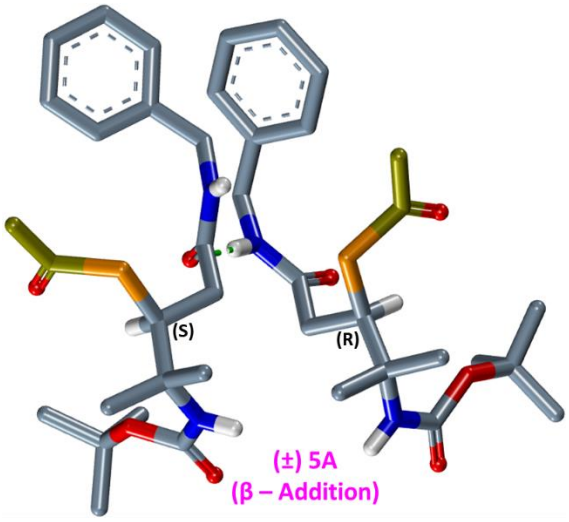


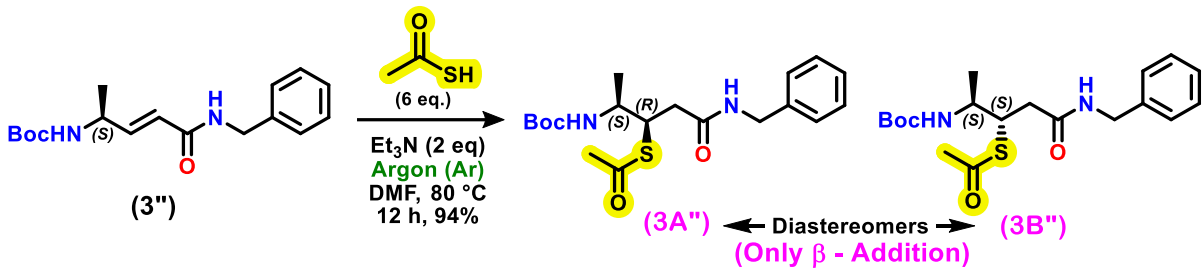
Figure 16: Crystal structures of thioacetic acid β-addition product (±) **5A**.

amide **5** with thioacetic acid, DMF solvent and stirred it for approximately 12 hours at 80 °C (Scheme 8). As observed in the previous reaction, this reaction also given only β-addition

products. We isolated a product and characterized it. As starting material amide **5** do not have any chiral center in it, the β-addition product is become the racemic mixture. Therefore in the reverse phase HPLC we observed only one peak for racemic mixture is shown in Figure 15. The crystal structure of product **5A** shows two enantiomers in its assymetric unit (Figure 16).

4.3.1.3. <u>Reaction Under Inert Atmosphere</u>: Only β addition products were observed in the reaction.

To comprehend the role of O_2 in the reaction, we conducted the reaction under inert conditions. The α,β-unsaturated amide **3''** was subjected to a conjugate addition reaction with thioacetic acid in the presence of a base, but under an inert Argon atmosphere. The reaction was stirred



Scheme 9: Conjugate addition of thioacetic acid on amide **3''** under an inert atmosphere. The reaction gave only β-addition products.

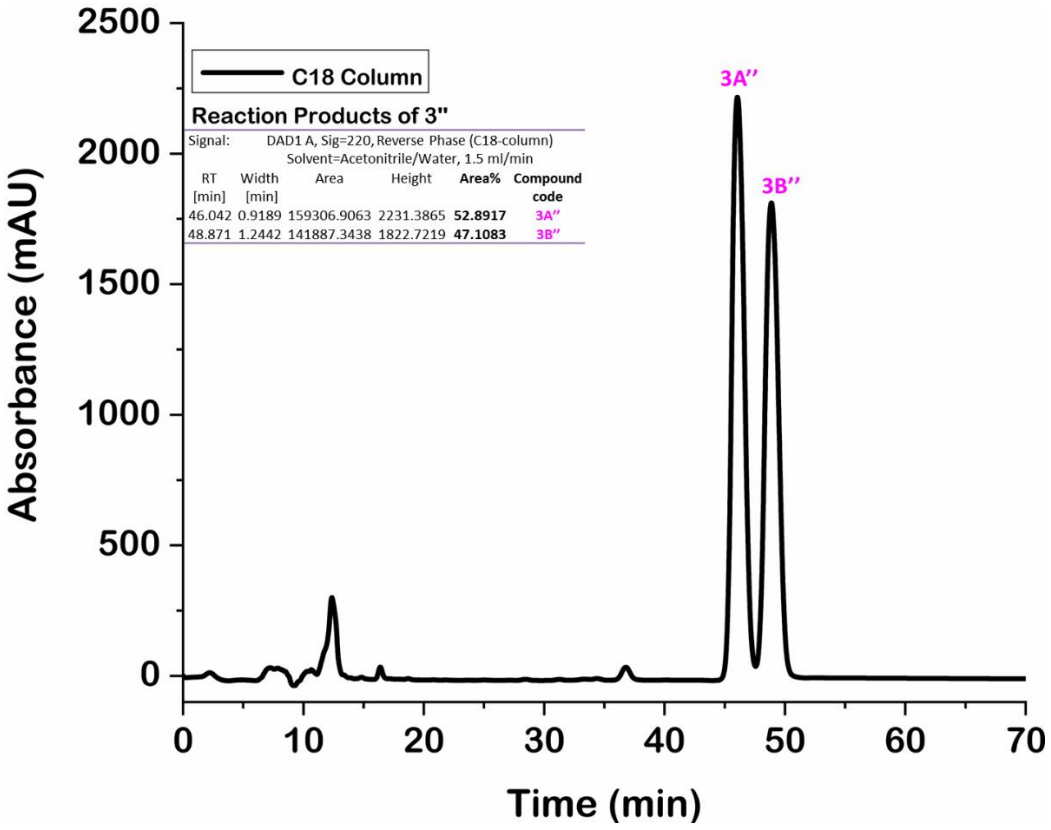
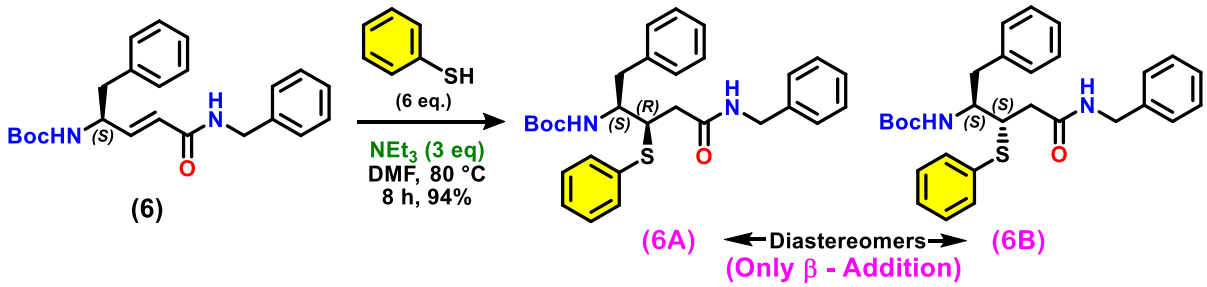


Figure 17: RP-HPLC profile depicting two diastereoisomers obtained in the conjugated addition reaction of amide **3''** with thioacetic acid under an inert argon atmosphere. Only β-addition products were isolated.

for approximately 12 hours at 80 °C. Upon completion and workup, we observed only β-addition products in the reaction, with no α-addition products detected. Scheme 9 illustrates a schematic representation of this reaction. RP-HPLC profile of the reaction mixture after work-up is shown in Figure 17.

4.3.2. Outcome of the Reaction between Thiophenol and BocNH-(*E*)-α,β-Unsaturated γ-Phenylalanine Benzyl Amides (6).

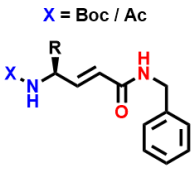
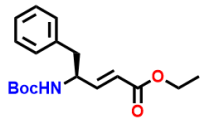
Inspired by the occurrence of both α- and β-addition products during the thioacid addition reaction, we sought to investigate whether the nucleophilic addition of other thiols could yield both α- and β-addition products. Under identical conditions, N-Boc-protected amide **6** subjected to a conjugated addition reaction with thiophenol. In contrast to the observation of both α- and β-addition products in thioacid conjugate addition reactions, we observed only β-addition products in the thiophenol conjugate addition reaction. This reaction confirmed that α-addition products are possible in the case of thioacid addition reactions. Scheme 10 illustrates a schematic representation of this reaction. Both diastereoisomers of the β-addition products were isolated and characterized.



Scheme 10: Conjugate addition of thiophenol on amide **6**. The reaction gave only β-addition products.

4.3.3. A concise overview of thioacid and thiol conjugate addition reactions conducted under diverse conditions with various substrates and plausible mechanisms inferred from the experiments.

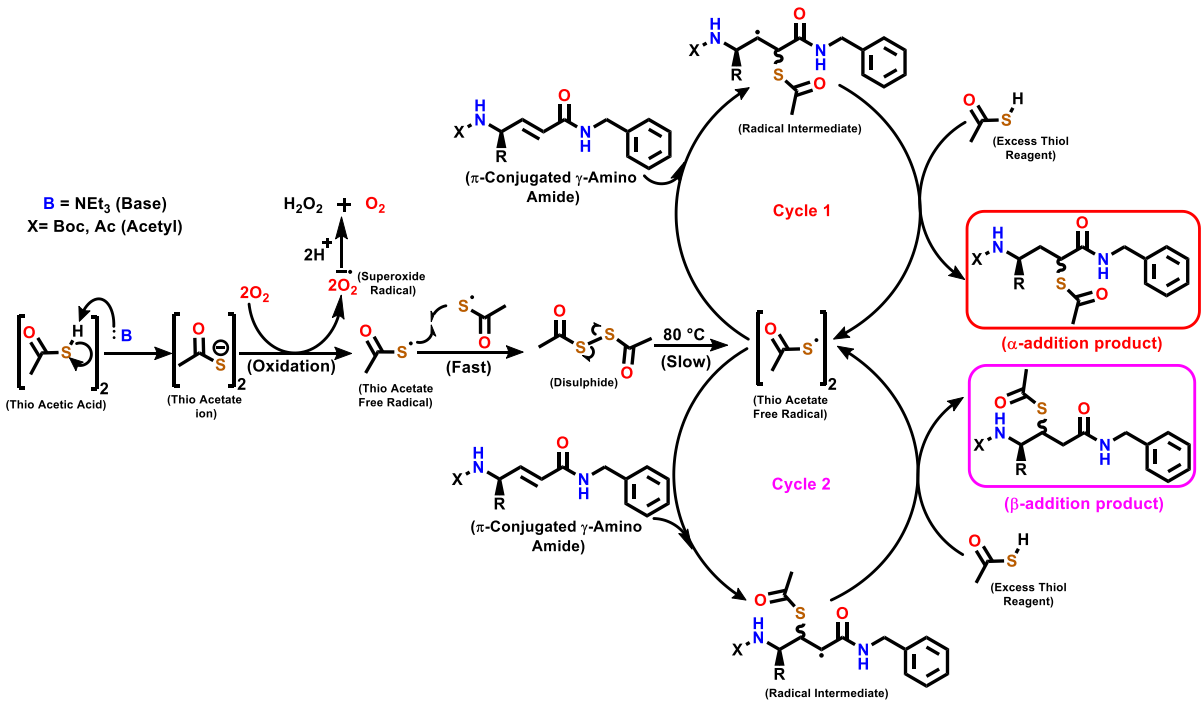
Table 1: Concise overview of thioacid and thiol conjugate addition reactions.

Substrate	Reaction	Thiol Reagent	Base	Reaction Condition	Product	No. of Examples
	(I)		**Et_3N**	**Open atm.** 80 °C	α- and β-Addition	4
	(II)		**In absence of Base**	Open atm. 80 °C	Only β - Addition	2
	(III)		Et_3N	**Inert (Argon) atm.** 80 °C	Only β - Addition	1
	(IV)		Et_3N	Open atm. 80 °C	Only β - Addition	1
	(V)		Et_3N	Open atm. Room Temp.	Only β - Addition	1

Upon an overall analysis of these reactions, two critical factors emerged as crucial for thioacetic α-addition. Firstly, the relatively lower reactivity of (*E*)-α,β-unsaturated γ-amides compared to their corresponding esters and aldehydes was evident. Secondly, the requirement of base and O_2 proved to be essential. Notably, no α-addition product was observed in (*E*)-α,β-unsaturated esters.

Based on the results gathered from various reaction conditions shown in Table 1, we propose a mechanism for the α-addition reaction of thioacetic acid. Scheme 11 illustrates a schematic representation of the proposed mechanism for the α-addition product.

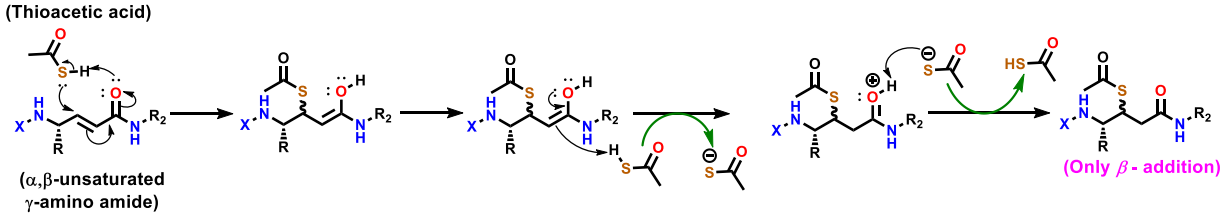
I) Mechanism for Reaction (I): <u>Reaction in the presence of a base and open atmoshere</u> (Both α and β addition products observed)



Scheme 11: Mechanism of the α-addition reaction of thioacetic acid on α,β-unsaturated γ-amides.

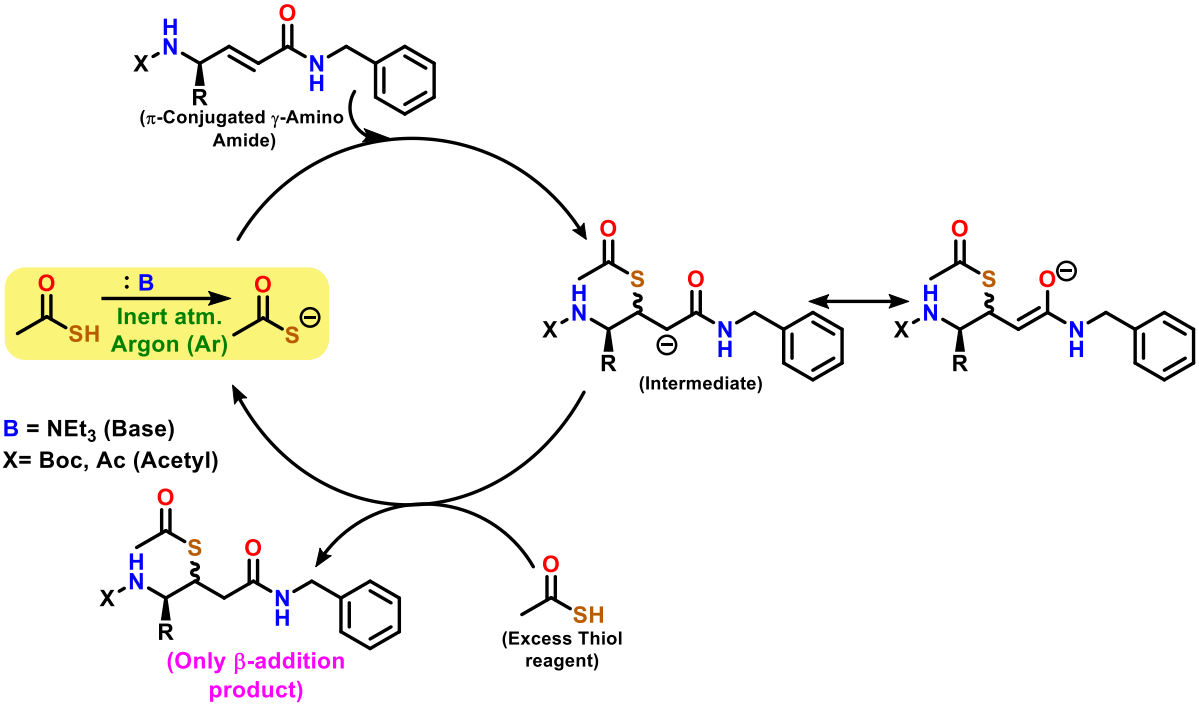
The oxidative dimerization of thioacetic acid in the presence of oxygen results in the formation of the corresponding anhydride, which subsequently breaks down into thioacid radicals. These thioacid radicals participate in addition reactions with relatively unreactive *E*-α,β-unsaturated γ-acid amides. The reactive thioacetic acid radicals exhibit equal reactivity at both the α- and β-positions, resulting in the formation of both α- and β-addition products.

II) Mechanism for Reaction (II): <u>Reaction in the absence of a base</u> (Only β addition products observed)



Scheme 12: Mechanism of the reaction in the absence of base.

III) Mechanism for Reaction (III): <u>Reaction in the Presence of a base and Inert atmosphere (Argon)</u> (Only β addition products observed)



Scheme 13: Mechanism of the reaction in the presence of base under inert argon atmoshere.

4.3.4. Outcome of the thioacetic acid and thiol (thiophenol / ethanethiol) addition reactions on peptide backbone containing (*E*)-α,β-unsaturated γ-amino acids.

Inspired by the α-addition of thioacetic acid in (*E*)-α,β-unsaturated γ-amino acid amides, we aimed to explore the same reaction in peptides containing (*E*)-α,β-unsaturated γ-amino acids. This investigation aimed to comprehend the reactivity of (*E*)-α,β-unsaturated amides within peptides. To this end, peptide **P1** was synthesized, purified, and thoroughly characterized. Peptide **P1** yielded single crystals upon the slow evaporation of its methanol solution. Crystal structure analysis revealed that the peptide adopted a two-helix motif, consistent with previous reports.[18-22]

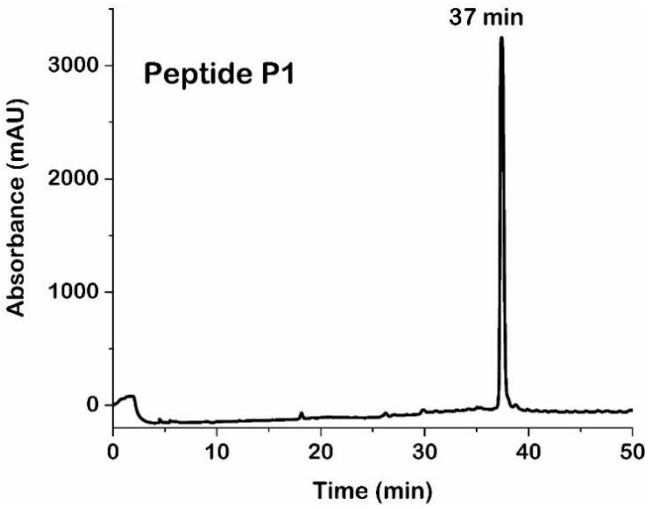


Figure 18: The RP-HPLC profile of starting peptide **P1**.

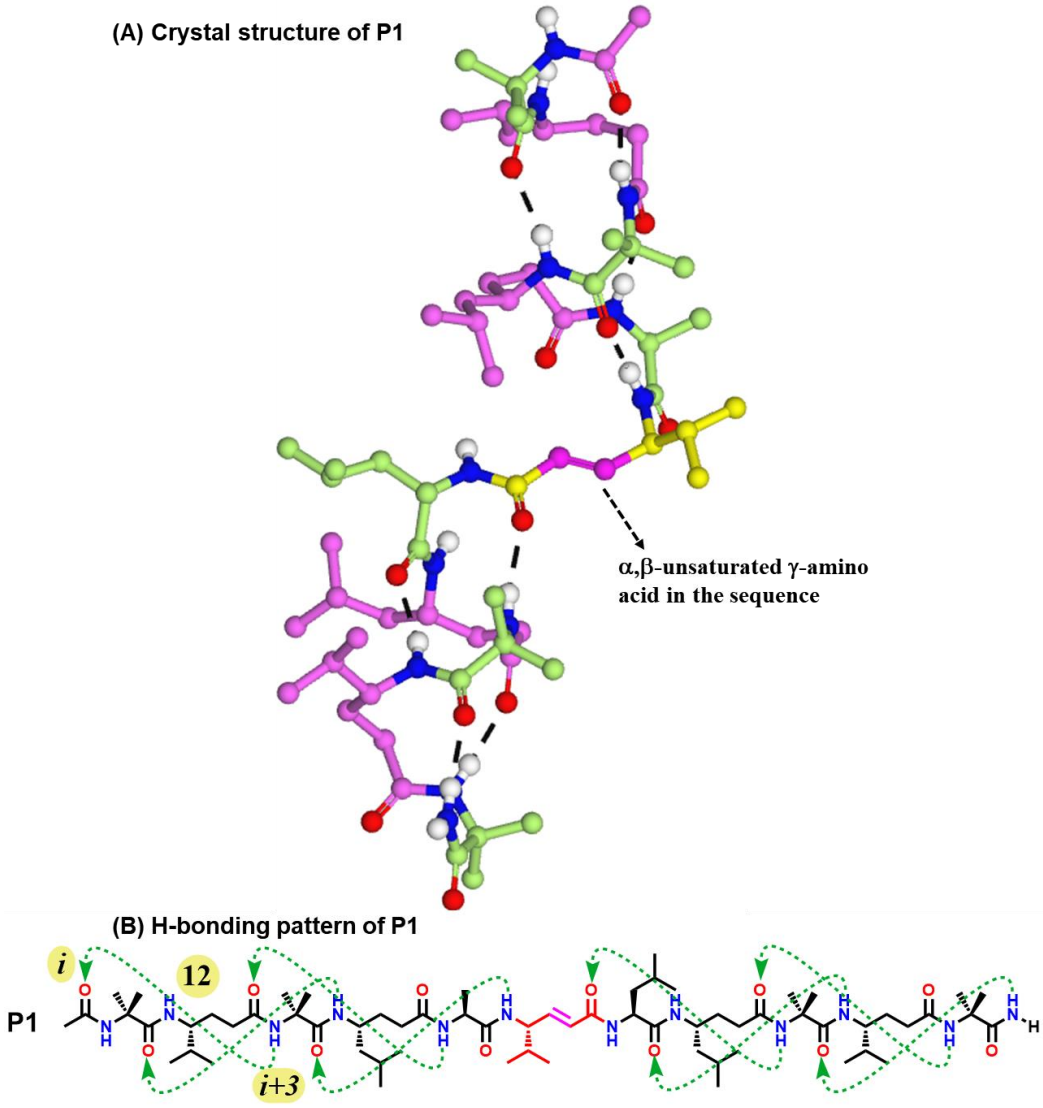


Figure 19: Crystal structures of peptide **P1**.

Table 2: Torsional Angle table of **P1**.

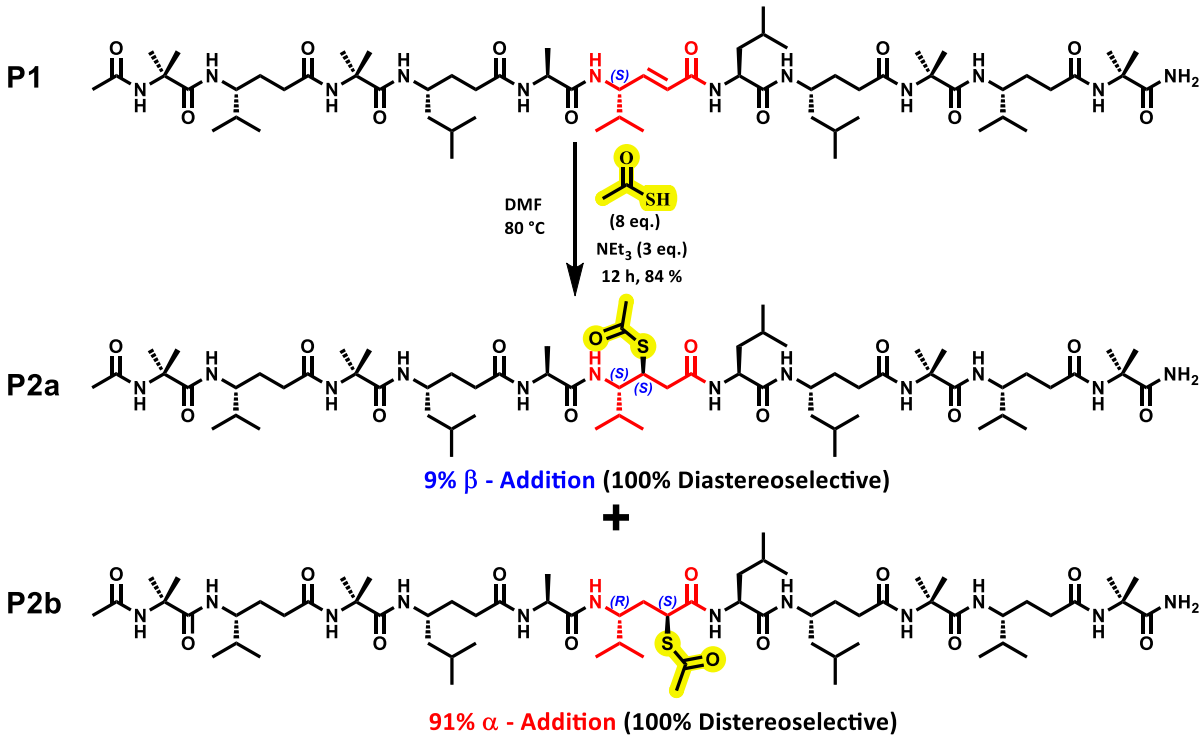
Peptide P1	ϕ	θ_1	θ_2	Ψ	ω
Aib (1)	-59	-	-	-39	-175
γVal (2)	-124	48	65	-118	-175
Aib (3)	-58	-	-	-45	-173
γLeu (4)	-119	49	62	-129	-164
Ala (5)	-69	-	-	-30	-170
dγVal (6)	**-110**	**6**	**-177**	**179**	**-172**
Leu (7)	-71	-	-	-30	-179
γLeu (8)	-126	49	60	-114	-174
Aib (9)	-55	-	-	-41	-172
γVal (10)	-128	53	61	-120	-172
Aib (11)	-57	-	-	-42	-

Table 3: H-bonding Parameters of Peptide **P1**

Intra-molecular H-bonds of peptide **P1**				
D-H.....A	**d(D-H)**	**d(H.....A) (Å)**	**d(D.....A) (Å)**	**<(N-H.....O) (°)**
N(3)-H(3).....O(1)	0.88	2.05	2.911	164.8
N(4)-H(4).....O(2)	0.88	2.04	2.902	166.6
N(5)-H(5).....O(3)	0.88	1.93	2.807	175.2
N(6)-H(6).....O(4)	0.88	2.03	2.872	159.7
N(9)-H(9).....O(7)	0.88	2.01	2.881	168.4
N(10)-H(10A).....O(8)	0.88	2.05	2.875	156.4
N(11)-H(11).....O(9)	0.88	2.04	2.918	172.3
N(12)-H(12D).....O(10)	0.88	1.99	2.850	165.7
Intermolecular H-bonds of peptide **P1**				
N(1)-H(1).....O(6)#	0.88	2.01	2.875	168.6
N(2)-H(2).....O(12)*	0.88	2.07	2.870	150.6
N(12)-H(12C).....O(6)$	0.88	2.12	2.993	170.7
N(7)-H(7).....O(14) (MeOH solvent)	0.88	2.07	2.941	172.8
(MeOH solvent)O(14)-H(14).....O(5)	0.84	1.87	2.671	157.8
Symmetry operations used to generate equivalent atoms: # x+1,y,z * x+1,y,z-1 $ x,y,z+1				

Both N- and C-terminal peptides adopted 12-helix structures, stabilized by four intramolecular H-bonds each. The γ-amino acids elegantly fit into the 12-helix by adopting a gauche+, gauche+ conformation along the backbone, as indicated by the torsion angles tabulated in Table 2. The parameters for the H-bonds are detailed in Table 3. Notably, the unsaturated amino acid acts as a linker, connecting the two helices, as illustrated in Figure 19 representing the crystal structure.

Following structural analysis, the peptide underwent a conjugate addition reaction with thioacetic acid in the presence of a base and DMF solvent. The reaction, heated to 80 °C and stirred for approximately 12 hours, yielded two distinct products, **P2a** and **P2b**, as depicted in Scheme 14. After standard acid and base workup procedures, the observation of these two products was evident.



Scheme 14: Conjugate addition reaction of thioacetic acid on peptide **P1** consisting of α,β-unsaturated γ-amino acid. Two products **P2a** and **P2b** were obtained in the reaction.

Following the reaction, the two resulting products were separated using RP-HPLC. The HPLC profile of the crude reaction mixture is depicted in Figure 20. Subsequently, both products, **P2a** and **P2b**, were isolated and subjected to structural analysis. This analysis aimed to confirm the site of thioacetic acid addition and determine the stereochemistry.

Among the two peptides, **P2b** was the major product, while **P2a** was obtained as the minor product with no other products detected in the reaction. To obtain precise structural details of the thioacetic acid-conjugated peptides **P2a** and **P2b**, we subjected them to crystallization under different solvent conditions. Both peptides were crystallized via slow evaporation from their solutions in aqueous methanol.

The single crystal structure of **P2b** is depicted in Figure 21. In contrast to the starting peptide

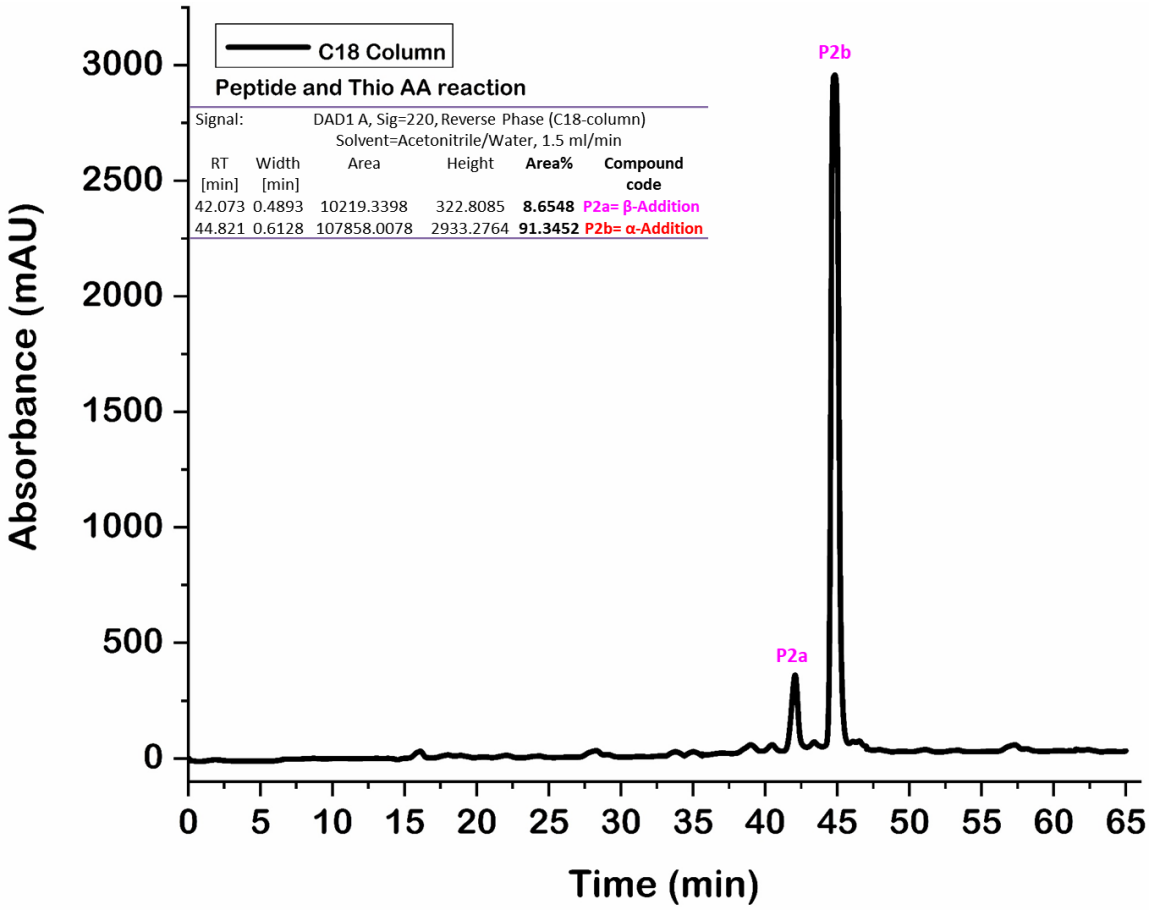


Figure 20: The RP-HPLC profile of crude reaction mixture consisting of **P2a** and **P2b**.

P1, **P2b** adopted a continuous 12-helix conformation in the single crystal after the conjugate addition. Structural analysis revealed that thioacetic acid was added to the α-position of the (*E*)-α,β-unsaturated γ-amino acid. Moreover, this reaction displayed high enantioselectivity, producing only the (*S*)-isomer without obtaining the (*R*)-isomer. This type of stereoselective α-addition in α,β-unsaturated carbonyl systems is exceptionally rare. Typically, α,β-unsaturated amides yield β-substituted products when reacting with nucleophiles due to the strong polarization of the substrate and the nucleophile. To our knowledge, this is the first example demonstrating thioacetic acid addition at the α-position of the α,β-unsaturated carbonyl system. However, in the biosynthesis of phenylalanine from cinnamic acid, phenylalanine ammonium lyase adds ammonia to the α-position.[23] In addition, Wang and team showed radical mediated α-borylation of α,β-unsaturated carbonyl compounds for direct synthesis of α-borylcarbonyl molecules.[24] Recently, Kang and colleagues reported a visible-light-promoted redox-neutral nucleophilic α-addition of nucleophiles to α,β-unsaturated amides.[25]

The 12-helix structure of **P2b** is stabilized by 10 intramolecular H-bonds between residues *i*

and *i*+3. H-bonding pattern is shown in Figure 21. All γ-residues, including the (α,*S*)-thioacetic acid substituted γ-residue, adopted gauche+, gauche+ conformations along the Cγ-Cβ and Cβ-

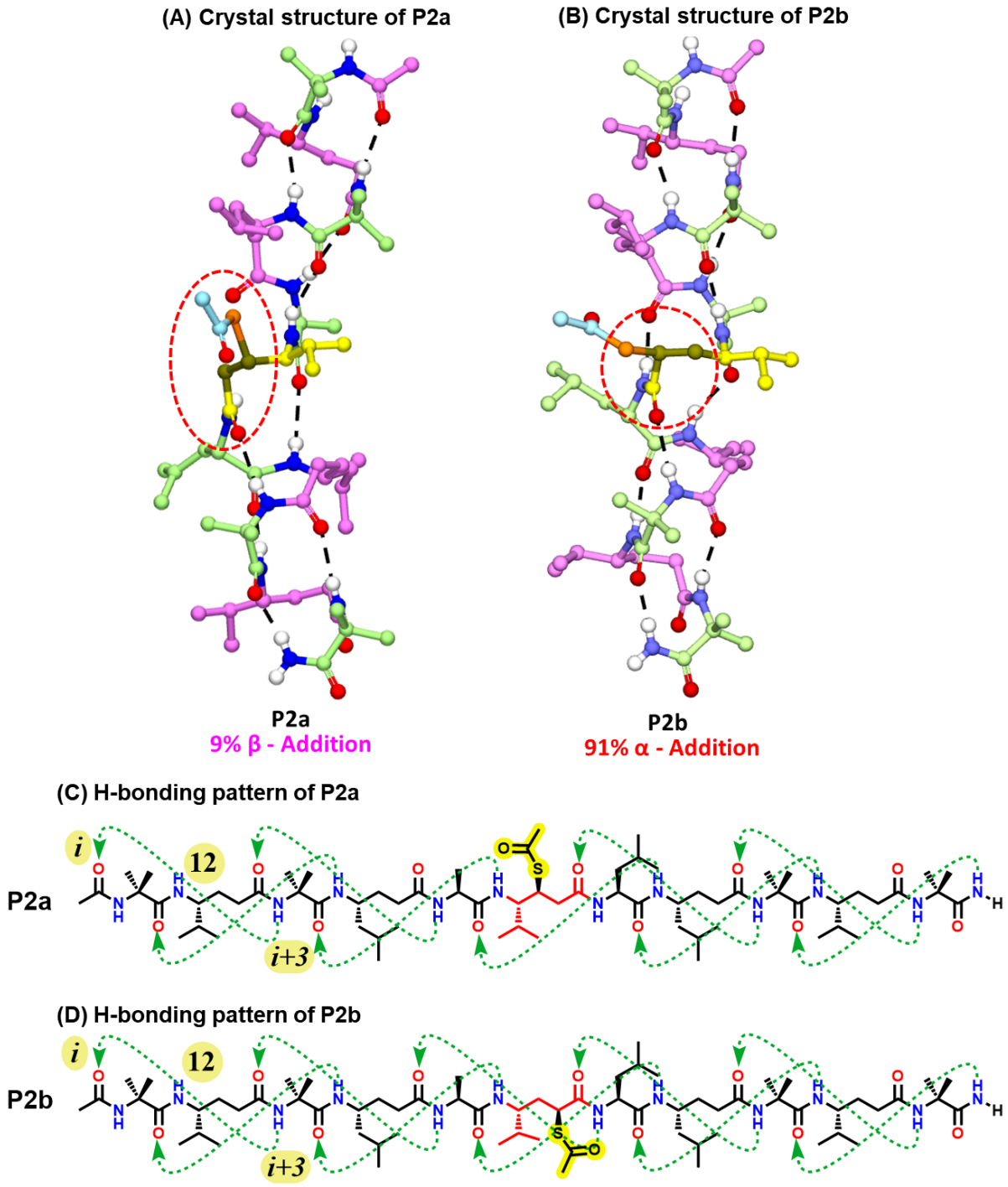


Figure 21: (A) Crystal structures of peptide **P2a.** (B) Crystal structures of peptide **P2b.** (C) Hydrogen bonding pattern of **P2a.** (D) Hydrogen bonding pattern of **P2b.**

Cα. Similar to other γ4-amino acids in the sequence, the α,γ-disubstituted γ-amino acid nicely accommodated within the helix. The accommodation of (α, *S*)-thioacetic acid in the helix is

consistent with the helix favoring γ, α(*S*)-disubstituted γ-amino acids. The H-bond parameters are detailed in Table 7, while the torsion angles of the **P2b** helix are tabulated and presented in Table 6.

The single crystal structure of peptide **P2a**, comprising (β, *S*)-thioacetic acid-substituted γ-amino acid in the middle, is depicted in Figure 21. While the peptide adopts an overall 12-helix structure, a noticeable kink is evident in the middle. This kink arises due to steric repulsion between the thioacetic acid side-chain and the γLeu4 side-chain. This repulsion disrupts the regular 12-membered H-bond between 4LeuCO and Leu7NH, resulting in a lack of H-bond

Table 4: Torsional Angle table of **P2a**.

Peptide P2a	ϕ	θ_1	θ_2	Ψ	ω
Aib (1)	-62	-	-	-35	-172
γVal (2)	-129	51	60	-113	-174
Aib (3)	-60	-	-	-46	-175
γLeu (4)	-116	50	67	-128	-166
Ala (5)	-79	-	-	-5	172
(β, *S*)-thioacetic acid γVal (6)	**-115**	**62**	**84**	**-147**	**-165**
Leu (7)	-85	-	-	-32	173
γLeu (8)	-108	43	60	-123	-167
Aib (9)	-53	-	-	-44	-171
γVal (10)	-130	53	56	-114	-179
Aib (11)	-53	-	-	-49	-

Table 5: H-bonding Parameters of Peptide **P2a**

Intra-molecular H-bonds of peptide **P2a**				
D-H.....A	**d(D-H)**	**d(H.....A) (Å)**	**d(D.....A) (Å)**	**<(N-H.....O) (°)**
N(3)-H(3).....O(1)	0.86	2.18	3.027	167
N(4)-H(4).....O(2)	0.86	2.10	2.924	161
N(5)-H(5).....O(3)	0.86	2.17	3.004	163
N(6)-H(6).....O(4)	0.86	2.14	2.924	152
N(8)-H(8).....O(6)	0.86	2.19	3.022	162
N(9)-H(9).....O(7)	0.86	2.11	2.939	164
N(10)-H(10A).....O(8)	0.86	1.93	2.771	164
N(11)-H(11).....O(9)	0.86	2.16	3.010	169
N(12)-H(12D).....O(10)	0.86	1.98	2.834	172
Intermolecular H-bonds of peptide **P2a**				
N(1)-H(1).....O(11)#	0.86	1.91	2.756	166
Symmetry operations used to generate equivalent atoms: #1.5-x,1-y,-1/2+z				

Table 6: Torsional Angle table of **P2b**.

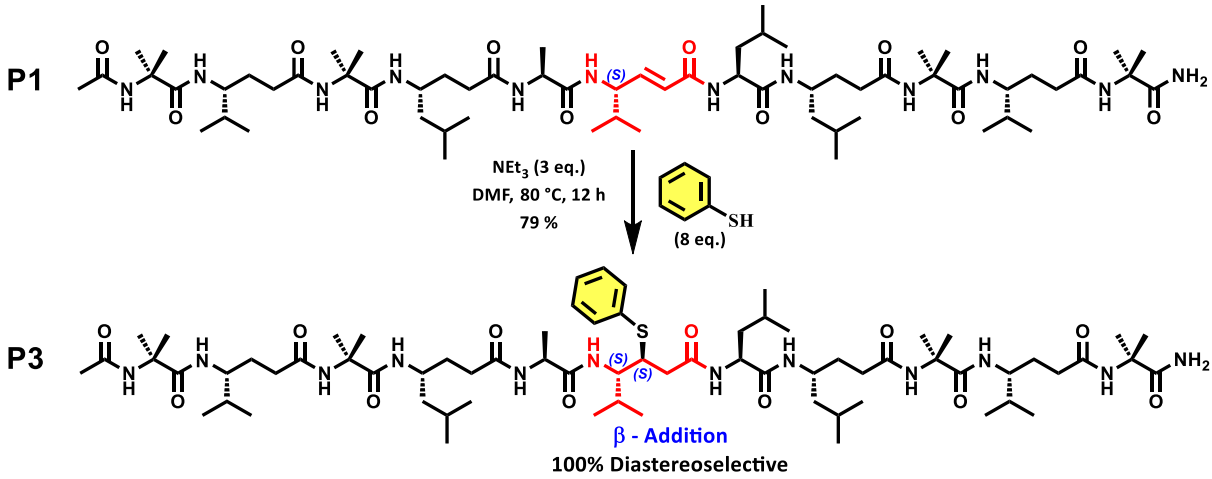
Peptide P2b	ϕ	θ_1	θ_2	Ψ	ω
Aib (1)	-60	-	-	-37	-175
γVal (2)	-122	50	62	-123	-169
Aib (3)	-61	-	-	-36	-171
γLeu (4)	-118	43	64	-125	-165
Ala (5)	-72	-	-	-29	-179
(α, *S*)-thioacetic acid γVal (6)	**-132**	**52**	**57**	**-126**	**-165**
Leu (7)	-79	-	-	-20	178
γLeu (8)	-121	46	61	-128	-163
Aib (9)	-62	-	-	-39	-171
γVal (10)	-135	54	58	-112	-175
Aib (11)	-54	-	-	-46	-

Table 7: H-bonding Parameters of Peptide **P2b**

Intra-molecular H-bonds of peptide **P2b**				
D-H.....A	**d(D-H)**	**d(H.....A) (Å)**	**d(D.....A) (Å)**	**<(N-H.....O) (°)**
N(3)-H(3).....O(1)	0.88	2.05	2.919	169
N(4)-H(4).....O(2)	0.88	1.97	2.804	158
N(5)-H(5).....O(3)	0.88	2.04	2.908	171
N(6)-H(6).....O(4)	0.88	1.98	2.819	160
N(7)-H(7).....O(5)	0.88	2.08	2.958	173
N(8)-H(8).....O(6)	0.88	1.98	2.781	151
N(9)-H(9).....O(7)	0.88	2.10	2.968	167
N(10)-H(10A).....O(8)	0.88	1.96	2.804	160
N(11)-H(11).....O(9)	0.88	2.12	2.982	167
N(12)-H(12D).....O(10)	0.88	2.02	2.880	165
Intermolecular H-bonds of peptide **P2b**				
N(1)-H(1).....O(11)#	0.88	2.03	2.890	166
N(2)-H(2).....O(12)*	0.88	2.18	2.921	142
Symmetry operations used to generate equivalent atoms: #2+x,y,-1+z *2+x,y,-1+z				

interaction and causing the structural kink. In contrast, continuous H-bonding between 4LeuCO and Leu7NH was observed in **P2b**. Additionally, the torsion angles of the (β, *S*)-substituted thioacetic acid γ-amino acid slightly deviate from other γ-amino acids in **P2a**, as well as from the (α, *S*)-thioacetic acid-substituted γ-amino acid in **P2b**. Overall, the (α, *S*) substitution appears to promote a better-formed helix compared to the (β, *S*)-substituted derivatives. H-bonding pattern is shown in Figure 21. Torsion angles and H-bond parameters are shown in Table 4 and Table 5 respectively.

To explore whether all thiol conjugate addition reactions can yield α-addition products, we subjected peptide **P1** to conjugate addition reactions with thiophenol and thioethanol. Scheme 15 illustrates the schematic representation of thiophenol addition. The reactions were conducted under identical conditions as those with thioacetic acid, at 80°C in the presence of a base.



Scheme 15: Conjugate addition reaction of thiophenol on peptide **P1** consisting of α,β-unsaturated γ-amino acid. Only one diastereoselective β-addition product **P3** is obtained in the reaction.

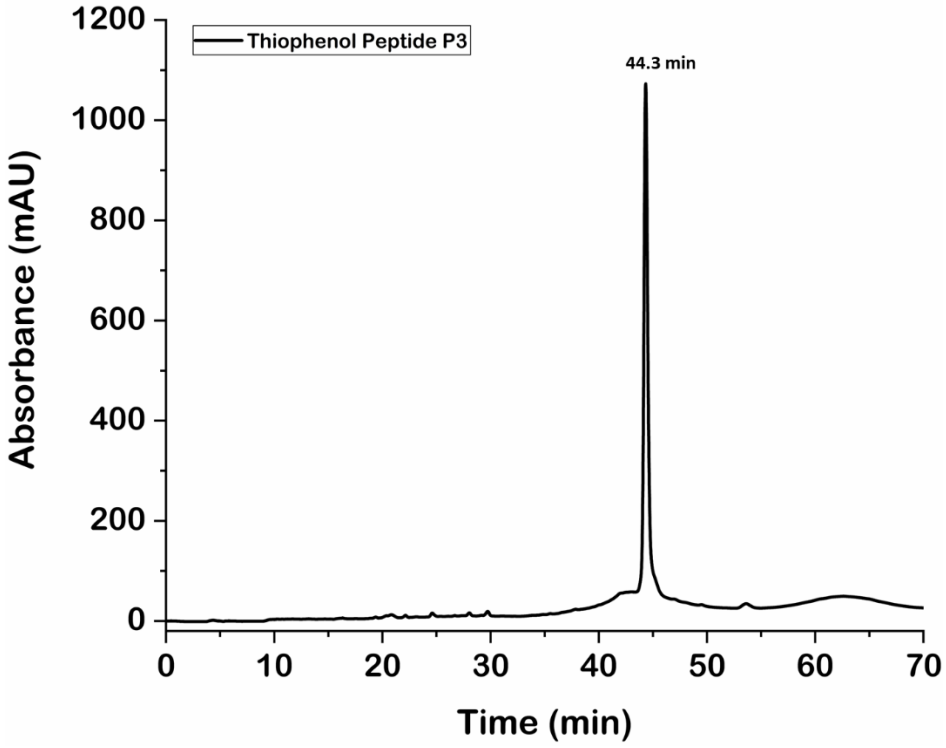


Figure 22: The RP-HPLC profile of crude reaction mixture consisting of **P3**.

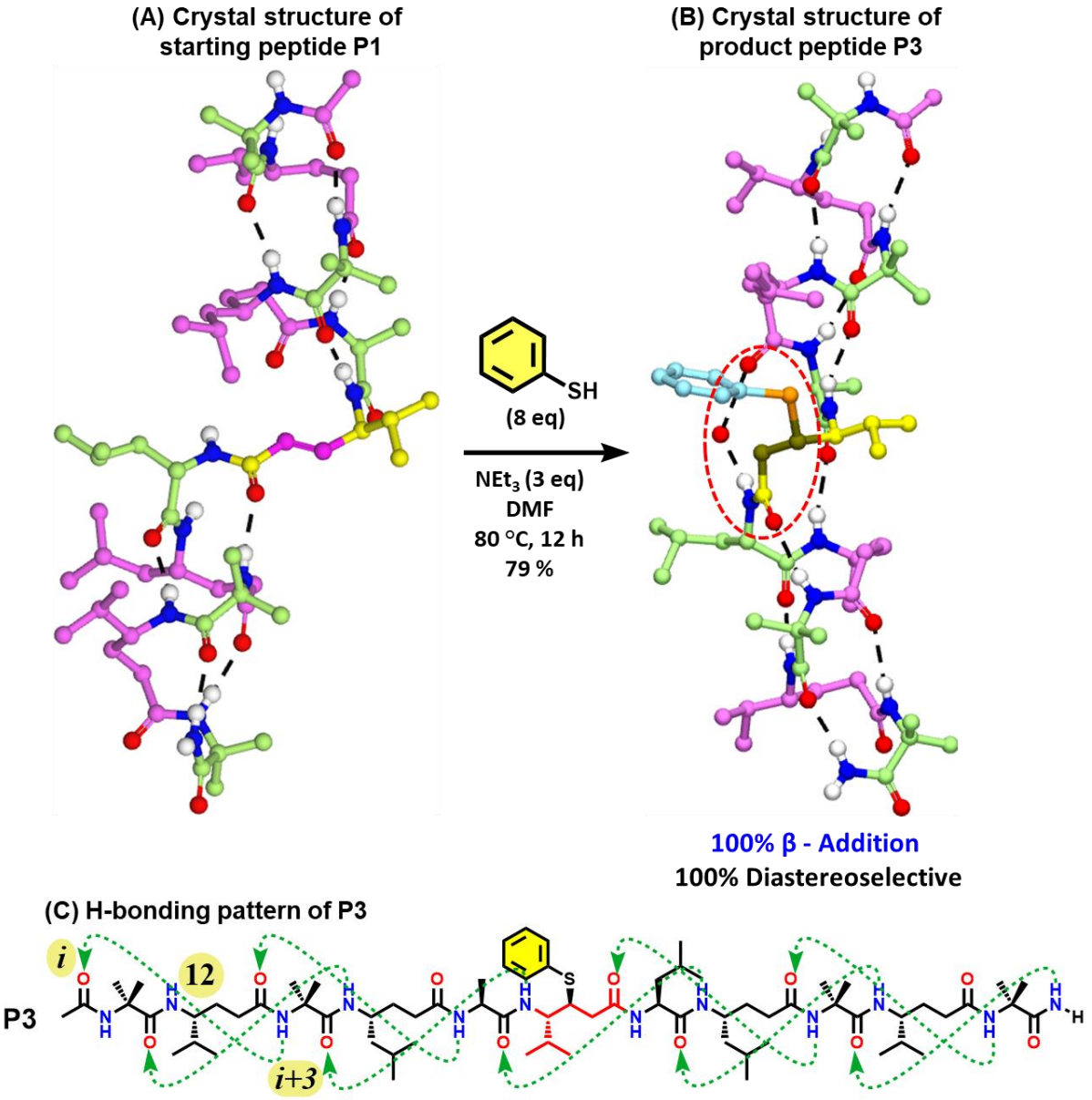


Figure 23: (A) Crystal structures of starting peptide **P1.** (B) Crystal structures of product peptide **P3.** (C) Hydrogen bonding pattern of **P3.**

In a sharp contrast to the thioacetic acid addition, thiophenol addition resulted in the formation of only one product. The RP-HPLC profile of the crude product post work-up is depicted in Figure 22. Notably, the conjugate addition reaction with thiophenol exhibited enantioselectivity.

To comprehend the regioselectivity, stereoselectivity, and achieve unambiguous conformation, we subjected product **P3** to crystallization using various solvent combinations. Peptide **P3** yielded single crystals through slow evaporation from its solution in aqueous methanol. The X-ray diffracted structure of peptide **P3** is depicted in Figure 23. Although the peptide adopted

an overall 12-helix structure, a noticeable kink was observed in the middle. The structure was stabilized by nine canonical *i*← *i*+3 H-bonds.

The examination of the crystal structure revealed the incorporation of thiophenol at the β-position with an (*S*)-configuration. Earlier investigations into conjugated addition reactions involving nitromethane suggested that the predominant product was β-addition anti to the side-chain, while a minor amount of β-addition syn to the side-chain was also observed.

The analysis of the crystal structure unveiled that the thiophenol added at the β-position with

Table 8: Torsional Angle Table of **P3.**

Peptide P3	ϕ	θ_1	θ_2	Ψ	ω
Aib (1)	-61	-	-	-37	-172
γVal (2)	-132	51	62	-112	-176
Aib (3)	-56	-	-	-48	-178
γLeu (4)	-111	59	68	-131	-166
Ala (5)	-76	-	-	-11	179
(β,*S*)-thiophenol γVal (6)	**-105**	**54**	**73**	**-140**	**-174**
Leu (7)	-69	-	-	-21	176
γLeu (8)	-117	49	57	-128	-164
Aib (9)	-57	-	-	-43	-175
γVal (10)	-128	53	63	-116	-179
Aib (11)	-53	-	-	-49	-

Table 9: H-bonding Parameters of Peptide **P3.**

Intra-molecular H-bonds of peptide **P3**				
D-H.....A	**d(D-H)**	**d(H.....A) (Å)**	**d(D.....A) (Å)**	**<(N-H.....O) (°)**
N(3)-H(3).....O(1)	0.86	2.17	3.022	169
N(4)-H(4).....O(2)	0.86	2.10	2.949	168
N(5)-H(5).....O(3)	0.86	2.11	2.944	165
N(6)-H(6).....O(4)	0.86	2.14	2.936	154
N(8)-H(8).....O(6)	0.86	2.13	2.968	165
N(9)-H(9).....O(7)	0.86	2.08	2.927	166
N(10)-H(10A).....O(8)	0.86	2.05	2.866	158
N(11)-H(11).....O(9)	0.86	2.18	3.024	165
N(12)-H(12D).....O(10)	0.86	2.01	2.859	168
Intermolecular H-bonds of peptide **P3**				
N(1)-H(1).....O(11)#	0.86	1.93	2.771	169
Symmetry operations used to generate equivalent atoms: #x,y,-1+z				

an (*S*)-configuration. Previous studies on conjugated addition reactions using nitromethane suggested that the major product was β-addition anti to the side-chain, while a minor amount of β-addition syn to the side-chain was also observed. For instance, in the case of amide **1**, the conjugate addition of thiophenol resulted in an almost equal mixture of (β, *R*) and (β, *S*)-addition products. However, in sharp contrast, **P1** exclusively yielded a (β, S)-addition product with thiophenol. No (β, *R*)-addition product or α-addition products were observed in case of thiophenol.

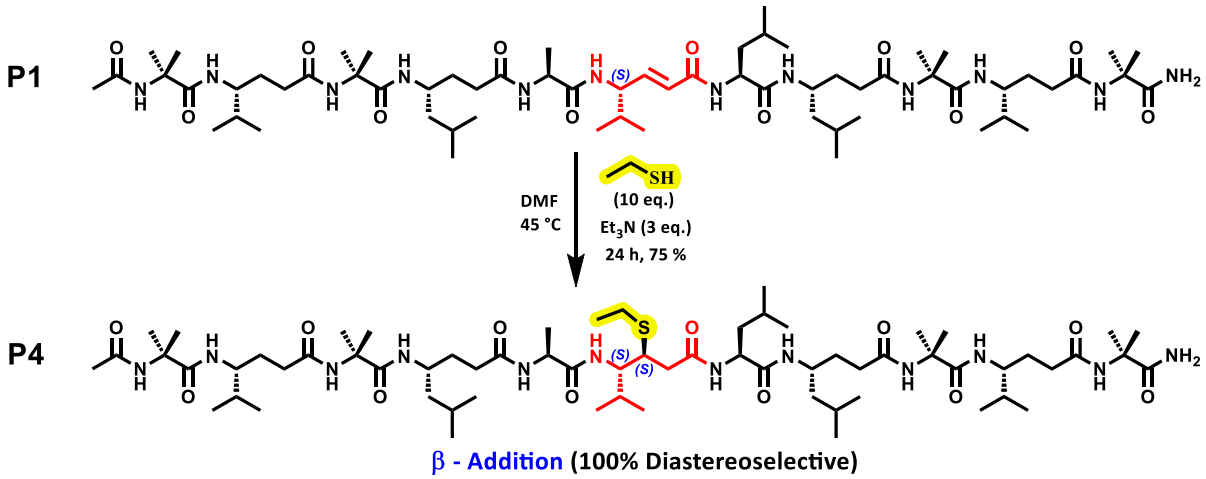
As thiophenol added to the same side of the alkyl side-chain's on carbon-carbon double bond, it induced steric repulsion with the 4-Leu side-chain in the helix. This steric clash caused distortion in the helix, leading to the disruption of the hydrogen bond between residue 4 γLeu CO and NH Leu 7; however, they were connected through H_2O-mediated H-bonds. Apart from the disrupted H-bond, the structure was stabilized by nine canonical H-bonds. Torsion angles for all residues in **P3** are presented in Table 8 and comprehensive hydrogen bond parameters are outlined in Table 9.

Motivated by the diastereoselective conjugate addition of thiophenol, we aimed to investigate the regio- and stereoselectivity of the conjugate addition with ethanethiol. This investigation sought to understand whether alkyl thiol can yield different products compared to thiophenol. To conduct this study, we subjected **P1** to a conjugate addition reaction with ethanethiol in the presence of triethylamine in DMF solvent. The reaction was maintained at 45°C and stirred for approximately 24 hours. Scheme 16 illustrates the schematic representation of the reaction. Following aqueous workup, the reaction mixture underwent RP-HPLC on a C18 column. The RP-HPLC analysis revealed a single product in the reaction (Figure 24).

The product **P4** underwent purification using reverse-phase HPLC, and the pure product was then subjected to crystallization to understand the regio- and stereoselectivity of the thiol conjugate addition. Single crystals of **P4** were obtained through the slow evaporation of the water / methanol solvent system, the crystal structure is shown in Figure 25. Similar to **P3**, peptide **P4** adopted a slightly distorted 12-helix structure.

The crystal structure analysis revealed that the ethanethiol was introduced at the β-position with an *S*-configuration (β, *S*). Similar to the phenyl group in **P3**, the syn addition of ethanethiol led to steric repulsion between the 4γLeu side-chain and the ethyl group. This repulsive interaction resulted in a distortion of the helical structure of **P4** and and contributed to the

discontinuity of the canonical H-bonds in the 12-helix. Similar to other (β, *S*)-conjugate thiol addition products, we observed a lack of H-bonding between 4Leu CO and NH Leu 7; however,



Scheme 16: Conjugate addition of ethanethiol on peptide **P1** consisting of α,β- unsaturated γ-amino acid. Only one diastereoselective β-addition product **P4** is obtained in the reaction.

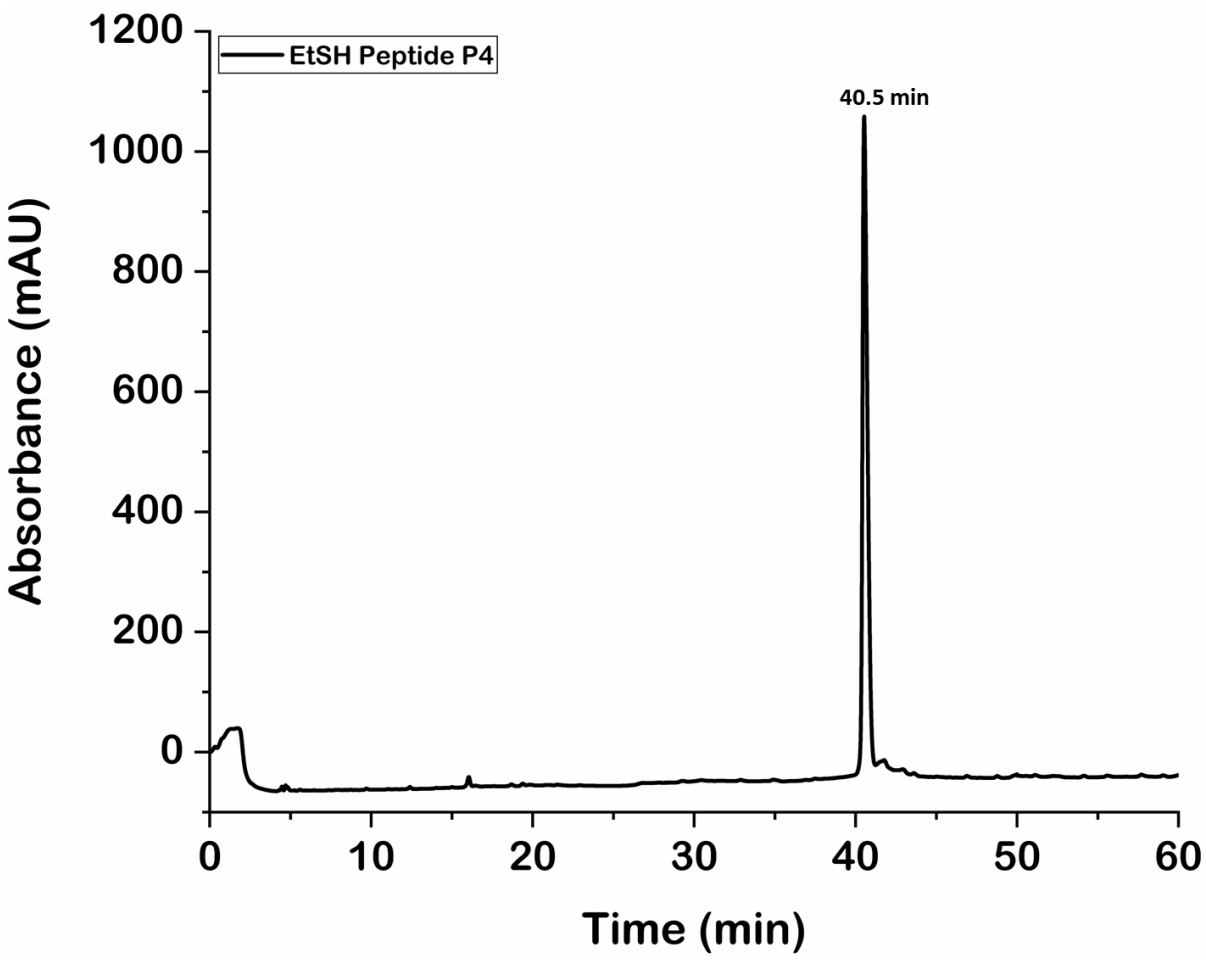


Figure 24: The RP-HPLC profile of crude reaction mixture consisting of **P4**.

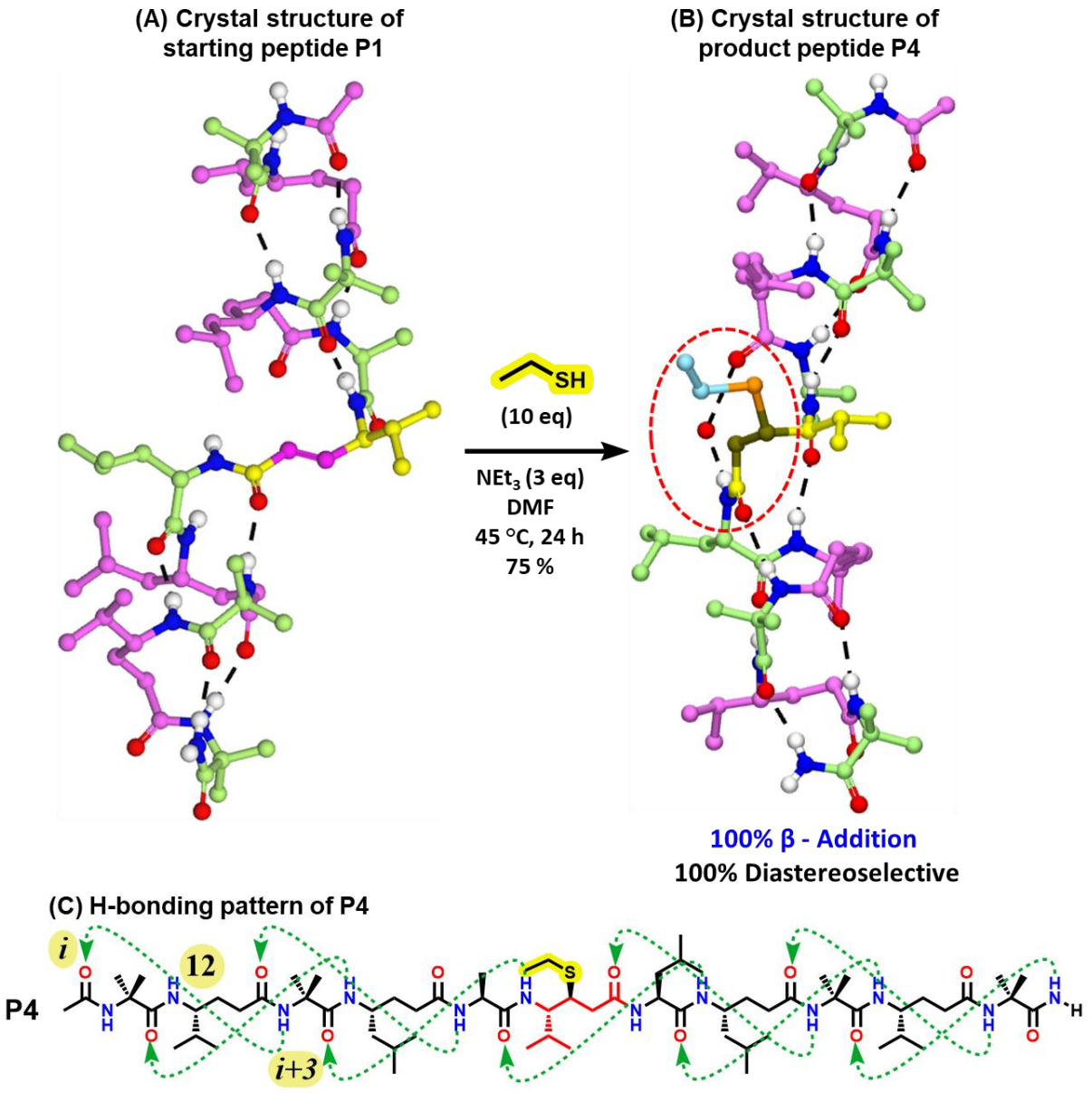


Figure 25: (A) Crystal structures of starting peptide **P1.** (B) Crystal structures of product peptide **P4.** (C) Hydrogen bonding pattern of **P4.**

Table 10: Torsional Angle table of **P4.**

Peptide P4	ϕ	θ_1	θ_2	Ψ	ω
Aib (1)	-64	-	-	-33	-174
γVal (2)	-130	49	63	-115	-173
Aib (3)	-57	-	-	-48	-174
γLeu (4)	-115	50	65	-125	-166
Ala (5)	-77	-	-	-9	174

(β, *S*)-ethanethiol γVal (6)	-100	51	77	-147	-175
Leu (7)	-66	-	-	-24	-179
γLeu (8)	-117	44	63	-125	-166
Aib (9)	-58	-	-	-43	-174
γVal (10)	-129	54	60	-116	-180
Aib (11)	-54	-	-	-49	-

Table 11: H-bonding Parameters of Peptide **P4.**

Intra-molecular H-bonds of peptide **P4**				
D-H.....A	**d(D-H)**	**d(H.....A) (Å)**	**d(D.....A) (Å)**	**<(N-H.....O) (°)**
N(3)-H(3).....O(1)	0.86	2.14	2.986	167
N(4)-H(4).....O(2)	0.86	2.07	2.914	165
N(5)-H(5).....O(3)	0.86	2.13	2.964	164
N(6)-H(6).....O(4)	0.86	2.11	2.893	152
N(8)-H(8).....O(6)	0.86	2.12	2.959	165
N(9)-H(9).....O(7)	0.86	2.10	2.945	167
N(10)-H(10A).....O(8)	0.86	2.04	2.865	161
N(11)-H(11).....O(9)	0.86	2.14	2.990	167
N(12)-H(12D).....O(10)	0.86	1.97	2.818	169
Intermolecular H-bonds of peptide **P4**				
N(1)-H(1).....O(11)#	0.86	1.93	2.77	164
Symmetry operations used to generate equivalent atoms: #1.5-x,1-y,-1/2+z				

they were connected through H_2O-mediated H-bonds. Additionally, the structure was stabilized by nine intramolecular H-bonds between residues *i* and *i*+3. Detailed H-bond parameters and torsion angles are tabulated in Tables 10 and 11, respectively.

Overall, these results reveal that ethanethiol conjugate addition can be performed on peptides composed of (*E*)-α,β-unsaturated γ-amino acids with 100% enantioselectivity and regioselectivity.

4.3.5. Ramachandran type plot of Peptides P2a, P2b, P3 and P4.

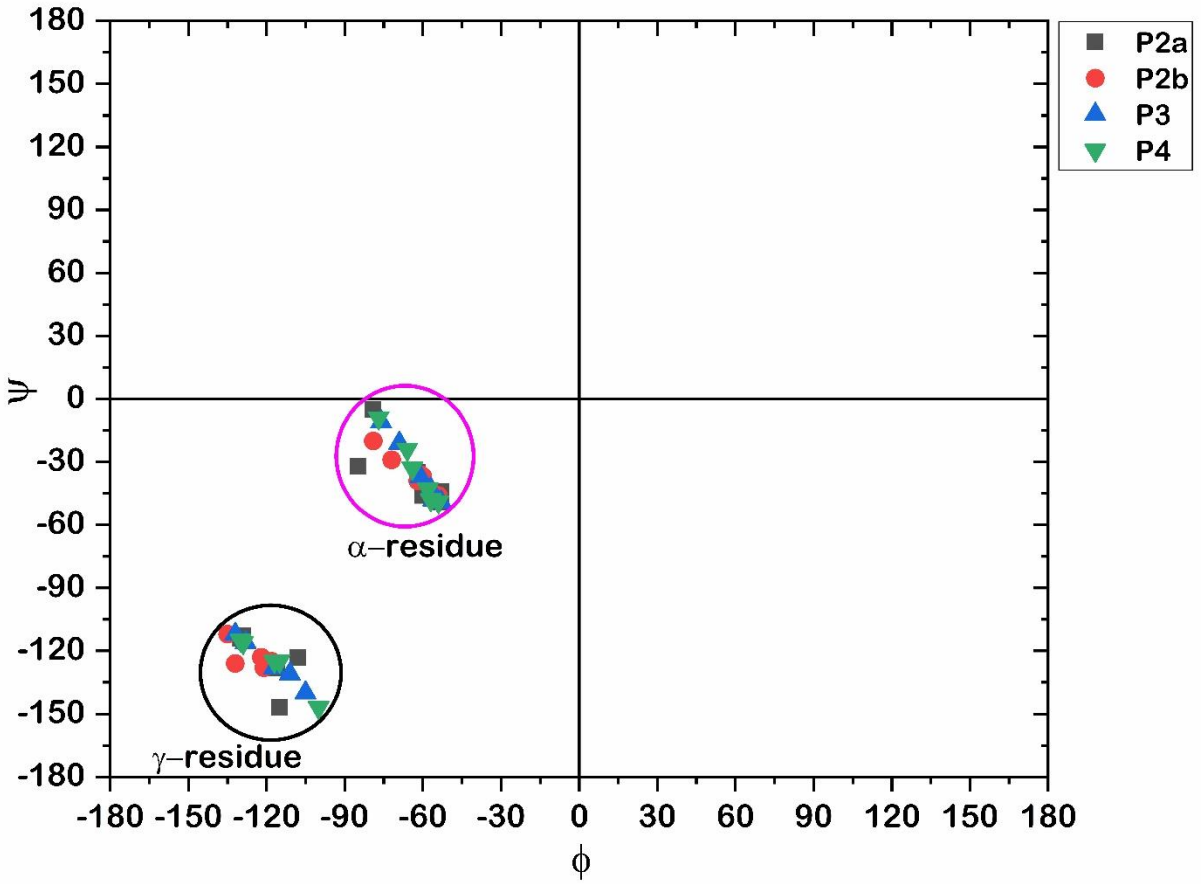


Figure 26: Two-dimensional ϕ and ψ plot of **P2a**, **P2b**, **P3** and **P4**.

4.3.6. CD Spectroscopy of peptides P2a, P2b, P3 and P4.

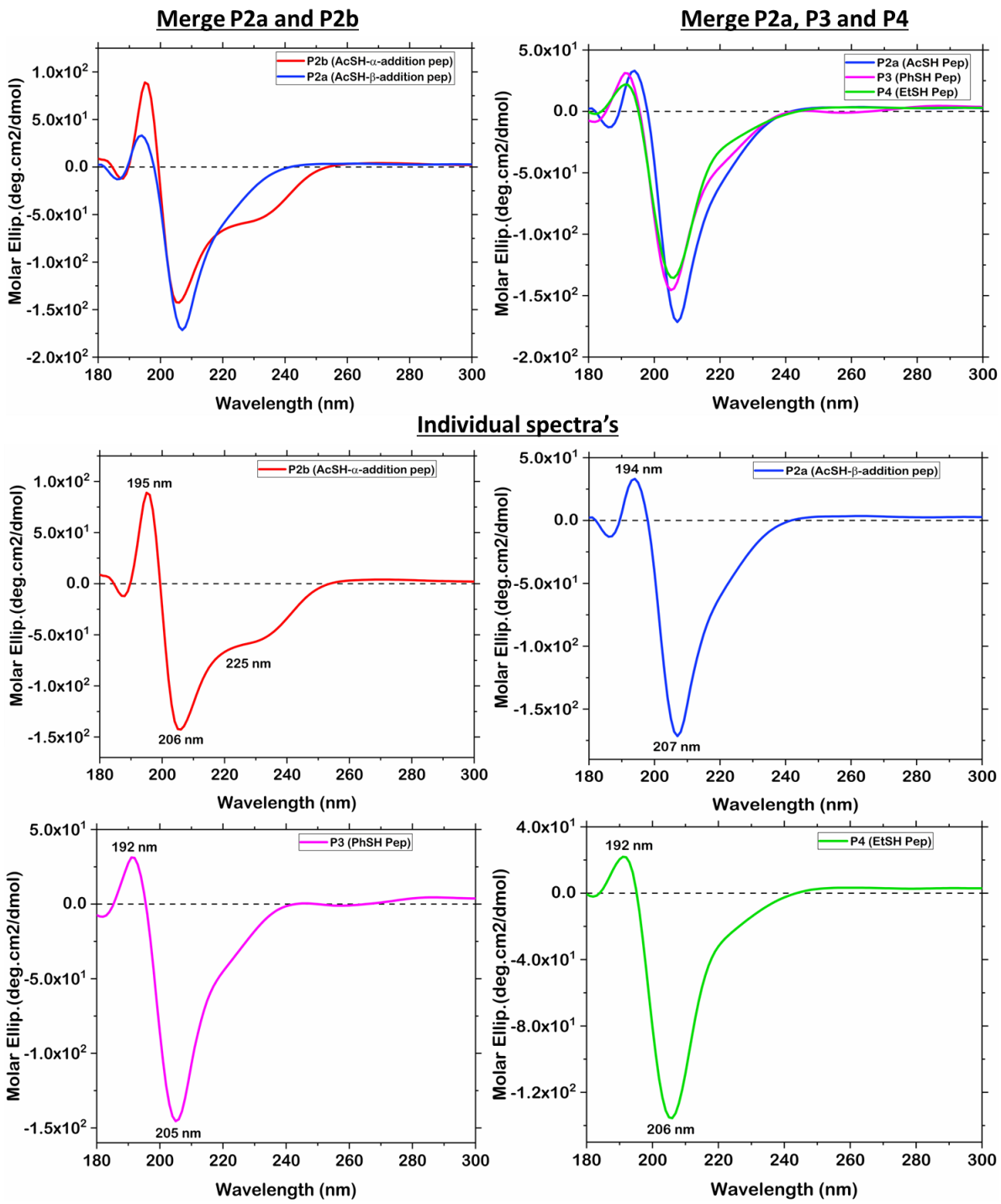


Figure 27: CD Spectra of peptides **P2a, P2b, P3**, and **P4** in methanol (CH_3OH) at a concentration of 1mg/mL.

The circular dichroism analysis revealed that the α-addition peptide **P2b** exhibited similar CD pattern to that of α-helix with CD maxima at 195 nm, significant minima at 206 nm and slight dips at 225 nm. In contrast, the β-addition peptides **P2a**, **P3** and **P4** exhibited CD spectra slightly different from **P2b,** possibly due to interrupted hydrogen bonding interactions within

the helix's midpoint. Additionally, a noticeable bend was observed in the middle of these 12-helical peptide sequences.

4.4. Conclusion

In this chapter, we demonstrated the conjugated addition of thioacetic acid, thiophenol, and ethanethiol onto N-protected *E*-α,β-unsaturated amides and peptides composed of *E*-α,β-unsaturated γ-amino acids. The conjugate addition of thioacetic acid onto α,β-unsaturated esters exclusively yielded β-addition products (β, *R* and β, *S*). In stark contrast, the addition of thiacetic acid to N-protected *E*-α,β-unsaturated γ-amino acid amides resulted in both β-addition products (β, *R* and β, *S*) and unusual α-addition products (α, *R*) and (α, *S*). Interestingly, upon reaction with either alkyl thiol or aryl thiol, (*E*)-α,β-unsaturated γ-amino acid amides exclusively gave β-addition products. Based on the observed results, we proposed that the poor reactivity of unsaturated amides, along with the oxidative dimerization of thioacetic acid and subsequent homolysis of it in the thioacetate free radicals, led to both α- and β-addition products.

The most unusual outcomes were obtained in the case of peptides composed of *E*-α,β-unsaturated γ-amino acids. The conjugate addition of thioacetic acid resulted in a major (α, *S*)-addition product and a minor (β, *S*)-addition product. Interestingly, the peptide with the (α, *S*)-addition product adopted a continuous 12-helix conformation, while the (β, *S*)-addition product displayed a slightly distorted 12-helix. Remarkably, highly diastereoselective (β, *S*)-substituted conjugate addition products were observed with both aromatic and aliphatic thiols. Crystal studies suggested that both structures adopted slightly distorted 12-helices.

Overall, our work highlighted uncommon conjugate addition products to unsaturated amides and peptides.

4.5. Experimental details

4.5.1. Materials, methods, and general experimental details

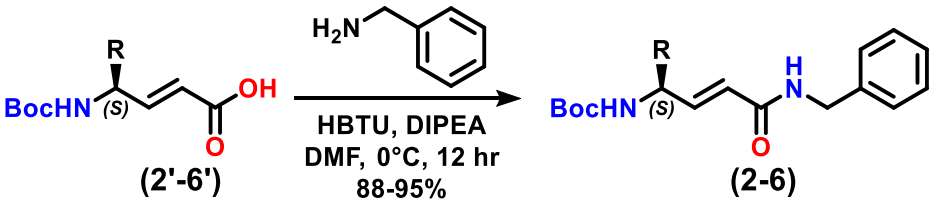
All amino acids, Di-tert-butyl dicarbonate, N,O-Dimethylhydroxylamine hydrochloride, DCC, HOBt, DIPEA, $LiAlH_4$, 2-iodoxybenzoic acid (IBX), PPh_3, Ethyl bromoacetate, HBTU, Benzyl amine, Acetic anhydride, N, N-Diisopropylethylamine(DIPEA), Triethyl amine, Thioacetic acid, Thiophenol, Ethanethiol, DMF, THF, DCM and Ethyl acetate were purchased from the commercial sources. THF was dried over sodium metal and distilled prior to use. DCM was also dried using CaH_2 and distilled under inert atmosphere before use. Pet-ether and

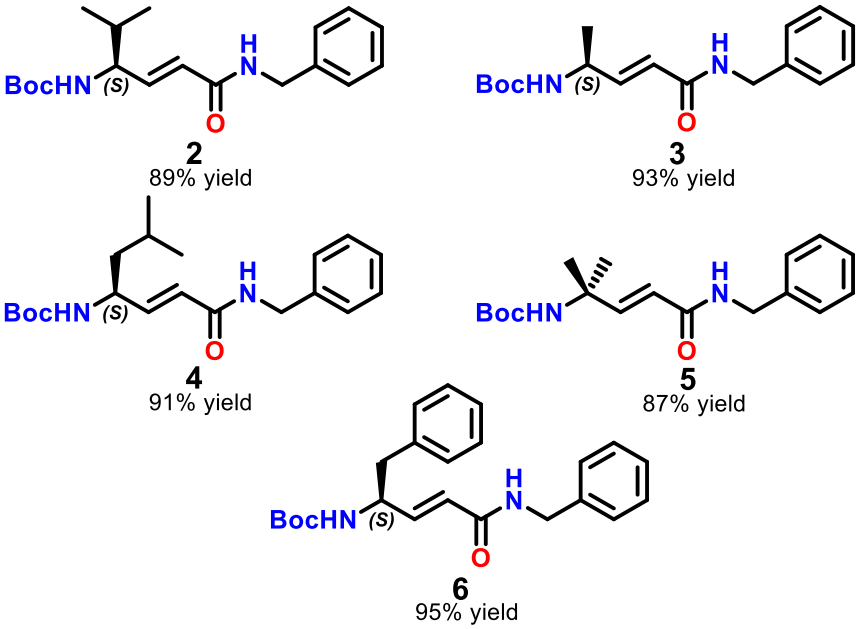
Ethyl acetate was distilled prior to use. Column chromatography was performed on silica gel (230-400 mesh). ^{1}H NMR and ^{13}C NMR spectra were recorded on 400 MHz and 100 MHz respectively using deuterated chloroform ($CDCl_3$) as the internal standard. The chemical shifts (δ) and coupling constants were reported in ppm and Hz respectively. The mass of all pure molecules was confirmed by high-resolution mass spectrometer (ESI-QTOF) and Matrix Assisted LASER Desorption Ionization mass spectrometer (MALDI-TOF/TOF). HPLC analysis was performed on Shimadju HPLC with Diode array detector(DAD). Specific rotations were recorded using chloroform solvent (Rudolph Analytical Research instrument). Single crystal XRD data for peptide structure determination were collected from an X-ray diffractometer using Mo-Kα (λ = 0.71073 Å) graphite monochromated radiation. Boc-(*E*)-α,β-unsaturated γ-amino esters (BocNH-(*E*)dγXaa-COOEt) and Boc-(*E*)-α,β-unsaturated γ-amino acids (BocNH-(*E*)dγXaa-COOH) were synthesized using our previously reported protocol.[15]

4.5.2. General Procedure for the Synthesis of (*E*)-α,β-Unsaturated γ-Amino Amides (1-6)

I) Synthesis of Boc-(*E*)-α,β-Unsaturated γ-Amino Amides (2-6)

The synthesis of boc-(*E*)-α,β-Unsaturated γ-Amino Amides (**2-6**) followed a documented procedure[26], commencing with Boc-(*E*)-α,β-unsaturated γ-amino acids (BocNH-(*E*)dγXaa-COOH).[1] Briefly, to a 5 mL solution of BocNH-(*E*)dγXaa-COOH (5 mmol) in dimethylformamide (DMF), diisopropylethylamine (DIPEA) (5 mmol), and benzylamine (5 mmol) were added. Subsequently, the mixture underwent treatment with HBTU (5 mmol) coupling reagent under ice-cold condition. The progression of the reaction was monitored using thin-layer chromatography (TLC). Upon completion, the reaction mixture was diluted with 200 mL of ethyl acetate (EtOAc) and subjected to washes with 5 % aq. HCl solution (3 × 150 ml), 10% aq. Na_2CO_3 (3 × 150 mL), and brine solution (1 × 150 mL). The organic layer was then



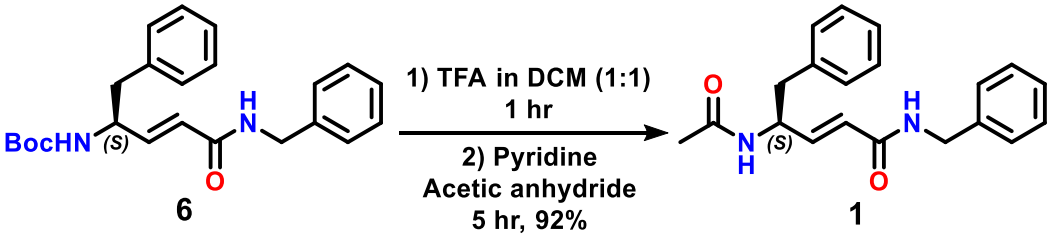


Scheme 17: Synthesis of Boc-(*E*)-α,β-Unsaturated γ-Amino Amides.

dried over anhydrous Na_2SO_4 and concentrated under reduced pressure. Purification of the crude product was achieved through column chromatography, utilizing a petroleum ether/EtOAc (80:20) solvent system to obtain the final pure amides (**2**-**6**).

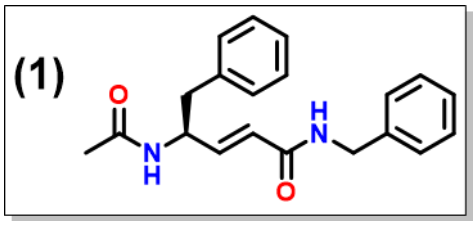
II) Synthesis of Ac-(*E*)-α,β-Unsaturated γ-Amino Amides (1)[26]

Boc-(*E*)-α,β-Unsaturated γ-Phenylalanine Benzyl Amide (**6**) (5 mmol) underwent deprotection using a 1:1 mixture of trifluoroacetic acid (TFA) and dichloromethane (DCM) (8 mL). Upon completion of the reaction, as monitored by TLC over 1 hour, the solvent was evaporated under reduced pressure to yield TFA.H_2N-(*E*)dγPhe-CONHBn. To the TFA salt, pyridine (2mL) and acetic anhydride (10 mmol) were added. The reaction mixture was stirred for approximately 5 hours, and the reaction progress was monitored by TLC. Following the completion of the reaction, the solvent was evaporated under reduced pressure to obtain crude products. The purification of pure compound AcHN-(*E*)dγPhe-CONHBn (**1**) was achieved through column chromatography using a petroleum ether/EtOAc (78:22) solvent system.

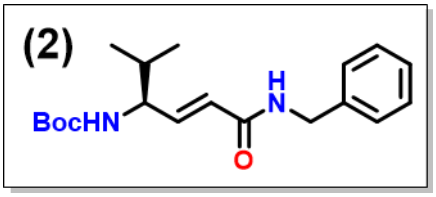


Scheme 18: Synthesis of AcHN-(*E*)dγPhe-CONHBn (**1**).

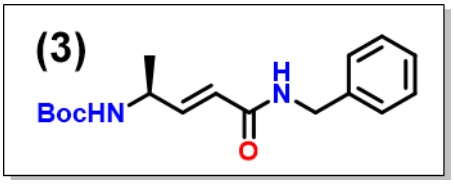
Characterization of (*E*)-α,β-Unsaturated γ-Amino Amides (1-6)



(S,E)-4-acetamido-N-benzyl-5-phenylpent-2-enamide (1): White solid, yield = 1.48 g (92%); mp 152−154°C; **^{1}H NMR** (400 MHz, DMSO-d_6) δ 8.52 (t, *J* = 6.0 Hz, 1H), 8.08 (d, *J* = 8.4 Hz, 1H), 7.32 – 7.20 (m, 10H), 6.63 (dd, *J* = 15.4, 5.5 Hz, 1H), 5.98 (dd, *J* = 15.4, 1.6 Hz, 1H), 4.62 (m, 1H), 4.32 (d, *J* = 5.9 Hz, 2H), 2.85 (dd, *J* = 13.6, 6.2 Hz, 1H), 2.74 (dd, *J* = 13.6, 8.6 Hz, 1H), 1.79 (s, 3H). **^{13}C NMR** (101 MHz, DMSO) δ 168.95, 165.00, 142.96, 139.88, 138.69, 129.60, 128.77, 128.63, 127.79, 127.28, 126.70, 124.01, 51.43, 42.60, 23.05. **HRMS** (ESI-QTOF) m/z calculated value for $C_{20}H_{22}N_2O_2$ is $[M+Na]^+$ 345.1579 and observed 345.1569.

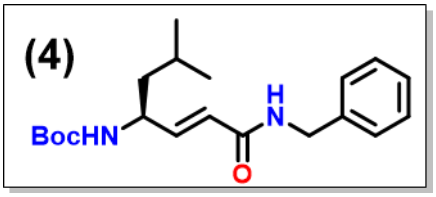


(S,E)-tert-butyl (6-(benzylamino)-2-methyl-6-oxohex-4-en-3-yl)carbamate (2): White solid, yield = 1.47 g (89%); mp 153−155°C; **^{1}H NMR** (400 MHz, Chloroform-*d*) δ 7.35 – 7.25 (m, 5H), 6.75 (dd, *J* = 15.2, 6.3 Hz, 1H), 6.02 (t, *J* = 6 Hz, 1H), 5.90 (dd, *J* = 15.2, 1.6 Hz, 1H), 4.63 (d, *J* = 9.4 Hz, 1H), 4.49 (d, *J* = 5.8 Hz, 2H), 4.11 (m, 1H), 1.84 – 1.80 (m, 1H), 1.43 (s, 9H), 0.92 (d, *J* = 7.2 Hz, 3H), 0.90 (d, *J* = 7.2 Hz, 3H). **^{13}C NMR** (101 MHz, $CDCl_3$) δ 165.24, 155.45, 143.31, 138.10, 128.72, 127.92, 127.55, 123.91, 79.61, 56.92, 43.72, 32.34, 28.39, 18.88, 18.12. **HRMS** (ESI-QTOF) m/z calculated value for $C_{19}H_{28}N_2O_3$ is $[M+H]^+$ 333.2178 and observed 333.2178.

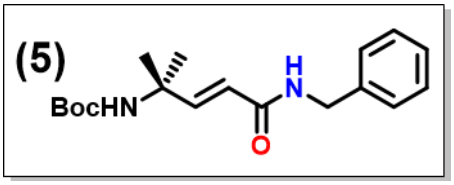


(S,E)-tert-butyl (5-(benzylamino)-5-oxopent-3-en-2-yl)carbamate (3): White solid, yield = 1.41 g (93%); mp 131−133°C; **^{1}H NMR** (400 MHz, Chloroform-*d*) δ 7.33 – 7.25 (m, 5H), 6.74 (dd, *J* = 15.2, 5.5 Hz, 1H), 5.94 (s, 1H), 5.86 (dd, *J* = 15.0, 1.6 Hz, 1H), 4.53 (d, *J* = 21.4 Hz,

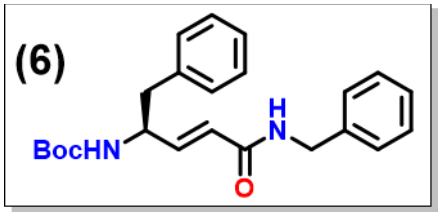
1H), 4.48 (d, *J* = 5.8 Hz, 2H), 4.38 – 4.29 (m, 1H), 1.41 (s, 9H), 1.23 (d, *J* = 6.7 Hz, 3H). **^{13}C NMR** (101 MHz, CHLOROFORM-*D*) δ 165.46, 155.07, 145.52, 138.18, 128.82, 128.01, 127.66, 122.55, 79.78, 47.20, 43.80, 28.47, 20.71. **HRMS** (ESI-QTOF) m/z calculated value for $C_{17}H_{24}N_2O_3$ is $[M+Na]^+$ 327.1685 and observed 327.1690.



(S,E)-tert-butyl (1-(benzylamino)-6-methyl-1-oxohept-2-en-4-yl)carbamate (4): White solid, yield = 1.57 g (91%); mp 142−144°C; **^{1}H NMR** ^{1}H NMR (400 MHz, Chloroform-*d*) δ 7.36 – 7.27 (m, 5H), 6.77 (dd, *J* = 15.2, 6.2 Hz, 1H), 5.89 (dd, *J* = 15.2, 1.6 Hz, 1H), 5.82 (t, *J* = 6 Hz, 1H), 4.56 (d, *J* = 9.5 Hz, 1H), 4.50 (d, *J* = 5.7 Hz, 2H), 4.11 (d, *J* = 8.3 Hz, 1H), 1.83 (qd, *J* = 6.9, 5.6 Hz, 1H), 1.64 (d, *J* = 6 Hz, 2H), 1.43 (s, 9H), 0.93 (d, *J* = 6.9 Hz, 3H), 0.91 (d, *J* = 6.7 Hz, 3H). **^{13}C NMR** (101 MHz, Chloroform-*d*) δ 165.50, 155.26, 144.91, 138.22, 128.79, 128.01, 127.62, 122.98, 79.66, 50.01, 44.08, 43.78, 28.47, 24.73, 22.71, 22.37. **HRMS** (ESI-QTOF) m/z calculated value for $C_{20}H_{30}N_2O_3$ is $[M+Na]^+$ 369.2149 and observed 369.2154.



(E)-tert-butyl (5-(benzylamino)-2-methyl-5-oxopent-3-en-2-yl)carbamate (5): White solid, yield = 1.38 g (87%); mp 152−154°C;**^{1}H NMR** (400 MHz, Chloroform-*d*) δ 7.34 – 7.26 (m, 5H), 6.86 (d, *J* = 15.5 Hz, 1H), 6.03 (s, 1H), 5.83 (d, *J* = 15.6 Hz, 1H), 4.68 (s, 1H), 4.49 (d, *J* = 5.8 Hz, 2H), 1.41 (s, 9H), 1.39 (s, 6H). **^{13}C NMR** (101 MHz, $CDCl_3$) δ 165.77, 154.30, 149.35, 138.21, 128.68, 127.93, 127.49, 120.67, 79.43, 52.80, 43.71, 28.40, 27.35. **HRMS** (ESI-QTOF) m/z calculated value for $C_{18}H_{26}N_2O_3$ is $[M+Na]^+$ 341.1841 and observed 341.1840.



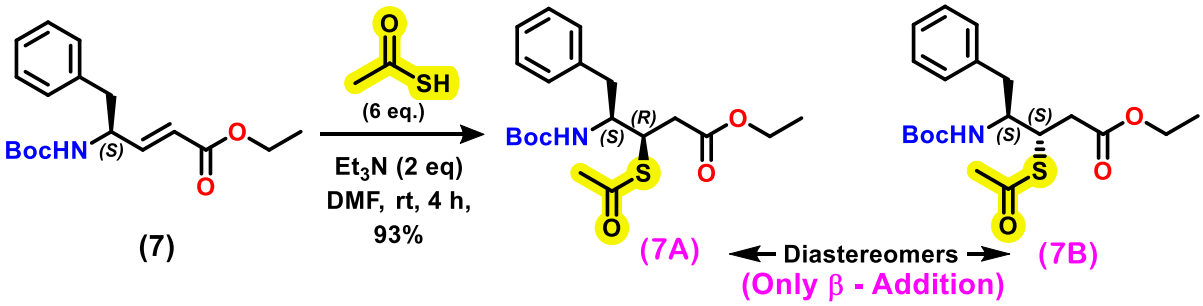
(S,E)-tert-butyl (5-(benzylamino)-5-oxo-1-phenylpent-3-en-2-yl)carbamate (6): White solid, yield = 1.80 g (95%); mp 139−141°C;**^{1}H NMR** (400 MHz, Chloroform-*d*) δ 7.33 – 7.25 (m, 7H (Aromatic)), 7.25 – 7.18 (m, 3H (Aromatic)), 7.16 (d, *J* = 1.7 Hz, 1H), 7.15 (m, 1H), 6.80 (d, *J* = 15.2 Hz, 1H), 5.79 (d, *J* = 15.2 Hz, 1H), 4.55 (s, 1H), 4.46 (d, *J* = 5.7 Hz, 2H), 2.84 (br, 2H), 1.36 (s, 9H). **^{13}C NMR** (101 MHz, CHLOROFORM-*D*) δ 165.16, 155.13, 143.78, 138.11, 136.68, 129.57, 128.82, 128.62, 127.96, 127.68, 126.87, 123.50, 79.90, 49.27, 43.80, 41.16, 28.40. **HRMS** (ESI-QTOF) m/z calculated value for $C_{23}H_{28}N_2O_3$ is $[M+Na]^+$ 381.2178 and observed 381.2182.

4.5.3. General Procedure for Thiol-ene Reaction between <u>Thioacetic acid</u> and (*E*)-α,β-Unsaturated γ-Amino Amides (1-5, 2'' and 3'') / BocNH-(*E*)-α,β-Unsaturated γ-Phenylalanine Ethyl Ester (7).

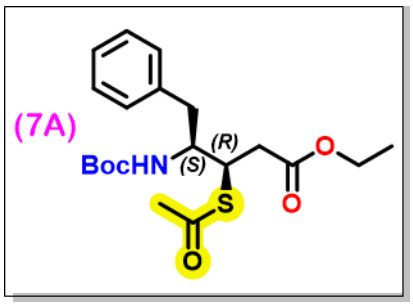
4.5.3.1. <u>Reaction in the presence of a base</u>: Each reaction of (*E*)-α,β-Unsaturated γ-Amino Amides (1-4) gave both α and β addition products (1A-1D, 2A-2D, 3A-3D and 4A-4D), and (*E*)-α,β-Unsaturated γ-Amino Esters (7) gave only β addition products (7A-7B).

General Procedure of reaction 1st to 5th : To a 2 ml solution of (*E*)-α,β-Unsaturated γ-Amino Amides (**1-4**) / (*E*)-α,β-Unsaturated γ-Amino Esters (**7**) (3 mmol) in dimethylformamide (DMF), thioacetic acid (CH_3COSH) (18 mmol) and triethylamine (Et_3N) (6 mmol) were added. Subsequently, the reaction mixture is heated for 80 °C for 12 hours using reflux condenser. (Amides reaction does not works at room temperature, it need heating to react. But esters reaction works at room temperature, it does not required heating to react) The progression of the reaction was monitored by using thin-layer chromatography (TLC) and MALDI TOF/TOF mass analysis. Upon completion, the reaction mixture was diluted with 200 mL of ethyl acetate (EtOAc) and subjected to washes with 5 % aq. HCl solution (3 × 150 ml), 15% aq. Na_2CO_3 (3 × 150 mL), and brine solution (2 × 150 mL). The organic layer was then dried over anhydrous Na_2SO_4 and concentrated under reduced pressure. Purification of the crude product was achieved through reverse phase HPLC on the C-18 column using water/acetonitrile gradient system (95% H_2O: 5% ACN and 5% H_2O: 95% ACN as gradient with 1.5 mL/min flow rate). Both α and β addition products were observed in each reaction, as illustrated below.

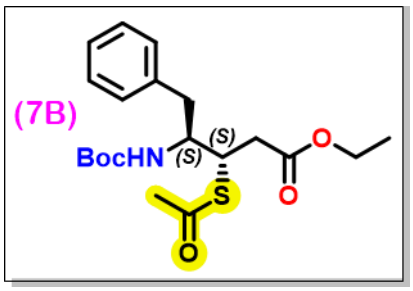
Reaction 1st :



Characterization data of thioacetic acid β- addition products (7A and 7B):



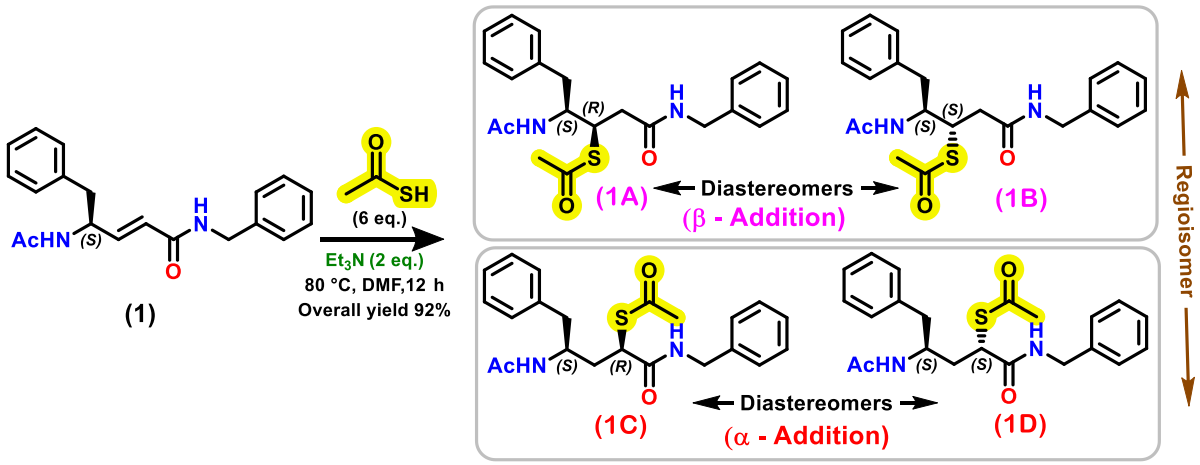
ethyl (3R,4S)-3-(acetylthio)-4-((tert-butoxycarbonyl)amino)-5-phenylpentanoate (7A): White solid, yield = 474 mg (40%); mp 76 − 78 °C; $[\alpha]_D^{25}$ = -7.082 (*c* 0.1, MeOH); **^{1}H NMR** (400 MHz, Chloroform-*d*) δ 7.30 – 7.27 (m, 2H (Aromatic)), 7.24 – 7.15 (m, 3H (Aromatic)), 4.58 (d, *J* = 9.4 Hz, 1H), 4.16 (m, 1H), 4.14 (q, *J* = 7.1 Hz, 2H), 4.07 (q, *J* = 6.7 Hz, 1H), 3.05 (dd, *J* = 14.1, 4.3 Hz, 1H), 2.73 (dd, *J* = 16.3, 6.0 Hz, 1H), 2.64 (dd, *J* = 14.1, 5.0 Hz, 1H), 2.64 (dd, *J* = 16.3, 6.5 Hz, 1H), 2.36 (s, 3H), 1.30 (s, 9H), 1.25 (t, *J* = 7.1 Hz, 3H). **^{13}C NMR** (101 MHz, CHLOROFORM-*D*) δ 194.07, 171.14, 155.19, 137.45, 129.16, 128.45, 126.54, 79.48, 60.91, 54.16, 43.94, 38.59, 37.23, 30.67, 28.20, 14.15. **HRMS** (ESI-QTOF) m/z calculated value for $C_{20}H_{29}NO_5S$ is $[M+Na]^+$ 418.1663 and observed 418.1660.



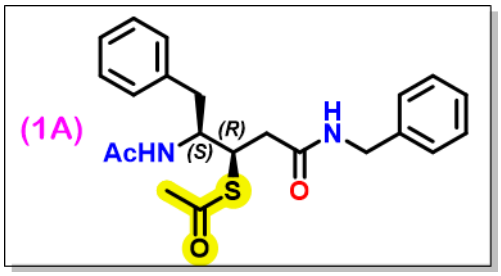
ethyl (3S,4S)-3-(acetylthio)-4-((tert-butoxycarbonyl)amino)-5-phenylpentanoate (7B): White solid, yield = 628 mg (53%); mp 82 − 84 °C; $[\alpha]_D^{25}$ = -10.401 (*c* 0.1, MeOH); **^{1}H NMR** (400 MHz, Chloroform-*d*) δ 7.28 (m, 2H (Aromatic)), 7.22 – 7.16 (m, 3H (Aromatic)), 4.44 (d, *J* = 9.9 Hz, 1H), 4.31 – 4.23 (br, 1H), 4.13 (q, *J* = 7.0 Hz, 2H), 4.13 (q, *J* = 6.6 Hz, 1H), 2.90 (dd, *J* = 14.2, 5.3 Hz, 1H), 2.80 (dd, *J* = 16.6, 6.9 Hz, 1H), 2.65 (dd, *J* = 14.2, 9.4 Hz, 1H), 2.62

(dd, *J* = 16.6, 7.7 Hz, 1H), 2.39 (s, 3H), 1.30 (s, 9H), 1.23 (t, *J* = 7.0 Hz, 3H). **^{13}C NMR** (101 MHz, CHLOROFORM-*D*) δ 193.78, 170.58, 155.44, 137.33, 129.16, 128.40, 126.50, 79.54, 60.78, 54.37, 45.24, 39.99, 38.32, 30.78, 28.18, 14.14. **HRMS** (ESI-QTOF) m/z calculated value for $C_{20}H_{29}NO_5S$ is $[M+Na]^+$ 418.1663 and observed 418.1656.

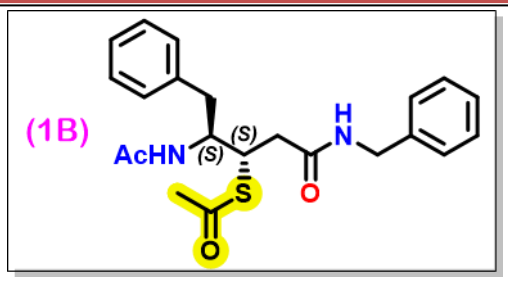
Reaction 2nd:



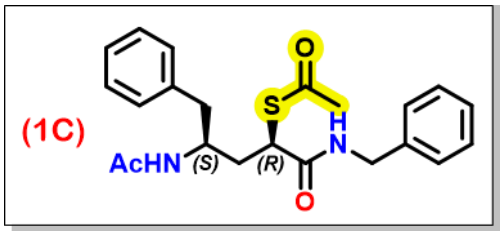
Characterization Data of α- & β- addition products of Thioacetic acid (1A-1D)



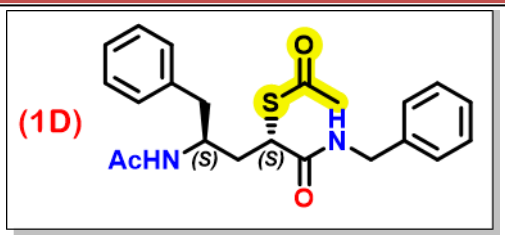
S-((3R,4S)-4-acetamido-1-(benzylamino)-1-oxo-5-phenylpentan-3-yl) ethanethioate (1A): White solid, yield = 240 mg (20%); mp 177−179°C; $[\alpha]_D^{25}$ = -21.604 (*c* 0.1, MeOH); **^{1}H NMR** (400 MHz, $CDCl_3$) δ 7.35 – 7.27 (m, 6H (Aromatic)), 7.25 – 7.15 (m, 4H (Aromatic)), 6.74 (d, *J* = 8.9 Hz, 1H), 6.33 (t, *J* = 5.1 Hz, 1H), 4.49 – 4.44 (m, 1H), 4.43 (d, *J* = 5.7 Hz, 2H), 3.98 (td, *J* = 6.9, 4.9 Hz, 1H), 2.98 (dd, *J* = 14.2, 6.1 Hz, 1H), 2.85 (dd, *J* = 14.2, 8.4 Hz, 1H), 2.71 (dd, *J* = 15.4, 4.9 Hz, 1H), 2.62 (dd, *J* = 15.3, 7.2 Hz, 1H), 2.29 (s, 3H), 1.84 (s, 3H). **^{13}C NMR** (101 MHz, $CDCl_3$) δ 195.07, 170.54, 170.23, 137.87, 137.33, 129.01, 128.74, 128.59, 127.85, 127.61, 126.73, 53.07, 43.83, 43.37, 38.63, 38.55, 30.66, 23.14. **HRMS** (ESI-QTOF) m/z calculated value for $C_{22}H_{26}N_2O_3S$ is $[M+H]^+$ 399.1742 and observed 399.1741.



S-((3S,4S)-4-acetamido-1-(benzylamino)-1-oxo-5-phenylpentan-3-yl) ethanethioate (1B): White solid, yield = 299 mg (25%); mp 171−173°C; $[\alpha]_D^{25}$ = -8.5 (*c* 0.1, MeOH); **^{1}H NMR** (400 MHz, Chloroform-*d*) δ 7.34 – 7.27 (m, 5H (Aromatic)), 7.26 – 7.18 (m, 3H (Aromatic)), 7.11 – 7.04 (m, 2H (Aromatic)), 7.03 (t, *J* = 5 Hz, 1H), 5.60 (d, *J* = 9.1 Hz, 1H), 4.56 – 4.52 (m, 1H), 4.50 (dd, *J* = 14.7, 3.6 Hz, 1H), 4.38 (dd, *J* = 14.7, 5.5 Hz, 1H), 4.11 (ddd, *J* = 9.5, 5.2, 2.5 Hz, 1H), 2.91 (dd, *J* = 14.5, 5.1 Hz, 1H), 2.66 (dd, *J* = 14.5, 9.9 Hz, 1H), 2.66 (dd, *J* = 14.0, 9.8 Hz, 1H), 2.50 (dd, *J* = 14.0, 5.1 Hz, 1H), 2.37 (s, 3H), 1.83 (s, 3H). **^{13}C NMR** (101 MHz, $CDCl_3$) δ 193.93, 170.86, 169.73, 138.42, 136.98, 128.81, 128.68, 128.58, 127.90, 127.39, 126.76, 52.83, 46.51, 43.66, 41.00, 39.32, 30.78, 23.14. **HRMS** (ESI-QTOF) m/z calculated value for $C_{22}H_{26}N_2O_3S$ is $[M+Na]^+$ 421.1562 and observed 421.1548.

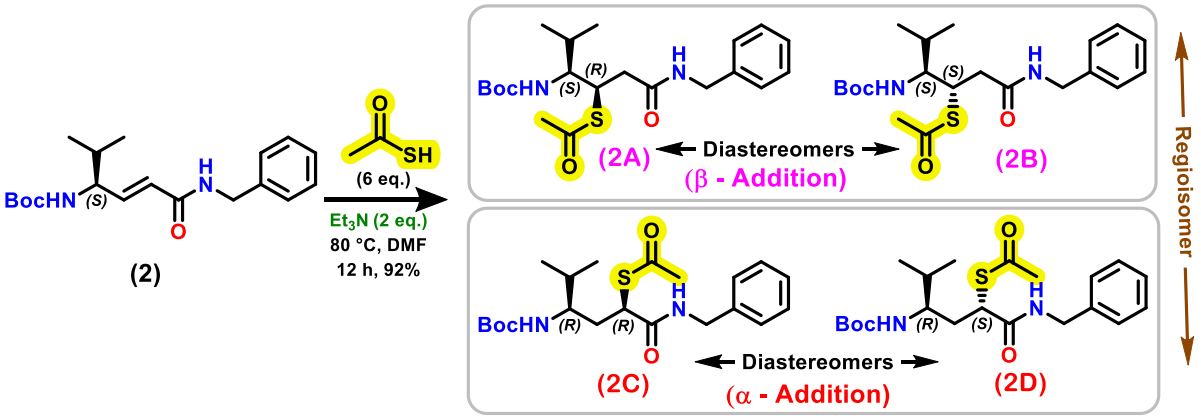


S-((2R,4S)-4-acetamido-1-(benzylamino)-1-oxo-5-phenylpentan-2-yl) ethanethioate (1C): White solid, yield = 284 mg (24%); mp 162−164°C; $[\alpha]_D^{25}$ = +32.315 (*c* 0.1, MeOH);**^{1}H NMR** (400 MHz, Chloroform-*d*) δ 7.33 – 7.27 (m, 4H Aromatic)), 7.26 – 7.14 (m, 6H Aromatic)), 6.70 (t, *J* = 5.9 Hz, 1H), 5.68 (d, *J* = 8.9 Hz, 1H), 4.44 (dd, *J* = 14.9, 6.2 Hz, 1H), 4.33 (m, 1H), 4.3 (dd, *J* = 14.9, 5.5 Hz, 1H), 3.97 (dd, *J* = 8.4, 6.0 Hz, 1H), 2.86 (dd, *J* = 13.6, 5.5 Hz, 1H), 2.71 (dd, *J* = 13.6, 7.4 Hz, 1H), 2.31 (s, 3H), 2.28 – 2.19 (m, 1H), 1.84 – 1.78 (m, 1H), 1.81 (s, 3H). **^{13}C NMR** (101 MHz, $CDCl_3$) δ 195.82, 171.32, 170.00, 137.67, 137.36, 129.46, 128.73, 128.55, 128.52, 127.55, 127.49, 127.23, 126.65, 49.59, 43.93, 43.78, 41.80, 33.81, 30.26, 23.22. **HRMS** (ESI-QTOF) m/z calculated value for $C_{22}H_{26}N_2O_3S$ is $[M+Na]^+$ 421.1562 and observed 421.1559.

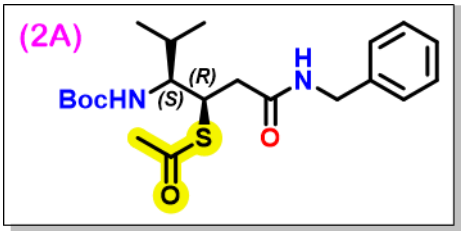


S-((2S,4S)-4-acetamido-1-(benzylamino)-1-oxo-5-phenylpentan-2-yl) ethanethioate (1D): White solid, yield = 275 mg (23%); mp 168−170°C; $[\alpha]_D^{25}$ = -11.136 (*c* 0.1, MeOH); **^{1}H NMR** (400 MHz, Chloroform-*d*) δ 7.62 (t, *J* = 5.7 Hz, 1H), 7.35 – 7.27 (m, 6H Aromatic)), 7.26 – 7.20 (m, 2H Aromatic)), 7.05 (d, *J* = 6.6 Hz, 2H Aromatic)), 5.86 (d, *J* = 9.1 Hz, 1H), 4.49 (dd, *J* = 14.8, 6.1 Hz, 1H), 4.40 (dd, *J* = 14.9, 5.8 Hz, 1H), 4.28 – 4.19 (m, 1H), 4.10 (dd, *J* = 11.0, 2.7 Hz, 1H), 2.76 (d, *J* = 6.6 Hz, 2H), 2.30 (s, 3H), 2.24 (ddd, *J* = 14.0, 11.0, 2.8 Hz, 1H), 1.97 (s, 3H), 1.70 (ddd, *J* = 14.0, 11.3, 2.8 Hz, 1H). **^{13}C NMR** (101 MHz, $CDCl_3$) δ 195.83, 171.55, 170.30, 138.08, 136.80, 129.08, 128.65, 128.63, 127.69, 127.37, 126.81, 48.78, 44.78, 43.84, 41.11, 38.69, 30.39, 23.24. **HRMS** (ESI-QTOF) m/z calculated value for $C_{22}H_{26}N_2O_3S$ is $[M+H]^+$ 399.1742 and observed 399.1746.

Reaction 3rd :

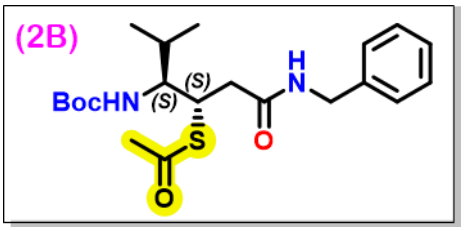


Characterization Data of α- & β- addition products of Thioacetic acid (2A-2D)

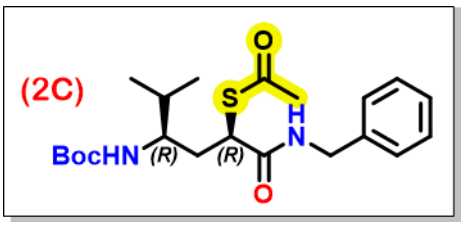


S-((3R,4S)-1-(benzylamino)-4-((tert-butoxycarbonyl)amino)-5-methyl-1-oxohexan-3-yl) ethanethioate (2A): White solid, yield = 232 mg (19%); mp 187−189°C; $[\alpha]_D^{25}$ = +17.005 (*c* 0.1, MeOH); **^{1}H NMR** (400 MHz, Chloroform-*d*) δ 7.34 – 7.27 (m, 4H (Aromatic)), 7.26 (d, *J*

= 3.1 Hz, 1H (Aromatic)), 6.40 (t, *J* = 5.6 Hz, 1H), 5.15 (d, *J* = 10.5 Hz, 1H), 4.46 (dd, *J* = 14.8, 5.9 Hz, 1H), 4.37 (dd, *J* = 14.8, 5.5 Hz, 1H), 4.02 (dt, *J* = 8.2, 6.4 Hz, 1H), 3.65 (ddd, *J* = 10.5, 8.2, 5.6 Hz, 1H), 2.68 (dd, *J* = 15.1, 6.2 Hz, 1H), 2.54 (dd, *J* = 15.1, 6.4 Hz, 1H), 2.25 (s, 3H), 2.04 – 1.98 (m, 1H), 1.42 (s, 9H), 0.93 (d, *J* = 6.7 Hz, 3H), 0.87 (d, *J* = 6.7 Hz, 3H). **^{13}C NMR** (101 MHz, CDCl3) δ 195.22, 170.62, 170.28, 156.38, 138.20, 128.61, 127.84, 127.42, 79.28, 58.15, 43.69, 42.89, 38.62, 30.59, 29.85, 28.39, 20.29, 16.95. **HRMS** (ESI-QTOF) m/z calculated value for $C_{21}H_{32}N_2O_4S$ is $[M+Na]^+$ 431.1980 and observed 431.1974.

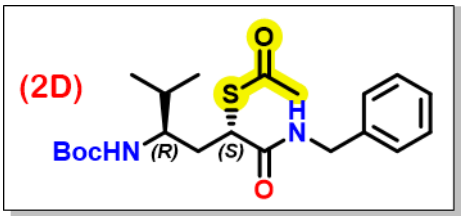


S-((3S,4S)-1-(benzylamino)-4-((tert-butoxycarbonyl)amino)-5-methyl-1-oxohexan-3-yl) ethanethioate (2B): White solid, yield = 269 mg (22%); mp 179−181°C; $[\alpha]_D^{25}$ = -9.502 (*c* 0.1, MeOH); **^{1}H NMR** (400 MHz, Chloroform-*d*) δ 7.34 – 7.29 (m, 4H (Aromatic)), 7.27 – 7.23 (m, 1H (Aromatic)), 6.89 (t, *J* = 5.8 Hz, 1H), 4.49 (d, *J* = 9.6 Hz, 1H), 4.47 (dd, *J* = 14.7, 5.9 Hz, 1H), 4.41 (dd, *J* = 14.7, 5.8 Hz, 1H), 4.23 (ddd, *J* = 8.9, 6.1, 2.9 Hz, 1H), 3.48 (td, *J* = 9.6, 2.9 Hz, 1H), 2.62 (dd, *J* = 14.1, 8.8 Hz, 1H), 2.47 (dd, *J* = 14.1, 6.1 Hz, 1H), 2.29 (s, 3H), 1.67 – 1.59 (m, 1H), 1.43 (s, 9H), 0.92 (d, *J* = 6.6 Hz, 3H), 0.88 (d, *J* = 6.7 Hz, 3H). **^{13}C NMR** (101 MHz, $CDCl_3$) δ 193.93, 169.71, 156.68, 138.56, 128.53, 127.95, 127.26, 79.76, 59.00, 44.82, 43.62, 41.49, 30.92, 30.69, 28.32, 20.16, 18.94. **HRMS** (ESI-QTOF) m/z calculated value for $C_{21}H_{32}N_2O_4S$ is $[M+Na]^+$ 431.1980 and observed 431.1982.



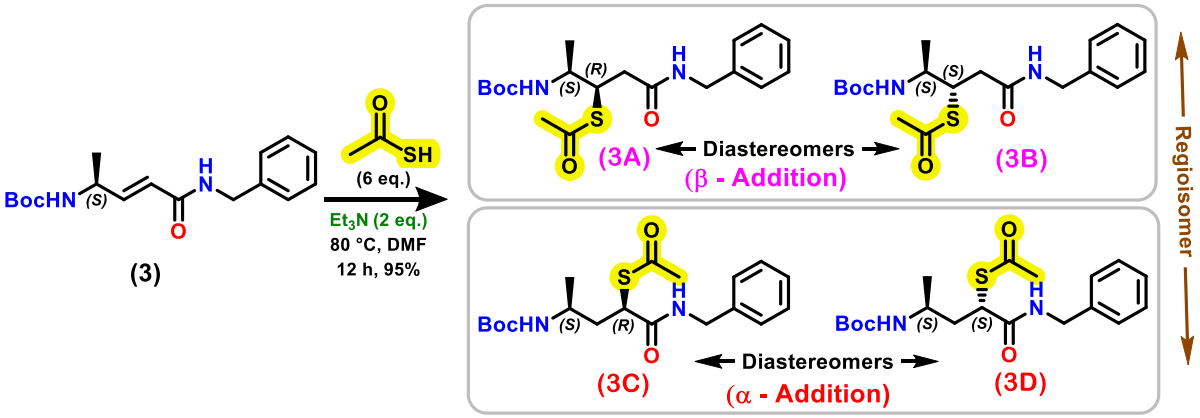
S-((2R,4R)-1-(benzylamino)-4-((tert-butoxycarbonyl)amino)-5-methyl-1-oxohexan-2-yl) ethanethioate (2C): White solid, yield = 294 mg (24%); mp 173−175°C; $[\alpha]_D^{25}$ = -15.471 (*c* 0.1, MeOH); **^{1}H NMR** (400 MHz, Chloroform-*d*) δ 7.34 – 7.28 (m, 3H (Aromatic)), 7.24 – 7.21 (m, 2H (Aromatic)), 6.62 (t, *J* = 5.9 Hz, 1H), 4.51 (dd, *J* = 14.9, 6.2 Hz, 1H), 4.37 (d, *J* = 10.2 Hz, 1H), 4.32 (dd, *J* = 14.9, 5.3 Hz, 1H), 4.06 (dd, *J* = 9.0, 5.7 Hz, 1H), 3.71 – 3.63 (m,

1H), 2.35 (s, 3H), 2.04 (ddd, *J* = 14.8, 11.7, 5.8 Hz, 1H), 1.88 (ddd, *J* = 14.8, 8.9, 3.2 Hz, 1H), 1.77 – 1.71 (m, 1H), 1.41 (s, 9H), 0.90 (d, *J* = 6.9 Hz, 3H), 0.88 (d, *J* = 6.7 Hz, 3H). **^{13}C NMR** (101 MHz, $CDCl_3$) δ 196.21, 171.48, 155.83, 137.93, 128.70, 127.56, 127.48, 79.19, 53.64, 43.98, 43.79, 33.07, 32.87, 32.14, 30.32, 28.38, 18.90, 17.88. **HRMS** (ESI-QTOF) m/z calculated value for $C_{21}H_{32}N_2O_4S$ is $[M+Na]^+$ 431.1980 and observed 431.1976.

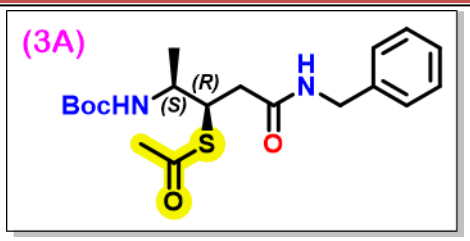


S-((2S,4R)-1-(benzylamino)-4-((tert-butoxycarbonyl)amino)-5-methyl-1-oxohexan-2-yl) ethanethioate (2D): White solid, yield = 331 mg (27%); mp 169−171°C; $[\alpha]_D^{25}$ = +18.384 (*c* 0.1, MeOH); **^{1}H NMR** (400 MHz, Chloroform-*d*) δ 7.43 (t, *J* = 5.8 Hz, 1H), 7.35 – 7.27 (m, 5H (Aromatic)), 4.53 (d, *J* = 10.1 Hz, 1H), 4.47 (d, *J* = 5.8 Hz, 2H), 4.14 (dd, *J* = 11.6, 3.1 Hz, 1H), 3.50 – 3.42 (m, 1H), 2.32 (s, 3H), 2.23 (ddd, *J* = 13.6, 11.9, 2.2 Hz, 1H), 1.71 – 1.66 (m, 1H), 1.53 (ddd, *J* = 13.6, 11.7, 3.0 Hz, 1H), 1.46 (s, 9H), 0.87 (d, *J* = 6.7 Hz, 3H), 0.84 (d, *J* = 6.9 Hz, 3H). **^{13}C NMR** (101 MHz, $CDCl_3$) δ 195.61, 170.52, 157.04, 138.24, 128.55, 127.71, 127.25, 79.80, 53.94, 44.87, 43.83, 37.13, 32.49, 30.35, 28.39, 19.10, 17.63. **HRMS** (ESI-QTOF) m/z calculated value for $C_{21}H_{32}N_2O_4S$ is $[M+Na]^+$ 431.1980 and observed 431.1980.

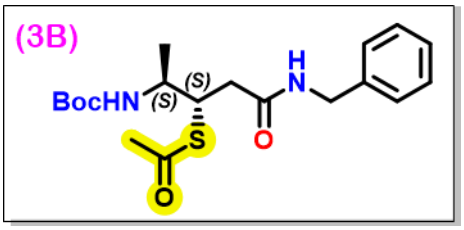
Reaction 4th :



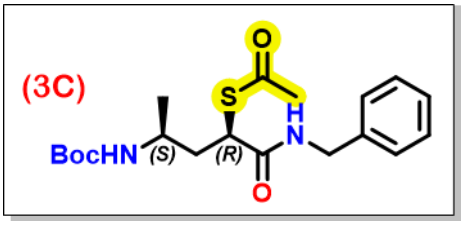
Characterization Data of α- & β- addition products of Thioacetic acid (3A-3D)



S-((3R,4S)-1-(benzylamino)-4-((tert-butoxycarbonyl)amino)-1-oxopentan-3-yl) ethanethioate (3A): White solid, yield = 239 mg (21%); mp 145 − 147 °C; $[\alpha]_D^{25}$ = -25.100 (*c* 0.1, MeOH); **^{1}H NMR** (400 MHz, Chloroform-*d*) δ 7.35 – 7.28 (m, 5H), 6.47 (s, 1H), 4.93 (d, *J* = 8.5 Hz, 1H), 4.44 (dd, *J* = 5.9, 2.4 Hz, 2H), 4.04 (q, *J* = 6.5 Hz, 1H), 3.98 – 3.89 (m, 1H), 2.64 (dd, *J* = 15.3, 6.8 Hz, 1H), 2.55 (dd, *J* = 15.3, 7.3 Hz, 1H), 2.29 (s, 3H), 1.43 (s, 9H), 1.17 (d, *J* = 6.7 Hz, 3H). **^{13}C NMR** (101 MHz, $CDCl_3$) δ 194.84, 169.75, 155.40, 138.12, 128.63, 127.93, 127.44, 79.72, 48.97, 45.64, 43.76, 39.35, 30.69, 28.36, 17.85. **HRMS** (ESI-QTOF) m/z calculated value for $C_{19}H_{28}N_2O_4S$ is $[M+Na]^+$ 403.1667 and observed 403.1663.

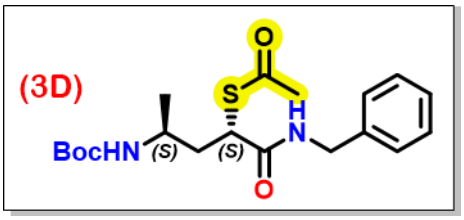


S-((3S,4S)-1-(benzylamino)-4-((tert-butoxycarbonyl)amino)-1-oxopentan-3-yl) ethanethioate (3B): White solid, yield = 251 mg (22%); mp 151 − 153 °C; $[\alpha]_D^{25}$ = -20.739 (*c* 0.1, MeOH); **^{1}H NMR** (400 MHz, Chloroform-*d*) δ 7.35 – 7.27 (m, 5H), 6.79 (s, 1H), 4.58 (d, *J* = 9.1 Hz, 1H), 4.49 (dd, *J* = 14.8, 5.9 Hz, 1H), 4.42 (dd, *J* = 14.8, 5.5 Hz, 1H), 4.07 – 4.04 (m, 1H), 4.03 – 4.01 (m, 1H), 2.66 (dd, *J* = 14.3, 8.5 Hz, 1H), 2.46 (dd, *J* = 14.3, 6.3 Hz, 1H), 2.32 (s, 3H), 1.42 (s, 9H), 1.15 (d, *J* = 6.6 Hz, 3H). **^{13}C NMR** (101 MHz, $CDCl_3$) δ 193.99, 169.85, 155.92, 138.29, 128.60, 127.83, 127.35, 79.91, 48.67, 47.80, 43.71, 40.68, 30.66, 28.32, 19.61. **HRMS** (ESI-QTOF) m/z calculated value for $C_{19}H_{28}N_2O_4S$ is $[M+Na]^+$ 403.1667 and observed 403.1666.



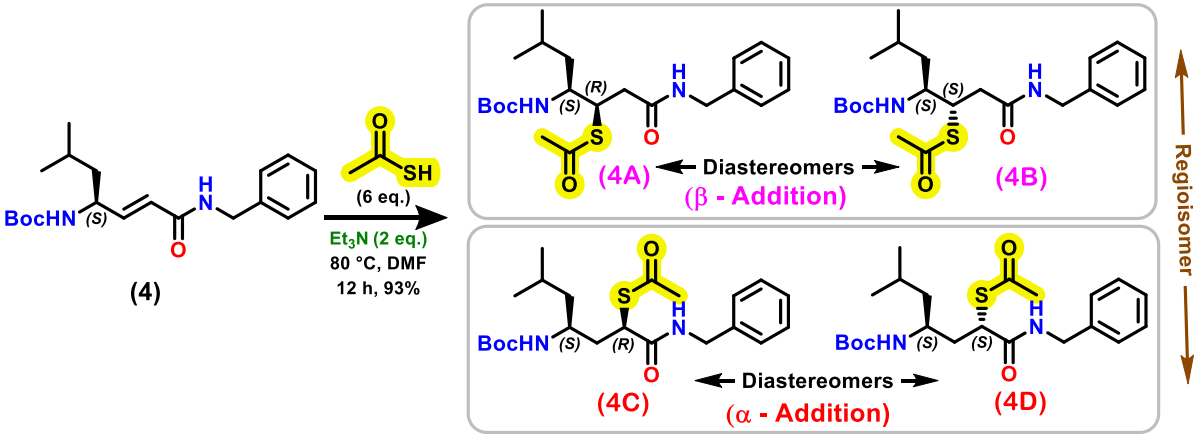
S-((2R,4S)-1-(benzylamino)-4-((tert-butoxycarbonyl)amino)-1-oxopentan-2-yl) ethanethioate (3C): White solid, yield = 285 mg (25%); mp 139 − 141°C; $[\alpha]_D^{25}$ = +37.178 (*c* 0.1, MeOH); **^{1}H NMR** (400 MHz, Chloroform-*d*) δ 7.40 (s, 1H), 7.33 – 7.26 (m, 5H), 4.53 (dd,

J = 7.6, 3.8 Hz, 1H), 4.49 (dd, *J* = 15.0, 5.9 Hz, 1H), 4.43 (dd, *J* = 15.0, 5.3 Hz, 1H), 4.16 (dd, *J* = 10.9, 3.8 Hz, 1H), 3.79 – 3.70 (m, 1H), 2.33 (s, 3H), 2.20 (ddd, *J* = 14.0, 10.8, 3.6 Hz, 1H), 1.65 (ddd, *J* = 14.0, 10.3, 3.9 Hz, 1H), 1.45 (s, 9H), 1.14 (d, *J* = 6.7 Hz, 3H). **^{13}C NMR** (101 MHz, $CDCl_3$) δ 195.65, 170.57, 156.26, 138.03, 128.58, 127.60, 127.29, 79.81, 44.96, 44.54, 43.83, 40.95, 30.32, 28.37, 21.61. **HRMS** (ESI-QTOF) m/z calculated value for $C_{19}H_{28}N_2O_4S$ is $[M+Na]^+$ 403.1667 and observed 403.1667.

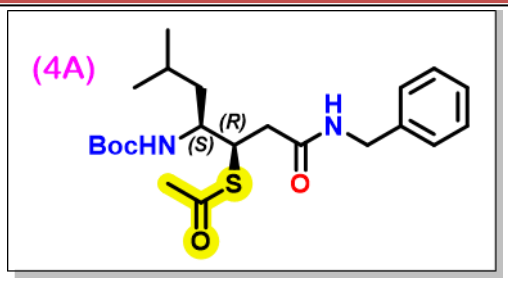


S-((2S,4S)-1-(benzylamino)-4-((tert-butoxycarbonyl)amino)-1-oxopentan-2-yl) ethanethioate (3D): White solid, yield = 308 mg (27%); mp 136 − 138°C; $[\alpha]_D^{25}$ = -26.394 (*c* 0.1, MeOH); **^{1}H NMR** (400 MHz, Chloroform-*d*) δ 7.35 – 7.26 (m, 3H (Aromatic)), 7.23 (dd, *J* = 8.1, 1.5 Hz, 2H (Aromatic)), 6.64 (s, 1H), 4.48 (dd, *J* = 14.9, 6.1 Hz, 1H), 4.42 (d, *J* = 8.5 Hz, 1H), 4.35 (dd, *J* = 14.9, 5.5 Hz, 1H), 4.06 (dd, *J* = 8.0, 6.6 Hz, 1H), 3.86 (br, 1H), 2.35 (s, 3H), 2.14 (ddd, *J* = 14.7, 10.4, 6.6 Hz, 1H), 1.84 (ddd, *J* = 14.5, 7.9, 3.8 Hz, 1H), 1.41 (s, 9H), 1.17 (d, *J* = 6.6 Hz, 3H). **^{13}C NMR** (101 MHz, $CDCl_3$) δ 196.11, 171.09, 155.36, 137.88, 128.68, 127.57, 127.47, 79.31, 44.97, 43.79, 43.73, 36.88, 30.29, 28.38, 22.09. **HRMS** (ESI-QTOF) m/z calculated value for $C_{19}H_{28}N_2O_4S$ is $[M+Na]^+$ 403.1667 and observed 403.1664.

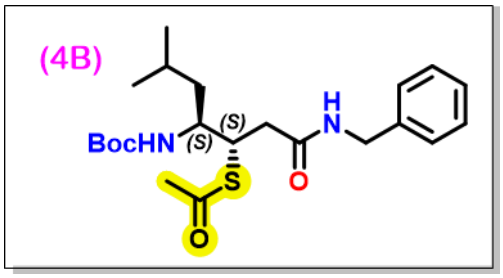
Reaction 5th :



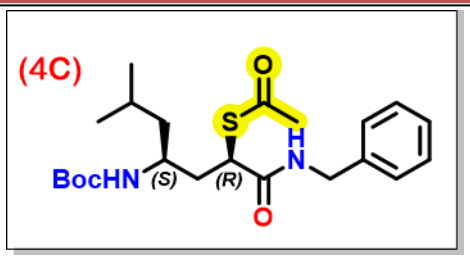
Characterization Data of α- & β- addition products of Thioacetic acid (4A-4D)



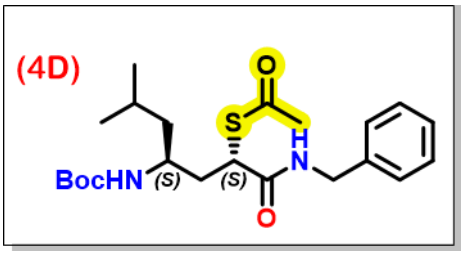
S-((3R,4S)-1-(benzylamino)-4-((tert-butoxycarbonyl)amino)-6-methyl-1-oxoheptan-3-yl) ethanethioate (4A): White solid, yield = 278 mg (22%); mp 155−157°C; $[\alpha]_D^{25}$ = -19.062 (*c* 0.1, MeOH); **^{1}H NMR** (400 MHz, Chloroform-*d*) δ 7.34 – 7.28 (m, 5H), 6.48 (t, *J* = 7.3 Hz, 1H), 4.80 (d, *J* = 9.3 Hz, 1H), 4.44 (d, *J* = 5.5 Hz, 2H), 4.02 – 3.97 (m, 1H), 3.91 – 3.85 (m, 1H), 2.64 (dd, *J* = 15.3, 6.7 Hz, 1H), 2.55 (dd, *J* = 15.3, 7.0 Hz, 1H), 2.28 (s, 3H), 1.63-1.59 (m, 1H), 1.43 (s, 9H), 1.35 – 1.30 (m, 2H), 0.91 (d, *J* = 6.7 Hz, 3H), 0.87 (d, *J* = 6.5 Hz, 3H). **^{13}C NMR** (101 MHz, $CDCl_3$) δ 194.95, 169.88, 155.83, 138.17, 128.63, 127.95, 127.42, 79.63, 51.42, 45.37, 43.75, 41.27, 39.08, 30.67, 28.36, 24.95, 23.44, 21.58. **HRMS** (ESI-QTOF) m/z calculated value for $C_{22}H_{34}N_2O_4S$ is $[M+Na]^+$ 445.2136 and observed 445.2130.



S-((3S,4S)-1-(benzylamino)-4-((tert-butoxycarbonyl)amino)-6-methyl-1-oxoheptan-3-yl) ethanethioate (4B): White solid, yield = 291 mg (23%); mp 160−162°C; $[\alpha]_D^{25}$ = +13.362 (*c* 0.1, MeOH); **^{1}H NMR** (400 MHz, Chloroform-*d*) δ 7.34 – 7.27 (m, 5H), 7.00 (t, *J* = 5.3 Hz, 1H), 4.49 (d, *J* = 8.9 Hz, 1H), 4.43 (dd, *J* = 13.5, 7.3 Hz, 2H), 4.06 - 4.02 (m, 1H), 3.97 (m, 1H), 2.65 (dd, *J* = 13.9, 9.4 Hz, 1H), 2.45 (dd, *J* = 14.0, 5.9 Hz, 1H), 2.32 (s, 3H), 1.63 – 1.56 (m, 1H), 1.42 (s, 9H), 1.35 – 1.27 (m, 2H), 0.86 (d, *J* = 6.7 Hz, 3H), 0.83 (d, *J* = 6.6 Hz, 3H). **^{13}C NMR** (101 MHz, $CDCl_3$) δ 193.67, 169.83, 156.40, 138.41, 128.56, 127.87, 127.26, 79.92, 51.06, 47.39, 43.67, 42.65, 41.19, 30.68, 28.30, 24.81, 23.02, 21.96. **HRMS** (ESI-QTOF) m/z calculated value for $C_{22}H_{34}N_2O_4S$ is $[M+Na]^+$ 445.2136 and observed 445.2136.



S-((2R,4S)-1-(benzylamino)-4-((tert-butoxycarbonyl)amino)-6-methyl-1-oxoheptan-2-yl) ethanethioate (4C): White solid, yield = 292 mg (23%); mp 154−156°C; $[\alpha]_D^{25}$ = +42.085 (*c* 0.1, MeOH); **^{1}H NMR** (400 MHz, Chloroform-*d*) δ 7.32 – 7.26 (m, 3H (Aromatic)), 7.21 (d, *J* = 6.8 Hz, 2H (Aromatic)), 6.64 (t, *J* = 6.5 Hz, 1H), 4.48 (dd, *J* = 14.8, 6.2 Hz, 1H), 4.31 (dd, *J* = 15.0, 5.5 Hz, 1H), 4.24 (d, *J* = 9.7 Hz, 1H), 4.07 (dd, *J* = 8.8, 5.9 Hz, 1H), 3.88 - 381 (m, 1H), 2.33 (s, 3H), 2.03 – 1.97 (m, 1H), 1.92 – 1.87 (m, 1H), 1.65 – 1.58 (m, 1H), 1.39 (s, 9H), 1.30 (dd, *J* = 8.5, 6.0 Hz, 2H), 0.90 (d, *J* = 2.7 Hz, 3H), 0.88 (d, *J* = 2.9 Hz, 3H). **^{13}C NMR** (101 MHz, CHLOROFORM-*D*) δ 196.32, 171.39, 155.57, 138.01, 128.74, 127.62, 127.52, 79.27, 47.07, 45.77, 43.83, 43.70, 35.69, 30.41, 29.78, 28.44, 24.99, 22.92, 22.79, 22.44. **HRMS** (ESI-QTOF) m/z calculated value for $C_{22}H_{34}N_2O_4S$ is $[M+Na]^+$ 445.2136 and observed 445.2133.

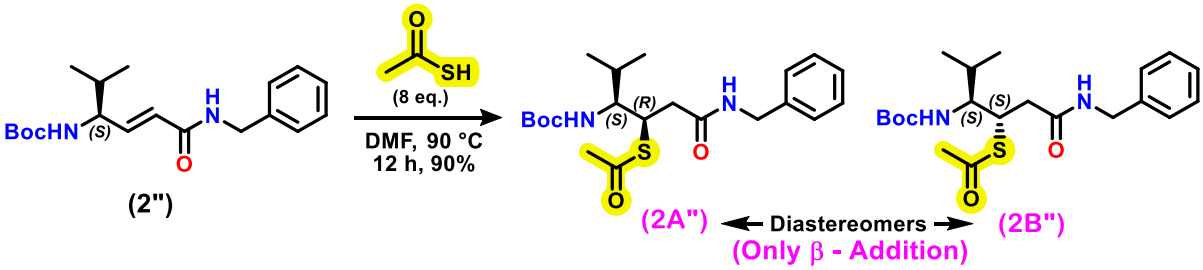


S-((2S,4S)-1-(benzylamino)-4-((tert-butoxycarbonyl)amino)-6-methyl-1-oxoheptan-2-yl) ethanethioate (4D): White solid, yield = 317 mg (25%); mp 149−151°C; $[\alpha]_D^{25}$ = -23.712 (*c* 0.1, MeOH); **^{1}H NMR** (400 MHz, Chloroform-*d*) δ 7.55 (t, *J* = 6.4 Hz, 1H), 7.27 – 7.21 (m, 3H (Aromatic)), 7.17 (m, 2H (Aromatic)), 4.40 (t, *J* = 5.1 Hz, 2H), 4.33 (d, *J* = 9.7 Hz, 1H), 4.11 (dd, *J* = 11.5, 3.2 Hz, 1H), 3.64 – 3.58 (m, 1H), 2.25 (s, 3H), 2.17 – 2.10 (m, 1H), 1.57 – 1.53 (m, 1H), 1.50 – 1.43 (m, 1H), 1.38 (s, 9H), 1.36 – 1.33 (m, 2H), 0.78 (d, *J* = 6.7 Hz, 3H), 0.76 (d, *J* = 6.5 Hz, 3H). **^{13}C NMR** (101 MHz, $CDCl_3$) δ 194.48, 169.46, 155.73, 137.19, 127.50, 126.62, 126.15, 78.79, 46.41, 43.87, 43.73, 42.77, 39.52, 29.29, 27.34, 23.86, 21.82, 20.97. **HRMS** (ESI-QTOF) m/z calculated value for $C_{22}H_{34}N_2O_4S$ is $[M+Na]^+$ 445.2136 and observed 445.2137.

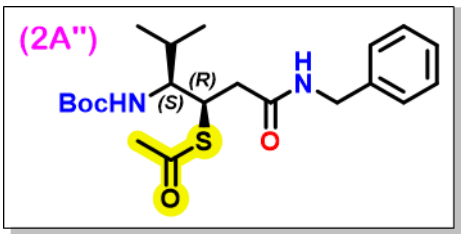
4.5.3.2. <u>Reaction in absence of a base</u>: Only β addition products were observed in each reactions (2A''-2B'' and 5A-5B).

General Procedure of reaction 6th and 7th : In a 2 ml solution of (*E*)-α,β-Unsaturated γ-Amino Amides (**2'' & 5**) (3 mmol) dissolved in dimethylformamide (DMF), thioacetic acid (CH3COSH) (18 mmol) was introduced. The reaction mixture was then subjected to heating at 90 °C for a duration of 12 hours using a reflux condenser. The advancement of the reaction was observed through thin-layer chromatography (TLC) and confirmed by MALDI TOF/TOF mass analysis. After completion, the reaction mixture was diluted with 200 mL of ethyl acetate (EtOAc) and subjected to washes with 5 % aq. HCl solution (3 × 150 ml), 15% aq. Na_2CO_3 (3 × 150 mL), and brine solution (2 × 150 mL). The organic layer was then dried over anhydrous Na_2SO_4 and concentrated under reduced pressure. The crude product was purified through reverse-phase HPLC on the C-18 column using water/acetonitrile gradient system (95% H_2O: 5% ACN and 5% H_2O: 95% ACN as gradient with 1.5 mL/min flow rate). Only β addition products were observed in each reactions, as illustrated below.

Reaction 6th :

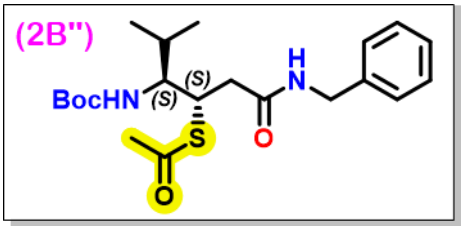


Characterization data of thioacetic acid β- addition products (2A'' and 2B'') in the absence of base.



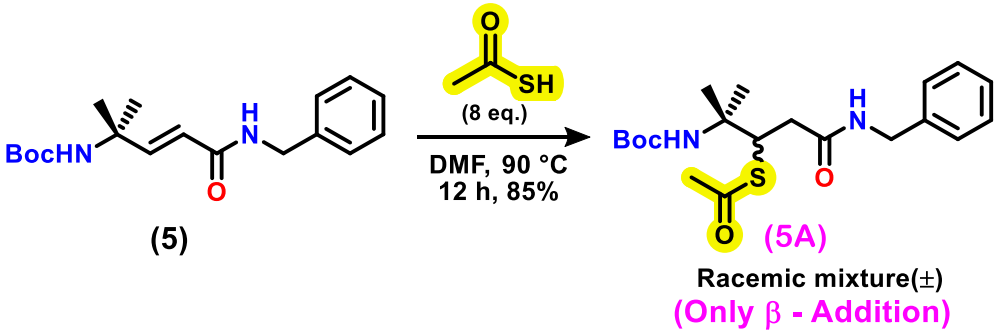
S-((3R,4S)-1-(benzylamino)-4-((tert-butoxycarbonyl)amino)-5-methyl-1-oxohexan-3-yl) ethanethioate (2A''): White solid, yield = 514 mg (42%); mp 187−189°C; $[\alpha]_D^{25}$ = +17.005 (*c* 0.1, MeOH); **^{1}H NMR** (400 MHz, Chloroform-*d*) δ 7.33 – 7.27 (m, 4H (Aromatic)), 7.25 (d, *J* = 3.1 Hz, 1H (Aromatic)), 6.40 (d, *J* = 7.7 Hz, 1H), 5.14 (dd, *J* = 10.7, 4.6 Hz, 1H), 4.45 (dd, *J* = 14.8, 5.9 Hz, 1H), 4.36 (dd, *J* = 14.8, 5.5 Hz, 1H), 4.01 (dt, *J* = 8.2, 6.4 Hz, 1H), 3.64 (ddd, *J* = 10.5, 8.1, 5.6 Hz, 1H), 2.67 (dd, *J* = 15.1, 6.2 Hz, 1H), 2.53 (dd, *J* = 15.1, 6.4 Hz, 1H), 2.24 (s, 3H), 1.99 (dq, *J* = 13.2, 6.7 Hz, 1H), 1.41 (s, 9H), 0.92 (d, *J* = 6.7 Hz, 3H), 0.86

(d, *J* = 6.7 Hz, 3H). **^{13}C NMR** (101 MHz, CHLOROFORM-*D*) δ 195.19, 170.75, 156.40, 138.00, 128.65, 127.86, 127.49, 79.44, 58.03, 43.81, 43.77, 42.87, 38.73, 30.63, 29.77, 28.36, 20.28, 16.81. **HRMS** (ESI-QTOF) m/z calculated value for $C_{21}H_{32}N_2O_4S$ is $[M+Na]^+$ 431.1980 and observed 431.1981.

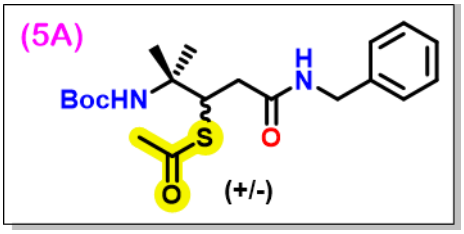


S-((3S,4S)-1-(benzylamino)-4-((tert-butoxycarbonyl)amino)-5-methyl-1-oxohexan-3-yl) ethanethioate (2B''): White solid, yield = 588 mg (48%); mp 179−181°C; $[\alpha]_D^{25}$ = -9.502 (*c* 0.1, MeOH); **^{1}H NMR** (400 MHz, Chloroform-*d*) δ δ 7.33 – 7.28 (m, 4H (Aromatic)), 7.27 – 7.23 (m, 1H (Aromatic)), 6.89 (t, *J* = 5.9 Hz, 1H), 4.49 (d, *J* = 9.6 Hz, 1H), 4.47 (dd, *J* = 14.7, 5.9 Hz, 1H), 4.41 (dd, *J* = 14.7, 5.8 Hz, 1H), 4.23 (ddd, *J* = 8.9, 6.1, 2.9 Hz, 1H), 3.48 (td, *J* = 9.6, 2.9 Hz, 1H), 2.62 (dd, *J* = 14.1, 8.8 Hz, 1H), 2.47 (dd, *J* = 14.1, 6.1 Hz, 1H), 2.29 (s, 3H), 1.67 – 1.59 (m, 1H), 1.43 (s, 9H), 0.92 (d, *J* = 6.6 Hz, 3H), 0.88 (d, *J* = 6.7 Hz, 3H). **^{13}C NMR** ^{13}C NMR (101 MHz, CHLOROFORM-*D*) δ 193.91, 170.22, 156.80, 138.29, 128.56, 127.93, 127.33, 79.96, 58.91, 44.79, 43.71, 41.50, 30.90, 30.69, 28.29, 20.08, 19.03. **HRMS** (ESI-QTOF) m/z calculated value for $C_{21}H_{32}N_2O_4S$ is $[M+Na]^+$ 431.1980 and observed 431.1984.

Reaction 7th :



Characterization data of thioacetic acid β- addition products (5A) in the absence of base.



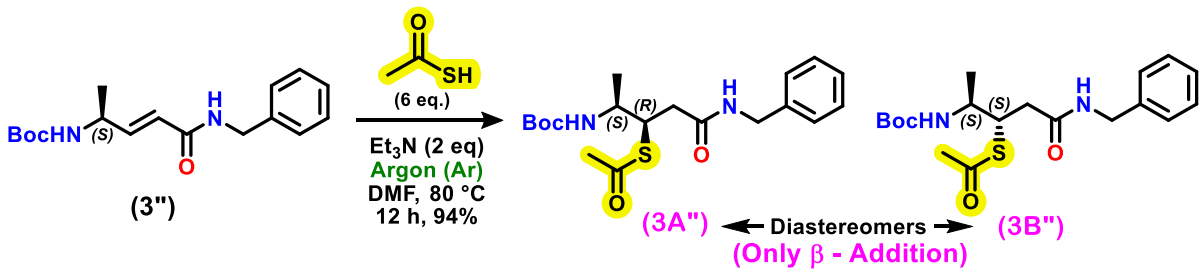
S-(1-(benzylamino)-4-((tert-butoxycarbonyl)amino)-4-methyl-1-oxopentan-3-yl) ethanethioate (5A): White solid, yield = 1 gm (85%); mp 119−121°C; **^{1}H NMR** (400 MHz,

Chloroform-*d*) δ 7.32 – 7.27 (m, 4H (Aromatic)), 7.25 – 7.22 (m, 1H (Aromatic)), 6.48 (s, 1H), 4.80 (s, 1H), 4.54 (dd, *J* = 10.3, 4.0 Hz, 1H), 4.40 (dd, *J* = 5.8, 4.0 Hz, 2H), 2.86 (dd, *J* = 15.2, 4.0 Hz, 1H), 2.40 (dd, *J* = 15.2, 10.3 Hz, 1H), 2.24 (s, 3H), 1.39 (s, 9H), 1.36 (s, 3H), 1.27 (s, 3H). **^{13}C NMR** ^{13}C NMR (101 MHz, $CDCl_3$) δ 194.90, 170.46, 154.59, 138.30, 128.57, 127.88, 127.32, 79.56, 55.65, 48.40, 43.68, 38.75, 30.47, 28.36, 25.19, 25.06. **HRMS** (ESI-QTOF) m/z calculated value for $C_{20}H_{30}N_2O_4S$ is $[M+Na]^+$ 417.1823 and observed 417.1823.

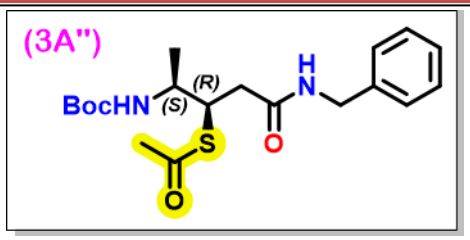
4.5.3.3. <u>Reaction Under Inert Atmosphere</u>: Only β addition products were observed in the reaction (3A''-3B'').

General Procedure of reaction 8th : In an oven-dried 5 ml round-bottom flask equipped with a stir bar and rubber septum, a mixture of BocNH-(*E*)-α,β-Unsaturated γ-Alanine Benzyl Amide **3''** (3 mmol), thioacetic acid (CH_3COSH) (18 mmol) and triethylamine (Et_3N) (6 mmol) in Dimethylformamide (DMF) (2 mL) was prepared under an inert atmosphere. The reaction mixture was purged with argon for 10 minutes initially to eliminate any dissolved air, and an oxygen-free atmosphere was maintained throughout the reaction using a argon filled balloon. The reaction mixture was then stirred under heating at 80 °C for a duration of 12 hours. The completion of the reaction was confirmed through thin-layer chromatography (TLC) and MALDI TOF/TOF mass analysis. after completion, the reaction mixture was diluted with 200 mL of ethyl acetate (EtOAc) and subjected to washes with 5 % aqueous HCl solution (3 × 100 ml), 15% aqueous Na_2CO_3 (3 × 100mL), and brine solution (1 × 100 mL). The organic layer was then dried over anhydrous Na_2SO_4 and concentrated under reduced pressure. Purification of the crude product was achieved through reverse phase HPLC on the C-18 column using water/acetonitrile gradient system (95% H_2O: 5% ACN and 5% H_2O: 95% ACN as gradient with 1.5 mL/min flow rate). Only β addition products were observed in the reaction, as illustrated below.

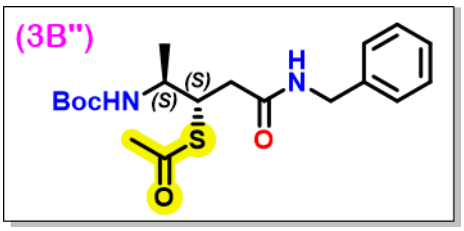
Reaction 8th :



Characterization data of thioacetic acid β- addition products (3A'' and 3B'') under Argon atm.



S-((3R,4S)-1-(benzylamino)-4-((tert-butoxycarbonyl)amino)-1-oxopentan-3-yl) ethanethioate (3A''): White solid, yield = 559 mg (49%); mp 145 − 147 °C; $[\alpha]_D^{25}$ = -25.100 (*c* 0.1, MeOH); **^{1}H NMR** ^{1}H NMR (400 MHz, Chloroform-*d*) δ 7.35 – 7.27 (m, 5H), 6.47 (s, 1H), 4.93 (d, *J* = 8.5 Hz, 1H), 4.44 (dd, *J* = 5.9, 2.5 Hz, 2H), 4.04 (q, *J* = 6.7 Hz, 1H), 3.97 – 3.90 (m, 1H), 2.64 (dd, *J* = 15.3, 6.8 Hz, 1H), 2.55 (dd, *J* = 15.3, 7.3 Hz, 1H), 2.29 (s, 3H), 1.43 (s, 9H), 1.17 (d, *J* = 6.7 Hz, 3H). **^{13}C NMR** (101 MHz, CHLOROFORM-*D*) δ 194.84, 170.03, 155.46, 138.00, 128.62, 127.88, 127.45, 79.76, 48.93, 45.55, 43.75, 39.20, 30.68, 28.34, 17.80. **HRMS** (ESI-QTOF) m/z calculated value for $C_{19}H_{28}N_2O_4S$ is $[M+Na]^+$ 403.1667 and observed 403.1669.



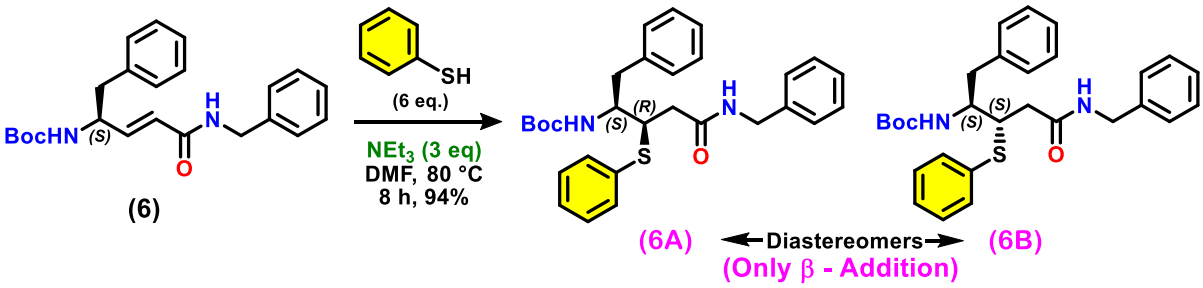
S-((3S,4S)-1-(benzylamino)-4-((tert-butoxycarbonyl)amino)-1-oxopentan-3-yl) ethanethioate (3B''): White solid, yield = 513 mg (45%); mp 151 − 153 °C; $[\alpha]_D^{25}$ = -20.739 (*c* 0.1, MeOH); **^{1}H NMR** (400 MHz, Chloroform-*d*) δ 7.35 – 7.27 (m, 5H), 6.79 (s, 1H), 4.58 (d, *J* = 9.1 Hz, 1H), 4.49 (dd, *J* = 14.8, 5.9 Hz, 1H), 4.42 (dd, *J* = 14.8, 5.5 Hz, 1H), 4.07 – 4.04 (m, 1H), 4.03 – 4.01 (m, 1H), 2.66 (dd, *J* = 14.3, 8.5 Hz, 1H), 2.46 (dd, *J* = 14.3, 6.3 Hz, 1H), 2.32 (s, 3H), 1.42 (s, 9H), 1.15 (d, *J* = 6.6 Hz, 3H). **^{13}C NMR** (101 MHz, CHLOROFORM-*D*) δ 194.03, 170.01, 155.95, 138.18, 128.60, 127.79, 127.37, 79.96, 48.61, 47.79, 43.71, 40.66, 30.66, 28.31, 19.59. **HRMS** (ESI-QTOF) m/z calculated value for $C_{19}H_{28}N_2O_4S$ is $[M+Na]^+$ 403.1667 and observed 403.1660.

4.5.4. General Procedure for Thiol-ene Reaction between Thiophenol and BocNH-(*E*)-α,β-Unsaturated γ-Phenylalanine Benzyl Amides (6); Only β addition products were observed in the reaction (6A-6B).

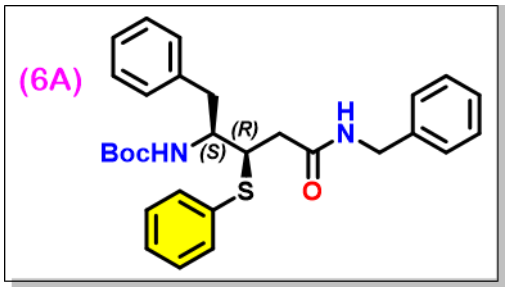
General Procedure of reaction 9th : To a solution of BocNH-(*E*)-α,β-Unsaturated γ-Phenylalanine Benzyl Amides **6** (3 mmol) in DMF (2 ml) was added thiophenol (Ph-SH) (18

mmol) and triethylamine (Et_3N) (9 mmol). The reaction mixture was stirred for 12 hours at 80 °C using a reflux condenser. The progress of the reaction was monitored using TLC in ethyl acetate in pet ether (35%) solvent system and MALDI TOF/TOF mass analysis.. After completion, the reaction mixture was diluted with 200 mL of ethyl acetate (EtOAc) and washed the ethyl acetate layer with 5 % aq. HCl solution (3 × 150 ml), 15% aq. Na_2CO_3 (3 × 150 mL), and brine solution (2 × 150 mL). The organic layer was then dried using anhydrous Na_2SO_4 and concentrated over rotary evaporator. The crude product was purified through reverse phase HPLC on the C-18 column using water/acetonitrile gradient system (95% H_2O: 5% ACN and 5% H_2O: 95% ACN as gradient with 1.5 mL/min flow rate). Only β addition products were observed the reaction, as illustrated below.

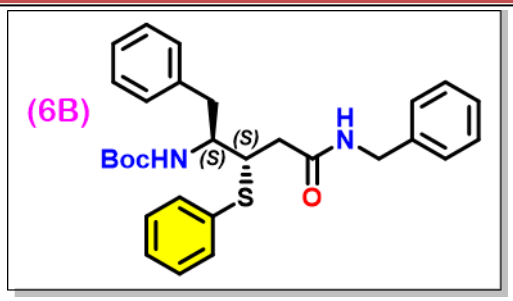
Reaction 9th :



Characterization data of thiophenol β- addition products (6A and 6B)



tert-butyl((2S,3R)-5-(benzylamino)-5-oxo-1-phenyl-3-(phenylthio)pentan-2-yl)carbamate (6A): White solid, yield = 632 mg (43%); mp 142 − 144 °C; $[\alpha]_D^{25}$ = +14.071 (*c* 0.1, MeOH); **^{1}H NMR** (400 MHz, Chloroform-*d*) δ 7.43 – 7.16 (m, 15H (Aromatic)), 6.03 (s, 1H), 4.84 (d, *J* = 9.4 Hz, 1H), 4.45 (dd, *J* = 14.9, 5.8 Hz, 1H), 4.34 (dd, *J* = 14.9, 5.3 Hz, 1H), 4.07 (m, 1H), 3.73 (q, *J* = 6.9 Hz, 1H), 3.19 (dd, 14.2, 4.6 Hz, 1H), 2.79 (dd, *J* = 14.2, 9.1 Hz, 1H), 2.63 (dd, *J* = 15.1, 6.3 Hz, 1H), 2.49 (dd, *J* = 15.1, 7.4 Hz, 1H), 1.29 (s, 9H). **^{13}C NMR** (101 MHz, $CDCl_3$) δ 170.53, 155.46, 137.93, 137.78, 134.36, 131.94, 129.29, 129.20, 128.68, 128.45, 127.89, 127.52, 127.37, 126.49, 79.44, 55.31, 49.95, 43.84, 40.06, 38.27, 28.24. **HRMS** (ESI-QTOF) m/z calculated value for $C_{29}H_{34}N_2O_3S$ is $[M+H]^+$ 491.2368 and observed 491.2367.



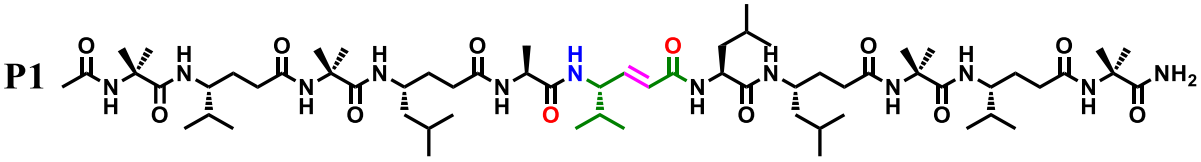
tert-butyl((2S,3S)-5-(benzylamino)-5-oxo-1-phenyl-3-(phenylthio)pentan-2-yl)carbamate (6B): White solid, yield = 750 mg (51%); mp 147 − 149 °C; $[\alpha]_D^{25}$ = +5.2 (*c* 0.1, MeOH); **^{1}H NMR** (400 MHz, Chloroform-*d*) δ 7.45 (d, *J* = 7.6 Hz, 2H (Aromatic)), 7.32 – 7.26 (m, 7H (Aromatic)), 7.23 – 7.15 (m, 4H (Aromatic)), 7.11 (d, *J* = 6.0 Hz, 1H (NH-Benzylic), 6.94 (d, *J* = 6.6 Hz, 2H (Aromatic)), 4.79 (d, *J* = 9.7 Hz, 1H), 4.48 (dd, *J* = 14.6, 5.9 Hz, 1H), 4.39 (dd, *J* = 14.6, 5.7 Hz, 1H), 4.25 – 4.18 (m, 1H), 3.65 (td, *J* = 6.2, 2.9 Hz, 1H), 2.92 – 2.83 (m, 2H), 2.61 (dd, *J* = 14.0, 8.6 Hz, 1H), 2.53 (dd, *J* = 14.0, 5.9 Hz, 1H), 1.35 (s, 9H). **^{13}C NMR** (101 MHz, $CDCl_3$) δ 170.44, 156.38, 138.28, 137.26, 134.50, 131.33, 129.25, 128.91, 128.59, 128.44, 127.87, 127.32, 127.17, 126.54, 80.03, 54.74, 51.31, 43.76, 41.68, 40.20, 28.23. **HRMS** (ESI-QTOF) m/z calculated value for $C_{29}H_{34}N_2O_3S$ is $[M+Na]^+$ 513.2187 and observed 513.2188.

4.5.5. General procedure for the solid phase synthesis of starting peptide P1:

Peptide **P1** was synthesized at 0.2 mmol scales on Knorr-Amide resin using standard Fmoc-chemistry. HBTU/HOBT was used as a standard coupling reagent. To avoid Michael addition of HOBT, we carried out-coupling reactions of *E*-vinylogous γ-amino acids only with HBTU.[27] Reaction time for Fmoc-deprotections and couplings of amino acids were 45 min and 1.5 h, respectively. The final Fmoc-deprotected amine was acylated using Acetic anhydride and pyridine base (Ac_2O/Py). After completion of the synthesis, peptide was cleaved from the resin using 20 mL of TFA/TIPS/Phenol/H_2O (88:2:5:5). After peptide cleavage, the resin was filtered out using the sintered funnel. The filtrate (which contains peptide) was evaporated under reduced pressure to give the crude peptide products. Peptide was further precipitated out using cold diethyl ether and purified through reverse phase HPLC on the C-18 column using MeOH/H_2O gradient. The purity of peptide was further confirmed using an analytical C-18 column in the same MeOH/H_2O gradient system. The mass of peptide was confirmed by MALDI TOF/TOF.

Characterization data of Peptide P1:

Peptide P1:



^{1}H NMR (600 MHz, $CDCl_3$) δ 8.80 (d, *J* = 6 Hz, 1H), 8.76 (s, 1H), 8.17 (d, *J* = 7.8 Hz, 1H), 8.09 (s, 1H), 8.06 (s, 1H), 8.04 (s, 1H), 7.92 (s, 1H), 7.84 (s, 1H), 7.75 (s, 1H), 7.14 (d, *J* = 8.4 Hz, 1H), 7.08 (d, *J* = 4.8 Hz, 1H), , 6.96 (dd, *J* = 15, 2.4 Hz, 1H), 6.78 (d, *J* = 8.4 Hz, 1H), 6.33 (d, *J* = 15 Hz, 1H), 5.10 (s, 1H), 4.29 (m, 1H), 4.19 (m, 1H), 4.09 (m, 1H), 3.95 (m, 1H), 3.93 (m, 1H), 3.68 (m, 1H), 3.54 (m, 1H), 2.65 (br, 1H), 2.41 (br, 1H), 2.26 (br, 4H), 2.17 (br, 1H), 2.08 (m, 4H), 2.05 (s, 3H), 2.00 (m, 3H), 1.79 (m, 2H), 1.67 (m, 6H), 1.57 (m, 2H), 1.50 (m, 22H), 1.41 (s, 3H), 1.35 (br, 3H), 1.21 (br, 2H), 1.11 (br, 1H), 1.07 (m, 6H), 0.99 (d, *J* = 6 Hz, 3H), 0.93 (d, *J* = 6 Hz, 3H), 0.85 (m, 21H), 0.75 (d, *J* = 6 Hz, 3H). **MALDI (TOF/TOF)** *m/z* calculated value for $C_{64}H_{116}N_{12}O_{12}$ [M+Na^+] is 1267.87 and observed at 1267.94.

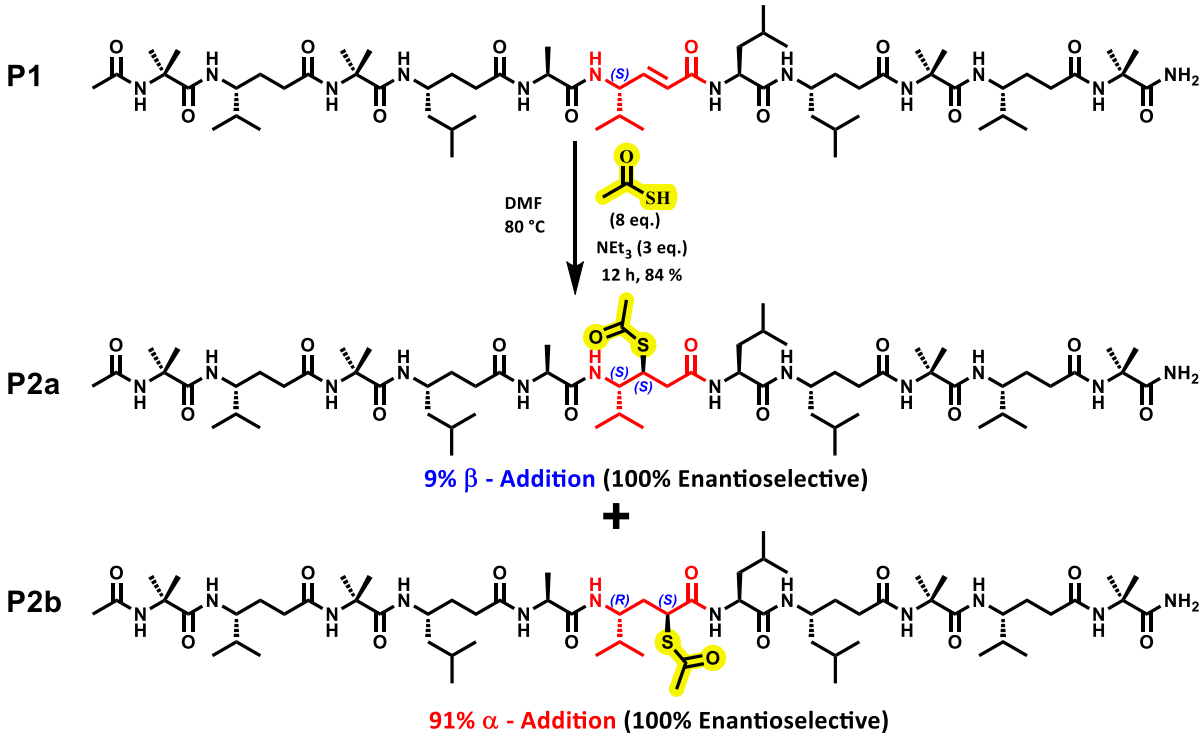
4.5.6. General Procedure for thioacetic acid / thiophenol / ethanethiol conjugate addition reactions on peptide backbone containing (*E*)-α,β-unsaturated γ-amino acids (Reaction 10th, 11th and 12th)

The peptide **P1** (0.1 mmol) was dissolved in 1 ml of dimethylformamide (DMF). Subsequently, thiol reagent (thioacetic acid / thiophenol) 0.8 mmol, (ethanethiol used 1 mmol) and triethylamine (Et_3N) 0.3 mmol were introduced to the peptide solution. Following this, the reaction mixture underwent heating at 80 °C for 12 hours using a reflux condenser (ethanethiol reaction performed at 45 °C for 24 hours). The progression of the reaction was tracked through MALDI TOF/TOF mass analysis. Upon completion, the reaction mixture was diluted with 100 mL of chloroform ($CHCl_3$) and subjected to sequential washes with a 5% aqueous hydrochloric acid solution (3 × 100 ml), 15% aqueous Na_2CO_3 (3 × 100 mL), and brine solution (2 × 100 mL). The organic layer was then dried over anhydrous Na_2SO_4 and concentrated under reduced pressure.

Purification of the crude product was carried out via reverse-phase HPLC on a C-18 column using a methanol/water gradient system (95% CH3OH : 5% H2O and 5% CH3OH : 95% H2O) with a flow rate of 2 mL/min. The purity of peptides was further confirmed using an analytical C-18 column in the MeOH/H_2O gradient system. The mass of peptides was confirmed by

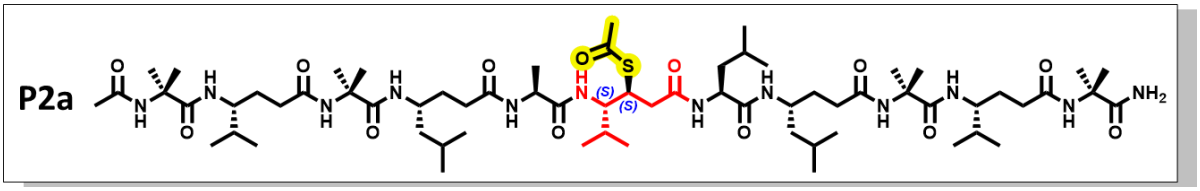
MALDI TOF/TOF. The outcomes of the reaction of peptide **P1** with each thioacetic acid, thiophenol, ethanethiol are provided below.

Reaction 10th : Peptide P1 Reaction with Thioacetic Acid (CH_3COSH) : 100% Diatereoselective α- addition (91%) and β- addition (9%) products observed.



Characterization data of Peptide P2a and P2b:

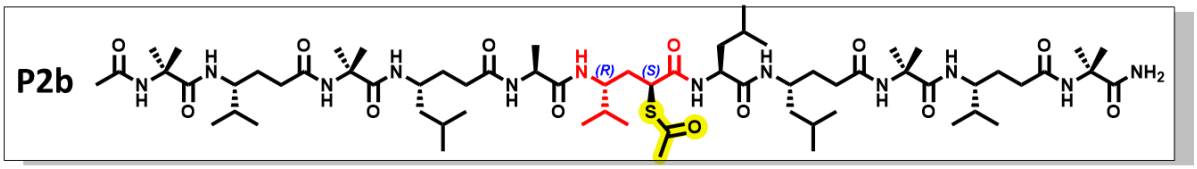
Peptide P2a:



White solid, yield = 10 mg (8%); **^{1}H NMR** (600 MHz, Chloroform-*d*) δ 8.71 (s, 1H), 8.45 (d, *J* = 9.3 Hz, 1H), 8.35 (d, *J* = 9.6 Hz, 1H), 8.24 (d, *J* = 9.7 Hz, 1H), 8.15 (d, *J* = 9.5 Hz, 1H), 8.04 (s, 1H), 7.86 (d, *J* = 4.0 Hz, 1H), 7.85 (s, 1H), 7.83 (s, 1H), 7.44 (d, *J* = 4.1 Hz, 1H), 7.14 (s, 1H), 6.58 (d, *J* = 10.0 Hz, 1H), 5.14 (s, 1H), 4.47 (dt, *J* = 12.3, 3.7 Hz, 1H), 4.18 (dt, *J* = 10.6, 5.2 Hz, 1H), 4.00 – 3.98 (m, 1H), 3.97 (s, 1H), 3.85 (td, *J* = 10.0, 3.6 Hz, 1H), 3.72 (d, *J* = 14.6 Hz, 1H), 3.57 (t, *J* = 11.2 Hz, 1H), 2.89 – 2.83 (m, 1H), 2.59 (dt, *J* = 13.6, 7.4 Hz, 1H), 2.54 – 2.48 (m, 1H), 2.44 (d, *J* = 3.5 Hz, 1H), 2.41 (d, *J* = 3.6 Hz, 1H), 2.34 (t, *J* = 7.5 Hz, 1H), 2.31 (s, 3H), 2.29 – 2.26 (m, 1H), 2.19 (s, 1H), 2.11 (d, *J* = 19.4 Hz, 2H), 2.07 (s, 3H), 2.02 (s, 1H), 1.98 – 1.95 (m, 1H), 1.81 (q, *J* = 7.0 Hz, 2H), 1.75 (d, *J* = 6.6 Hz, 1H), 1.65 (s, 5H), 1.55

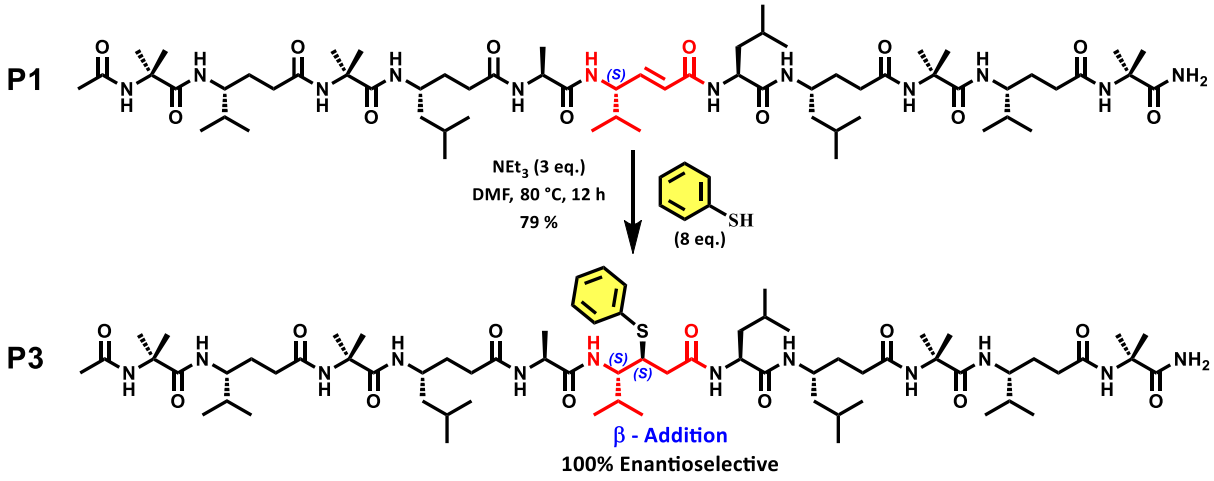
(d, *J* = 6.5 Hz, 6H), 1.53 (s, 2H), 1.51 (d, *J* = 2.3 Hz, 6H), 1.49 (d, *J* = 6.0 Hz, 6H), 1.45 (s, 5H), 1.37 (d, *J* = 2.5 Hz, 1H), 1.28 (d, *J* = 4.9 Hz, 2H), 1.20 (t, *J* = 10.0 Hz, 2H), 0.94 – 0.92 (m, 10H), 0.90 – 0.86 (m, 30H), 0.83 (d, *J* = 6.5 Hz, 3H). **MALDI (TOF/TOF)** *m/z* calculated value for $C_{66}H_{120}N_{12}O_{13}S$ [M+Na$^+$] is 1344.8068 and observed at 1344.5659.

Peptide P2b:



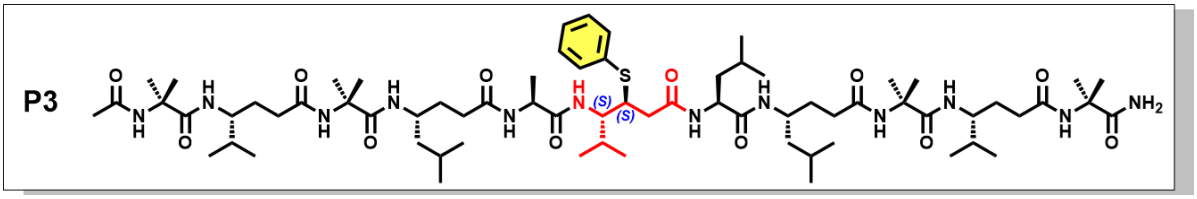
White solid, yield = 100 mg (76%); **^{1}H NMR** (600 MHz, Chloroform-*d*) δ 8.73 (s, 1H), 8.57 (d, *J* = 9.5 Hz, 1H), 8.48 (d, *J* = 9.5 Hz, 1H), 8.34 (d, *J* = 9.3 Hz, 1H), 8.16 (d, *J* = 8.2 Hz, 2H), 8.02 (s, 1H), 7.97 (s, 1H), 7.87 (s, 1H), 7.74 (s, 1H), 7.24 (s, 1H), 6.65 (d, *J* = 9.8 Hz, 1H), 5.16 (s, 1H), 4.27 (d, *J* = 14.0 Hz, 1H), 3.96 (d, *J* = 8.0 Hz, 1H), 3.93 (s, 1H), 3.91 (d, *J* = 7.8 Hz, 1H), 3.89 – 3.84 (m, 1H), 3.72 (t, *J* = 13.5 Hz, 1H), 3.64 (s, 1H), 3.56 (d, *J* = 15.5 Hz, 1H), 2.55 (t, *J* = 13.9 Hz, 1H), 2.42 (d, *J* = 13.8 Hz, 2H), 2.34 (t, *J* = 7.3 Hz, 1H), 2.29 (s, 3H), 2.26 (d, *J* = 11.1 Hz, 1H), 2.19 (s, 1H), 2.14 – 2.10 (m, 2H), 2.07 (s, 3H), 2.00 (d, *J* = 15.4 Hz, 1H), 1.88 – 1.83 (m, 2H), 1.76 (q, *J* = 6.6 Hz, 2H), 1.70 – 1.66 (m, 6H), 1.60 (s, 3H), 1.52 (t, *J* = 4.9 Hz, 10H), 1.49 (d, *J* = 6.7 Hz, 7H), 1.46 (d, *J* = 7.0 Hz, 3H), 1.41 (s, 2H), 1.30 – 1.28 (m, 2H), 1.19 (d, *J* = 9.8 Hz, 2H), 1.08 (t, *J* = 11.1 Hz, 2H), 0.94 (d, *J* = 6.3 Hz, 3H), 0.86 (ddd, *J* = 25.5, 15.1, 6.0 Hz, 40H). **MALDI (TOF/TOF)** *m/z* calculated value for $C_{66}H_{120}N_{12}O_{13}S$ [M+Na$^+$] is 1344.8068 and observed at 1344.6921.

Reaction 11th : <u>Peptide P1 Reaction with Thiophenol (Ph-SH)</u>: 100% Diastereoselective β-addition product only observed.



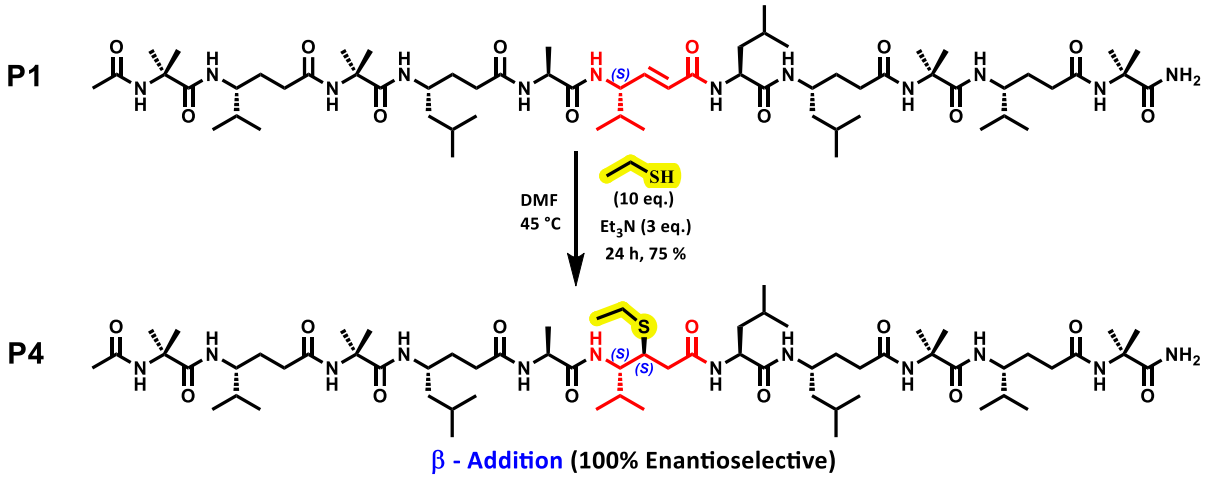
Characterization data of Peptide P3:

Peptide P3:



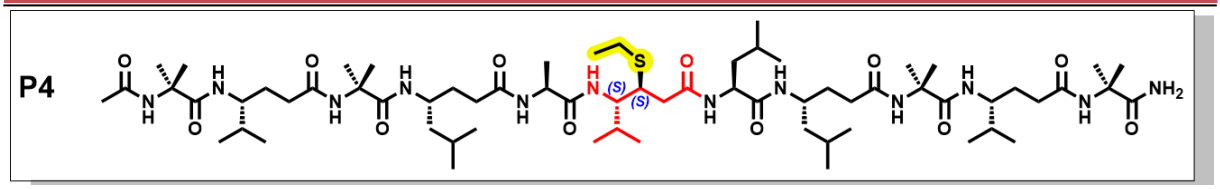
White solid, yield = 107 mg (79 %); **^{1}H NMR** (500 MHz, Chloroform-*d*) δ 8.71 (s, 1H), 8.37 (d, *J* = 9.5 Hz, 1H), 8.29 (d, *J* = 9.6 Hz, 1H), 8.13 (d, *J* = 9.7 Hz, 1H), 8.06 – 8.04 (m, 1H), 8.02 (s, 1H), 7.83 (s, 1H), 7.66 (s, 1H), 7.48 – 7.46 (m, 2H), 7.34 (dd, *J* = 8.3, 6.8 Hz, 3H), 7.27 (d, *J* = 2.1 Hz, 1H), 7.25 (t, *J* = 1.4 Hz, 1H), 6.69 – 6.62 (m, 1H), 5.19 (s, 1H), 4.40 (s, 1H), 4.06 – 4.03 (m, 1H), 4.03 (d, *J* = 3.3 Hz, 1H), 4.00 (s, 1H), 3.94 (d, *J* = 7.3 Hz, 1H), 3.84 – 3.80 (m, 1H), 3.74 (s, 1H), 3.61 (s, 1H), 2.84 – 2.78 (m, 1H), 2.65 (s, 1H), 2.53 (s, 1H), 2.48 (s, 1H), 2.44 (s, 1H), 2.39 – 2.35 (m, 1H), 2.31 (d, *J* = 3.9 Hz, 1H), 2.30 – 2.27 (m, 1H), 2.19 (d, *J* = 4.7 Hz, 2H), 2.16 (d, *J* = 4.3 Hz, 1H), 2.09 (s, 3H), 2.03 (s, 1H), 1.81 – 1.76 (m, 3H), 1.65 (s, 6H), 1.54 (s, 7H), 1.52 – 1.50 (m, 10H), 1.48 – 1.47 (m, 6H), 1.32 (dd, *J* = 5.5, 3.5 Hz, 6H), 1.01 (d, *J* = 6.4 Hz, 3H), 0.94 (d, *J* = 6.4 Hz, 5H), 0.90 – 0.84 (m, 36H). **MALDI (TOF/TOF)** *m/z* calculated value for $C_{66}H_{120}N_{12}O_{13}S$ [M+Na$^+$] is 1378.8678 and observed at 1378.161.

Reaction 12th : <u>Peptide P1 Reaction with Ethanethiol (Et-SH)</u>: 100% Diastereoselective β-addition product only observed



Characterization data of Peptide P4:

Peptide P4:



White solid, yield = 98 mg (75%); **^{1}H NMR** (600 MHz, Chloroform-*d*) δ 8.74 (s, 1H), 8.42 (d, *J* = 9.7 Hz, 1H), 8.28 (d, *J* = 9.6 Hz, 1H), 8.13 – 8.08 (m, 2H), 8.05 (s, 1H), 7.81 (s, 1H), 7.75 (d, *J* = 9.5 Hz, 1H), 7.73 (s, 1H), 7.48 (d, *J* = 4.5 Hz, 1H), 7.32 (s, 1H), 6.69 (d, *J* = 10.1 Hz, 1H), 5.19 (s, 1H), 4.32 – 4.27 (m, 1H), 4.24 – 4.12 (m, 1H), 4.05 – 3.89 (m, 4H), 3.72 (ddd, *J* = 13.7, 9.5, 4.0 Hz, 2H), 3.62 – 3.57 (m, 1H), 3.51 (s, 1H), 2.72 (dd, *J* = 14.5, 11.8 Hz, 1H), 2.60 (ttd, *J* = 14.3, 11.0, 4.8 Hz, 4H), 2.48 – 2.42 (m, 2H), 2.38 – 2.25 (m, 3H), 2.14 (td, *J* = 9.3, 8.3, 3.7 Hz, 4H), 2.09 (d, *J* = 10.4 Hz, 6H), 1.85 – 1.77 (m, 5H), 1.66 – 1.63 (m, 4H), 1.57 – 1.49 (m, 31H), 1.45 (s, 5H), 1.36 – 1.26 (m, 28H), 1.02 – 0.94 (m, 9H), 0.94 – 0.87 (m, 36H), 0.84 (d, *J* = 6.4 Hz, 4H). **MALDI (TOF/TOF)** *m/z* calculated value for $C_{66}H_{122}N_{12}O_{12}S$ [M+Na^+] is 1330.8238 and observed at 1330.362.

4.6. References

1. (a) O. Boutureira, G. J. L. Bernardes, *Chem. Rev.* **2015**, *115*, 2174−2195; (b) N. Stephanopoulos, M. B. Francis, *Nat. Chem. Biol.* **2011**, *7*, 876-884.
2. (a) E. Basle, N. Joubert, M. Pucheault, *Chem. Biol.* **2010**, *17*, 213−227; (b) C. P. R. Hackenberger, D. Schwarzer, *Angew. Chem., Int. Ed.* **2008**, *47*, 10030−10074.
3. (a) C. T. Walsh, S. Garneau-Tsodikova, J. Gregory J. Gatto, *Angew. Chem., Int. Ed.* **2005**, *44*, 7342-7372; (b) J. N. deGruyter, L. R. Malins, P. S. Baran, *Biochemistry* **2017**, *56*, 3863−3873; (c) J. M. Chalker, G. J. L. Bernardes, Y. A. Lin, B. G. Davis, *Chem. Asian J.* **2009**, *4*, 630−640; (d) J. C. M. van Hest, F. L. van Delft, *ChemBioChem* **2011**, *12*, 1309−1312.
4. (a) N. Stephanopoulos, M. B. Francis, *Nat. Chem. Biol.* **2011**, *7*, 876−884; (b) E. M. Sletten, C. R. Bertozzi, *Angew. Chem., Int. Ed.* **2009**, *48*, 6974−6998; (c) J.-M. Kee, T. W. Muir, *ACS Chem. Biol.* **2012**, *7*, 44−51; (d) G. J. L. Bernardes, J. M. Chalker, B. G. Davis, *Chemical Protein Modification*; Wiley-VCH Verlag GmbH & Co. KGaA: Weinheim, Germany, **2010**.
5. (a) S. B. Sun, P. G. Schultz, C. H. Kim, *ChemBioChem.* **2014**, *15*, 1721−1729; (b) S. Zalipsky, *Bioconjugate Chem.*, **1995**, *6*, 150–165; (c) M. Steiner, I. Hartmann, E. Perrino, G. Casi, S. Brighton, I. Jelesarov, G. J. L. Bernardes, D. Neri, *Chem. Sci.* **2013**, *4*, 297−302;

(d) S. J. Bell, C. M. Fam, E. A. Chlipala, S. J. Carlson, J. I. Lee, M. S. Rosendahl, D. H. Doherty, G. N. Cox, *Bioconjugate Chem.*, **2008**, *19*, 299–305.

6. (a) J. M. Harris, R. B. Chess, *Nat. Rev. Drug Discovery*, **2003**, *2*, 214–221; (b) D. P. Baker, E. Y. Lin, K. Lin, M. Pellegrini, R. C. Petter, L. L. Chen, R. M. Arduini, M. Brickelmaier, D. Wen, D. M. Hess, L. Chen, D. Grant, A. Whitty, A. Gill, D. J. Lindner, R. B. Pepinsky, *Bioconjugate Chem.*, **2006**, *17*, 179–188.
7. (a) Q. Wang, T. Lin, L. Tang, J. E. Johnson, M. G. Finn, *Angew. Chem., Int. Ed.*, **2002**, *41*, 459‑462; (b) J. C. Smith, K.-B. Lee, Q. Wang, M. G. Finn, J. E. Johnson, M. Mrksich, C. A. Mirkin, *Nano Lett.*, **2003**, *3*, 883‑886; (c) D. W. P. M. Lo¨wik, I. O. Shklyarevskiy, L. Ruizendaal, P. C. M. Christianen, J. C. Maan, J. C. M. van Hest, *Adv. Mater.*, **2007**, *19*, 1191‑1195; (d) K. L. Christman, R. M. Broyer, Z. P. Tolstyka, H. D. Maynard, *J. Mater. Chem.*, **2007**, *17*, 2021‑2027; (e) M. J. Abedin, L. Liepold, P. Suci, M. Young, T. Douglas, *J. Am. Chem. Soc.*, **2009**, *131*, 4346‑4354; (f) L. S. Witus, M. B. Francis, *Acc. Chem. Res.*, **2011**, *44*, 774–783.
8. (a) Y.-L. Huang, C.-Y. Wu, *Expert Rev. Vaccines*, **2010**, *9*, 1257–1274; (b) S. Aggarwal, *Nat. Biotechnol.*, **2010**, *28*, 1165–1171; (c) A. Mullard, *Nat. Rev. Drug Discovery*, **2013**, *12*, 329–332; Y.-L. Huang, J.-T. Hung, S. K. C. Cheung, H.-Y. Lee, K.-C. Chu, S.-T. Li, Y.-C. Lin, C.-T. Ren, T.-J. R. Cheng, T.-L. Hsu, A. L. Yu, C.-Y. Wu, C.-H. Wong, *Proc. Natl. Acad. Sci. U. S. A.*, **2013**, *110*, 2517–2522; (d) R. Adamo, A. Nilo, B. Castagner, O. Boutureira, F. Berti, G. J. L. Bernardes, *Chem. Sci.*, **2013**, *4*, 2995–3008.
9. (a) J. R. Fraústo da Silva, R. J. P. Williams, *The Biological Chemistry of the Elements*, Oxford University Press, New York, **2001**; b) A. Nudelman, *The Chemistry of Optically Active Sulfur Compounds*, Gordon and Breach, New York, **1984**; c) *Sulphur-Containing Drugs and Related Organic Compounds*, (Ed.: L. A. Damani), Wiley, New York, **1989**.
10. a) N. A. McGrath, M. Brichacek, J. T. A. Njardarson, *J. Chem. Educ.* **2010**, 87, 1348–1349; b) K. A. Scott, J. T. Njardarson, *Top. Curr. Chem.* **2018**, *376*, 1–34.
11. (a) O. Koniev, A. Wagner, *Chem. Soc. Rev.* **2015**, *44*, 5495−5551; (b) J. M. Chalker, G. J. L. Bernardes, Y. A. Lin, B. G. Davis, *Chem. - Asian J.* **2009**, *4*, 630−640; (c) J. Liu, R. Cheng, H. Wu, S. Li, P. G. Wang, W. F. DeGrado, S. Rozovsky, L. Wang, *Angew. Chem., Int. Ed.* **2018**, *57*, 12702−12706; (d) G.-P. Li, K. Zhang, P.-F. Zhang, W.-N. Liu, W.-Q. Tong, L. Hou, Y.-Y. Wang, *Inorganic Chemistry*, **2019**, *58*, 3409-3415.

12. J. S. Plummer, L. A. Emery, M. A. Stier, M. J. Suto, *Tetrahedron Lett*. **1993**, *34*, 7529-7532.
13. M. Ganesh Kumar, S. M. Mali, K. M. Raja, H. N. Gopi, *Org Lett.* **2015**, *17*, 230-233.
14. S. A. Nalawade, M. Singh, D. R. Puneeth Kumar, S. Dey, H. N. Gopi, *Org. Biomol. Chem.* 2**023**, *21*, 2586–2595.
15. S. M. Mali, A. Bandyopadhyay, S. V. Jadhav, M. Ganesh Kumar, H. N. Gopi, *Org. Biomol. Chem*., **2011**, *9*, 6566–6574.
16. A. Bandyopadhyay, S. V. Jadhav, H. N. Gopi, *Chem. Commun*. **2012**, *48*, 7170-7172.
17. S. V. Jadhav, A. Bandyopadhyay, H. N. Gopi, *Org. Biomol. Chem*. **2013**, *11*, 509-514.
18. (a) I. L. Karle, A. Banerjee and P. Balaram, *Folding Des.*, **1997**, *2*, 203–210; (b) A. Banerjee, S. Raghothama and P. Balaram, *J. Chem. Soc., Perkin Trans. 1*, **1997**, *2*, 2087–2094.
19. I. L. Karle, J. L. Flippen-Anderson, M. Sukumar, K. Uma, P. BaIaram, *J. Am. Chem. Soc*., **1991**, *113*, 3952–3956.
20. G. V. M. Sharma, V. Subash, K. Narsimulu, A. R. Sankar and A. C. Kunwar, *Angew. Chem., Int. Ed.*, **2006**, *45*, 8207–8210.
21. U. A. Ramagopal, S. Ramakumar, D. Sahal and V. S. Chauhan, *Proc. Natl. Acad. Sci. U. S. A.*, **2001**, *98*, 870–874.
22. I. L. Karle, C. Das and P. Balaram, *Proc. Natl. Acad. Sci. U. S. A.*, **2000**, *97*, 3034–3037.
23. S. Yamada, K. Nabe, N. Izuo, K, Nakamich, I. Chibata, *Appl Environ Microbiol.* **1981** *42*, 773-778.
24. Z.-H, Luan, J.-P. Qu, Y.-B. Kang, *J. Am. Chem. Soc.* **2020**, *142*, 20942-20947.
25. S.-C. Ren, F.-L. Zhang, A.-Q. Xu, Y. Yang, M. Zheng, X. Zhou, Y. Fu, Y.-F. Wang, *Nat Commun.* **2019**, *10*, 1934
26. M. Ganesh Kumar, V. Kuruva, S. A. Nalawade, R. V. Nithun, H. N. Gopi, *J. Org. Chem.* **2019**, *84*, 15145-15153.
27. S. M. Mali, M. Ganesh Kumar, M. M. Katariya, H. N. Gopi, *Org. Biomol. Chem*. **2014**, *2*, 8462-8472.
28. (a) G. M. Sheldrick, *Acta Crystallogr. Sect A.* **1990**, *46*, 467-473; (b) G. M. Sheldrick, SHELXL-97, Program for Crystal Structure Solution and Refinement, Universität Göttingen (Germany) **1997**.
29. (a) G. M. Sheldrick, Phase annealing in *SHELX*-90: direct methods for larger structures. *Acta Crystallogr*. **1990**, *A46*, 467-473; (b) G. M.Sheldrick, SHELXL-97, Program for Crystal Structure Solution and Refinement, Universität Göttingen (Germany) **1997**.

30. A. L. Spek, *Acta Crystallogr*. PLATON, an integrated tool for the analysis of the results of a single crystal structure determination. **1990**, *A46*, C34.
31. The solvent mask (void determination) in OLEX is based on: J.- S. Jiang, A. T. Brünger, Protein hydration observed by X-ray diffraction. Solvation properties of penicillopepsin and neuraminidase crystal structures. *J. Mol. Biol*. **1994**, *243*, 100-115.

4.7. Appendix

S. No	Content	Page No
4.7.1.	Ortep plot and crystallographic information of peptide 7B, 1A, 1C, 2C, 2D, 3C, 4C, 2A'', 5A, P1, P2a, P2b, P3 and P4.	230
4.7.2	^{1}H NMR, ^{13}C NMR, HRMS and MALDI spectra of all compounds and peptides	244

4.7.1. Ortep plot and crystallographic information of compounds and peptides 7B, 1A, 1C, 2C, 2D, 3C, 4C, 2A'', 5A, P1, P2a, P2b, P3 and P4.

4.7.1.1. ORTEP diagrams of peptides 7B, 1A, 1C, 2C, 2D, 3C, 4C, 2A'', 5A, P1, P2a, P2b, P3 and P4.

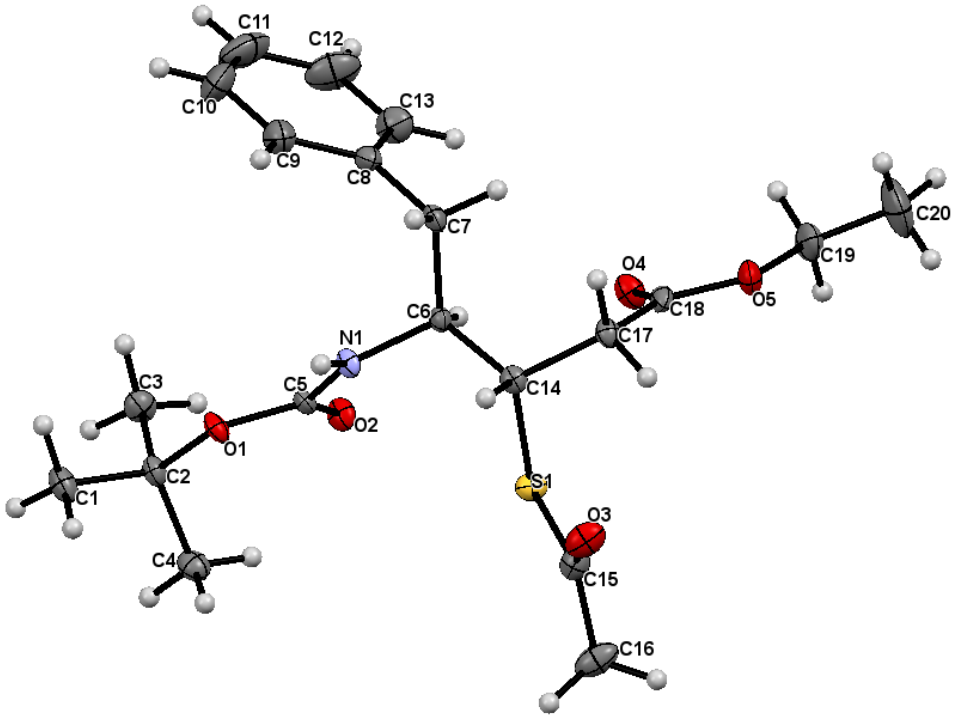


Figure 28: ORTEP diagram of compound **7B**. All H-atoms are not labeled for clarity. Ellipsoids are drawn at 50% probability.

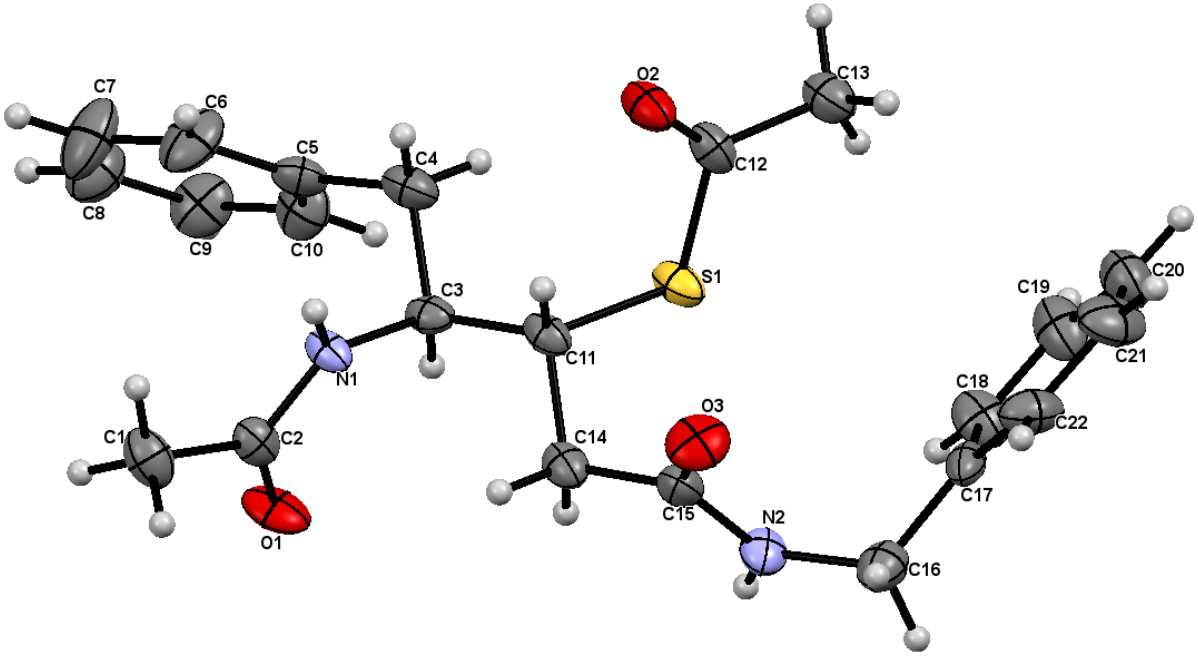


Figure 29: ORTEP diagram of compound **1A**. All H-atoms are not labeled for clarity. Ellipsoids are drawn at 50% probability.

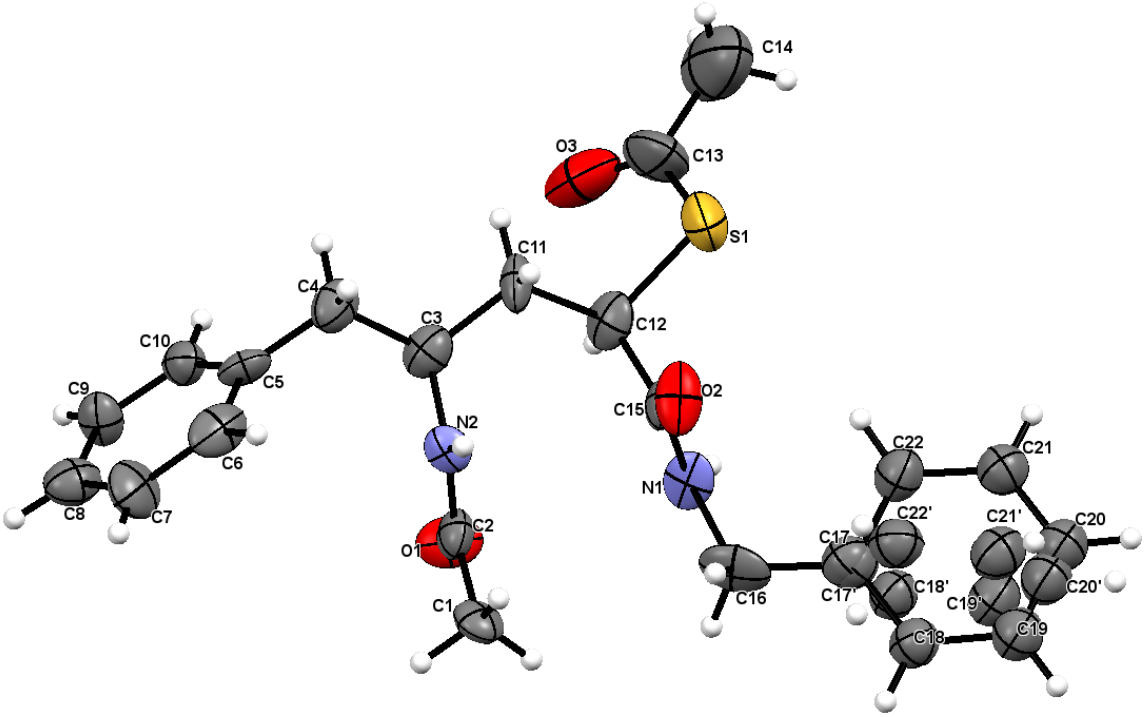


Figure 30: ORTEP diagram of compound **1C**. All H-atoms are not labeled for clarity. Ellipsoids are drawn at 50% probability.

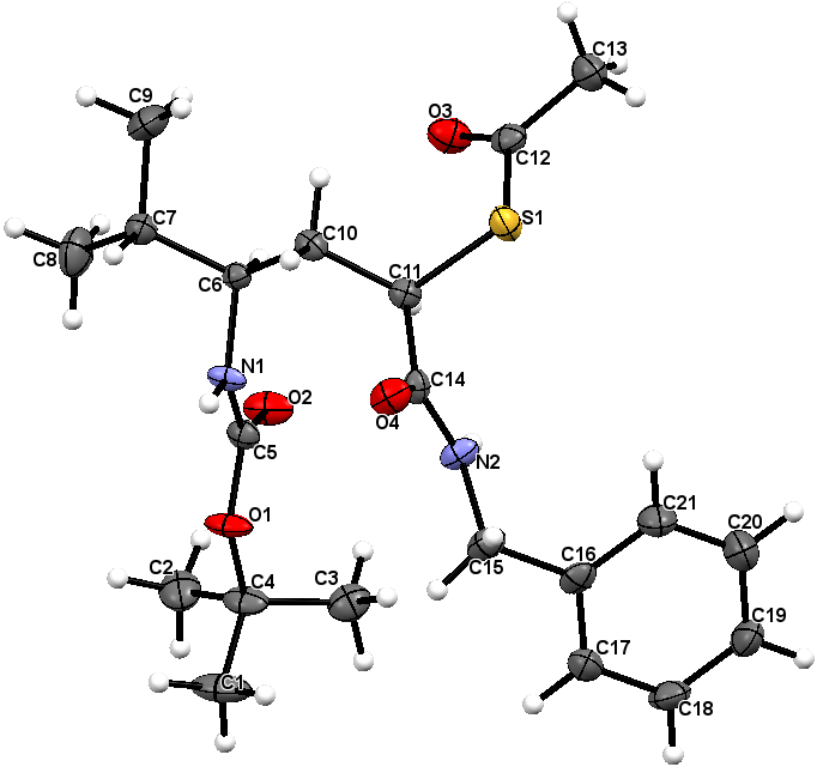


Figure 31: ORTEP diagram of compound **2C**. All H-atoms are not labeled for clarity. Ellipsoids are drawn at 50% probability.

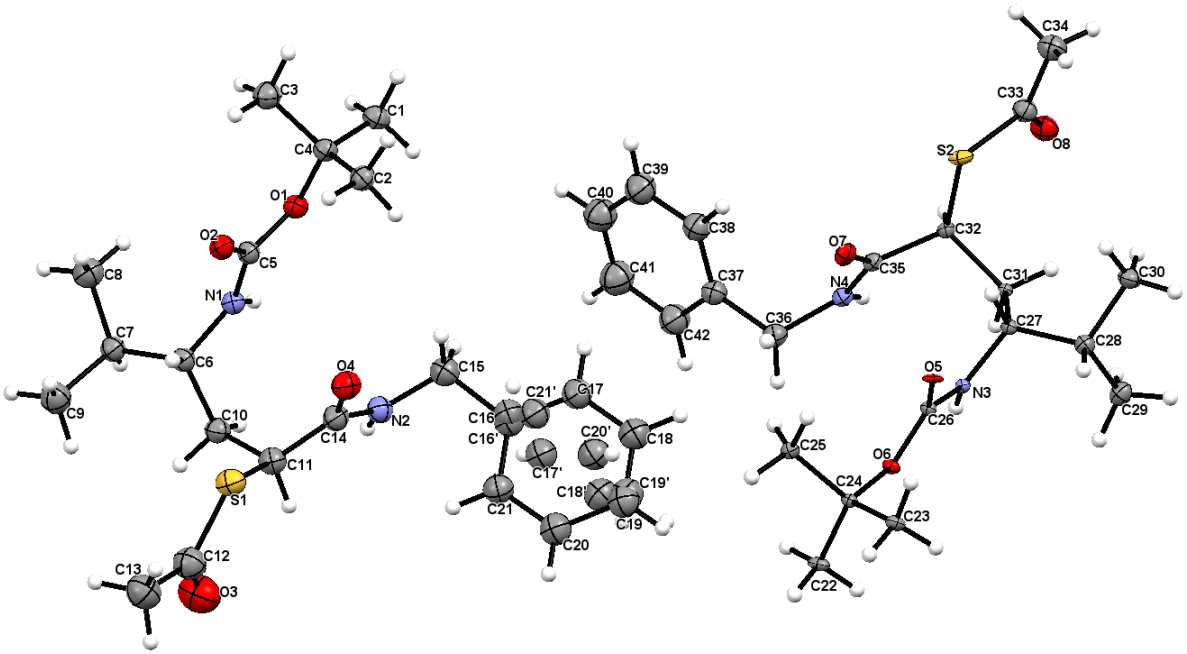


Figure 32: ORTEP diagram of compound **2D**. All H-atoms are not labeled for clarity. Ellipsoids are drawn at 50% probability.

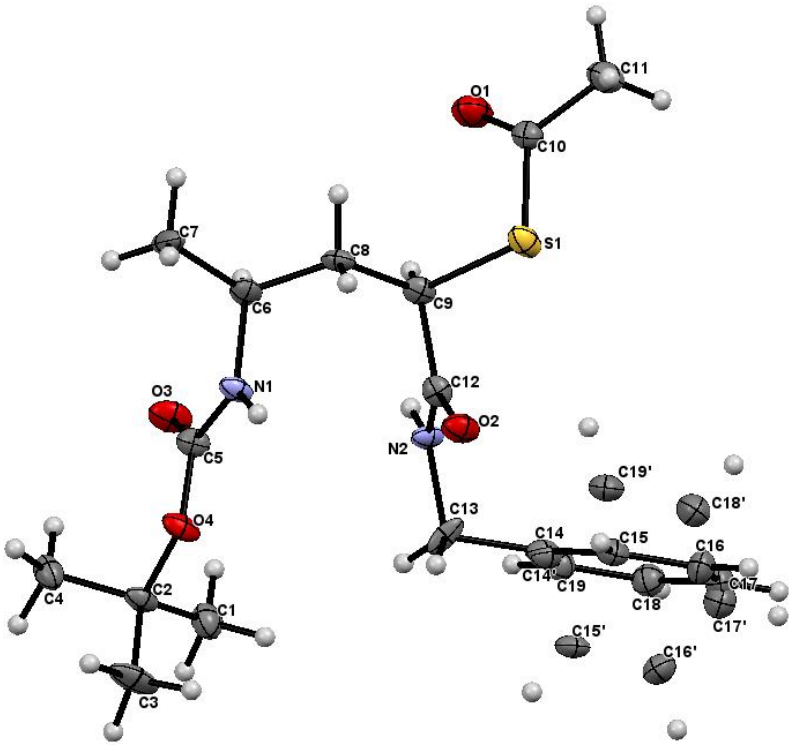


Figure 33: ORTEP diagram of compound **3C**. All H-atoms are not labeled for clarity. Ellipsoids are drawn at 50% probability.

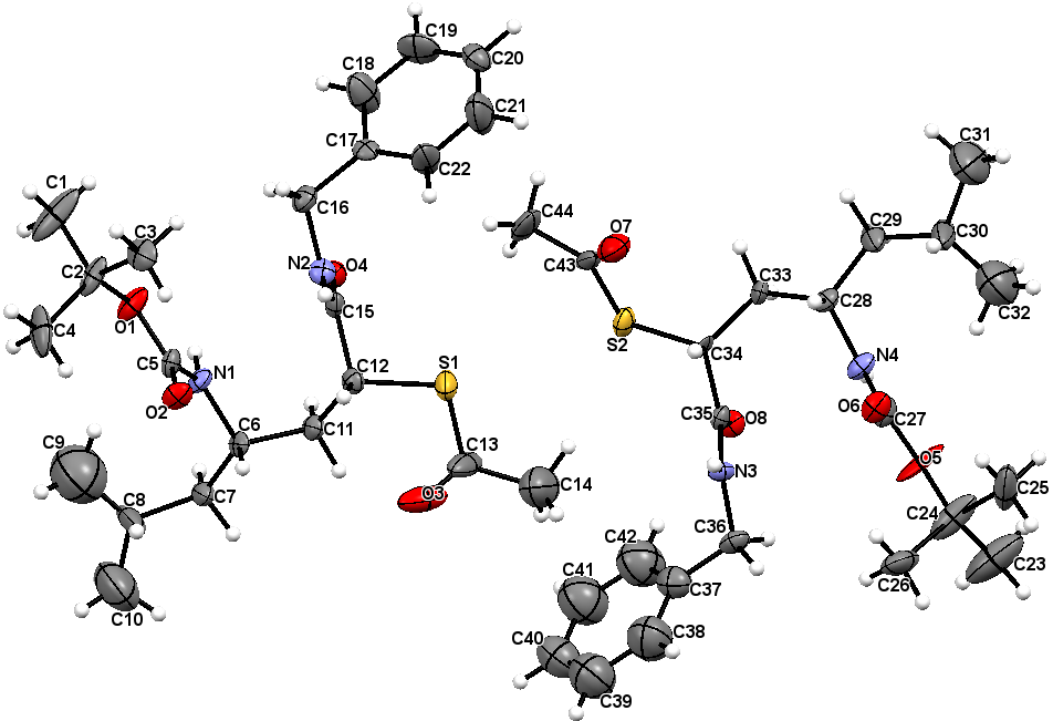


Figure 34: ORTEP diagram of compound **4C**. All H-atoms are not labeled for clarity. Ellipsoids are drawn at 50% probability.

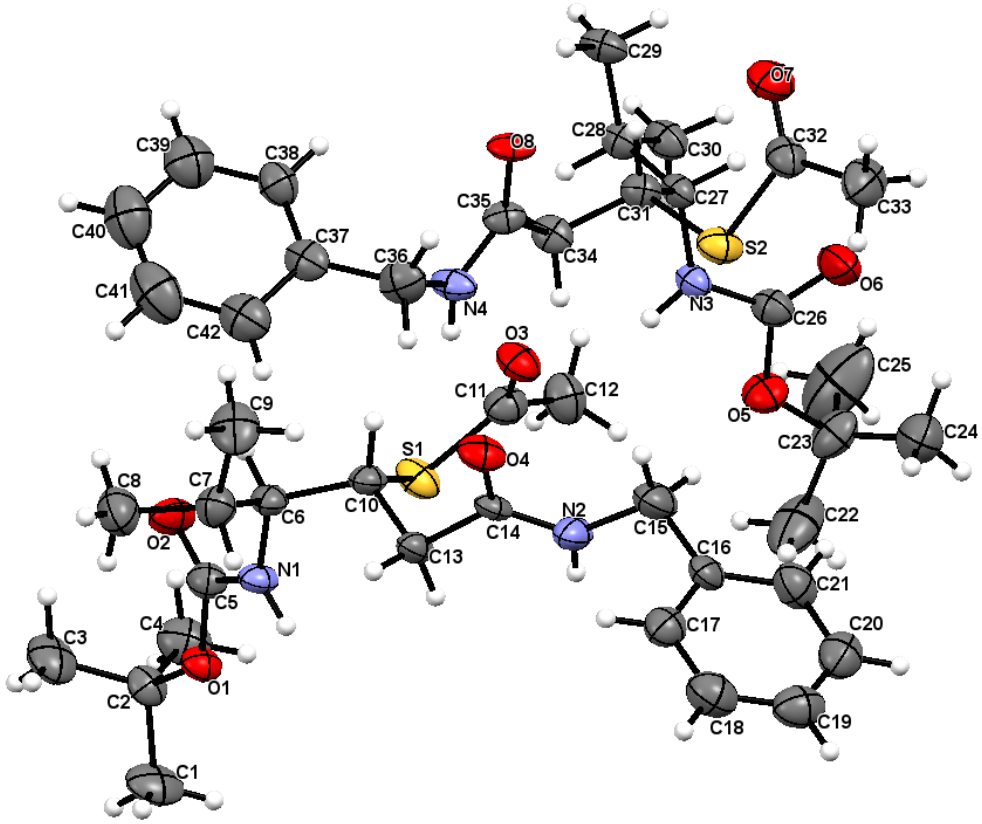


Figure 35: ORTEP diagram of compound **2A''**. All H-atoms are not labeled for clarity. Ellipsoids are drawn at 50% probability.

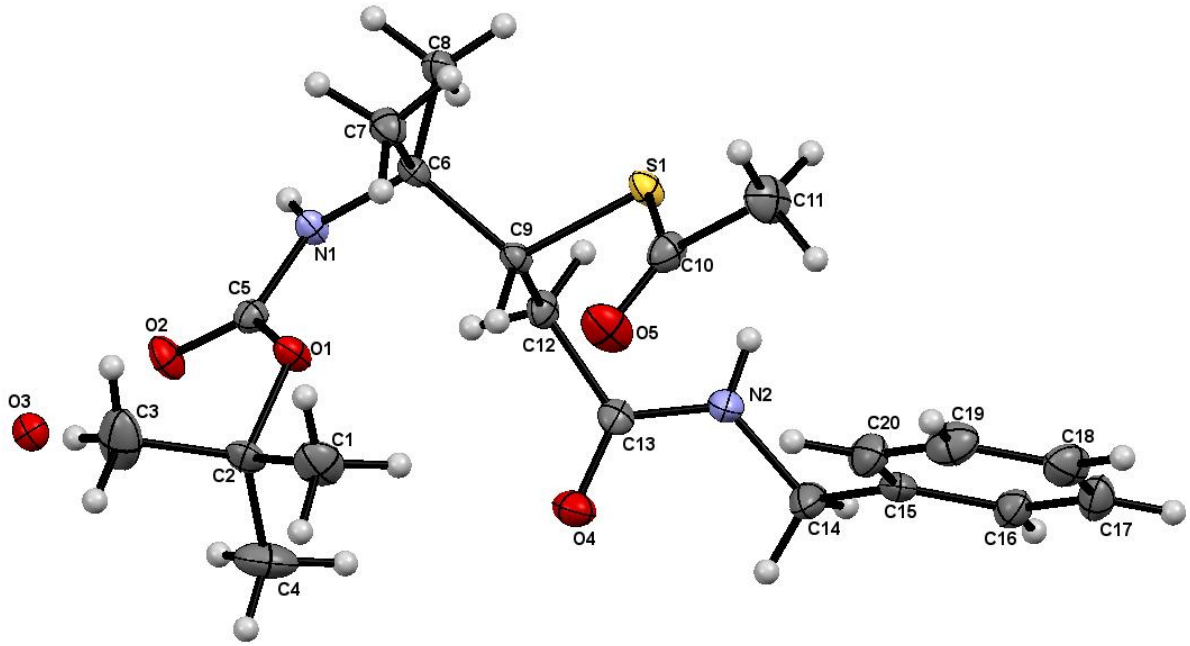


Figure 36: ORTEP diagram of compound **5A**. All H-atoms are not labeled for clarity. Ellipsoids are drawn at 50% probability.

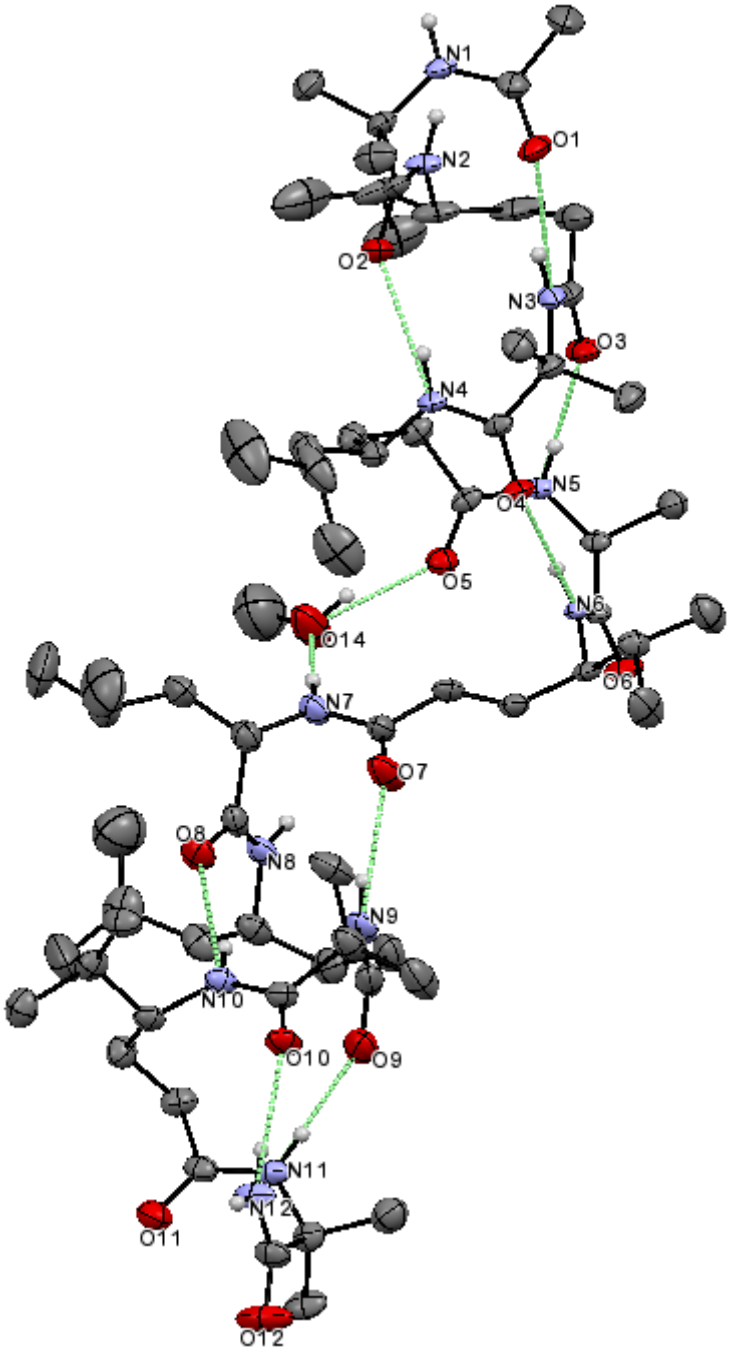


Figure 37: ORTEP diagram of **P1** [Ac-Aib-*γ*Val-Aib-*γ*Leu-Ala-(*E*)d*γ*Val-Leu-*γ*Leu-Aib-*γ*Val-Aib-$CONH_2$], with labelled heteroatoms. H-bonding is represented by dotted lines in light green colour. The side-chain and backbone H-atoms are not shown for clarity (except N-H). Ellipsoids are drawn at 50% probability. (symmetry operations: N1 = -1+x,y,z; N2 = -1+x,y,1+z; N12 = x,y,-1+z; O6 = x,y,1+z); O12 = 1+x,y,-1+z; O6 = 1+x,y,z). [(*E*)d*γ*Val = (*E*)-α, β-unsaturated γ-Valine[1]]

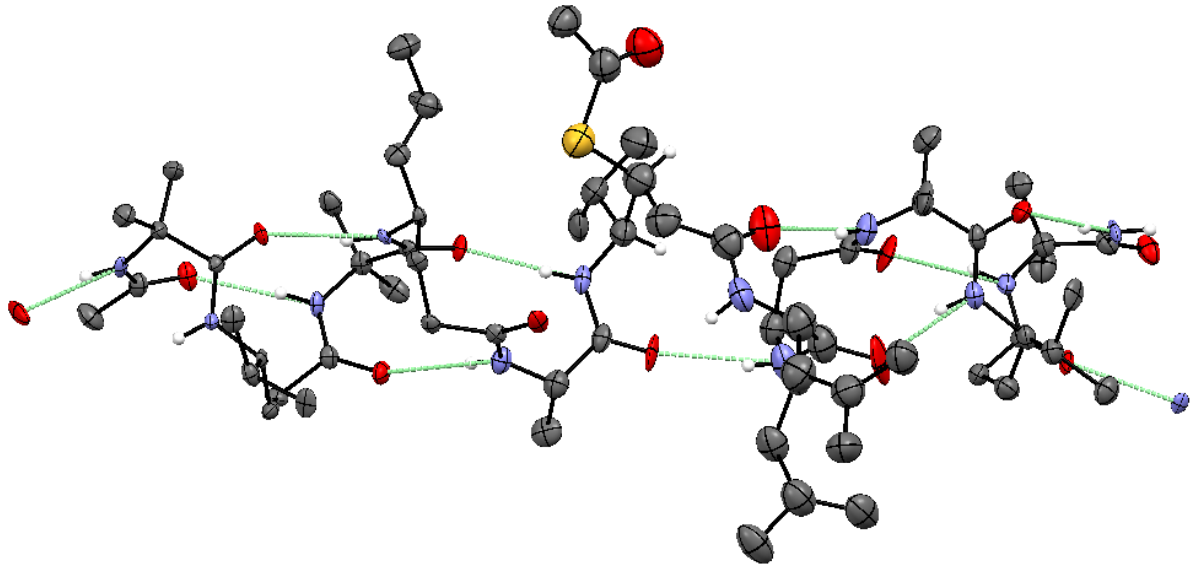


Figure 38: ORTEP diagram of Peptide **P2a** [Ac-Aib-γVal-Aib-γLeu-Ala-γ- *(β -SCOCH$_3$)* Val-Leu-γLeu-Aib-γVal-Aib-CONH$_2$]. H-bonding is represented by dotted lines. The side-chain and backbone H-atoms are not shown for clarity. Ellipsoids are drawn at 50% probability.

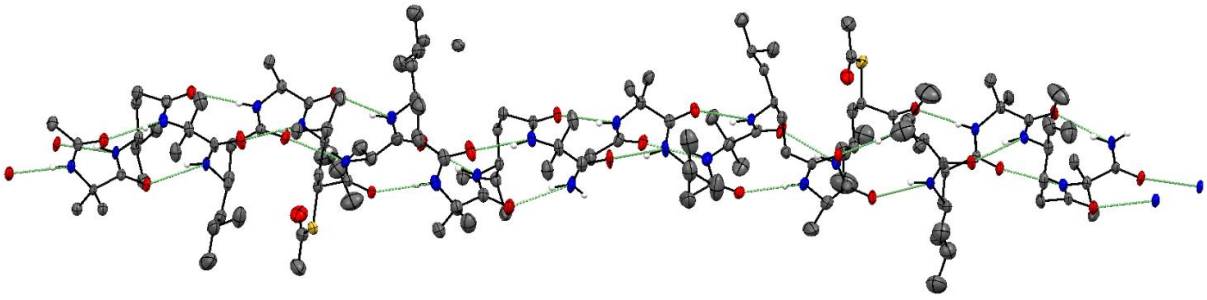


Figure 39: ORTEP diagram of Peptide **P2b** [Ac-Aib-γVal-Aib-γLeu-Ala-γ- *(α -SCOCH$_3$)* Val-Leu-γLeu-Aib-γVal-Aib-CONH$_2$]. H-bonding is represented by dotted lines. The side-chain and backbone H-atoms are not shown for clarity. Ellipsoids are drawn at 50% probability.

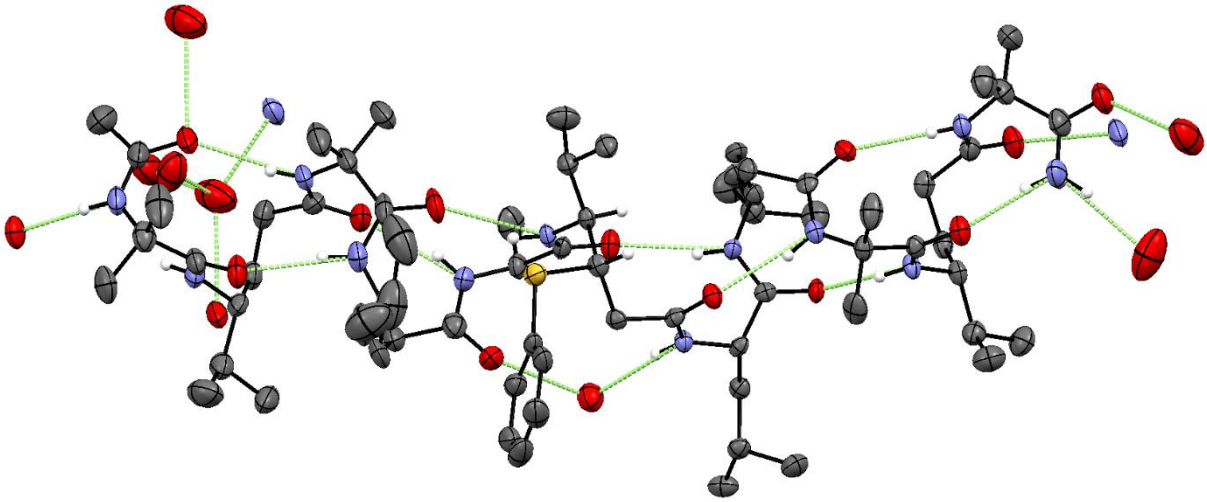


Figure 40: ORTEP diagram of Peptide **P3** [Ac-Aib-*γ*Val-Aib-*γ*Leu-Ala-*γ*- *(β* -*SPh*) Val-Leu-*γ*Leu-Aib-*γ*Val-Aib-$CONH_2$]. H-bonding is represented by dotted lines. The side-chain and backbone H-atoms are not shown for clarity. Ellipsoids are drawn at 50% probability.

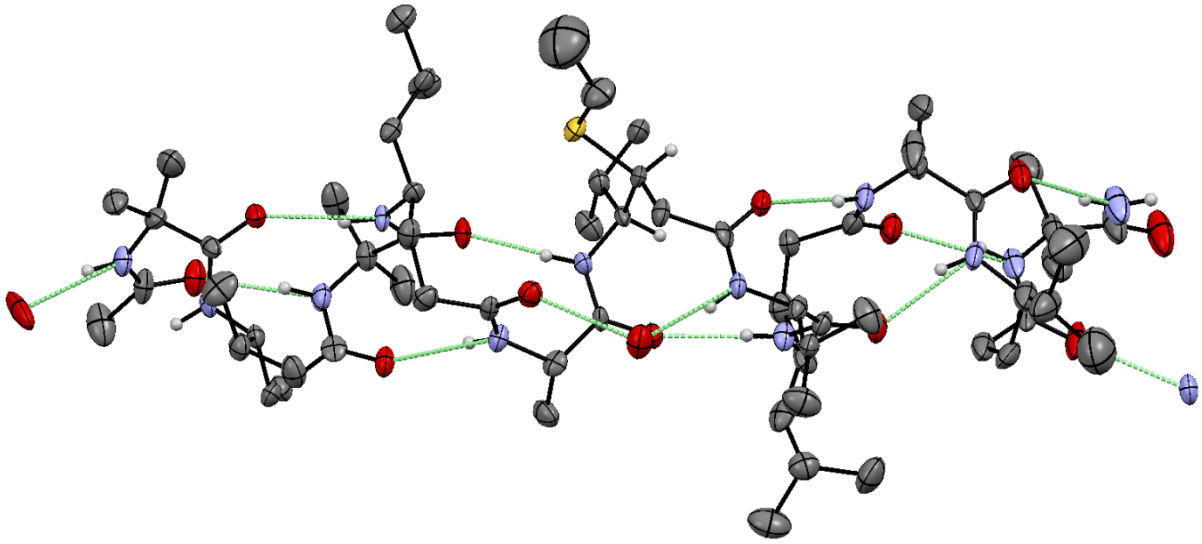


Figure 41: ORTEP diagram of Peptide **P4** [Ac-Aib-*γ*Val-Aib-*γ*Leu-Ala-*γ*- *(β* -SCH_2CH_3) Val-Leu-*γ*Leu-Aib-*γ*Val-Aib-$CONH_2$]. H-bonding is represented by dotted lines. The side-chain and backbone H-atoms are not shown for clarity. Ellipsoids are drawn at 50% probability.

4.7.1.2. Crystallographic information of 7B, 1A, 1C, 2C, 2D, 3C, 4C, 2A'', 5A, P1, P2a, P2b, P3 and P4.

Crystallographic information of 7B: Colourless plate shape Crystals of **7B** were grown by slow evaporation from an aqueous solution of methanol. A good quality single crystal (0.2 × 0.1 × 0.07mm) was mounted on the head of a goniometer using a loop with a small amount of paraffin oil. The X-ray diffraction data of a single crystal were collected at 100K temperature on a Bruker APEX(II) DUO CCD diffractometer using Mo Kα radiation (λ = 0.71073 Å), *ω*-scans (2*θ* = 56.612), for a total of 15866 independent reflections. Space group P 1, a = 5.2206(11), b = 10.011(2), c = 10.968(2), *β* = 78.447(7), V = 534.9(2) $Å^3$, triclinic, Z = 1 for chemical formula $C_{20}H_{29}NO_5S$ with one molecule in asymmetric unit; *ρ* calcd = 1.228 gcm^{-3}, *μ* = 0.180 mm^{-1}, F (000) = 212.0, Rint= 0.0467. The structure was obtained by direct methods using SHELXL-97.[29] The final R value was 0.0476 (wR2 = 0.1169) 4643 observed reflections (*F0* ≥ 4*σ* (|F0|)) and 250 variables, S = 1.050. The largest difference peak and hole were 1.023 and -0.356 $eÅ^3$, respectively.

Crystallographic information of 1C: Colourless block shape Crystals of **1C** were grown by slow evaporation of chloroform and n-heptane solvent system. A good quality single crystal

(0.3 × 0.2 × 0.2mm) was mounted on the head of a goniometer using a loop with a small amount of paraffin oil. The X-ray diffraction data of a single crystal were collected at 100K temperature on a Bruker APEX(II) DUO CCD diffractometer using Mo Kα radiation (λ = 0.71073 Å), *ω*-scans (2*θ* = 41.48), for a total of 4315 independent reflections. Space group P 21 21 21, a = 23.955(3), b = 4.9885(6), c = 20.837(3), *β* = 90, V = 2490.0(6) Å^3, orthorhombic, Z = 4 for chemical formula C_{22} H_{26} N2 O_3 S with one molecule in asymmetric unit; *ρ* calcd = 1.063 gcm^{-3}, *μ* = 0.151mm^{-1}, F (000) = 848.0, Rint= 0.0630. The structure was obtained by direct methods using SHELXL-97.[29] The final R value was 0.0987 (wR2 = 0.2294) 2389 observed reflections (*F0* ≥ 4*σ* (|F0|)) and 321 variables, S = 0.967. The largest difference peak and hole were 0.334 and -0.282 eÅ^3, respectively.

The diffracted single crystal was a small-sized and the quality of diffraction was poor. Several datasets were collected on single crystals from different groups and one of the highest quality is reported herein.

There is some partially occupied solvent molecule also present in the asymmetric unit. A significant amount of time was invested in identifying and refining the disordered molecule. Option SQUEEZE of program PLATON[30] was used to correct the diffraction data for diffuse scattering effects and to remove the contributions of the disordered solvent molecules from the structure factors. PLATON calculated the upper limit of volume that can be occupied by the solvent to be 511 Å^3 of the unit cell volume. The program calculated 179 electrons in the unit cell for the diffuse species. No data are given for the diffusely scattering species. Outputs of the SQUEEZE report are appended in CIF file **1C**.

Crystallographic information of 2A: Colourless cubic shape Crystals of **2A** were grown by slow evaporation from an aqueous solution of methanol. A good quality single crystal (0.1 × 0.08 × 0.05mm) was mounted on the head of a goniometer using a loop with a small amount of paraffin oil. The X-ray diffraction data of a single crystal were collected at 100K temperature on a Bruker APEX(II) DUO CCD diffractometer using Mo Kα radiation (λ = 0.71073 Å), *ω*-scans (2*θ* = 56.874), for a total of 23048 independent reflections. Space group P 1, a = 8.592(5), b = 10.288(6), c = 13.693(9), *β* = 80.183(16), V = 1131.4(12) Å^3, triclinic, Z = 2 for chemical formula C_{21} H_{32} N_2 O_4 S with two molecules in asymmetric unit; *ρ* calcd = 1.199 gcm^{-3}, *μ* = 0.170 mm^{-1}, F (000) = 440.0, Rint= 0.1237. The structure was obtained by direct methods using SHELXL-97.[29] The final R value was 0.0658 (wR2 = 0.1084) 9503 observed reflections (*F0* ≥

4σ (|F0|)) and 518 variables, S = 1.032. The largest difference peak and hole were 0.304 and -0.261 eÅ^3, respectively.

Crystallographic information of 2C: Colourless needle shape Crystals of **2C** were grown by slow evaporation from an aqueous solution of methanol. A good quality single crystal (0.1 × 0.02 × 0.02 mm) was mounted on the head of a goniometer using a loop with a small amount of paraffin oil. The X-ray diffraction data of a single crystal were collected at 100K temperature on a Bruker APEX(II) DUO CCD diffractometer using Mo Kα radiation (λ = 0.71073 Å), ω-scans (2θ = 56.438), for a total of 25037 independent reflections. Space group P 21 21 21, a = 4.9952(4), b = 20.2046(16), c = 22.2560(19), β = 90, V = 2246.2(3) Å^3, orthorhombic, Z = 4 for chemical formula $C_{21}H_{32}N_2O_4S$ with one molecule in asymmetric unit; ρ calcd = 1.208 gcm^{-3}, μ = 0.171 mm^{-1}, F (000) = 880.0, Rint= 0.0972. The structure was obtained by direct methods using SHELXL-97.[29] The final R value was 0.0565 (wR2 = 0.0831) 5533 observed reflections ($F0 \geq 4\sigma$ (|F0|)) and 260 variables, S = 1.043. The largest difference peak and hole were 0.270 and -0.281eÅ^3, respectively.

Crystallographic information of 2D: Colourless needle shape Crystals of **2D** were grown by slow evaporation from an aqueous solution of methanol. A good quality single crystal (0.15 × 0.025 × 0.012 mm) was mounted on the head of a goniometer using a loop with a small amount of paraffin oil. The X-ray diffraction data of a single crystal were collected at 100K temperature on a Bruker APEX(II) DUO CCD diffractometer using Mo Kα radiation (λ = 0.71073 Å), ω-scans (2θ = 34.992), for a total of 6028 independent reflections. Space group P 21 21 2, a = 19.237(3), b = 44.765(7), c = 5.1536(8), β = 90, V = 4437.9(12) Å^3, orthorhombic, Z = 8 for chemical formula $C_{21}H_{32}N_2O_4S$ with two molecules in asymmetric unit; ρ calcd = 1.223 gcm^{-3}, μ = 0.174 mm^{-1}, F (000) = 1760.0, Rint= 0.0832. The structure was obtained by direct methods using SHELXL-97.[29] The final R value was 0.1000 (wR2 = 0.2186) 2673 observed reflections ($F0 \geq 4\sigma$ (|F0|)) and 548 variables, S = 1.032. The largest difference peak and hole were 0.461 and -0.304 eÅ^3, respectively.

Crystallographic information of 3C: Colourless spherulites shape Crystals of **3C** were grown by slow evaporation from an aqueous solution of methanol. A good quality single crystal (0.03 × 0.02 × 0.01 mm) was mounted on the head of a goniometer using a loop with a small amount of paraffin oil. The X-ray diffraction data of a single crystal were collected at 100K temperature on a Bruker APEX(II) DUO CCD diffractometer using Mo Kα radiation (λ = 0.71073 Å), ω-scans (2θ = 47.994), for a total of 9509 independent reflections. Space group C 2, a = 40.942(4),

b = 5.1243(5), c = 9.7473(10), β = 100.178(4), V = 2012.8(4) Å^3, monoclinic, Z = 4 for chemical formula $C_{19}H_{28}N_2O_4S$ with one molecule in asymmetric unit; ρ calcd = 1.256 gcm^{-3}, μ = 0.186 mm^{-1}, F (000) = 816.0, Rint= 0.0697. The structure was obtained by direct methods using SHELXL-97.[29] The final R value was 0.0715 (wR2 = 0.1557) 3122 observed reflections ($F0 \geq 4\sigma$ (|F0|)) and 265 variables, S = 0.998. The largest difference peak and hole were 1.203 and -0.265 eÅ^3, respectively.

Crystallographic information of 4C: Colourless plate shape Crystals of **4C** were grown by slow evaporation from an aqueous solution of methanol. A good quality single crystal (0.05 × 0.03 × 0.01 mm) was mounted on the head of a goniometer using a loop with a small amount of paraffin oil. The X-ray diffraction data of a single crystal were collected at 100K temperature on a Bruker APEX(II) DUO CCD diffractometer using Mo Kα radiation (λ = 0.71073 Å), ω-scans (2θ = 46.09), for a total of 31773 independent reflections. Space group P 21, a = 21.503(5), b = 5.0700(13), c = 22.072(5), β = 104.278(8), V = 2332.0(10) Å^3, monoclinic, Z = 4 for chemical formula $C_{22}H_{34}N_2O_4S$ with two molecules in asymmetric unit; ρ calcd = 1.204 gcm^{-3}, μ = 0.167 mm^{-1}, F (000) = 912.0, Rint= 0.0611. The structure was obtained by direct methods using SHELXL-97.[29] The final R value was 0.0998 (wR2 = 0.2441) 6533 observed reflections ($F0 \geq 4\sigma$ (|F0|)) and 524 variables, S = 1.002. The largest difference peak and hole were 1.660 and -0.932 eÅ^3, respectively.

Crystallographic information of 5A: Colourless plate shape Crystals of **5A** were grown by slow evaporation from an aqueous solution of methanol. A good quality single crystal (0.07 × 0.06 × 0.05 mm) was mounted on the head of a goniometer using a loop with a small amount of paraffin oil. The X-ray diffraction data of a single crystal were collected at 100K temperature on a Bruker APEX(II) DUO CCD diffractometer using Mo Kα radiation (λ = 0.71073 Å), ω-scans (2θ = 57.16), for a total of 108483 independent reflections. Space group P b c n, a = 37.951(6), b = 12.621(2), c = 8.9556(14), β = 90, V = 4289.6(12) Å^3, orthorhombic, Z = 4 for chemical formula 2(C20 H30 N2 O4 S), O with one molecule in asymmetric unit; ρ calcd = 1.247 gcm^{-3}, μ = 0.180 mm^{-1}, F (000) = 1728.0, Rint= 0.1765. The structure was obtained by direct methods using SHELXL-97.[29] The final R value was 0.0591 (wR2 = 0.1098) 5420 observed reflections ($F0 \geq 4\sigma$ (|F0|)) and 256 variables, S = 1.046. The largest difference peak and hole were 0.722 and -0.427 eÅ^3, respectively.

Crystallographic information of P1: Colourless plate shape Crystals of **P1** were grown by slow evaporation from the aqueous solution of methanol. A good quality single crystal (0.25 ×

0.12 × 0.1 mm) was mounted on the head of a goniometer using a loop with a small amount of paraffin oil. The X-ray diffraction data of a single crystal were collected at 100K temperature on a Bruker APEX(II) DUO CCD diffractometer using Mo Kα radiation (λ = 0.71073 Å), *ω*-scans (2*θ* = 56.65), for a total of 43572 independent reflections. Space group P 21, a = 14.637(8), b = 19.378(9), c = 16.197(7), *β* = 104.947(16), V = 4439(4) Å^3, Monoclinic, Z = 2 for chemical formula C_{64} H_{116} N_{12} O_{12}, C H_4 O with one methanol molecule in asymmetric unit; *ρ* calcd = 0.956 gcm^{-3}, *μ* = 0.067mm^{-1}, F (000) = 1396, Rint= 0.0384. The crystal structure was solved by direct methods using SHELXL-97.[4] The final R value was 0.0531 (wR2 = 0.1158) 21737 observed reflections (*F0* ≥ 4*σ* (|F0|)) and 837 variables, S = 1.053. The largest difference peak and hole were 0.442 and -0.275 eÅ^3, respectively.

There is some partially occupied solvent molecule also present in the asymmetric unit. A significant amount of time was invested in identifying and refining the disordered molecule. The solvent masks option in program Olex2-1.2[6] serves as an alternative to SQUEEZE which is implemented in PLATON[5]. The solvent masks option in program Olex2-1.2[6] was used to correct the diffraction data for diffuse scattering effects and to remove the contributions of the disordered solvent molecules from the structure factors. The Olex2-solvent mask calculated the upper limit of volume that can be occupied by the solvent to be 1193 Å^3, or 26.9% of the unit cell volume. The program calculated 159 electrons in the unit cell for the diffuse species. No data are given for the diffusely scattering species. Outputs of the Olex2-solvent mask (SQUEEZE) report are appended in CIF file **P1**.

Crystallographic information of P2a: Colourless plate shape Crystals of **P2a** were grown by slow evaporation from the aqueous solution of methanol. A good quality single crystal (0.04 × 0.02 × 0.01 mm) was mounted on the head of a goniometer using a loop with a small amount of paraffin oil. The X-ray diffraction data of a single crystal were collected at 100K temperature on a Bruker APEX(II) DUO CCD diffractometer using Mo Kα radiation (λ = 0.71073 Å), *ω*-scans (2*θ* = 47.998), for a total of 238061 independent reflections. Space group P 21 21 21, a = 9.0575(13), b = 18.075(3), c = 48.440(7), *β* = 90, V = 7930.3(19) Å^3, orthorhombic, Z = 4 for chemical formula C_{66} H_{120} N_{12} O_{13}, S with one molecule in asymmetric unit; *ρ* calcd = 1.107 gcm^{-3}, *μ* = 0.102 mm^{-1}, F (000) = 2880.0, Rint= 0.0749. The crystal structure was solved by direct methods using SHELXL-97.[29] The final R value was 0.1961 (wR2 = 0.5056) 12461 observed reflections (*F0* ≥ 4*σ* (|F0|)) and 853 variables, S = 2.707. The largest difference peak and hole were 7.341 and -1.509 eÅ^3, respectively.

The diffracted single crystal was a small-sized and the quality of diffraction was poor. Several datasets were collected on single crystals from different groups and one of the highest quality is reported herein.

There is some partially occupied solvent molecule also present in the asymmetric unit. A significant amount of time was invested in identifying and refining the disordered molecule. Option SQUEEZE of program PLATON[30] was used to correct the diffraction data for diffuse scattering effects and to remove the contributions of the disordered solvent molecules from the structure factors. PLATON calculated the upper limit of volume that can be occupied by the solvent to be 834 $Å^3$ of the unit cell volume. The program calculated 206 electrons in the unit cell for the diffuse species. No data are given for the diffusely scattering species. Outputs of the SQUEEZE report are appended in CIF file **P2a**.

Crystallographic information of P2b: Colourless block shape Crystals of **P2b** were grown by slow evaporation from the aqueous solution of methanol. A good quality single crystal (0.12 × 0.10 × 0.08 mm) was mounted on the head of a goniometer using a loop with a small amount of paraffin oil. The X-ray diffraction data of a single crystal were collected at 100K temperature on a Bruker APEX(II) DUO CCD diffractometer using Mo Kα radiation (λ = 0.71073 Å), ω-scans (2θ = 52.884), for a total of 357153 independent reflections. Space group P 21, a = 12.285(2), b = 17.804(3), c = 37.493(6), β = 99.245(6), V = 8094(2) $Å^3$, monoclinic, Z = 4 for chemical formula C_{66} H_{120} N_{12} O_{13}, S with two molecules in asymmetric unit; ρ calcd = 1.085 gcm^{-3}, μ = 0.100 mm^{-1}, F (000) = 2880.0, Rint= 0.1243. The crystal structure was solved by direct methods using SHELXL-97.[29] The final R value was 0.0813 (wR2 = 0.2139) 33225 observed reflections ($F0 \geq 4\sigma$ (|F0|)) and 1732 variables, S = 1.119. The largest difference peak and hole were 1.112 and -0.434 $eÅ^3$, respectively.

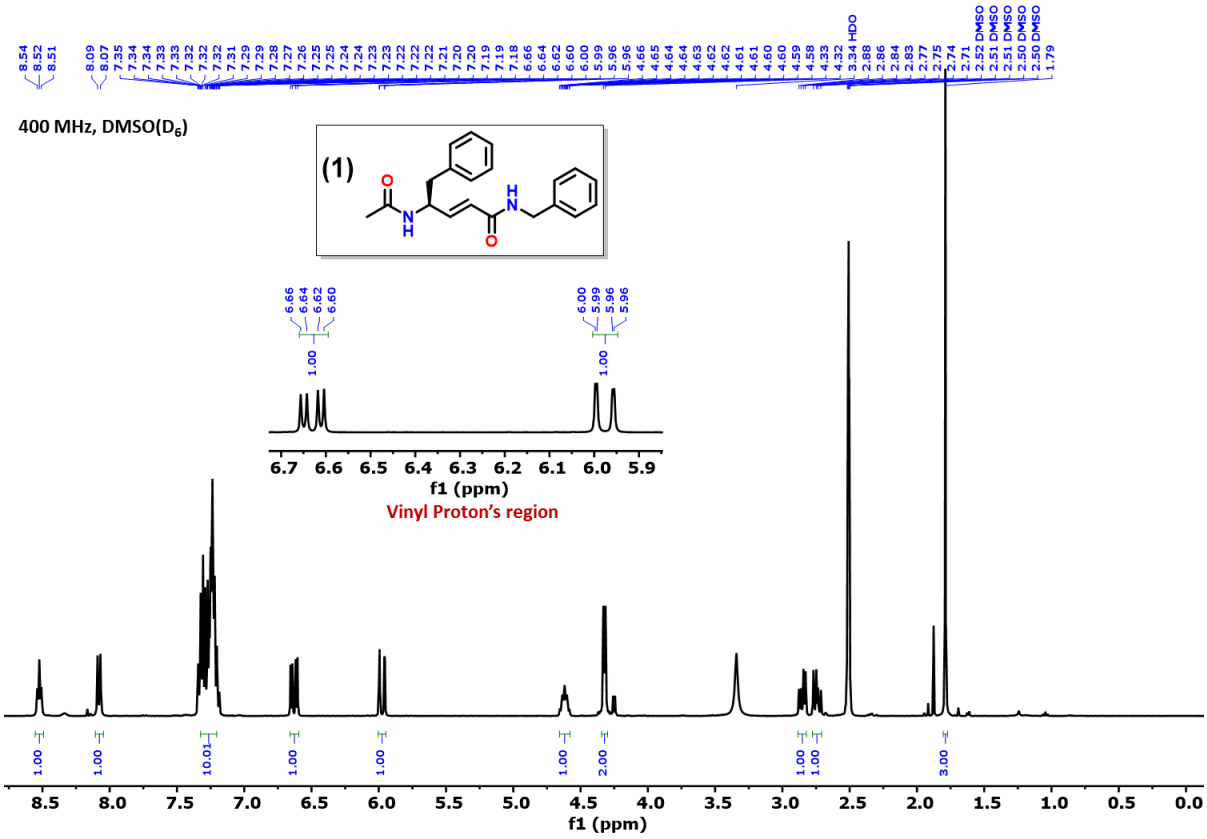
There is some partially occupied solvent molecule also present in the asymmetric unit. A significant amount of time was invested in identifying and refining the disordered molecule. Option SQUEEZE of program PLATON[30] was used to correct the diffraction data for diffuse scattering effects and to remove the contributions of the disordered solvent molecules from the structure factors. PLATON calculated the upper limit of volume that can be occupied by the solvent to be 938 $Å^3$ of the unit cell volume. The program calculated 489 electrons in the unit cell for the diffuse species. No data are given for the diffusely scattering species. Outputs of the SQUEEZE report are appended in CIF file **P2b**.

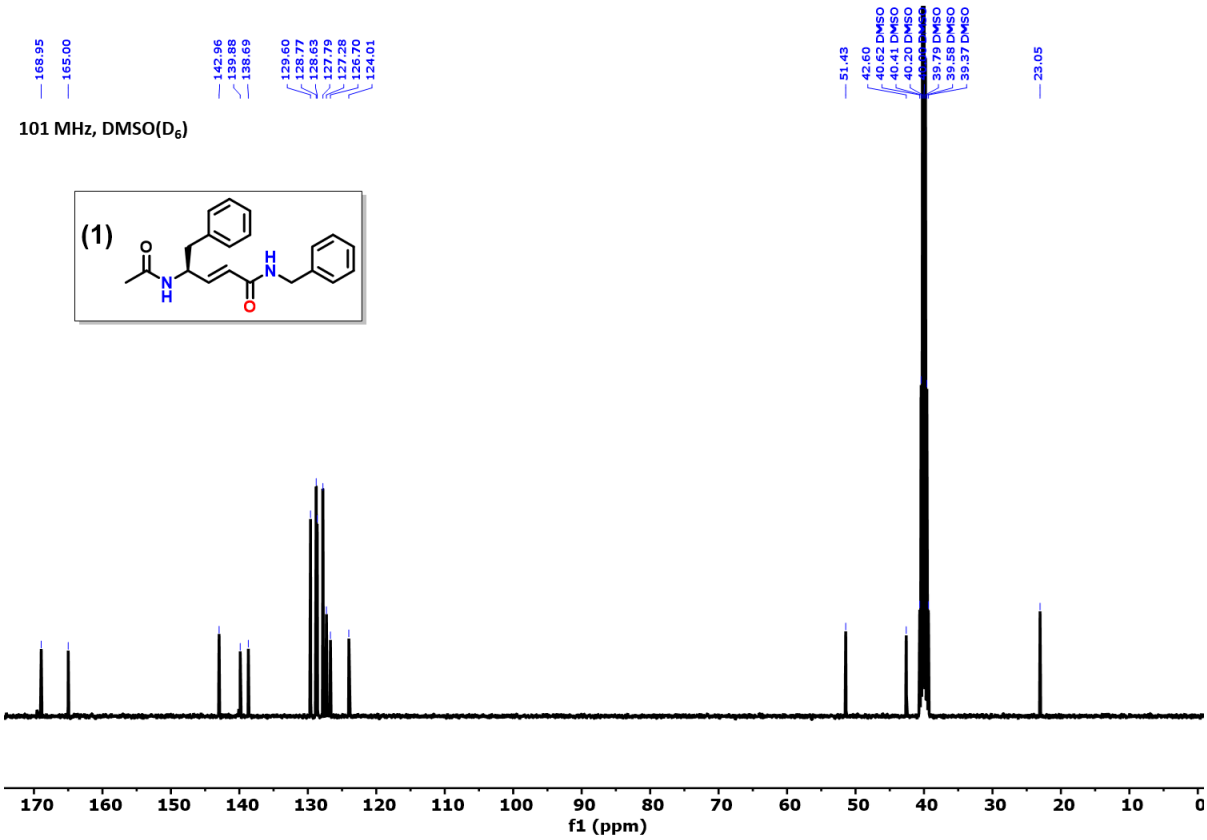
Crystallographic information of P3: Colourless plate shape Crystals of **P3** were grown by slow evaporation from the aqueous solution of methanol. A good quality single crystal (0.6 × 0.4 × 0.2 mm) was mounted on the head of a goniometer using a loop with a small amount of paraffin oil. The X-ray diffraction data of a single crystal were collected at 100K temperature on a Bruker APEX(II) DUO CCD diffractometer using Mo Kα radiation (λ = 0.71073 Å), *ω*-scans (2*θ* = 56.68), for a total of 207565 independent reflections. Space group P 21 21 21, a = 8.782(4), b = 19.400(8), c = 48.35(2), *β* = 90, V = 8239(6) Å^3, monoclinic, Z = 4 for chemical formula 'C_{70} H_{122} N_{12} O_{12}, S, 3(O)' with one molecule in asymmetric unit; *ρ* calcd = 1.132 gcm^{-3}, *μ* = 0.104 mm^{-1}, F (000) = 3048.0, Rint= 0.1522. The crystal structure was solved by direct methods using SHELXL-97.[29] The final R value was 0.0906 (wR2 = 0.1827) 20089 observed reflections (*F0* ≥ 4*σ* (|F0|)) and 906 variables, S = 1.057. The largest difference peak and hole were 0.851 and -0.304 eÅ^3, respectively.

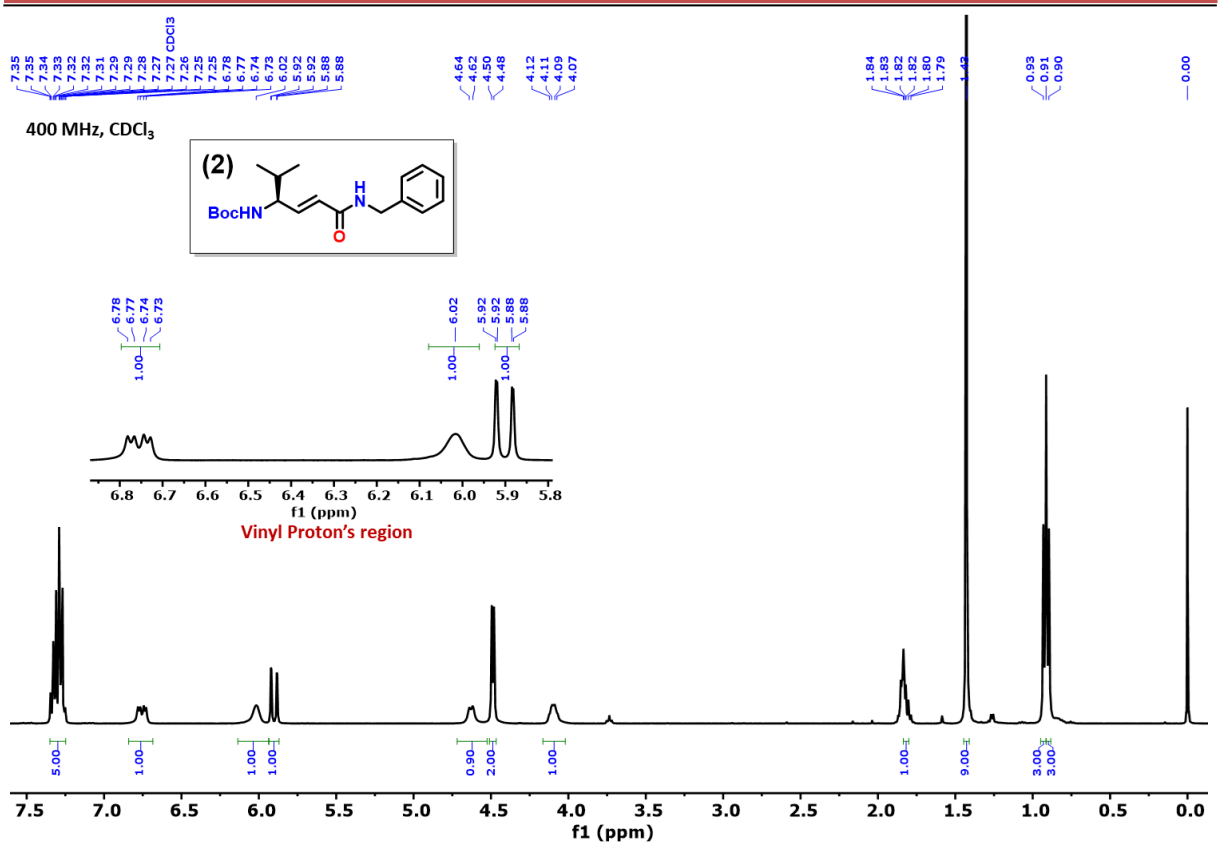
Crystallographic information of P4: Colourless plate shape Crystals of **P4** were grown by slow evaporation from the aqueous solution of methanol. A good quality single crystal (0.08 × 0.05 × 0.03 mm) was mounted on the head of a goniometer using a loop with a small amount of paraffin oil. The X-ray diffraction data of a single crystal were collected at 100K temperature on a Bruker APEX(II) DUO CCD diffractometer using Mo Kα radiation (λ = 0.71073 Å), *ω*-scans (2*θ* = 48.3), for a total of 48524 independent reflections. Space group P 21 21 21, a = 9.0676(10), b = 18.507(2), c = 48.002(6), *β* = 90, V = 8055.6(16) Å^3, orthorhombic, Z = 4 for chemical formula 'C_{66} H_{122} N_{12} O_{12}, S, O' with one molecule in asymmetric unit; *ρ* calcd = 1.092 gcm^{-3}, *μ* = 0.101 mm^{-1}, F (000) = 2888.0, Rint= 0.0918. The crystal structure was solved by direct methods using SHELXL-97.[29] The final R value was 0.0751 (wR2 = 0.1785) 12106 observed reflections (*F0* ≥ 4*σ* (|F0|)) and 853 variables, S = 1.052. The largest difference peak and hole were 0.825 and -0.335 eÅ^3, respectively.

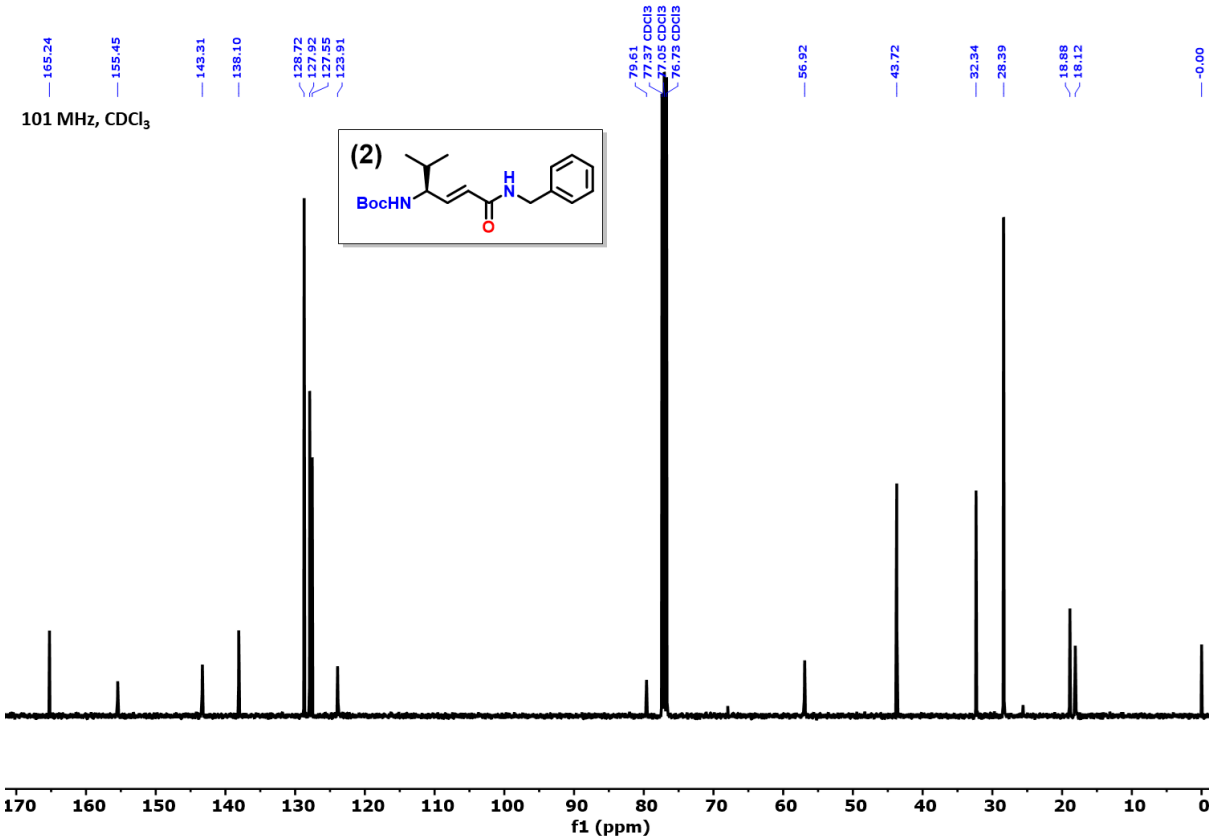
There is some partially occupied solvent molecule also present in the asymmetric unit. A significant amount of time was invested in identifying and refining the disordered molecule. Option SQUEEZE of program PLATON[30] was used to correct the diffraction data for diffuse scattering effects and to remove the contributions of the disordered solvent molecules from the structure factors. PLATON calculated the upper limit of volume that can be occupied by the solvent to be 733 Å^3 of the unit cell volume. The program calculated 170 electrons in the unit cell for the diffuse species. No data are given for the diffusely scattering species. Outputs of the SQUEEZE report are appended in CIF file **P4**.

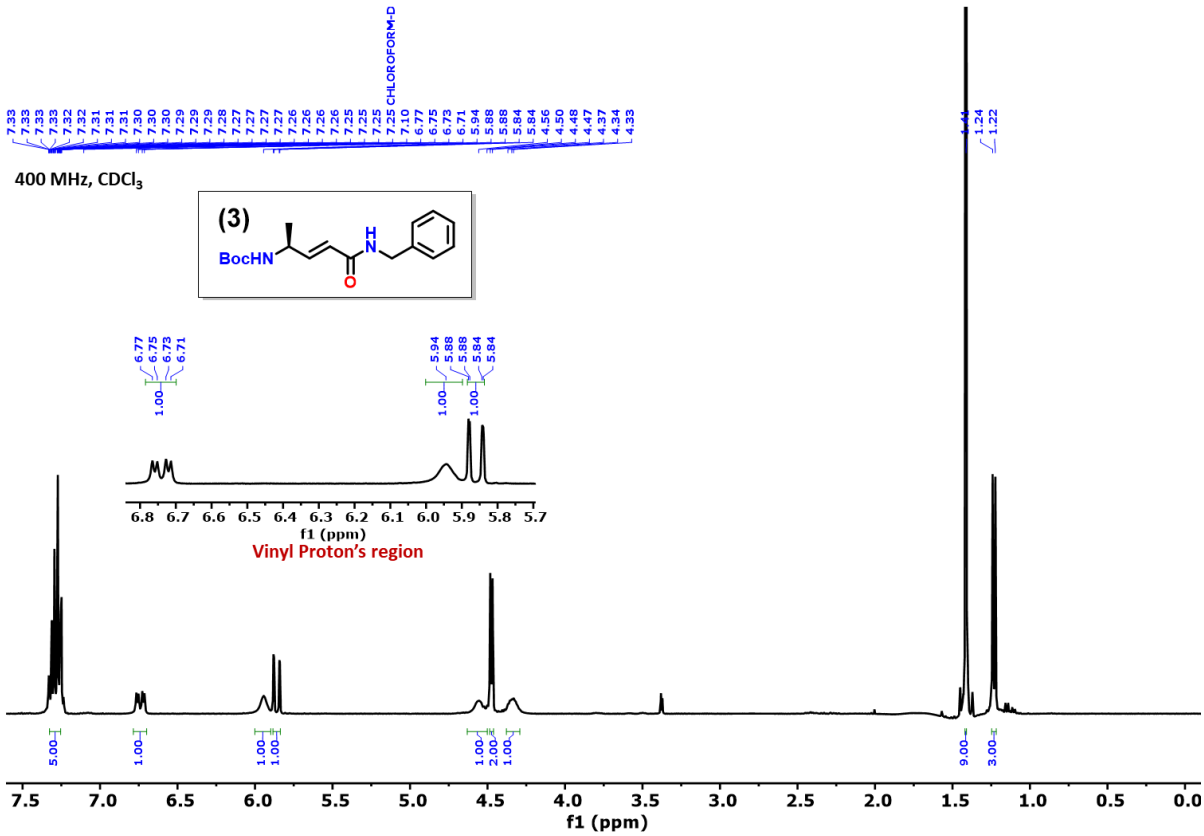
4.7.2. ^{1}H NMR, ^{13}C NMR, HRMS and MALDI spectra of all compounds and peptides

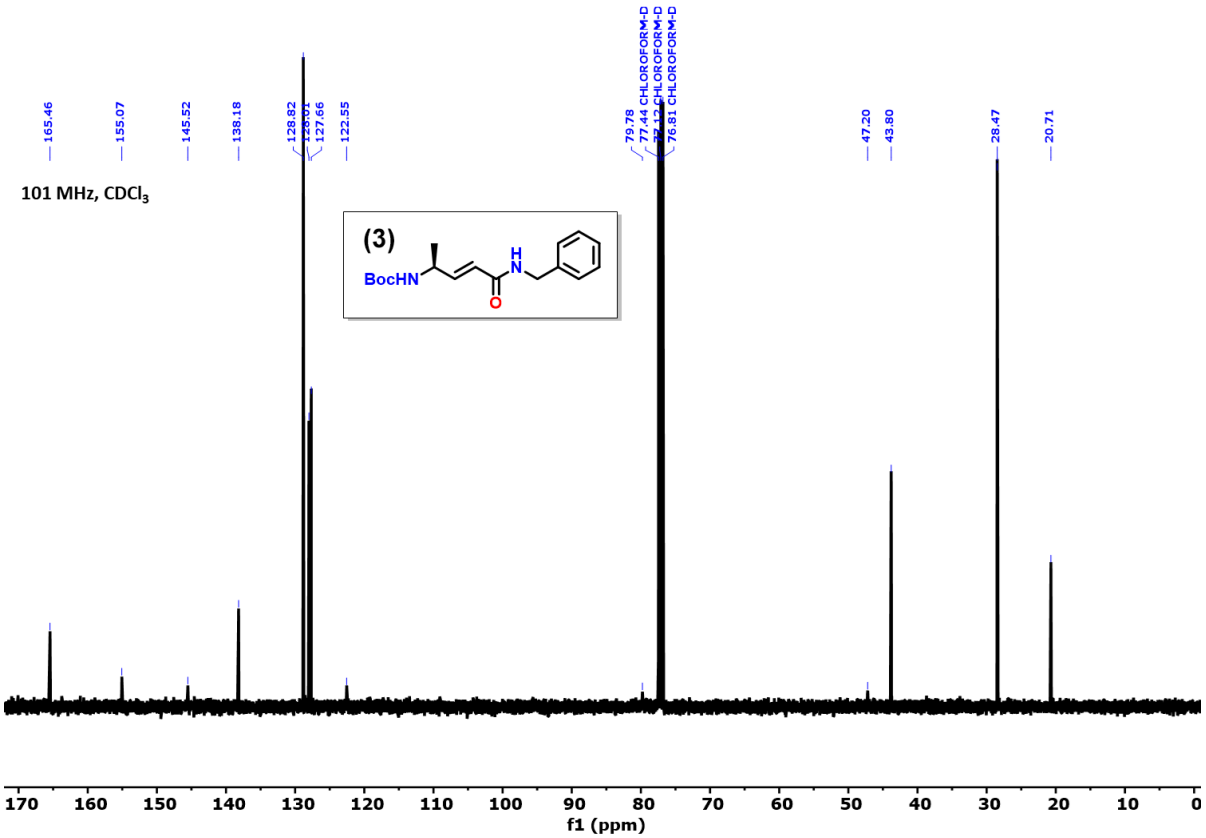


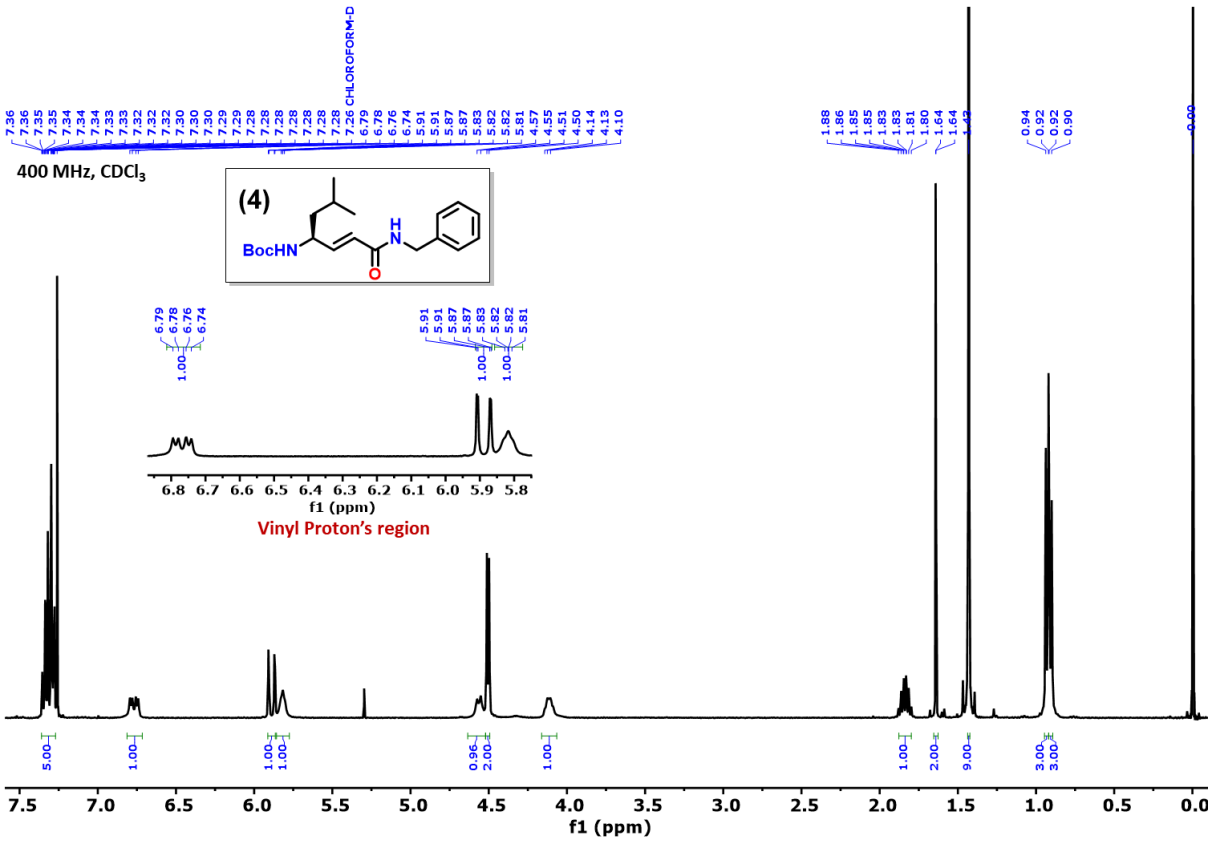


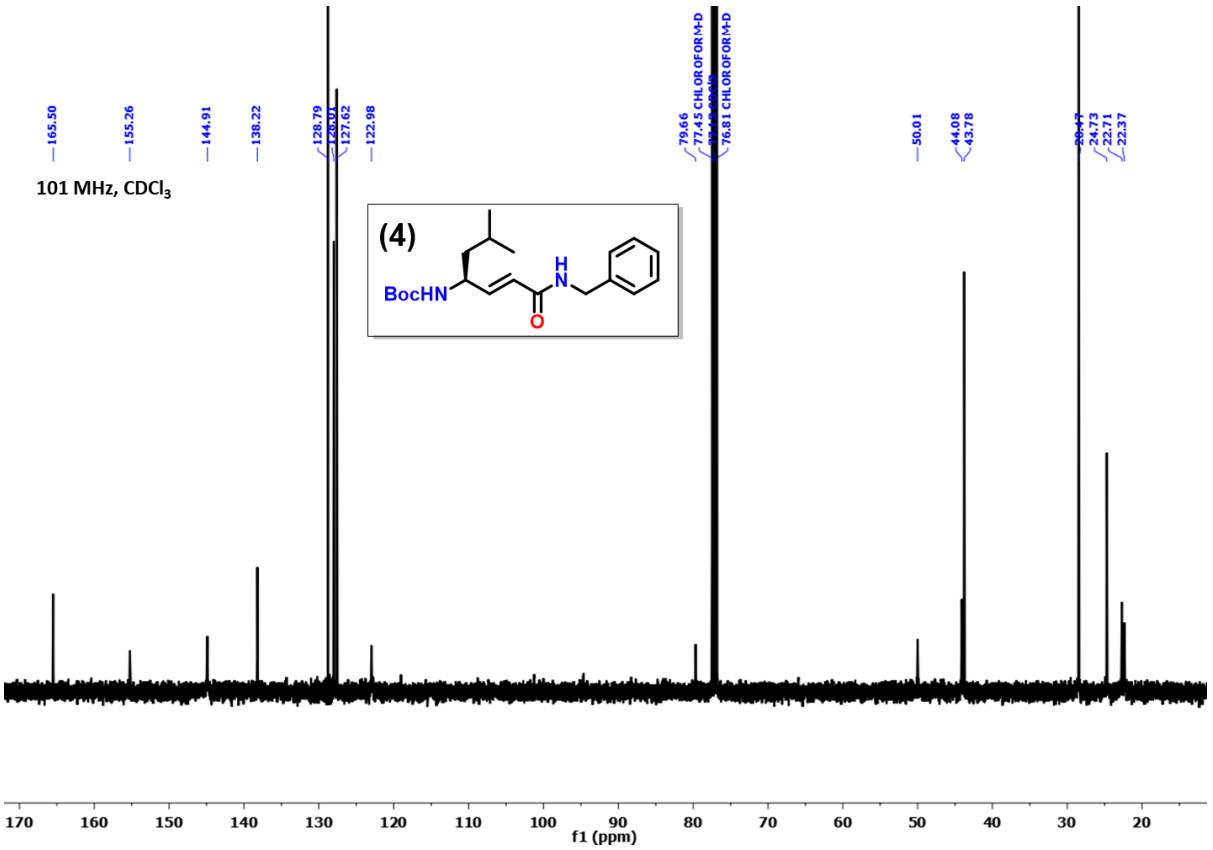

400 MHz, CDCl3
(2)
BocHN
H
N
O
Vinyl Proton's region
f1 (ppm)

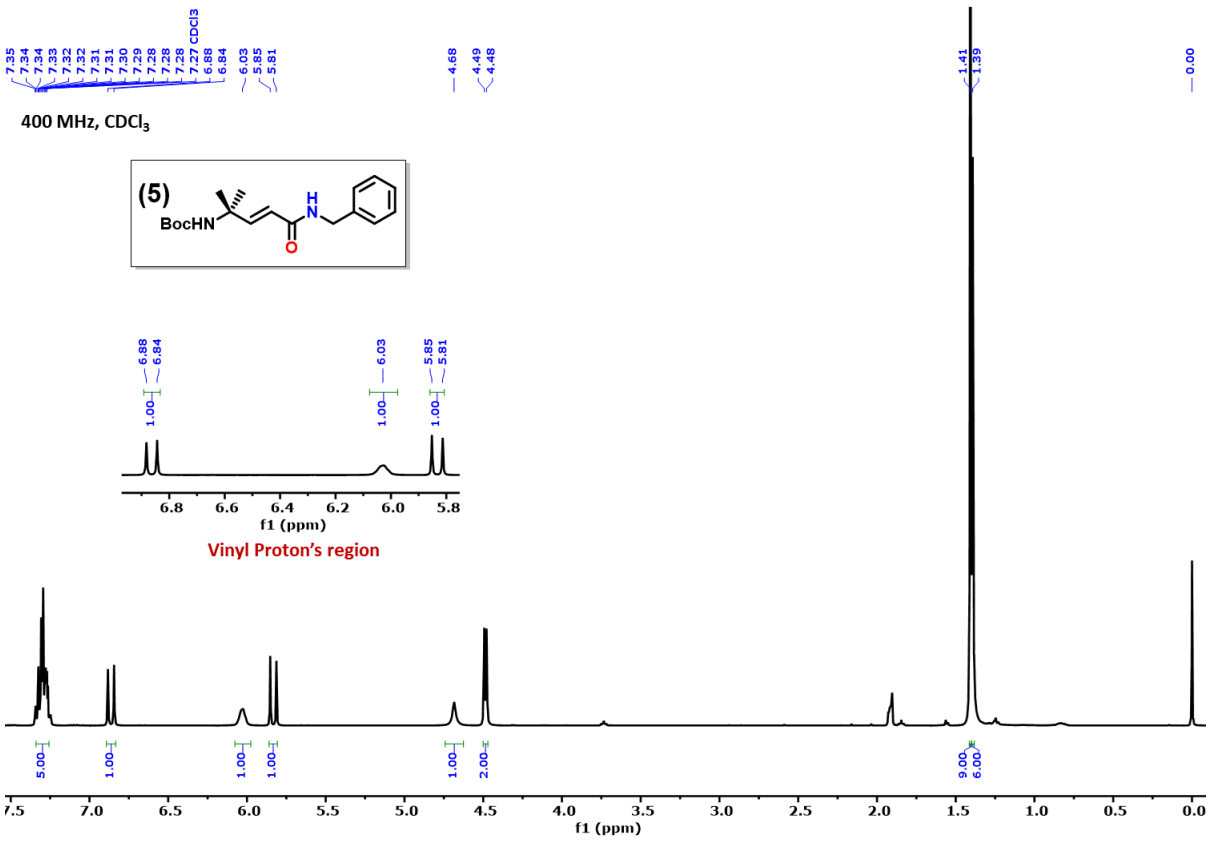

101 MHz, CDCl3
(2)
BocHN
H
N
O
f1 (ppm)

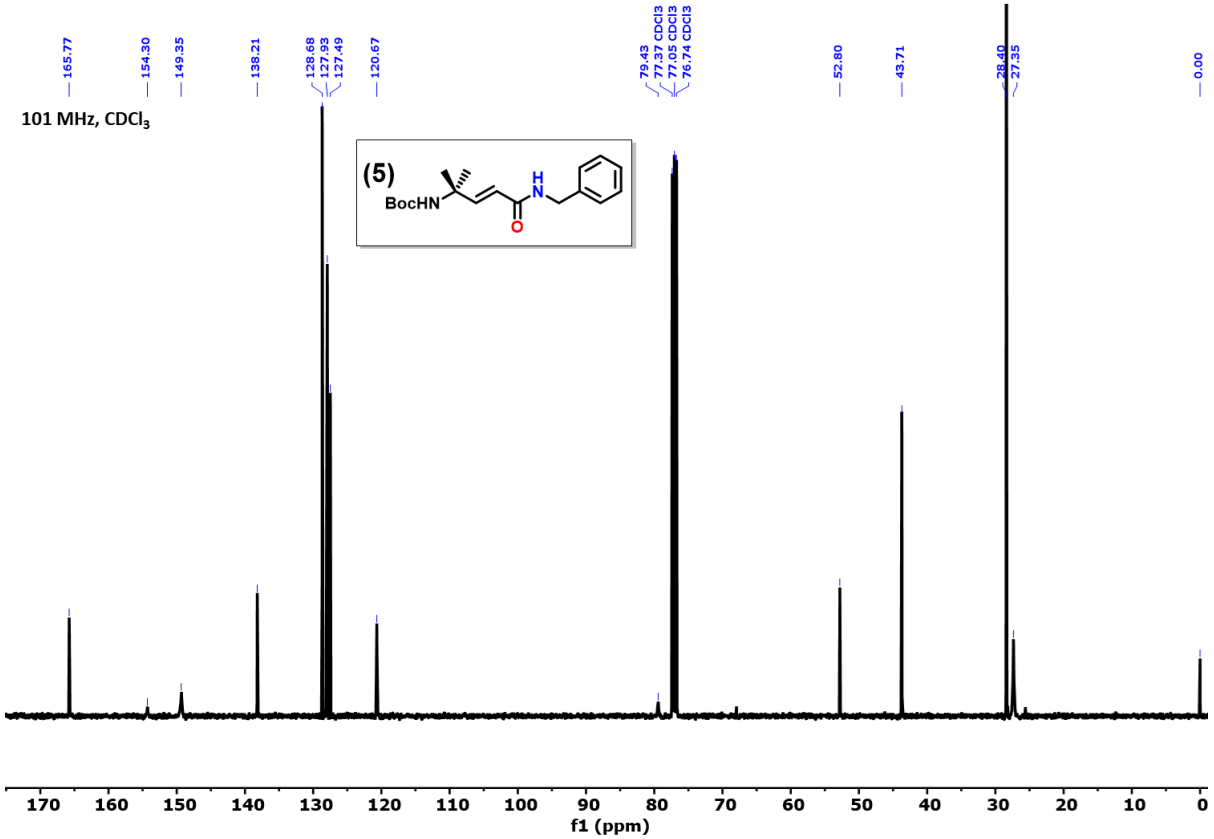

400 MHz, CDCl3
(3)
BocHN
Vinyl Proton's region
f1 (ppm)

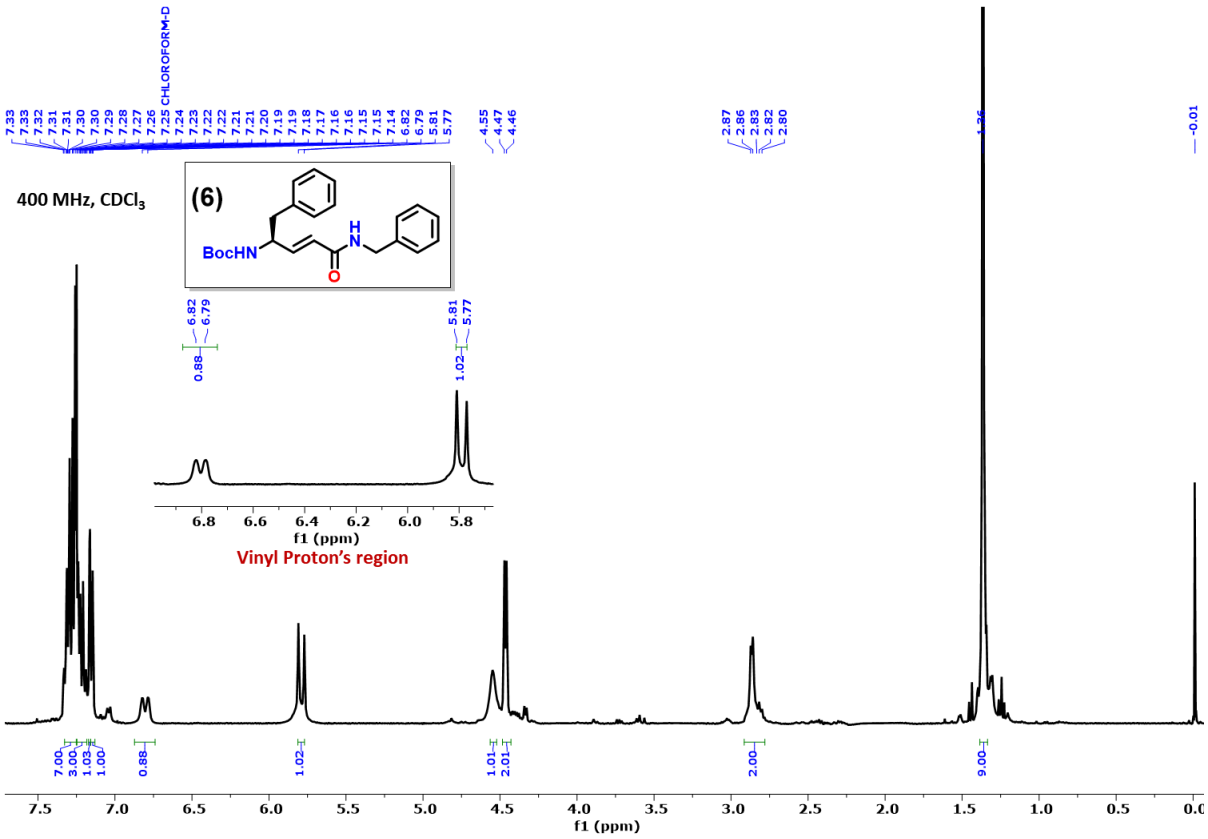

101 MHz, CDCl3
(3)
BocHN
f1 (ppm)

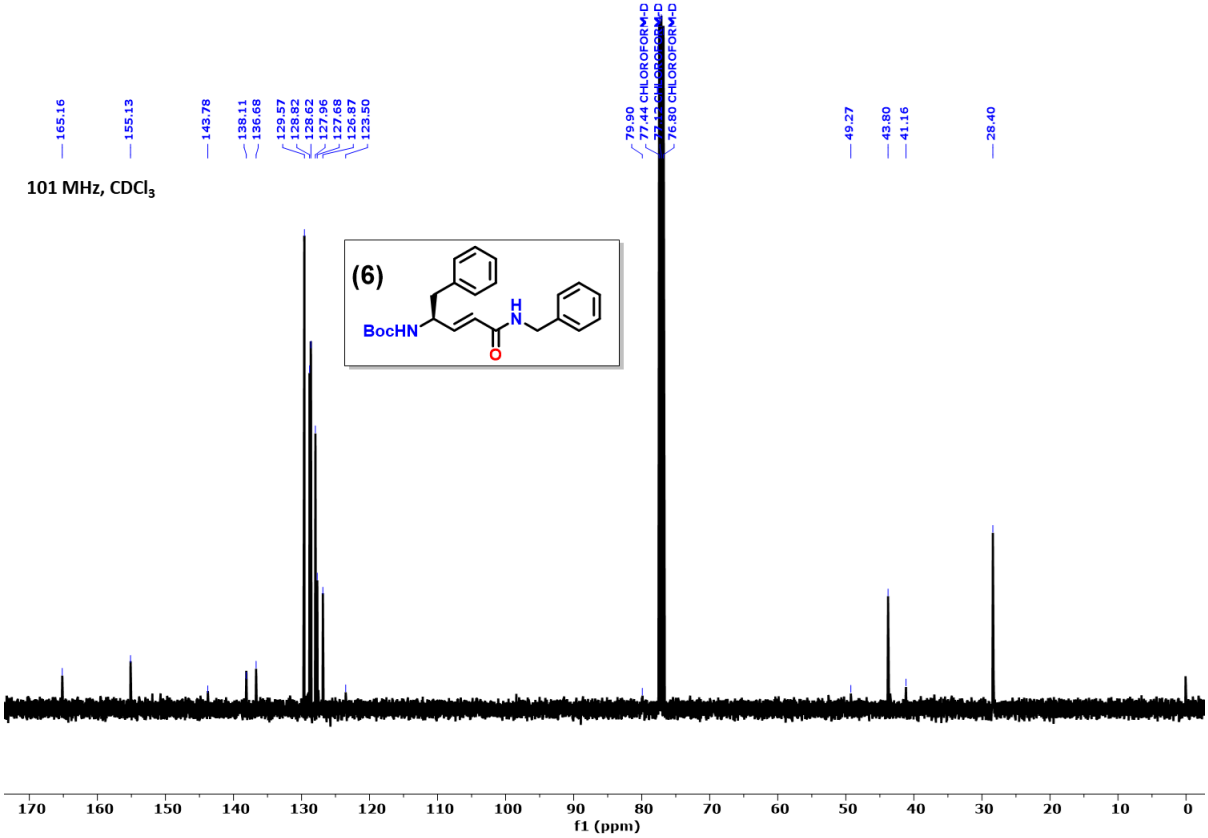

400 MHz, CDCl3
(4)
BocHN
H
N
O
Vinyl Proton's region
f1 (ppm)

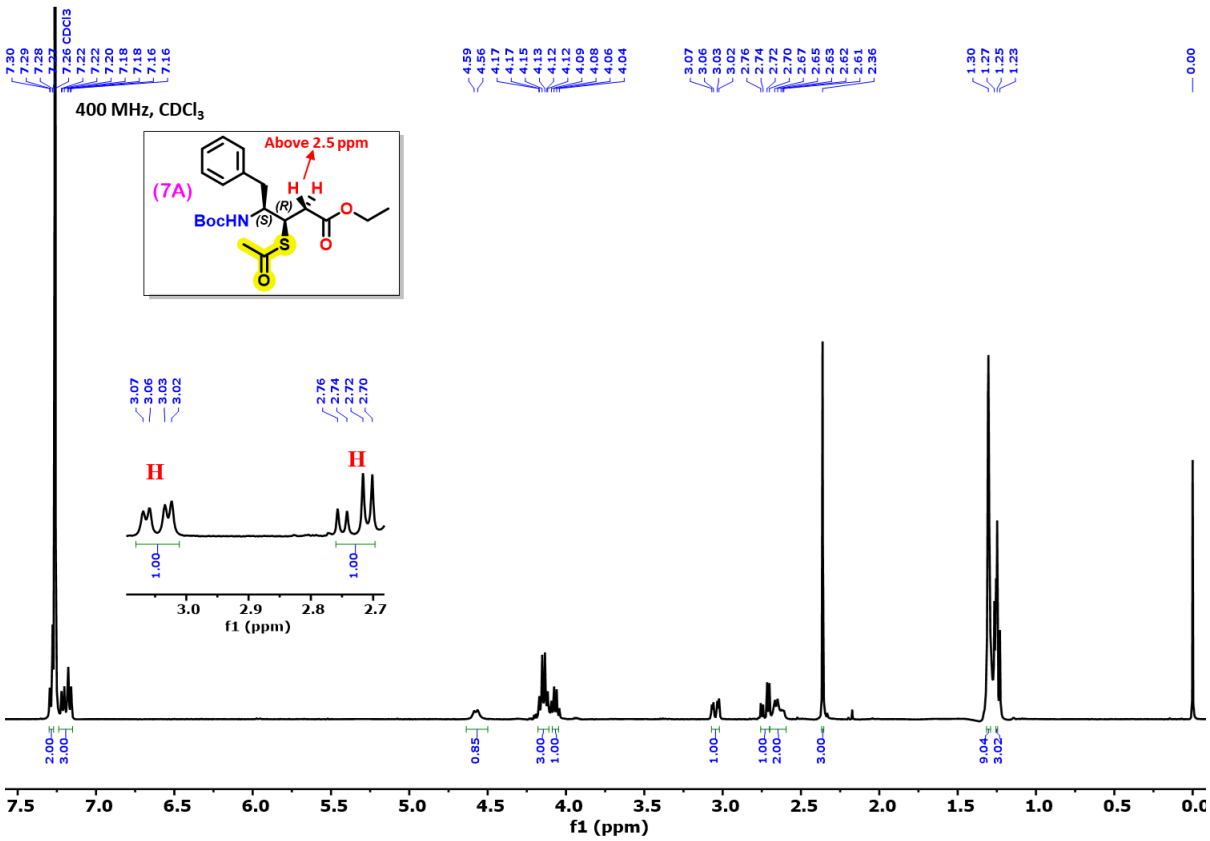

101 MHz, CDCl3
(4)
BocHN
H
N
O
f1 (ppm)

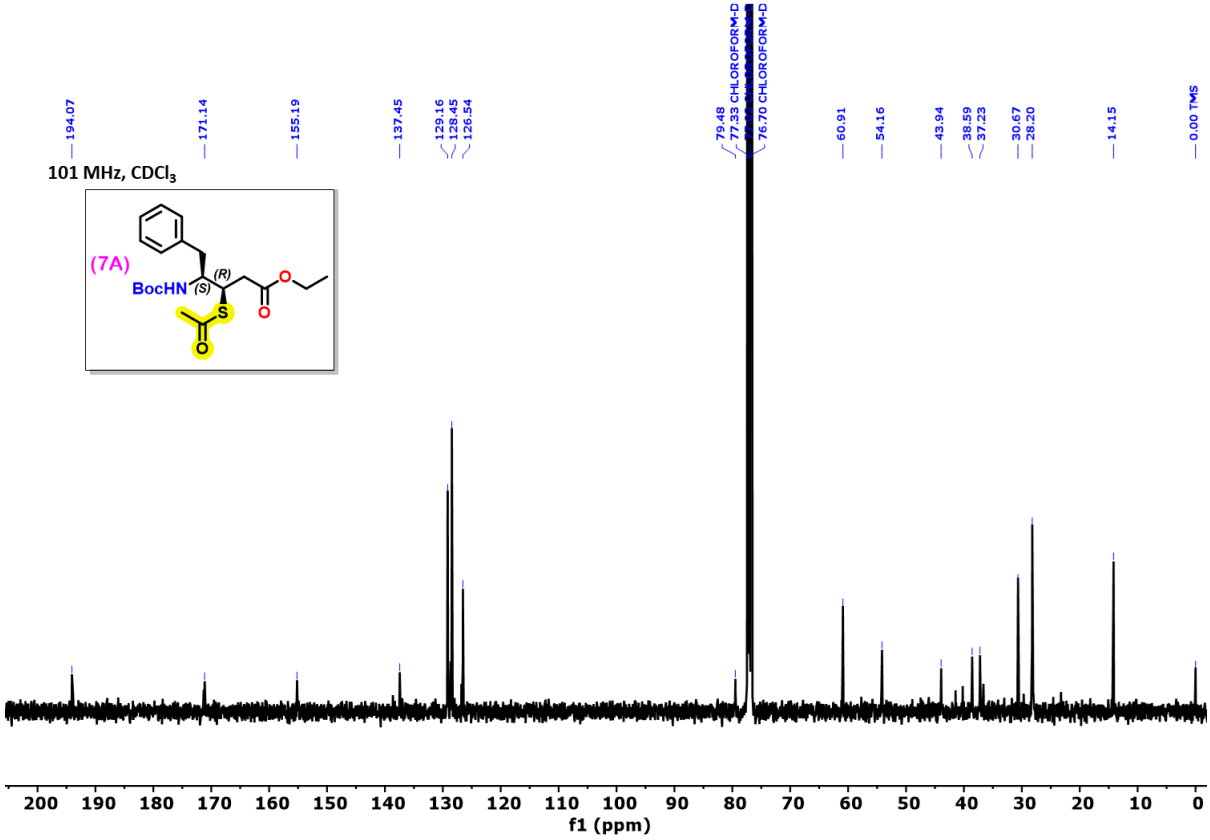

400 MHz, CDCl3
(5)
BocHN
H
N
O
Vinyl Proton's region
f1 (ppm)

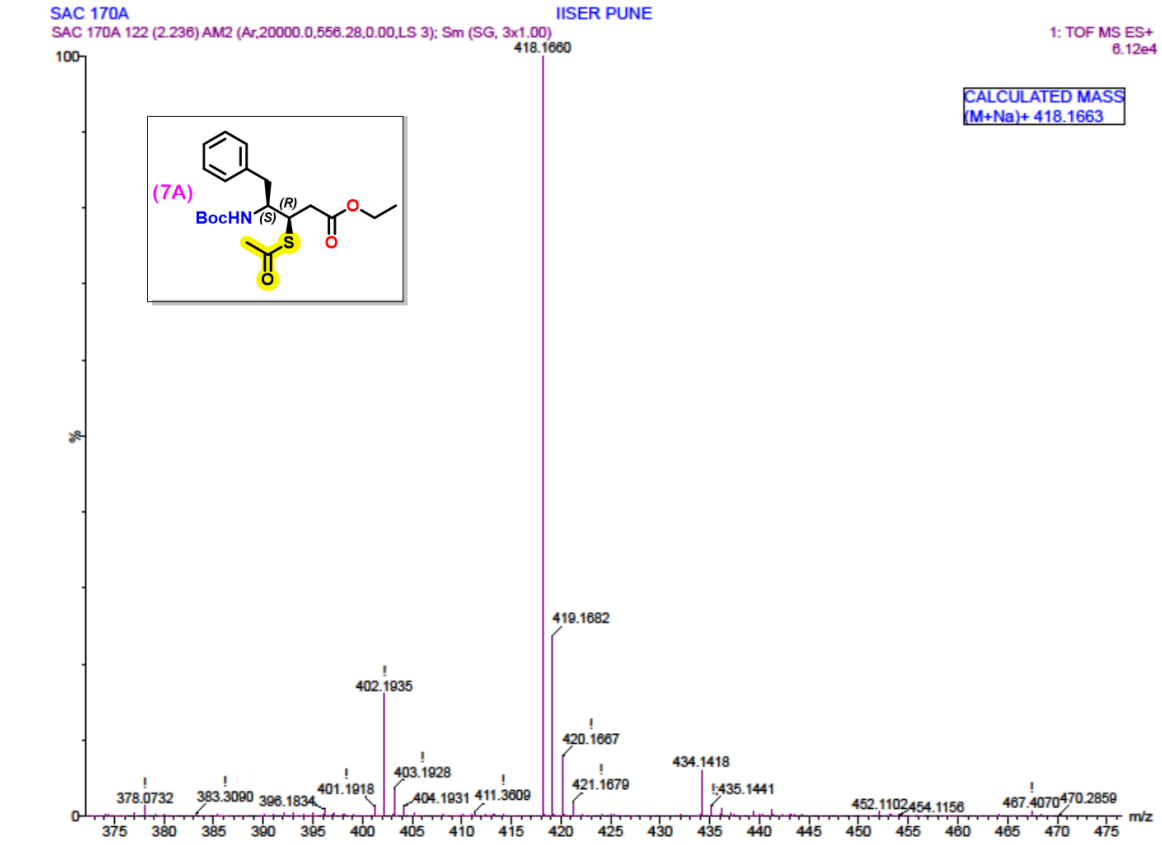

101 MHz, CDCl3
(5)
BocHN
H
N
O
f1 (ppm)

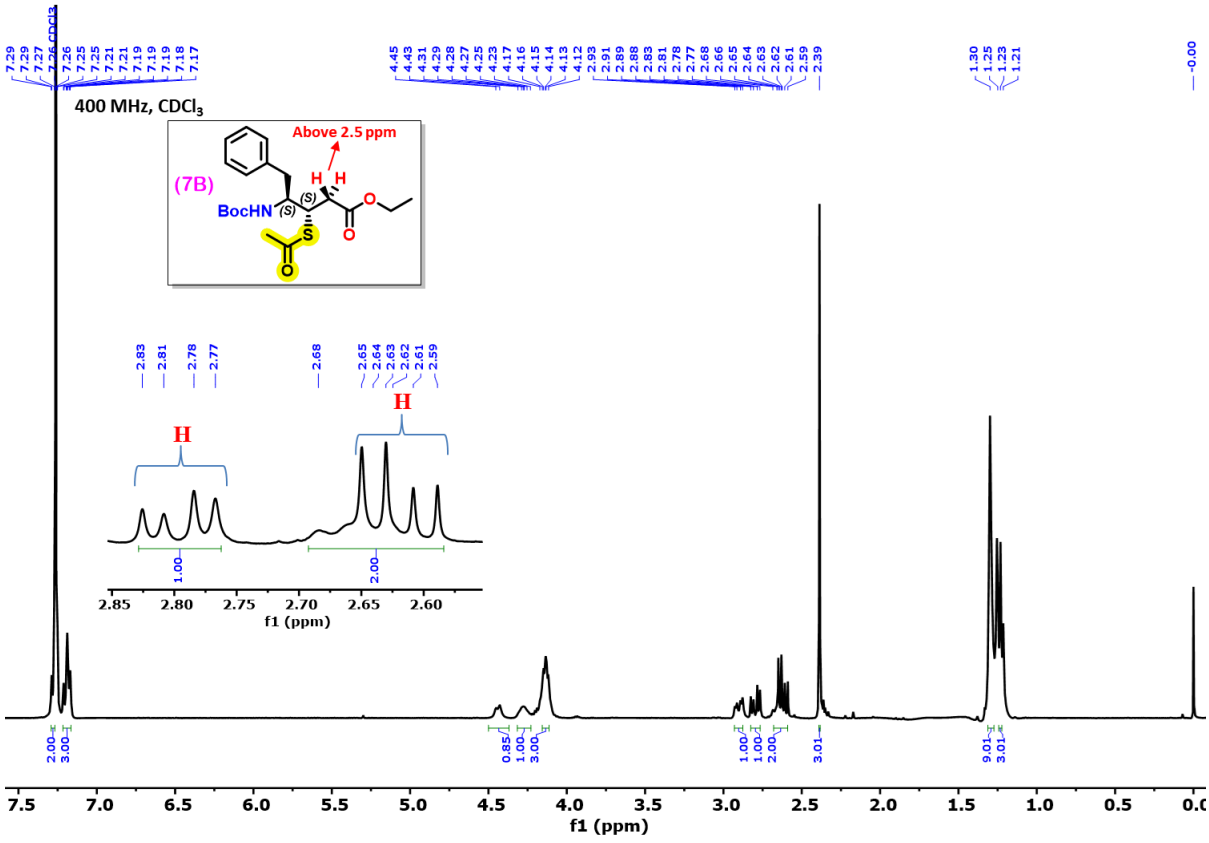

400 MHz, CDCl3
(6)
BocHN
H
N
O
Vinyl Proton's region
f1 (ppm)

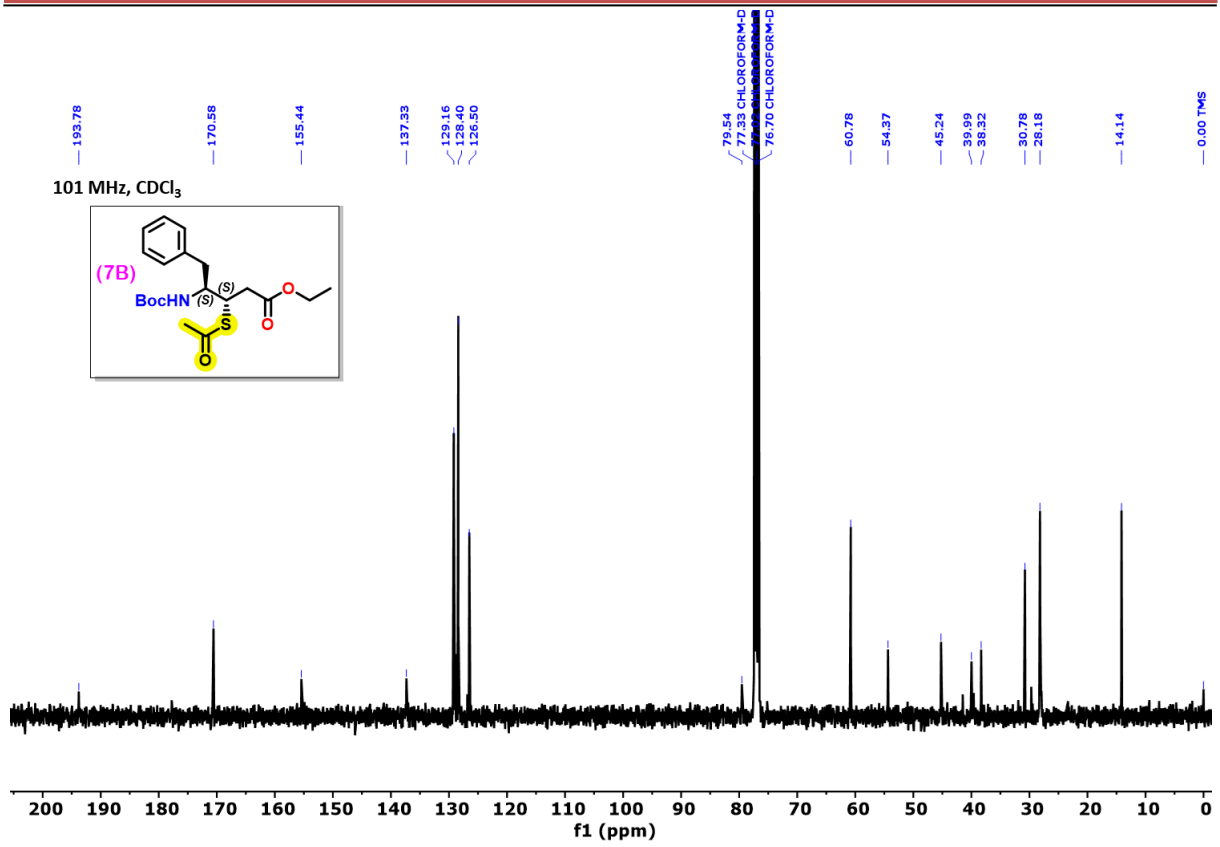

101 MHz, CDCl3
(6)
BocHN
H
N
O
f1 (ppm)

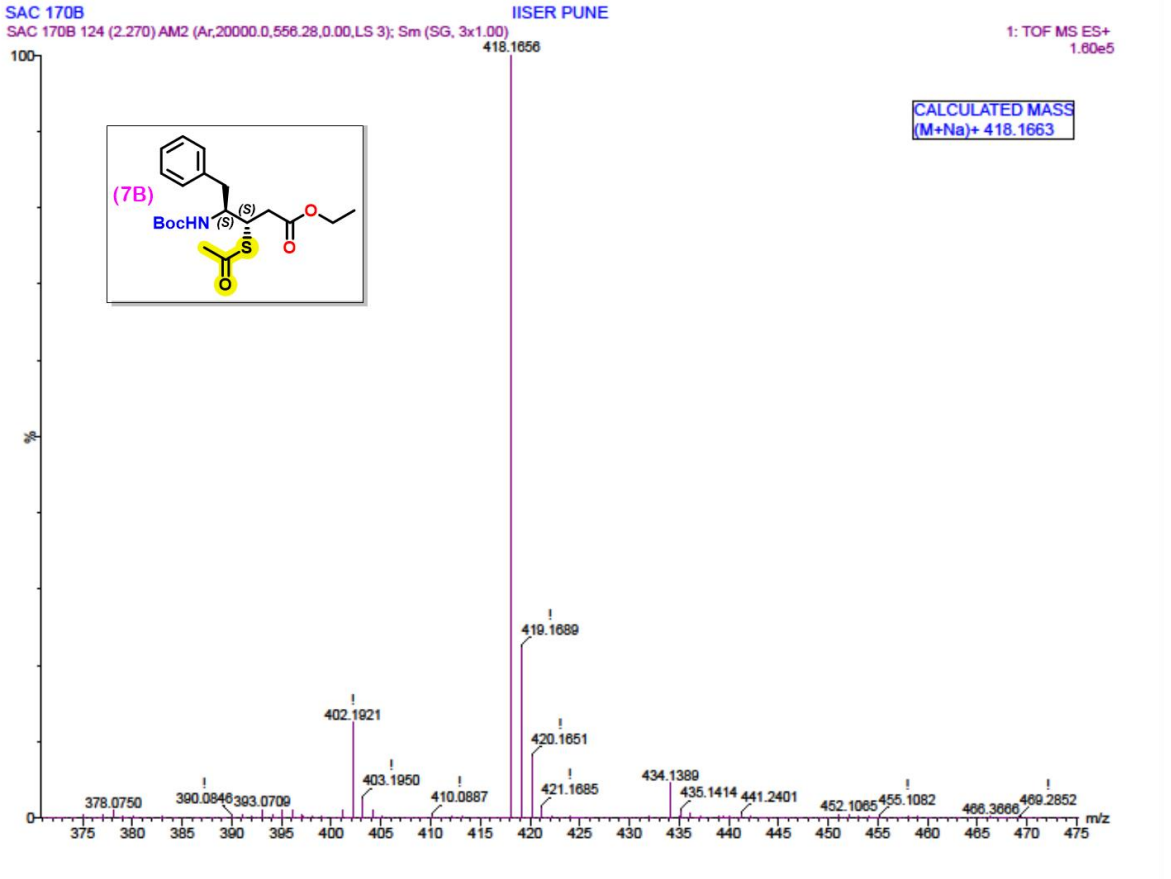

400 MHz, CDCl3
Above 2.5 ppm
(7A)
BocHN
f1 (ppm)

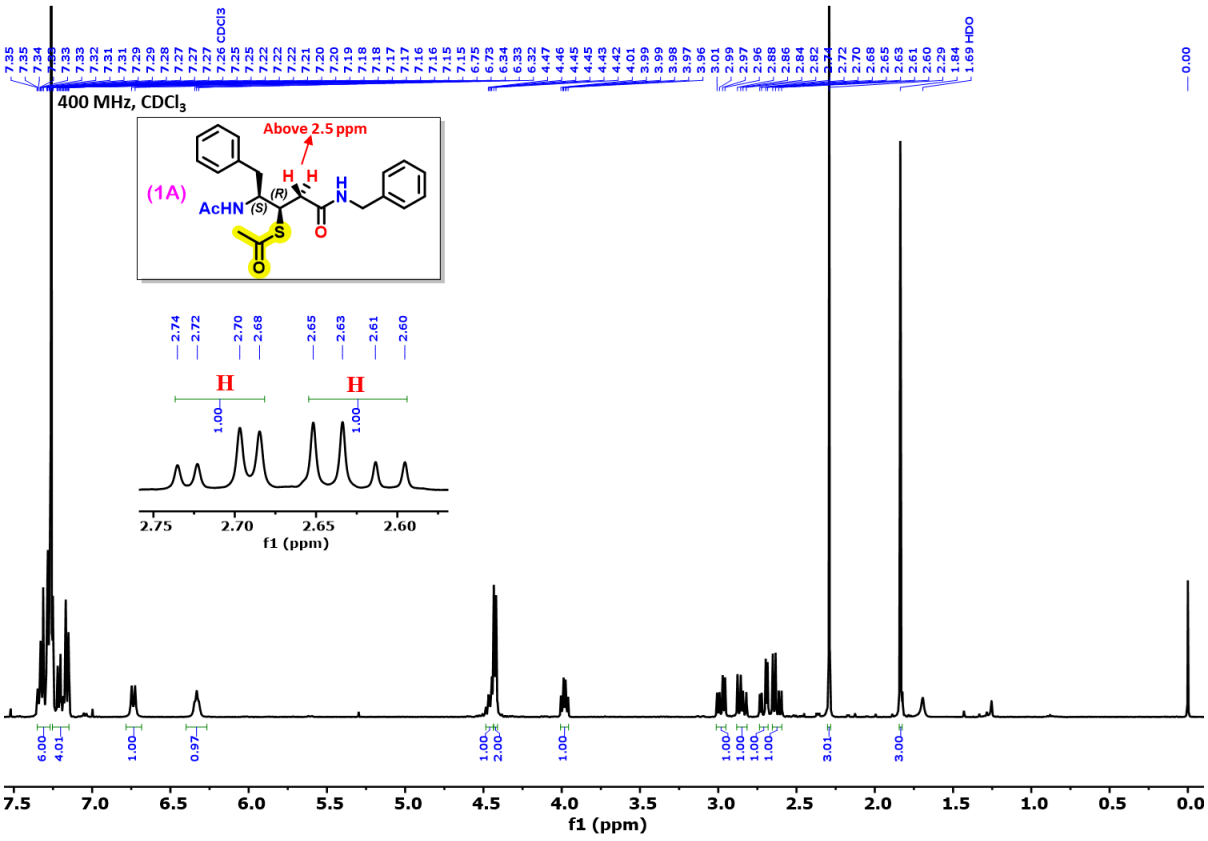

101 MHz, CDCl3
(7A)
BocHN
f1 (ppm)

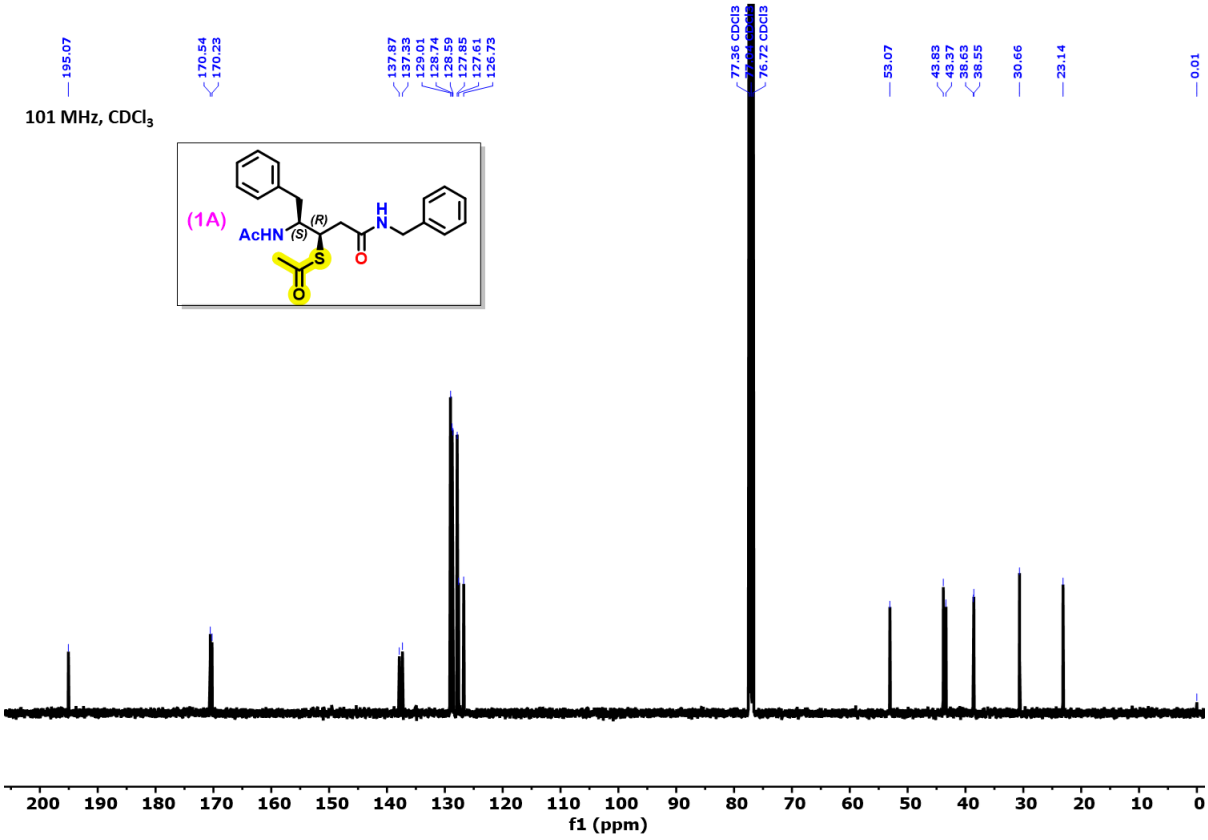

SAC 170A
IISER PUNE
SAC 170A 122 (2.236) AM2 (Ar,20000.0,556.28,0.00,LS 3); Sm (SG, 3x1.00)
1: TOF MS ES+
6.12e4
CALCULATED MASS
(M+Na)+ 418.1663
(7A)
BocHN
418.1660
419.1682
402.1935
420.1667
403.1928
434.1418
421.1679
401.1918
435.1441
404.1931
411.3609
378.0732
383.3090
396.1834
452.1102
454.1156
467.4070
470.2859
m/z

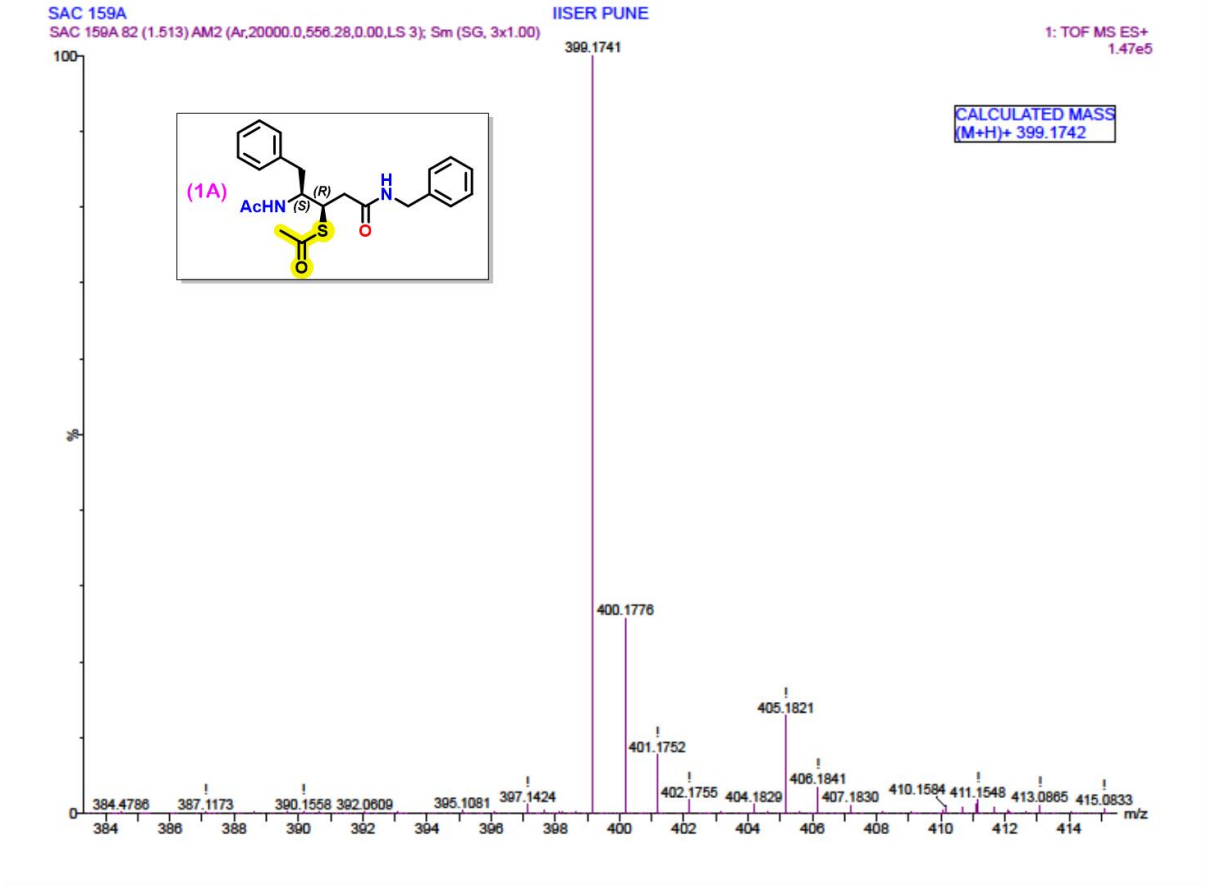

400 MHz, CDCl3
Above 2.5 ppm
(7B)
BocHN
H
H
f1 (ppm)

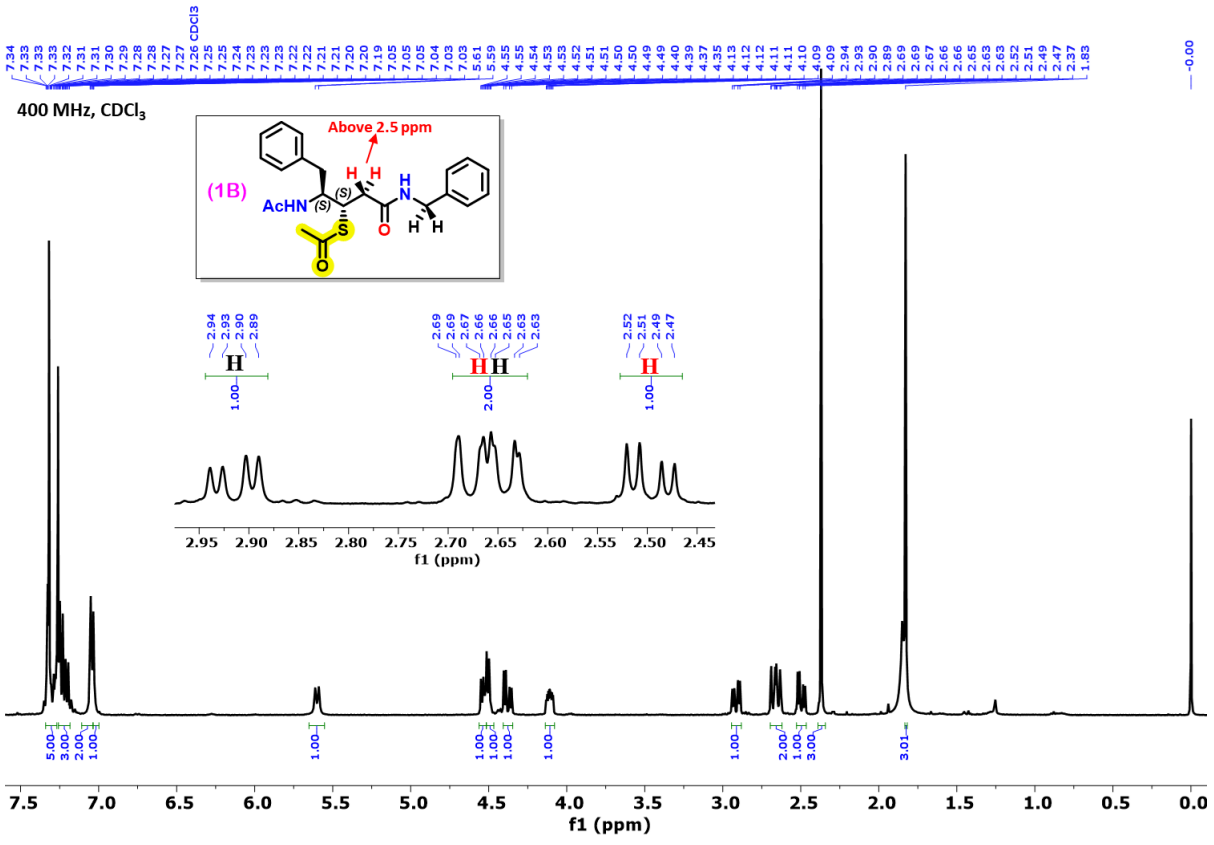

193.78
170.58
155.44
137.33
129.16
128.40
126.50
79.54
77.33 CHLOROFORM-D
76.70 CHLOROFORM-D
60.78
54.37
45.24
39.99
38.32
30.78
28.18
14.14
0.00 TMS
101 MHz, CDCl3
(7B)
BocHN
(S)
(S)
S
O
O
O
200 190 180 170 160 150 140 130 120 110 100 90 80 70 60 50 40 30 20 10 0
f1 (ppm)

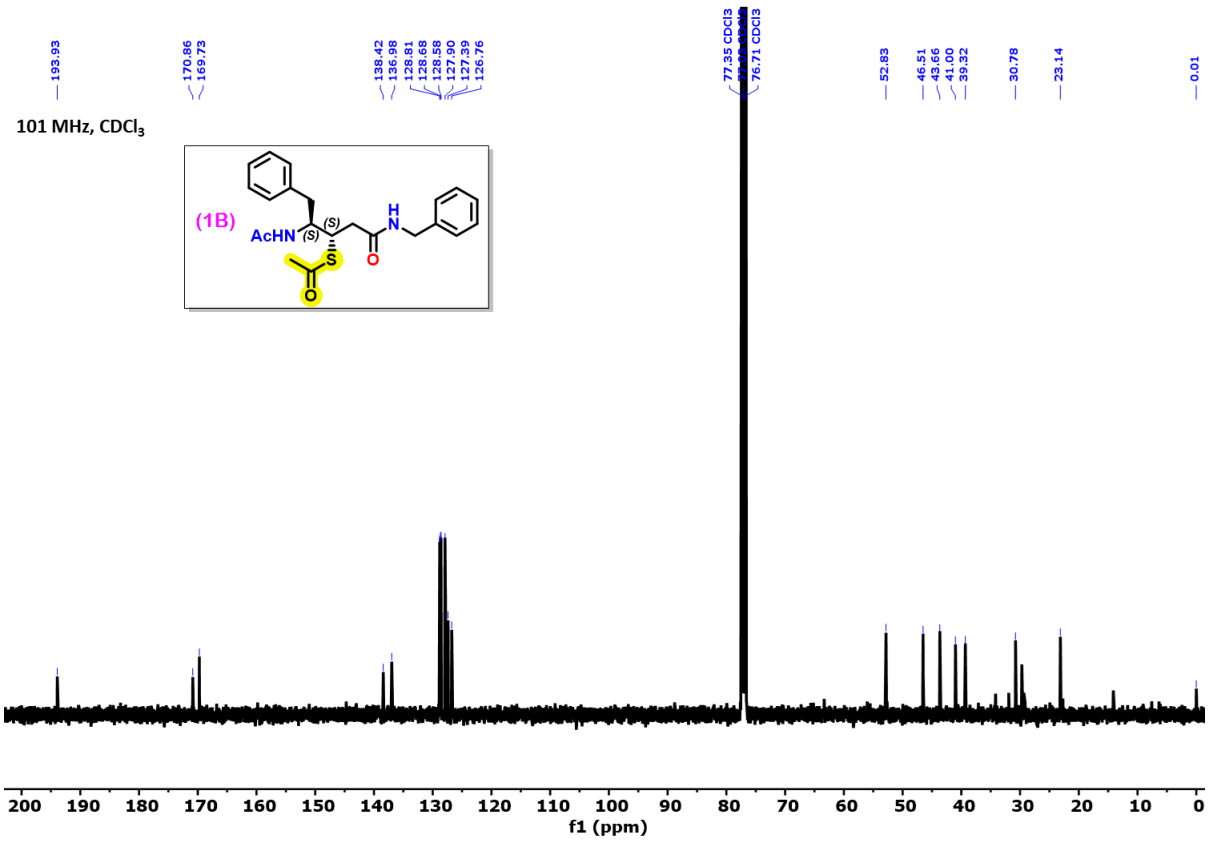

SAC 170B
IISER PUNE
SAC 170B 124 (2.270) AM2 (Ar,20000.0,556.28,0.00,LS 3); Sm (SG, 3x1.00)
1: TOF MS ES+
1.60e5
100
%
0
418.1656
CALCULATED MASS
(M+Na)+ 418.1663
(7B)
BocHN
(S)
(S)
S
O
O
O
419.1689
402.1921
420.1651
403.1950
421.1685
410.0887
434.1389
435.1414
441.2401
378.0750
390.0846
393.0709
452.1065
455.1082
466.3666
469.2852
375 380 385 390 395 400 405 410 415 420 425 430 435 440 445 450 455 460 465 470 475
m/z

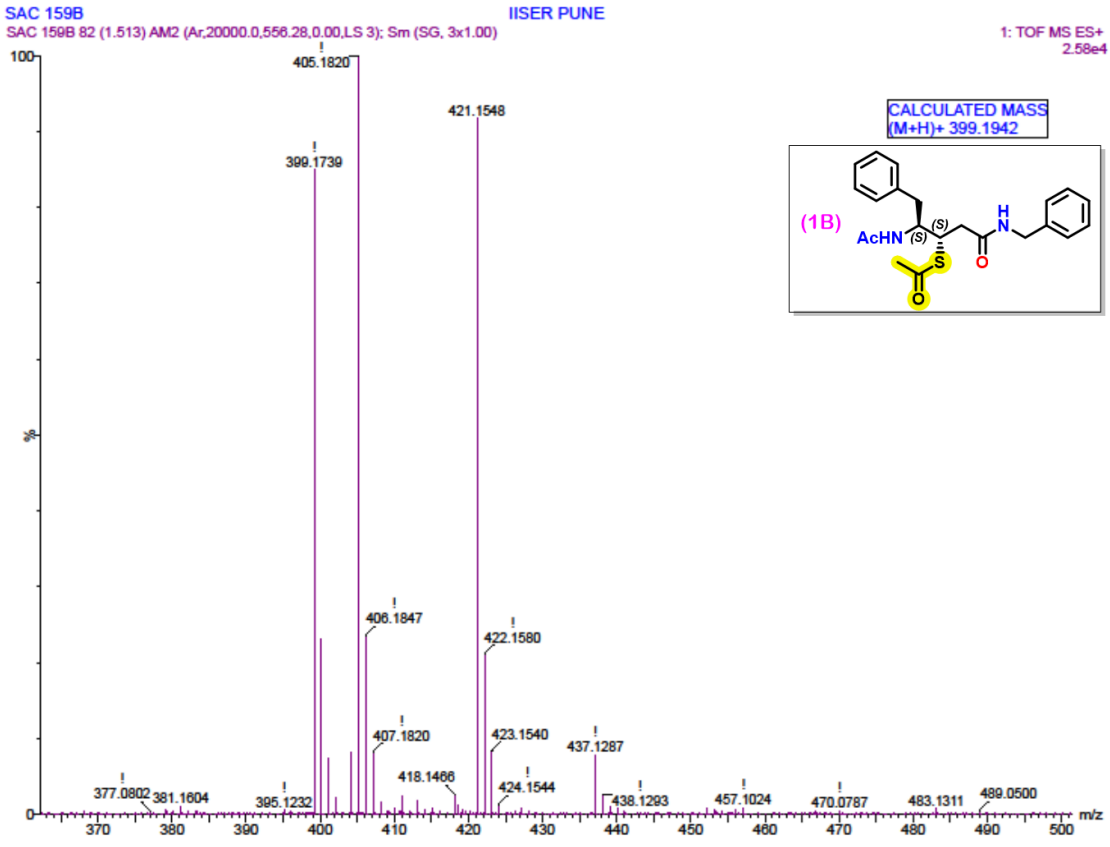

400 MHz, CDCl3
Above 2.5 ppm
(1A)
AcHN
(S)
(R)
H
H
N
S
O
f1 (ppm)

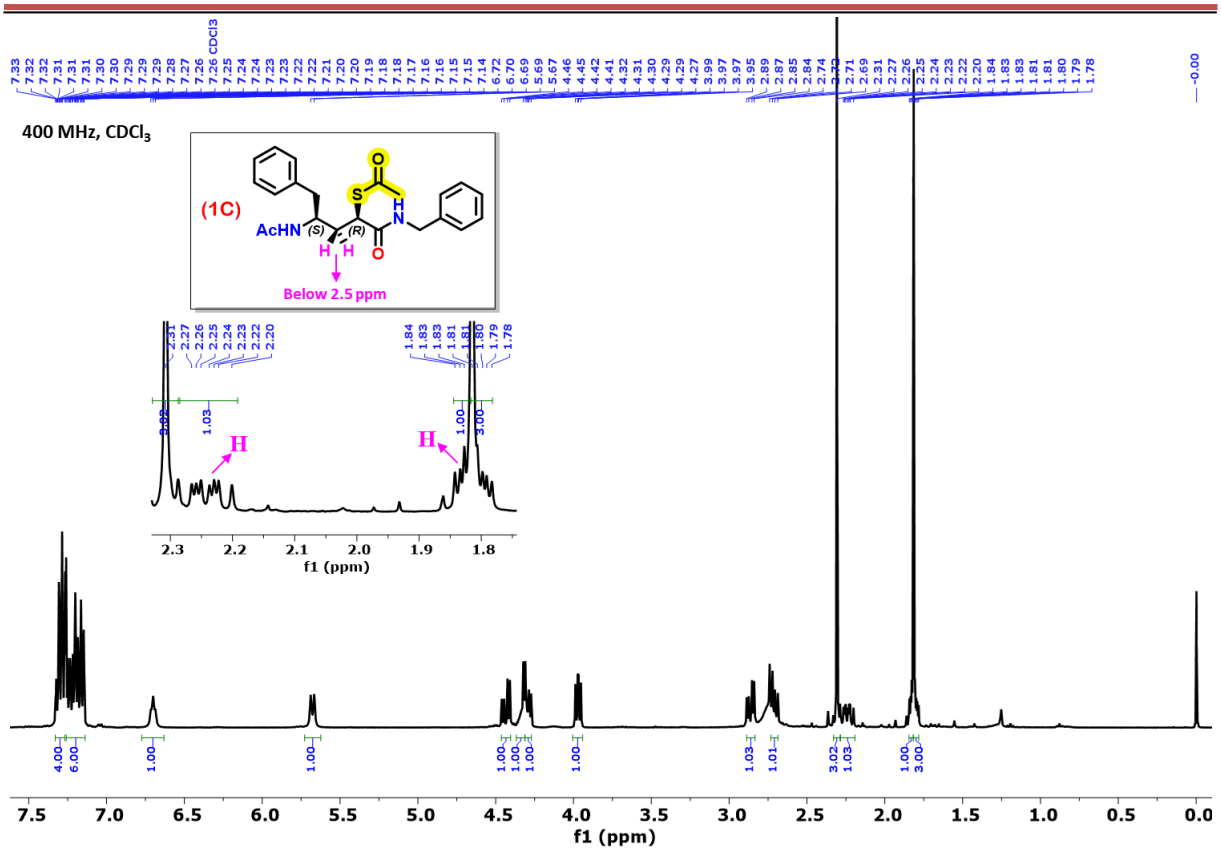

101 MHz, CDCl3
(1A)
AcHN
(S)
(R)
f1 (ppm)

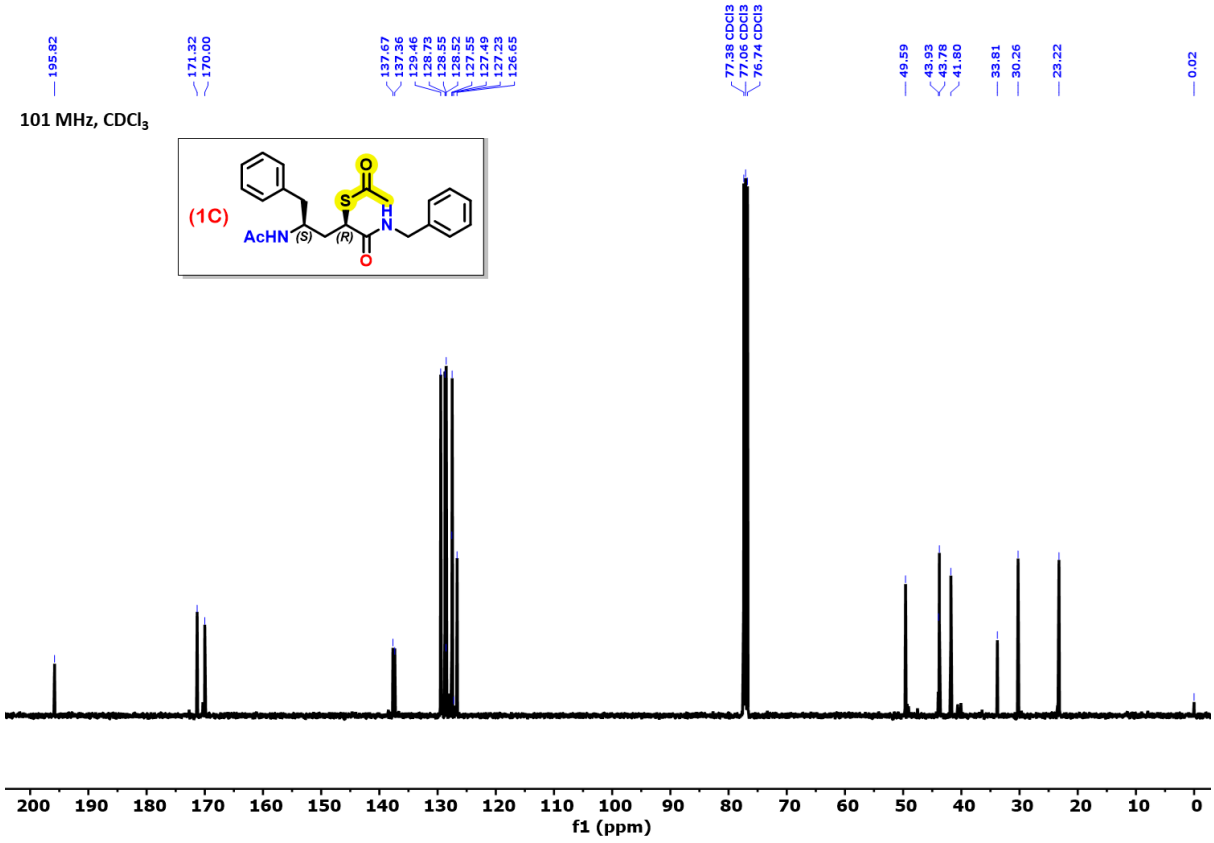

SAC 159A
SAC 159A 82 (1.513) AM2 (Ar,20000.0,556.28,0.00,LS 3); Sm (SG, 3x1.00)
IISER PUNE
1: TOF MS ES+
1.47e5
399.1741
CALCULATED MASS
(M+H)+ 399.1742
(1A)
AcHN
400.1776
405.1821
401.1752
406.1841
402.1755
404.1829
407.1830
410.1584
411.1548
413.0865
415.0833
384.4786
387.1173
390.1558
392.0609
395.1081
397.1424
m/z

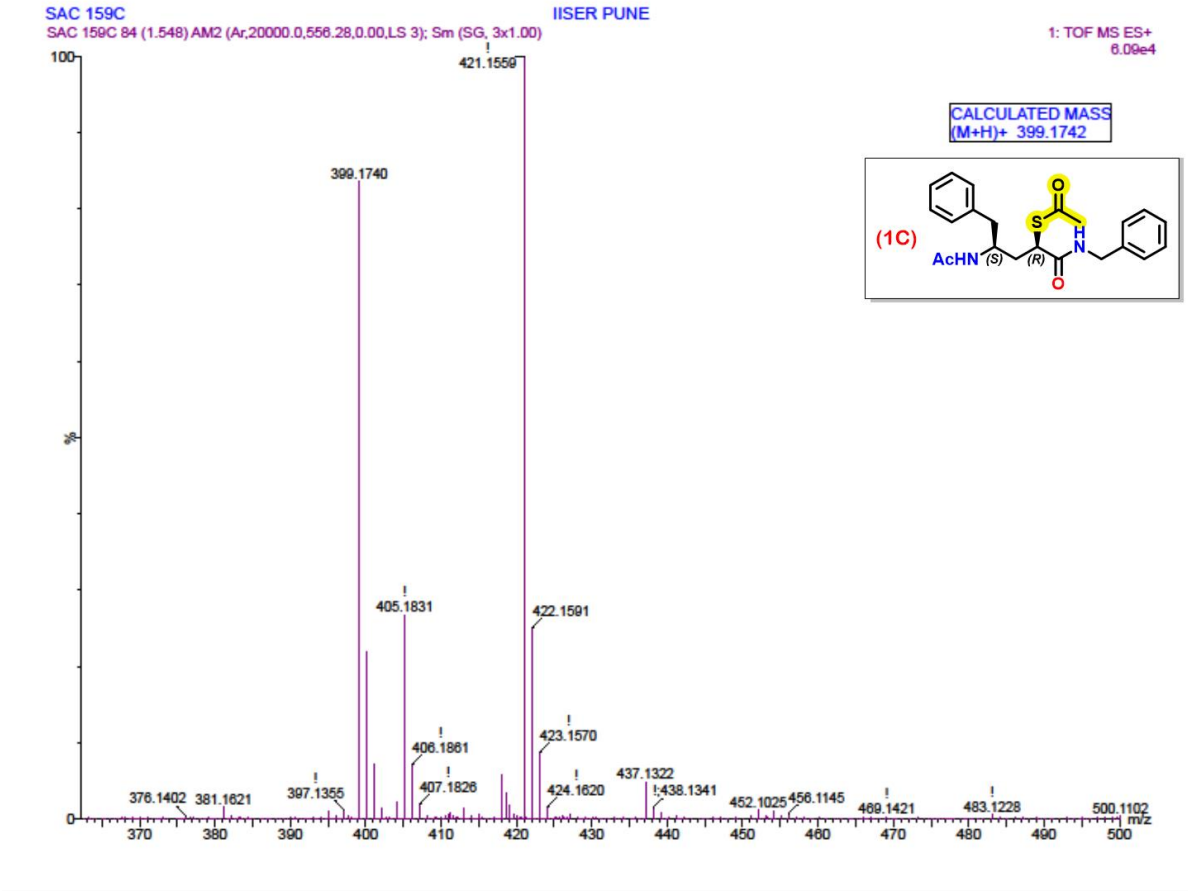

400 MHz, CDCl3
(1B)
AcHN
Above 2.5 ppm
f1 (ppm)

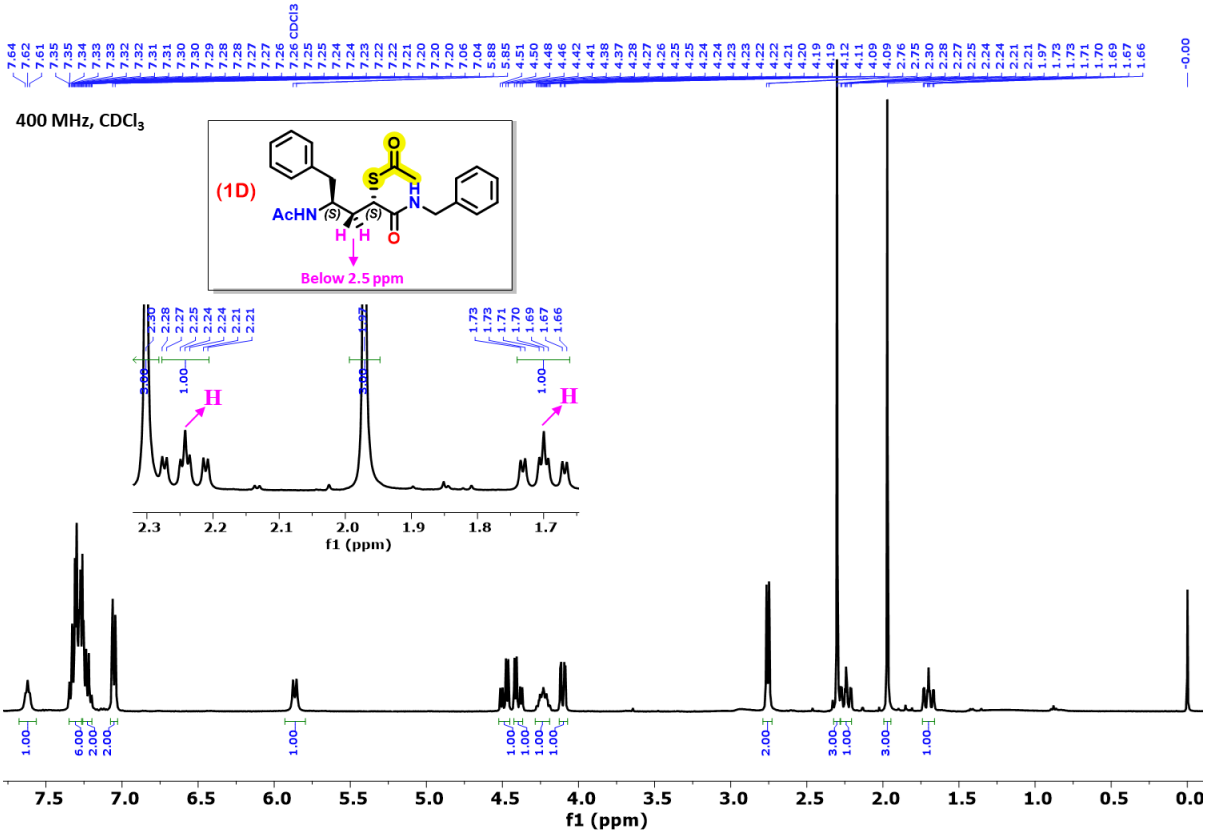

193.93
170.86
169.73
138.42
136.98
128.81
128.68
128.58
127.90
127.39
126.76
77.35 CDCl3
76.71 CDCl3
52.83
46.51
43.66
41.00
39.32
30.78
23.14
0.01
101 MHz, CDCl3
(1B)
AcHN
(S)
(S)
H
N
O
S
O
200 190 180 170 160 150 140 130 120 110 100 90 80 70 60 50 40 30 20 10 0
f1 (ppm)

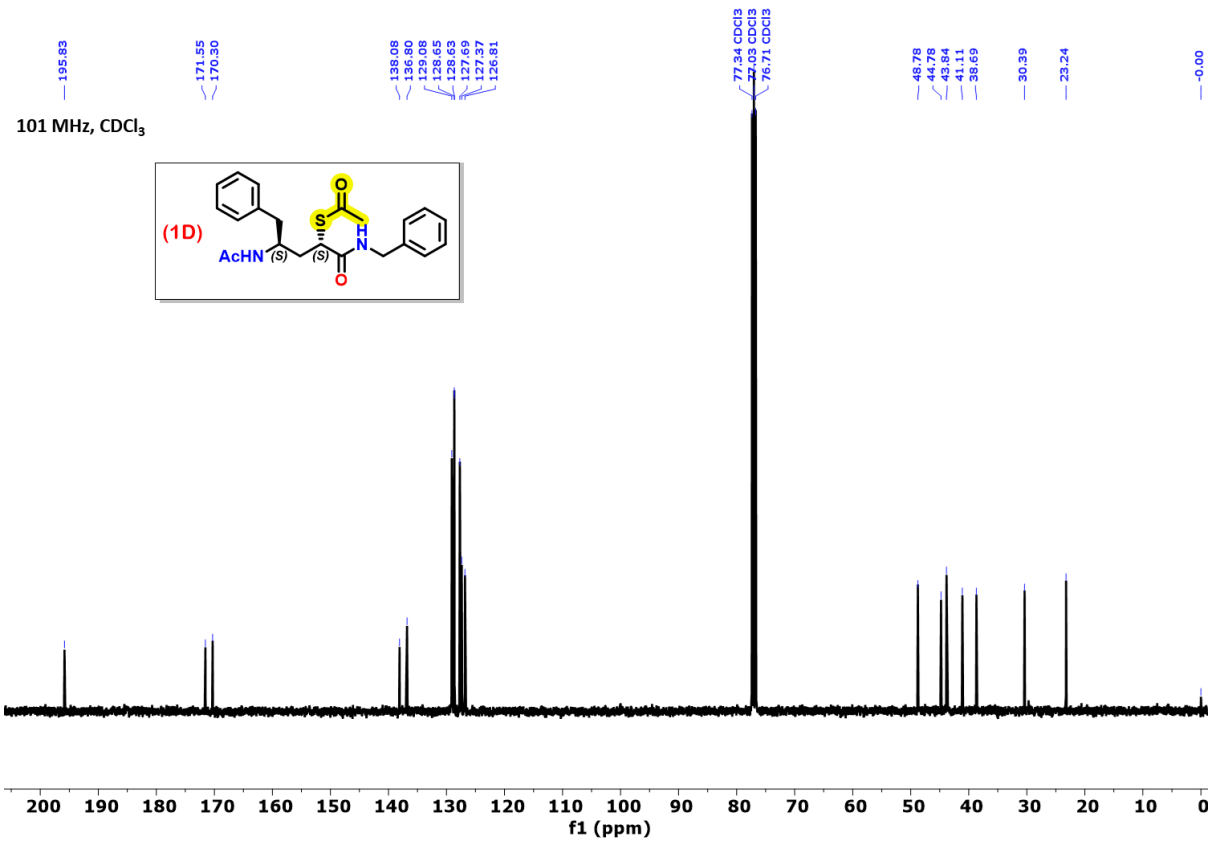

SAC 159B
IISER PUNE
SAC 159B 82 (1.513) AM2 (Ar,20000.0,556.28,0.00,LS 3); Sm (SG, 3x1.00)
1: TOF MS ES+
2.58e4
100
%
0
405.1820
421.1548
399.1739
406.1847
422.1580
407.1820
423.1540
437.1287
418.1466
424.1544
377.0802
381.1604
395.1232
438.1293
457.1024
470.0787
483.1311
489.0500
370 380 390 400 410 420 430 440 450 460 470 480 490 500
m/z
CALCULATED MASS
(M+H)+ 399.1942
(1B)
AcHN
(S)
(S)
H
N
O
S
O

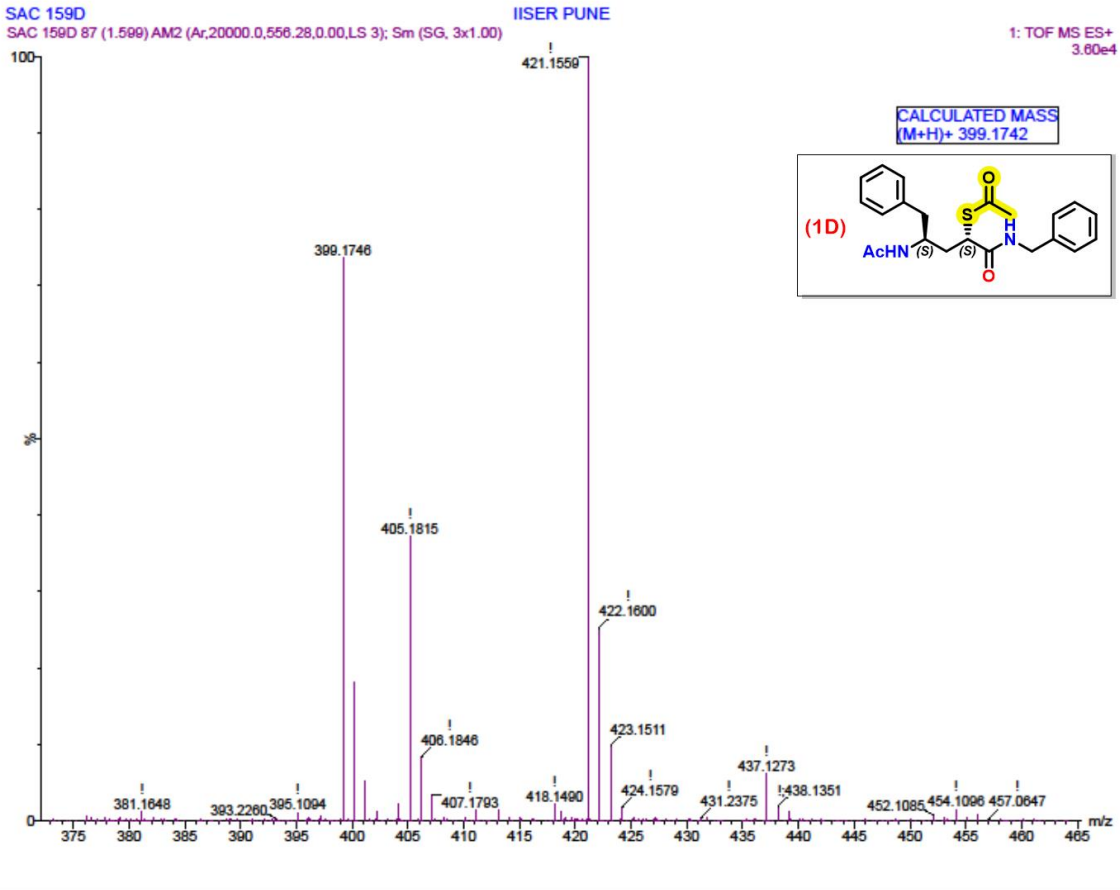

400 MHz, CDCl3
(1C)
AcHN
Below 2.5 ppm
f1 (ppm)

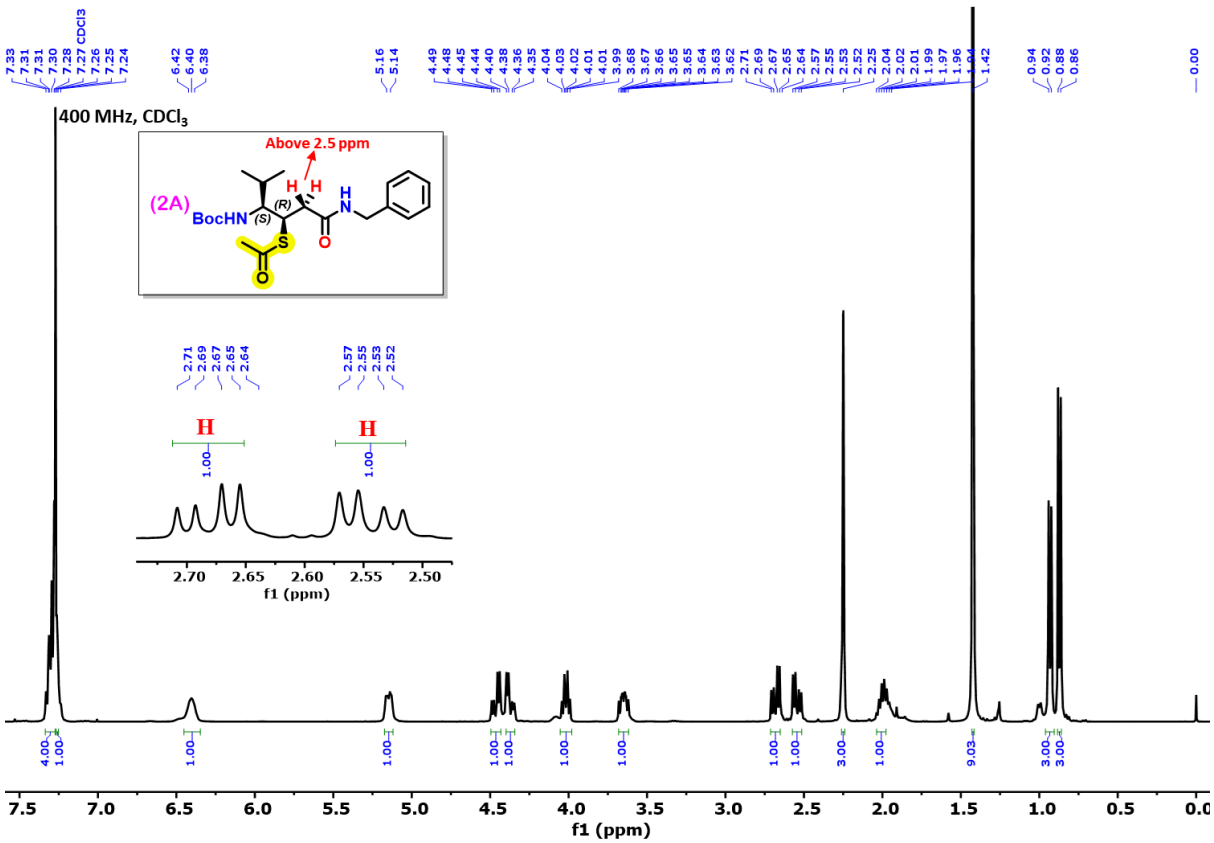

101 MHz, CDCl3
(1C)
AcHN
f1 (ppm)

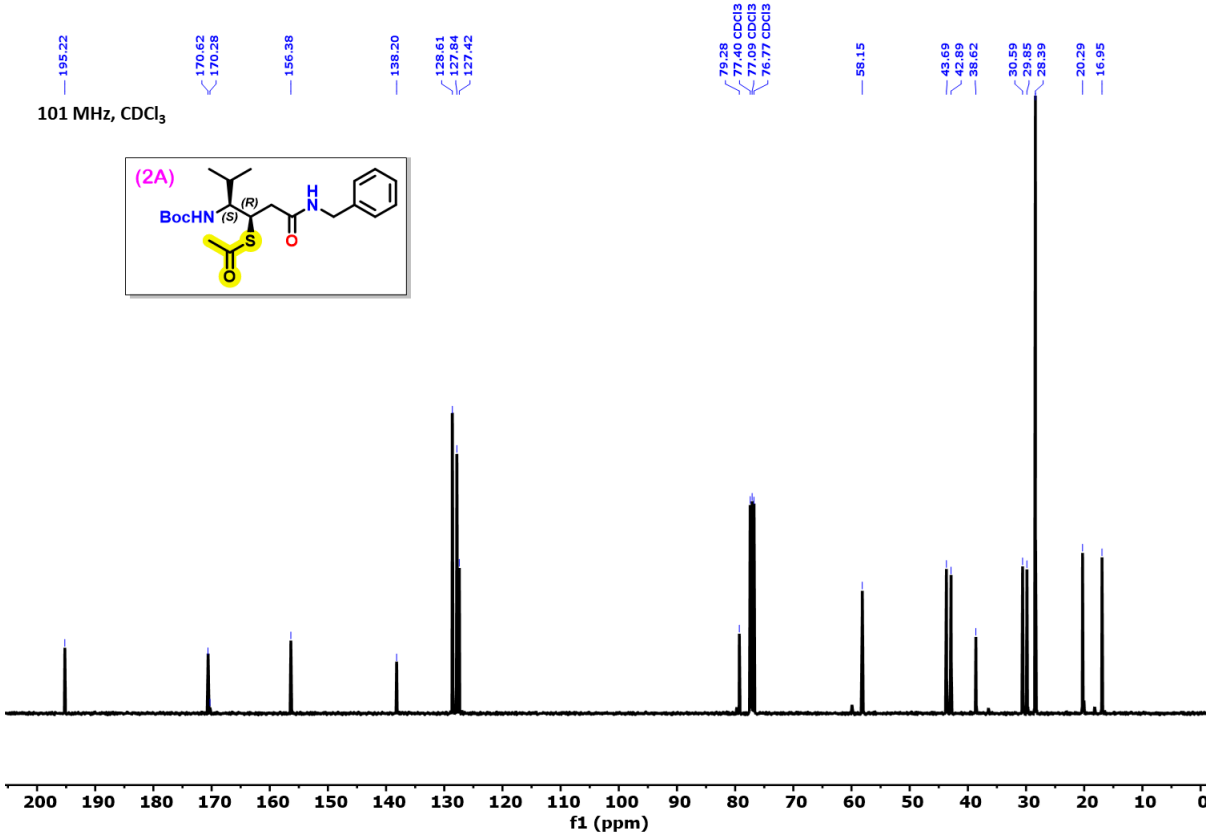

SAC 159C
IISER PUNE
SAC 159C 84 (1.548) AM2 (Ar,20000.0,556.28,0.00,LS 3); Sm (SG, 3x1.00)
1: TOF MS ES+
6.09e4
CALCULATED MASS
(M+H)+ 399.1742
(1C)
AcHN
421.1559
399.1740
405.1831
422.1591
406.1861
423.1570
407.1826
424.1620
437.1322
438.1341
376.1402
381.1621
397.1355
452.1025
456.1145
469.1421
483.1228
500.1102
m/z

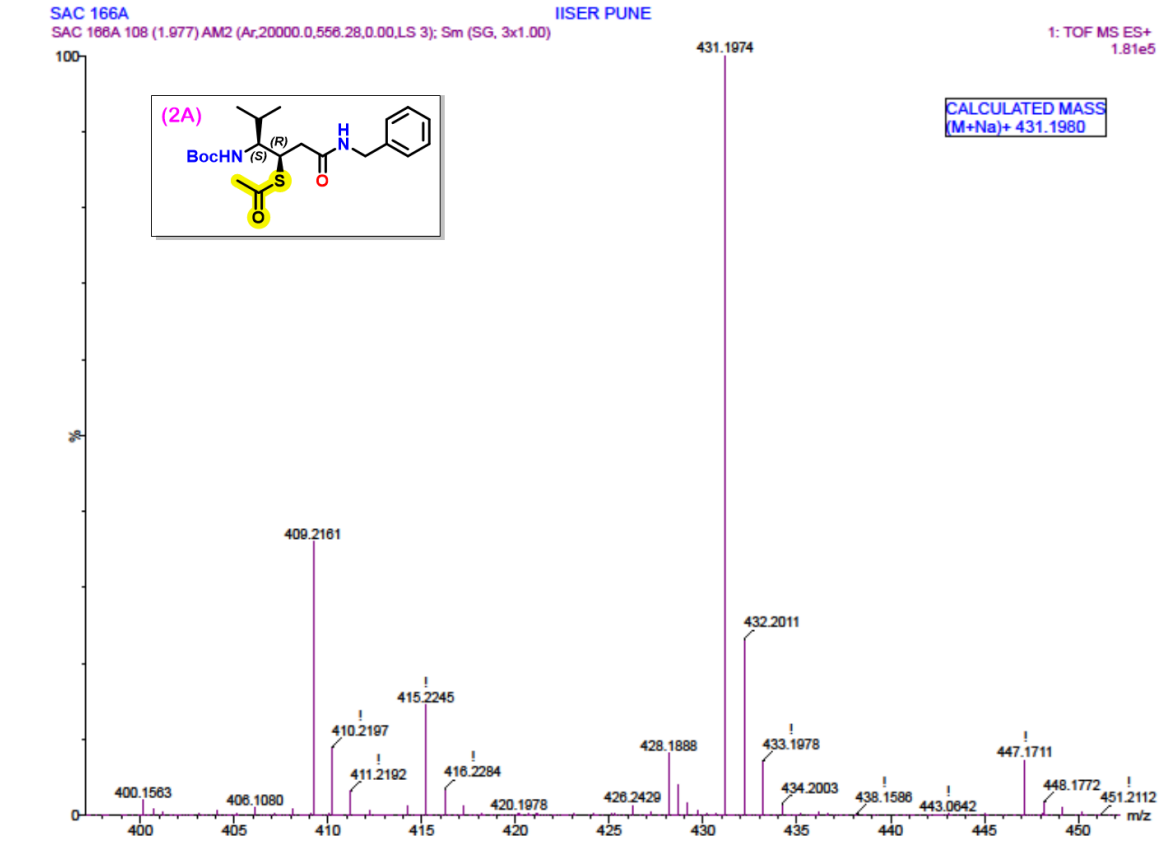

400 MHz, CDCl3
(1D)
AcHN
Below 2.5 ppm
f1 (ppm)

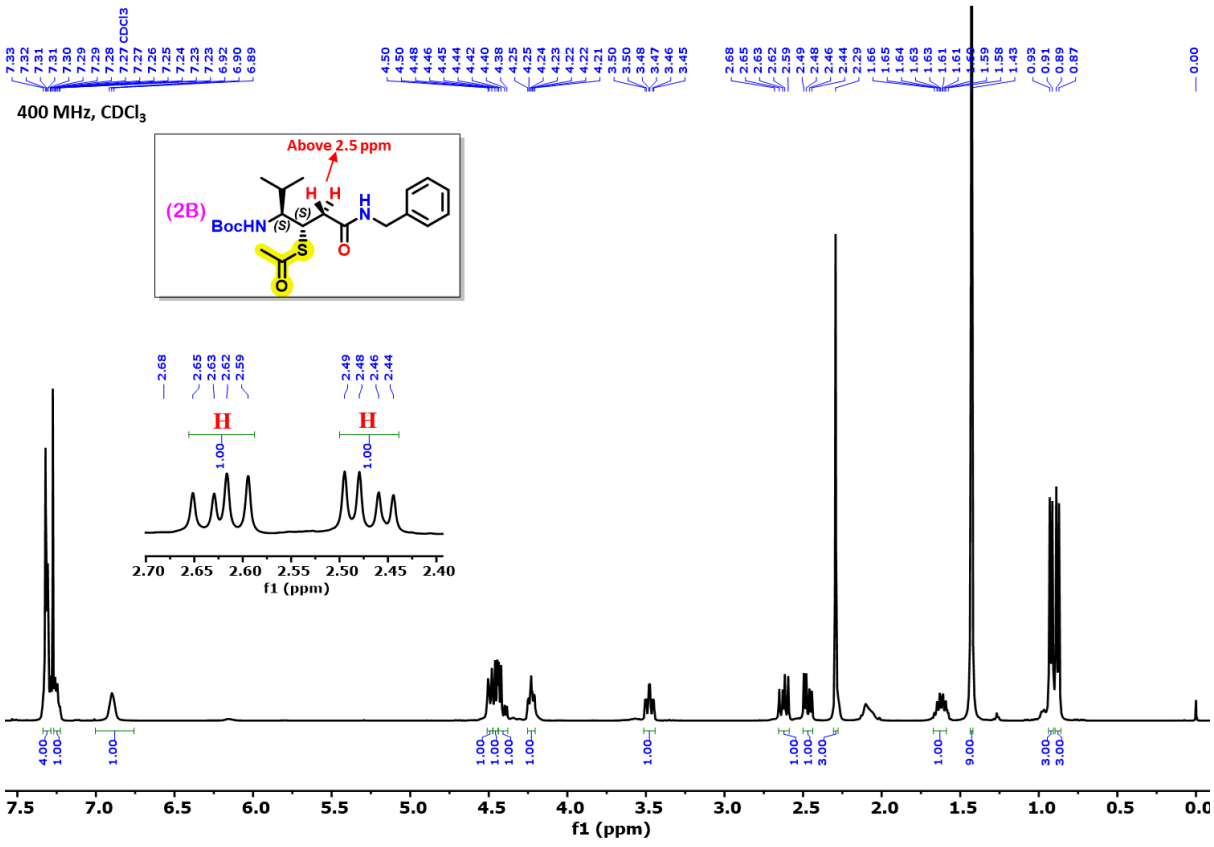

195.83
171.55
170.30
138.08
136.80
129.08
128.65
128.63
127.69
127.37
126.81
77.34 CDCl3
77.03 CDCl3
76.71 CDCl3
48.78
44.78
43.64
41.11
38.69
30.39
23.24
-0.00
101 MHz, CDCl3
(1D)
AcHN
(S)
(S)
f1 (ppm)

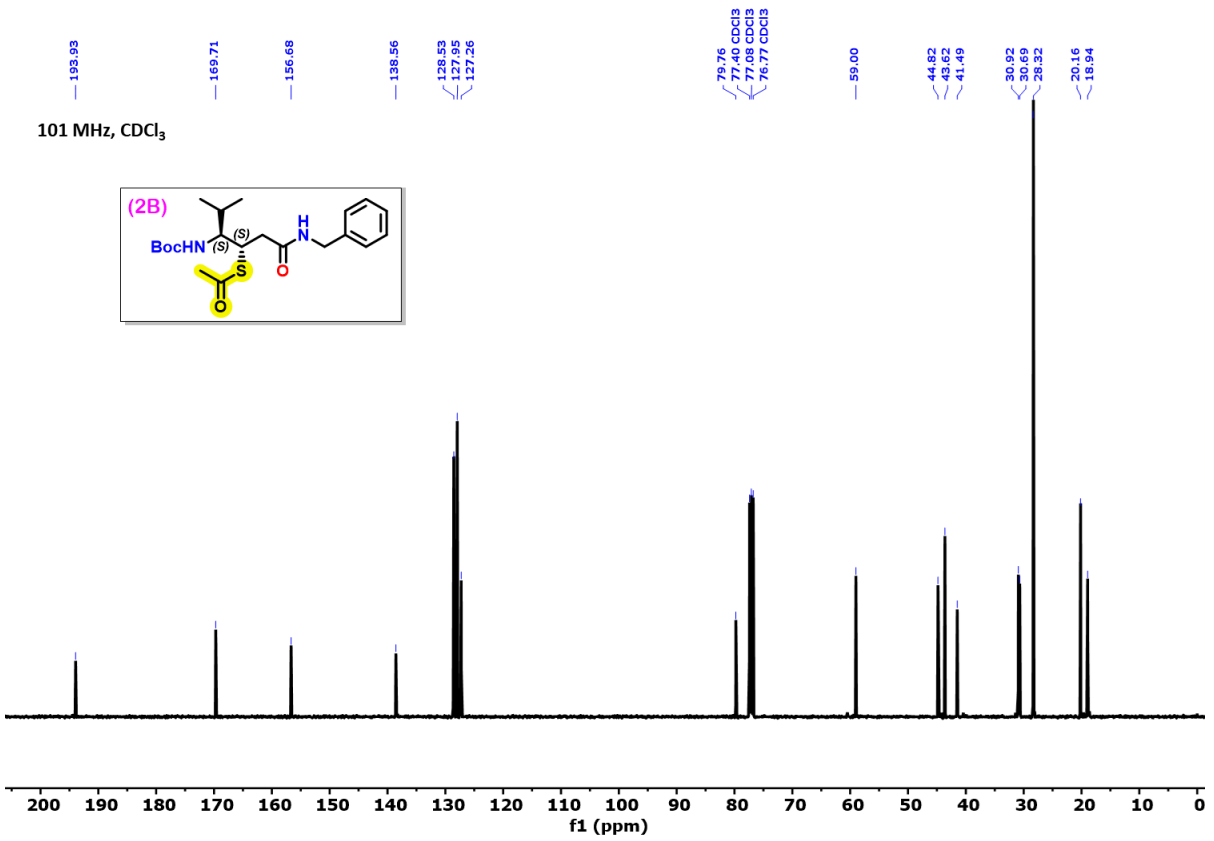

SAC 159D
SAC 159D 87 (1.599) AM2 (Ar,20000.0,556.28,0.00,LS 3); Sm (SG, 3x1.00)
IISER PUNE
1: TOF MS ES+
3.60e4
CALCULATED MASS
(M+H)+ 399.1742
(1D)
AcHN
421.1559
399.1746
405.1815
422.1600
406.1846
423.1511
437.1273
381.1648
393.2260
395.1094
407.1793
418.1490
424.1579
431.2375
438.1351
452.1085
454.1096
457.0647
%
m/z

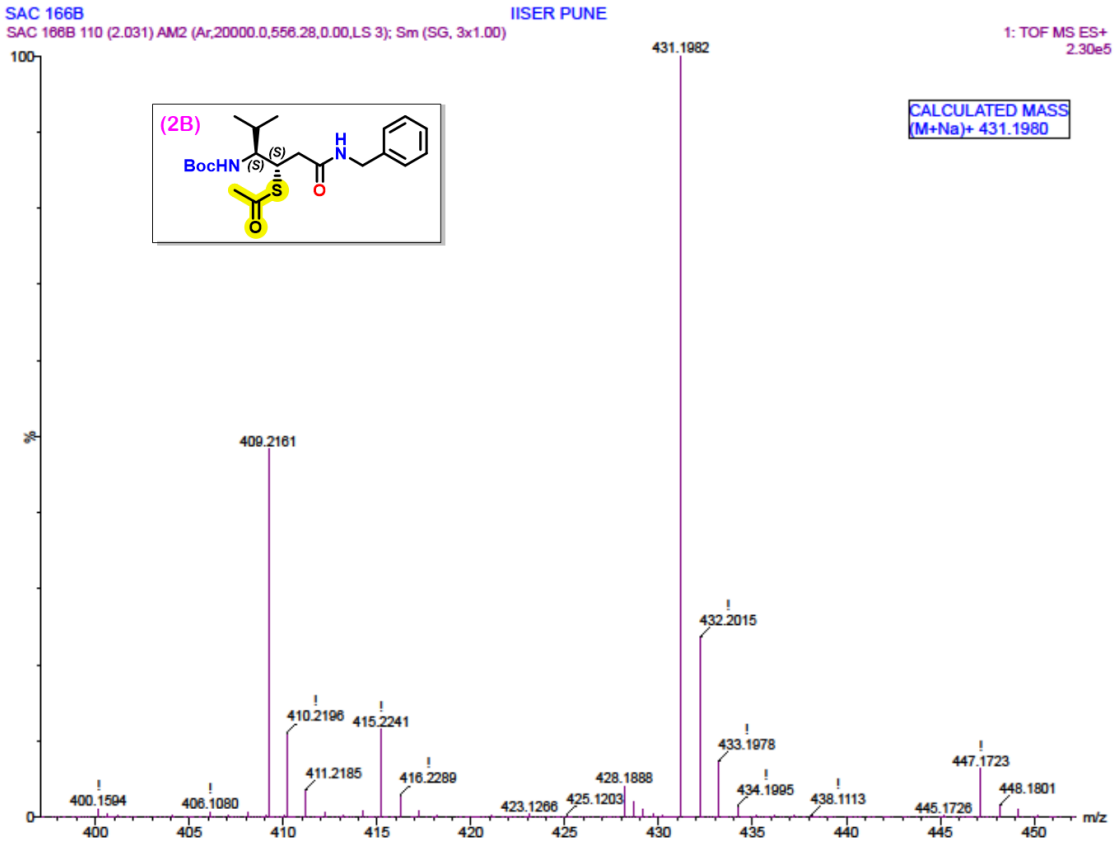

400 MHz, CDCl3
Above 2.5 ppm
(2A)
BocHN
f1 (ppm)

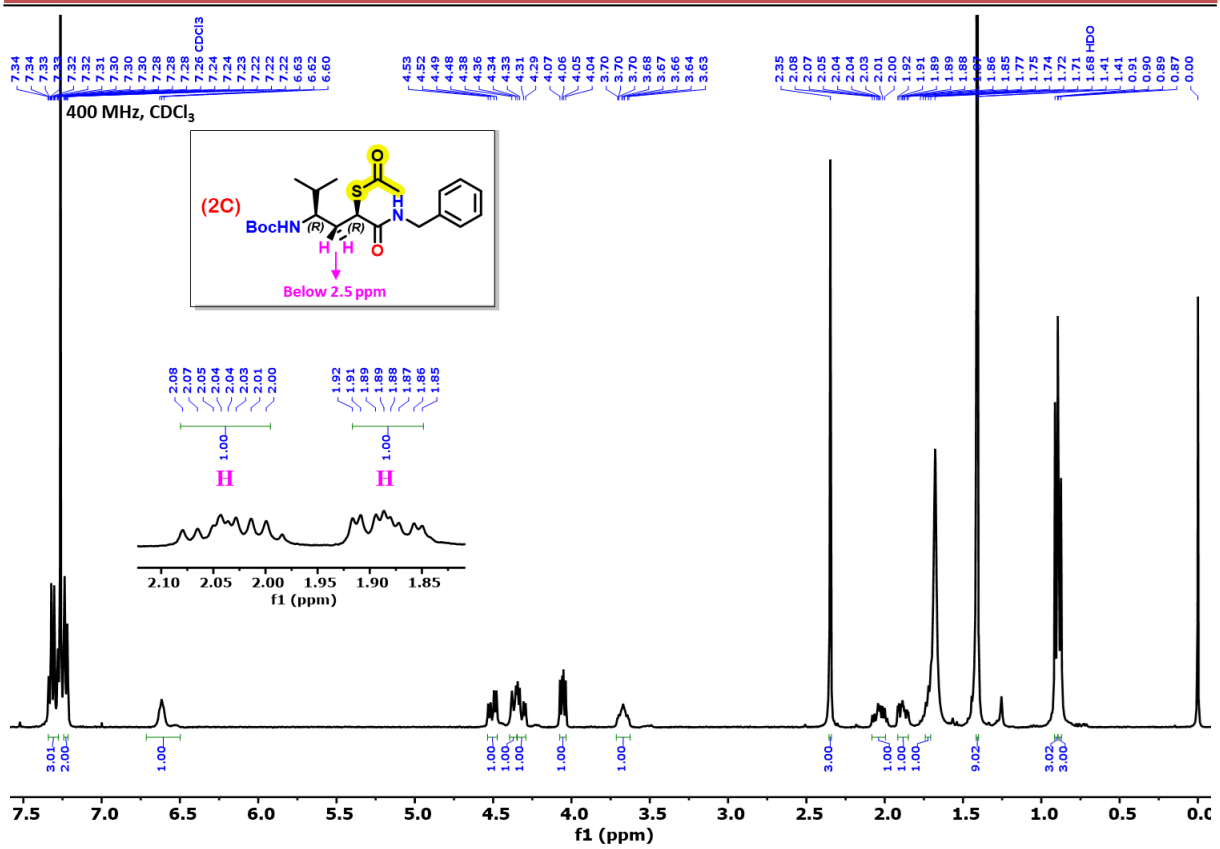

101 MHz, CDCl3
(2A)
BocHN
f1 (ppm)

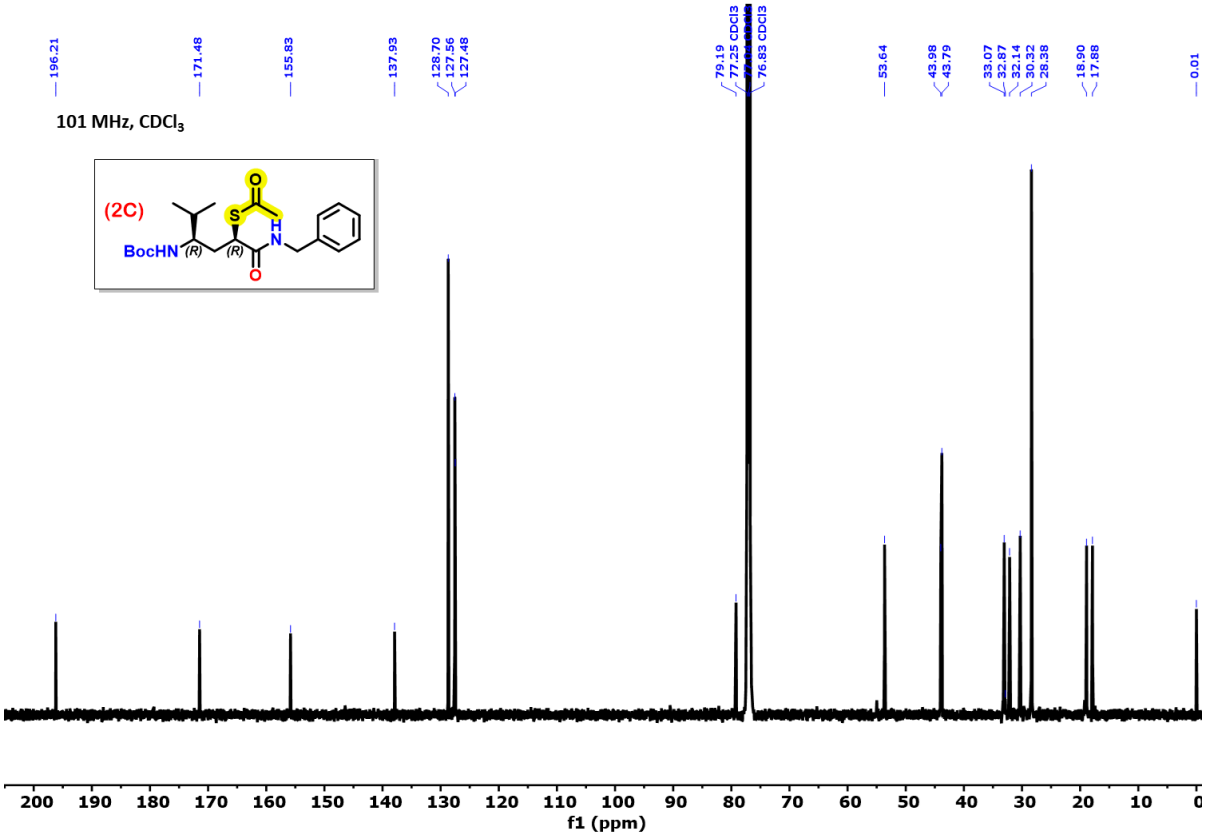

SAC 166A
IISER PUNE
SAC 166A 108 (1.977) AM2 (Ar,20000.0,556.28,0.00,LS 3); Sm (SG, 3x1.00)
1: TOF MS ES+
1.81e5
(2A)
CALCULATED MASS
(M+Na)+ 431.1980
431.1974
409.2161
432.2011
415.2245
410.2197
411.2192
416.2284
428.1888
433.1978
447.1711
400.1563
406.1080
420.1978
426.2429
434.2003
438.1586
443.0642
448.1772
451.2112
m/z

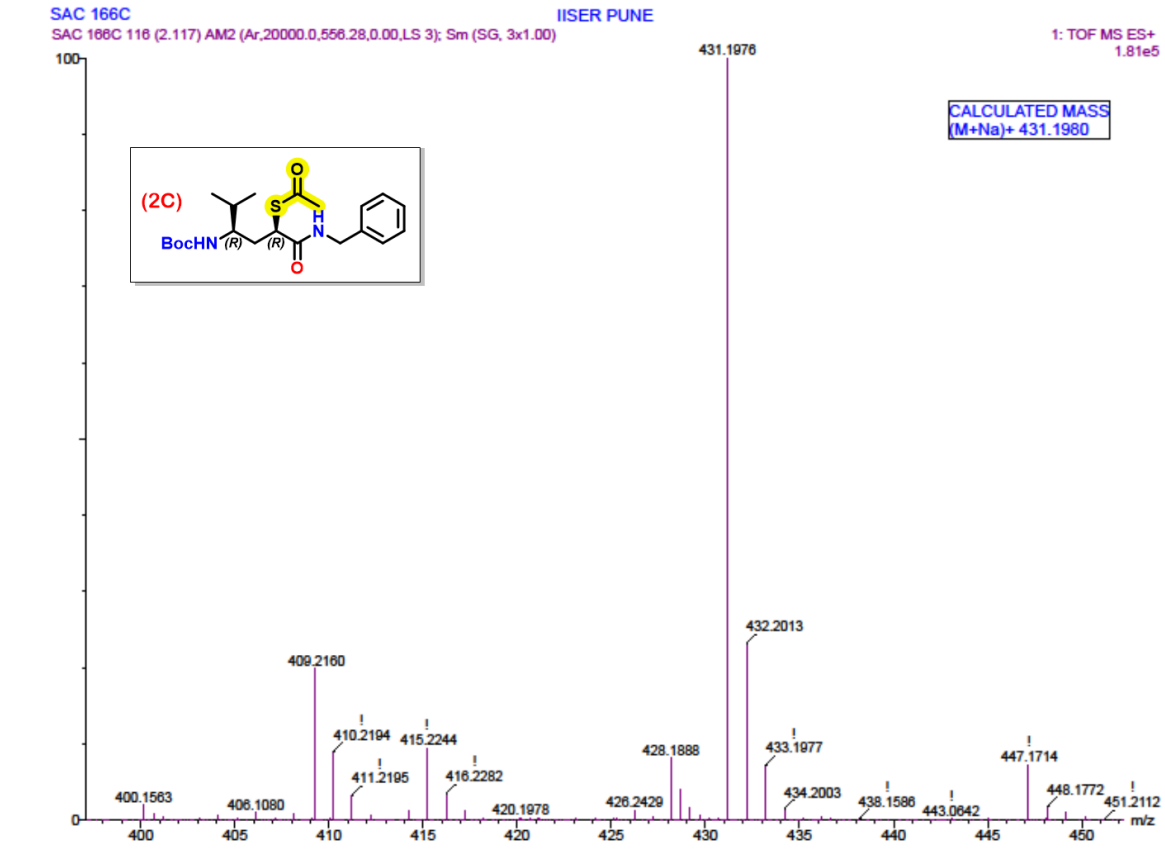

400 MHz, CDCl3
(2B)
Above 2.5 ppm
f1 (ppm)

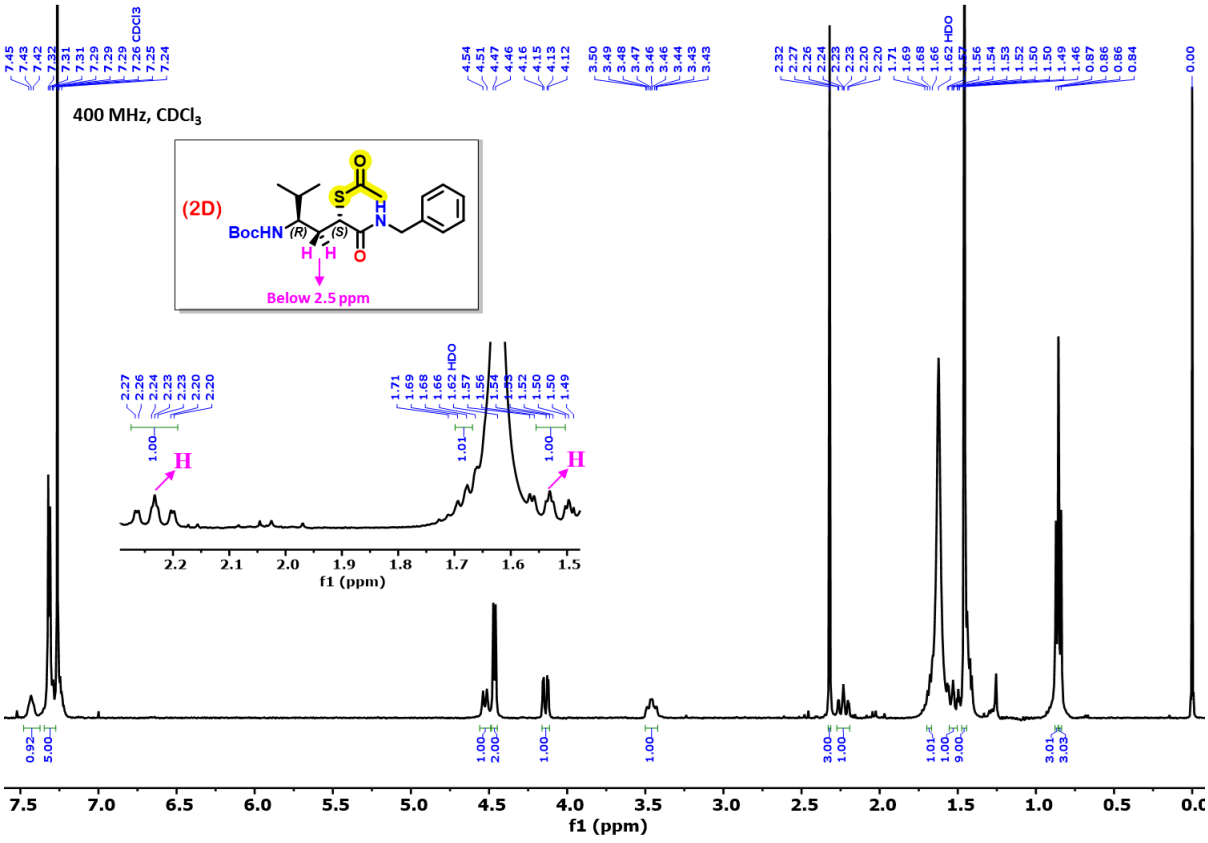

193.93
169.71
156.68
138.56
128.53
127.95
127.26
79.76
77.40 CDCl3
77.08 CDCl3
76.77 CDCl3
59.00
44.82
43.62
41.49
30.92
30.69
28.32
20.16
18.94
101 MHz, CDCl3
(2B)
BocHN
(S)
(S)
H
N
O
S
O
200 190 180 170 160 150 140 130 120 110 100 90 80 70 60 50 40 30 20 10 0
f1 (ppm)

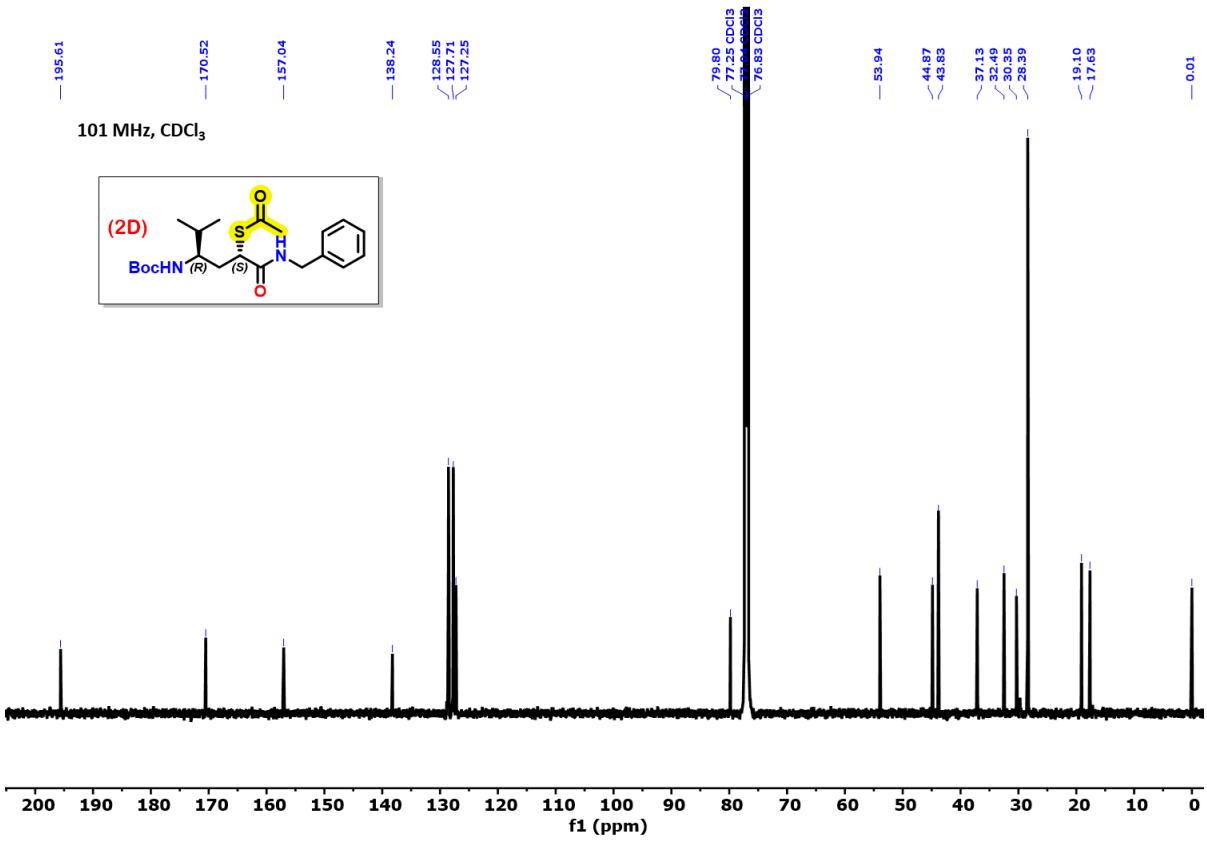

SAC 166B
IISER PUNE
SAC 166B 110 (2.031) AM2 (Ar,20000.0,556.28,0.00,LS 3); Sm (SG, 3x1.00)
1: TOF MS ES+
2.30e5
100
%
0
(2B)
BocHN
(S)
(S)
H
N
O
S
O
CALCULATED MASS
(M+Na)+ 431.1980
431.1982
409.2161
432.2015
410.2196
415.2241
433.1978
411.2185
416.2289
428.1888
434.1995
447.1723
448.1801
400.1594
406.1080
423.1266
425.1203
438.1113
445.1726
400 405 410 415 420 425 430 435 440 445 450
m/z

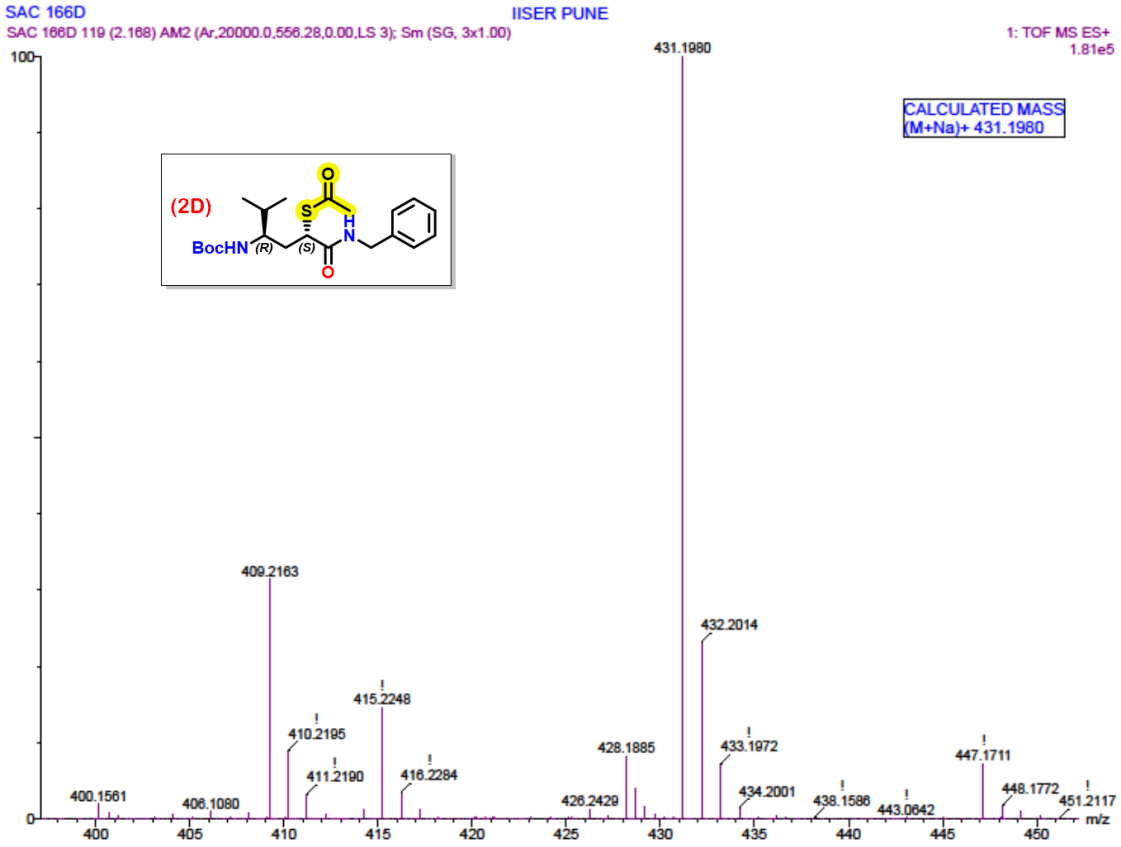

400 MHz, CDCl3
(2C)
BocHN
Below 2.5 ppm
H
H
f1 (ppm)

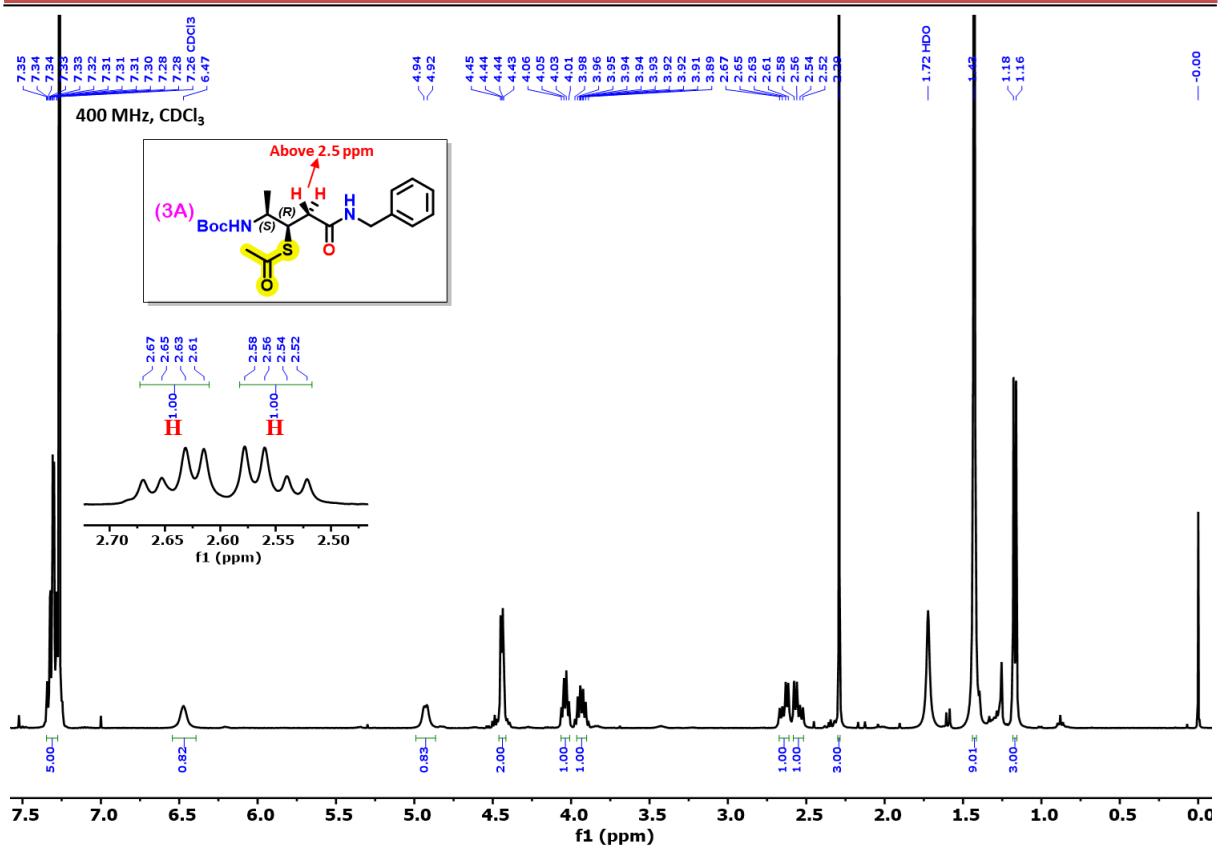

101 MHz, CDCl3
(2C)
BocHN
f1 (ppm)

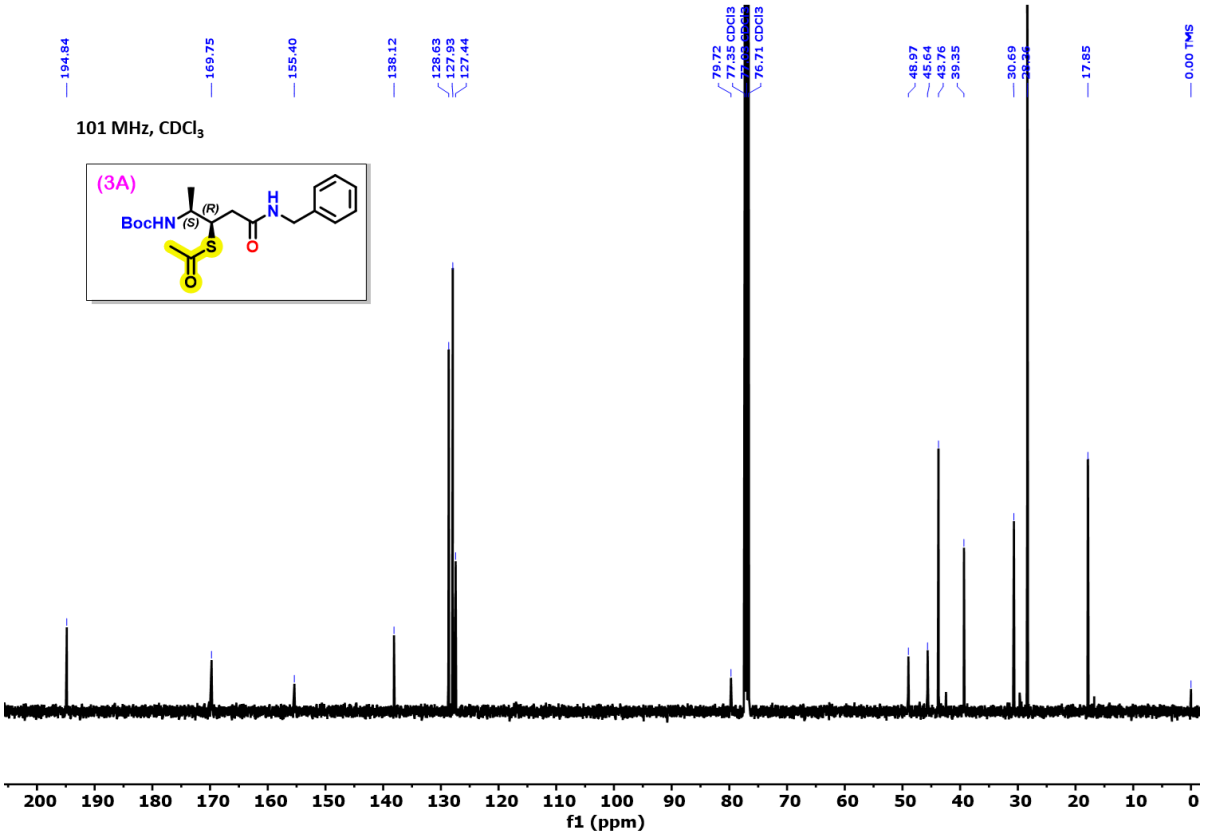

SAC 166C
IISER PUNE
SAC 166C 116 (2.117) AM2 (Ar,20000.0,556.28,0.00,LS 3); Sm (SG, 3x1.00)
1: TOF MS ES+
1.81e5
CALCULATED MASS
(M+Na)+ 431.1980
(2C)
BocHN
431.1976
432.2013
409.2160
410.2194
415.2244
411.2195
416.2282
428.1888
433.1977
447.1714
400.1563
406.1080
420.1978
426.2429
434.2003
438.1586
443.0642
448.1772
451.2112
m/z

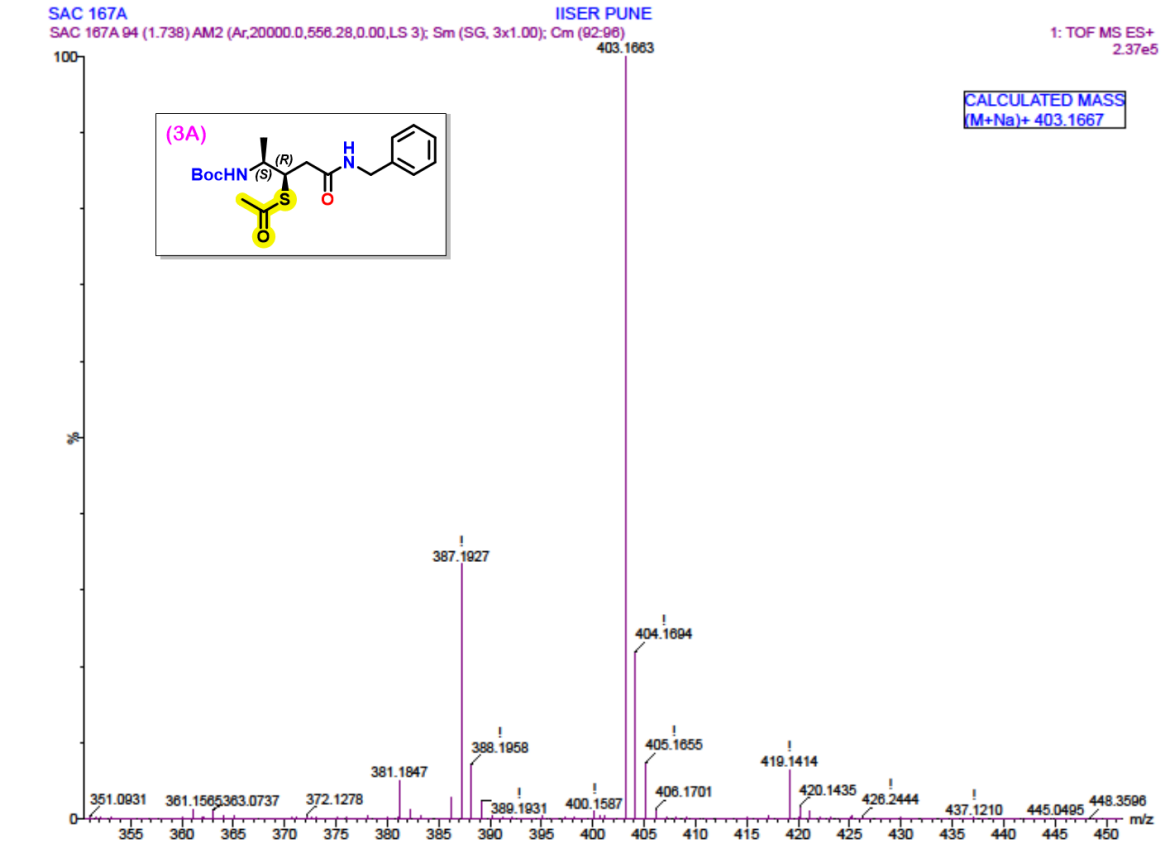

400 MHz, CDCl3
(2D)
BocHN
Below 2.5 ppm
f1 (ppm)

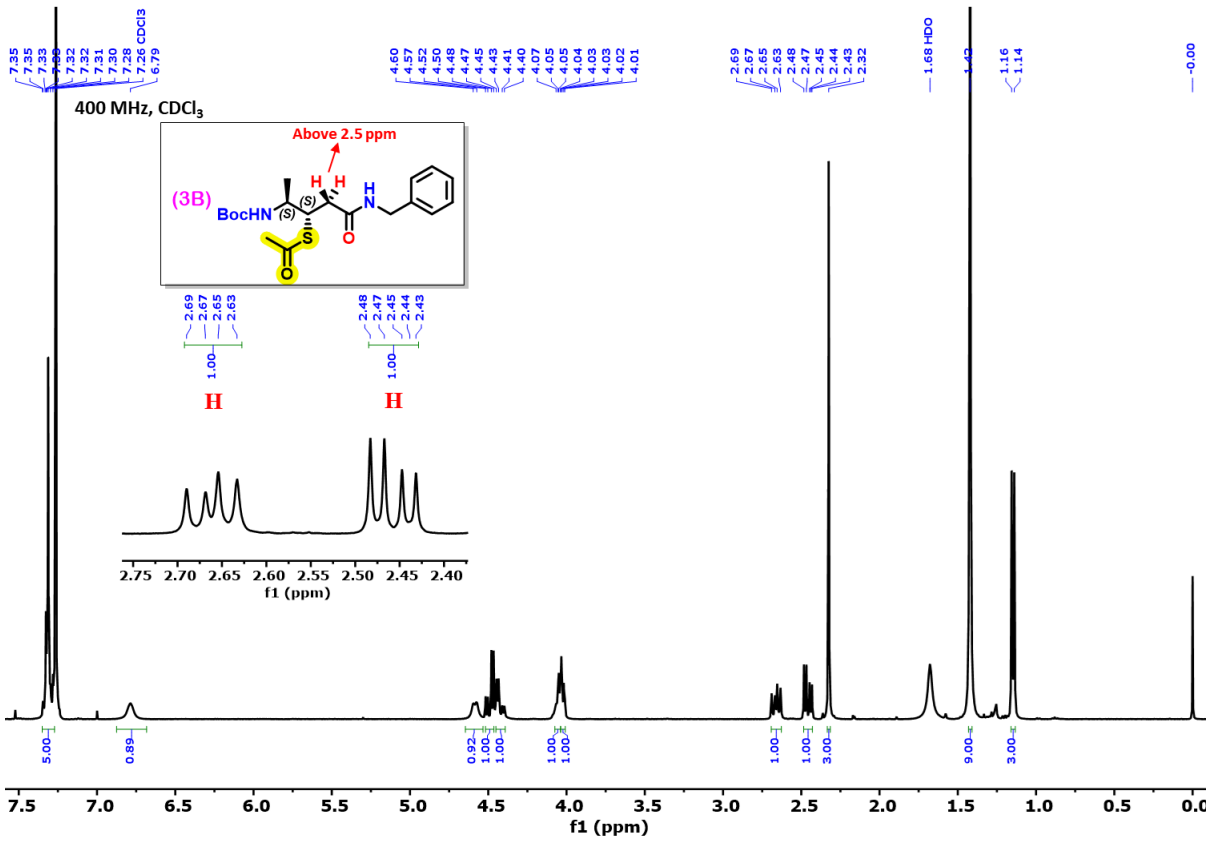

195.61
170.52
157.04
138.24
128.55
127.71
127.25
79.80
77.25 CDCl3
76.83 CDCl3
53.94
44.87
43.83
37.13
32.49
30.35
28.39
19.10
17.63
0.01
101 MHz, CDCl3
(2D)
BocHN
(R)
(S)
f1 (ppm)

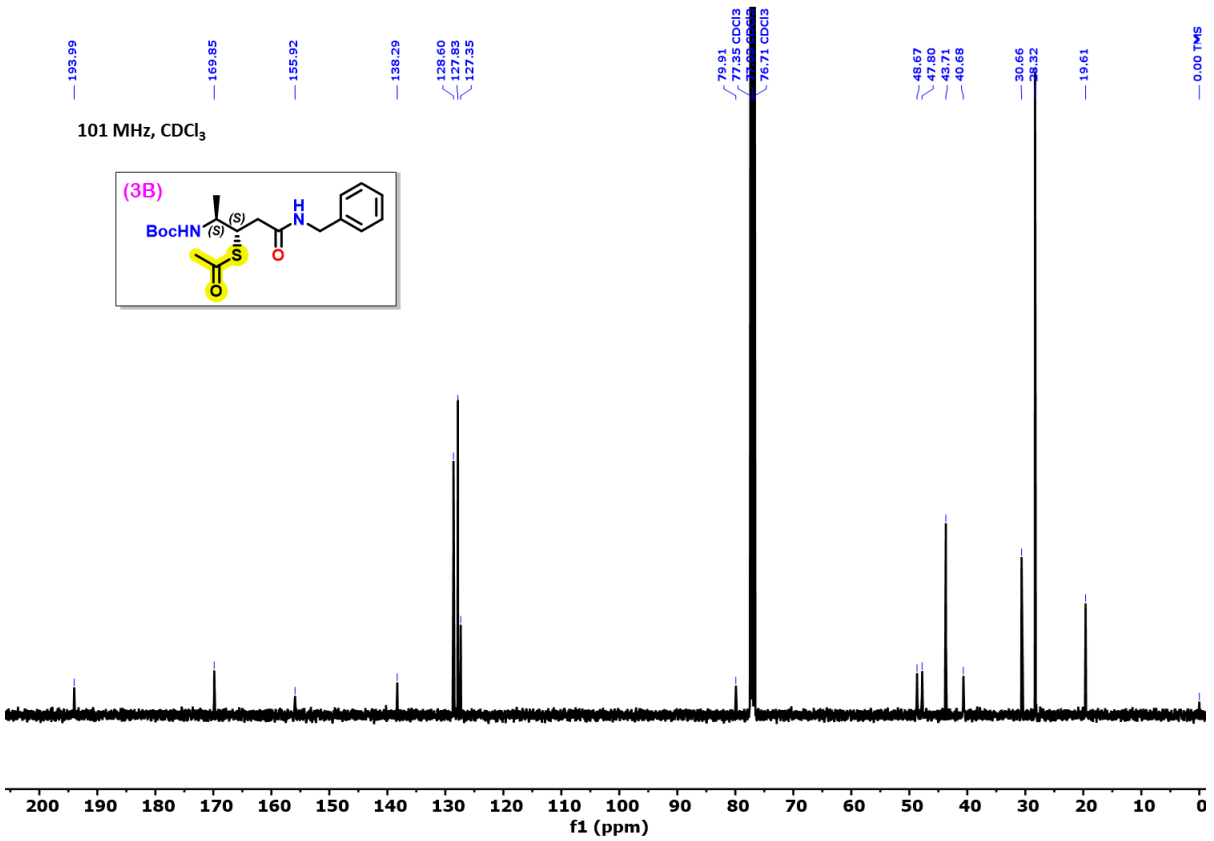

SAC 166D
IISER PUNE
SAC 166D 119 (2.168) AM2 (Ar,20000.0,556.28,0.00,LS 3); Sm (SG, 3x1.00)
1: TOF MS ES+
1.81e5
CALCULATED MASS
(M+Na)+ 431.1980
(2D)
BocHN
(R)
(S)
431.1980
409.2163
432.2014
415.2248
410.2195
433.1972
428.1885
411.2190
416.2284
447.1711
434.2001
400.1561
406.1080
426.2429
438.1586
443.0642
448.1772
451.2117
m/z

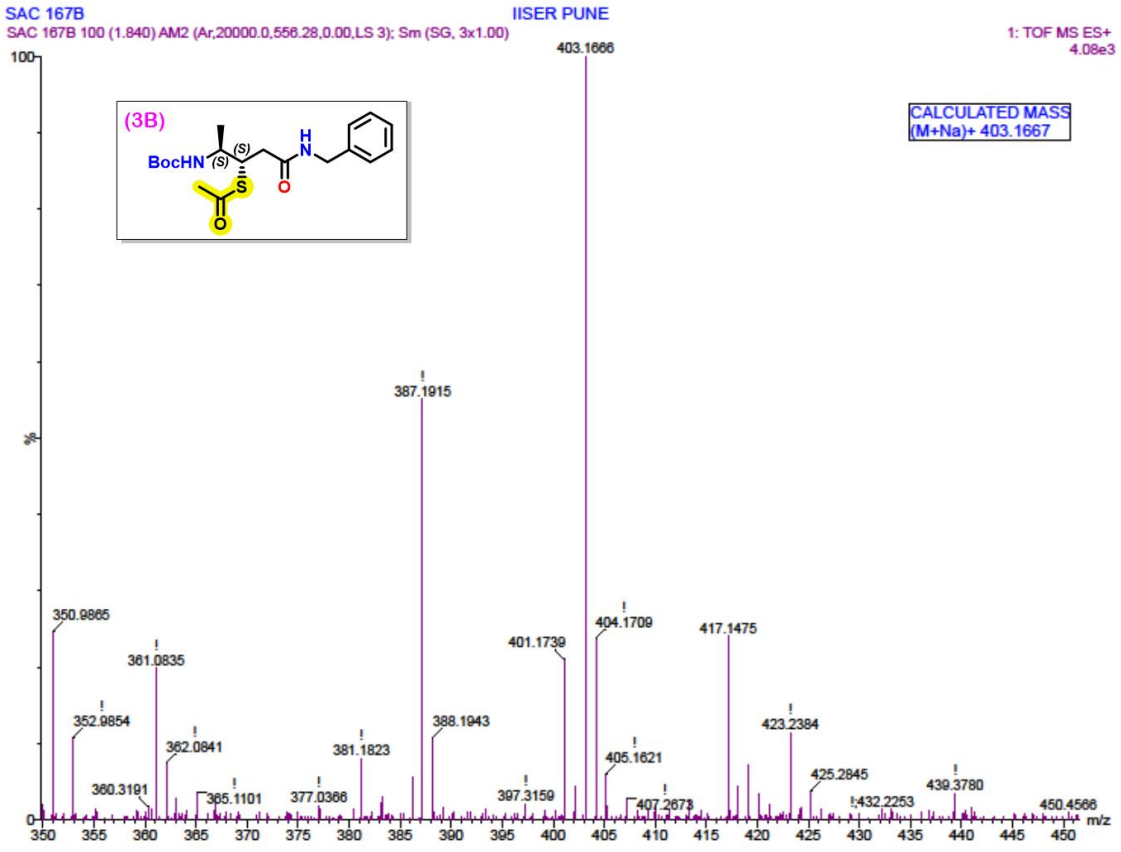

400 MHz, CDCl3
Above 2.5 ppm
(3A)
BocHN
f1 (ppm)

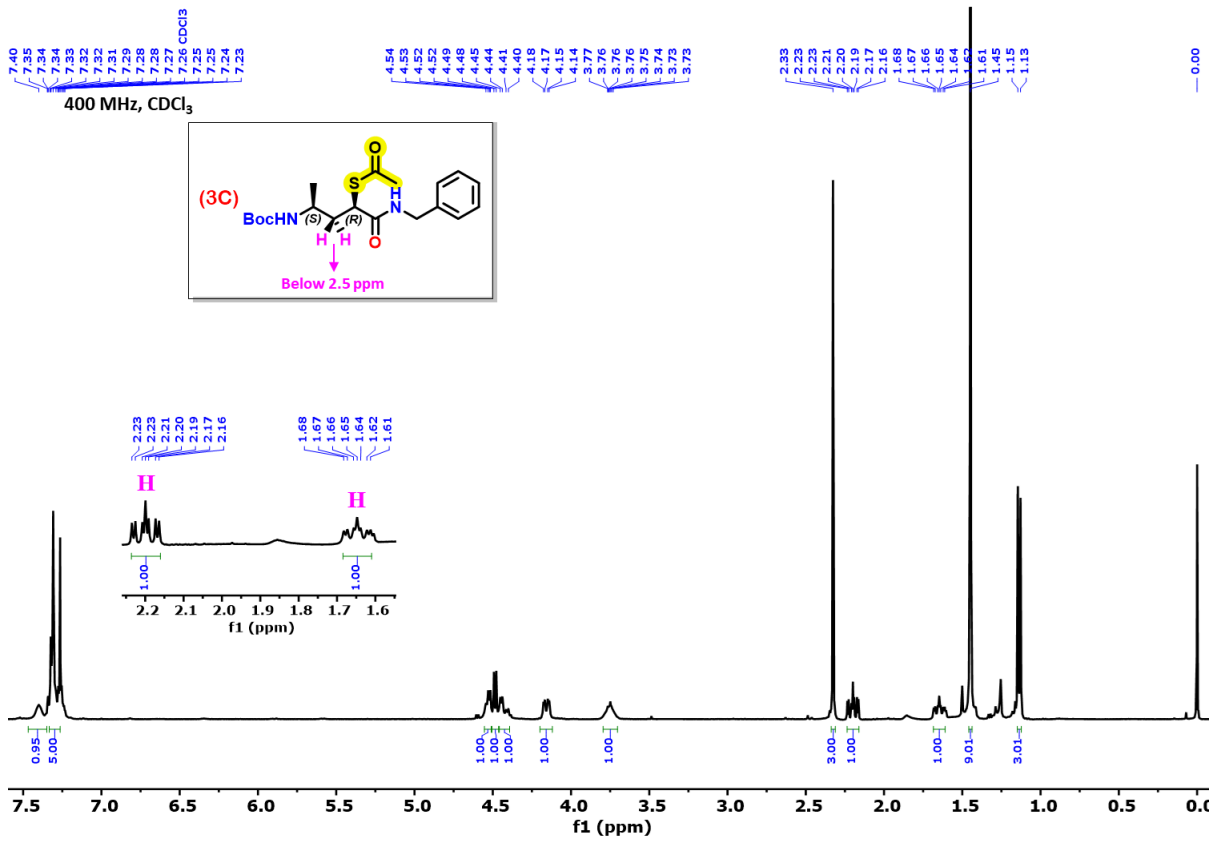

101 MHz, CDCl3
(3A)
BocHN
f1 (ppm)

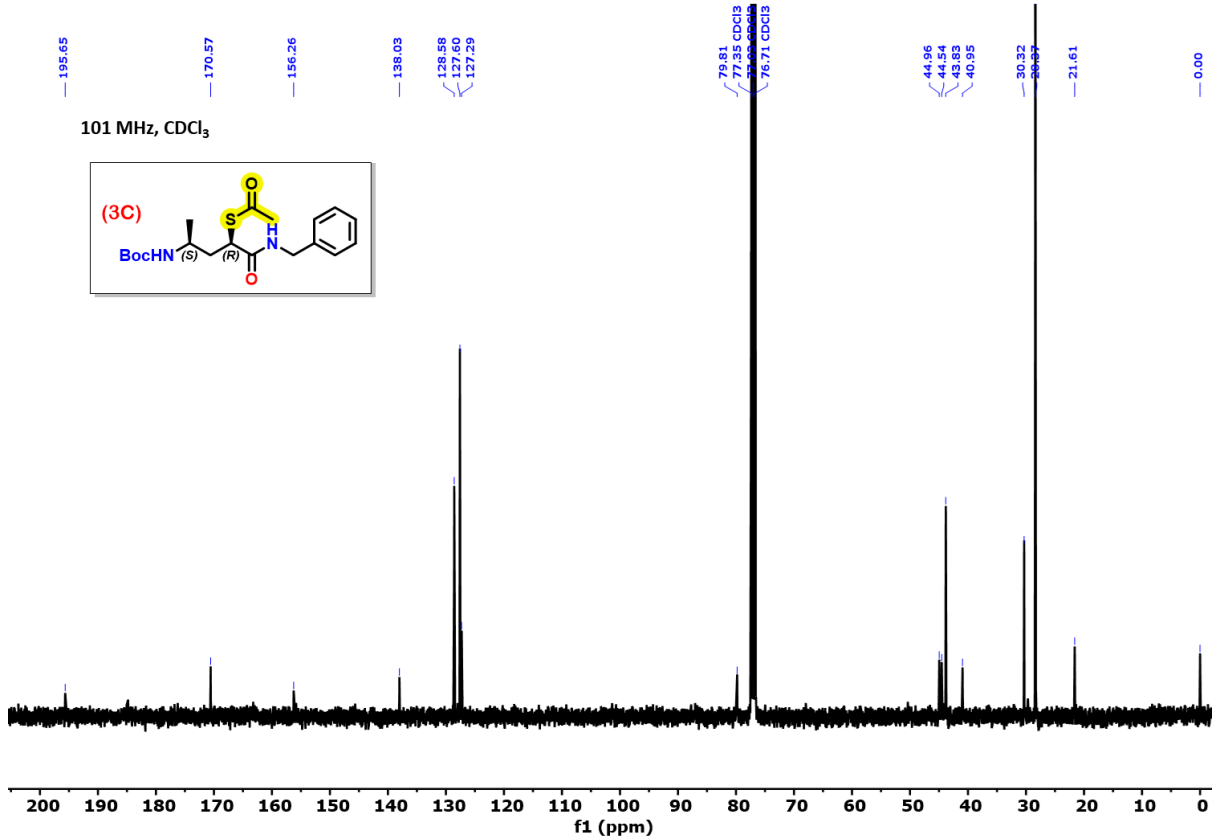

SAC 167A
IISER PUNE
SAC 167A 94 (1.738) AM2 (Ar,20000.0,556.28,0.00,LS 3); Sm (SG, 3x1.00); Cm (92:96)
1: TOF MS ES+
2.37e5
CALCULATED MASS
(M+Na)+ 403.1667
(3A)
BocHN
403.1663
387.1927
404.1694
388.1958
405.1655
419.1414
381.1847
420.1435
426.2444
351.0931
361.1565
363.0737
372.1278
389.1931
400.1587
406.1701
437.1210
445.0495
448.3596
m/z

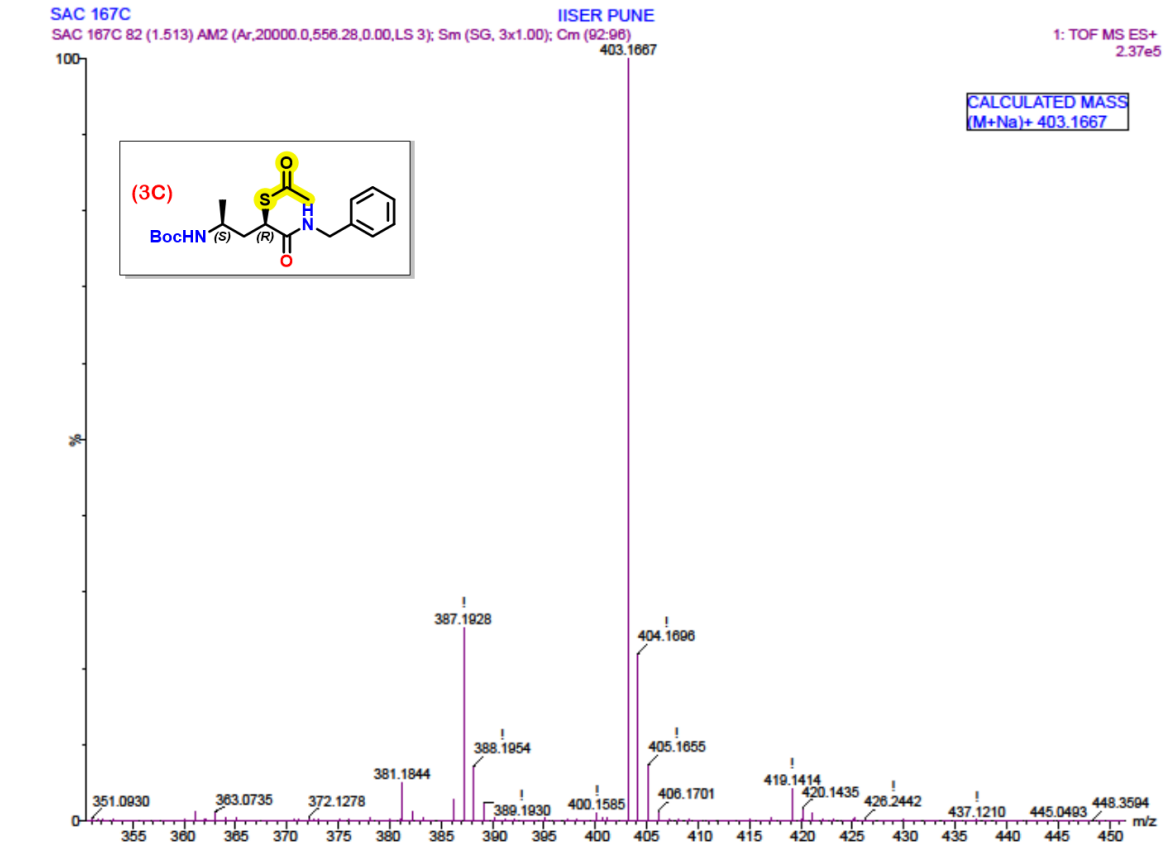

400 MHz, CDCl3
Above 2.5 ppm
(3B)
BocHN
H
H
f1 (ppm)

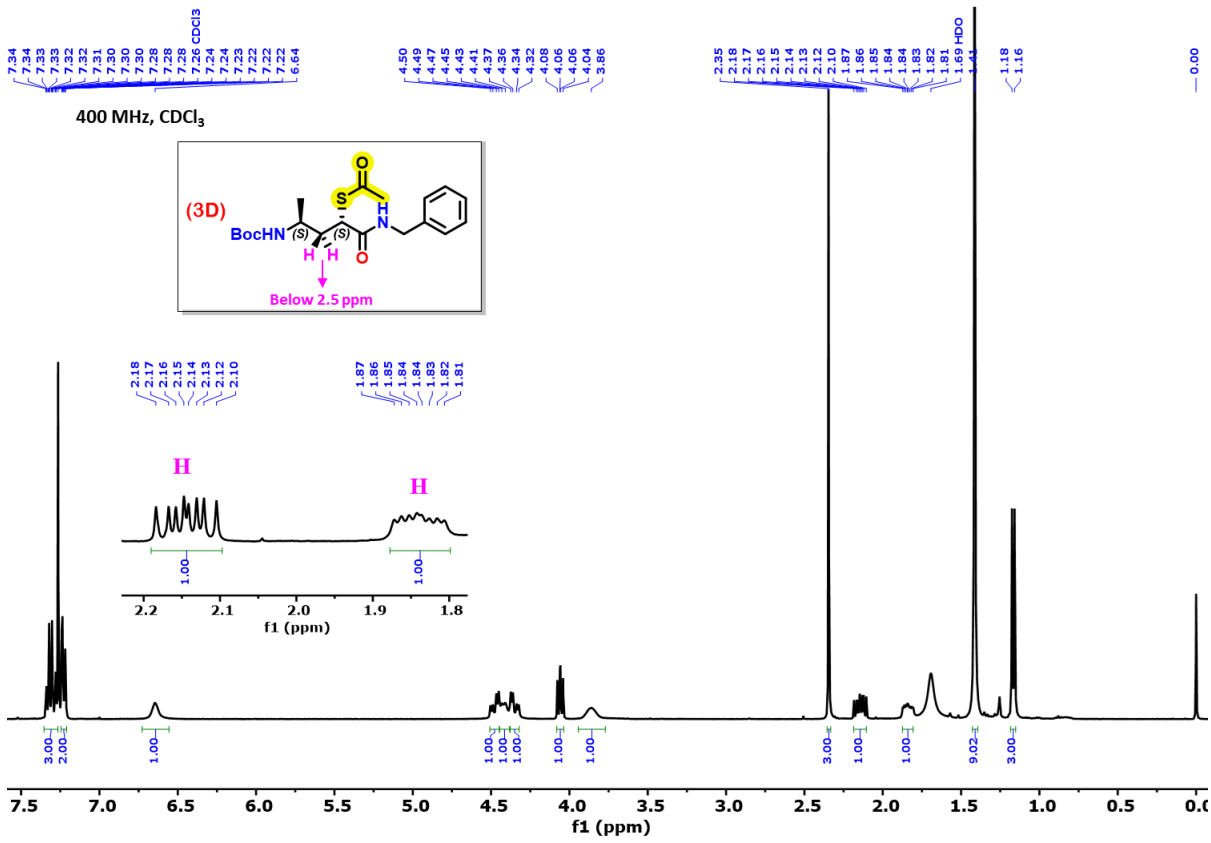

193.99
169.85
155.92
138.29
128.60
127.83
127.35
79.91
77.35 CDCl3
76.71 CDCl3
48.67
47.80
43.71
40.68
30.66
28.32
19.61
0.00 TMS
101 MHz, CDCl3
(3B)
BocHN
(S)
(S)
S
O
H
N
O
200 190 180 170 160 150 140 130 120 110 100 90 80 70 60 50 40 30 20 10 0
f1 (ppm)

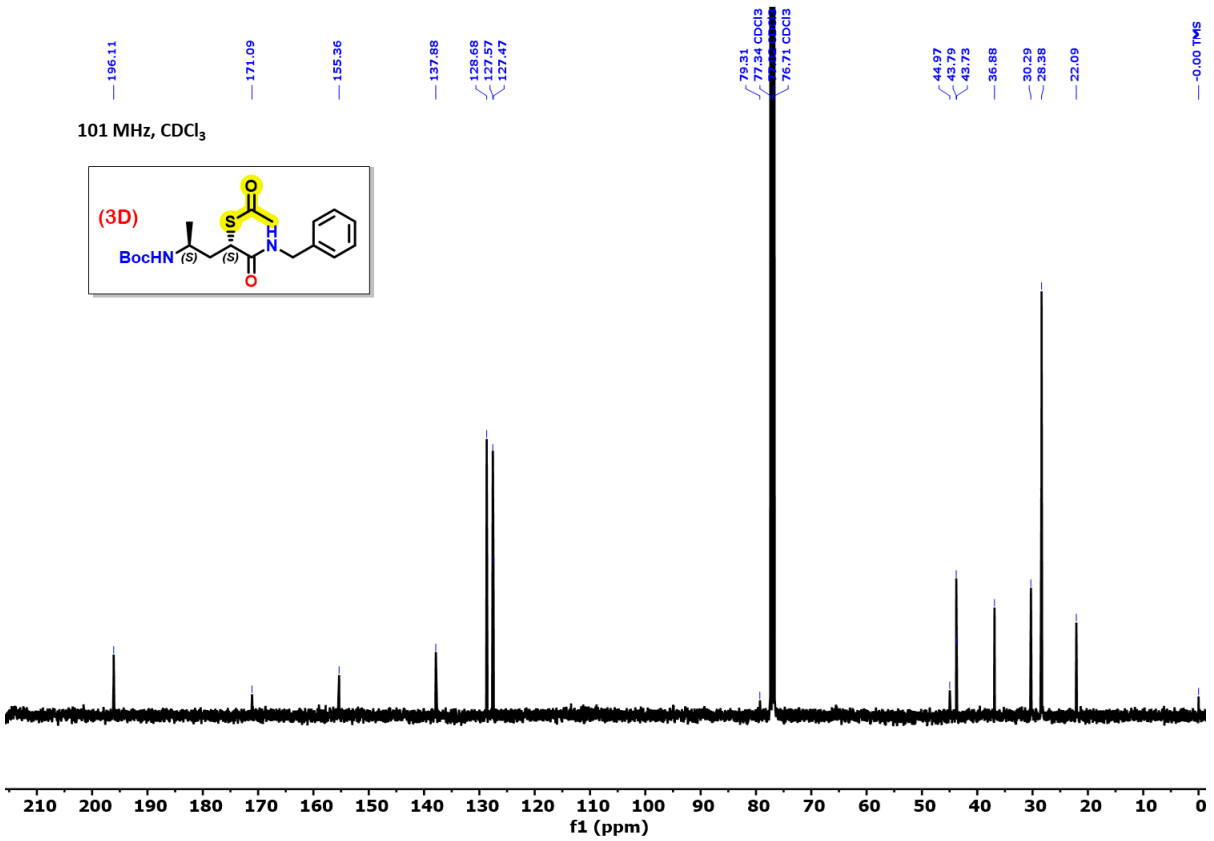

SAC 167B
IISER PUNE
SAC 167B 100 (1.840) AM2 (Ar,20000.0,556.28,0.00,LS 3); Sm (SG, 3x1.00)
1: TOF MS ES+
4.08e3
CALCULATED MASS
(M+Na)+ 403.1667
(3B)
BocHN
(S)
(S)
S
O
H
N
O
100
%
0
403.1666
387.1915
350.9865
361.0835
352.9854
362.0841
360.3191
365.1101
377.0366
381.1823
388.1943
397.3159
401.1739
404.1709
405.1621
407.2673
417.1475
423.2384
425.2845
432.2253
439.3780
450.4566
350 355 360 365 370 375 380 385 390 395 400 405 410 415 420 425 430 435 440 445 450
m/z

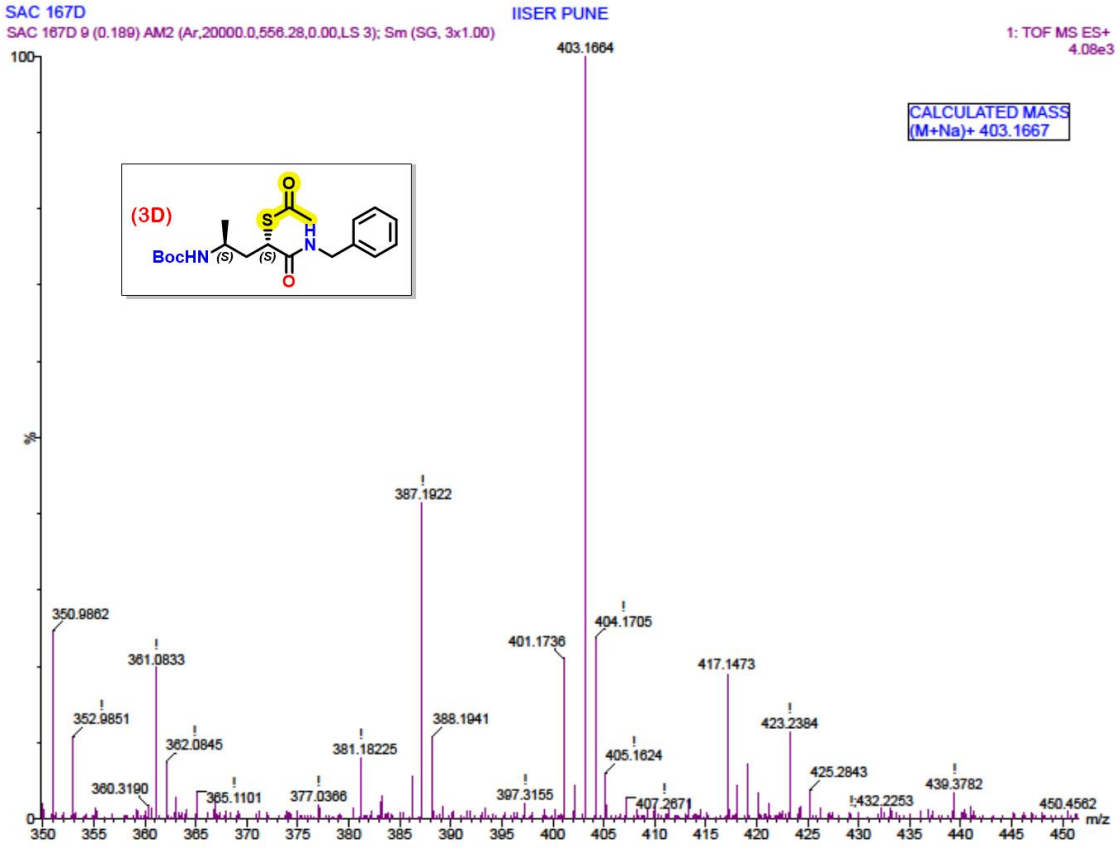

400 MHz, CDCl3
(3C)
BocHN
(S)
(R)
H H
O
Below 2.5 ppm
H
H
1.00
1.00
2.2 2.1 2.0 1.9 1.8 1.7 1.6
f1 (ppm)
0.95
5.00
1.00
1.00
1.00
1.00
1.00
3.00
1.00
1.00
9.01
3.01
7.5 7.0 6.5 6.0 5.5 5.0 4.5 4.0 3.5 3.0 2.5 2.0 1.5 1.0 0.5
f1 (ppm)

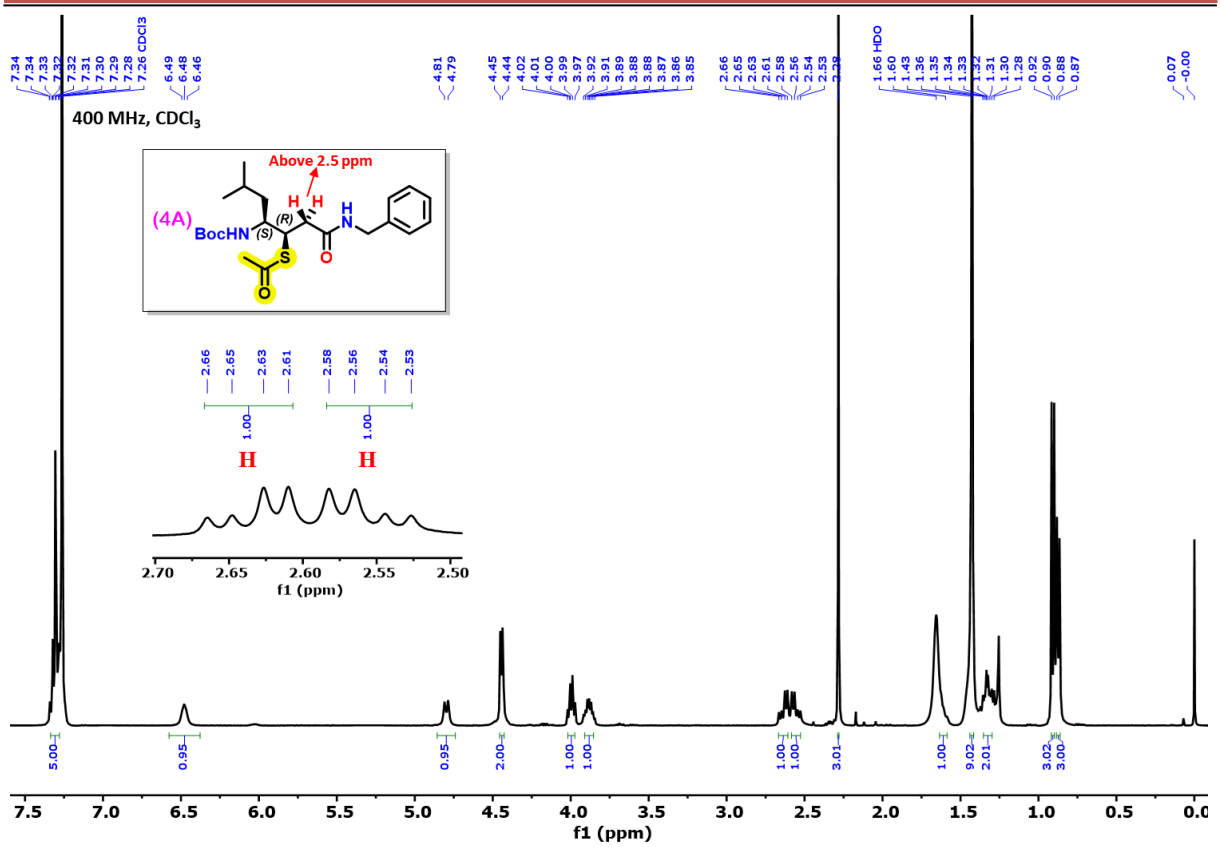

195.65
170.57
156.26
138.03
128.58
127.60
127.29
79.81
77.35 CDCl3
76.71 CDCl3
44.96
44.54
43.83
40.95
30.32
21.61
0.00
101 MHz, CDCl3
(3C)
BocHN
(S)
(R)
200 190 180 170 160 150 140 130 120 110 100 90 80 70 60 50 40 30 20 10 0
f1 (ppm)

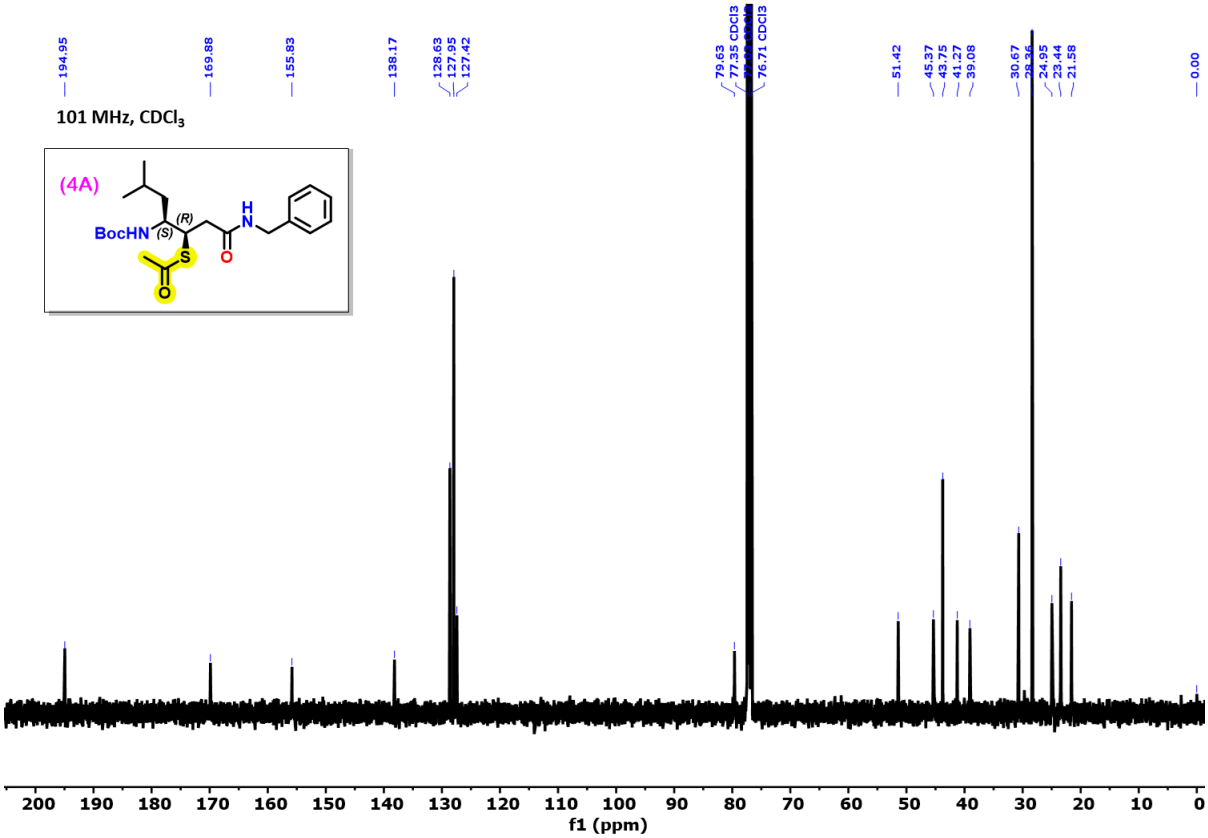

SAC 167C
IISER PUNE
SAC 167C 82 (1.513) AM2 (Ar,20000.0,556.28,0.00,LS 3); Sm (SG, 3x1.00); Cm (92:96)
1: TOF MS ES+
2.37e5
403.1667
CALCULATED MASS
(M+Na)+ 403.1667
(3C)
BocHN
(S)
(R)
387.1928
404.1696
388.1954
405.1655
381.1844
419.1414
420.1435
406.1701
351.0930
363.0735
372.1278
389.1930
400.1585
426.2442
437.1210
445.0493
448.3594
m/z

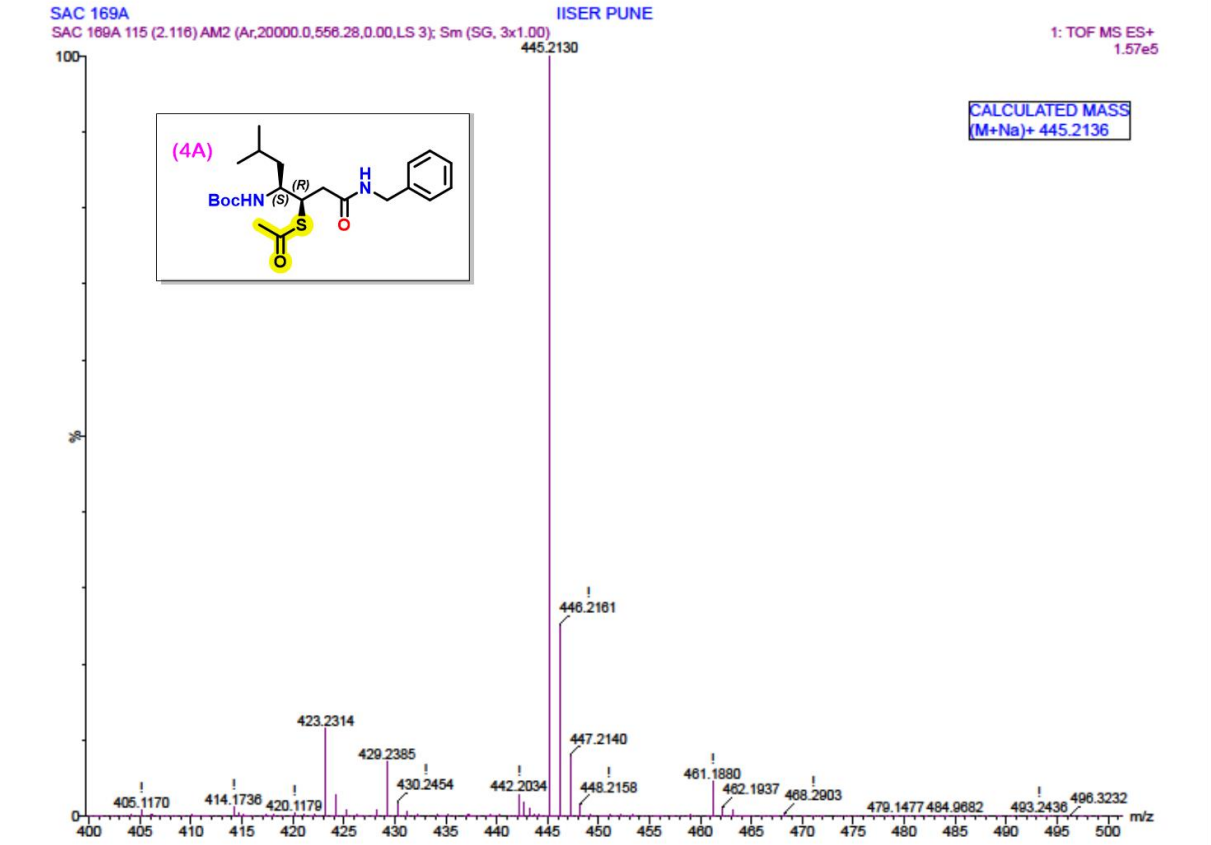

400 MHz, CDCl3
(3D)
BocHN
(S)
(S)
H H
O
Below 2.5 ppm
H
H
f1 (ppm)
f1 (ppm)

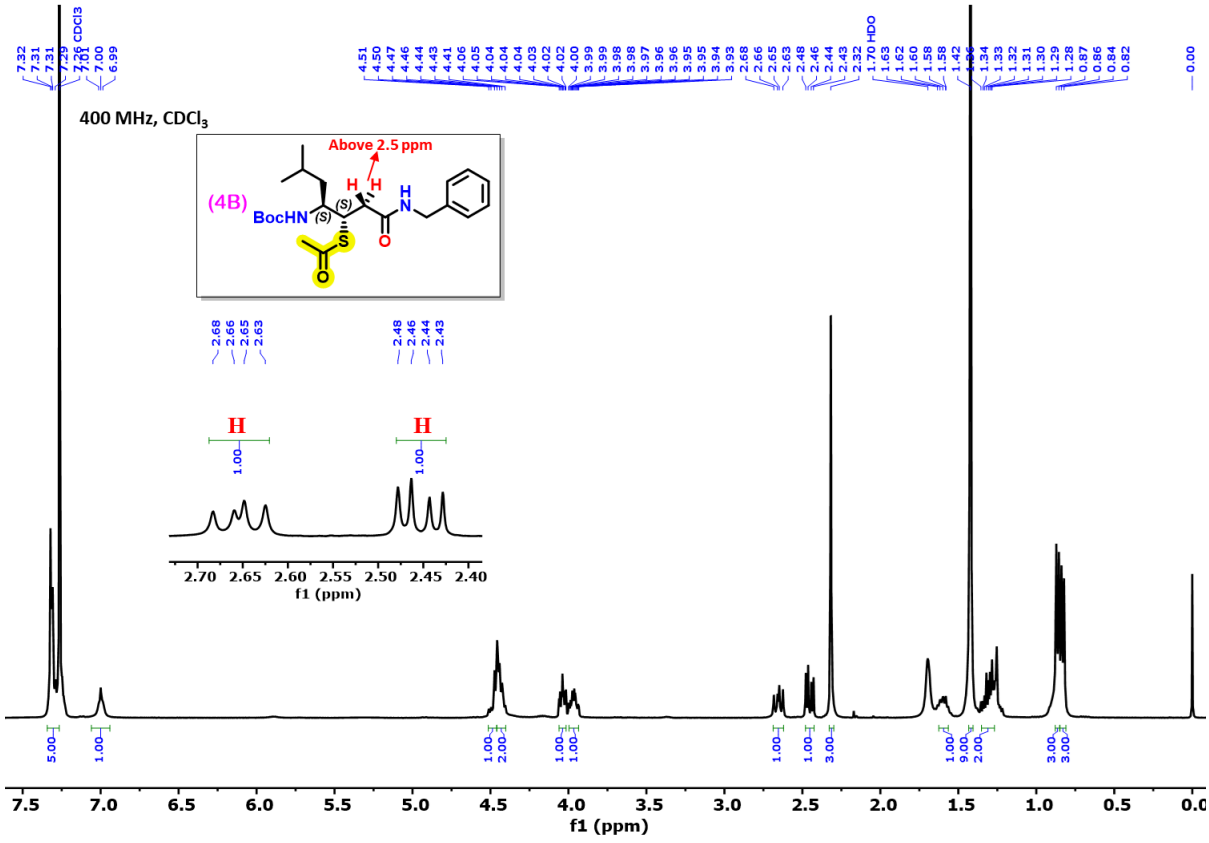

196.11
171.09
155.36
137.88
128.68
127.57
127.47
79.31
77.34 CDCl3
76.71 CDCl3
44.97
43.79
43.73
36.88
30.29
28.38
22.09
-0.00 TMS
101 MHz, CDCl3
(3D)
BocHN
(S)
(S)
O
S
H
N
O
210 200 190 180 170 160 150 140 130 120 110 100 90 80 70 60 50 40 30 20 10 0
f1 (ppm)

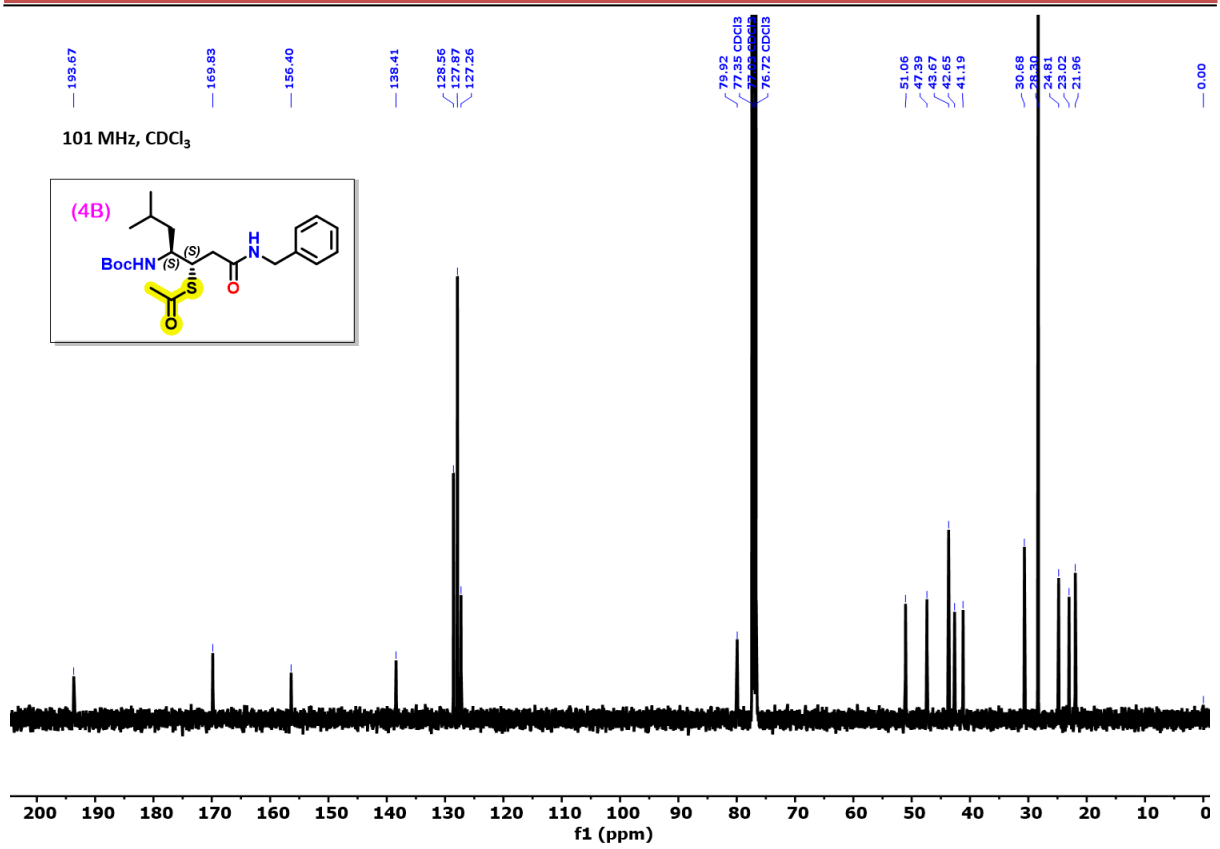

SAC 167D
SAC 167D 9 (0.189) AM2 (Ar,20000.0,556.28,0.00,LS 3); Sm (SG, 3x1.00)
IISER PUNE
1: TOF MS ES+
4.08e3
CALCULATED MASS
(M+Na)+ 403.1667
(3D)
BocHN
(S)
(S)
403.1664
387.1922
350.9862
404.1705
401.1736
361.0833
417.1473
352.9851
388.1941
423.2384
362.0845
381.18225
405.1624
425.2843
360.3190
365.1101
377.0366
397.3155
407.2671
432.2253
439.3782
450.4562
%
m/z

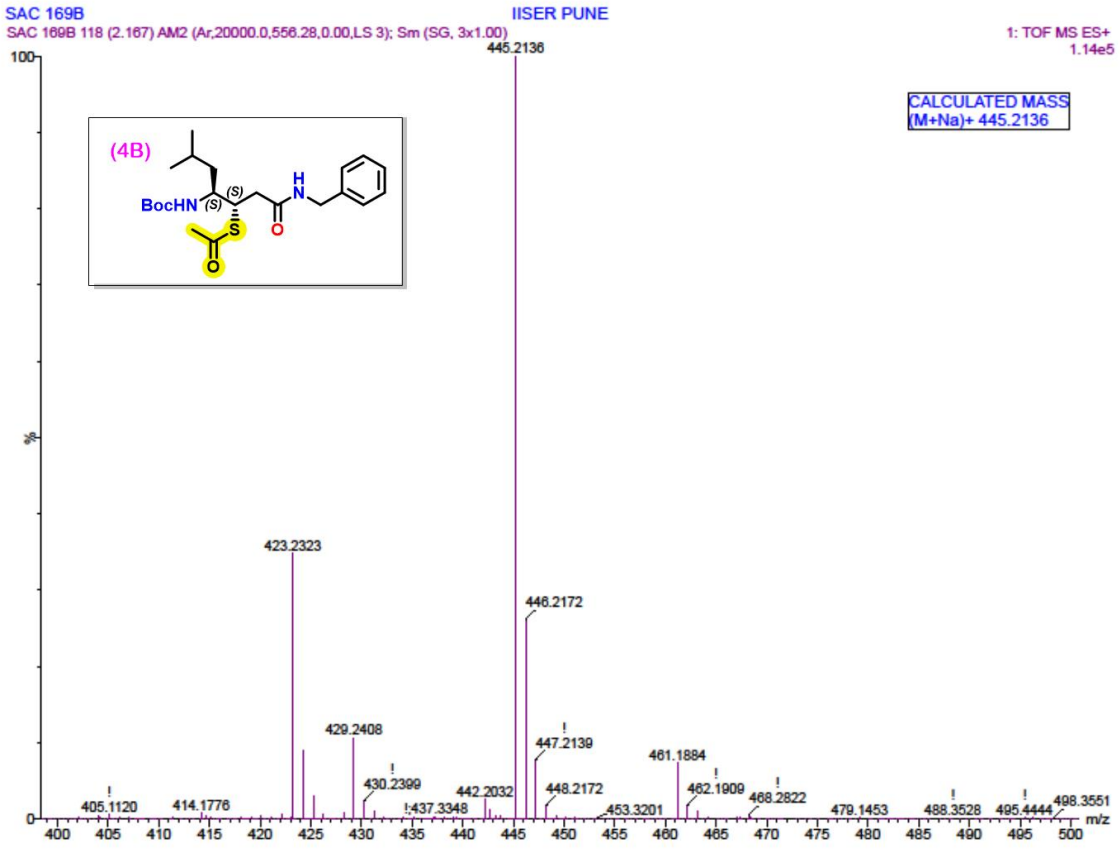

400 MHz, CDCl3
Above 2.5 ppm
(4A)
BocHN
f1 (ppm)

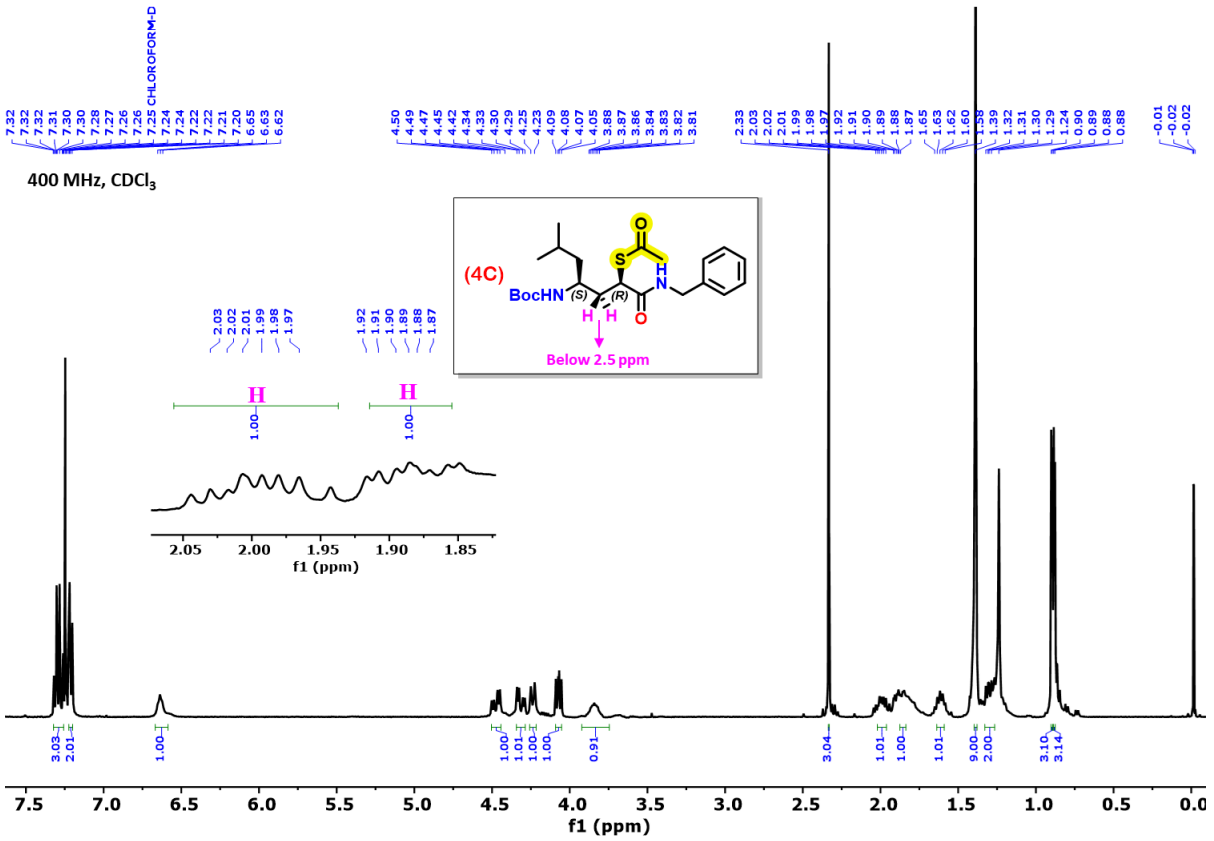

101 MHz, CDCl3
(4A)
BocHN
f1 (ppm)

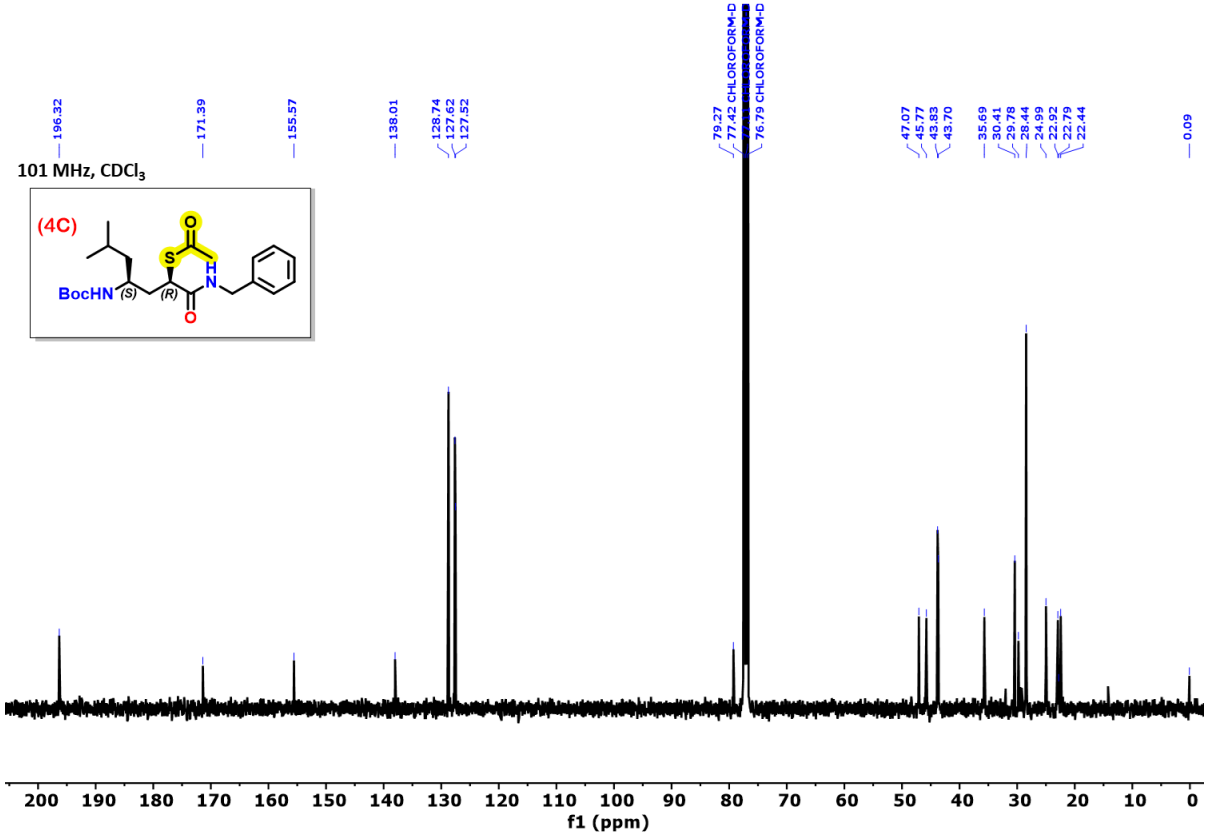

SAC 169A
IISER PUNE
SAC 169A 115 (2.116) AM2 (Ar,20000.0,556.28,0.00,LS 3); Sm (SG, 3x1.00)
1: TOF MS ES+
1.57e5
(4A)
BocHN
CALCULATED MASS
(M+Na)+ 445.2136
445.2130
446.2161
423.2314
429.2385
447.2140
430.2454
442.2034
448.2158
461.1880
462.1937
468.2903
405.1170
414.1736
420.1179
479.1477
484.9682
493.2436
496.3232
m/z

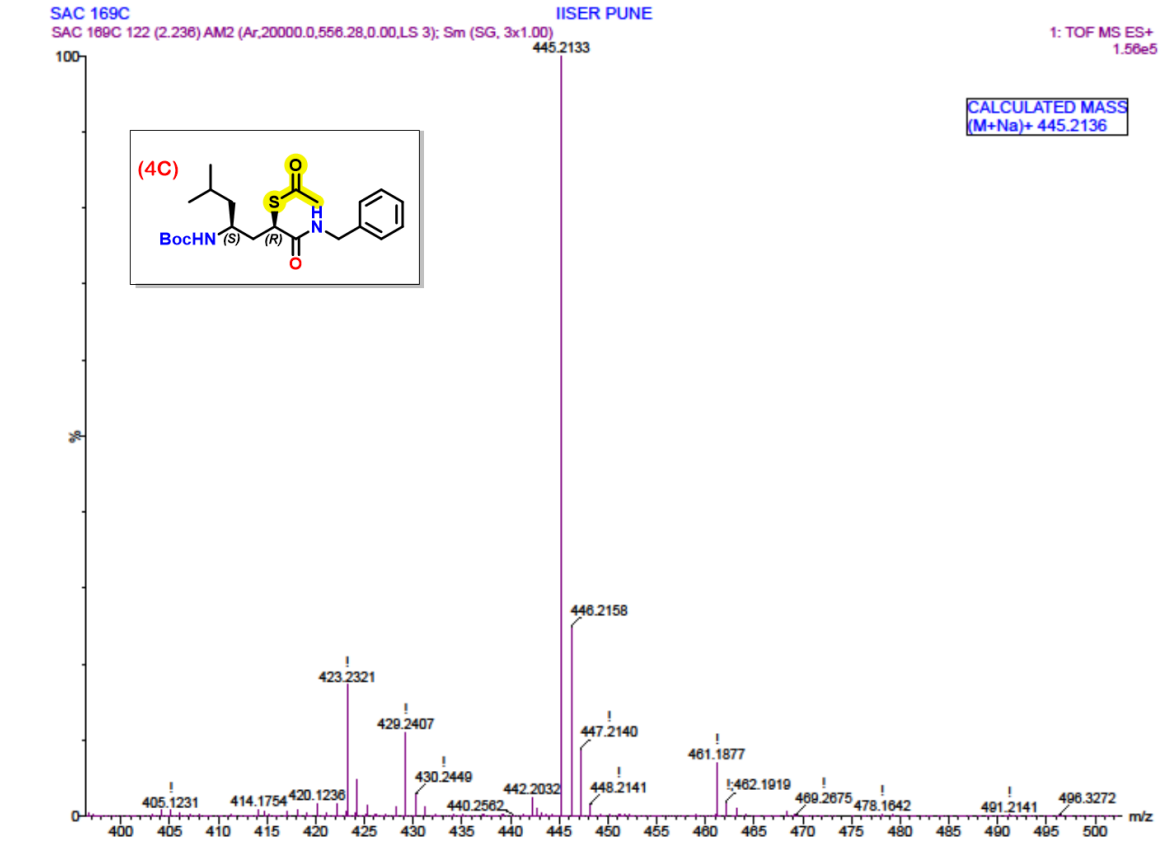

400 MHz, CDCl3
(4B)
BocHN
Above 2.5 ppm
H
H
f1 (ppm)

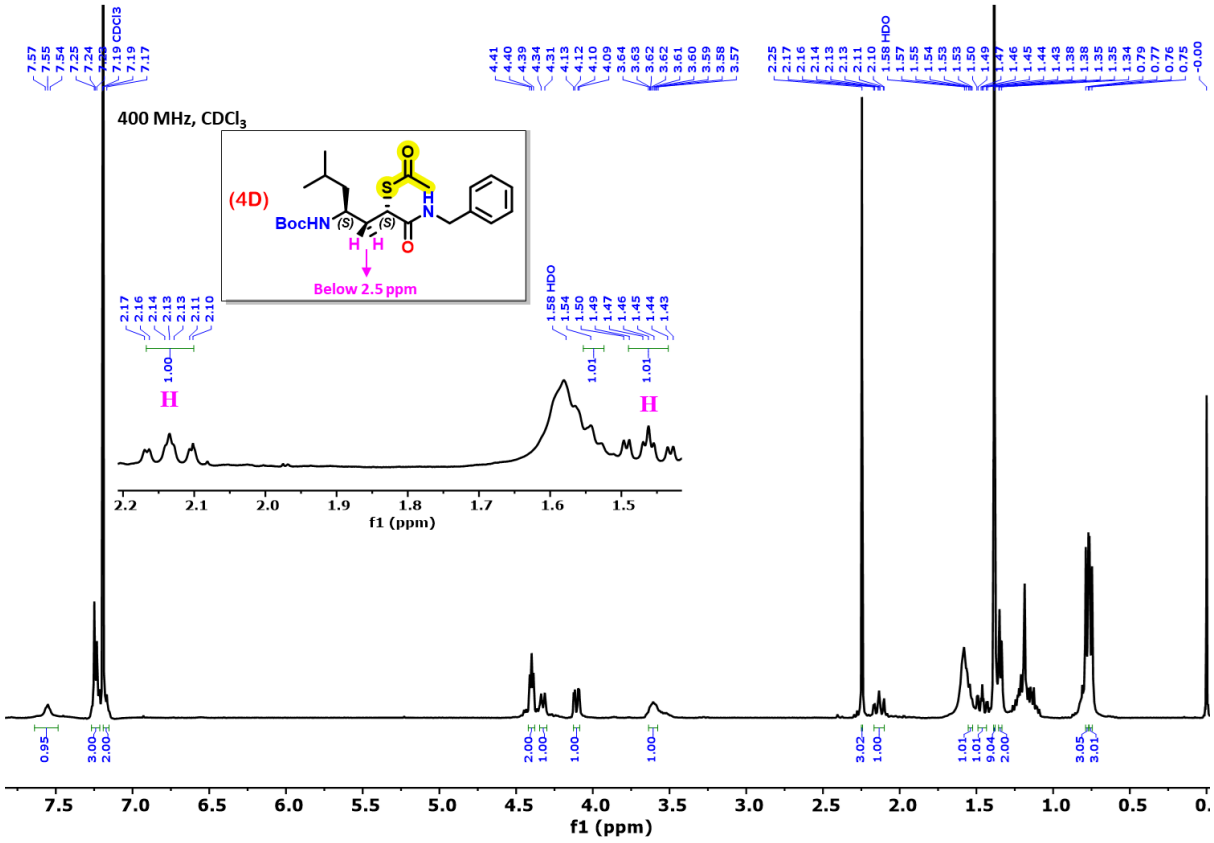

193.67
169.83
156.40
138.41
128.56
127.87
127.26
79.92
77.35 CDCl3
76.72 CDCl3
51.06
47.39
43.67
42.65
41.19
30.68
28.30
24.81
23.02
21.96
0.00
101 MHz, CDCl3
(4B)
BocHN
(S)
(S)
H
N
S
O
O
200 190 180 170 160 150 140 130 120 110 100 90 80 70 60 50 40 30 20 10 0
f1 (ppm)

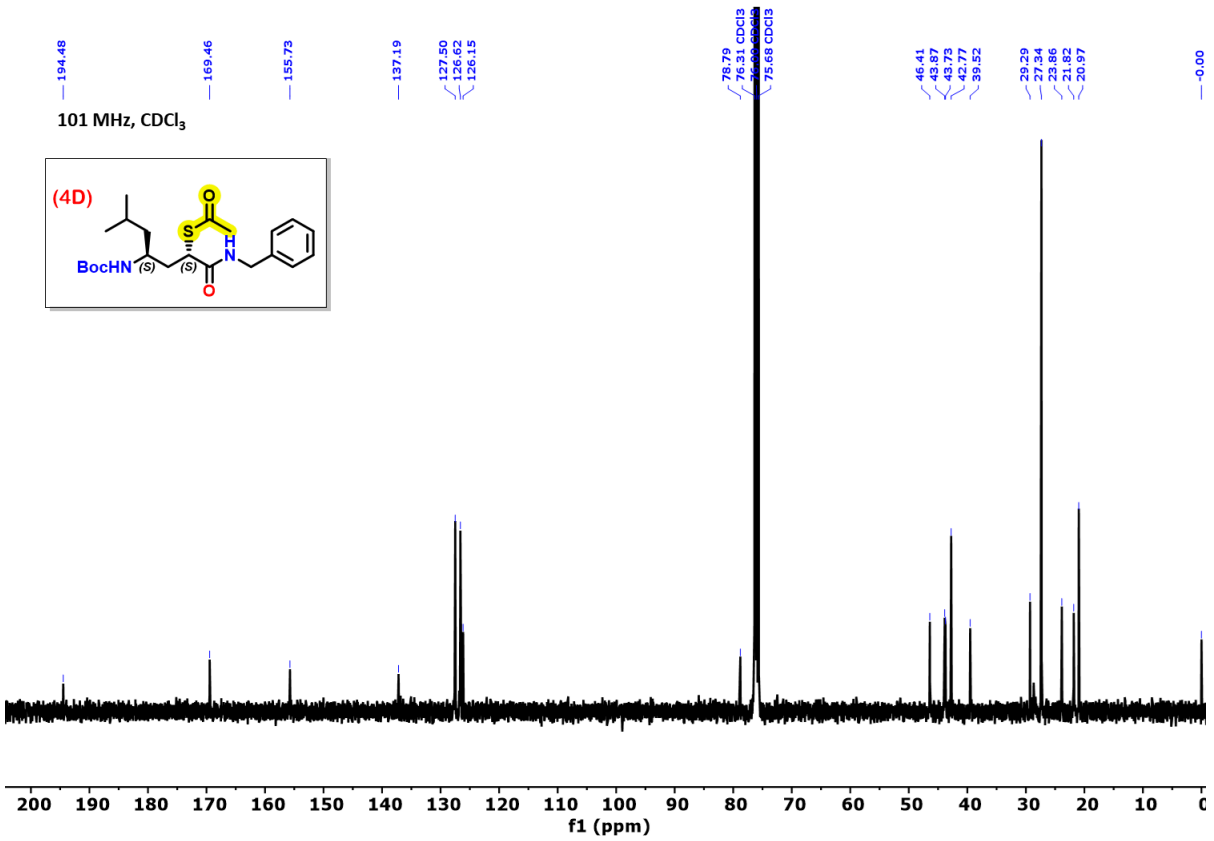

SAC 169B
IISER PUNE
SAC 169B 118 (2.167) AM2 (Ar,20000.0,556.28,0.00,LS 3); Sm (SG, 3x1.00)
1: TOF MS ES+
1.14e5
CALCULATED MASS
(M+Na)+ 445.2136
(4B)
BocHN
(S)
(S)
H
N
S
O
O
100
%
0
445.2136
423.2323
446.2172
429.2408
447.2139
461.1884
430.2399
462.1909
468.2822
405.1120
414.1776
437.3348
442.2032
448.2172
453.3201
479.1453
488.3528
495.4444
498.3551
400 405 410 415 420 425 430 435 440 445 450 455 460 465 470 475 480 485 490 495 500
m/z

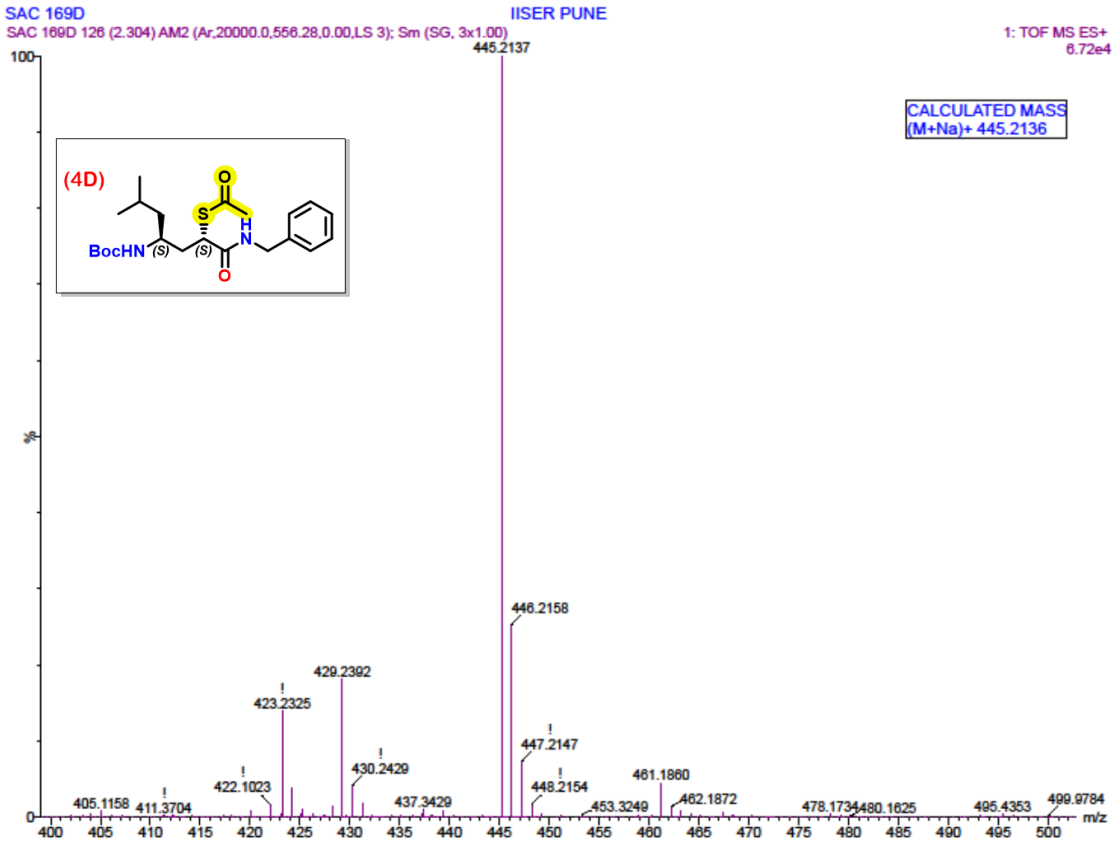

400 MHz, CDCl3
(4C)
BocHN (S) (R)
Below 2.5 ppm
f1 (ppm)

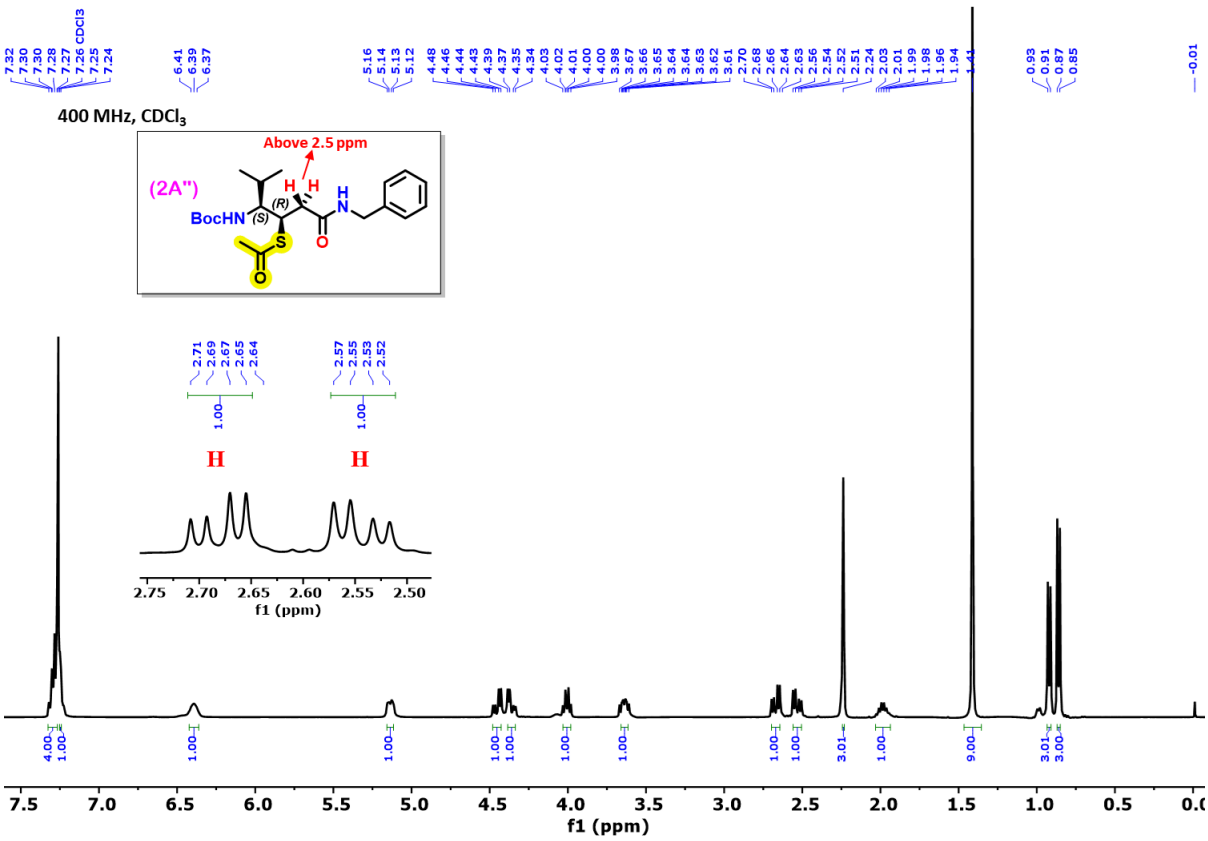

101 MHz, CDCl3
(4C)
BocHN (S) (R)
f1 (ppm)

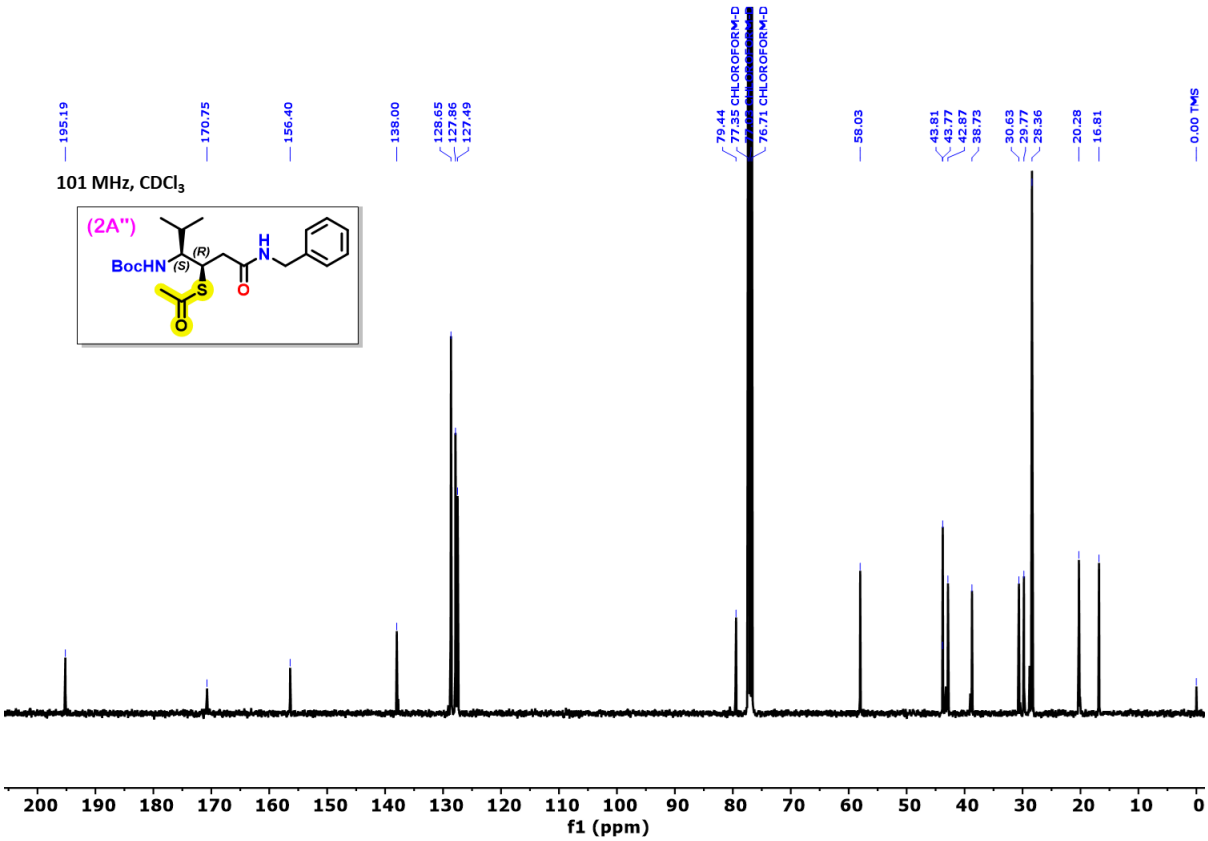

SAC 169C
IISER PUNE
SAC 169C 122 (2.236) AM2 (Ar,20000.0,556.28,0.00,LS 3); Sm (SG, 3x1.00)
1: TOF MS ES+
1.56e5
CALCULATED MASS
(M+Na)+ 445.2136
(4C)
BocHN (S) (R)
445.2133
446.2158
423.2321
429.2407
447.2140
461.1877
430.2449
448.2141
462.1919
405.1231
414.1754
420.1236
440.2562
442.2032
469.2675
478.1642
491.2141
496.3272
m/z

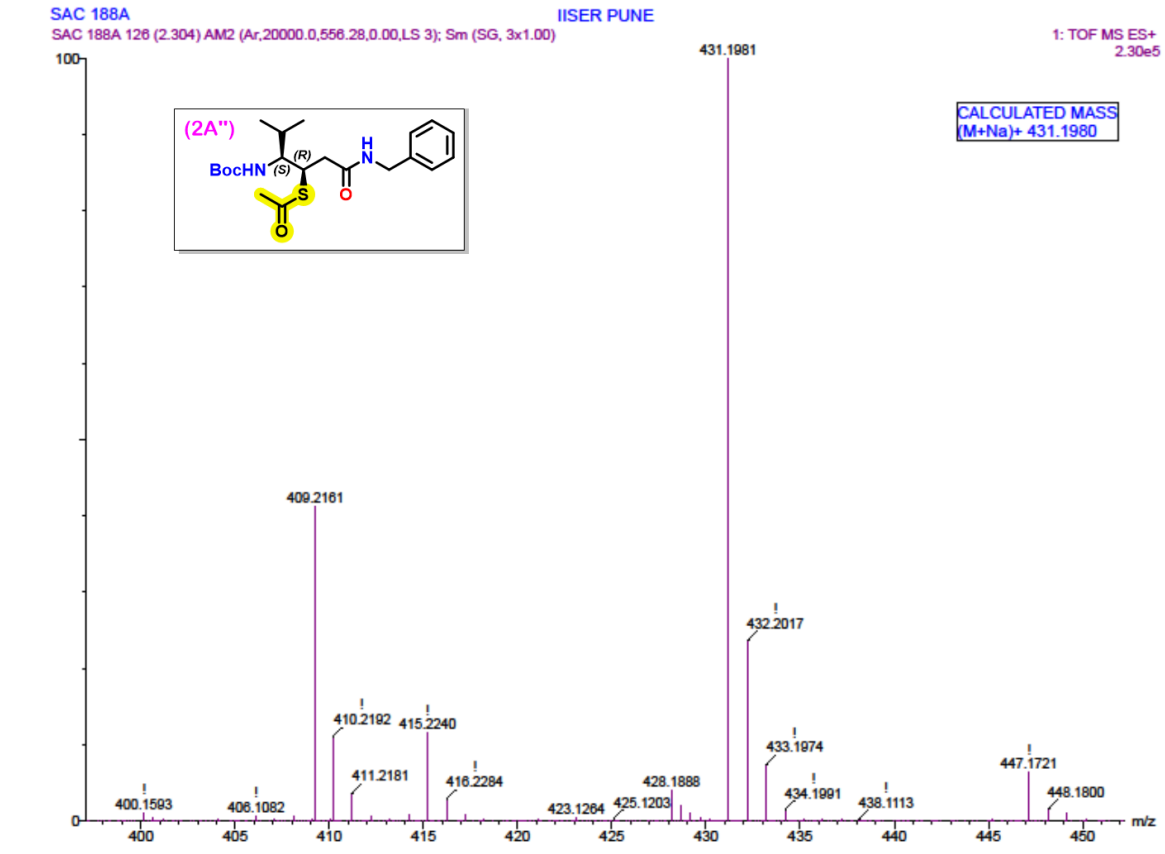

400 MHz, CDCl3
(4D)
BocHN (S) (S)
Below 2.5 ppm
HDO
CDCl3
f1 (ppm)

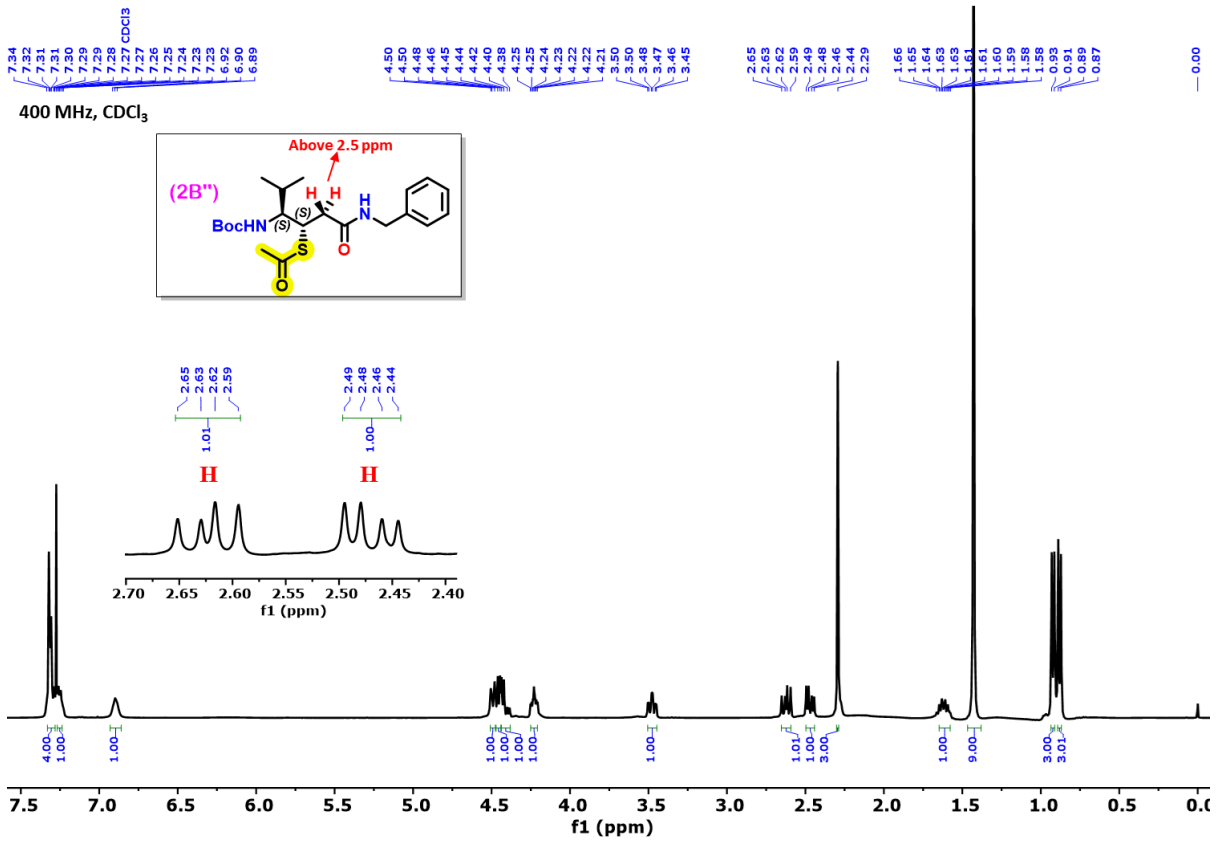

194.48
169.46
155.73
137.19
127.50
126.62
126.15
78.79
76.31 CDCl3
75.68 CDCl3
46.41
43.87
43.73
42.77
39.52
29.29
27.34
23.86
21.82
20.97
-0.00
101 MHz, CDCl3
(4D)
BocHN
f1 (ppm)

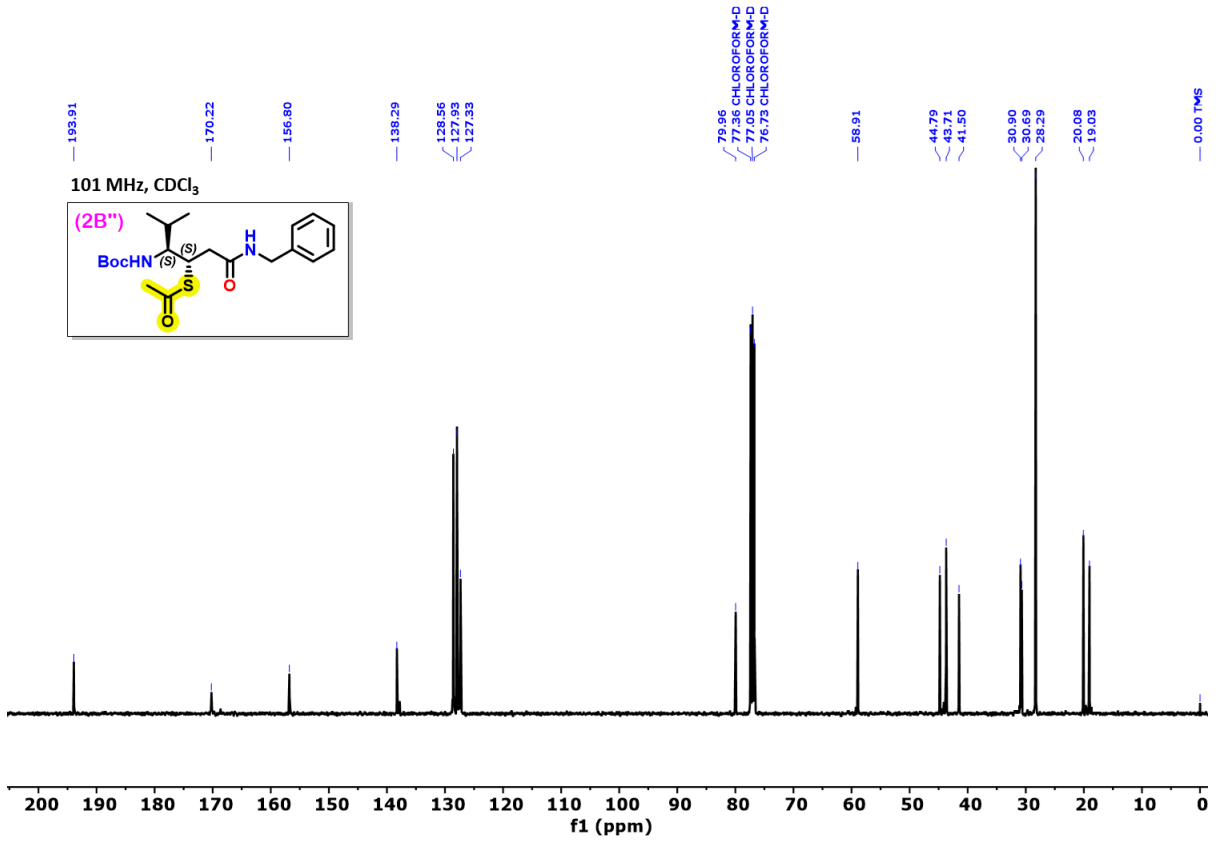

SAC 169D
IISER PUNE
SAC 169D 126 (2.304) AM2 (Ar,20000.0,556.28,0.00,LS 3); Sm (SG, 3x1.00)
1: TOF MS ES+
6.72e4
CALCULATED MASS
(M+Na)+ 445.2136
(4D)
BocHN
445.2137
446.2158
447.2147
448.2154
429.2392
423.2325
430.2429
422.1023
405.1158
411.3704
437.3429
453.3249
461.1860
462.1872
478.1734
480.1625
495.4353
499.9784
%
m/z

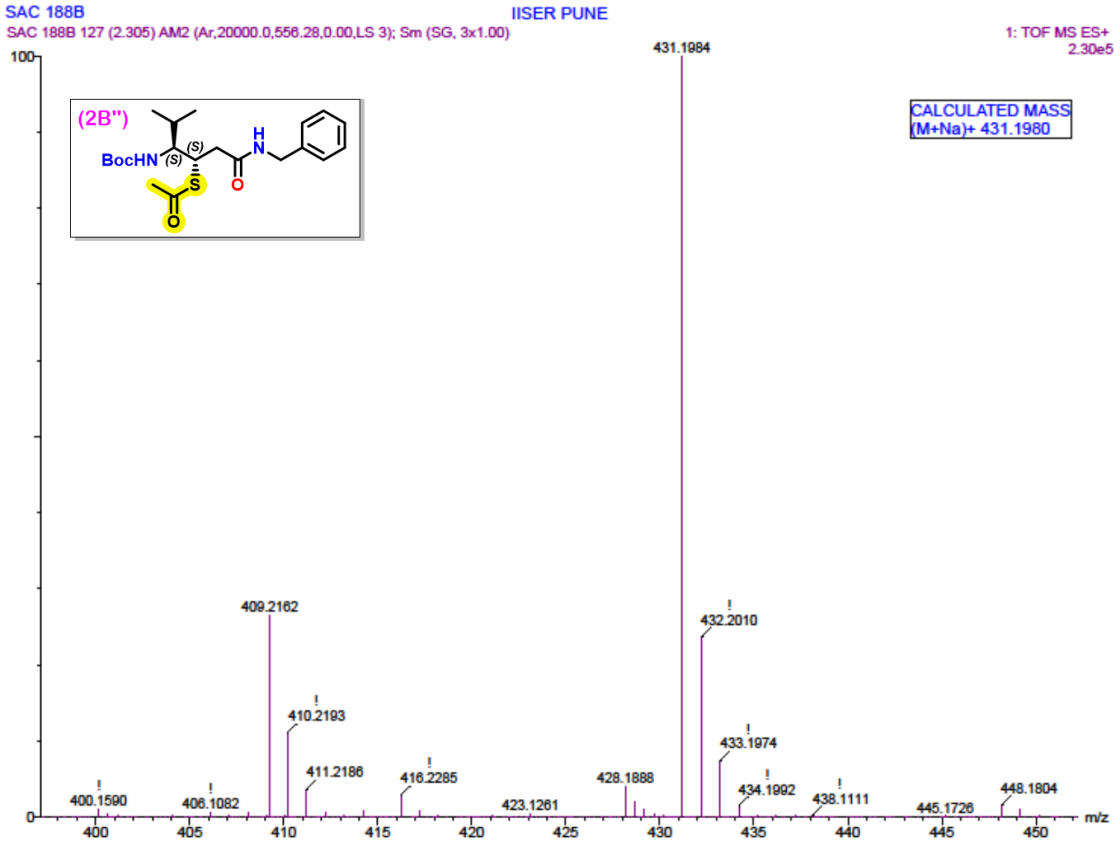

400 MHz, CDCl3
Above 2.5 ppm
(2A")
BocHN
(S)
(R)
H
H
N
S
O
O
f1 (ppm)

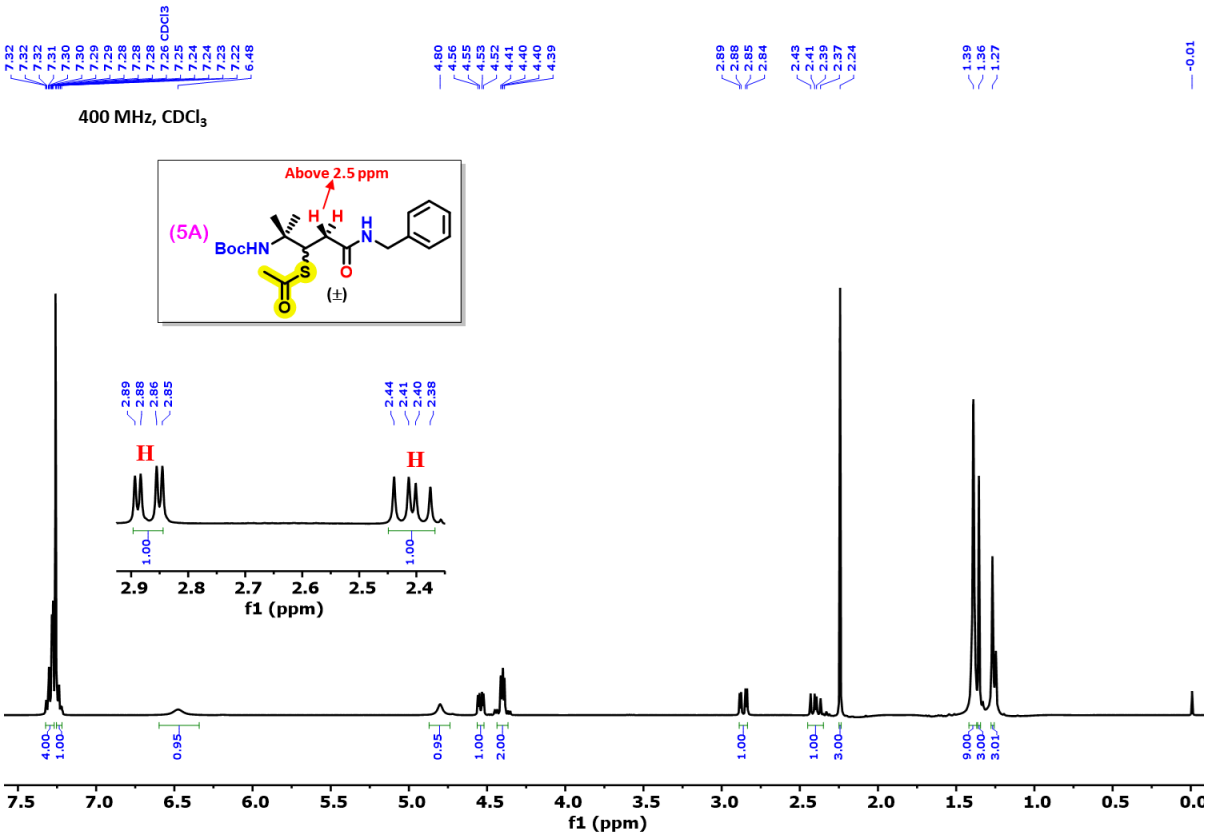

101 MHz, CDCl3
(2A")
BocHN
(S)
(R)
H
N
S
O
O
f1 (ppm)

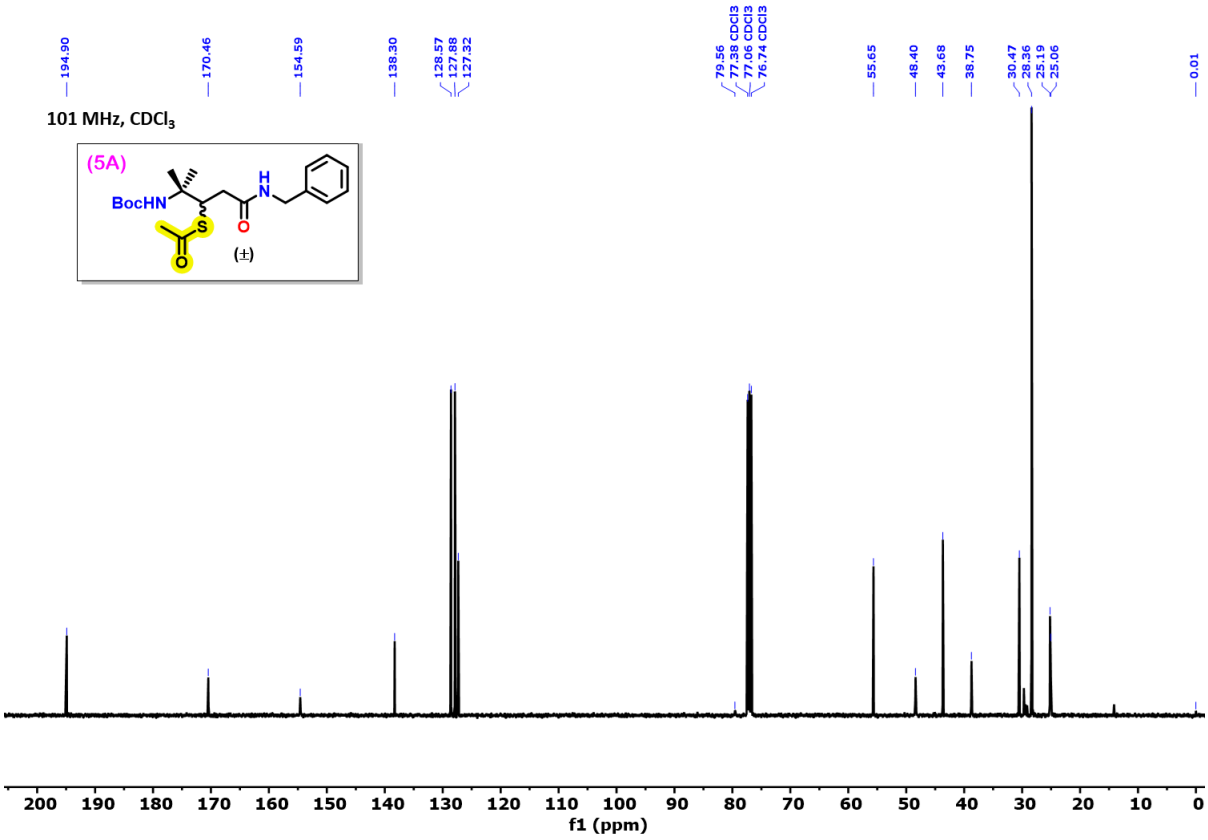

SAC 188A
IISER PUNE
SAC 188A 126 (2.304) AM2 (Ar,20000.0,556.28,0.00,LS 3); Sm (SG, 3x1.00)
1: TOF MS ES+
2.30e5
(2A")
CALCULATED MASS
(M+Na)+ 431.1980
431.1981
409.2161
432.2017
410.2192
415.2240
433.1974
411.2181
416.2284
447.1721
428.1888
434.1991
400.1593
406.1082
423.1264
425.1203
438.1113
448.1800
m/z

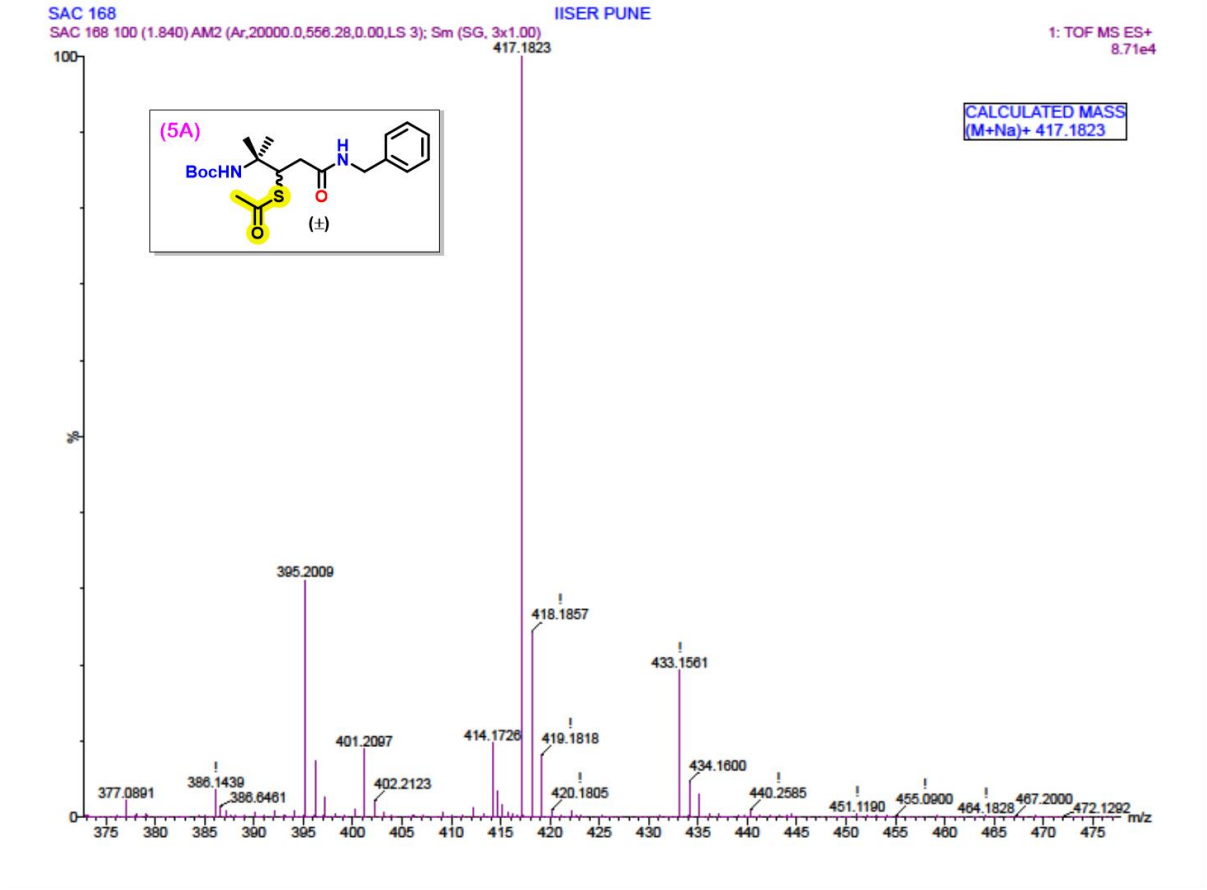

400 MHz, CDCl3
Above 2.5 ppm
(2B")
f1 (ppm)

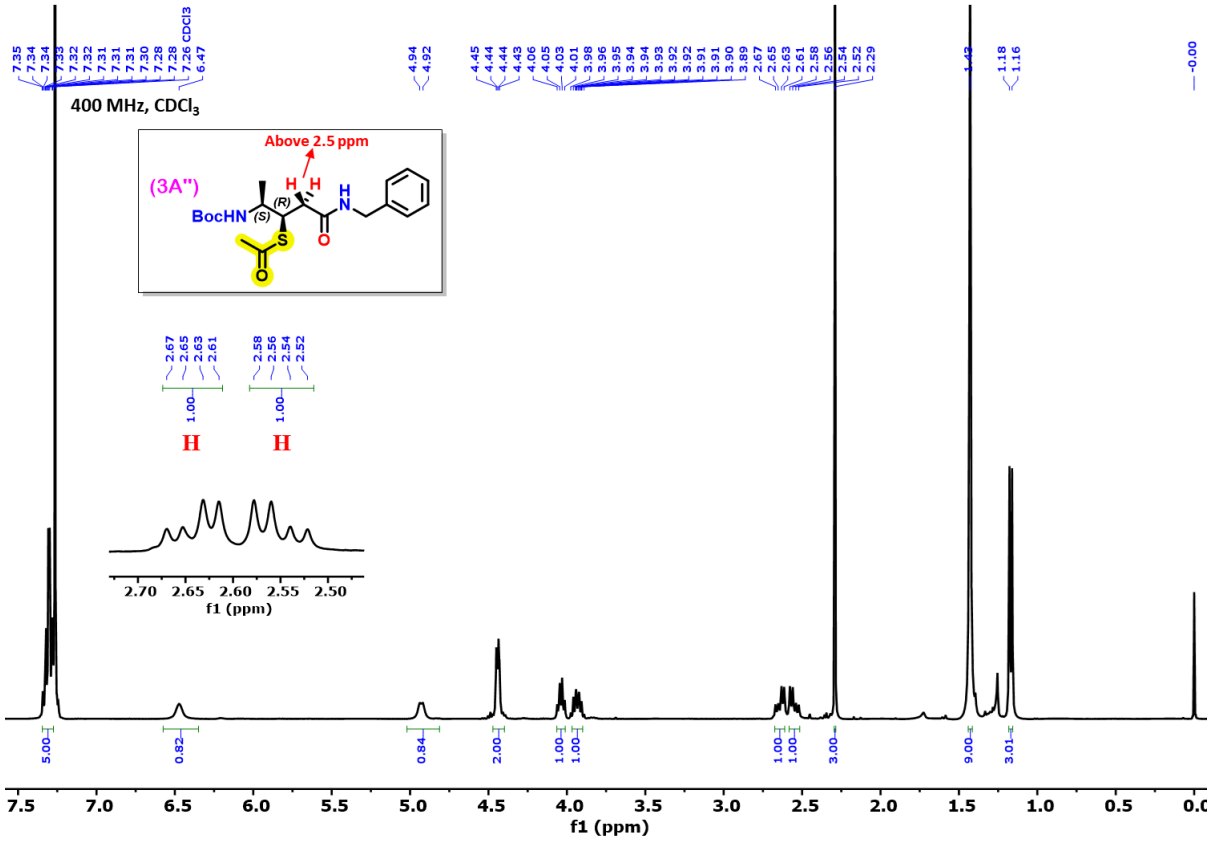

193.91
170.22
156.80
138.29
128.56
127.93
127.33
79.96 CHLOROFORM-D
77.36 CHLOROFORM-D
77.05 CHLOROFORM-D
76.73 CHLOROFORM-D
58.91
44.79
43.71
41.50
30.90
30.69
28.29
20.08
19.03
0.00 TMS
101 MHz, CDCl3
(2B'')
BocHN
f1 (ppm)

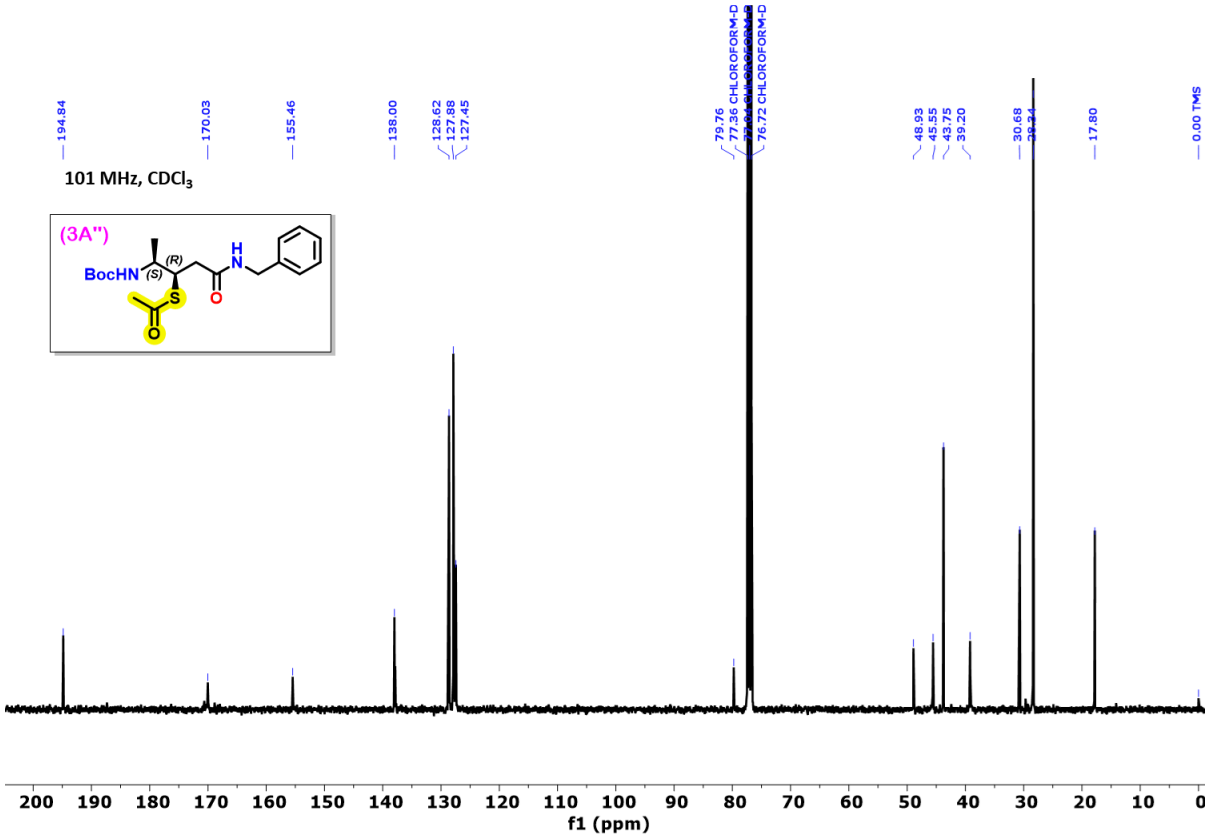

SAC 188B
IISER PUNE
SAC 188B 127 (2.305) AM2 (Ar,20000.0,556.28,0.00,LS 3); Sm (SG, 3x1.00)
1: TOF MS ES+
2.30e5
CALCULATED MASS
(M+Na)+ 431.1980
(2B'')
BocHN
431.1984
409.2162
410.2193
411.2186
416.2285
400.1590
406.1082
423.1261
428.1888
432.2010
433.1974
434.1992
438.1111
445.1726
448.1804
m/z

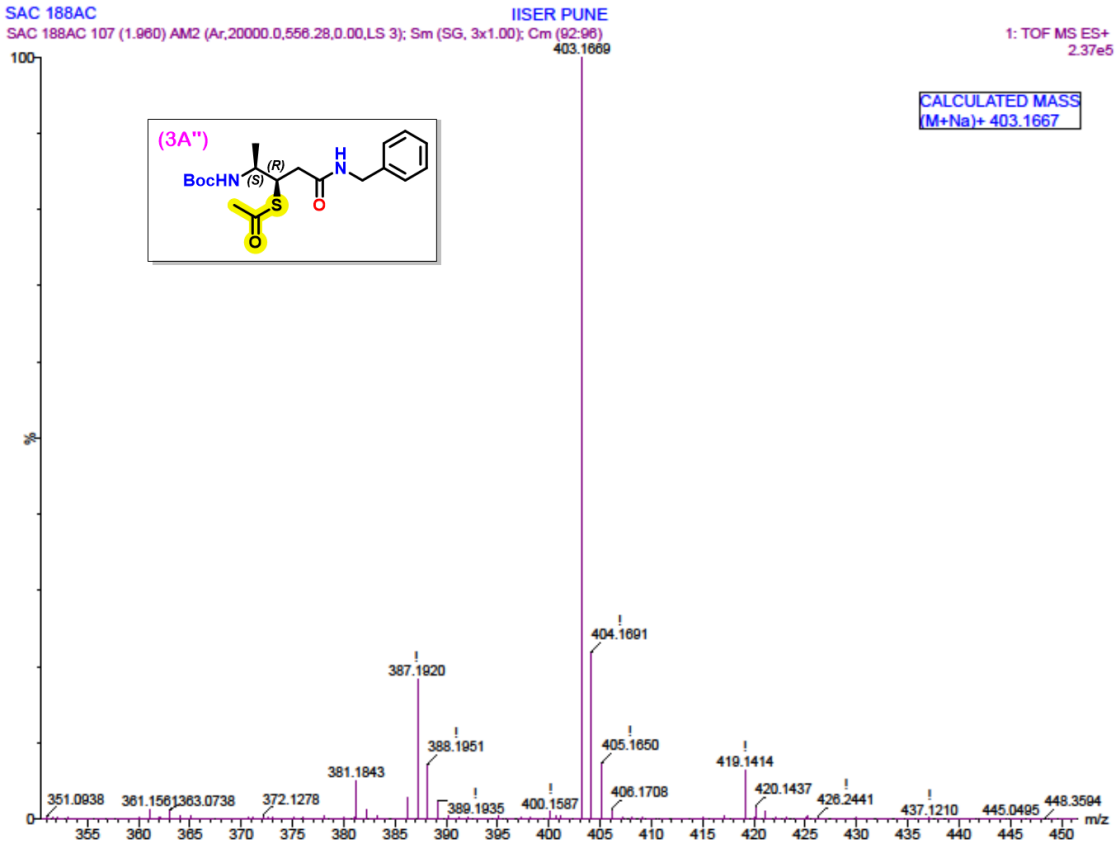

400 MHz, CDCl3
Above 2.5 ppm
(5A)
BocHN
(±)
f1 (ppm)

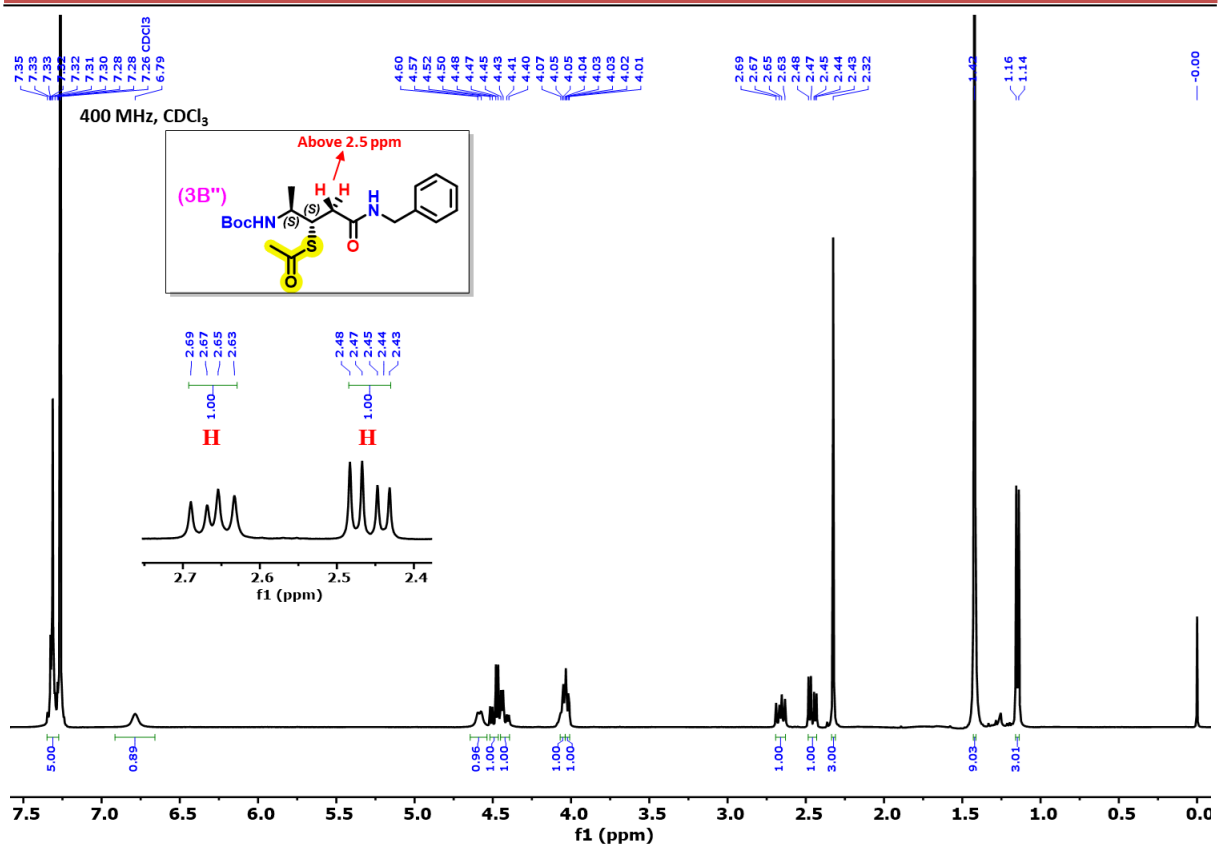

101 MHz, CDCl3
(5A)
BocHN
(±)
f1 (ppm)

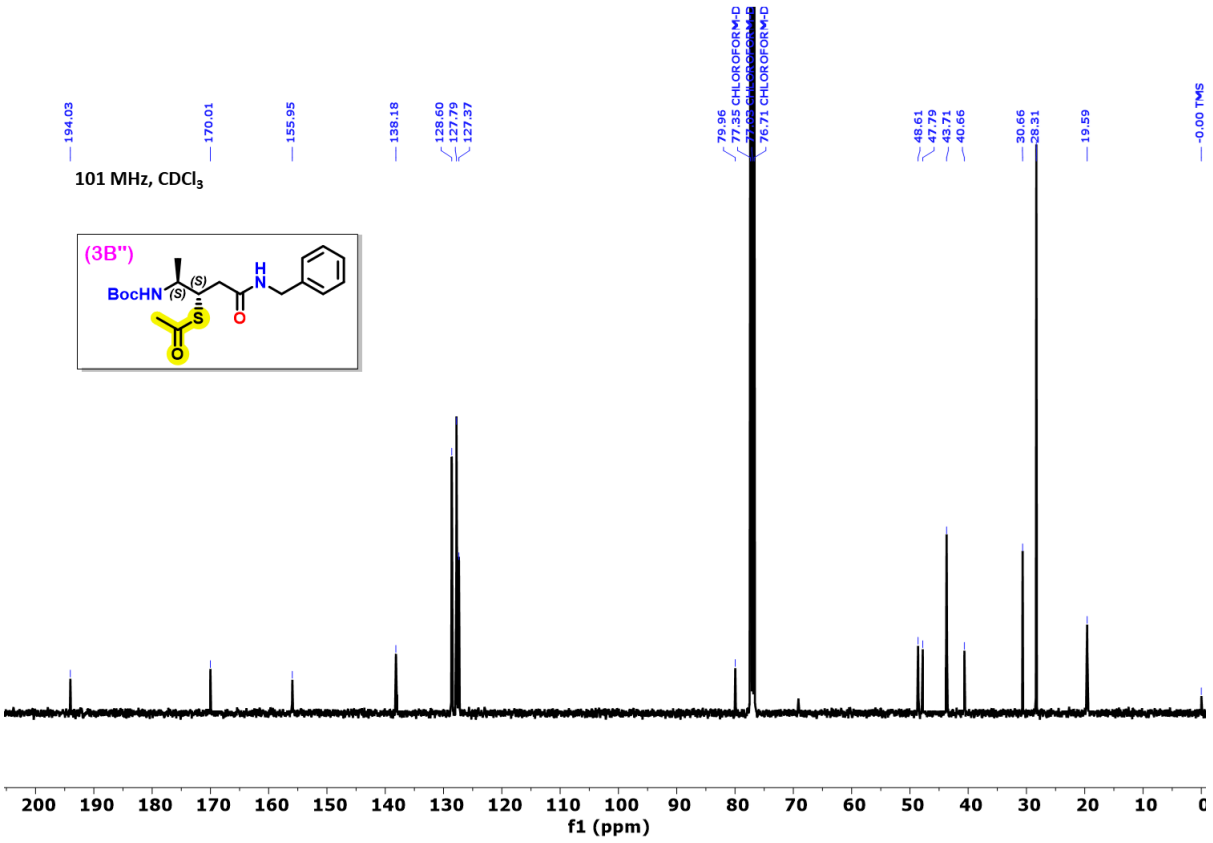

SAC 168
IISER PUNE
SAC 168 100 (1.840) AM2 (Ar,20000.0,556.28,0.00,LS 3); Sm (SG, 3x1.00)
1: TOF MS ES+
8.71e4
CALCULATED MASS
(M+Na)+ 417.1823
(5A)
BocHN
(±)
417.1823
395.2009
418.1857
433.1561
401.2097
414.1726
419.1818
434.1600
377.0891
386.1439
386.6461
402.2123
420.1805
440.2585
451.1190
455.0900
464.1828
467.2000
472.1292
m/z

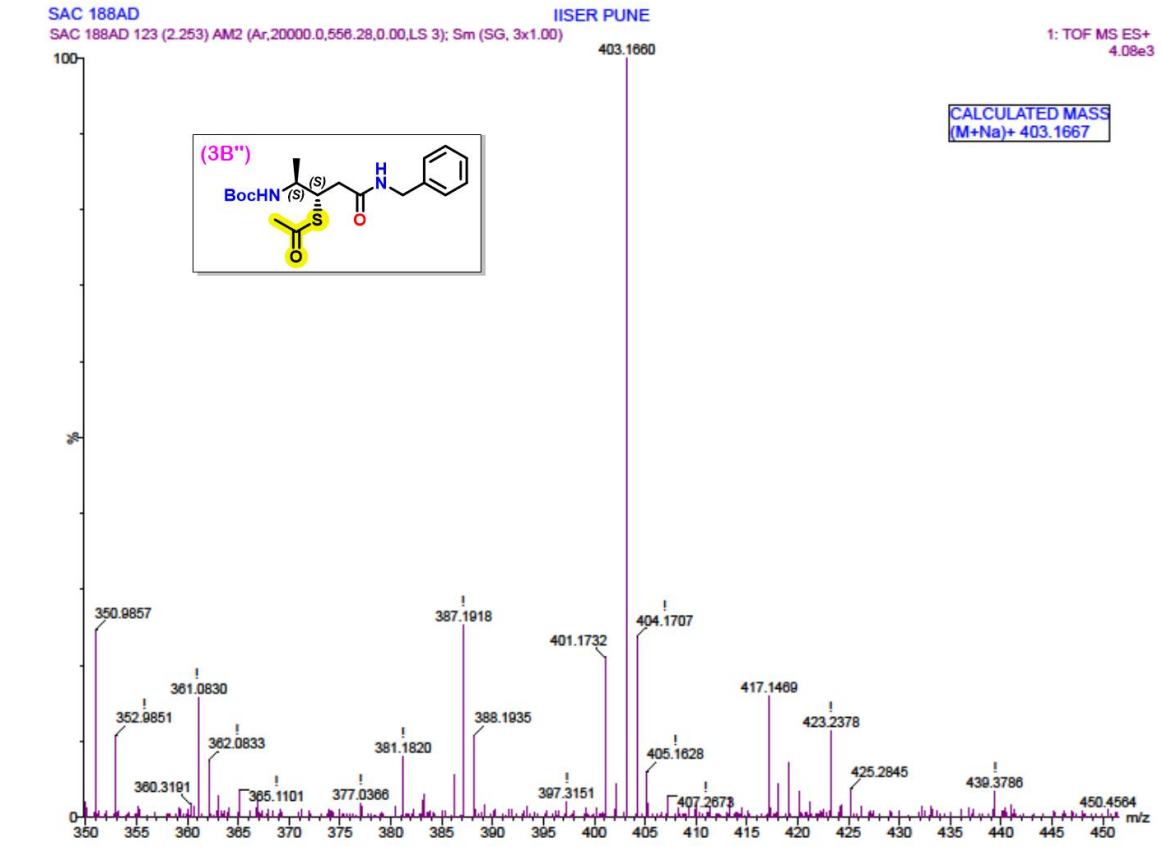

400 MHz, CDCl3
Above 2.5 ppm
(3A")
BocHN
(S)
(R)
H
H
f1 (ppm)

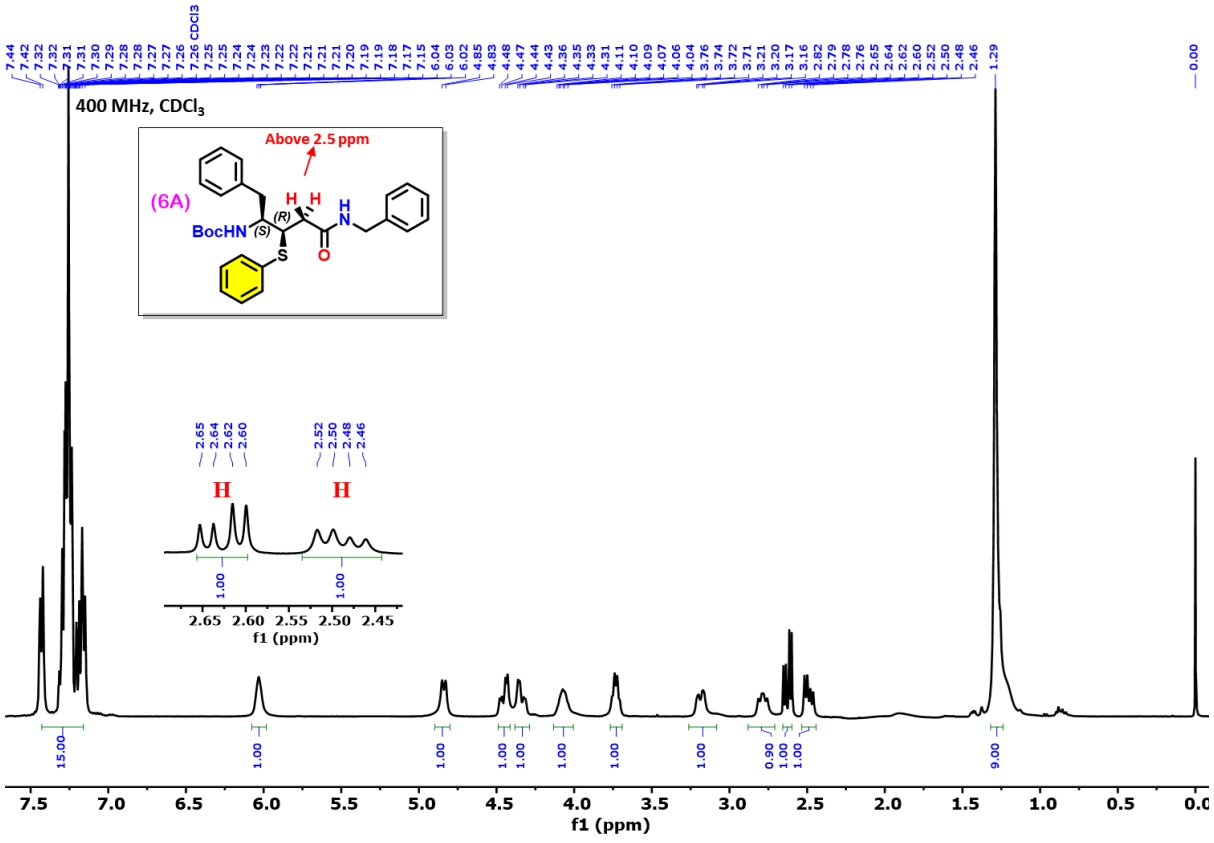

194.84
170.03
155.46
138.00
128.62
127.88
127.45
79.76
77.36 CHLOROFORM-D
76.72 CHLOROFORM-D
48.93
45.55
43.75
39.20
30.68
28.24
17.80
0.00 TMS
101 MHz, CDCl3
(3A'')
BocHN
(S)
(R)
H
N
S
O
O
200 190 180 170 160 150 140 130 120 110 100 90 80 70 60 50 40 30 20 10 0
f1 (ppm)

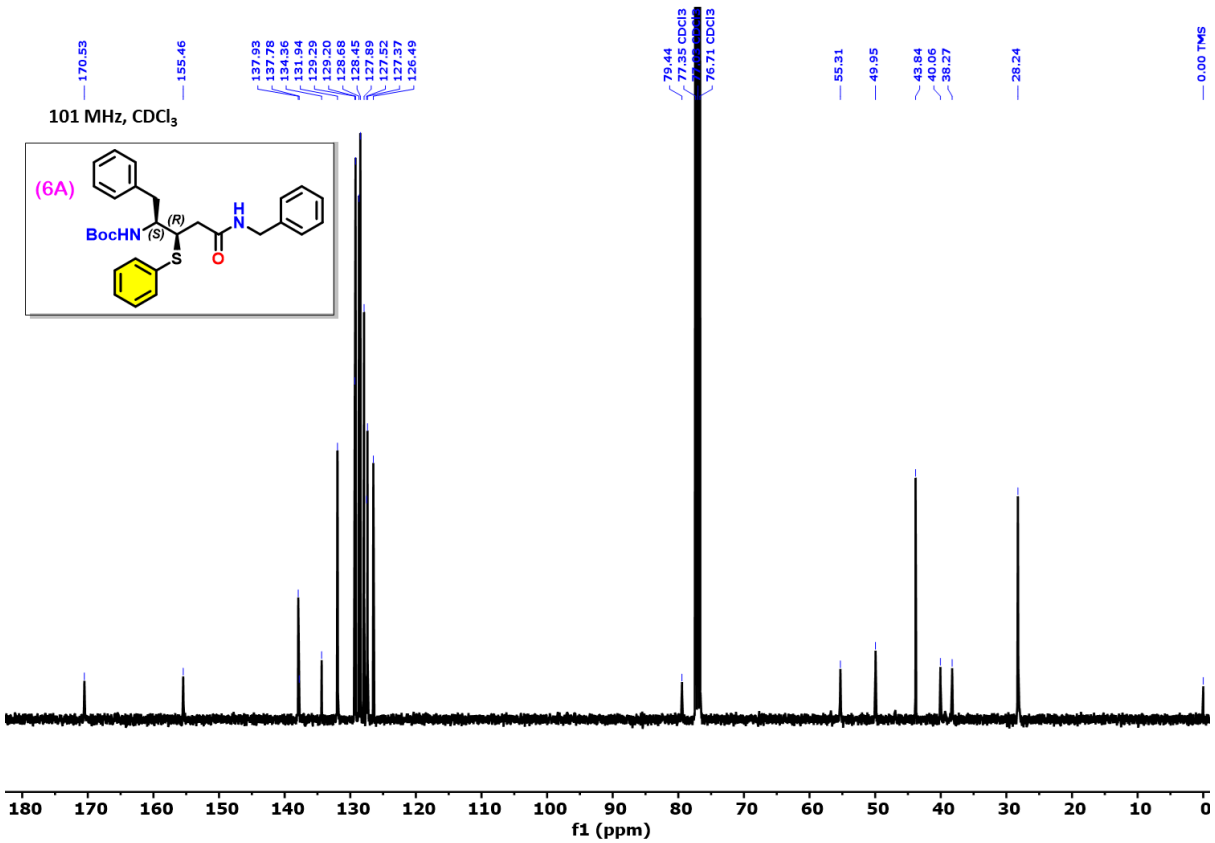

SAC 188AC
IISER PUNE
SAC 188AC 107 (1.960) AM2 (Ar,20000.0,556.28,0.00,LS 3); Sm (SG, 3x1.00); Cm (92:96)
1: TOF MS ES+
2.37e5
CALCULATED MASS
(M+Na)+ 403.1667
(3A'')
BocHN
(S)
(R)
H
N
S
O
O
100
%
0
403.1669
404.1691
387.1920
388.1951
405.1650
381.1843
419.1414
420.1437
426.2441
351.0938
361.1561
363.0738
372.1278
389.1935
400.1587
406.1708
437.1210
445.0495
448.3594
355 360 365 370 375 380 385 390 395 400 405 410 415 420 425 430 435 440 445 450
m/z

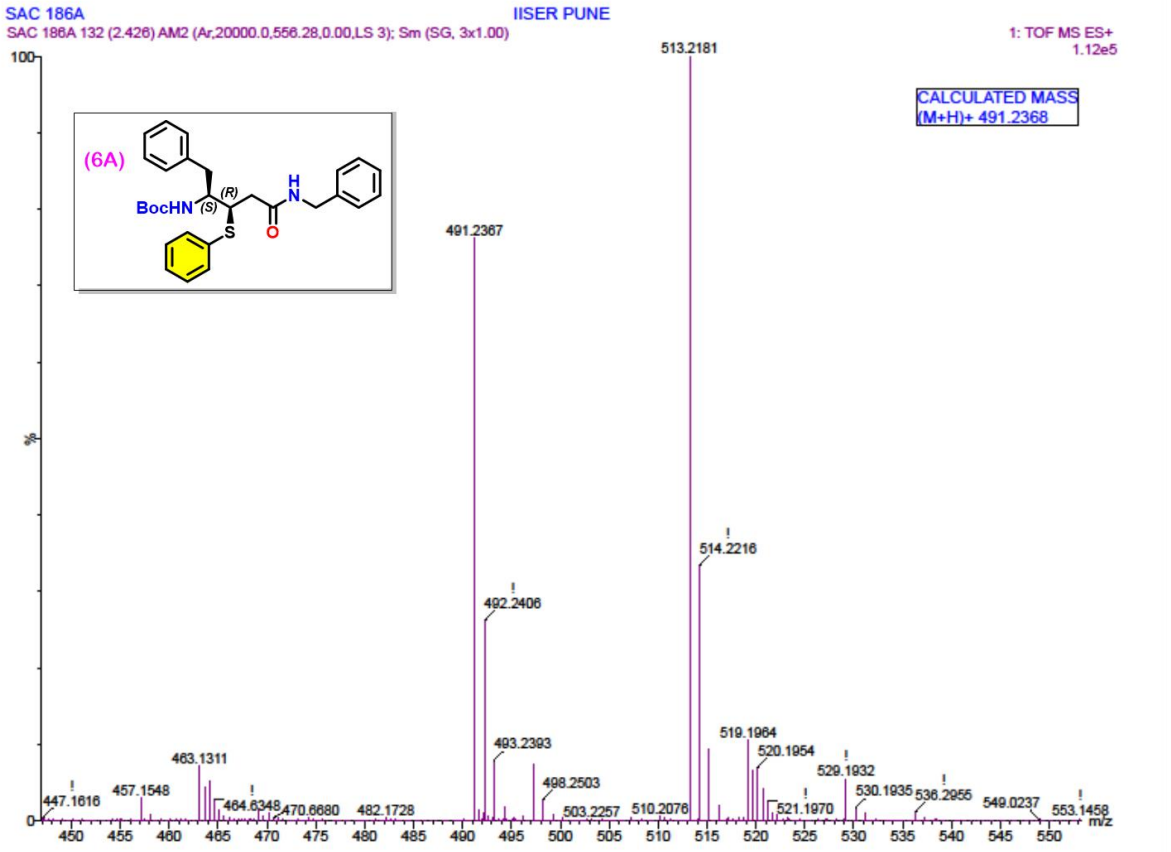

400 MHz, CDCl3
Above 2.5 ppm
(3B")
BocHN
f1 (ppm)

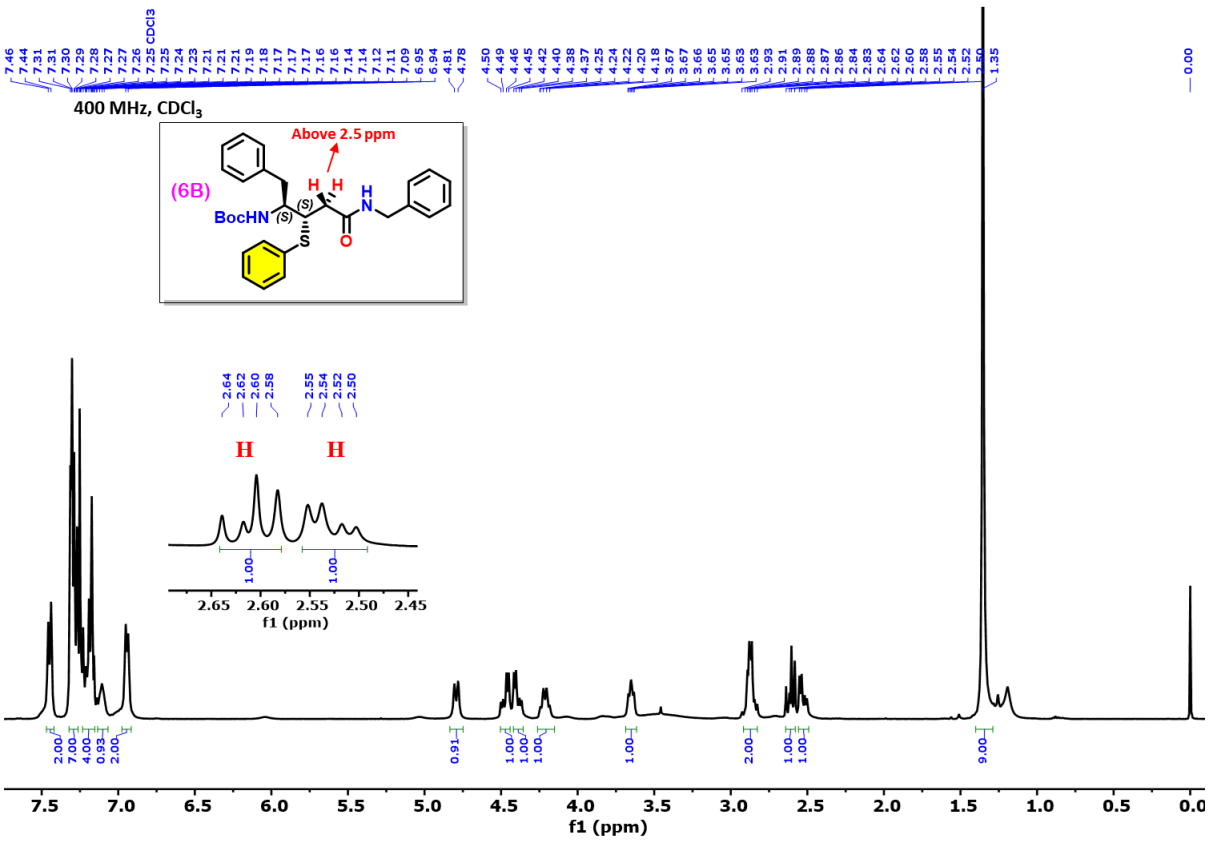

101 MHz, CDCl3
(3B")
BocHN
f1 (ppm)

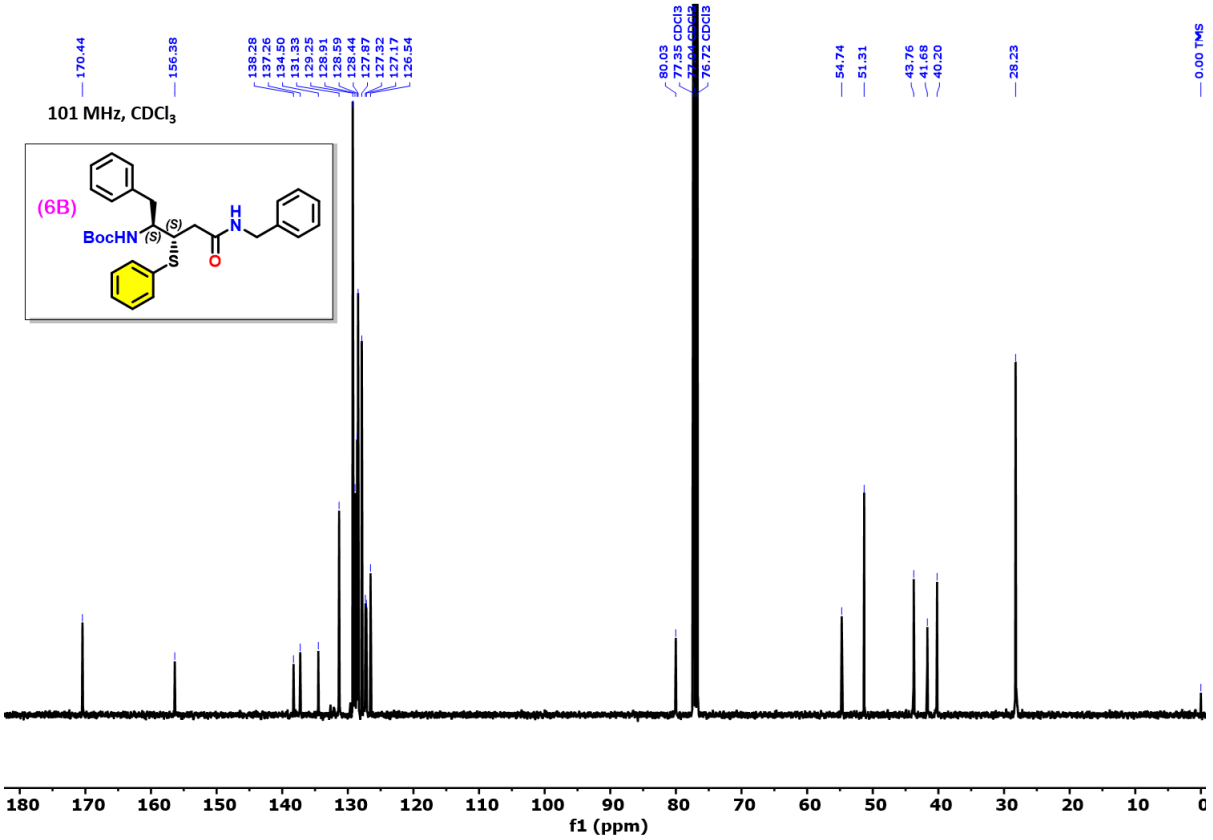

SAC 188AD
IISER PUNE
SAC 188AD 123 (2.253) AM2 (Ar,20000.0,556.28,0.00,LS 3); Sm (SG, 3x1.00)
1: TOF MS ES+
4.08e3
403.1660
CALCULATED MASS
(M+Na)+ 403.1667
(3B")
BocHN
(S)
(S)
H
N
O
S
O
%
350.9857
387.1918
401.1732
404.1707
361.0830
417.1469
352.9851
423.2378
388.1935
362.0833
381.1820
405.1628
425.2845
360.3191
365.1101
377.0366
397.3151
439.3786
407.2673
450.4564
m/z
350 355 360 365 370 375 380 385 390 395 400 405 410 415 420 425 430 435 440 445 450

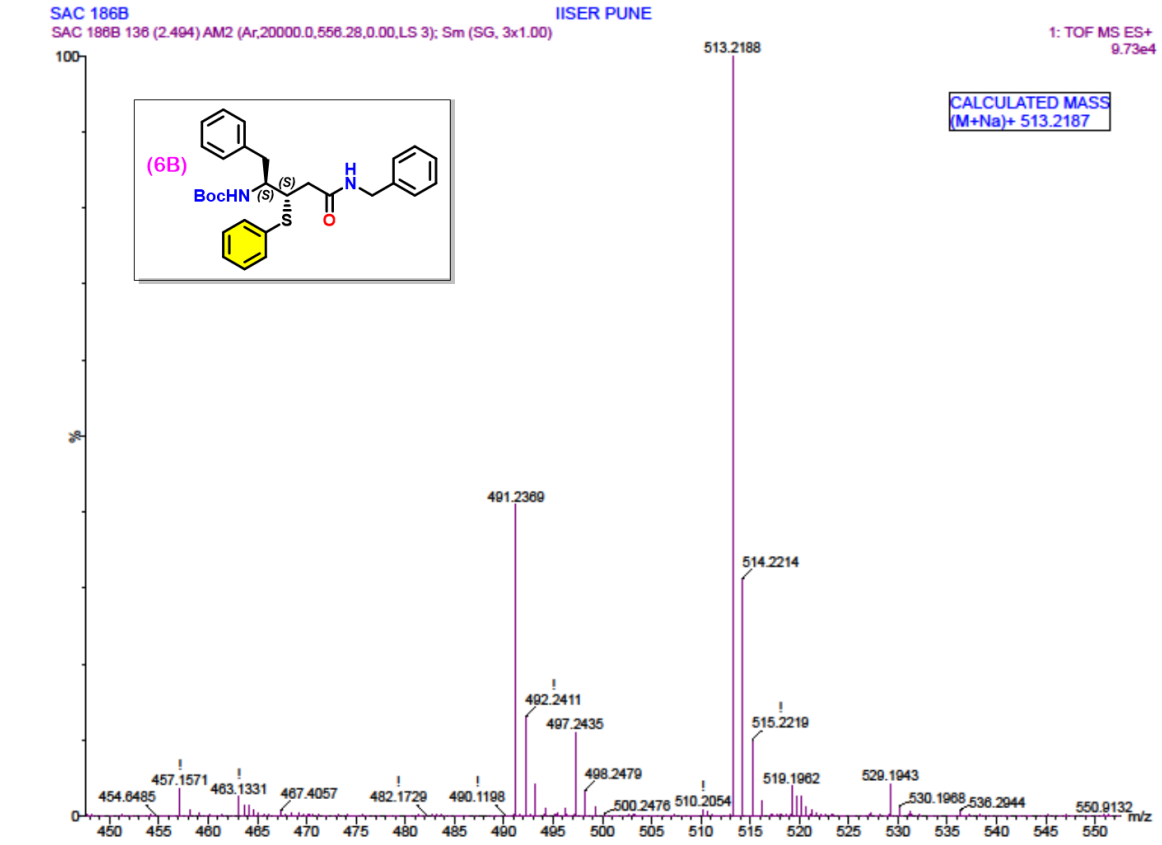

400 MHz, CDCl3
Above 2.5 ppm
(6A)
H
H
H
BocHN
(S)
(R)
S
O
2.65 2.64 2.62 2.60
2.52 2.50 2.48 2.46
H
H
1.00
1.00
2.65 2.60 2.55 2.50 2.45
f1 (ppm)
15.00
1.00
1.00
1.00
1.00
1.00
1.00
1.00
0.90
1.00
1.00
9.00
7.5 7.0 6.5 6.0 5.5 5.0 4.5 4.0 3.5 3.0 2.5 2.0 1.5 1.0 0.5 0.0
f1 (ppm)

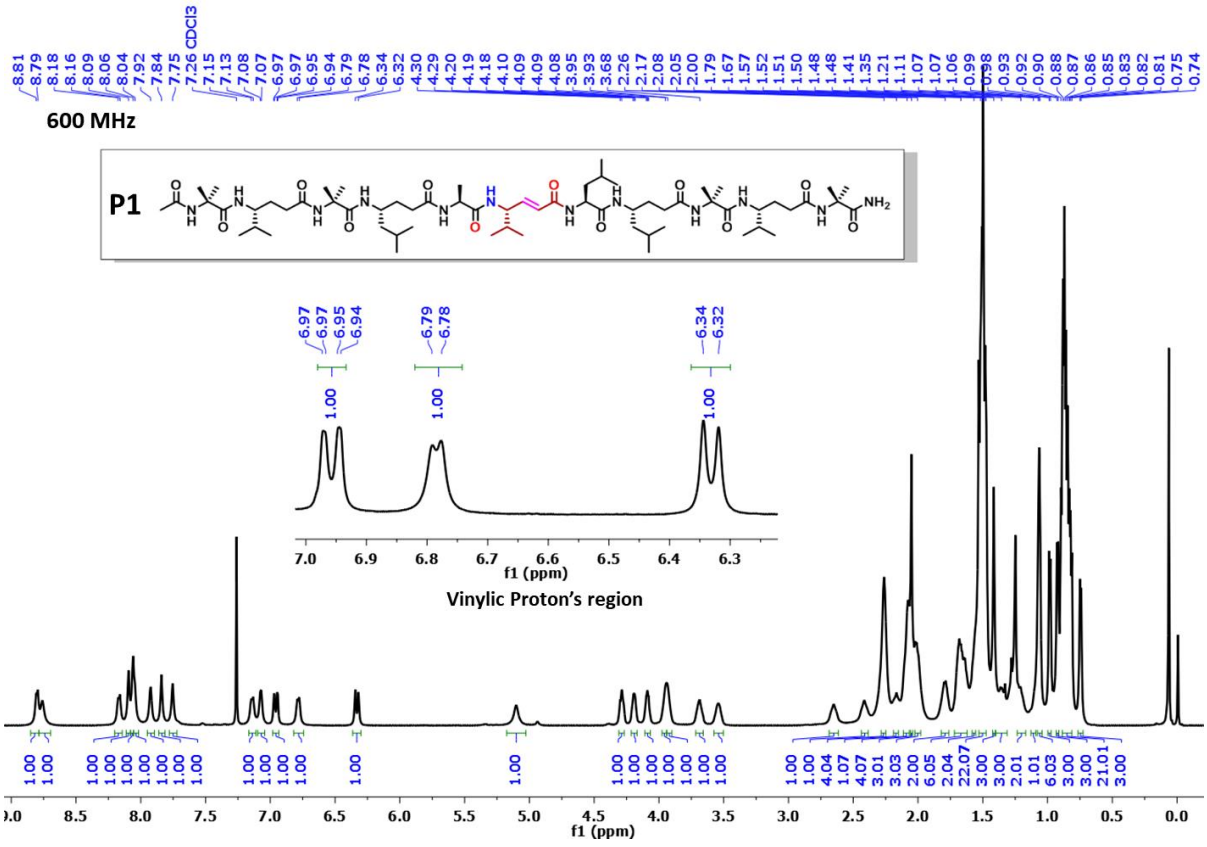

101 MHz, CDCl3
(6A)
BocHN
(S)
(R)
S
H
N
O
170.53
155.46
137.93
137.78
134.36
131.94
129.29
129.20
128.68
128.45
127.89
127.52
127.37
126.49
79.44
77.35 CDCl3
76.71 CDCl3
55.31
49.95
43.84
40.06
38.27
28.24
0.00 TMS
f1 (ppm)


SAC 186A
IISER PUNE
SAC 186A 132 (2.426) AM2 (Ar,20000.0,556.28,0.00,LS 3); Sm (SG, 3x1.00)
1: TOF MS ES+
1.12e5
CALCULATED MASS
(M+H)+ 491.2368
(6A)
BocHN
(S)
(R)
S
H
N
O
513.2181
491.2367
514.2216
492.2406
493.2393
519.1964
520.1954
529.1932
530.1935
536.2955
549.0237
553.1458
463.1311
457.1548
447.1616
464.6348
470.6680
482.1728
498.2503
503.2257
510.2076
521.1970
%
m/z


400 MHz, CDCl3
Above 2.5 ppm
(6B)
BocHN
H H
f1 (ppm)

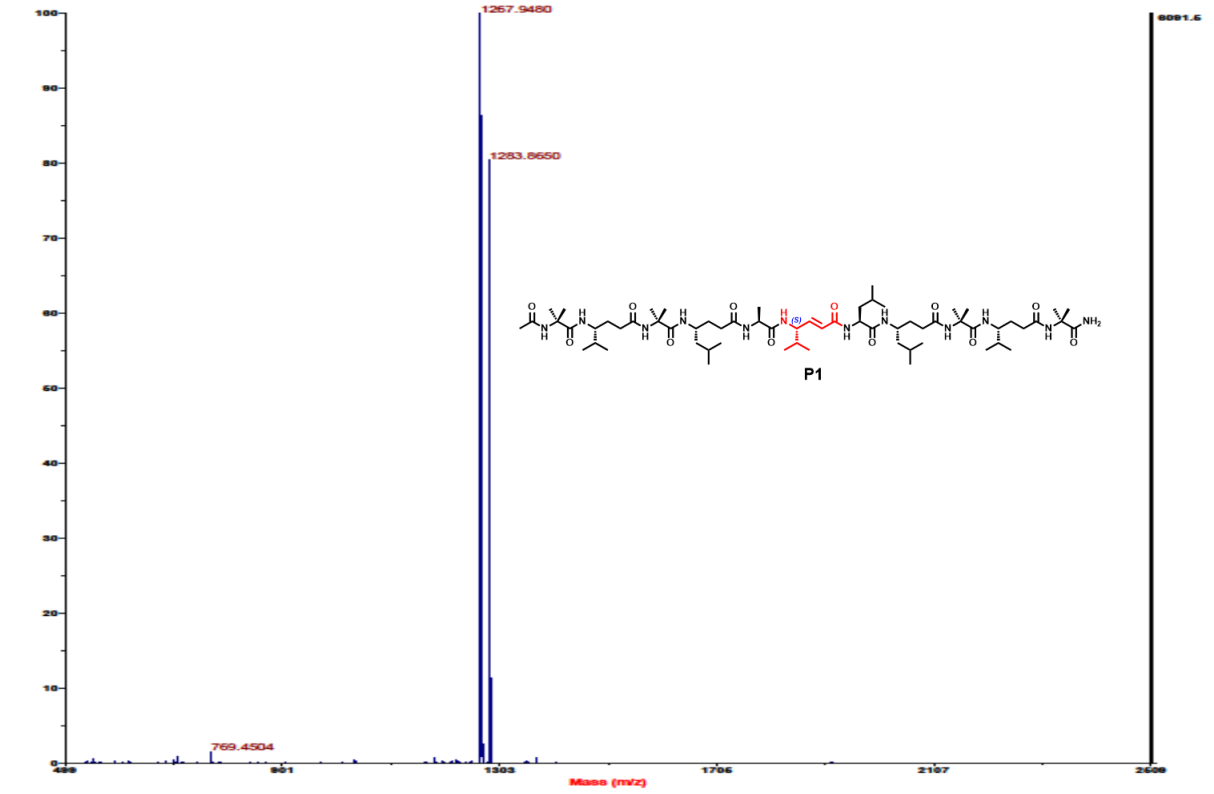

101 MHz, CDCl3
(6B)
BocHN
f1 (ppm)


SAC 186B
IISER PUNE
SAC 186B 136 (2.494) AM2 (Ar,20000.0,556.28,0.00,LS 3); Sm (SG, 3x1.00)
1: TOF MS ES+
9.73e4
100
%
0
(6B)
BocHN
(S)
(S)
H
N
O
S
CALCULATED MASS
(M+Na)+ 513.2187
513.2188
491.2369
514.2214
492.2411
497.2435
515.2219
498.2479
519.1962
529.1943
457.1571
463.1331
467.4057
454.6485
482.1729
490.1198
500.2476
510.2054
530.1968
536.2944
550.9132
m/z
450
455
460
465
470
475
480
485
490
495
500
505
510
515
520
525
530
535
540
545
550

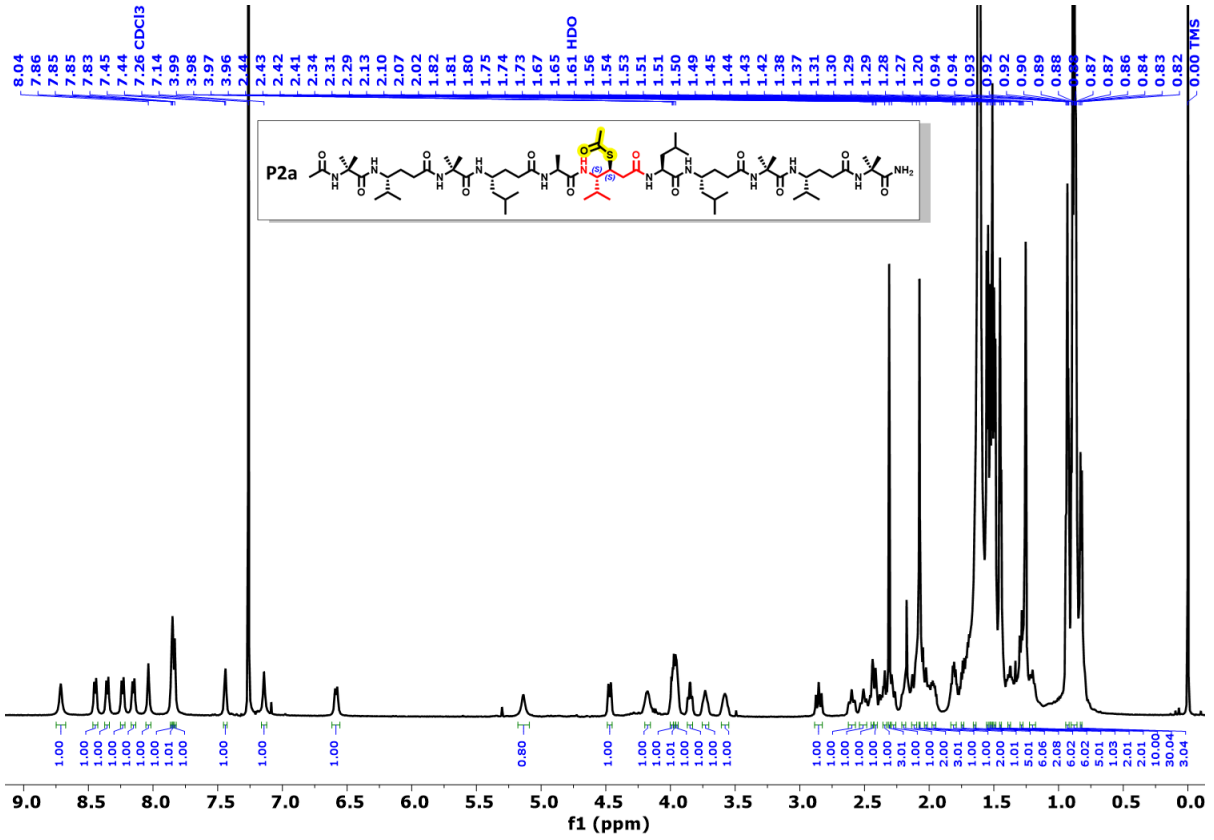

CDCl3
600 MHz
P1
NH2
6.97
6.97
6.95
6.94
6.79
6.78
6.34
6.32
1.00
1.00
1.00
7.0
6.9
6.8
6.7
6.6
6.5
6.4
6.3
f1 (ppm)
Vinylic Proton's region
f1 (ppm)

Spectrum Report

Final - Shota 600 - IISER-96-2-2018; Run #411; Label A9

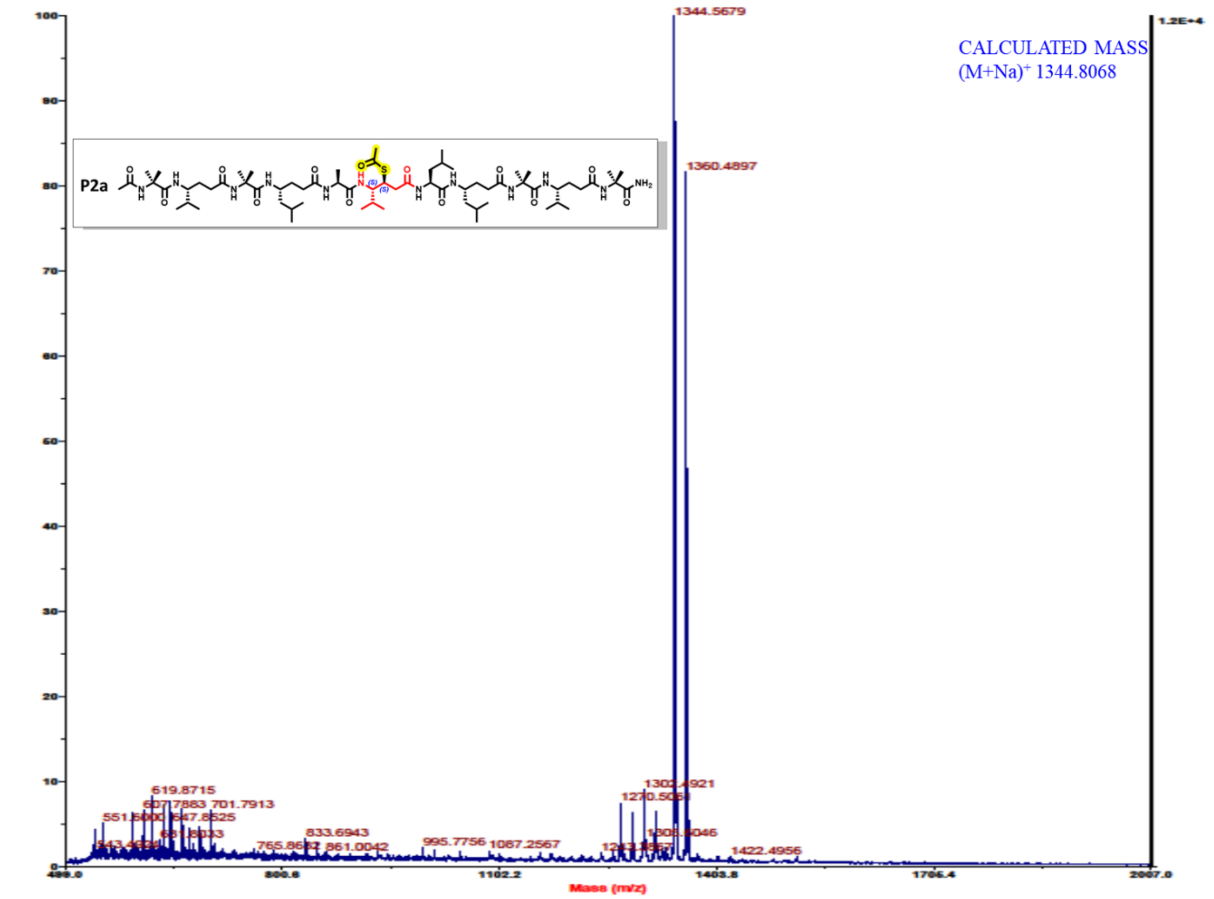


2018\IISER-96-2-2018 Label A9 Run # 411 Page 1 12/28/2018 11:28:14 AM

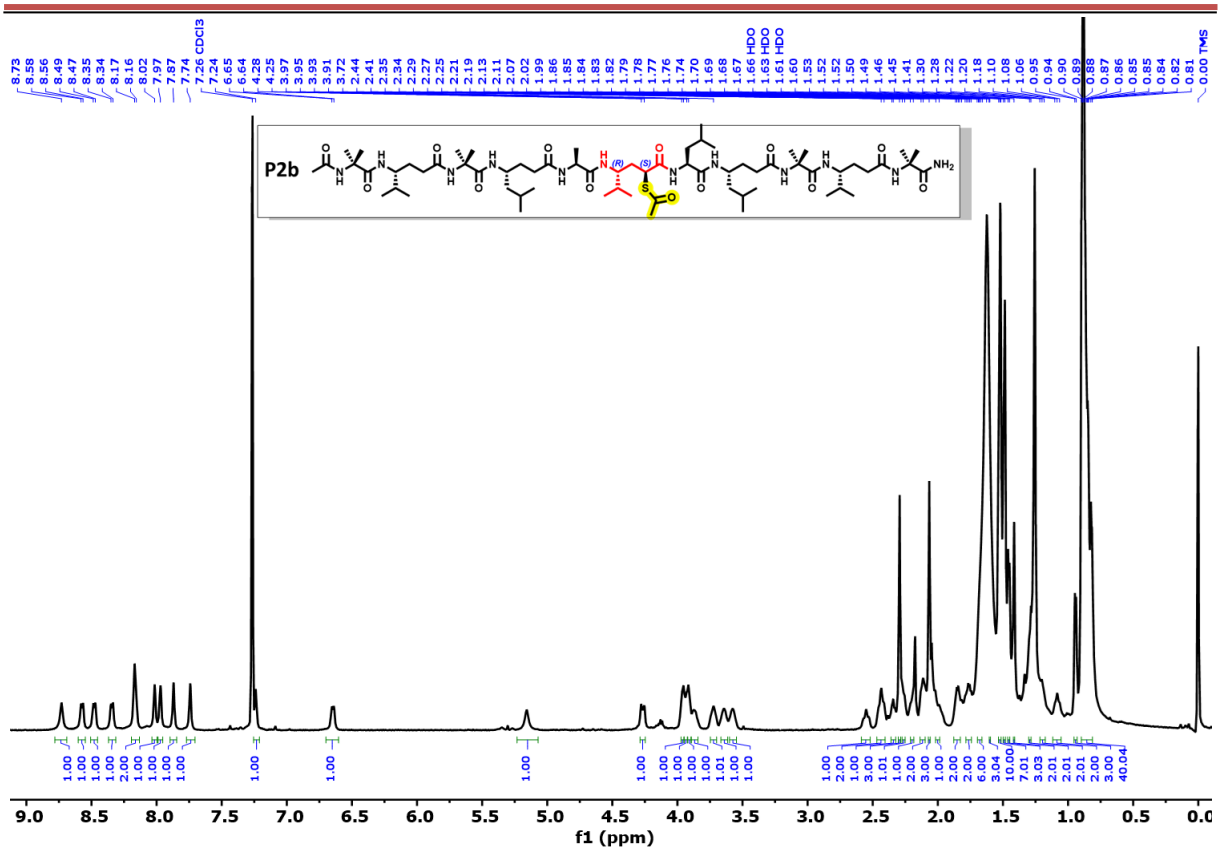


Spectrum Report

Final - Shots 2000 - IISER-96-2-2020; Label G3

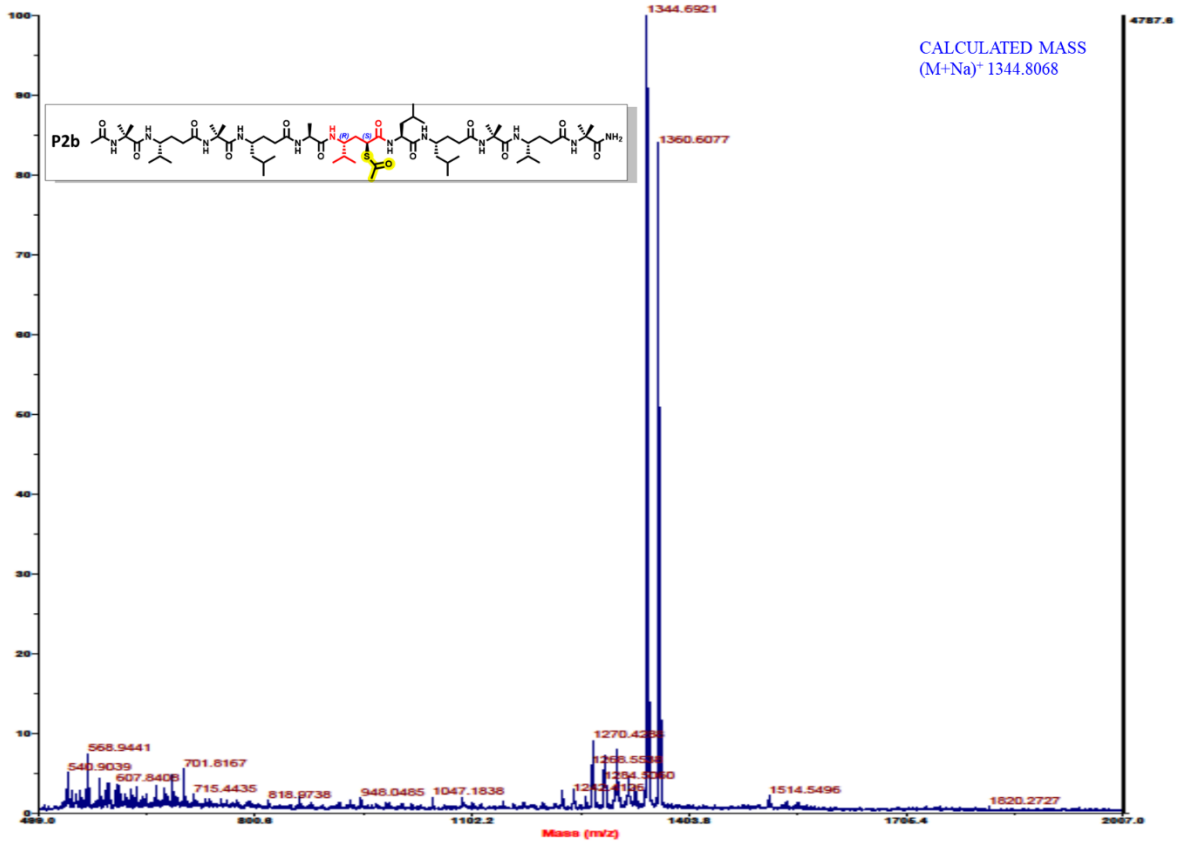


2020\IISER-96-2-2020 Label G3 Run # 31 Page 1 12/16/2020 4:02:32 PM

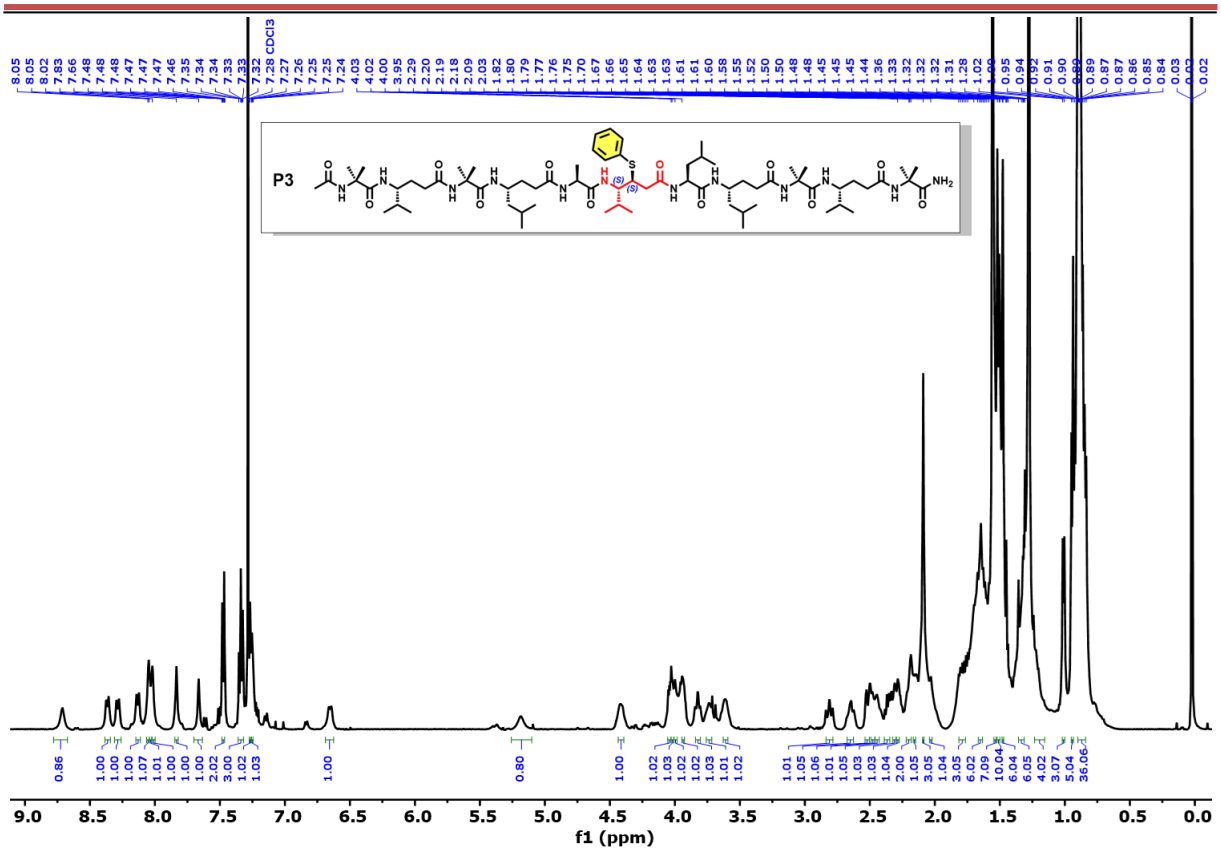


Spectrum Report

Final - Shots 2000 - IISER-96-2-2020; Label G4

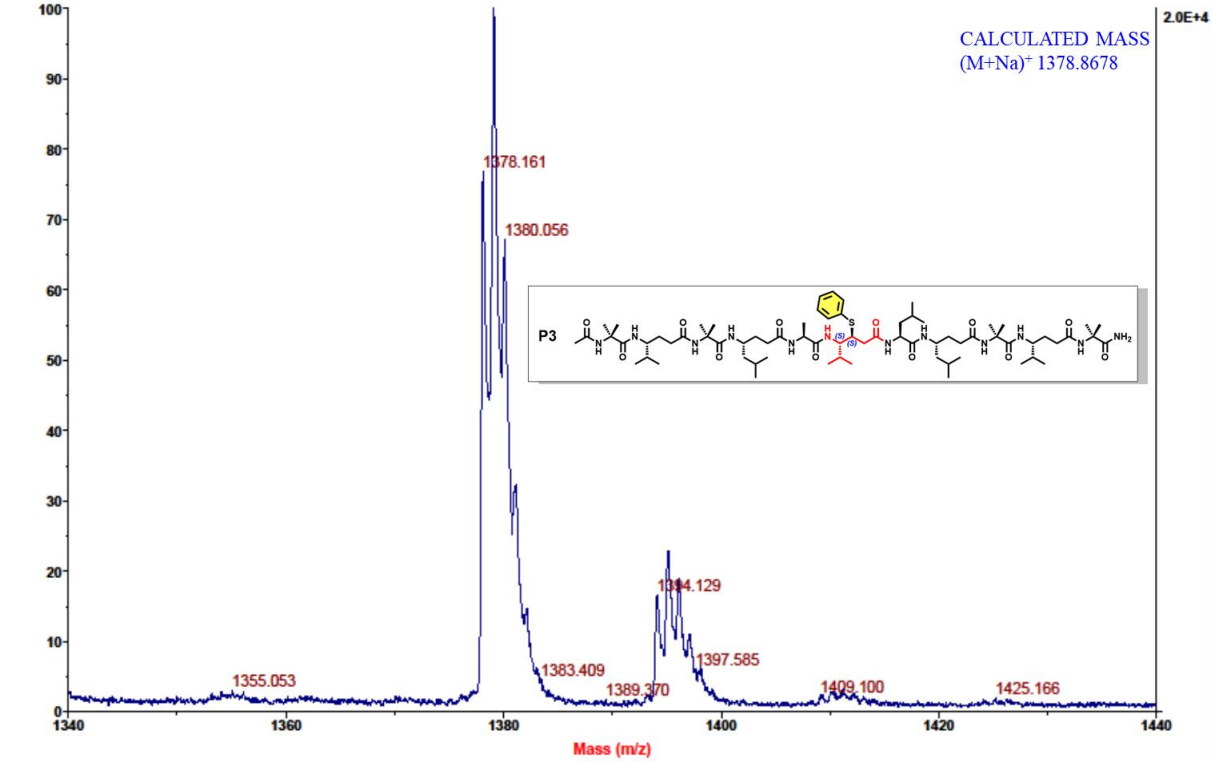


2020\IISER-96-2-2020 Label G4 Run # 31 Page 1 12/16/2020 4:03:16 PM

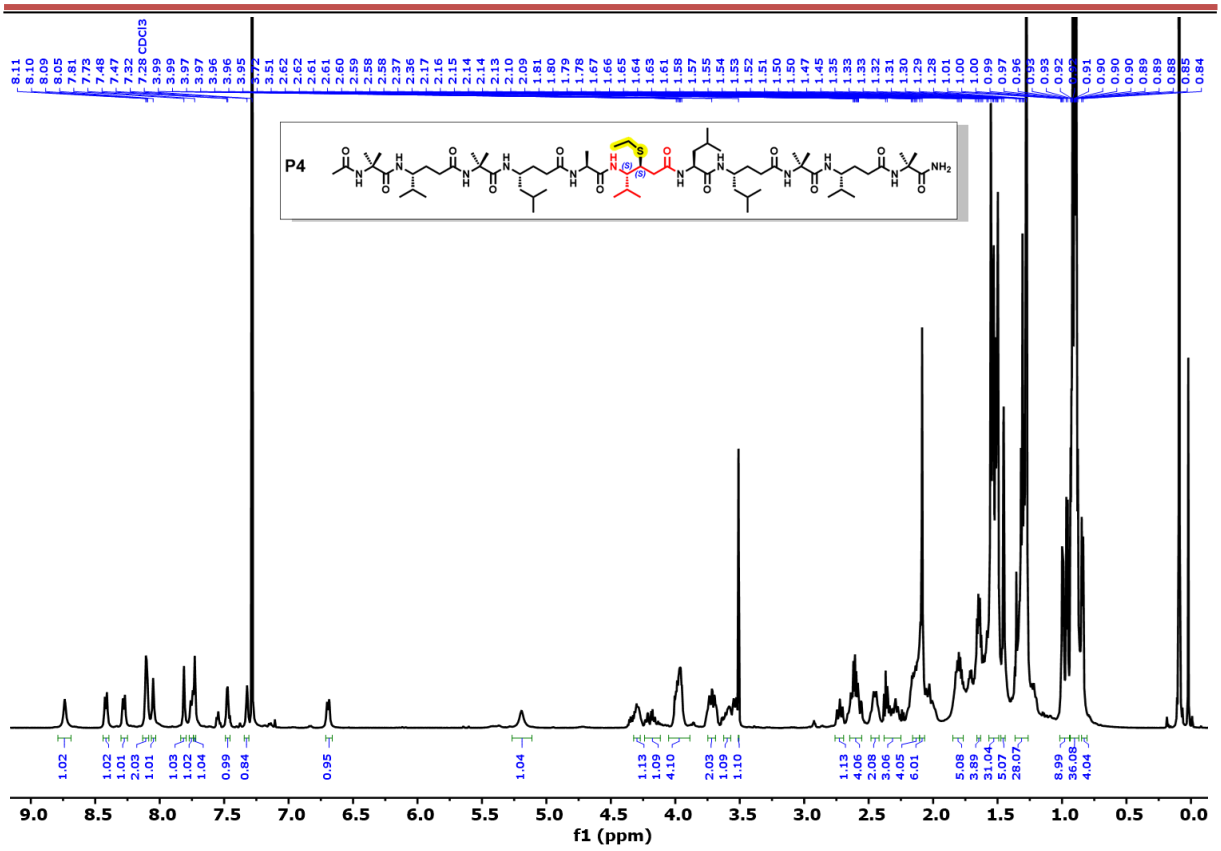


Spectrum Report

Final - Shots 500 - IISER-96-2-2021; Run #18; Label B4

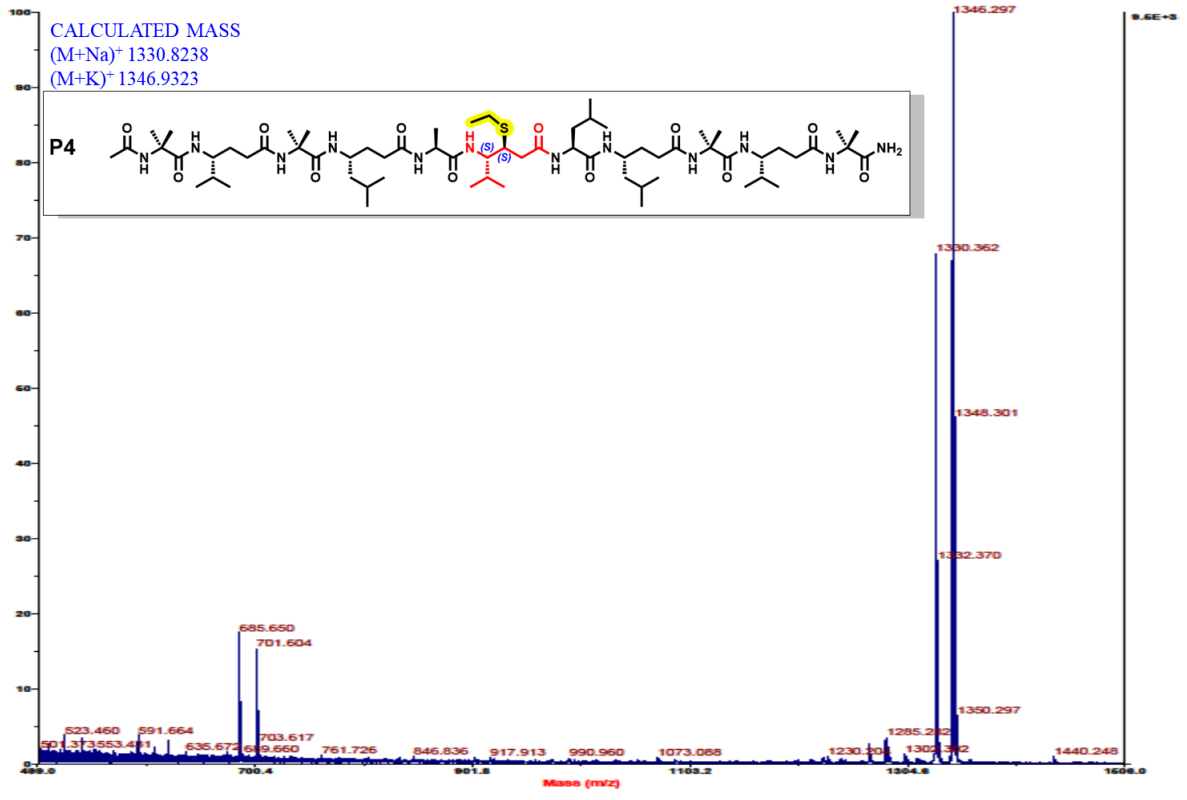


2021\IISER-96-2-2021 Label B4 Run # 18 Page 1 11/11/2021 5:53:44 PM



Spectrum Report

Final - Shots 200 - IISER-96-1-2023; Run #82; Label E1



IISER-2023\IISER-96-1-2023 Label E1 Run # 82 Page 1 10/18/2023 2:37:54 PM

Chapter 5

α, γ-Hybrid Peptide Foldamers Consisting of γ-Amino Acid with Aromatic Backbone: Role of Chiral and Achiral Amino Acids in Folding Patterns of Hybrid Peptides

5.1. Introduction

The oligomers of synthetic building blocks, encompassing β-, γ-, and higher homologous amino acids, exhibit reproducible helical structures. This phenomenon introduces a completely new dimension to the design of protein secondary structure mimetics.[1,2] In nature, there are instances where hybrid peptides with biological activity are derived by incorporating either β- or γ-amino acids alongside α-amino acids (see Figure 1). In contrast to homooligomers composed solely of β- and γ-amino acids, mixed sequences incorporating α-, β-, γ-amino acids, and higher homologues have demonstrated the ability to adopt diverse helical patterns characterized by distinct intramolecular H-bonding pseudocycles.[3-5] In their pioneering work, Gellman and colleagues conducted a comprehensive exploration of the conformational properties and biological activities of αβ-hybrid peptides.[6,7] Similar to αβ-hybrid peptides, the literature reflects substantial endeavors to comprehend the conformations of αγ-hybrid peptides. Both theoretical[8] and experimental[9] studies indicate that the 12-helix represents a stable conformation for α,γ-hybrid peptides. The design of helical foldamers has been explored using various γ-amino acids, including double homologated γ[4]-amino acids, 2,2-dialkyl γ-amino acids,[10] 3,3-dialkyl γ-amino acids,[11,12] 4,4-dialkyl γ-amino acids,[13] cyclic-γ-amino acids,[14] 3,4-disubstituted γ-amino acids,[15] 2,3,4-trisubstituted γ-amino acids,[16] γ-carboamino acids,[17] and 3-hydroxy-γ-amino acids.[18] In addition to the previously mentioned saturated γ-amino acids, (*Z*)-α,β-unsaturated γ-amino acids[19] and (*E*)-α,β-unsaturated γ-amino acids have also been incorporated into helical foldamers.[20] Recently, we demonstrated the existence of 12- and 15/17-helical conformations featuring unidirectional H-bonds in α,γ-hybrid peptides

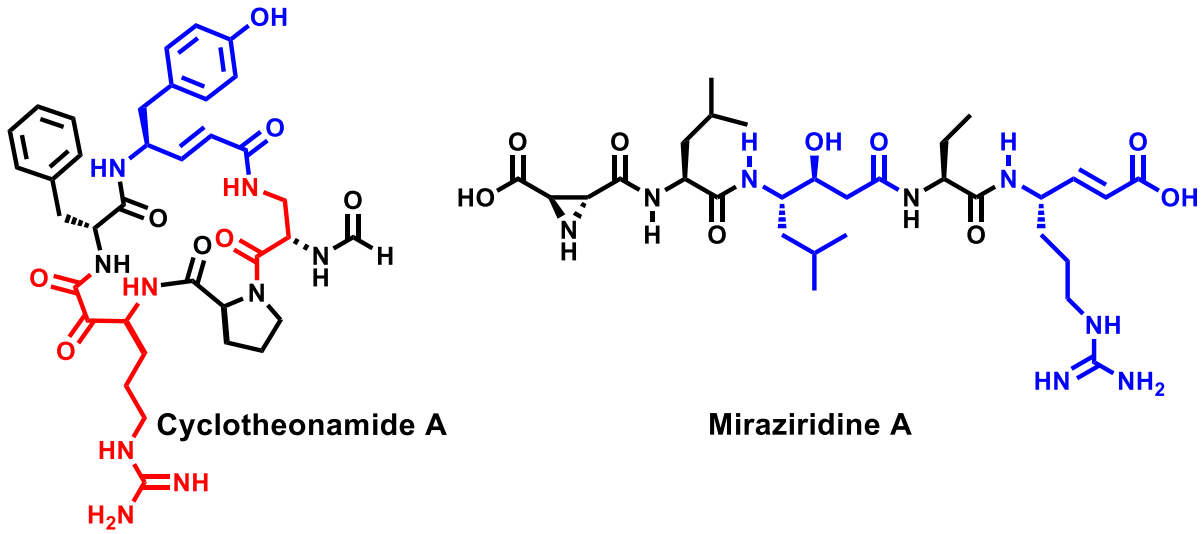


Figure 1: Peptide natural products consisting of β- and γ-amino acids.

composed of gem-dialkyl substituted γ-amino acids.[13a] The oligomers composed of (*Z*)-α,β-unsaturated γ-amino acids have been observed to adopt 9-helix conformations,[21] whereas α,γ-hybrid peptides exhibit a 12-helix conformation.[22] Homooligomers composed of (*E*)-α,β-unsaturated γ-amino acids have demonstrated the adoption of a β-double helix[23] conformation. On the other hand, α,γ-hybrid peptides containing (*E*)-α,β-unsaturated γ-amino acids exhibited planar structures.[24] Notably, these planar structures underwent a transformation into 12-helix structures upon treatment with a strong base, involving α,β ➔ β,γ-double bond migration.[25] Importantly, the (*E*)-double bond in the initial peptide converted into a (*Z*)-double bond during the double bond migration in the resulting product (see Figure 2).

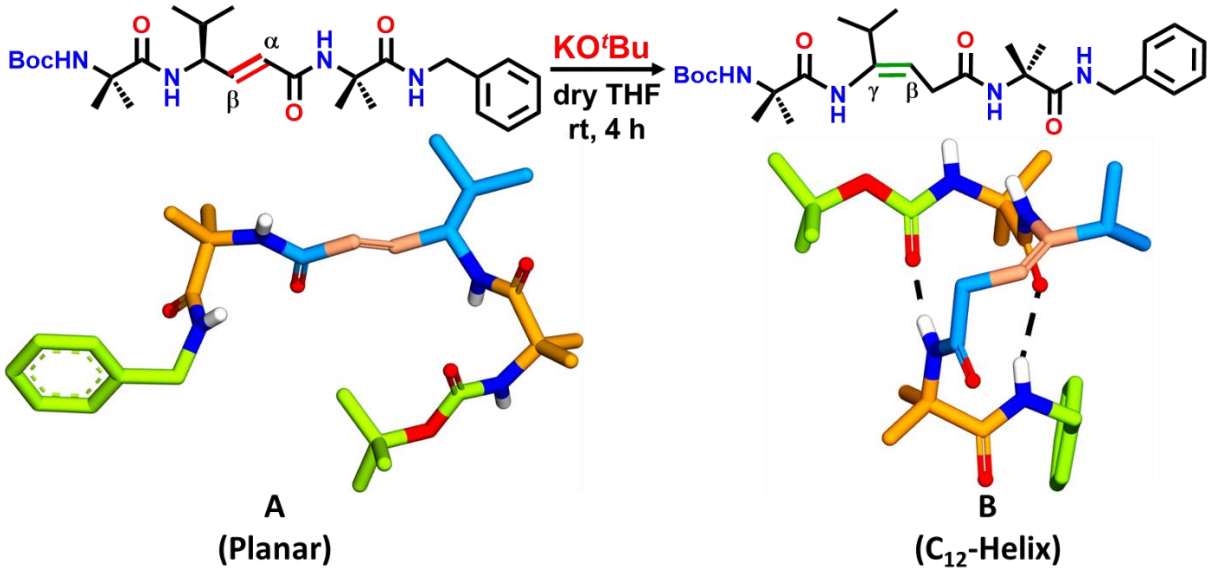


Figure 2: Transformation of planar structure to the 12-helical structure via KO^{t}Bu mediated α,β → β,γ-double bond migration.

The stability of the 12-helix in structure B is maintained through intramolecular H-bonds. Motivated by this 12-helix conformation, we initially aimed to explore α,γ-hybrid peptides incorporating (*Z*)-β,γ-unsaturated γ-amino acids. However, these amino acids proved to be unstable under mild acidic conditions. Subsequently, considering the instability of (*Z*)-β,γ-unsaturated γ-amino acids in acidic conditions, our focus shifted to investigating (2-aminophenyl)acetic acid (Apa) as a γ-amino acid surrogate that mimics the (*Z*)-β,γ-unsaturated γ-amino acid. Our objective was to study the conformations of α,γ-hybrid peptides incorporating Apa. In this report, we present the synthesis and elucidate the single crystal as well as solution conformations of α,γ-hybrid peptides incorporating (2-aminophenyl)acetic acid as the γ-amino acid. We have employed both sterically constrained achiral Aib and chiral

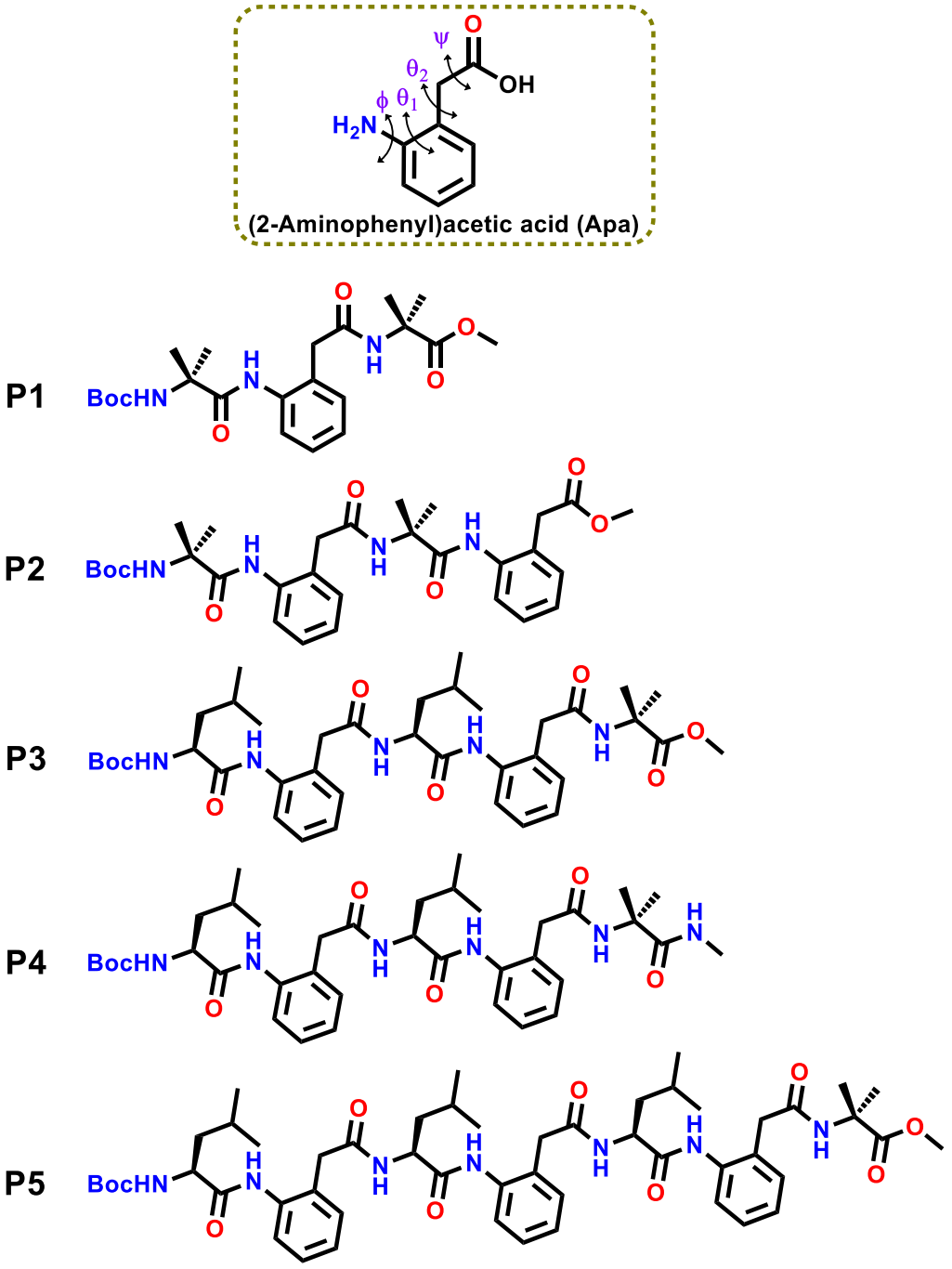
α-amino acids alongside Apa to investigate their respective influences on the conformations of α,γ-hybrid peptides.

5.2. Objective of the current Work

The α-helix stands as one of the predominant secondary structures in proteins, characterized by stabilization through unidirectional intramolecular hydrogen bonds. Considerable efforts have been devoted in the literature to design mimetics of the α-helix, employing a diverse array of synthetic building blocks. This report introduces diverse helical conformations derived from α,γ-hybrid peptides incorporating (2-aminophenyl)acetic acid (Apa) as the γ-amino acid. Apa shares similarities with (*Z*)- β,γ-unsaturated γ-amino acids. The single crystal conformations of α,γ-hybrid tri- and tetrapeptides, composed of alternated sterically constrained Aib and Apa amino acids, indicate that the tripeptide assumed a helical twist conformation without inter-residue hydrogen bonds, while the tetrapeptide adopted a regular 12-helix conformation. On the contrary, the conformational analysis in both single crystal and solution states for α,γ-hybrid pentapeptides, and the solution conformation of a heptapeptide containing proteinogenic chiral amino acid Leu and Aib at the C-terminus, unveiled an unusual 12/10-helix conformation with alternating hydrogen bond directionality. Overall, the results presented in this study provide valuable insights into the construction of continuous 12/10-helix conformations characterized by alternating hydrogen bond directionality.

5.3. Results and Discussion

In order to comprehend the folding tendencies of α,γ-hybrid peptides incorporating the aromatic amino acid Apa, we formulated peptides **P1-P5**. The sequences of these designed peptides are illustrated in Scheme 1. The sequences of these peptides we designed are presented in Scheme 1. Apa amino acid was synthesized starting from o-nitrophenylacetic acid through the reduction of the nitro group using catalytic hydrogenation. The free amine and carboxylic acid groups were protected with the Boc group and methyl esters, respectively. We encountered challenges in conducting the coupling reaction between Boc-Aib and free amine Apa using standard coupling conditions involving HBTU and HOBt. However, we established that the mixed anhydride method,[26] employing Ibc-Cl and DIPEA, was more effective for coupling Boc-Aib and Apa. Chiral amino acids and Apa were coupled using HBTU and HOBt as coupling reagents. All peptides were synthesized through the solution-phase method, purified via column chromatography, and characterized using mass spectrometry.



Scheme 1. Designed sequences of α,γ-hybrid peptides consisting of Apa as γ-amino acids.

In order to understand the unambiguous conformations, we attempted crystallizations of all peptides, **P1-P5**, using different solvent combinations. However, only **P1**, **P2**, and **P3** produced single crystals via slow evaporation of their respective peptide solutions in ethyl acetate.

5.3.1. Crystal structure analysis of P1

The single crystals of **P1** were obtained through slow evaporation of its solution in ethyl acetate, and its X-ray diffracted structure is depicted in Figure 3. In the asymmetric unit, two

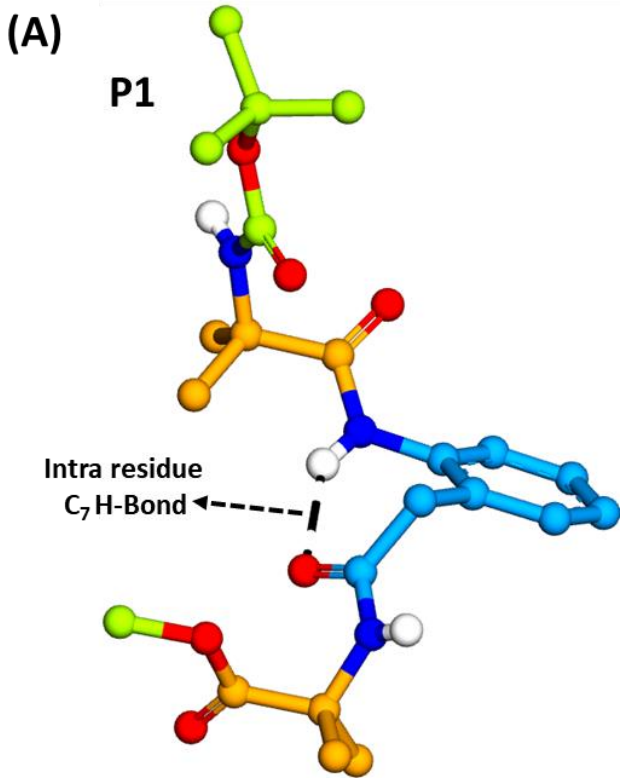


Figure 3: (A) X-ray crystal structure of **P1**. All hydrogen atoms (except N-H) are omitted.

Table 1: Torsional Angle Parameters of **P1**.

Peptide P1	ϕ	θ_1	θ_2	ψ	ω
Aib1	61	-	-	-139	179
Apa2	-127	0	-77	-114	173
Aib3	49	-	-	47	176

Table 2: Hydrogen Bonding Parameters of **P1.**

D-H.....A	**d(D.....A) (Å)**	**d(H.....A) (Å)**	**<(N-H.....O) (°)**
Intramolecular H-bonds			
N(2)-H(2).....O(4)	2.89	2.17	141
Intermolecular H-bonds			
N(1)-H(1).....O(3)*	3.00	2.23	150
N(1)#-H(1).....O(3)	3.00	2.23	150
N(3)-H(1).....O(5)!	2.95	2.11	165
N(3)$-H(1).....O(5)	2.95	2.11	165
Symmetry operations: # -x, -y, -z; * -x, -y, -z; ! 1+x, y, z; $ -1+x, y, z			

molecules were identified, both adopting overall helical type conformations with opposite handedness. However, no inter-residue hydrogen bonds were observed. Nevertheless, a single intra-residue seven-membered hydrogen bond between NH---OC is observed in the γ-residues. Table 2 displays the Hydrogen Bonding Parameters of **P1**. Torsion angle analysis indicated that the Aib at the N-terminus adopted a polyproline (II) type conformation, while the Aib at the C-terminus adopted a helical type conformation (refer to Table 1). The ϕ, θ_2 and ψ values of Apa were found to be ±124, ±77, and ±113, respectively, being it as aromatic backbone the value of θ_1 is zero.

5.3.2. Crystal structure analysis of P2

The structure of tetra-peptide **P2**, derived from its single crystals, is illustrated in Figure 4. Within the asymmetric unit, two molecules addopted a 12-helix conformation with opposite handedness. The 12-helix of **P2** is stabilized by two intramolecular 12-membered hydrogen bonds between the residues *i* (CO) → *i*+3 (NH). The hydrogen bonding observed in the 12-helix aligns with the pattern found in α,γ-hybrid peptides containing (Z)-β,γ-unsaturated γ-amino acids.[25] The H-bonding pattern observed in **P2** is illustrated in Figure 4.

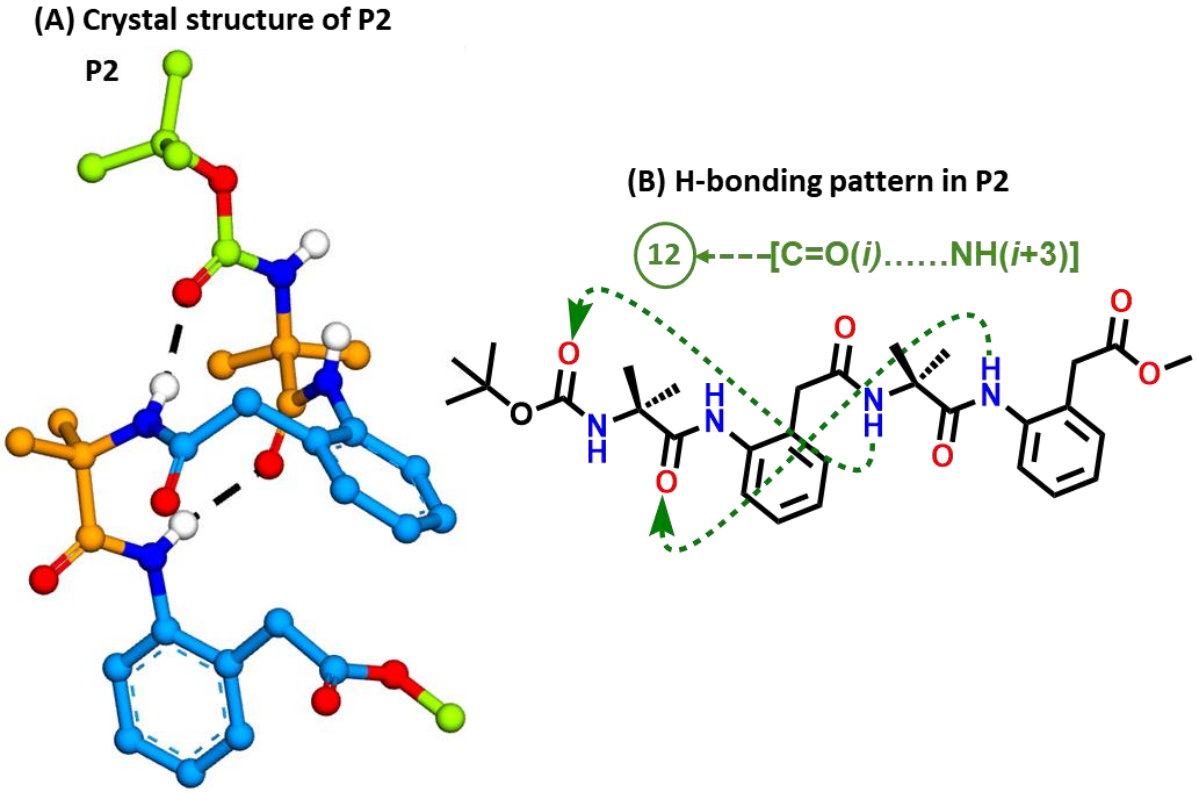


Figure 4. (A) X-ray crystal structure of **P2**. (B) Schematic representation of intramolecular hydrogen bonding pattern in 12-helix peptide **P2**.

Table 3: Torsional Angle Parameters of **P2.**

Peptide P2	ϕ	θ_1	θ_2	ψ	ω
Aib1	-63	-	-	-33	-164
Apa2	-102	4	91	-108	-175
Aib3	-54	-	-	-44	-176
Apa4	-123	2	168	91	-

Table 4: Hydrogen Bonding Parameters of **P2.**

D-H.....A	**d(D.....A) (Å)**	**d(H.....A) (Å)**	**<(N-H.....O) (°)**
Intramolecular H-bonds			
N(3)-H(3).....O(2)	2.87	2.02	169
N(4)-H(4).....O(3)	2.93	2.09	167

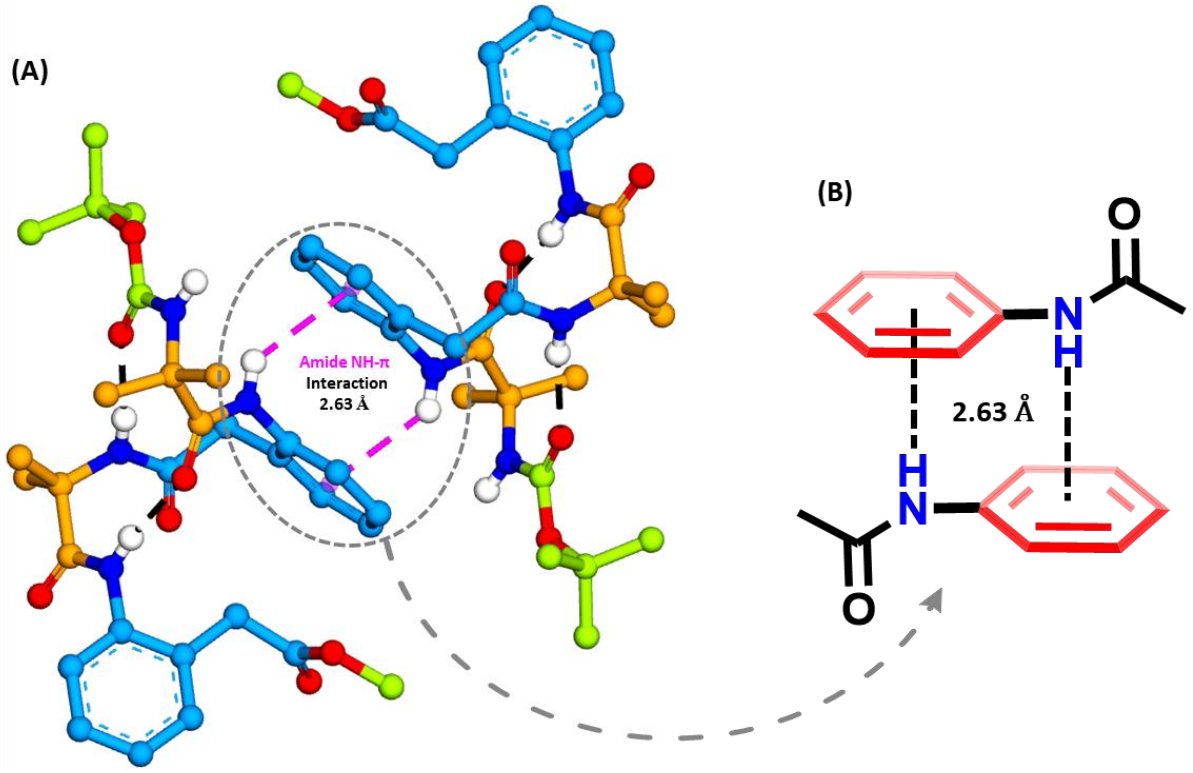


Figure 5. (A) Crystal structure of **P2** depicting the amide NH-π interactions. (B) Schematic representation of amide NH-π interactions. All hydrogen atoms (except N-H) are omitted for clarity.

Torsion angle analysis indicated that both Aib residues conformed to regular helical structures.

In the right-handed helix, the values of ϕ, θ2, and ψ for Apa2 were found to be -102, +91, and -108, respectively, whereas similar values with opposite sign were found in the left-handed helix. The torsion angles and hydrogen bonding parameters of **P2** were tabulated in the Table 3 and Table 4 respectively. The C-terminal ester carbonyl group did not take part in the helical fold, deviates away from the helix. In addition to the 12-helix conformation, we noted a robust intermolecular amide NH---π interaction between the amide NH and the aromatic backbone of Apa2 from two different helices. The interaction between the amide NH and the aromatic π system is depicted in Figure 5. This interaction likely arises from the absence of steric hindrance between the amide NH and the planar aromatic group.

5.3.3. Crystal structure analysis of P3

As peptide **P2** adopted a 12-helix conformation similar to that of hybrid peptides containing (*Z*)-β,γ-unsaturated γ-amino acids, we aimed to explore the impact of Aib on the 12-helix conformation by substituting it with chiral α-amino acids. In this context, we designed the penta-peptide **P3**, consisting α-Leu residues, except one Aib at the C-terminus (refer to Scheme 1). The X-ray diffracted single crystal structure of **P3** is depicted in Figure 6.

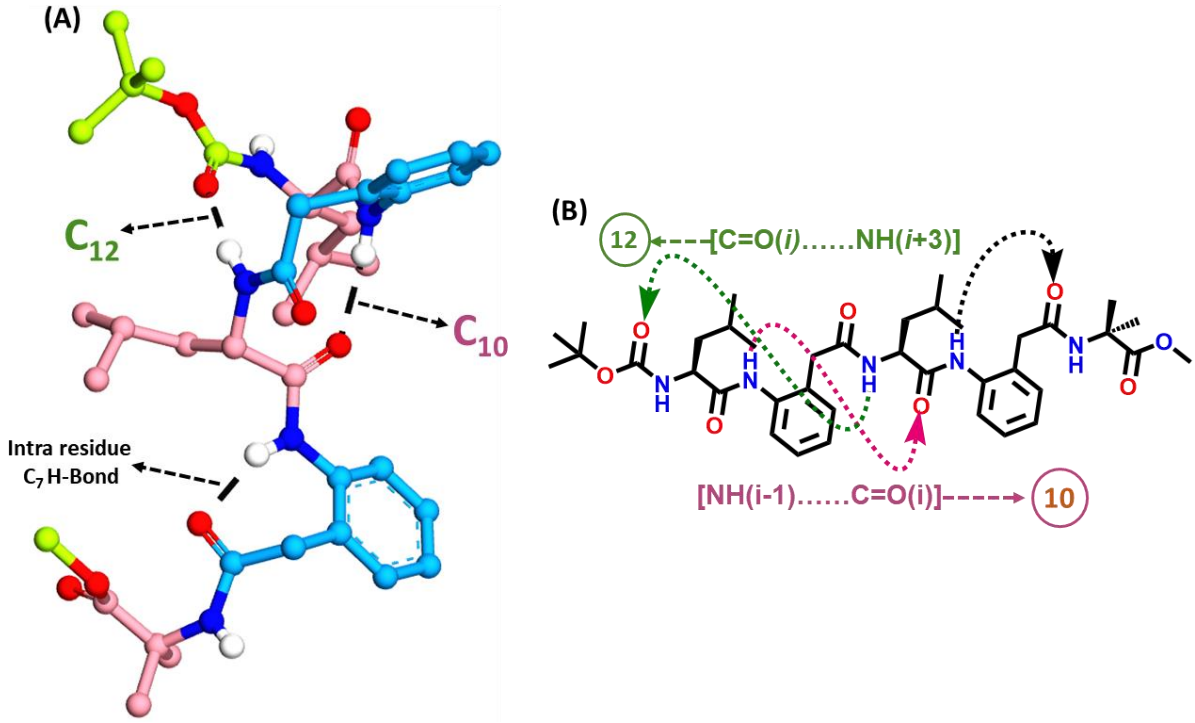


Figure 6. (A) Single-crystal X-ray diffracted structure of **P3**. 12/10 helical conformation of peptide **P3** in single crystal with alternate hydrogen bonding. All hydrogen atoms (except N-H) are omitted for clarity. (B) Schematic representation of intramolecular hydrogen bonding pattern in 12/10-helix peptide **P3**.

Table 5: Torsional Angle Parameters of **P3.**

Peptide P3	ϕ	θ_1	θ_2	ψ	ω
Leu1	-71	-	-	142	172
Apa2	103	-4	70	-120	173
Leu3	-72	-	-	-155	-173
Apa4	155	-11	79	116	-172
Aib5	-58	-	-	-41	-

Table 6: Hydrogen Bonding Parameters of **P3.**

D-H.....A	**d(D.....A) Å**	**d(H.....A) (Å)**	**<(N-H…..O)**
Intramolecular H-bonds			
N(2)-H(2)**.....**O(2)	2.82	1.94	175
N(1)-H(1)**.....**O(6)	2.90	1.90	171
N(3)-H(3)**.....**O(7)	2.82	2.02	150
Intermolecular H-bonds			
N(4)-H(4)**.....**O(5)*	2.93	2.15	147
#N(4)-H(4)**.....**O(5)	2.93	2.15	147
Symmetry operations: # -x, -1/2+y, -z; * -x, 1/2+y, -z			

The peptide adopted an unusual helical conformation. The initial three residues adopted a 12/10-helical conformation characterized with alternating hydrogen bond directionality, while the two residues at the C-terminus adopted a γ-helix type conformation with a single seven-membered intra-residue H-bond between NH and CO of Apa2. The torsion angles adopted by the α-Leu residues are consistent with those reported in previous α,γ-hybrid peptides. The distinction between the γ-amino acid residue Apa in the mixed helices is represented by θ1. The Apa4 is not participated in the mixed helix conformation, exhibiting different torsion angles. Furthermore, the C-terminal Aib5 adopted a right-handed helix conformation, but it does not participated in the intramolecular H-bonding, instead it involved intermolecular H-bonding. The torsion angles and hydrogen bonding parameters of **P3** were tabulated in the Table 5 and Table 6 respectively.

5.3.4. NMR structure analysis of peptides P3, P4 and P5 using 2D NMR (TOCSY & ROESY) analysis and DMSO-d_6 titration

Additionally, we synthesized peptide **P4** from **P3** by changing the methyl ester into a methyl amide. In parallel, a seven-residue peptide, **P5**, was synthesized. Unfortunately, attempts to obtain single crystals for Peptides **P4** and **P5** were unsuccessful. To gain insights into the solution conformation of these peptides, we conducted 2D-NMR analysis, employing TOCSY and ROESY techniques. Furthermore, DMSO-*d6* titration was employed for Peptide **P3** and **P4**, temperature dependent experiment conducted for peptide **P5**. Utilizing the crucial NOEs identified in the 2D-NMR spectra, we generated models representing the energy-minimized solution conformations of Peptides **P3**, **P4**, and **P5**. This modeling process was carried out using the Insight II (version 97.0) / Discover program on a Silicon Graphics Octane workstation. The structural analyses of Peptides **P3**, **P4**, and **P5** based on NMR data are sequentially presented below.

5.3.4.1. Peptide P3 and P4 NMR structure analysis, using 2D NMR (TOCSY and ROESY) and DMSO-d_6 titration

The ROESY analysis of **P3** revealed sequential weak NH(*i*)↔NH(*i*+1) NOEs, strong NH(*i*+1) ↔ $C^{\alpha}H$ (*i*) NOEs, strong NOEs between Leu3NH↔Leu1$C^{\alpha}H$ and Apa4NH↔Leu3$C^{\alpha}H$. Further, ROESY analysis also revealed Leu3H ↔Aib5 CH_3, Leu3 $C^{\alpha}H$↔Aib5CH_3 medium NOEs and strong NOE between Leu1$C^{\alpha}H$↔ Leu3$C^{\beta}H$ (refer Figure 9). All NOEs observed in the ROESY analysis of **P3** are tabulated in the Table 8. Further, the DMSO titration analysis revealed downfield shift of Leu1NH and Apa4NH with increasing concentrations of DMSO suggesting that these two amide NH groups are exposed to solvent compared to other three amide NH groups (refer Table 7 and Figure 10). Probably, these three NH groups are involved in H-bonding with the backbone carbonyl groups.

Further, ROESY analysis of peptide **P4** revealed the similar type of NOE pattern as observed in **P3**. The weak NOEs between Leu1NH↔Apa2NH, Apa2NH↔Leu3NH, Aib5NH↔6NHMe, strong NOEs between Apa2NH↔Leu1$C^{\alpha}H$, Apa4NH↔Leu3$C^{\alpha}H$, Leu3H↔Apa2$C^{\alpha}H$, Aib5NH↔Apa4$C^{\alpha}H$ and Apa4NH↔Aib5CH_3 (refer Figure 13). In addition, medium NOEs between Leu3NH↔Leu1$C^{\alpha}H$, Apa4NH↔Leu3 $C^{\beta}H$ and other inter-residue NOEs are observed. All these crucial NOEs are tabulated in the Table 10. The DMSO titrations studies further revealed the down field chemical shifts in Leu1NH and 6NHCH_3 groups (refer Table 9 and Figure 14). Based on the NOEs observed in the 2D-NMR analysis and DMSO titration experiments, energy minimized solution conformations of **P3** and **P4** are

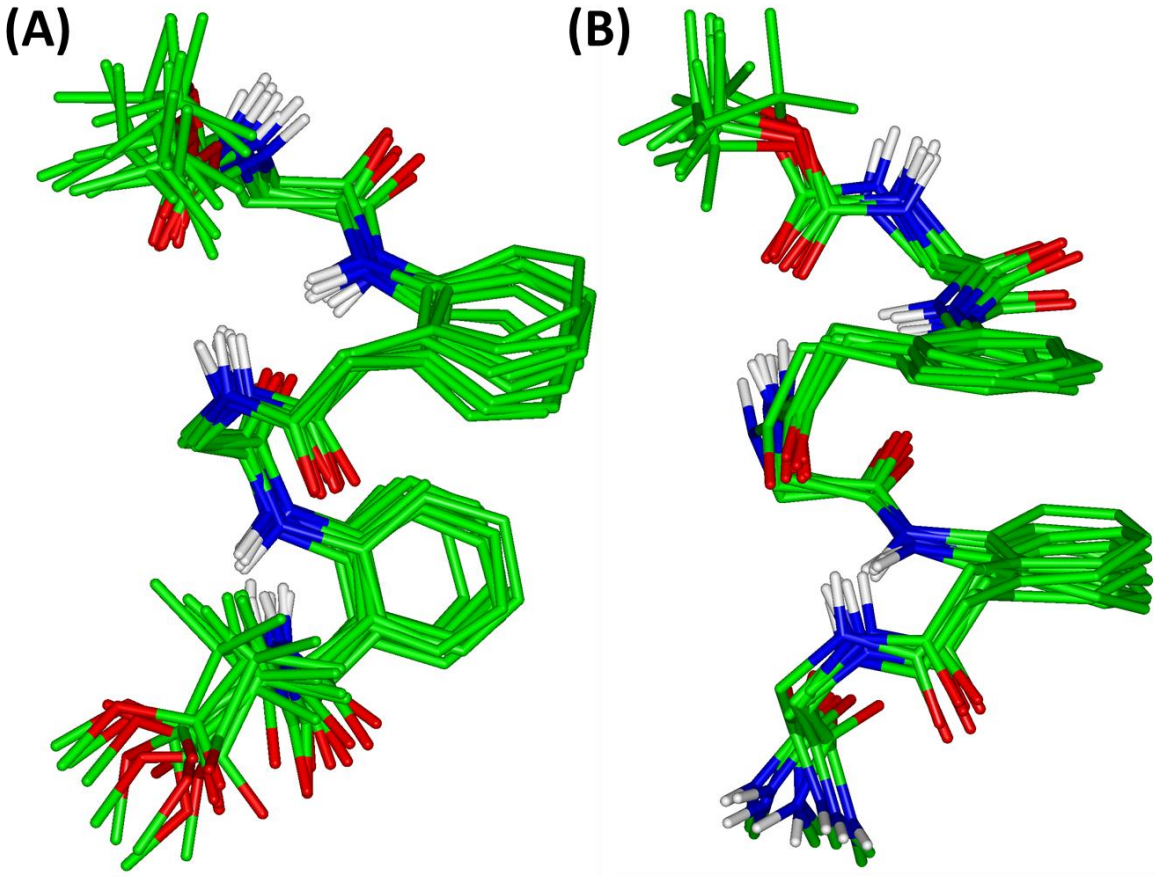


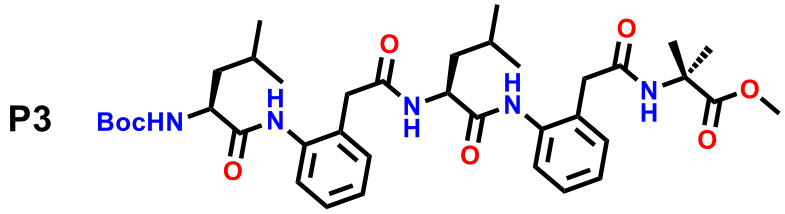
Figure 7: Solution conformations of peptides **P3** and **P4**. Peptide **P3** and **P4** adopt 12/10 helical conformations in solution with alternate hydrogen bonding.

shown in the Figure 7. The comparison of the crystal structure and solution structure of **P3** revealed that the mixed 12/10-helix observed at N-terminus in the crystal structure continues throughout the peptide in solution structure. These results also suggested that the fragility of the 12/10-helix structure.

Peptide P3 NMR (TOCSY and ROESY) analysis and DMSO-d_6 titration

A) Partial TOCSY spectrum analysis of peptide P3 in $CDCl_3$

Below partial TOCSY spectrum showing the amino acid residues in peptide **P3**



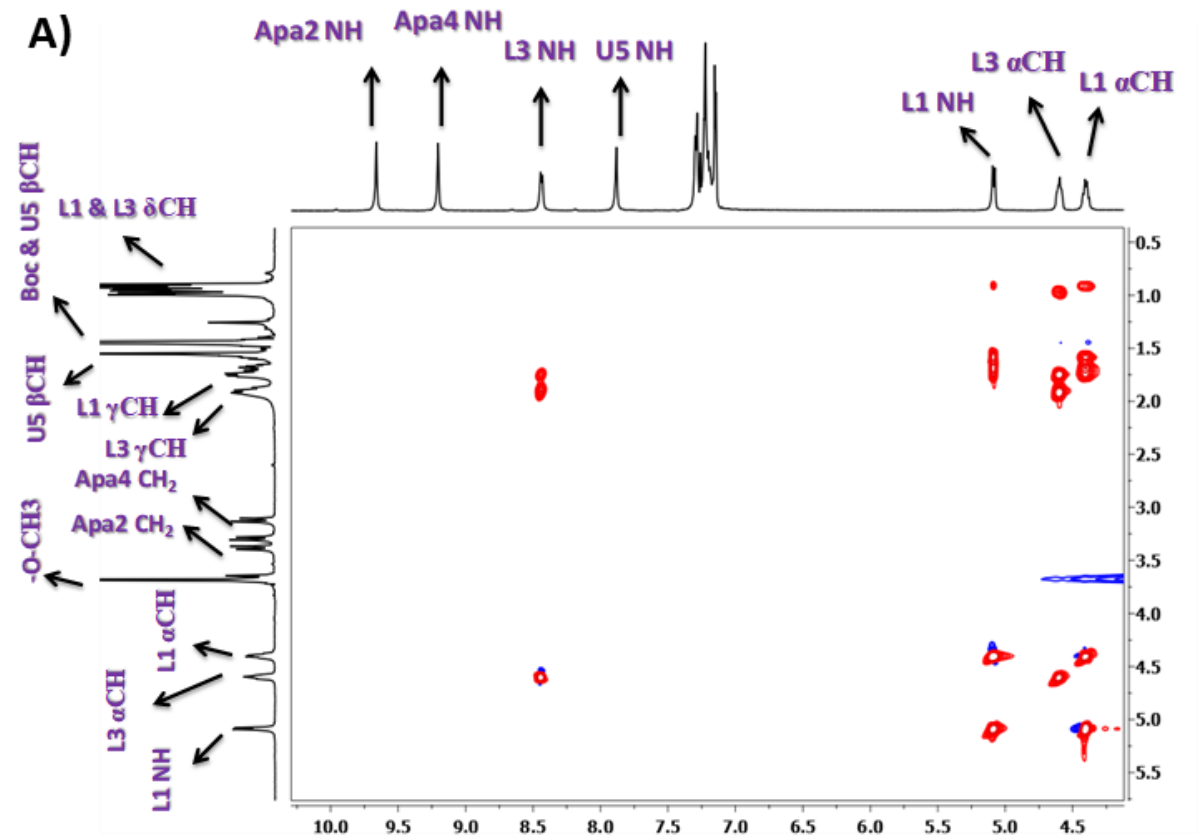
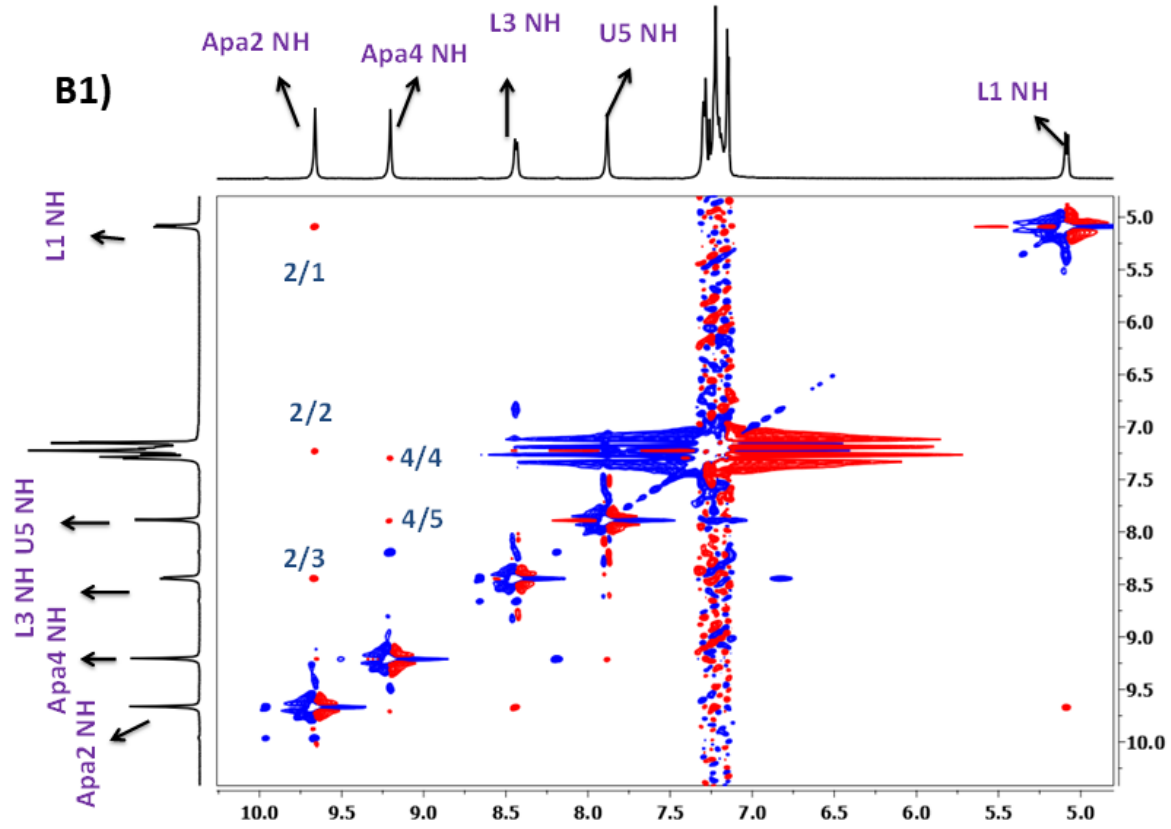
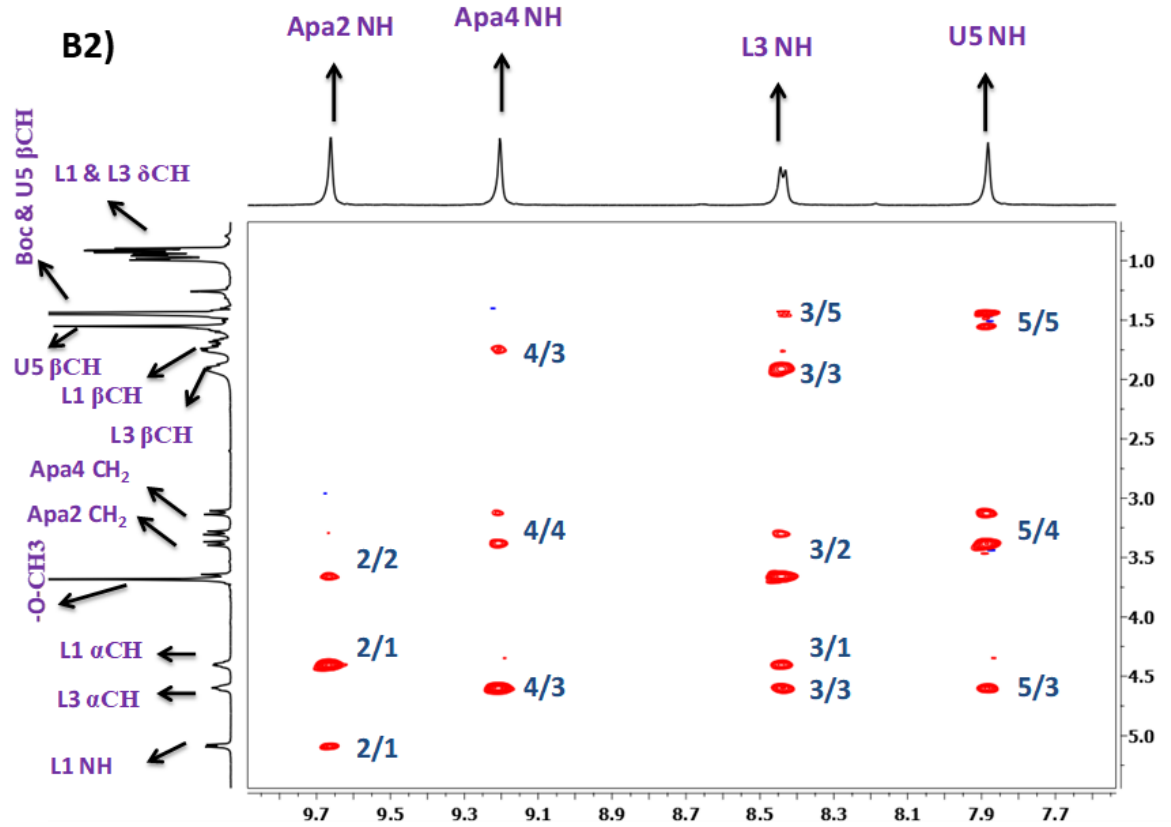


Figure 8: (A) Partial TOCSY spectra of peptide **P3** in $CDCl_3$. The TOCSY spectrum was used to identify amino acids in the peptide sequence. The sequential assignments of amino acids were performed using ROESY.

B) Partial ROESY spectrum analysis of Peptide P3 in $CDCl_3$


B1)
Apa2 NH
Apa4 NH
L3 NH
U5 NH
L1 NH
L1 NH
L3 NH U5 NH
Apa4 NH
Apa2 NH
2/1
2/2
4/4
4/5
2/3
10.0
9.5
9.0
8.5
8.0
7.5
7.0
6.5
6.0
5.5
5.0


B2)
Apa2 NH
Apa4 NH
L3 NH
U5 NH
Boc & U5 βCH
L1 & L3 δCH
U5 βCH
L1 βCH
L3 βCH
Apa4 CH2
Apa2 CH2
-O-CH3
L1 αCH
L3 αCH
L1 NH
4/3
3/5
3/3
5/5
4/4
3/2
5/4
2/2
2/1
3/1
3/3
5/3
4/3
2/1
9.7
9.5
9.3
9.1
8.9
8.7
8.5
8.3
8.1
7.9
7.7
1.0
1.5
2.0
2.5
3.0
3.5
4.0
4.5
5.0

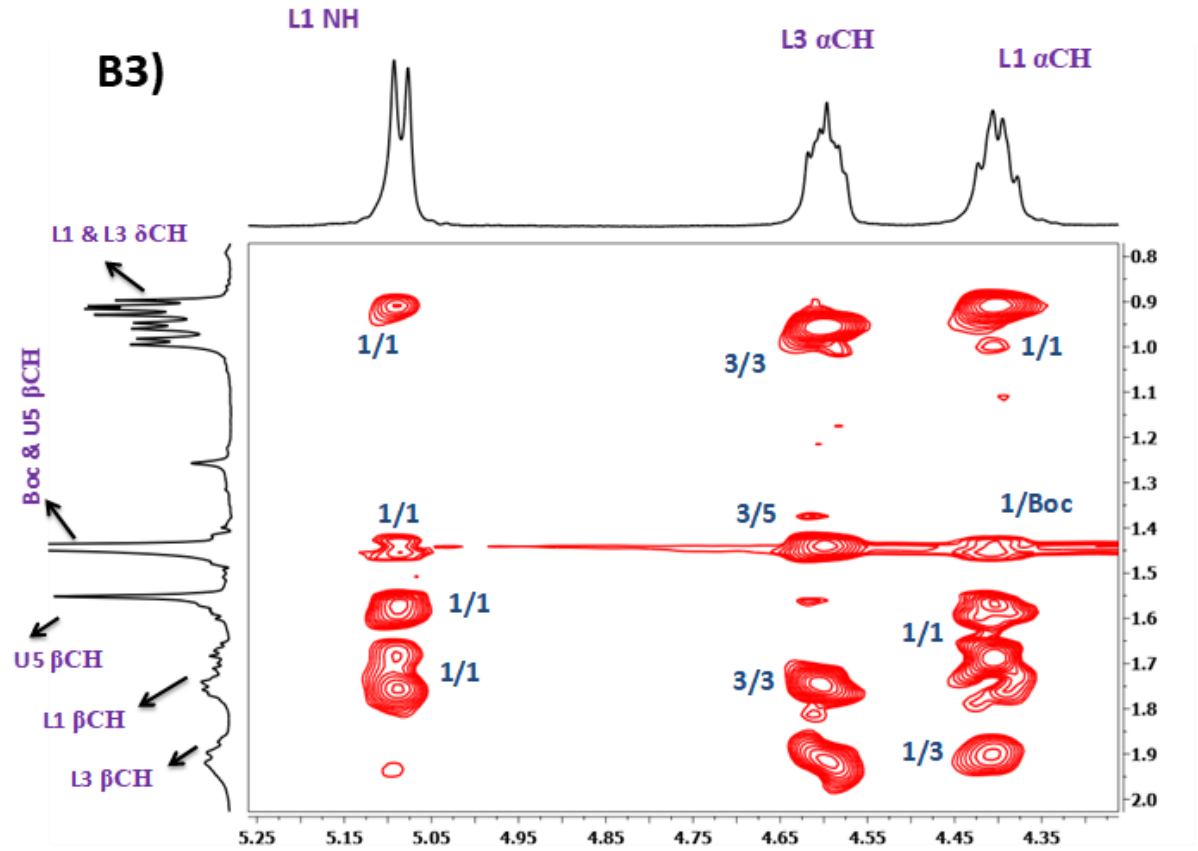
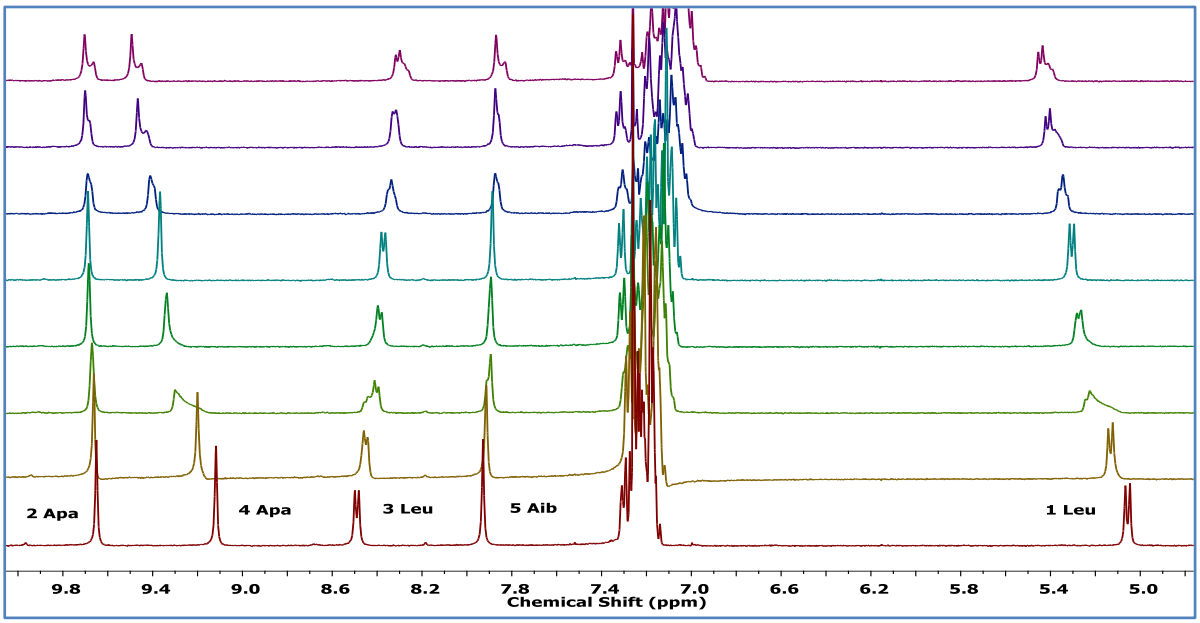


Figure 9: Partial ROESY spectrum of **P3** showing sequential NOEs of (B1) NH↔NH, (B2) NH↔$C_{\alpha}H$ and NH↔side-chain, (B3) $C_{\alpha}H$ ↔ sidechain.

C) <u>DMSO titration Experiment of peptide P3</u>



<u>Figure 10:</u> <u>NHs chemical shift of Peptide **P3** solution in $CDCl_3$ at varying concentration of DMSO-d_6</u>

Table 7: DMSO-d_6 titration experiment table of peptide **P3**.

Residue	*Chemical Shift Change (Δδ)*								*dδ/dv*	$^3J_{NH\text{-}C^{\alpha}H}$ *(30 °C)*
DMSO vol.	**0 µL**	**5 µL**	**10 µL**	**15 µL**	**20 µL**	**25 µL**	**30 µL**	**35 µL**		
1 NH	5.06	5.13	5.23	5.27	5.30	5.34	5.41	5.44	0.011	6.4
2 NH	9.65	9.66	9.67	9.68	9.69	9.69	9.70	9.70	0.001	-
3 NH	8.49	8.45	8.40	8.39	8.37	8.34	8.32	8.31	-0.005	5.2
4 NH	9.12	9.20	9.30	9.34	9.37	9.41	9.47	9.49	0.010	-
5 NH	7.93	7.91	7.89	7.89	7.89	7.87	7.87	7.87	-0.002	-

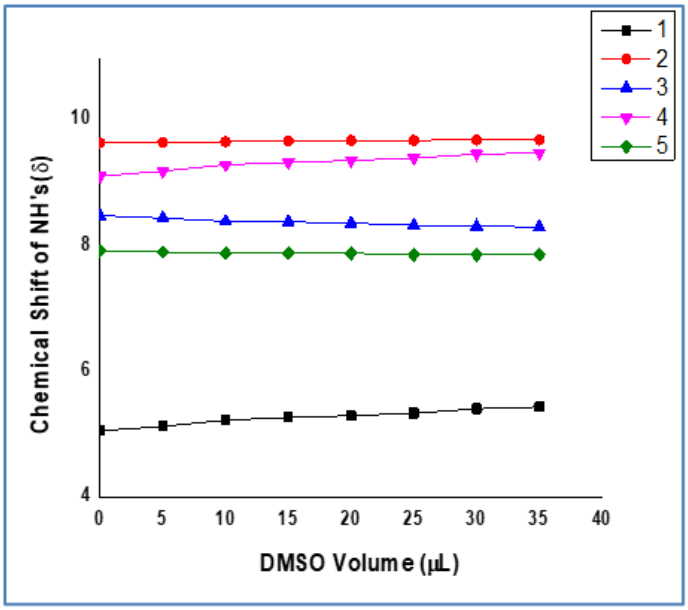


Figure 11: DMSO-d6 titration plots of peptide **P3** solution in $CDCl_3$. Peptide P3 showing negligible change in the NH chemical shifts except Leu1NH and Apa4NH shown in black color block and pink color triangle respectively.

Table 8: List of NOEs used for MD calculation for peptide **P3.**

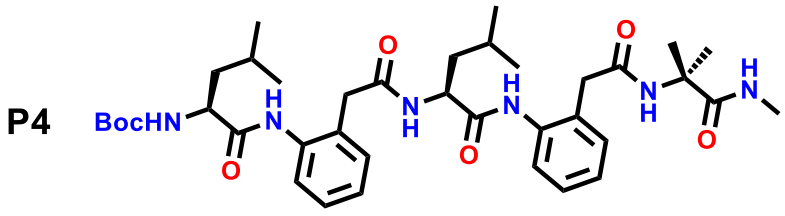
Residue	**H-atom**	**Residue**	**H-atom**	**NOE**
Apa4	NH	Leu3	βCH	Medium
Apa2	NH	Apa2	αCH_2	Medium
Apa2	NH	Leu1	αCH_2	Strong
Apa2	NH	Leu1	NH	Medium
Apa4	NH	Apa4	αCH_2	Medium
Apa4	NH	Leu3	αCH_2	Strong
Leu3	NH	Aib5	CH_3	Medium
Leu3	NH	Leu3	βCH_2	Strong

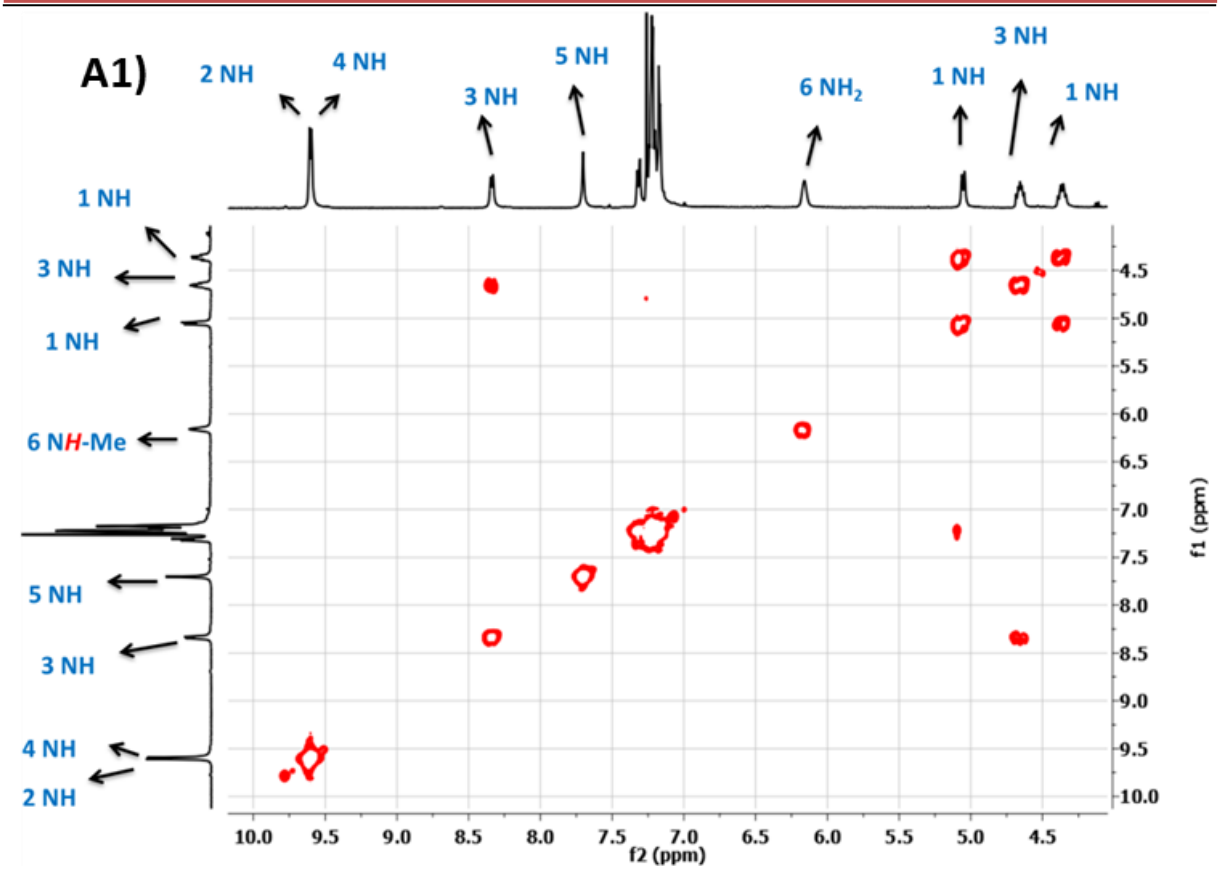
Leu3	NH	Apa2	αCH$_2$	Medium
Leu3	NH	Leu1	αCH	Strong
Leu3	NH	Leu3	αCH	Strong
Aib5	NH	Aib5	CH$_3$	Strong
Aib5	NH	Apa4	αCH$_2$	Strong
Aib5	NH	Leu3	αCH	Strong
Leu1	NH	Leu1	δCH$_2$	Medium
Leu1	NH	Boc-	CH$_3$	Medium
Leu1	NH	Leu1	βCH$_2$	Strong
Leu1	NH	Leu1	γCH	Strong
Leu3	αCH	Leu3	βCH$_2$	Strong
Leu3	αCH	Leu3	δCH$_2$	Medium
Leu3	αCH	Aib5	CH$_3$	Medium
Leu1	αCH	Leu1	βCH$_2$	Strong
Leu1	αCH	Boc-	CH$_3$	Medium
Leu1	αCH	Leu3	βCH$_2$	Strong
Leu 1	NH	Apa 2	NH	Weak
Apa2	NH	Leu 3	NH	Weak
Apa4	NH	Aib5	NH	Weak
Apa2	NH	Apa2	Ar-H	Weak
Apa4	NH	Apa4	Ar-H	Weak

Peptide P4 NMR (TOCSY and ROESY) analysis and DMSO-*d*$_6$ titration

A) Partial TOCSY spectrum analysis of peptide P4 in CDCl$_3$

Below partial TOCSY spectrum showing the amino acid residues in peptide **P4**




A1)
2 NH
4 NH
3 NH
5 NH
6 NH2
1 NH
3 NH
1 NH
1 NH
3 NH
1 NH
6 NH-Me
5 NH
3 NH
4 NH
2 NH
10.0 9.5 9.0 8.5 8.0 7.5 7.0 6.5 6.0 5.5 5.0 4.5
f2 (ppm)
4.5 5.0 5.5 6.0 6.5 7.0 7.5 8.0 8.5 9.0 9.5 10.0
f1 (ppm)

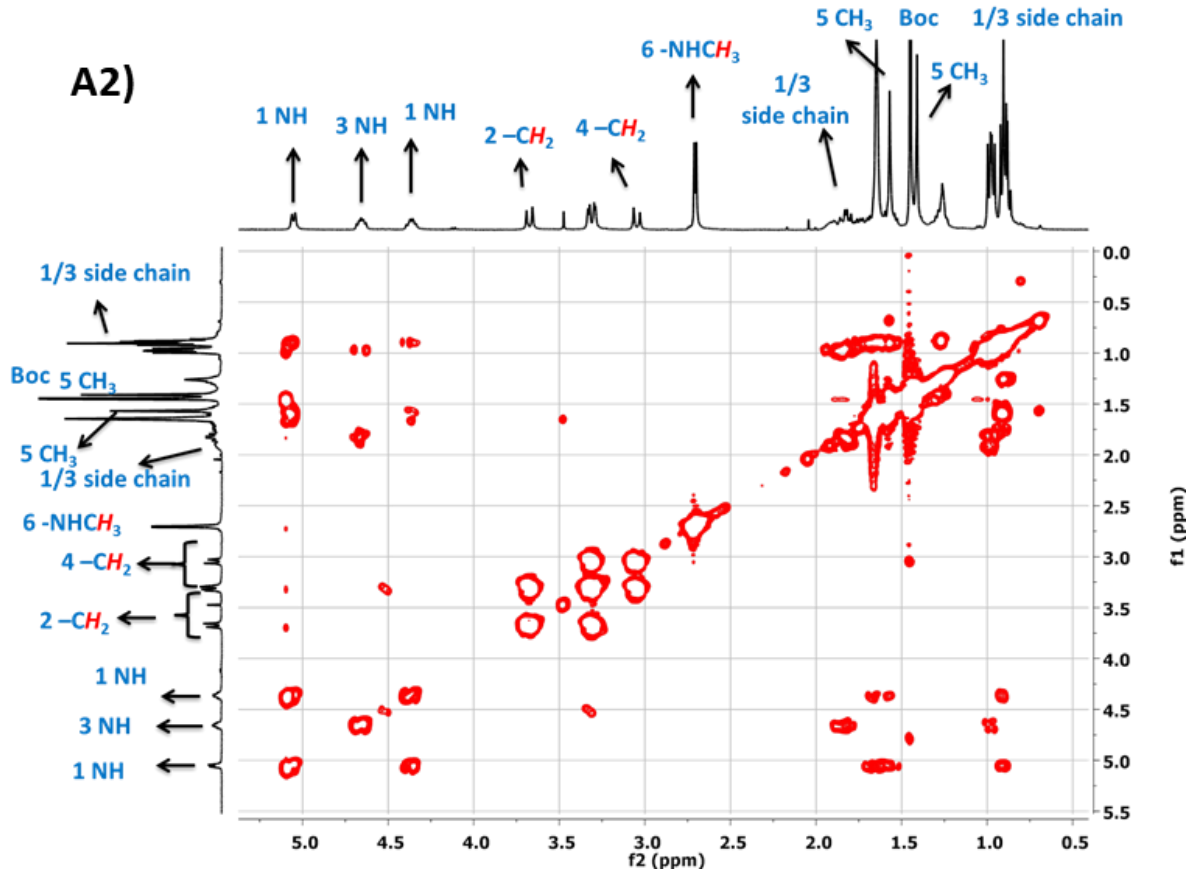
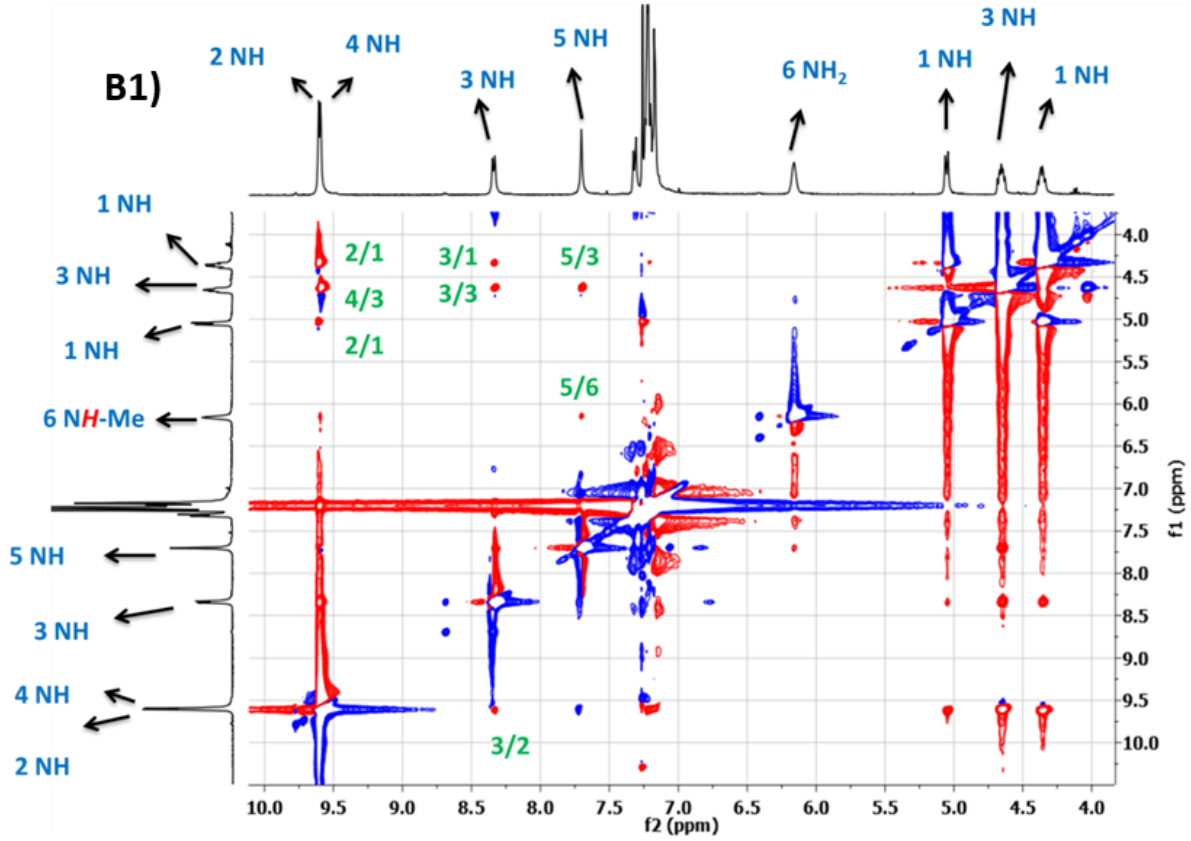

A2)
5 CH3
Boc
1/3 side chain
6 -NHCH3
1/3
side chain
5 CH3
1 NH
3 NH
1 NH
2 –CH2
4 –CH2
1/3 side chain
Boc 5 CH3
5 CH3
1/3 side chain
6 -NHCH3
4 –CH2
2 –CH2
1 NH
3 NH
1 NH
5.0 4.5 4.0 3.5 3.0 2.5 2.0 1.5 1.0 0.5
f2 (ppm)
0.0 0.5 1.0 1.5 2.0 2.5 3.0 3.5 4.0 4.5 5.0 5.5
f1 (ppm)

Figure 12: (A1) and (A2) are partial TOCSY spectra of peptide **P4** in $CDCl_3$. The TOCSY spectrum was used to identify amino acids in the peptide sequence. The sequential assignments of amino acids were performed using ROESY.

B) Partial ROESY spectrum analysis of Peptide P4 in $CDCl_3$



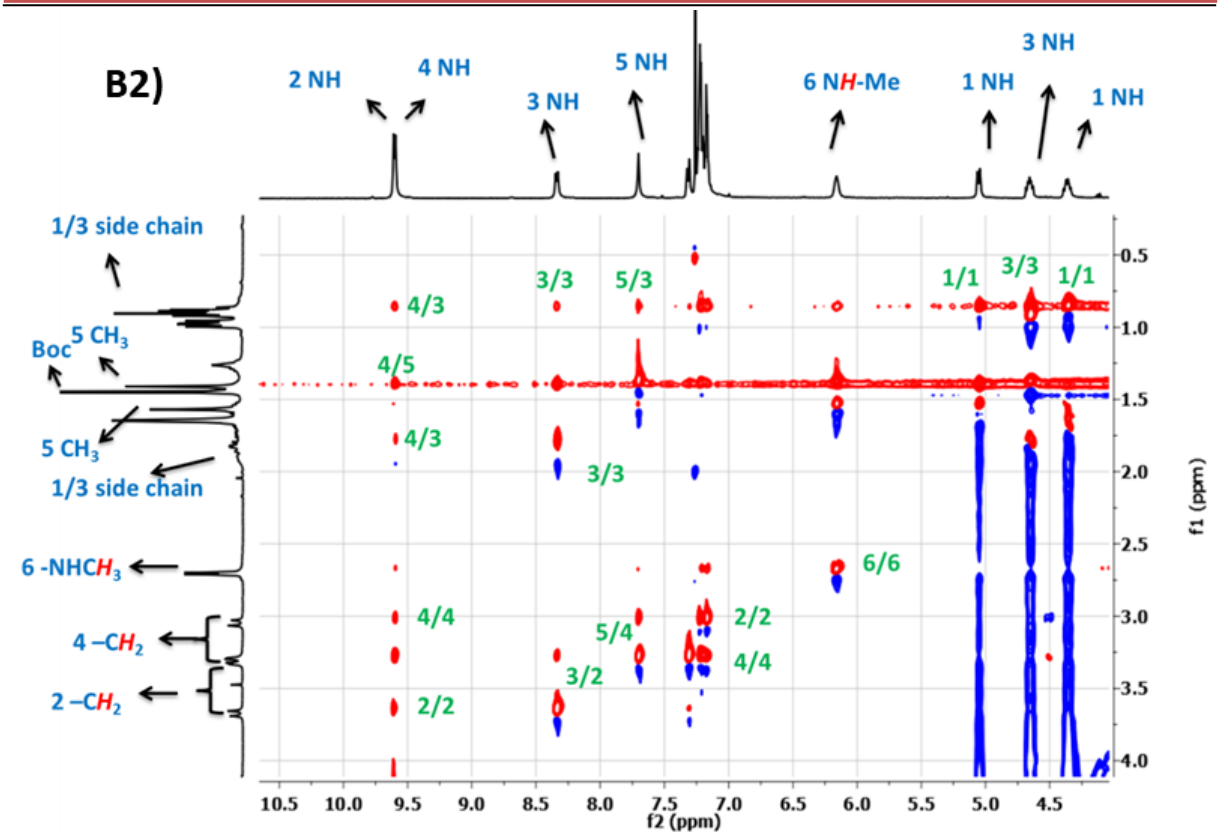


Figure 13: Partial ROESY spectrum of **P4** showing sequential NOEs of (B1) NH↔NH, (B2) NH↔C_{α}H and NH↔side-chain.

C) <u>DMSO titration Experiment of peptide P4</u>

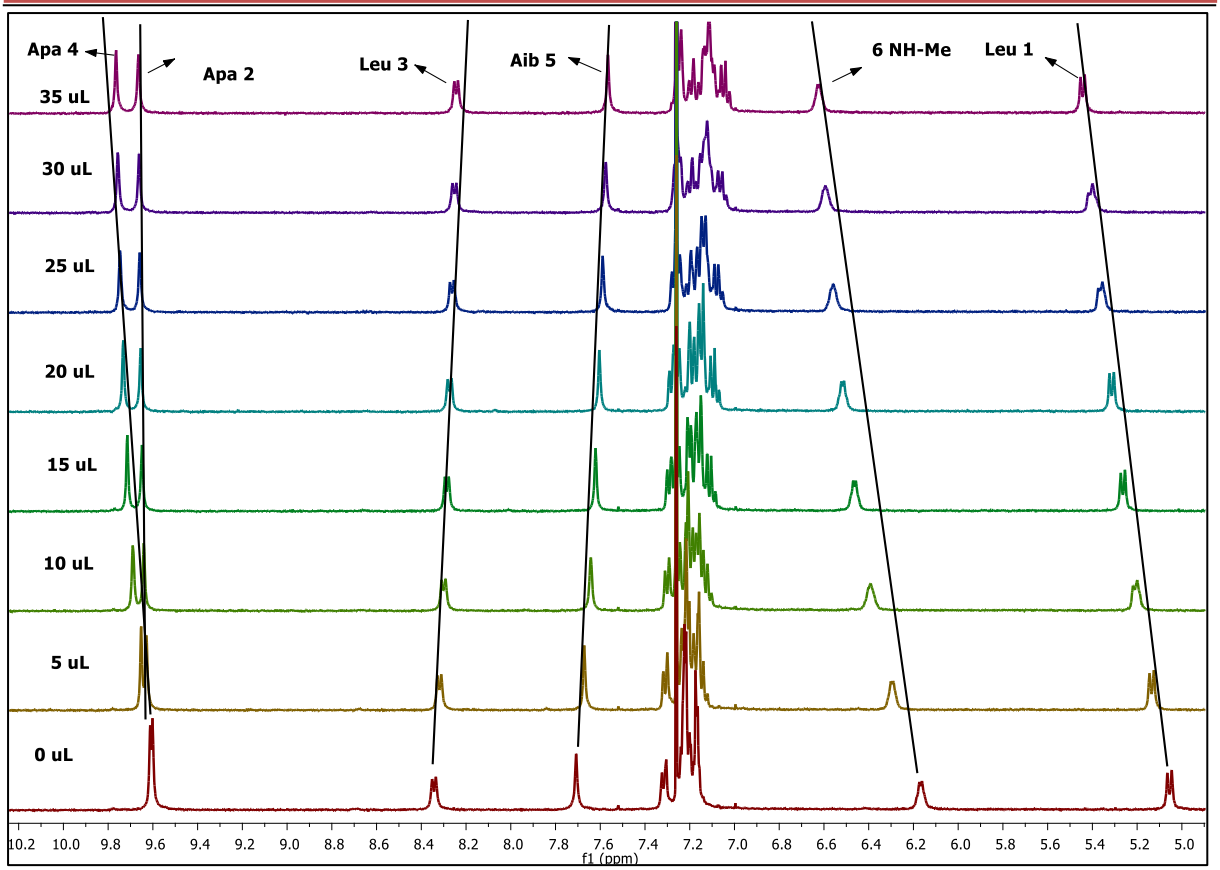


Figure 14: NHs chemical shift of Peptide **P4** solution in $CDCl_3$ at varying concentration of DMSO-d_6

Table 9: DMSO-d_6 titration experiment Table of peptide **P4**.

Chemical Shift (Δδ)									*dδ/dV*	$J^3_{NH\text{-}C^{\alpha}H}$ *(Hz) 30 °C*
DMSO titration (µL)	**0**	**5**	**10**	**15**	**20**	**25**	**30**	**35**		
Leu 1	5.06	5.14	5.21	5.26	5.31	5.36	5.40	5.44	0.011	7.6
Apa 2	9.61	9.63	9.64	9.65	9.66	9.66	9.66	9.67	0.002	-
Leu 3	8.43	8.32	8.30	8.29	8.27	8.26	8.25	8.24	-0.004	6.8
Apa 4	9.60	9.65	9.69	9.72	9.73	9.75	9.76	9.77	0.005	-
Aib 5	7.71	7.67	7.64	7.62	7.60	7.59	7.58	7.57	-0.004	-
NHMe-6	6.17	6.30	6.40	6.46	6.52	6.56	6.59	6.62	0.012	-

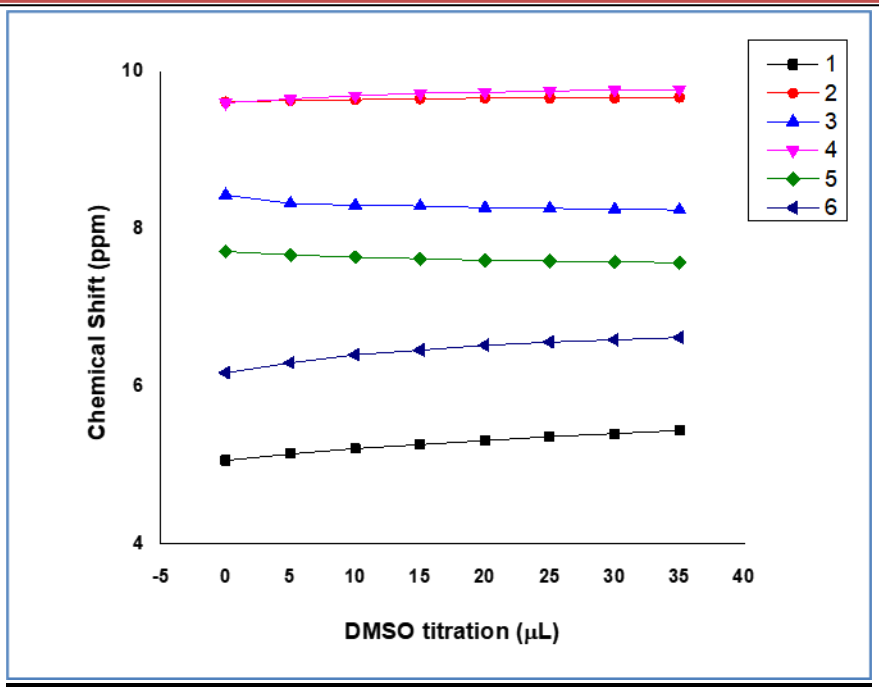


Figure 15: DMSO-d6 titration plots of peptide **P4** solution in $CDCl_3$. Peptide **P4** showing negligible change in the NH chemical shifts except Leu1NH and 6$NHCH_3$ groups shown in black color block and dark blue color triangle respectively.

Table 10: List of NOEs used for MD calculation for peptide **P4.**

Residue	H-atom	Residue	H-atom	NOE
Leu 1	NH	Apa 2	NH	Strong
Apa 2	NH	Leu 1	αCH	Strong
Apa 4	NH	Leu 3	αCH	Strong
Leu 3	NH	Leu 1	αCH	Medium
Leu 3	NH	Leu 3	αCH	Medium
Leu 3	NH	Apa 2	NH	Weak
Aib 5	NH	Leu 3	αCH	Medium
Aib 5	NH	6 NH-Me	NH	Weak
Apa 4	NH	Leu 3	Side chain CH	Medium
Apa 4	NH	Aib 5	CH_3	strong
Apa 4	NH	Leu 3	βCH_2	Medium
Apa 4	NH	Apa 4	αCH_2	Medium
Apa 2	NH	Apa 2	αCH_2	Medium
Leu 3	NH	Apa 2	αCH_2	Strong
Aib 5	NH	Leu 3	Side chain CH	Weak
Aib 5	NH	Apa 4	αCH_2	Strong
Apa 2	αCH_2	Apa 2	Ar-CH	Strong
Apa 4	αCH_2	Apa 4	Ar-CH	Strong

5.3.4.2. Peptide P5 NMR structure analysis, using 2D NMR (TOCSY and ROESY) and DMSO-d_6 titration.

In addtion, we synthesized a seven-residue peptide **P5** and studied its solution conformation using 2D-NMR. As peptide gave good ^{1}H spectrum in CD_3OH, we recorded the 2D-NMR (TOCSY and ROESY) in CD_3OH. The ROSEY analysis revealed crucial strong NOEs between Leu1NH↔Apa2NH, Leu3NH↔Apa4NH and Leu5NH↔Apa6NH, strong NOEs between NH(*i*+1)↔C$^{\alpha}$H(*i*), and medium NOEs between Apa4NH↔Leu3CβH and Apa6NH↔Leu5C$^{\beta}$H (Figure 18). All observed NOEs are tabulated in the Table 12. The temperature dependent NMR analysis suggested the downfield shift in the amide NH groups with increasing temperature. Based on the observed NOEs NMR solution structure was calculated using Insight II. The superimposed lowest energy conformers of peptide **P5** are shown in Figure 16.

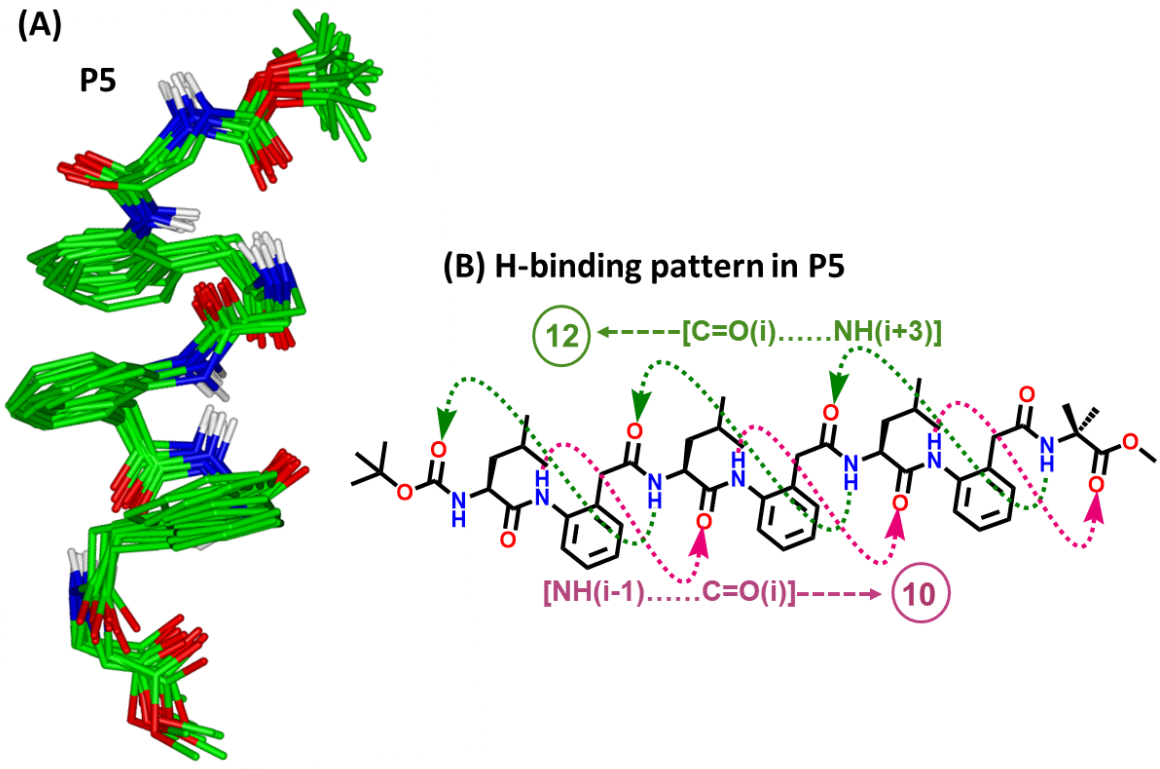


Figure 16. (A) Solution conformation of peptide **P5**. Peptide **P5** adopt 12/10 helical conformations in solution with alternate hydrogen bonding. (B) Schematic representation Intramolecular hydrogen bonding in the 12/10-helix of peptide **P5**.

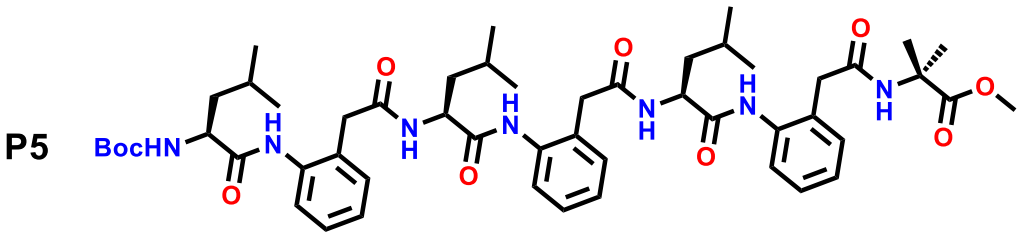
The peptide adopted a continuous 12/10-mixed helix conformation. Hofmann and colleagues, in their pioneering work, identified 12/10 as the second stable conformation of α,γ-hybrid

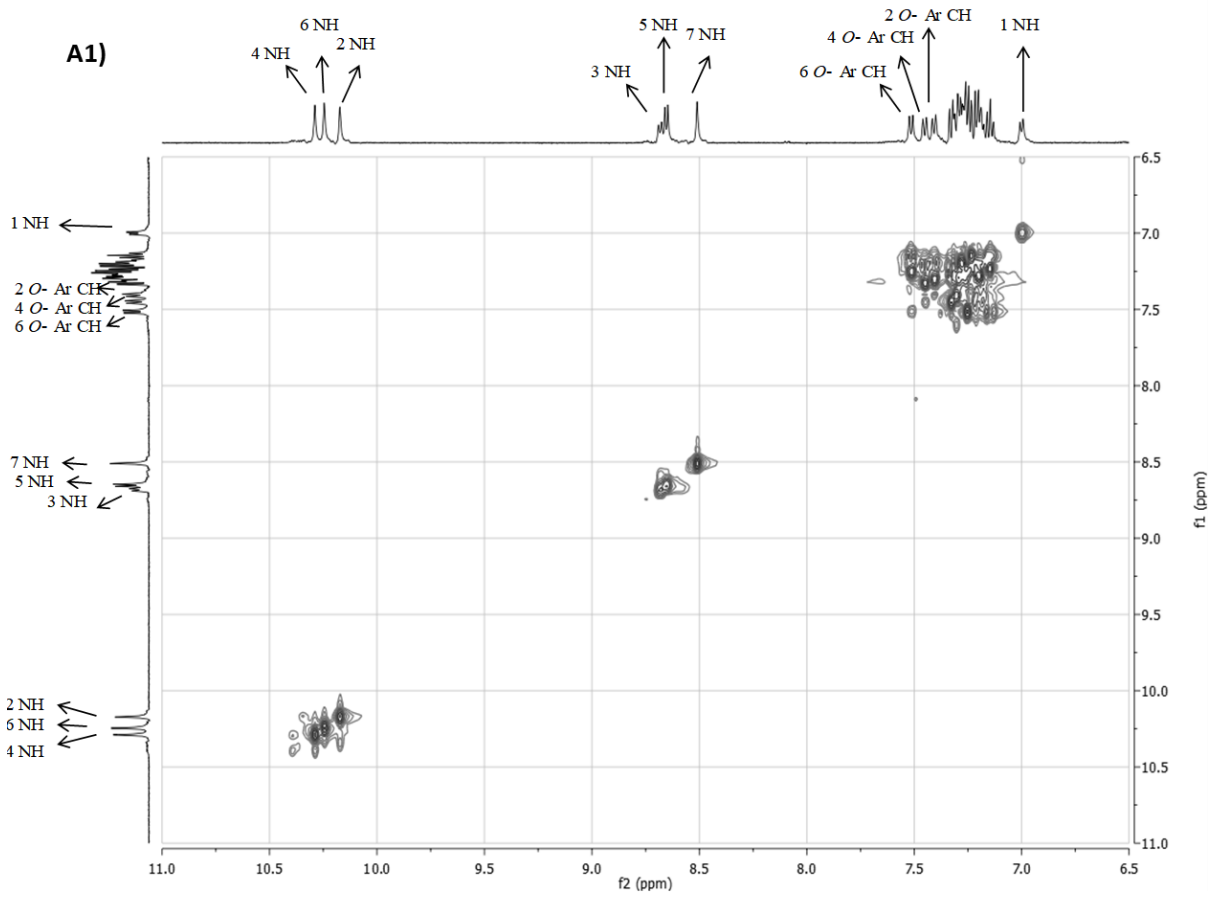
peptides.[8a] Recently, we demonstrated the stable 12/10-mixed helical conformations by incorporating α-residues and 4,4-dialkyl substituted γ-amino acids.[13b] These findings indicate that α,γ-hybrid peptides comprising sterically hindered α-amino acids and Apa result in a 12-helix conformation. In contrast, α,γ-hybrid peptides composed of common α-amino acids, such as Leu, along with Apa, exhibit a 12/10-helix conformation characterized with alternating H-bond directionality.

Upon structural comparison, it was observed that α,γ-hybrid peptides containing (*Z*)-β,γ-unsaturated γ-amino acids and those comprising Apa both adopt 12-helix conformations in the presence of sterically hindered Aib residues. As 12/10-helix conformation required the chiral amino acids, it difficult to introduce chiral amino acids in the α,γ-hybrid peptides consisting of (*Z*)-β,γ-unsaturated γ-amino acids because the strong base used for the double bond migration will also deprotonate the chiral amino acids. In addition, the 12/10-mixed helix conformation has also been observed in the hybrid peptides consisting of α-amino acids and Gpn (gabapentin) and also hybrid peptides consisting the γ-carbo amino acids. Overall, these studies suggested that α,γ-hybrid peptides with Apa as γ-amino acid can adopt either 12-helix with unidirectional H-bonds and 12/10-helix with alternating H-bond directionality.

A) Partial TOCSY spectrum analysis of peptide P5 in CD_3OH

Below partial TOCSY spectrum showing the amino acid residues in peptide **P5**




A1)
6 NH
4 NH
2 NH
5 NH
7 NH
3 NH
2 O- Ar CH
4 O- Ar CH
6 O- Ar CH
1 NH
1 NH
2 O- Ar CH
4 O- Ar CH
6 O- Ar CH
7 NH
5 NH
3 NH
2 NH
6 NH
4 NH
f2 (ppm)
f1 (ppm)

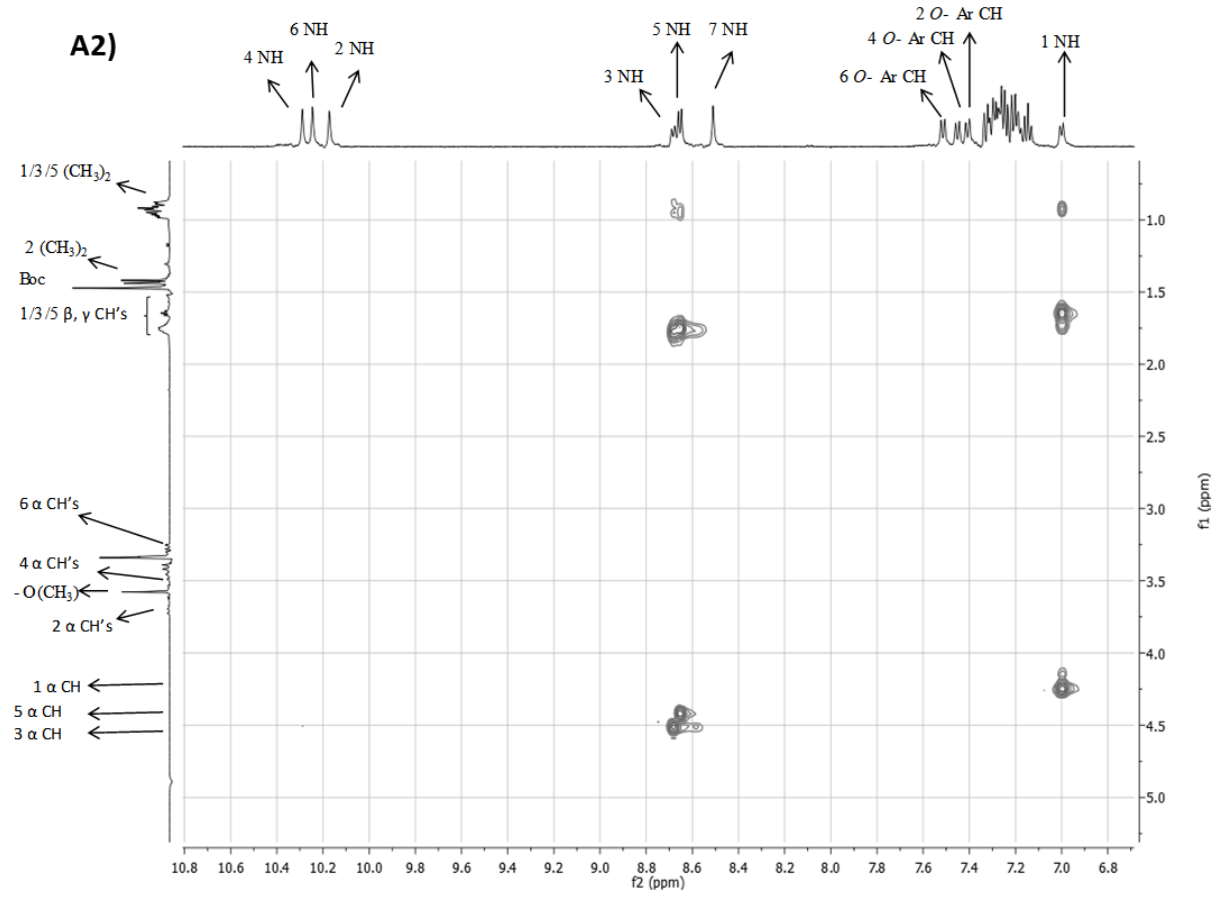
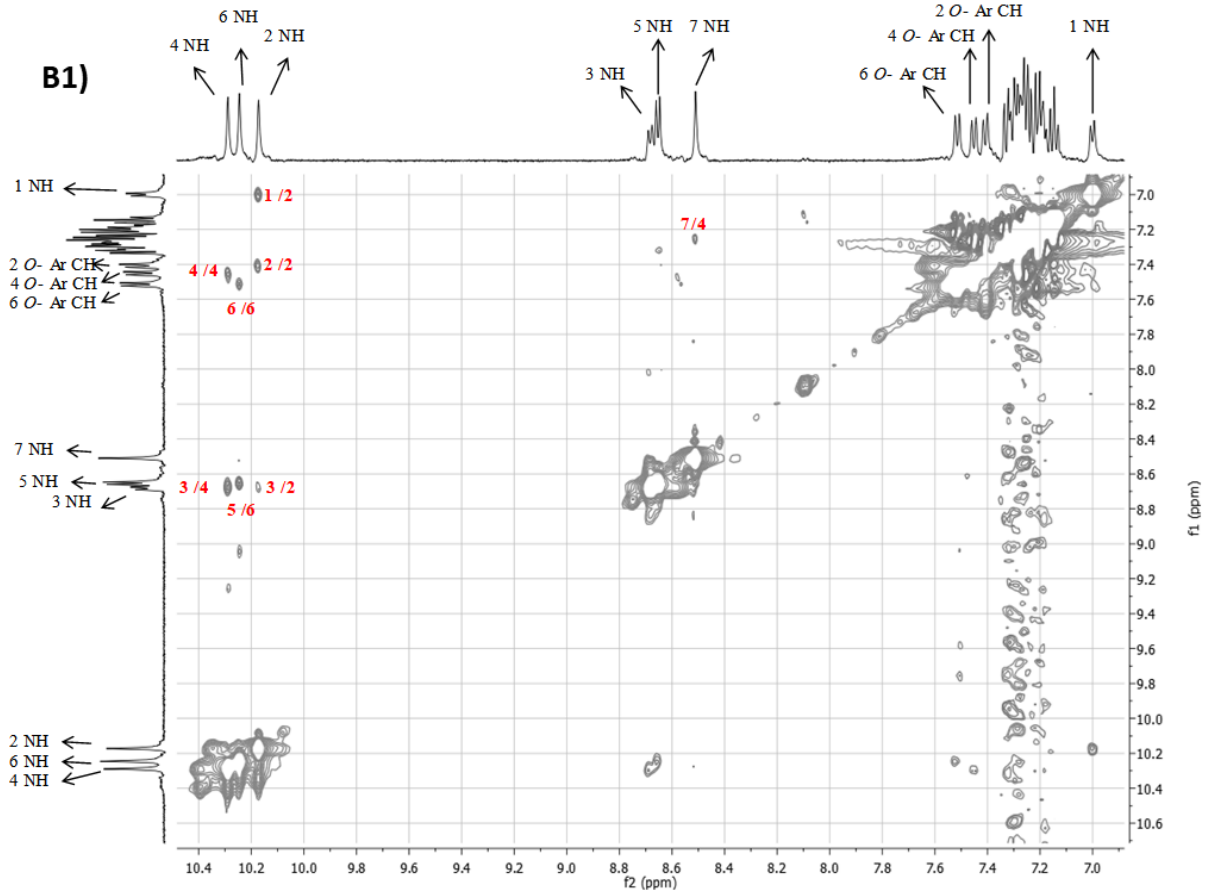

A2)
6 NH
4 NH
2 NH
5 NH
7 NH
3 NH
2 O- Ar CH
4 O- Ar CH
6 O- Ar CH
1 NH
1/3/5 (CH3)2
2 (CH3)2
Boc
1/3/5 β, γ CH's
6 α CH's
4 α CH's
-O(CH3)
2 α CH's
1 α CH
5 α CH
3 α CH
f2 (ppm)
f1 (ppm)

Figure 17: (A1) and (A2) are partial TOCSY spectra of peptide **P5** in CD_3OH. The TOCSY spectrum was used to identify amino acids in the peptide sequence. The sequential assignments of amino acids were performed using ROESY.

B) Partial ROESY spectrum analysis of Peptide P5 in CD_3OH



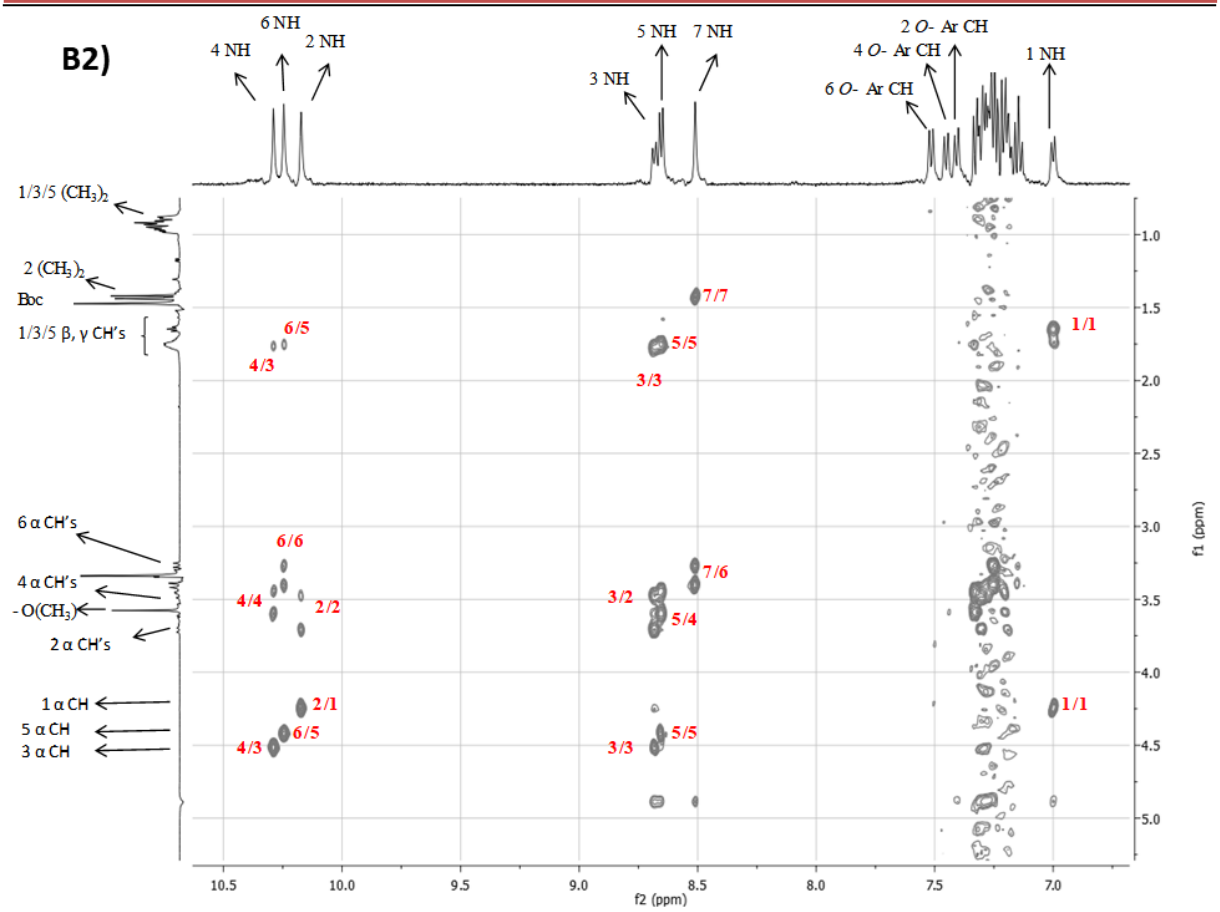


Figure 18: Partial ROESY spectrum of **P5** showing sequential NOEs of (B1) NH↔NH, (B2) NH↔$C_{\alpha}H$ and NH↔side-chain.

C) Variable Temperature NMR study of peptide P5

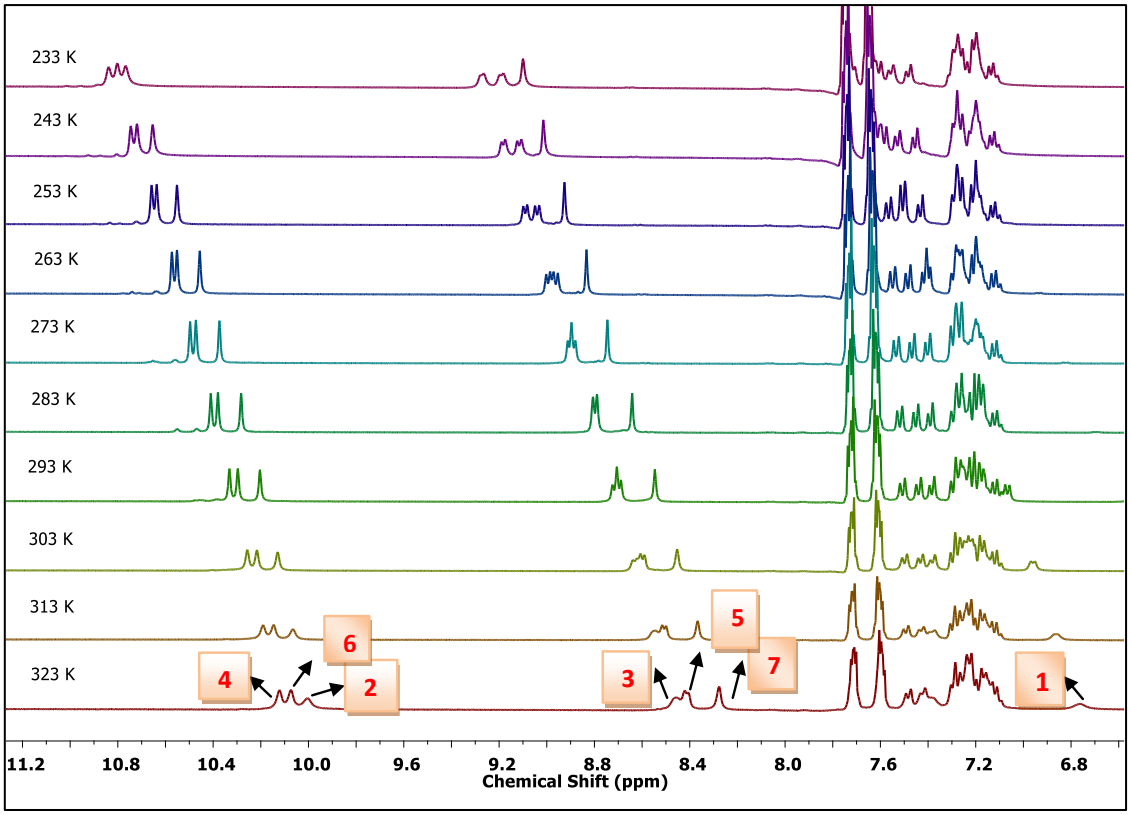


Figure 19: Temperature dependent ^{1}H NMR spectra of amide NH region of peptide **P5**.

Table 11: Chemical shift (in ppm) of amide NHs of peptide **P5**.

Temp (K)	1 NH	2 NH	3 NH	4 NH	5 NH	6 NH	7 NH
233	7.72	10.77	9.27	10.84	9.19	10.8	9.10
243	7.61	10.65	9.18	10.75	9.12	10.72	9.01
253	7.51	10.55	9.09	10.66	9.04	10.64	8.93
263	7.40	10.46	9.00	10.57	8.96	10.55	8.83
273	7.3	10.37	8.91	10.50	8.99	10.47	8.75
283	7.2	10.28	8.80	10.41	8.80	10.38	8.64
293	7.07	10.20	8.72	10.33	8.70	10.30	8.55
303	6.96	10.13	8.63	10.26	8.60	10.22	8.45
313	6.87	10.07	8.54	10.19	8.51	10.15	8.37
323	6.76	10.00	8.46	10.12	8.42	10.07	8.28
dδ/dT (ppb K^{-1})	**-0.01**	**-0.008**	**-0.009**	**-0.008**	**-0.009**	**-0.008**	**-0.009**
$^{3}J_{NH\text{-}C^{\alpha}H}$ (Hz) (30 °C)	**6.8**	**-**	**7.2**	**-**	**6.4**	**-**	**-**

Table 12: List of NOEs used for MD calculation for peptide **P5**.

Residue	H-atom	Residue	H-atom	NOE observed

Leu (1)	NH	Apa (2)	NH	Strong
Leu (1)	NH	Leu (1)	β, γ CH	Strong
Leu (1)	NH	Leu (1)	α CH	Strong
Apa (2)	NH	Apa (2)	Ortho-Ar CH	Strong
Apa (2)	NH	Leu (1)	α CH	Strong
Apa (2)	NH	Apa (2)	α CH	Strong
Leu (3)	NH	Apa (2)	α CH	Strong
Leu (3)	NH	Leu (3)	β, γ CH	Strong
Leu (3)	NH	Leu (3)	α CH	Strong
Leu (3)	NH	Apa (4)	NH	Strong
Leu (3)	NH	Apa (2)	NH	Medium
Apa (4)	NH	Apa (4)	α CH	Strong
Apa (4)	NH	Apa (4)	Ortho-Ar CH	Strong
Apa (4)	NH	Leu (3)	β CH	Medium
Apa (4)	NH	Leu (3)	α CH	Strong
Leu (5)	NH	Apa (4)	α CH	Strong
Leu (5)	NH	Leu (5)	β, γ CH	Strong
Leu (5)	NH	Leu (5)	α CH	Strong
Leu (5)	NH	Apa (6)	NH	Strong
Apa (6)	NH	Apa (6)	α CH	Strong
Apa (6)	NH	Apa (6)	Ortho-Ar CH	Strong
Apa (6)	NH	Leu (5)	β CH	Medium
Apa (6)	NH	Leu (5)	α CH	Strong
Aib (7)	NH	Apa (6)	α CH	Strong
Aib (7)	NH	Apa (4)	Ar CH	Medium
Aib (7)	NH	Aib (7)	$(CH_3)_2$	Strong

5.4. Conclusion

We have demonstrated the synthesis and conformations of α,γ-hybrid peptides composed of 2-aminophenyl acetic acid. The tetrapeptide consisting of 1:1 alternating Aib and Apa adopted a 12-helix conformation. When Aib residues are substituted with Leu, the resulting peptide exhibits a 12/10-helix conformation. In contrast, sterically constrained alpha amino acid is not

required to design 12-helix structures if the γ-amino acids consists of proteinogenic amino acid side-chains. The comparison of crystal structure and solution structure of penta and hexapeptide revealed that it is possible to construct the continuous 12/10-helix conformations. This type of helical peptides with alternating H-bond directionality is uncommon in proteins. In comparison, the torsion angles observed in α,γ-hybrid peptides reported here are consist with the previously reported 12/10-helices. In contrast to the acid labile α,γ-hybrid peptides consisting of (*Z*)-β,γ-unsaturated γ-amino acids, the α,γ-hybrid peptides reported here yield a stable 12- and 12/10-helical conformations. Furthermore, the aromatic amino acid backbone in peptides provides a versatile platform for introducing diverse functionalities onto the peptide backbone.

5.5. Experimental details

5.5.1. General Information: All amino acids and reagents, including Di-tert-butyl dicarbonate, *o*-Nitrophenylacetic acid, Pd-C, $SOCl_2$, TFA, HOBt, HATU, DIPEA, THF, DMF, Ethyl acetate, petroleum ether, ethanol, methanol, sodium hydroxide (NaOH), were procured from commercial sources. Pet-ether and Ethyl acetate were distilled earlier to use. Silica gel (120-200 mesh) was employed for column chromatography. The ultimate purification of peptides was carried out using reverse-phase HPLC with a C18 column and a gradient of MeOH/H2O (60:40-95:5), operating at a flow rate of 3.00 mL/min. ^{1}H spectra were captured at 500 MHz (or ^{13}C at 125 MHz) and 400 MHz (or ^{13}C at 100 MHz) utilizing residual solvents as internal standards ($CDCl_3$: δ_H 7.26 *ppm*, δ_C 77.3 *ppm*; CD_3OH : δ_H 3.31 *ppm*, δ_C 49.0 *ppm*). Chemical shifts (δ) and coupling constants were expressed in ppm and Hz, respectively. ^{1}H NMR and ^{13}C NMR spectra were recorded at 400 MHz and 100 MHz, respectively, with deuterated chloroform ($CDCl_3$) serving as the internal standard. Chemical shifts (δ) and coupling constants were reported in ppm and Hz, respectively. The mass verification of all pure peptides was conducted using a Matrix Assisted LASER Desorption Ionization mass spectrometer (MALDI-TOF/TOF). Single crystal XRD data for peptide structure determination were collected from an X-ray diffractometer utilizing Mo-Kα (λ = 0.71073 Å) graphite monochromated radiation.

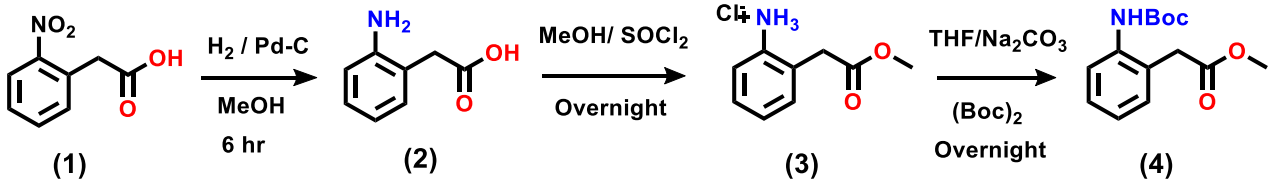
NMR spectroscopy: NMR investigations were performed on Bruker AVANCE^{III}-400 and 500 MHz spectrometers. Resonance assignments were acquired through TOCSY and ROESY analyses. Phase-sensitive mode was employed for collecting all two-dimensional data, utilizing the time-proportional phase incrementation (TPPI) method. The t_2 and t_1 dimensions utilized

sets of 1024 and 512 data points, respectively. For TOCSY analysis, 32 transients were collected, while 72 transients were acquired for ROESY analysis. A spectral width of 6007 Hz was employed in both dimensions. ROESY spectra were obtained with a spin-lock time of 256 ms. Zero-filling was implemented, resulting in a final dataset of 2 K × 1 K. Prior to processing, a shifted square-sine-bell window was applied.

Molecular Dynamics (MD): The NMR model building and molecular dynamics simulation for **P3**, **P4**, and **P5** were conducted following the established protocol as reported.[27]

5.5.2. Procedure for the synthesis of 2-aminophenyl acetic acid

A solution of o-Nitrophenylacetic acid (**1**) (1.81 g, 10 mmol) in 20 mL of MeOH, treated under a nitrogen atmosphere with 10% w/w Pd-C and then hydrogen gas was supplied through a balloon. The mixture was stirred for 6 hours, followed by filtration to remove the catalyst. The resulting solution was evaporated to dryness under reduced pressure, yielding o-Aminephenylacetic acid (**2**). Compound **2** was then dissolved in dry MeOH (100 mL) and treated with $SOCl_2$ (3 eq.). The reaction mixture was stirred overnight at room temperature, and upon completion, methanol was evaporated under reduced pressure to obtain 2-amino-methyl phenyl acetate (**3**).

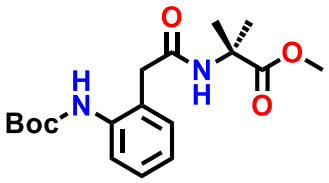


5.5.3. Synthesis of hybrid peptides containing 2-aminophenyl acetic acid

5.5.3.1. Boc-Apa-Aib-OMe (5a): To a solution of Boc-Apa-COOH (5 mmol) and HCl.NH_2-Aib-OMe (6.5 mmol, 1.3 eq) in 5 mL of DMF, HBTU (5 mmol), HOBt (5 mmol), and DIPEA (10 mmol) were added at 0 °C. The reaction was then stirred at room temperature for approximately 12 hours, with the progress monitored by TLC. Upon completion, EtOAc (150 mL) was introduced to the reaction mixture. The organic layer underwent sequential washing with 0.5 N HCl (3×50 mL), 10% Na_2CO_3 (3×50 mL), and brine solution (1×80 mL). Following this, the organic layer was dried over anhydrous Na_2SO_4, concentrated under reduced pressure, and the crude mixture was purified by column chromatography to yield pure peptide **5a** (90%).

White solid, Yield 90%; ^{1}H NMR (400 MHz, $CDCl_3$) δ 7.97 (s, 1H), 7.73 (d, J = 8 Hz, 1H), 7.29-7.04 (m, 4H), 6.37 (s, 1H), 3.70 (s, 3H), 3.49 (s, 2H), 1.52 (s, 9H), 1.50 (s, 6H);^{13}C NMR

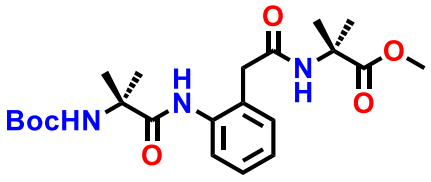
(100 MHz, $CDCl_3$) δ 175.1, 170.9, 154.2, 137.4, 130.4, 128.3, 127.2, 124.6, 124.3, 80.4, 56.9, 52.9, 41.4, 28.5, 24.7; HR-MS *m/z* calculated for $C_{18}H_{26}N_2O_5$ is 350.1842 and observed 350.1833.



5a

5.5.3.2. Boc-Aib-Apa-Aib-OMe (P1): The solution of Boc-Apa-Aib-OMe, **5a** (3.6 mmol, 1.2 eq), in 3 mL of DCM was cooled to 0 °C in an ice bath, and neat 5 mL of TFA was then added. After the reaction was complete (~30 minutes), the solvent was evaporated under reduced pressure. The resulting residue was diluted with water, and solid Na_2CO_3 was introduced at 0 °C until the solution reached a pH of approximately 10. The aqueous layer was subjected to extraction with EtOAc (3 × 50 mL). The combined organic layer was washed with 50 mL of brine solution, dried over anhydrous Na_2SO_4, and concentrated under reduced pressure to approximately 2 mL.

Coupling strategy: Boc-Aib-OH (3 mmol) was dissolved in 5 mL of dry DCM and cooled in an ice salt bath. DIPEA (6 mmol) and IBCF[26] (3 mmol) were introduced into the reaction mixture under a nitrogen atmosphere. After stirring for approximately 10 minutes, a pre-cooled solution of NH_2-Apa-Aib-OMe (2 mL) was added, and the reaction mixture was stirred overnight at room temperature. Subsequently, 100 mL of DCM was added to the reaction mixture, followed by successive washings with 5% HCl (3 × 40 mL), 10% $NaHCO_3$ (3 × 40 mL), and brine (2 × 40 mL). The combined organic layer was dried over anhydrous sodium sulfate and evaporated under vacuum. The crude product was purified by column chromatography to obtain pure peptide **P1** (52%).



P1

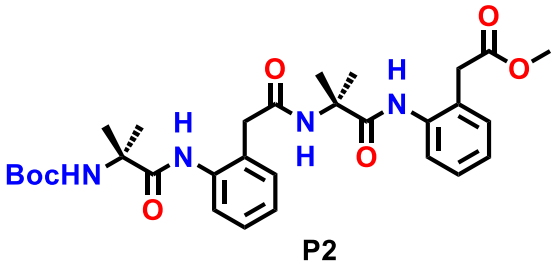
White solid, Yield 52%; ^{1}H NMR (400 MHz, $CDCl_3$) δ 9.58 (s, 1H), 7.69 (s, 1H), 7.29-7.09 (m, 3H), 6.66 (s, 1H), 5.28 (s, 1H), 3.68 (s, 1H), 3.46 (s, 1H), 1.61 (s, 6H), 1.51 (s, 6H), 1.44 (s, 9H); ^{13}C NMR (100 MHz, $CDCl_3$) δ 175.2, 174.1, 171.1, 154.8, 136.8, 130.4, 128.2, 125.6, 57.2, 56.9, 52.8, 41.0, 28.5, 25.7, 24.7; HR-MS *m/z* calculated for $C_{22}H_{33}N_3O_6$ is 435.2369, observed 435.2357.

5.5.3.3. Boc-Aib-Apa-Aib-Apa-OMe (P2): The Boc-Aib-Apa-Aib-OMe, **P1** (1.5 mmol), was dissolved in 15 mL methanol, and 1N NaOH was slowly added. The reaction mixture was stirred for approximately 4 hours, with the progress monitored by TLC. Upon completion, methanol was evaporated under reduced pressure. The resulting residue was then diluted with water (60 mL), acidified (pH ~ 4) with 0.5 N HCl, and the compound was extracted with EtOAc (3 × 60 mL). The combined organic layer was washed with a 50 mL brine solution, dried over anhydrous Na_2SO_4, and concentrated under reduced pressure to obtain the free carboxylic acid (95%). The carboxylic acids were directly utilized for peptide synthesis without further purification.

The solution of Boc-Apa-OMe, **4** (2 mmol), in 2 mL of DCM was cooled to 0 °C in an ice bath, and neat 2 mL of TFA was then added. After the reaction was complete (~30 minutes), the solvent was evaporated under reduced pressure. The resulting residue was diluted with water, and solid Na_2CO_3 was introduced at 0 °C until the solution reached a pH of approximately 10. The aqueous layer was subjected to extraction with EtOAc (3 × 50 mL). The combined organic layer was washed with 50 mL of brine solution, dried over anhydrous Na_2SO_4, and concentrated under reduced pressure to approximately 2 mL.

Coupling strategy: Dissolved Boc-Aib-Apa-Aib-COOH (1.43 mmol) in 5 mL of dry DCM and cooled it in an ice salt bath, DIPEA (3 mmol) and IBCF (1.43 mmol) were introduced to the reaction mixture under a nitrogen atmosphere. After stirring for approximately 10 minutes, a pre-cooled solution of TFA.NH_2-Apa-OMe (2 mL) was added. The pH of the solution was further adjusted to ~8 using DIPEA, and the reaction mixture was stirred overnight at room temperature. Following the completion of the reaction, 100 mL of DCM was added to the reaction mixture, and it was successively washed with 5% HCl (3 × 40 mL), 10% $NaHCO_3$ (3 × 40 mL), and brine (2 × 40 mL). The combined organic layer was dried over anhydrous sodium sulfate and evaporated under vacuum. The crude product underwent purification by column chromatography to yield pure peptide **P2** (55%).

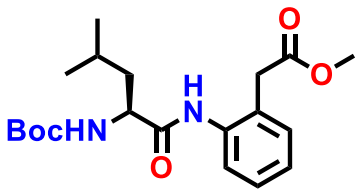
White solid, Yield 55%; ^{1}H NMR (400 MHz, $CDCl_3$) δ 9.53 (bs, 1H), 9.24 (s, 1H), 7.64 (bd, J = 4 Hz, 1H), 7.14-7.02 (m, 8H), 5.30 (s, 1H), 3.66 (s, 3H), 3.50 (s, 2H), 3.42 (s, 2H), 1.63 (s, 6H), 1.56 (s, 6H), 1.42 (s, 9H); ^{13}C NMR (100 MHz, $CDCl_3$) δ 174.3, 173.4, 173.0, 154.8, 136.4, 130.6, 128.2, 128.1, 128.0, 125.4, 125.1, 79.9, 57.7, 56.9, 52.5, 40.8, 38.0, 28.3, 25.5, 25.0; HR-MS *m/z* calculated for $C_{30}H_{40}N_4O_7$ is 568.2897, observed 568.2899.



P2

5.5.3.4. Boc-Leu-Apa-OMe (**6a**): To a solution of Boc-Leu-COOH (5 mmol) and HCl.NH_2-Apa-OMe (6 mmol) in 3 mL of DMF, HBTU (5 mmol), HOBt (5 mmol), and DIPEA (10 mmol) were added at 0 °C. The reaction was stirred at room temperature for approximately 12 hours, and the progress of the reaction was monitored by TLC. Upon completion, EtOAc (150 mL) was introduced to the reaction mixture. The organic layer was subsequently washed with 0.5 N HCl (3×50 mL), 10% Na_2CO_3 (3×50 mL), and brine solution (1×80 mL). After drying over anhydrous Na_2SO_4 and concentrating under reduced pressure, the crude mixture underwent column chromatography to obtain pure peptide **6a** (92%).

White solid, Yield 92%; ^{1}H NMR (400 MHz, $CDCl_3$) δ 9.12 (s, 1H), 7.80 (d, J = 8 Hz, 1H), 7.32-7.09 (m, 3H), 4.99 (d, J = 8 Hz, 1H), 4.28 (m, 1H), 3.73 (s, 3H), 3.63 (s, 2H), 1.79 (m, 2H), 1.61 (m, 1H), 1.45 (s, 9H), 0.99 (m, 6H);^{13}C NMR (100 MHz, $CDCl_3$) δ 172.9, 171.4, 155.8, 136.3, 130.9, 128.5, 125.6, 125.0, 80.2, 54.2, 52.7, 41.6, 38.5, 28.4, 25.1, 23.1, 22.1; HR-MS *m/z* calculated for $C_{20}H_{30}N_2O_5$ is 378.2155, observed 378.2148.



6a

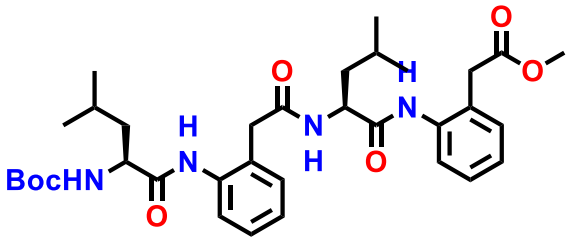
5.5.3.5. Boc-Leu-Apa-Leu-Apa-OMe (6b): The Boc-Leu-Apa-OMe, **6a** (2 mmol), was dissolved in 15 mL of methanol, followed by the slow addition of 1N NaOH. The reaction mixture was stirred for approximately 4 hours, and the progress of the reaction was monitored

by TLC. Upon completion, methanol was evaporated under reduced pressure. The resulting residue was diluted with water (60 mL), acidified (pH ~ 4) with 0.5 N HCl, and the compound was extracted with EtOAc (3 × 60 mL). The combined organic layer was washed with a 50 mL brine solution, dried over anhydrous Na_2SO_4, and concentrated under reduced pressure to obtain free carboxylic acid (2 mmol). The carboxylic acids were directly utilized for peptide synthesis without further purification.

The solution of Boc-Leu-Apa-OMe, **6a** (2.4 mmol), in 3 mL of DCM was cooled to 0 °C in an ice bath, and neat 5 mL of TFA was then added. After the reaction was complete (~30 minutes), the solvent was evaporated under reduced pressure. The resulting residue was diluted with water, and solid Na_2CO_3 was introduced at 0 °C until the solution reached a pH of approximately 10. The aqueous layer was subjected to extraction with EtOAc (3 × 50 mL). The combined organic layer was washed with 50 mL of brine solution, dried over anhydrous Na_2SO_4, and concentrated under reduced pressure to approximately 2 mL.

Coupling strategy: To a solution of Boc-Leu-Apa-COOH (2 mmol) and NH2-Leu-Apa-OMe (2 mL) in 3 mL of DMF, HBTU (2 mmol), HOBt (2 mmol), and DIPEA (4 mmol) were added at 0 °C. The reaction was then stirred at room temperature for about 12 hours, with the progress monitored by TLC. After completion of the reaction, EtOAc (150 mL) was introduced to the reaction mixture. The organic layer was subsequently washed with 0.5 N HCl (3×50 mL), 10% Na_2CO_3 (3×50 mL), and brine solution (1×80 mL), respectively. After drying over anhydrous Na_2SO_4 and concentrating under reduced pressure, the crude mixture underwent column chromatography to obtain pure peptide **6b** (75%).

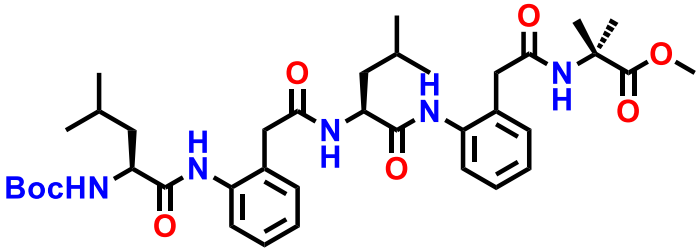
White solid, Yield 75%; ^{1}H NMR (400 MHz, $CDCl_3$) δ 9.45 (s, 1H), 9.06 (s, 1H), 8.01 (d, J = 4 Hz, 1H), 7.68 (d, J = 8 Hz, 1H), 7.31-7.08 (m, 7H), 5.18 (d, J = 8 Hz, 1H), 4.58 (m, 1H), 4.43 (m, 1H), 3.68 (s, 3H), 3.65-3.33 (m, 4H), 1.88-1.71 (m, 6H), 1.46 (s, 9H), 0.98 (m, 12H); 13C NMR (100 MHz, $CDCl_3$) δ 172.8, 172.7, 172.4, 172.3, 156.6, 136.5, 131.6, 130.5, 128.5, 128.1, 127.8, 127.1, 125.7, 125.2, 80.4, 53.6, 41.1, 29.8, 28.5, 26.6, 25.2, 25.0, 23.3, 22.9, 22.2, 21.5; HR-MS *m/z* calculated for $C_{34}H_{48}N_4O_7$ is 624.3523, observed 624.3518.



6b

5.5.3.6. Boc-Leu-Apa-Leu-Apa-Aib-OMe (**P3**): To the solution of Boc-Leu-Apa-Leu-Apa-COOH (1.5 mmol) and HCl.NH_2-Aib-OMe (2 mmol) in 3 mL of DMF, HBTU (1.5 mmol), HOBt (1.5 mmol), and DIPEA (3 mmol) were added at 0 °C. The reaction was stirred at room temperature for about 12 hours, with the progress monitored by TLC. After completion of the reaction, EtOAc (150 mL) was introduced to the reaction mixture. The organic layer was subsequently washed with 0.5 N HCl (3×50 mL), 10% Na_2CO_3 (3×50 mL), and brine solution (1×80 mL), respectively. After drying over anhydrous Na_2SO_4 and concentrating under reduced pressure, the crude mixture underwent column chromatography to obtain pure peptide **P3** (83%).

White solid, Yield 83%; ^{1}H NMR (400 MHz, $CDCl_3$) δ 9.67 (s, 1H), 9.17 (s, 1H), 8.49 (d, J = 4 Hz, 1H), 7.93 (s, 1H), 7.22 (m, 8H), 5.08 (d, J = 8 Hz, 1H), 4.60 (m, 1H), 4.39 (m, 1H), 3.69 (s, 3H), 3.64-3.10 (m, 4H), 1.89 (m, 3H), 1.70 (m, 3H), 1.56 (s, 3H), 1.44 (s, 12H), 0.94 (m, 12H); ^{13}C NMR (100 MHz, $CDCl_3$) δ 176.1, 173.4, 172.9, 172.4, 171.6, 156.7, 135.9, 132.2, 131.6, 131.2, 128.3, 127.8, 127.7, 127.2, 127.0, 126.8, 80.2, 56.6, 53.5, 53.3, 52.7, 40.9, 40.5, 29.7, 28.3, 25.7, 24.9, 24.8, 24.0, 23.4, 22.9, 21.8, 21.0; HR-MS *m/z* calculated for $C_{38}H_{55}N_5O_8$ is 709.4051, observed 709.4042.

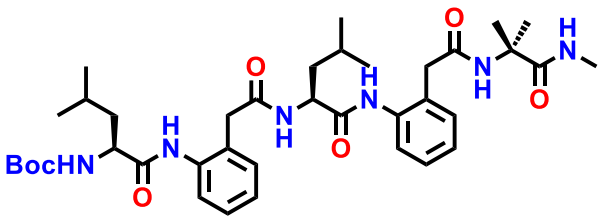


P3

5.5.3.7. Boc-Leu-Apa-Leu-Apa-Aib-NHMe (**P4**): Boc-Leu-Apa-Leu-Apa-Aib-OMe (**P3**) (0.05 g, 0.064 mmol) was dissolved in 50 mL of MeOH, and the solution was bubbled with methylamine gas in cold conditions until a volume increase of 5 mL was observed. The flask was then stored under a nitrogen atmosphere for one day at room temperature. Upon completion of the reaction, methanol was evaporated, and the product was diluted with EtOAc

(50 mL). The organic layer underwent washing with 5% HCl (3 × 25 mL) and brine solution (1 × 25 mL). Subsequently, the organic layer was dried over anhydrous Na_2SO_4 and concentrated under reduced pressure. The crude product was purified through RP-HPLC on a C18 column using a methanol/water gradient system to obtain pure compound **P4** (90%).

White solid, Yield 90%; ^{1}H NMR (400 MHz, $CDCl_3$) δ 9.61 (d, J = 4 Hz, 2H), 8.34 (d, J = 8 Hz, 1H), 7.70 (s, 1H), 7.33-7.16 (m, 8H), 6.16 (bs, 1H), 5.05 (d, J = 8 Hz, 1H), 4.66 (m, 1H), 4.37 (m, 1H), 3.69-3.03 (m, 4H), 2.71 (d, J = 4 Hz, 3H), 1.95-1.65 (m, 6H), 1.57 (s, 3H), 1.45 (s, 9H), 1.41 (s, 3H), 1.00-0.86 (m, 12H); 13C NMR (100 MHz, $CDCl_3$) δ 175.6, 173.3, 173.1, 172.3, 171.3, 156.6, 135.9, 135.7, 131.9, 131.5, 131.0, 127.8, 127.6, 127.0, 126.6, 80.1; 57.0, 53.8, 53.5, 40.7, 40.3, 28.3, 26.6, 26.3, 24.9, 24.7, 24.2, 23.3, 22.8, 21.7, 21.1; HR-MS *m/z* calculated for $C_{38}H_{56}N_6O_7$ is 708.4210, observed 708.4207.



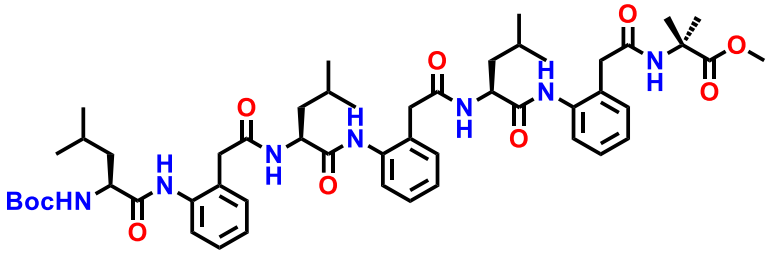
P4

5.5.3.8. Boc-Leu-Apa-Leu-Apa-Leu-Apa-Aib-OMe (P5): The Boc-Leu-Apa-OMe, **6a** (0.5 mmol), was dissolved in 15 mL methanol, followed by the slow addition of 1N NaOH. The reaction mixture was stirred for about 4 hours, with the progress monitored by TLC. After completion of the reaction, methanol was evaporated under reduced pressure. The resulting residue was diluted with water (60 mL), acidified (pH~ 4) with 0.5 N HCl, and the compound was extracted with EtOAc (3×60 mL). The combined organic layer was washed with 50 mL brine solution, dried over anhydrous Na_2SO_4, and concentrated under reduced pressure to obtain free carboxylic acid. The carboxylic acids were directly utilized for peptide synthesis without further purification.

The solution of Boc-Leu-Apa-Leu-Apa-Aib-OMe, **P3** (0.6 mmol, 1.2 eq), in 3 mL of DCM was cooled to 0 °C in an ice bath, followed by the addition of neat 5 mL of TFA. After the reaction was complete (~30 minutes), the solvent was evaporated under reduced pressure. The resulting residue was diluted with water, and solid Na_2CO_3 was introduced at 0 °C until the pH of the solution reached ~10. The aqueous layer was extracted with EtOAc (3×50 mL). The combined organic layer was washed with 50 mL of brine solution, dried over anhydrous Na_2SO_4, and concentrated under reduced pressure to approximately 2 mL.

Coupling strategy: To a solution of Boc-Leu-Apa-COOH (0.5 mmol) and NH_2-Leu-Apa-Leu-Apa-Aib-OMe (2 mL) in 3 mL of DMF, HBTU (0.5 mmol), HOBt (0.5 mmol), and DIPEA (1 mmol) were added at 0 °C. The reaction was stirred at room temperature for about 12 hours, with the progress monitored by TLC. After completion of the reaction, EtOAc (150 mL) was introduced to the reaction mixture. The organic layer was subsequently washed with 0.5 N HCl (3 × 50 mL), 10% Na_2CO_3 (3×50 mL), and brine solution (1×80 mL), respectively. The organic layer was dried over anhydrous Na_2SO_4 and concentrated under reduced pressure. The crude mixture underwent purification through HPLC to obtain pure peptide **P5** (65%).

White solid, Yield 65%; ^{1}H NMR (400 MHz, CD_3OH) δ 10.26 (s, 1H), 10.22 (s, 1H), 10.14 (s, 1H), 8.66 (d, *J* = 4Hz, 1H), 8.63 (d, *J* = 4 Hz, 1H), 8.48 (s, 1H), 7.49 (d, *J* = 4 Hz, 1H), 7.42 (d, *J* = 8 Hz, 1H), 7.38 (d, *J* = 8 Hz, 1H), 7.31-7.10 (m, 12H), 6.97 (d, *J* = 8 Hz, 1H), 4.23 (m, 1H), 4.41 (m, 1H), 4.50 (m, 1H), 3.69 (m, 1H), 3.55 (s, 3H), 3.46-3.22 (m, 5H), 1.73-1.60 (m, 10H), 1.44 (s, 9H), 1.41 (s, 3H), 1.39 (s, 3H), 0.96-0.85 (m, 24H); HR-MS *m/z* calculated value for $C_{52}H_{73}N_7O_{10}$ is 955.5419, observed 955.5420.



P5

5.6. References

CCDC numbers 2310842 (for **P1**), 2310843 (for **P2**), and 2310844 (for **P3**).

1. (a) S. H. Gellman, *Acc. Chem. Res*. **1998**, *31*, 173-180; (b) J. Venkatraman, S. C. Shankaramma, P. Balaram, *Chem. Rev*. **2001**, *101*, 3131-3152; (c) D. Seebach, A. K. Beck, D. J. Bierbaum, *Chem. Biodiversity*, **2004**, *1*,1111-1239; (d) R. P. Cheng, S. H. Gellman, W. F. De Grado, *Chem. Rev*. **2001**, *101*, 3219-3232; (e) D. J. Hill, M. J. Mio, R. B. Prince, T. S. Hughes, J. S. Moore, *Chem. Rev.* **2001**, *101*, 3893–4012; (f) F. Fülöp, T. A. Martinek, G. K. Tóth, *Chem. Soc. Rev*. **2006**, *35*, 323-334; (g) S. Hecht, I.Huc, *Foldamers: Structure, Properties and Applications*, Wiley-VCH, Weinheim, **2007**; (h) C. M. Goodman, S. Choi, S. Shandler, W. F. DeGrado, *Nat. Chem. Biol*. **2007**, *3*, 252-262; (i) W. S. Horne, S. H. Gellman, *Acc. Chem. Res*. **2008**, *41*, 1399-1408; (j) D. Seebach, J. Gardiner, *Acc. Chem. Res*. **2008**, *41*, 1366-1375.

2. (a) I. Saraogi, A. D. Hamilton, *Chem. Soc. Rev*. **2009**, *38*, 1726-1743; (b) P. G. Vasudev, S. Chatterjee, N. Shamala, P. Balaram, *Acc. Chem. Res*. **2009**, *42*, 1628-1639; (c) G. Guichard, I. Huc, *Chem. Commun*. **2011**, *47*, 5933-5941; (d) P. G. Vasudev, S. Chatterjee, N. Shamala, P. Balaram, *Chem. Rev*. **2011**, *111*, 657-687; (e) F. Bouillère, S. Thétiot-Laurent, C. Kouklovsky, V. Alezra, Amino Acids, **2011**, *41*, 687-707; (f) L. K. A. Pilsl, O. Reiser, Amino Acids, **2011**, *41*, 709-718; (g) C. Baldauf, H.-J. Hofmann, *Helv. Chim. Acta*, **2012**, *95*, 2348-2383; (h) T. A. Martinek, F. Fülöp, *Chem. Soc. Rev*. **2012**, *41*, 687-702; (i) S. H. Yoo, H. -S. Lee, *Acc. Chem. Res.* **2017**, *50*, 832–841.

3. (a) A. Hayen, M. A. Schmitt, F. N. Ngassa, K. A. Thomasson, S. H. Gellman, *Angew. Chem. Int. Ed*. **2004**, *43*, 505-510; *Angew. Chem*. **2004**, *116*, 511-516; (b) G. V. M. Sharma, P. Nagendar, P. Jayaprakash, P. R. Krishna, K. V. S. Ramakrishna, A. C. Kunwar, *Angew. Chem. Int. Ed*. **2005**, *44*, 5878-5882; *Angew. Chem*. **2005**, *117*, 6028-6032; (c) S. De Pol, C. Zorn, C. D. Klein, O. Zerbe, O. Reiser, *Angew. Chem. Int. Ed*. **2004**, *43*, 511-514; *Angew. Chem*. **2004**, *116*, 517-520; (d) M. A. Schmitt, S. H. Choi, I. A. Guzei, S. H. Gellman, *J. Am. Chem. Soc*. **2005**, *127*, 13130-13131; (e) G. Srinivasulu, S. K. Kumar, G. V. M. Sharma, A. C. Kunwar, *J. Org. Chem*. **2006**, *71*, 8395-8400; (f) G. Angelici, G. Luppi, B. Kaptein, Q. B. Broxtermann, H.-J. Hofmann, C. Tomasini, *Eur. J. Org. Chem*. **2007**,2713-2721; (g) C. Baldauf, R. Günthe, H.-J. Hofmann, *Biopolymers* **2006**, *84*, 408-413; (h) B. Jagadeesh, A. Prabakhar, G. D. Sharma, S. Chandrasekhar, M. S. Reddy, B. Jagannadh, *Chem. Commun*. **2007**, 371-373; (i) S. H. Choi, I. A. Guzei, S. H. Gellman, *J. Am. Chem. Soc*. **2007**, *129*, 13780-13781.

4. (a) P. G. Vasudev, K. Ananda, S. Chatterjee, S. Aravinda, N. Shamala, P. Balaram, *J. Am. Chem. Soc*. **2007**, *129*, 4039-4048; (b) S. Chatterjee, P. G. Vasudev, K. Ananda, S. Raghothama, N. Shamala, P. Balaram, *J. Org. Chem*. **2008**, *73*, 6595-6606; (c) S. Chatterjee, P. G. Vasudev, S. Ragothama, N. Shamala, P. Balaram, *Biopolymers* **2008**, *90*, 759-771; (d) S. H. Choi, I. A. Guzei, L. C. Spencer, S. H. Gellman, *J. Am. Chem. Soc*. **2008**, *130*, 6544-6550; (e) M. Lee, J. Shim, P. Kang, I. A. Guzei, S. H. Choi, *Angew. Chem. Int. Ed*. **2013**, *52*, 12564-12567; *Angew. Chem*. **2013**, *125*, 12796-12799; (f) B. Legrand, C. André, L. Moulat, E. Wenger, C. Didierjean, E. Aubert, M. C. Averlant-Petit, J. Martinez, M. Calmes, M. Amblard, *Angew. Chem. Int. Ed*. **2014**, *53*, 13131-13135; *Angew. Chem*. **2014**, *126*, 13347-13351; (g) D. Balamurugan, K. M. Muraleedharan, *Chem. Eur. J*. **2015**, *21*, 9332-9338; (h) N. A. Wani, S. Raghothama, U. P. Singh, R. Rai, *Chem. Eur. J*. **2017**, *23*, 8364–8370.

5. (a) L. Guo, A. M. Almeida, W. Zhang, A. G. Reidenbach, S. H. Choi, I. A. Guzei, S. H. Gellman, *J. Am. Chem. Soc*. **2010**, *132*, 7868-7869; (b) K. Basuroy, B. Dinesh, N. Shamala, P. Balaram, *Angew. Chem. Int. Ed*. **2012**, *51*, 8736-8739; *Angew*. *Chem*. **2012**, *124*, 8866-8869; (c) A. Bandyopadhyay, S. V. Jadhav, H. N. Gopi, *Chem. Commun*. **2012**, *48*, 7170-7172; (d) K. Basuroy, B. Dinesh, N. Shamala, P. Balaram, *Angew. Chem. Int. Ed*. **2013**, *52*, 3136-3139; *Angew. Chem*. **2013**, *125*, 3218-3221; (e) S. V. Jadhav, A. Bandyopadhyay, H. N. Gopi, *Org. Biomol. Chem*. **2013**, *11*, 509-514; (f) R. Sonti, B. Dinesh, K. Basuroy, S. Raghothama, N. Shamala, P. Balaram, *Org. Lett*. **2014**, *16*, 1656-1659; (g) R. Misra, A. Saseendran, G. George, K. Veeresh, K. M. P. Raja, S. Raghothama, H.-J. Hofmann, H. N. Gopi, *Chem. Eur. J*. **2017**, *23*, 3764-3772.

6. (a) W. S. Horne, M. D. Boersman, M. A. Windsor, S. H. Gellman, *Angew. Chem. Int. Ed*. **2008**, *47*, 2853-2856; *Angew. Chem*. **2008**, *120*, 2895-2898; (b) W. S. Horne, L. M. Johnson, T. J. Ketas, P. J. Klasse, M. Lu, J. P. Moore, S. H. Gellman, *Proc. Natl. Acad. Sci. USA* **2009**, *106*, 14751-14756.

7. (a) E. F. Lee, J. D. Sadowsky, B. J. Smith, P. E. Czabotar, K. J. Peterson-Kaufman, P. M. Colman, S. H. Gellman, W. D. Fairlie, *Angew. Chem. Int. Ed*. **2009**, *48*, 4318-4322; *Angew. Chem*. **2009**, *121*, 4382-4386; (b) H. S. Haase, K. J. Peterson-Kaufman, S. K. Lan Levengood, J. W. Checco, W. L. Murphy, S. H. Gellman, *J. Am. Chem. Soc*. **2012**, *134*, 7652-7655; (c) M. Werner, W. S. Horne, *Curr. Opin. Chem. Biol*. **2015**, *28*, 75-82.

8. (a) C. Baldauf, R. Günthe, H.-J. Hofmann, *J. Org. Chem*. **2006**, *71*, 1200-1208; (b) C. Baldauf, R. Günthe, H.-J. Hofmann, *Biopolymers*, **2006**, *84*, 408-413.

9. (a) S. Chatterjee, P. G. Vasudev, S. Raghothama, C. Ramakrishnan, N. Shamala, P. Balaram, *J. Am. Chem. Soc*. **2009**, *131*, 5956-5965; (b) L. Guo, Y. Chi, A. M. Almeida, I. A. Guzei, B. K. Parker, S. H. Gellman, *J. Am. Chem. Soc*. **2009**, *131*, 16018-16020; (c) A. Bandyopadhyay, S. V. Jadhav, H. N. Gopi, *Chem. Commun*. **2012**, *48*, 7170-7172; (d) S. V. Jadhav, A. Bandyopadhyay, H. N. Gopi, *Org. Biomol. Chem*. **2013**, *11*, 509-514; (e) G. V. M. Sharma, N. Chandramouli, M. Choudhary, P. Nagendar, K. V. S. Ramakrishna, A. C. Kunwar, P. Schramm, H.-J. Hofmann, *J. Am. Chem. Soc*. **2009**, *131*, 17335-17344; (f) B. F. Fisher, L. Guo, B. S. Dolinar, I. A. Guzei, S. H. Gellman, *J. Am. Chem. Soc*. **2015**, *137*, 6484-6487; (g) B. F. Fisher, S. H. Gellman, *J. Am. Chem. Soc*. **2016**, *138*, 10766-10769.

10. S. Debnath, S. Ghosh, G. Pandit, P. Satpati, S. Chatterjee, *J. Org. Chem*. **2021**, *86*, 11310-11323.

11. (a) P. G. Vasudev, S. Chatterjee, K. Ananda, N. Shamala, P. Balaram, *Angew. Chem. Int. Ed*. **2008**, *47*, 6430-6432; *Angew. Chem*. **2008**, *120*, 6530-6532; (b) K. Ananda, P. G. Vasudev, A. Sengupta, K. M. P. Raja, N. Shamala, P. Balaram, *J. Am. Chem. Soc*. **2005**, 127, 16668-16674.
12. (a) R. Misra, G. George, A. Saseendran, S. Raghothama, H. N. Gopi, *Chem. Asian J*. **2019**, *14*, 4408-4414; (b) R. Misra, G. George, R. M. Reja, S. Dey, S. Raghothama, H. N. Gopi, *Chem. Commun*. **2020**, *56*, 2171-2173.
13. (a) R. Misra, A. Saseendran, G. George, K. Veeresh, K. M. P. Raja, S. Raghothama, H.-J. Hofmann, H. N. Gopi, *Chem. Eur. J*. **2017**, *23*, 3764-3772; (b) R. Misra, K. M. P. Raja, H.-J. Hofmann, H. N. Gopi, *Chem. Eur. J*. **2017**, *23*, 16644-16652; (c) S. V. Jadhav, H. N. Gopi, *Chem. Commun*. **2013**, *49*, 9179-9181.
14. (a) M. W. Giuliano, S. J. Maynard, A. M. Almeida, L. Guo, I. A. Guzei, L. C. Spencer, S. H. Gellman, *J. Am. Chem. Soc*. **2014**, *136*, 15046-15053; (b) B. F. Fisher, L. Guo, B. S. Dolinar, I. A. Guzei, S. H. Gellman, *J. Am. Chem. Soc*. **2015**, *137*, 6484-6487; (c) L. Guo, W. Zhang, I. A. Guzei, L. C. Spencer, S. H. Gellman, *Org. Lett*. **2012**, *14*, 2582-2585.
15. (a) M. Ganesh Kumar, H. N. Gopi, Org. Lett. 2015, 17, 4738-4741; (b) M. Ganesh Kumar, S. M. Mali, H. N. Gopi, *Org. Biomol. Chem*. **2013**,*11*, 803-813.
16. (a) D. Seebach, M. Brenner, M. Rueping, B. Schweizer, B. Jaun, *Chem. Commun*. **2001**, 207-208; (b) D. Seebach, M. Brenner, M. Rueping, B. Jaun, *Chem. Eur. J*. **2002**, *8*, 573-584; (c) M. Brenner, D. Seebach, *Helv. Chim. Acta*, **2001**, *84*, 1181-1189; (d) S. Hanessian, X. Luo, R. Schaum, S. Michnick, *J. Am. Chem. Soc*. **1998**, *120*, 8569-8570.
17. G. V. M. Sharma, V. B. Jadhav, K. V. S. Ramakrishna, P. Jayaprakash, K. Narsimulu, V. Subash, A. C. Kunwar, *J. Am. Chem. Soc*. **2006**, *128*, 14657-14668.
18. (a) A. Bandyopadhyay, A. Malik, M. G. Kumar, H. N. Gopi, *Org. Lett*. **2014**, *16*, 294-297; (b) A. Malik, M. G. Kumar, A. Bandyopadhyay, H. N. Gopi, *Peptide Science*, **2017**, *108*, e22978.
19. C. Baldauf, R. Günther, H.-J. Hofmann, *J. Org. Chem*. **2005**, *70*, 5351-536.
20. C. Baldauf, R. Günther, H.-J. Hofmann, *Helv. Chim. Acta*, **2003**, *86*, 2573-2588.
21. L. Mathieu, B. Legrand, C. Deng, L. Vezenkov, E. Wenger, C. Didierjean, M. Amblard, M.-C. Averlant-Petit, N. Masurier, V. Lisowski, J. Martinez, L.T. Maillard, *Angew. Chem. Int. Ed*. **2013**, *52*, 6006-6010; *Angew. Chem*, **2013**, *125*, 6122-6126.
22. M. Ganesh Kumar, V. J. Thombare, M. M. Katariya, K. Veeresh, K. M. P. Raja, H. N. Gopi, *Angew. Chem. Int. Ed*. **2016**, *55*, 7847-7851.
23. R. Misra, S. Dey, R. M. Reja, H. N. Gopi, *Angew. Chem., Int. Ed*. **2018**, *57*, 1057-1061.

24. (a) A. Bandyopadhyay, H. N. Gopi, *Org. Lett*. **2012**, *14*, 2770-2773; (b) S. M. Mali, A. Bandyopadhyay, S. V. Jadhav, M. Ganesh Kumar, H. N. Gopi, *Org. Biomol. Chem*. **2011**, *9*, 6566-6574.
25. K. Veeresh, H. N. Gopi, *Org. Lett*. **2019**, *21*, 4500-4504.
26. (a) A. El-Faham, F. Albericio, *Chem. Rev*. **2011**, *111*, 6557−6602; (b) E. Valeur, M. Bradley, *Chem. Soc. Rev*. **2009**, *38*, 606−631; (c) J. R. Dunetz, J. Magano, G. A. Weisenburger, *Org. Process Res. Dev*. **2016**, *20*, 140−177.
27. S. C. Shankaramma, S. Kumar Singh, A. Sathyamurthy, P. Balaram, *J. Am. Chem. Soc.* **1999**, *121*, 5360-5363.
28. (a) G. M. Sheldrick, Phase annealing in SHELX-90: direct methods for larger structures. Acta Crystallogr. **1990**, *A46*, 467-473; (b) G. M. Sheldrick, SHELXL-97, Program for Crystal Structure Solution and Refinement, Universität Göttingen, Göttingen (Germany), **1997**.
29. A. L. Spek, Acta Crystallogr. PLATON, an integrated tool for the analysis of the results of a single crystal structure determination. **1990**, *A46*, C34.

5.7. Appendix

S. No	Content	Page No
5.7.1.	**Ortep plot and crystallographic information of 5a, P1, P2 and P3**	**334**
5.7.2	**^{1}H NMR and ^{13}C NMR spectra of all compounds**	**339**

5.7.1. Ortep plot and crystallographic information of 5a, P1, P2 and P3

5.7.1.1. Ortep plot of 5a, P1, P2 and P3

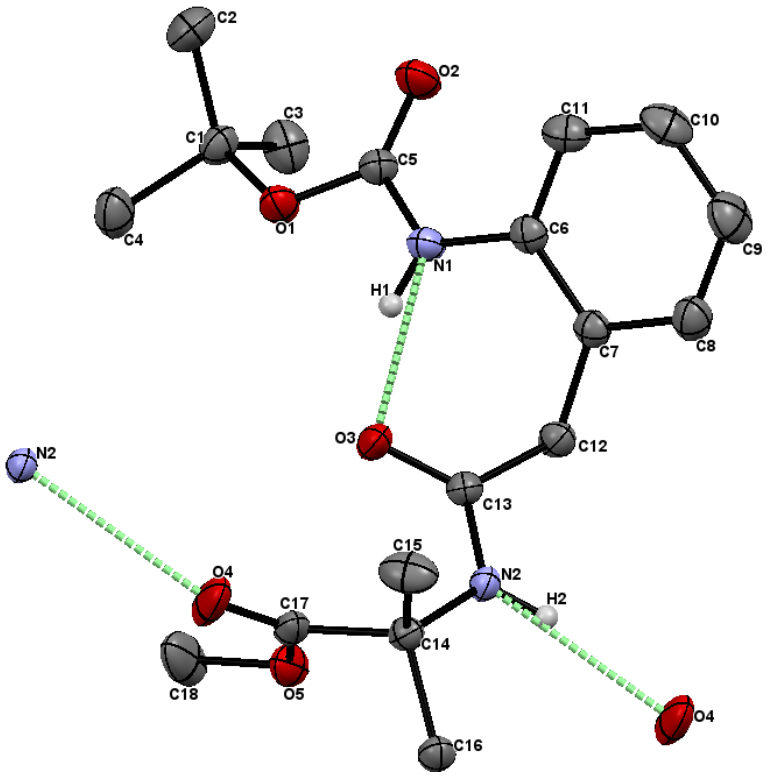


Figure 20: ORTEP diagram of peptide **5a** (Boc-Apa-Aib-OMe). Ellipsoids are drawn at 50% probability. H-atoms are omitted for clarity. [Apa = 2-Aminophenyl Acetic Acid] (**CCDC no : 2310876**)

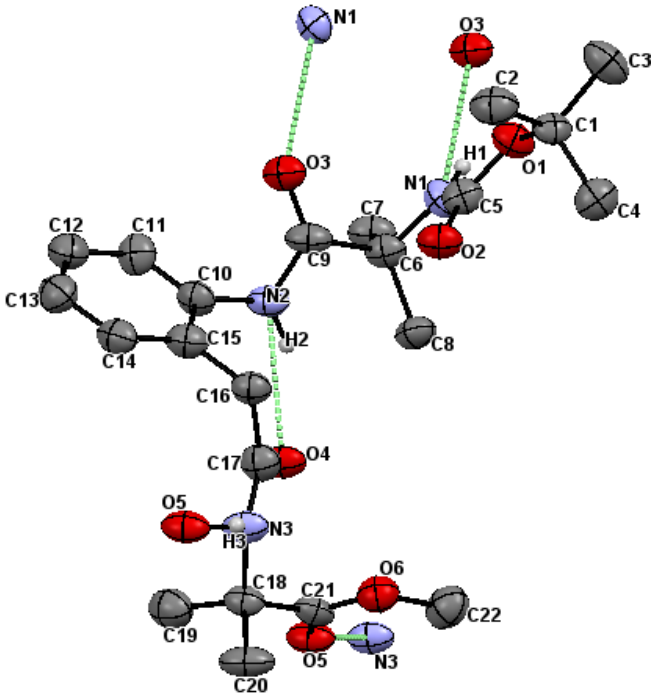


Figure 21: ORTEP diagram of peptide **P1** (Boc-Aib-Apa-Aib-OMe). Ellipsoids are drawn at 50% probability. H-atoms are omitted for clarity. [Apa = 2-Aminophenyl Acetic Acid] (**CCDC no : 2310842**)

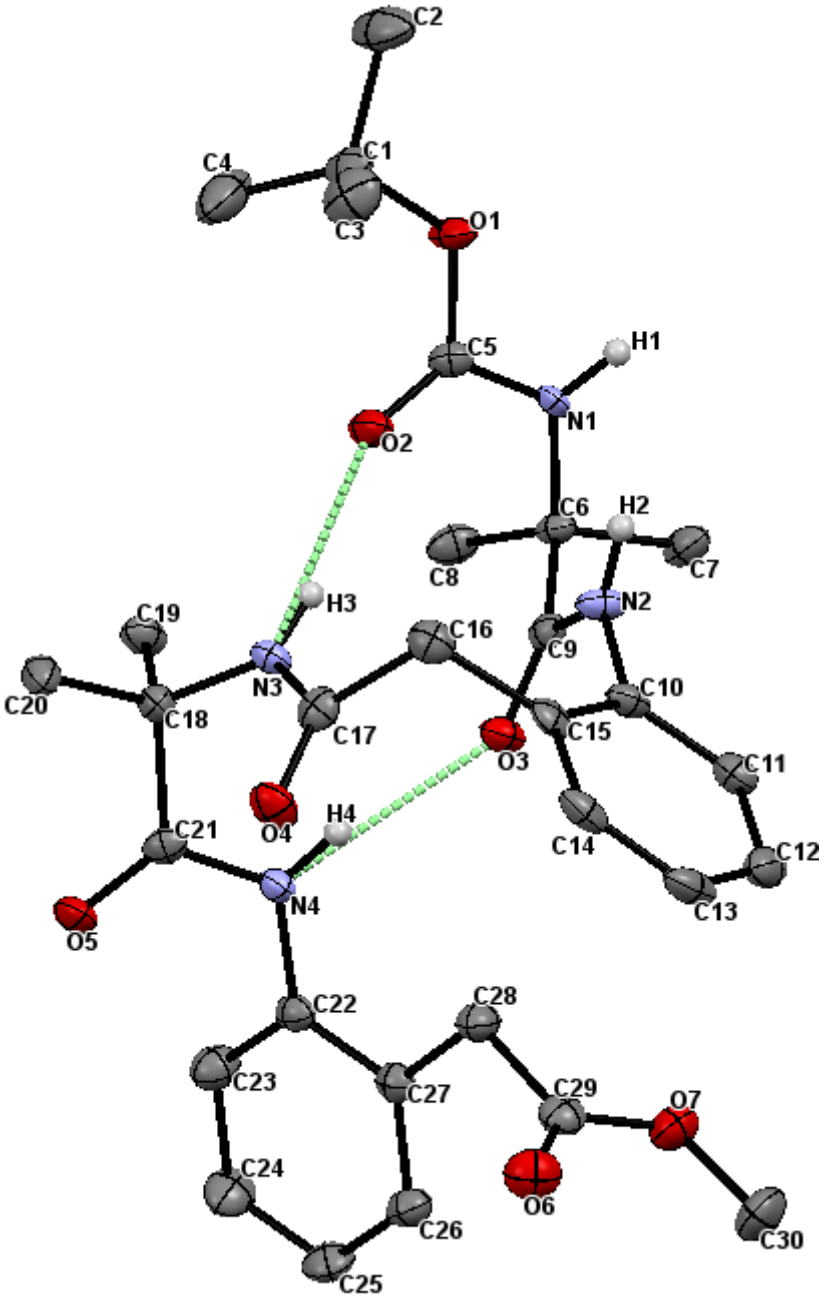


Figure 22: ORTEP diagram of peptide **P2** (Boc-Aib-Apa-Aib-Apa-OMe). Ellipsoids are drawn at 50% probability. H-atoms are omitted for clarity. (**CCDC no : 2310843**)

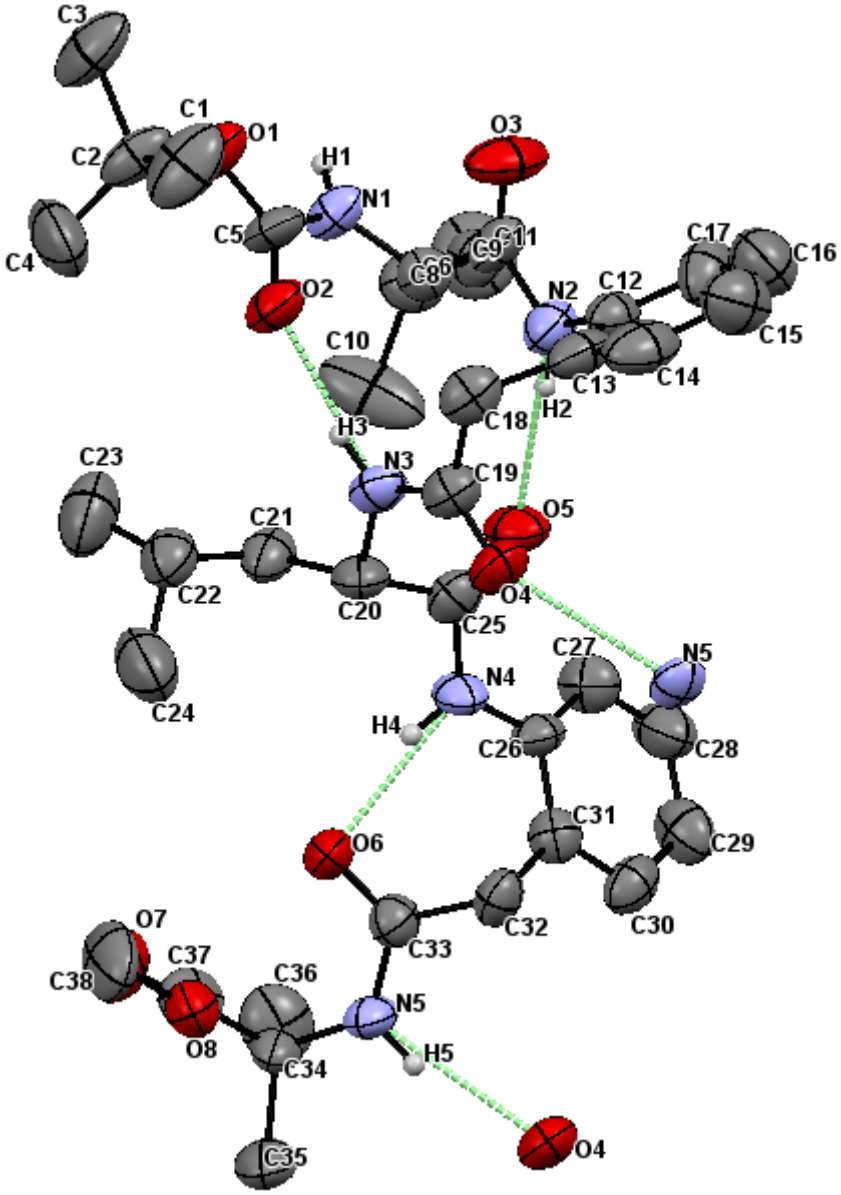


Figure 23: ORTEP diagram of peptide **P3** (Boc-Leu-Apa-Leu-Apa-Aib-OMe). Ellipsoids are drawn at 50% probability. H-atoms are omitted for clarity. (**CCDC no : 2310844**)

5.7.1.2. Crystallographic information of 5a, P1, P2 and P3

Boc-Apa-Aib-OMe (5a): Crystals of Boc-Apa-Aib-OMe (**5a**) were grown by slow evaporation from a solution of ethyl acetate. A single crystal (0.1 × 0.06 × 0.03 mm) was mounted on loop with a small amount of the paraffin oil. The X-ray data were collected at 100K temperature on a Bruker APEX(II) DUO CCD diffractometer using Mo K_α radiation (λ = 0.71073 Å), ω-scans (2θ = 56.94), for a total of 35337 independent reflections. Space group P21/c, a = 5.9366(5), b = 14.0149(12), c = 22.808(2), β = 91.91(2), V = 1896.6 (3) $Å^3$,

Monoclinic, Z = 4 for chemical formula C_{18} H_{26} N_2 O_5, with one molecule in asymmetric unit; ρcalcd = 1.227 gcm^{-3}, μ = 0.09 mm^{-1}, F (000) = 752, R_{int} = 0.0674. The structure was obtained by direct methods using SHELXS-97.[27] The final R value was 0.0499 (wR2 = 0.1458) 4770 observed reflections ($F_0 \geq 4\sigma$ (|F_0|)) and 232 variables, S = 1.091. The largest difference peak and hole were 0.240 and -0.277 eÅ^3, respectively.

Boc-Aib-Apa-Aib-OMe (P1): Crystals of Boc-Aib-Apa-Aib-OMe (**P1**) were grown by slow evaporation from a solution of ethyl acetate. A single crystal (0.7 × 0.6 × 0.5 mm) was mounted on loop with a small amount of the paraffin oil. The X-ray data were collected at 100K temperature on a Bruker APEX(II) DUO CCD diffractometer using Mo K_α radiation (λ = 0.71073 Å), ω-scans (2θ = 60.24), for a total of 16410 independent reflections. Space group P -1, a = 6.198(6), b = 12.654(13), c = 15.616(16), β = 93.310(17), V = 1213(2) Å^3, Triclinic, Z = 2 for chemical formula C_{22} H_{33} N_3 O_6, with one molecule in asymmetric unit; ρcalcd = 1.192 gcm^{-3}, μ = 0.087 mm^{-1}, F (000) = 468, R_{int} = 0.3219. The structure was obtained by direct methods using SHELXS-97.[28] The final R value was 0.1204 (wR2 = 0.2327) 6716 observed reflections ($F_0 \geq 4\sigma$ (|F_0|)) and 232 variables, S = 0.899. The largest difference peak and hole were 0.444 and -0.409 eÅ^3, respectively.

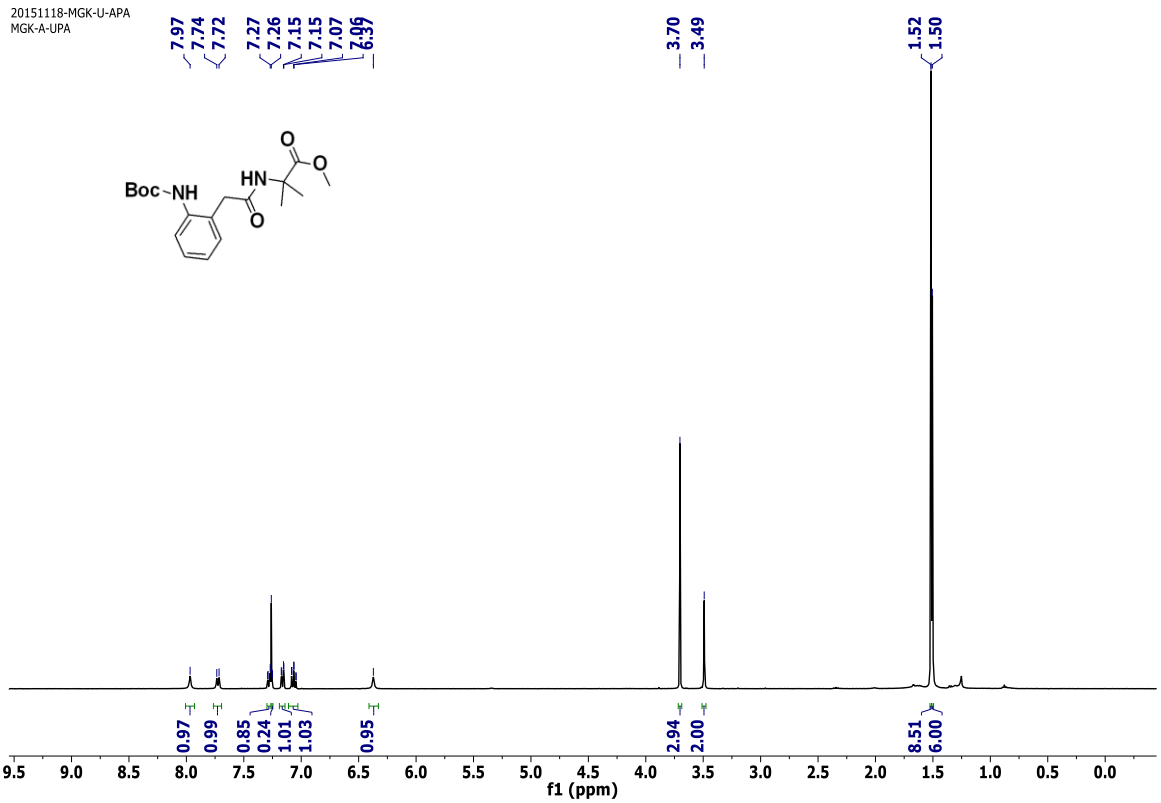
Boc-Aib-Apa-Aib-Apa-OMe (P2): Crystals of Boc-Aib-Apa-Aib-Apa-OMe (**P2**) were grown by slow evaporation from a solution of ethyl acetate. A single crystal (0.2 × 0.1 × 0.04 mm) was mounted on loop with a small amount of the paraffin oil. The X-ray data were collected at 100K temperature on a Bruker APEX(II) DUO CCD diffractometer using Mo K_α radiation (λ = 0.71073 Å), ω-scans (2θ = 56.6), for a total of 7315 independent reflections. Space group P -1, a = 9.7523(15), b = 10.4724(18), c = 15.048(3), β = 90.28(4), V = 1489.2 (4) Å^3, triclinic, Z = 2 for chemical formula $C_{30}H_{40}N_4O_7$, with one molecule in asymmetric unit; ρcalcd = 1.268 gcm^{-3}, μ = 0.091 mm^{-1}, F (000) = 608, R_{int} = 0.0249. The structure was obtained by direct methods using SHELXS-97.[28] The final R value was 0.0483 (wR2 = 0.1309) 5681 observed reflections ($F_0 \geq 4\sigma$ (|F_0|)) and 378 variables, S = 0.934. The largest difference peak and hole were 0.343 and -0.311 eÅ^3, respectively.

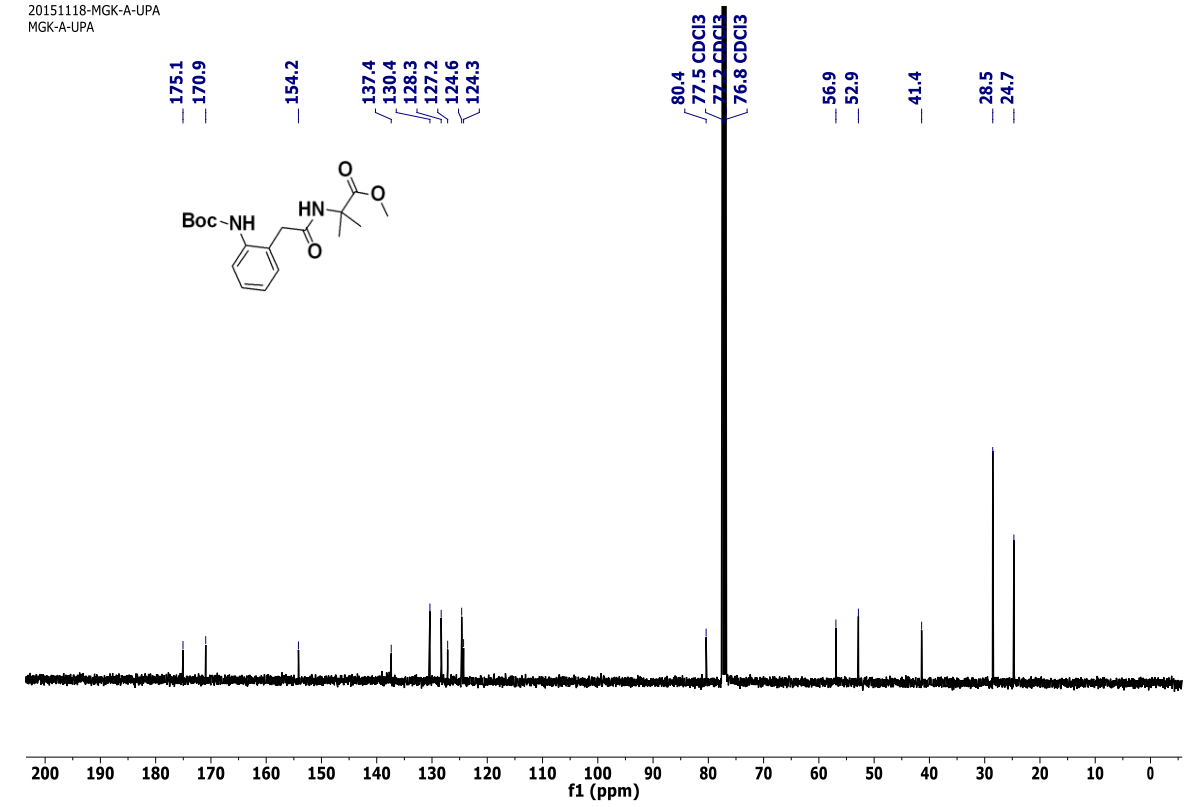
Boc-Leu-Apa-Leu-Apa-OMe (P3): Crystals of Boc-Leu-Apa-Leu-Apa-Aib-OMe (**P3**) were grown by slow evaporation from a solution of ethyl acetate. A single crystal (0.4 × 0.1 × 0.03 mm) was mounted on loop with a small amount of the paraffin oil. The X-ray data were collected at 100K temperature on a Bruker APEX(II) DUO CCD diffractometer using Cu K_α radiation (λ = 1.54178 Å), ω-scans (2θ = 64.44), for a total of 25671 independent reflections. Space group P 21, a = 14.6260(17), b = 10.2963(13), c = 19.187(2), β = 97.049(7), V = 2867.5(6) Å^3, Monoclinic, Z = 2 for chemical formula $C_{38}H_{55}N_5O_8$, with one molecule in

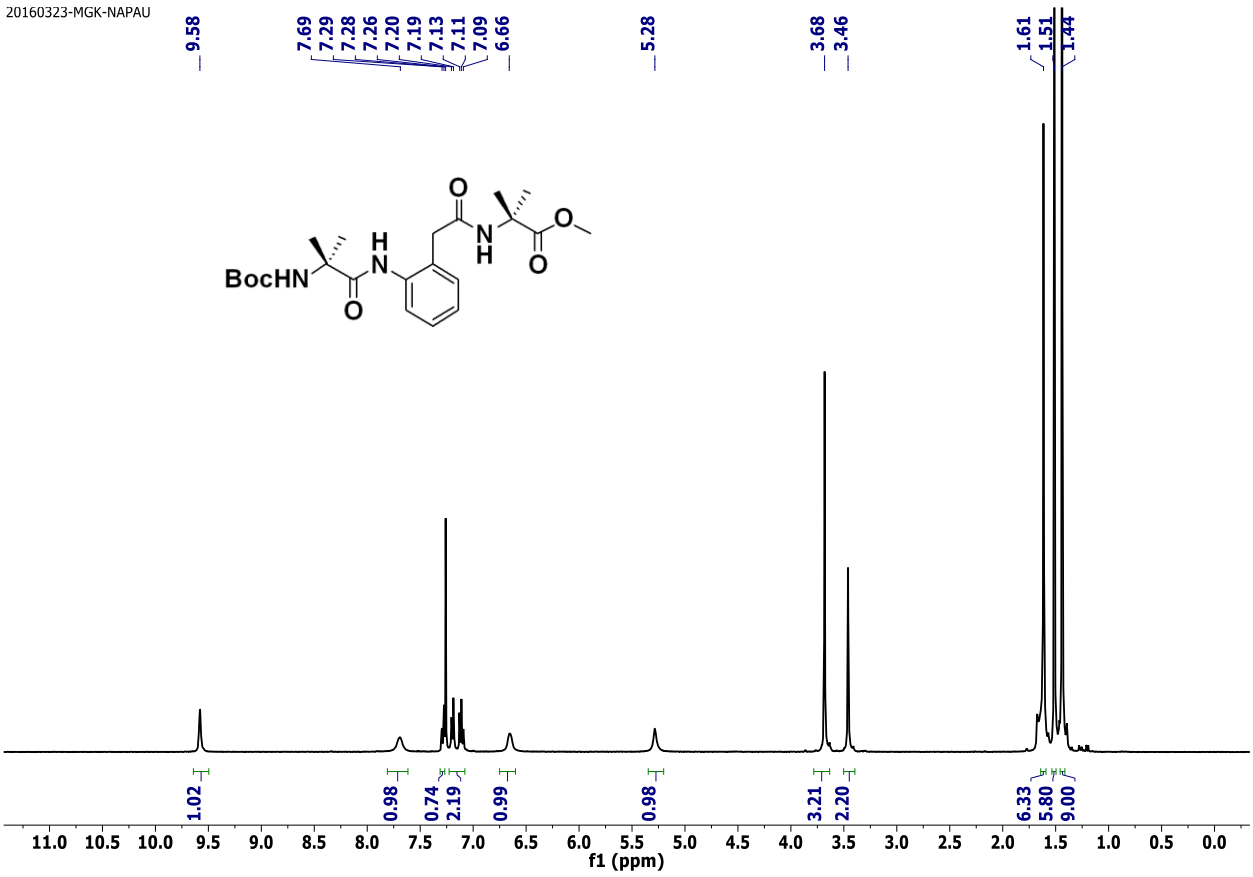
asymmetric unit; ρcalcd = 0.822 gcm^{-3}, μ = 0.0471 mm^{-1}, F (000) = 764, R_{int} = 0.11. The structure was obtained by direct methods using SHELXS-97.[28] The final R value was 0.1252 (wR2 = 0.32) 6706 observed reflections ($F_0 \geq 4\sigma(|F_0|)$) and 447 variables, S = 1.067. The largest difference peak and hole were 0.299 and -0.306 eÅ^3, respectively.

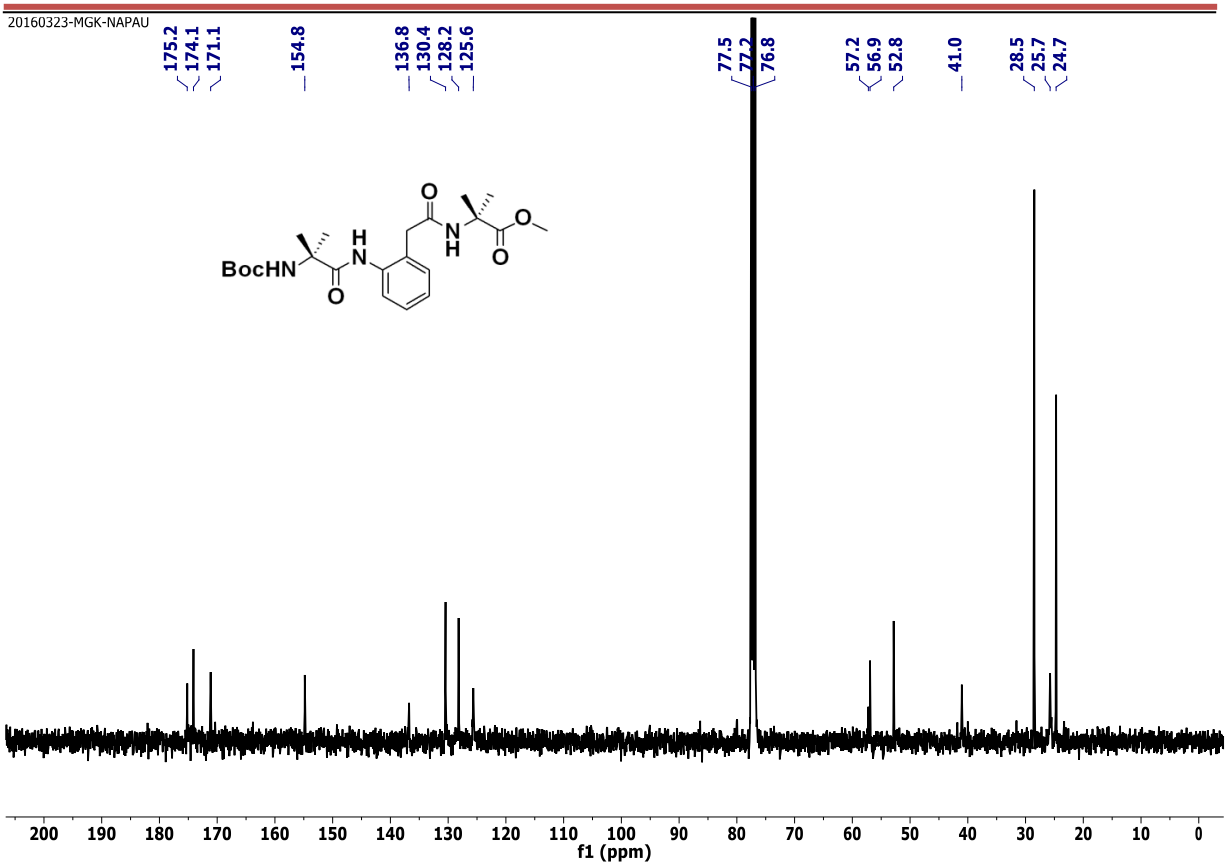
There is some partially occupied solvent molecule also present in the asymmetric unit. A significant amount of time was invested in identifying and refining the disordered molecule. Option SQUEEZE of program PLATON[29] was used to correct the diffraction data for diffuse scattering effects and to identify the solvent molecule. PLATON calculated the upper limit of volume that can be occupied by the solvent to be 1148.5 Å^3. No data are given for the diffusely scattering species. Outputs of SQUEEZE report are appended in CIF file **P3**.

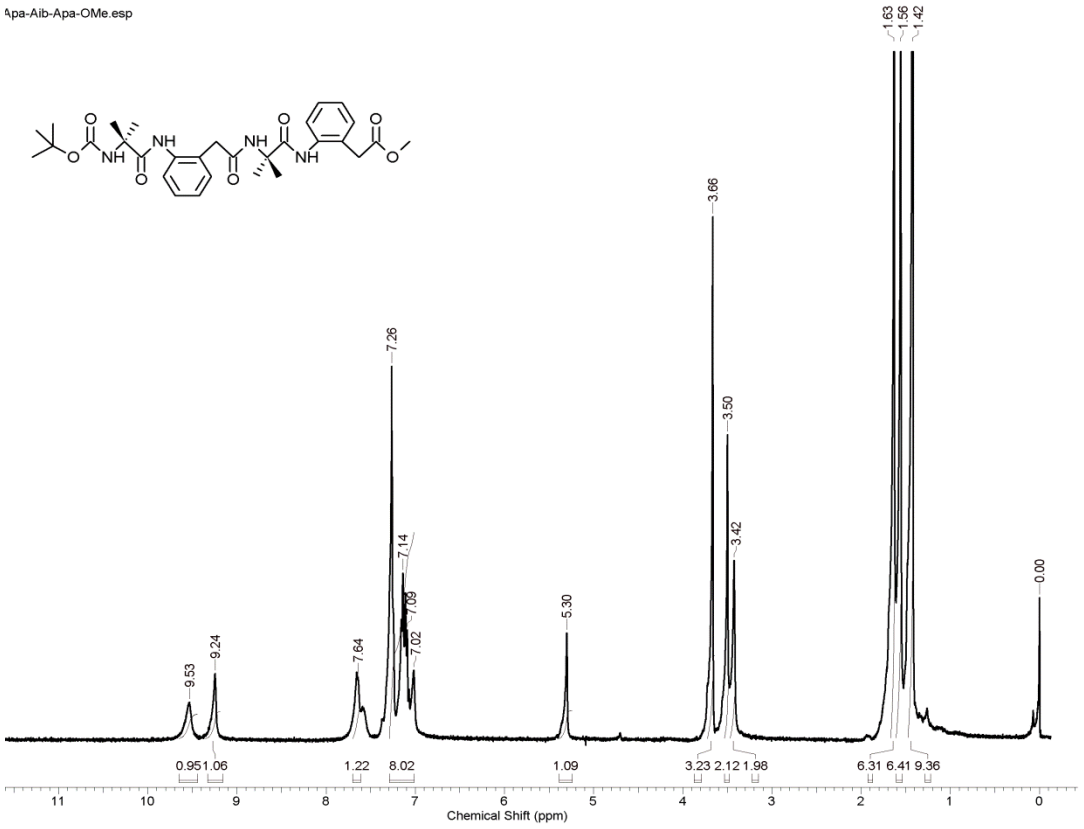
5.7.2. ^{1}H NMR and ^{13}C NMR spectra of all compounds

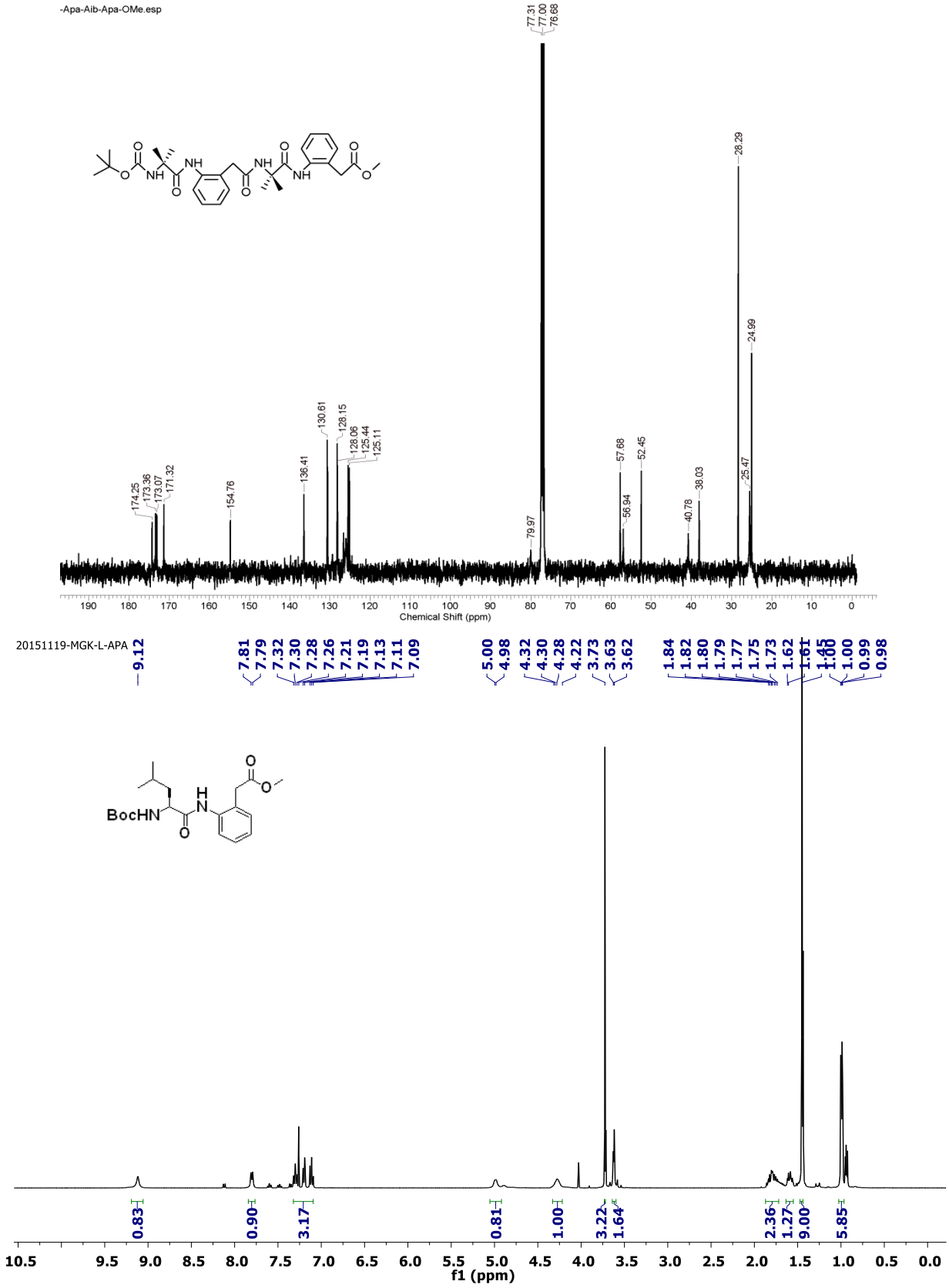


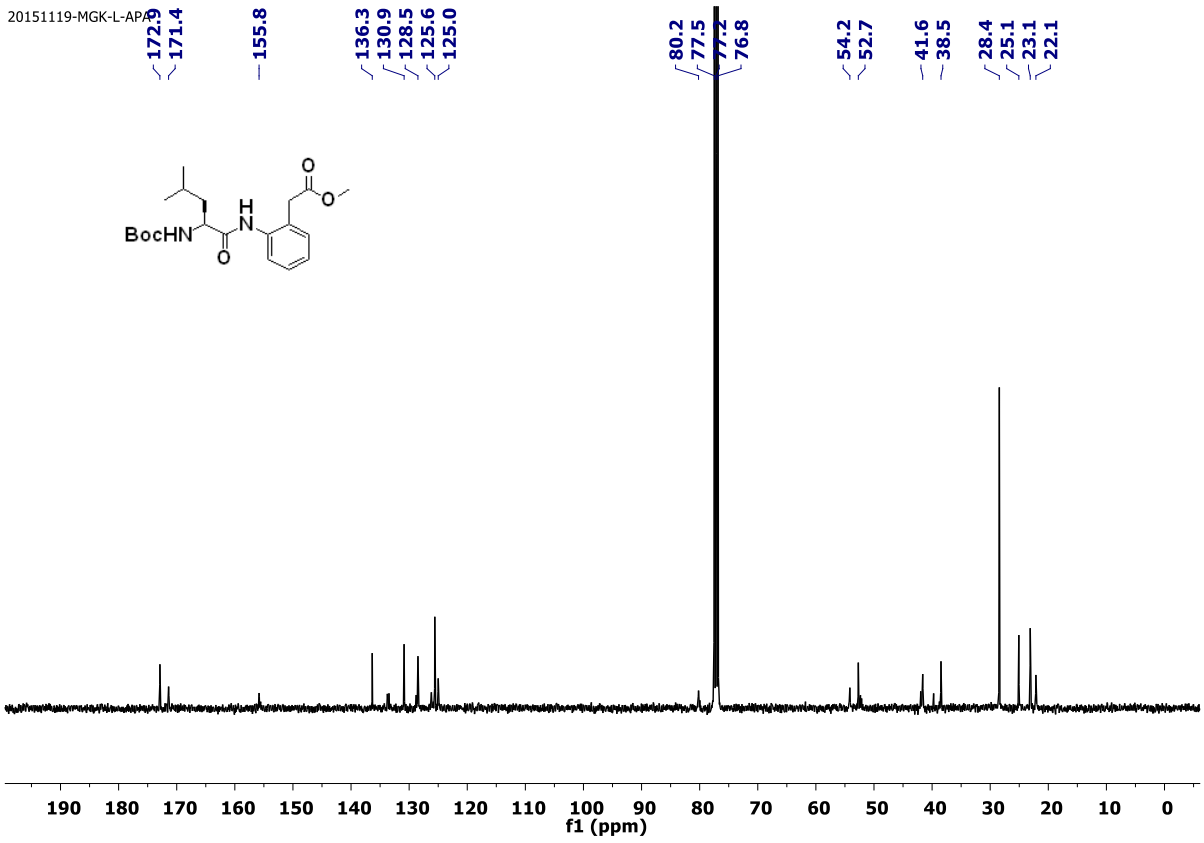

20151118-MGK-A-UPA
MGK-A-UPA
175.1
170.9
154.2
137.4
130.4
128.3
127.2
124.6
124.3
80.4
77.5 CDCl3
77.2 CDCl3
76.8 CDCl3
56.9
52.9
41.4
28.5
24.7
Boc-NH
HN
O
O
O
O
200 190 180 170 160 150 140 130 120 110 100 90 80 70 60 50 40 30 20 10 0
f1 (ppm)

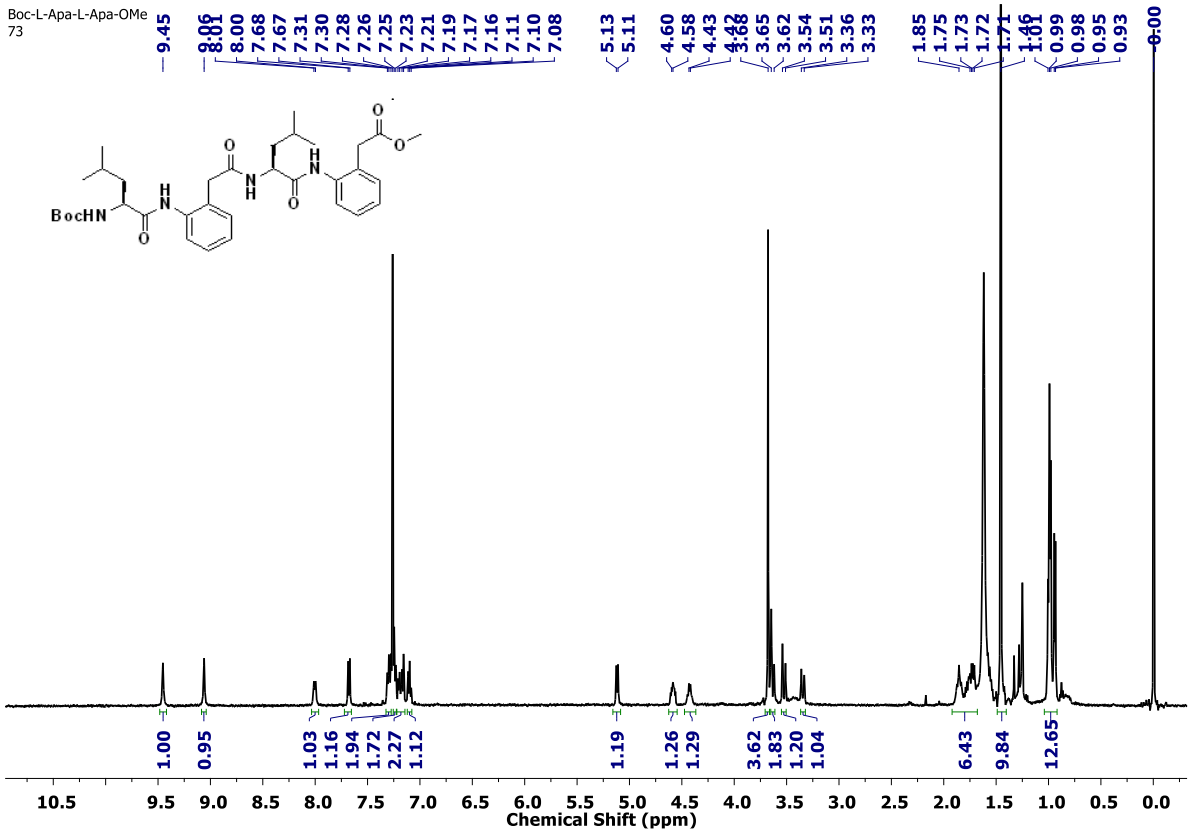

20160323-MGK-NAPAU
9.58
7.69
7.29
7.28
7.26
7.20
7.19
7.13
7.11
7.09
6.66
5.28
3.68
3.46
1.61
1.51
1.44
BocHN
H
N
O
N
H
O
O
1.02
0.98
0.74
2.19
0.99
0.98
3.21
2.20
6.33
5.80
9.00
11.0 10.5 10.0 9.5 9.0 8.5 8.0 7.5 7.0 6.5 6.0 5.5 5.0 4.5 4.0 3.5 3.0 2.5 2.0 1.5 1.0 0.5 0.0
f1 (ppm)

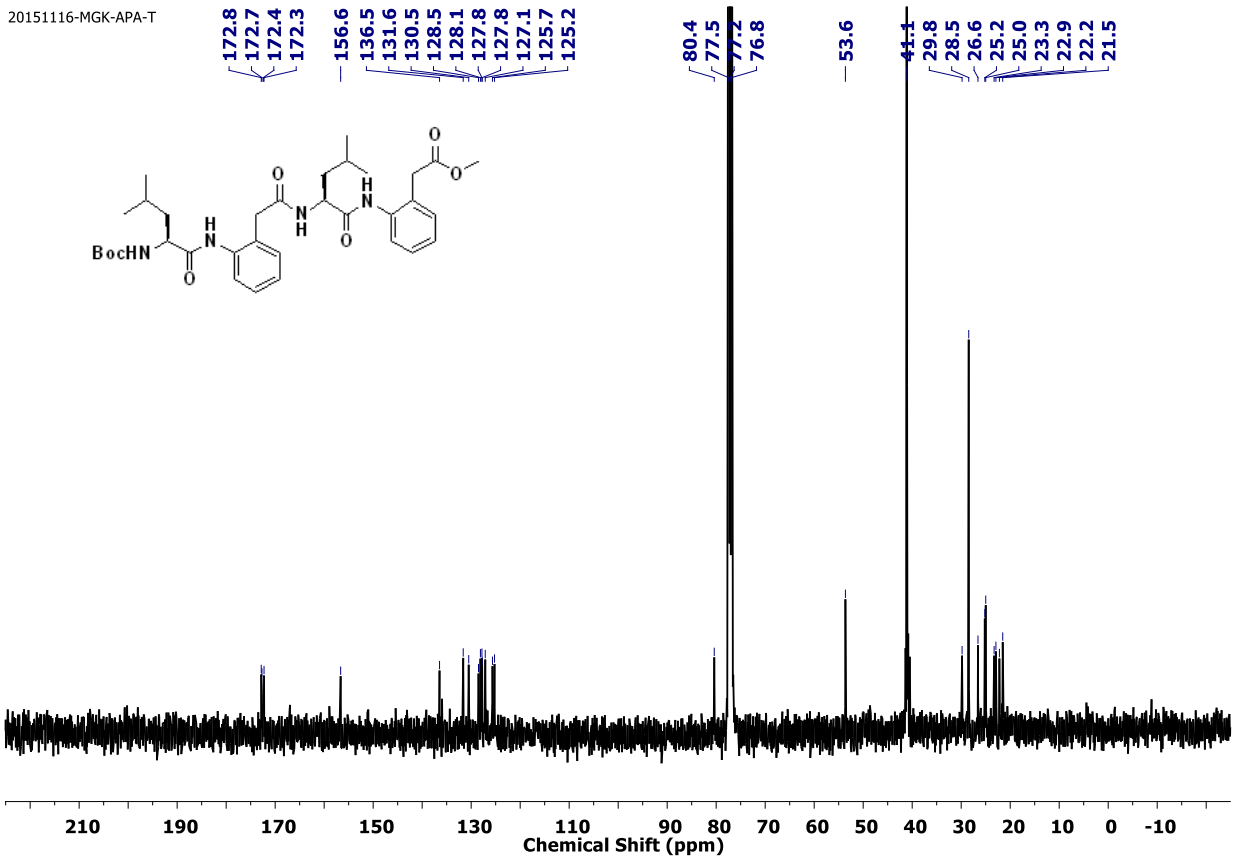

20160323-MGK-NAPAU
175.2
174.1
171.1
154.8
136.8
130.4
128.2
125.6
77.5
77.2
76.8
57.2
56.9
52.8
41.0
28.5
25.7
24.7
BocHN
f1 (ppm)

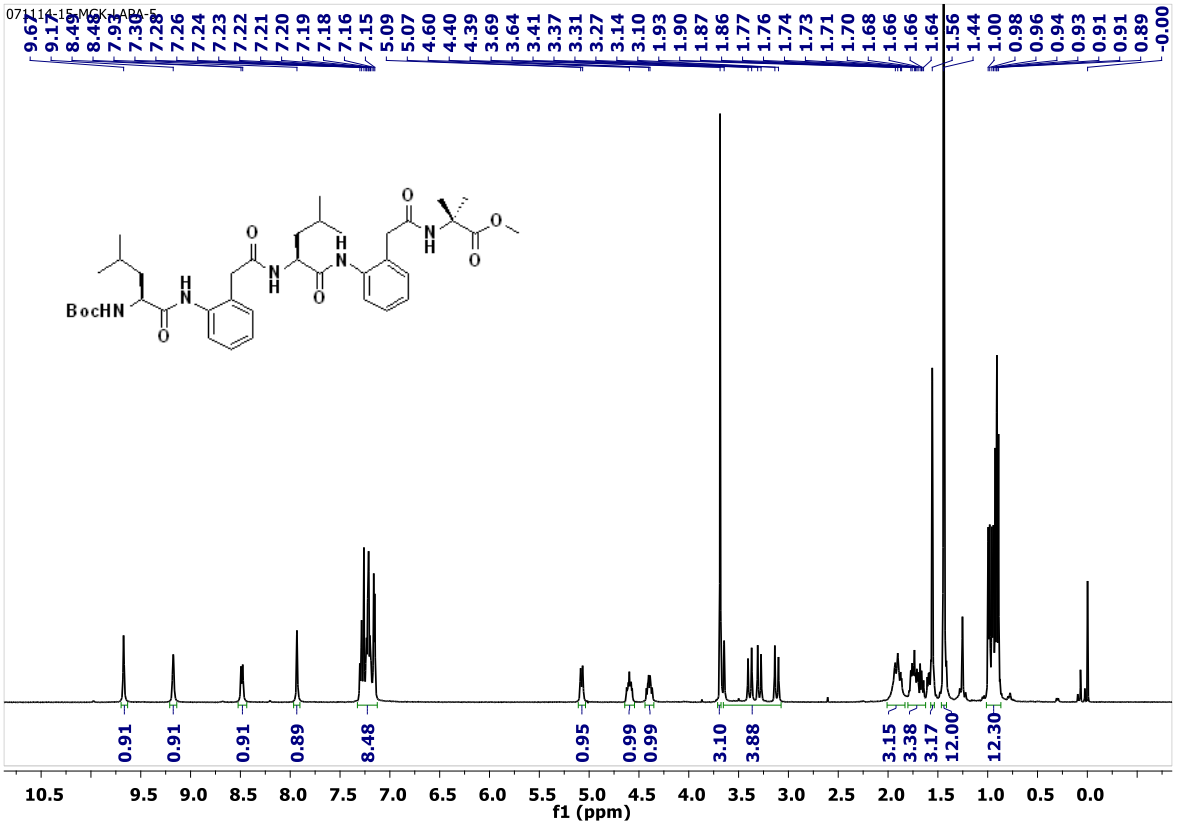

Apa-Aib-Apa-OMe.esp
1.63
1.56
1.42
3.66
3.50
3.42
7.26
7.14
7.09
7.02
9.53
9.24
7.64
5.30
0.00
0.95 1.06
1.22
8.02
1.09
3.23 2.12 1.98
6.31 6.41 9.36
Chemical Shift (ppm)

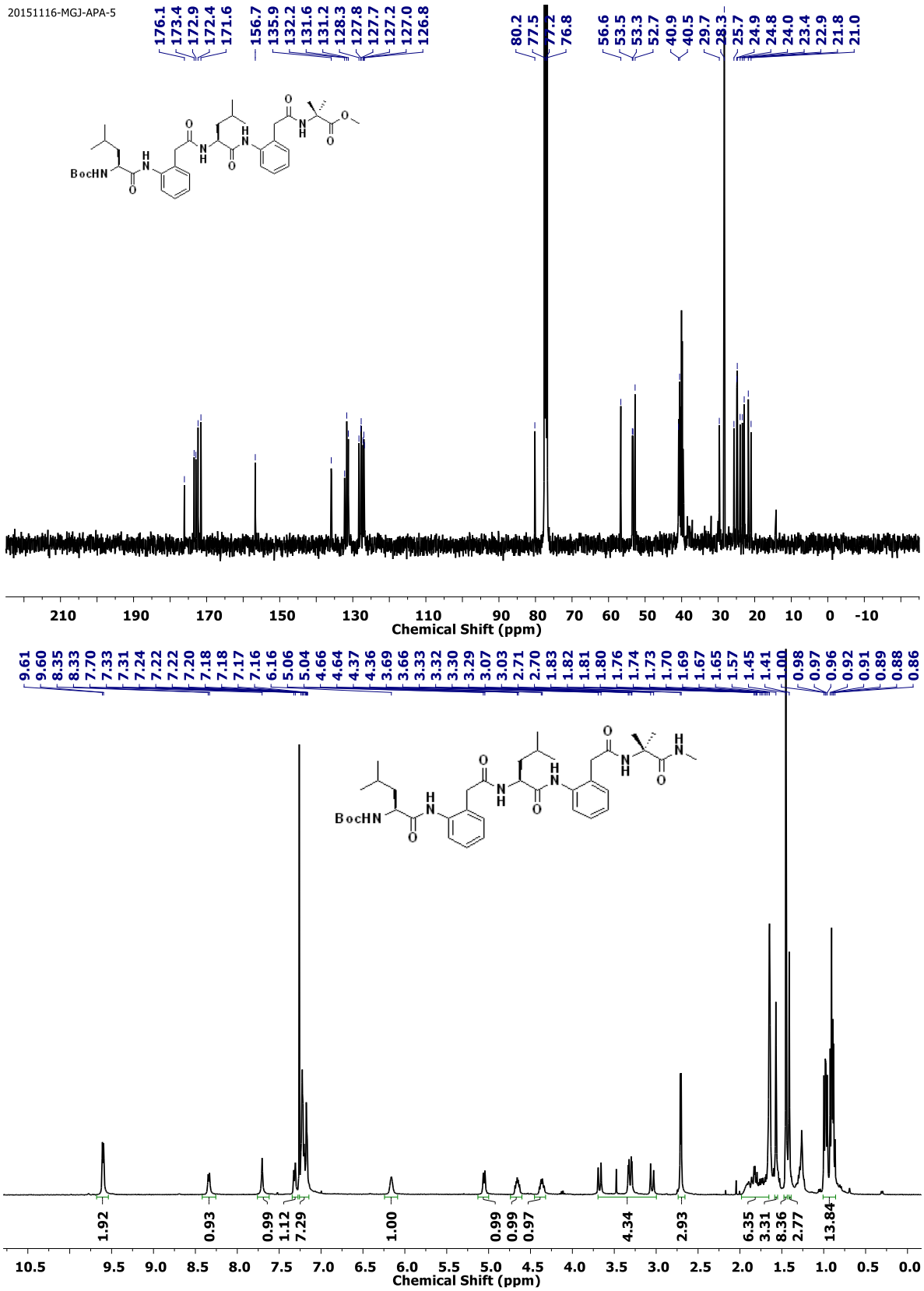

-Apa-Aib-Apa-OMe.esp
77.31
77.00
76.68
28.29
24.99
130.61
128.15
128.06
125.44
125.11
136.41
174.25
173.36
173.07
171.32
154.76
79.97
57.68
52.45
56.94
40.78
38.03
25.47
Chemical Shift (ppm)
20151119-MGK-L-APA
9.12
7.81
7.79
7.32
7.30
7.28
7.26
7.21
7.19
7.13
7.11
7.09
5.00
4.98
4.32
4.30
4.28
4.22
3.73
3.63
3.62
1.84
1.82
1.80
1.79
1.77
1.75
1.73
1.62
1.61
1.00
0.99
0.98
BocHN
0.83
0.90
3.17
0.81
1.00
3.22
1.64
2.36
1.27
9.00
5.85
f1 (ppm)

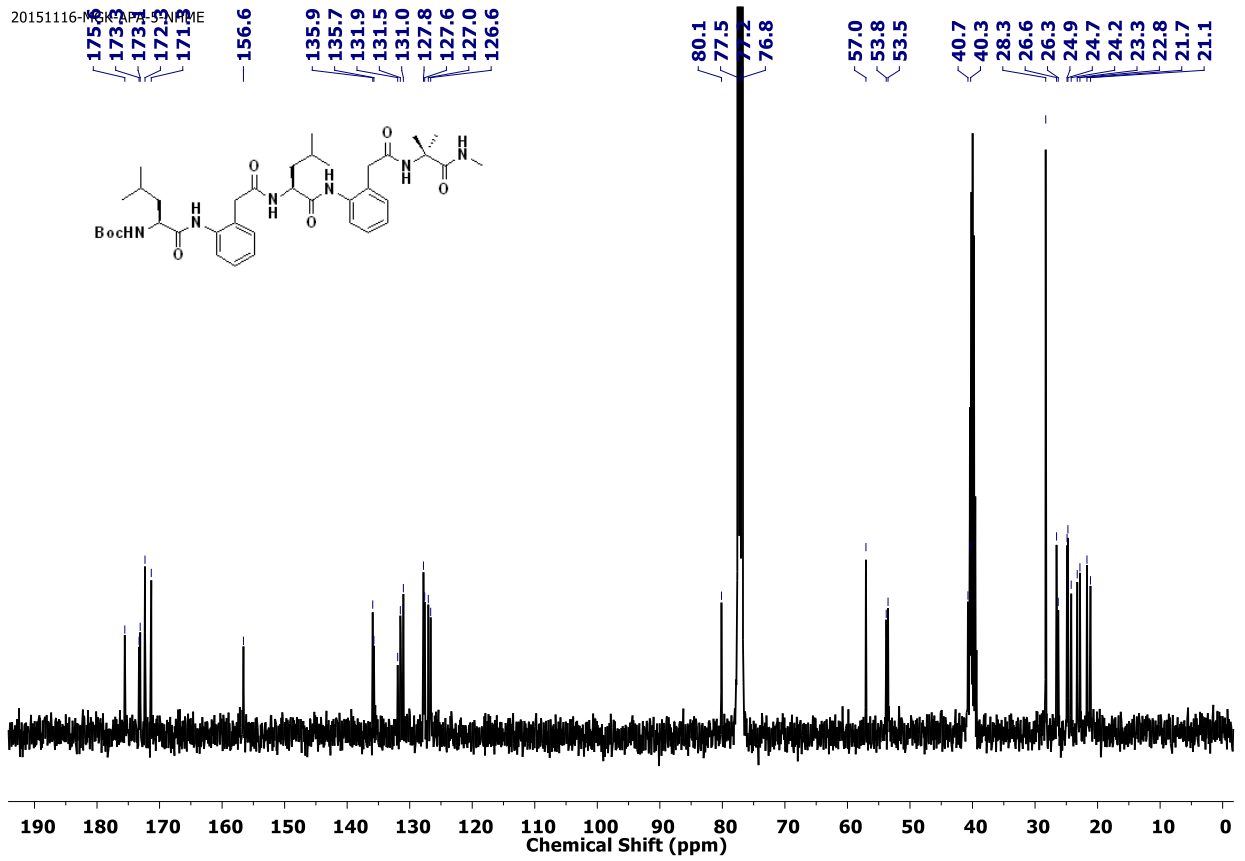

20151119-MGK-L-APA
172.9
171.4
155.8
136.3
130.9
128.5
125.6
125.0
80.2
77.5
77.2
76.8
54.2
52.7
41.6
38.5
28.4
25.1
23.1
22.1
BocHN
f1 (ppm)

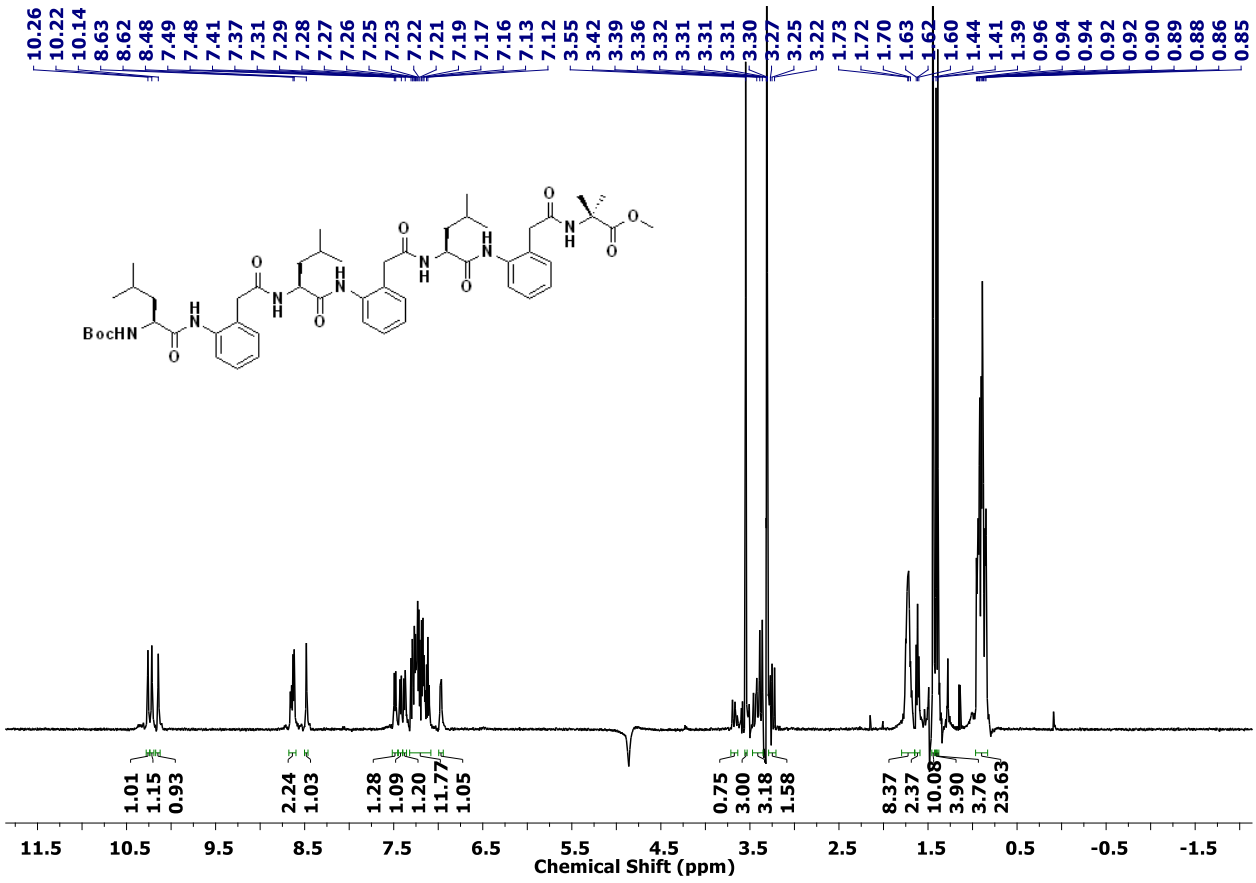

Boc-L-Apa-L-Apa-OMe
73
9.45
8.06
8.01
8.00
7.68
7.67
7.31
7.30
7.28
7.26
7.25
7.23
7.21
7.19
7.17
7.16
7.11
7.10
7.08
5.13
5.11
4.60
4.58
4.43
4.42
3.68
3.65
3.62
3.54
3.51
3.36
3.33
1.85
1.75
1.73
1.72
1.71
1.46
1.01
0.99
0.98
0.95
0.93
0.00
BocHN
1.00
0.95
1.03
1.16
1.94
1.72
2.27
1.12
1.19
1.26
1.29
3.62
1.83
1.20
1.04
6.43
9.84
12.65
Chemical Shift (ppm)


20151116-MGK-APA-T
172.8
172.7
172.4
172.3
156.6
136.5
131.6
130.5
128.5
128.1
127.8
127.8
127.1
125.7
125.2
80.4
77.5
77.2
76.8
53.6
44.1
29.8
28.5
26.6
25.2
25.0
23.3
22.9
22.2
21.5
BocHN
Chemical Shift (ppm)


071114-15-MGK-APA-5
9.67
9.17
8.49
8.48
7.93
7.30
7.28
7.26
7.24
7.23
7.22
7.21
7.20
7.19
7.18
7.16
7.15
5.09
5.07
4.60
4.40
4.39
3.69
3.64
3.41
3.37
3.31
3.27
3.14
3.10
1.93
1.90
1.87
1.86
1.77
1.76
1.74
1.73
1.71
1.70
1.68
1.66
1.66
1.64
1.56
1.44
1.00
0.98
0.96
0.94
0.93
0.91
0.91
0.89
-0.00
BocHN
0.91
0.91
0.91
0.89
8.48
0.95
0.99
0.99
3.10
3.88
3.15
3.38
3.17
12.00
12.30
f1 (ppm)


20151116-MGJ-APA-5
176.1
173.4
172.9
172.4
171.6
156.7
135.9
132.2
131.6
131.2
128.3
127.8
127.7
127.2
127.0
126.8
80.2
77.5
77.2
76.8
56.6
53.5
53.3
52.7
40.9
40.5
29.7
28.3
25.7
24.9
24.8
24.0
23.4
22.9
21.8
21.0
BocHN
Chemical Shift (ppm)
9.61
9.60
8.35
8.33
7.70
7.33
7.31
7.24
7.22
7.22
7.20
7.18
7.18
7.17
7.16
6.16
5.06
5.04
4.66
4.64
4.37
4.36
3.69
3.66
3.33
3.32
3.30
3.29
3.07
3.03
2.71
2.70
1.83
1.82
1.81
1.80
1.76
1.74
1.73
1.70
1.69
1.67
1.65
1.57
1.45
1.41
1.00
0.98
0.97
0.96
0.92
0.91
0.89
0.88
0.86
BocHN
1.92
0.93
0.99
1.12
7.29
1.00
0.99
0.99
0.97
4.34
2.93
6.35
3.31
8.36
2.77
13.84
Chemical Shift (ppm)


20151116-MSK-AP4-5-NME
175.3
173.3
173.1
172.3
171.2
156.6
135.9
135.7
131.9
131.5
131.0
127.8
127.6
127.0
126.6
80.1
77.5
77.2
76.8
57.0
53.8
53.5
40.7
40.3
28.3
26.6
26.3
24.9
24.7
24.2
23.3
22.8
21.7
21.1
BocHN
Chemical Shift (ppm)


10.26
10.22
10.14
8.63
8.62
8.48
7.49
7.48
7.41
7.37
7.31
7.29
7.28
7.27
7.26
7.25
7.23
7.22
7.21
7.19
7.17
7.16
7.13
7.12
3.55
3.42
3.39
3.36
3.32
3.31
3.31
3.31
3.30
3.27
3.25
3.22
1.73
1.72
1.70
1.63
1.62
1.60
1.44
1.41
1.39
0.96
0.94
0.94
0.92
0.92
0.90
0.89
0.88
0.86
0.85
BocHN
1.01
1.15
0.93
2.24
1.03
1.28
1.09
1.20
11.77
1.05
0.75
3.00
3.18
1.58
8.37
2.37
10.08
3.90
3.76
23.63
Chemical Shift (ppm)